DISSERTATION ZUR ERLANGUNG DES DOKTORGRADES
DER FAKULTÄT FÜR CHEMIE UND PHARMAZIE
DER LUDWIG-MAXIMILIANS-UNIVERSITÄT MÜNCHEN

ENERGETIC MATERIALS CONTAINING THE TRINITROMETHYL PSEUDOHALIDE FUNCTIONALITY

MICHAEL GÖBEL
AUS
LANDAU / PFALZ
2009

Erklärung

Diese Dissertation wurde im Sinne von § 1 Abs. 3 bzw. 4 der Promotionsordnung vom 29. Januar 1998 von Herrn Prof. Dr. Thomas M. Klapötke betreut.

Ehrenwörtliche Versicherung

Diese Dissertation wurde selbstständig, ohne unerlaubte Hilfe erarbeitet.

München, den 18.11.2009

_____

Michael Göbel

Dissertation eingereicht am 20.11.2009

1. Gutachter: Prof. Dr. Thomas M. Klapötke
2. Gutachter: Prof. Dr. Wolfgang Beck

Mündliche Prüfung am 18.12.2009

Contents

Scope

Chapter 1 represents the introduction and is composed of three major parts. Part 1 is an introduction into general aspects of energetic materials. It covers important definitions of energetic materials as well as frequently used test methods used to assess their properties. Part 2 is an introduction into the chemistry related to the trinitromethyl group and describes important features related to this group. Part 3 of the introduction contains the conceptual formulation and objectives of this thesis and covers safety regulations mandatory for laboratory work.

Chapter 2 contains the results obtained during this dissertation together with their discussion. It is comprised of two parts: ionic energetic compounds and energetic molecules. The ionic compounds contain anions of trinitromethane or 3,5-diamino-2,4,6-trinitrophenol as well as some simple acids. The second part of Chapter 2 contains energetic molecules and is comprised of compounds carrying the trinitroethyl moiety followed by a chapter about valuable precursor molecules for the synthesis of novel energetic materials. The final part of Chapter 2 contains a selection of simple molecules containing pseudohalide functionalities. The chapter about mercury fulminate represents in large parts the original publication with a shared authorship.

A summary of important results obtained within the scope of this thesis is provided in **Chapter 3**.

Additional data include abbreviations, general safety regulations, a summary of standard operating procedures, frequency analyses, single crystal X-ray data, constitute the appendix to this thesis denoted as **Chapter 4**.

Chapter 1

Introduction

The development and testing of energetic materials is an exciting and challenging area of chemistry both as far as fundamental and applied aspects are concerned. Though the development of this kind of materials, which include high explosives, propellants, and pyrotechnics has a long standing tradition in the chemical sciences, research and efforts are undertaken world-wide as never before, foremost driven by the prospect of outstanding materials properties in general, and in order to discover new representatives having significant advantages over compounds currently used. Environmental considerations and safety requirements are important driving factors next to higher performance and tailored properties for special applications. Due to their unique properties, these materials are useful for manifold and highly diverse applications ranging from military to civilian areas in many industries including but not limited to construction, mining, oil exploration as well as space exploration. Solid high explosives produce a velocity of detonation of up to three times the velocity of sound in the explosive (9000 m s^{-1}), a high liberated energy density of about 6 megajoules per kilogram (MJ kg^{-1}) and an initial material density of about 2000 kilograms per cubic meter (kg m^{-3}). The product of these quantities corresponds to a power density of 1 x 10^{10} W cm^{-2}. By comparison, a detonating explosive having a surface of 100 cm^2 operates at a power level of 1.000.000 MW which is equal to the total average electric generating capacity of the United States in the year 2007. [1] This very rapid rate of energy liberation is what makes explosives unique. [2] Obtaining such materials is complex owing to the fact that several different and mutually exclusive appearing material properties have to be met to find the molecule fulfilling all the qualification criteria in order to become widely accepted. The development of energetic materials is a whole world of trade-offs between energy content of a molecule and other desirable properties like higher performance, insensitivity against accidental initiation, thermal stability as well as a non-toxic and non-polluting behaviour when exposed to the environment

next to other additional properties. The traditional procedure for formulating new materials has been largely guided by intuition, experience and testing, relying foremost on trial and error. In turn, a better understanding of the basic principles is highly desirable to yield a more rational design process. However, exploiting these possibilities requires an understanding of the properties of the individual molecules, their interaction amongst each other as well as to surrounding matter next to an understanding of kinetic energy release and dynamics of initiation and decomposition processes. This *bottom-up* approach to energetic materials would allow for a more fundamental understanding of the evolution of properties with the size of the system as well as an understanding of the effects of the interaction of matter at different molecular-length scale with external stimuli and finally a detailed understanding of the functionalities of matter at molecular-length scale. The information obtained could provide breakthroughs not only in the area of energetic materials but additionally also in all areas of material science and chemistry in general both as far as fundamental and applied aspects are concerned. Energetic materials, due to their very nature, can offer a variety of unique insights into structure and matter. For example, detonations of high explosives produce thousands of Kelvins and a few hundred thousand atmospheres thus providing a unique means of elucidating the exotic chemical reactivity of matter under extreme conditions - similar to the conditions in the interiors of giant planets. In this context it has recently been reported that water formed during the detonation of the high explosive pentaerythritol tetranitrate (PETN) displays catalytic behaviour challenging the traditional view of water in high-explosives chemistry where water was considered to be one of the stable detonation products next to carbon dioxide and dinitrogen. These novel findings suggest that water may catalyse reactions in other explosives and in planetary interiours. [3] At the same time, the extreme conditions inside a detonating explosive have made it extremely difficult to perform measurements and consequently the detailed chemical reactions that cause a detonation are largely not understood. [4] Empirical observations are important to gain a better understanding of the final chemical composition after detonation and the corresponding reaction mechanisms are still not known for many explosives rendering this science to be very young and advances to be likely with the

advent of novel techniques allowing to acquire experimental information previously not available. [5]

As mentioned above, it is important to discover new representatives having significant advantages over compounds currently used not only for military but also for civilian purpose. As far as the military is concerned, U.S. Defense Secretary Robert M. Gates recently announced to spend less money on traditional weapon systems for conventional warfare against large nations like China and Russia and shift more money to counterterrorism in Iraq and Afghanistan representing the first broad rethinking of American military strategy under the Obama administration. [6] Under this program a combination of evolutionary and novel technologies are under development to facilitate intelligence and surveillance using unmanned vehicles like the Predator or Reaper drones currently used in Pakistan, Afghanistan and Iraq. Today these systems rely on munitions made up of yesterday's explosives and propellants. In contrast, novel energetic materials with increased performance, tailored energy release and insensitivity to unintended initiation would significantly improve existing systems and additionally enable new technology.

As well as performance properties, the desired criteria for a new material in order to become widely accepted are insensitivity towards destructive stimuli such as electrostatic discharge, heat, friction, and impact to ensure safe handling procedures and enhance controllability of kinetic energy release and further low water solubility and hydrolytic stability for environmental reasons, as well as longevity- and compatibility questions and other criteria addressing high-priority ecological toxicity requirements.

New high explosives – energetic materials with very high energy density - developed at our laboratories should display the following properties:

Table 1.1. Goals for the preparation of new High Energy Density Materials (HEDM):

parameter	desired property	value
performance	velocity of detonation	> 8500 m s^{-1}
	Koenen test (steel shell)	> 8 mm
thermal stability		> 200°C
sensitivity	impact	> 7J
	friction	> 120N
water solubility	low (no) solubility	
water stability	hydrolytically stable	
longevity		> 15 years
compatibility	chemically stable against:	
	binders: GAP / HTPB	
	plasticizer: nitro ester / NQ	
number of components	oxidizer and fuel	one
combustion	smokeless	
toxicity	low (no)	
environmental concerns	low (no)	
yield	high	
reaction medium / solvent	water	
price	low	

Notes. GAP = glycidyl azide polymer; HTPB = hydroxyl terminated polybutadiene; NQ = nitroguanidine.

In this context, the scope of this thesis was defined by two major issues:

1. Gaining a deeper understanding of the basic principles of structure and matter as key to a more rational design process and the directed synthesis of novel compounds with tailored properties.

2. Development of a molecule with potential to replace RDX (Research Department Explosive, 1,3,5-trinitro-1,3,5-triazine), which currently serves as the most important military explosive produced on a large scale today.

The primary objective of this thesis was to develop a new energetic compound with potential to replace the most important high explosive currently used in the United States and world-wide. RDX can chemically be classified as a nitramine. Nitramines generally are highly energetic compounds having found wide acceptance as explosives or rocket propellants. The most common nitramines in use today are RDX and HMX (Fig. 1.1).

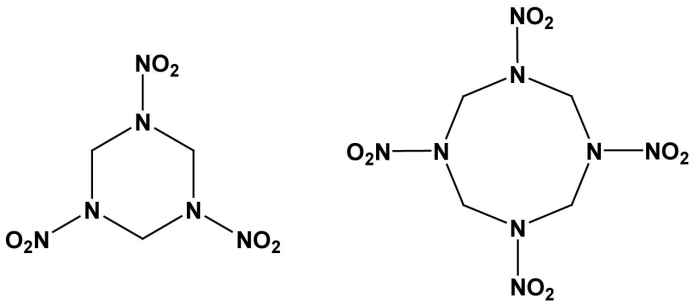

Figure 1.1. Molecular structures of RDX (1,3,5-trinitro-1,3,5-triaza-cyclohexane) and HMX (1,3,5,7-tetranitro-1,3,5,7-tetraaza-cyclooctane).

The acceptance of RDX and HMX is generally attributed to the high energetic performance and the high energy density possessed by these compounds. In essence, RDX and HMX are the standards of energetic performance and energy density by which other energetic compounds are measured. RDX was first prepared by Henning in 1899 intended for medicinal use, its explosive properties have been realized in 1920 by Herz. [7] As with most explosives, RDX can be used alone or as a component in explosive compositions like C-4 (when mixed with plasticizers) or Semtex (a combination of RDX and PETN, pentaerythritol tetranitrate), or as a base charge in detonators and high explosives. A drawback to RDX and HMX is that these nitramine compounds are relatively sensitive to shock, friction, and impact. The high sensitivities associated with RDX and HMX make these nitramine compounds less desirable for some applications, especially in an environment where external stimuli on RDX or HMX can lead to catastrophic damage with destruction of surrounding objects and loss of human life. Processing of neat RDX or HMX can be difficult due to their high melting points rendering melt casting to be dangerous.

A breakthrough in energetic materials research was the development of CL-20 (2,4,6,8,10,12-hexanitrohexaazaisowurtzitane, HNIW), a caged polynitramine compound that is 20 percent more powerful than HMX. It was first synthesised by A. Nielson in 1987 using a novel chemical reaction to construct the CL-20 cage in a single step thereby establishing a new type of amine glyoxal chemistry. While there have been several other new ingredients over the years, none of them have been successfully scaled up to mass production levels.

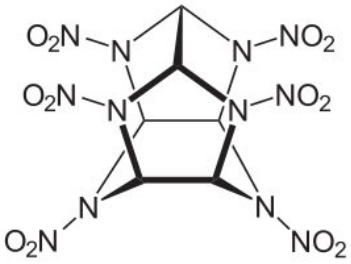

Figure 1.2. Molecular Structure of CL-20.

In contrast, CL-20 has been called the most significant energetic ingredient in energetic materials research since the discovery of RDX and HMX because it has made the jump from laboratory scale synthesis to scale up and finally to mass production levels. Its major limitations are due to the rather high costs of its production involving expensive reagents like nitronium tetrafluoroborate or a palladium catalyst. In the best case the potential of CL-20 stimulates increased demand leading to improved production processes. Availability will go up and cost will go down. Next to above mentioned criteria that may prevent the widespread use or even the development of an energetic material, both explosive and environmental safety issues are of major impact. Regarding the safety of the material, recent and growing interest in less sensitive energetic materials can be seen to be a consequence of national and international insensitive munitions policies [8] as well as additions to UN transport regulations. [9] According to BAM (Bundesanstalt für Materialprüfung), a compound can be classified as being insensitive, less sensitive, sensitive, very sensitive or extremely sensitive. According to their friction and impact sensitivity data, RDX and HMX are sensitive whereas CL-20 has been found to be very sensitive.

At our laboratories we aim to develop energetic materials that will enable the design of novel insensitive high-energy propellants and explosives with tailored energy release. Our approach to these materials is based on compounds that combine both high oxygen and nitrogen contents allowing not only to obtain superior performance characteristics but additionally compounds that are more environmentally benign and less toxic - during storage or use and also during their preparation. High nitrogen compounds are highly desirable due to their high heats of formation and the formation of environmentally friendly and toxicologically harmless dinitrogen. Nitrogen is unique amongst all other elements of the periodic table in so far that the bond energy per two-electron bond increases from a single over a double to a triple bond resulting in dinitrogen being more stable than any other polynitrogen species. [10] Compounds that preferentially contain only nitrogen can be very useful in propellants, but their use as high explosives is limited. The heat of formation of dinitrogen equals zero and consequently the products formed on decomposition of high nitrogen compounds display less negative values of their heats of formation resulting in lower heats of detonation (see page 30) and less thermochemical energy produced during detonation and usable for the work to be done by the explosive. To overcome this drawback but at the same time benefit from the advantages of high nitrogen compounds we are trying to develop new energetic materials preferentially containing both high nitrogen and oxygen content. These compounds release energy not only due to the high heats of formation of high nitrogen compounds but additionally through the release of energy produced from the oxidation-products formed during detonation. Within the scope of this thesis we were interested in developing oxygen rich energetic derivatives of high nitrogen compounds.

Traditional representatives of high oxygen explosives (HOX) have been reported in public literature as research reports initiated by the *Office of Naval Research* (ONR) became declassified in the early seventies of the twentieth century; however, relevant data were published mainly in the patent literature, often without giving information about synthetic procedures or specifying the physicochemical characteristics of the compounds obtained. [11] Some of the most promising materials initially considered were polynitroaliphatic compounds containing the dinitromethyl, fluorodinitromethyl and

trinitromethyl groups. [12] Among them, the trinitromethyl compounds were found to have the most favourable heats of detonation and oxygen balance values. However, thermal stability was reported to be generally limited to 150°C when solid and 100°C when molten reversing further investigation into trinitromethyl substituted compounds. [13] We have now investigated both compounds mentioned in the literature and we have developed and tested novel compounds carrying the trinitromethyl functionality in order to explore its potential for the design of next generation energetic materials trying to enhance the thermal stability of this class of compounds and finding the molecule offering the best trade-off between energy capability and thermal stability.

1.1 General Characteristics of Energetic Materials

1.1.1 Types of Energetic Materials

Energetic materials are chemical compounds, or mixtures of chemical compounds, that are divided into three classes according to use:

- Explosives
- Propellants
- Pyrotechnics

Explosives and propellants that have been properly initiated evolve large volumes of hot gas in a short time. The difference between explosives and propellants is the rate at which the reaction proceeds. In explosives, a fast reaction produces a very high pressure shock in the surrounding medium. This shock is capable of shattering objects. In propellants, a slower reaction produces lower pressure over a longer period of time. This lower, sustained pressure is used to propel objects. Pyrotechnics evolve large amounts of heat but much less gas than propellants or explosives. The exothermic chemical reactions occurring in pyrotechnics are generally speaking non-explosive, relatively slow, self-sustaining, and self-contained.

1.1.2 Classification of Energetic Materials

There is considerable variation among the properties of the compounds that constitute each of the three major classifications of energetic materials, explosives, propellants and pyrotechnics. Generally, they can be divided into composites and monomolecular energetic materials. Composites like black powder are obtained on physically mixing solid oxidizers and fuels whereas in monomolecular energetic materials like TNT (2,4,6-trinitrotoluene), each molecule contains an oxidizing component and a fuel component.

Explosives. An explosive is defined as a material that can be initiated to undergo very rapid, self-propagating decomposition that results in the formation of more stable material, the liberation of heat, or the development of a sudden pressure effect through the action of heat on produced or adjacent gases. A chemical explosive is a compound or a mixture of compounds which, when subjected to heat, impact, friction, or shock, undergoes very rapid, self-propagating, heat- producing decomposition. This decomposition produces gases that exert tremendous pressures as they expand at the high temperature of the reaction. The work done by an explosive depends primarily on the amount of heat given off during the explosion. The term detonation indicates that the reaction is moving through the explosive faster than the speed of sound in the unreacted explosive; whereas, deflagration indicates a slower reaction (rapid burning). Denser explosives usually give higher detonation velocities and pressures.

A high explosive will detonate; a low explosive will deflagrate. Low-order explosives (LE) create a subsonic explosion and lack the over-pressurization wave generated by high explosives. Low-order explosives with lower density like ANFO (Ammonium Nitrate Fuel Oil) will suffice in easily fragmented or closely jointed rocks and are preferred for quarrying coarse material for mining and construction purpose. A High Explosive (HE) is a compound or mixture which, when initiated, is capable of sustaining a detonation shockwave to produce a powerful blast effect. A detonation is the powerful explosive effect caused by the propagation of a high-speed shockwave through a high explosive compound or mixture. During the process of detonation, the high explosive is largely decomposed into hot, rapidly expanding gas. These high density explosives may be desirable for difficult blasting conditions or where fine fragmentation is required. Ingredients of high explosives are classified as explosive bases, combustibles, oxygen carriers, antacids, and absorbents. Some ingredients perform more than one function. An explosive base is a solid or liquid which, upon the application of sufficient heat or shock, decomposes to gases with an accompanying release of considerable heat. A combustible combines with excess oxygen to reduce the formation of nitrogen oxides. An oxygen carrier assures complete oxidation of the carbon to reduce the formation of carbon monoxide. The formation of nitrogen oxides or carbon

monoxide, in addition to being undesirable from the standpoint of fumes, results in lower heat of explosion and efficiency than when carbon dioxide and nitrogen are formed. Antacids increase stability in storage, and absorbents absorb liquid explosive bases.

Explosives are classified as primary or secondary based on their susceptibility to initiation. Primary explosives, which include lead azide and lead styphnate, are highly susceptible to initiation. Primary explosives often are referred to as initiating explosives because they can be used to ignite secondary explosives. Secondary explosives include nitroaromatics and nitramines and are formulated to detonate only under specific circumstances. Secondary explosives often are used as main charge. Secondary explosives can be loosely categorized into melt-castable explosives, which are based on nitroaromatics such as TNT, and plastic-bonded explosives which are based on a binder and crystalline explosive such as RDX.

Propellants can be divided into four classes:

(I) composites (II) single-base (III) double-base (IV) triple-base

Propellants include both rocket and gun propellants. The choice of a propellant for a specific use is determined by ballistic and physical requirements rather than on the basis of composition. A given propellant composition may be suitable for use in several applications.

(I) Most rocket propellants are composites. They generally consist of a physical mixture of a fuel such as metallic aluminum, a binder which is normally an organic polymer (generally a synthetic rubber which is also a fuel), and an inorganic oxidizing agent such as ammonium perchlorate. These are heterogeneous physical structures.

(II) One group of gun propellants are called single-base and principally consist of nitrocellulose.

(III) Double-base propellants usually consist of nitrocellulose and nitroglycerine. In general, double-base propellants contain nitrocellulose and a liquid organic nitrate which will gelatinize nitrocellulose.

(IV) The term triple-base applies to propellants containing three explosive ingredients, usually with nitroguanidine as the major ingredient. The other two explosive ingredients frequently used are nitroglycerine and nitrocellulose. As in the double-base propellant, other gelatinizers may be substituted for the nitroglycerine. The nitroguanidine in the formulation produces a lower flame temperature and a greater amount of gaseous combustion products. The lower flame temperature considerably reduces erosion of gun barrels and the greater amounts of gas produce a greater force on the projectile.

Pyrotechnics include illuminating flares, signalling flares, colored and white smoke generators, tracers, incendiary delays, fuses, and photo-flash compounds. Pyrotechnics usually are composed of an inorganic oxidizer and metal powder in a binder. Illuminating flares contain sodium nitrate, magnesium, and a binder. Signaling flares contain barium, strontium, or other metal nitrates. Flares burn to produce intense light that is used for illumination. Signals produce colored flames that can exemplarily be used for recognition purpose during emergencies. Colored smoke is used for signalling while white smoke is used for screening. Tracers and fumers are small, smoke producing charges that are placed in projectiles. During the flight of the projectile, the charge burns. In a tracer, the smoke is used to track the flight of the projectile. A fumer produces smoke at the proper rate to fill the partial vacuum that movement through the air creates behind the projectile. This cuts drag and increases range. Incendiaries produce large amounts of heat that cause fires. A delay is an element that consists of an initiator, a delay column, and an output charge or relay in a specially designed inert housing. The delay column burns for a predetermined amount of time. Delays are used to provide an interval between initiation and functioning of a device. A fuse is a cord of combustible material commonly used in demolition. Photoflash powders are loose mixtures of oxidizers with metallic fuels. When ignited, these mixtures burn with explosive violence in a very short time. Igniters and initiators are used to ignite propellant charges and initiate detonation in explosive charges.

1.1.3 Properties of Energetic Materials

Chemical properties of individual energetic materials are discussed in the appropriate chapters of this thesis. The basic definitions and properties discussed for these materials include the following:

Brisance. Brisance is the shattering capability of an explosive. Several tests are commonly used to determine brisance. In the sand test 0.400 grams of the explosive are placed in 200 grams of sand and detonated. The amount of sand crushed by the explosive is a measure of brisance. The plate dent test, in which a sample of the explosive is detonated in close proximity to a metal plate, is

also used to measure brisance. The size of the dent is proportional to the brisance. Another method of measurement involves detonating a sample of explosive on top of a cylinder made of copper and measuring the contraction in length of the cylinder. The number, size distribution, and velocity of fragments produced by an explosive in a projectile is also related to the brisance of the explosive. With a limited number of exceptions, increased detonation velocity increases brisance.

Burning. The process of exothermic redox reactions taking place in energetic materials without introduction of atmospheric oxygen is preferably denoted as burning. The reaction is self-sustaining after an initial activating energy has been applied. Many explosives are capable of burning without detonation, if unconfined.

Burning Rate. The burning rate is defined as the rate at which the burning surface consumes a compound grain in a direction normal to the grain surface. The velocity of the linear burning reaction is dependent on heat production and heat transfer to reach ignition temperature within the material. The rate of heat transfer by conduction, convection and radiation depends on the pressure of the combustion products. These phenomena are described in the Vieille equation (Fig. 1.3), where A is a constant and n is the burning rate index.

$$r = \frac{dx}{dt} = Ap^n$$

Figure 1.3. Vieille equation for linear burning rate. r: linear burning rate; A: calibration factor; p: pressure; n: burning rate index.

The value of the constant A depends on the pressure units used and the burning rate index n, which is an experimentally determined parameter typically varying between 0.3 and 1.0 for a certain explosive. [14]

The equation shown in Figure 1.4 allows the mass of explosive consumed per unit time to be calculated provided that the burning surface area and the density are known. The surface area of fine powders becomes very large and due to the enhanced convective heat transfer mechanism, the risk of a change from a burning reaction turning into a deflagration or detonation reaction is enhanced. [15]

$$\frac{dm}{dt} = S(t)\ \rho\ r$$

Figure 1.4. Mass consumption of a burning reaction. m: mass; t: time; S: surface; ρ: density; r: linear burning rate.

Chapman-Jouget Theory. The Chapman-Jouget (CJ) theory is a fluid dynamical model of detonations and is used to calculate performance characteristics of an explosive expressed by the four parameters velocity of propagation (D), pressure (p), density (ρ) and particle velocity (u) behind the wave front. The performance of a chemical explosive or its usable energy is determined by the expansion of product gases arising from the chemical reactions taking place during detonation. The variation of pressure depends on the particle velocity of the product gases during adiabatic or free expansion and in order to describe this behaviour and calculate performance, the state (that is the pressure and particle velocity) of the materials at the end of the reaction zone and their equation of state (describing the pressure variation with the particle velocity during adiabatic or free expansion) have to be known. The CJ theory relates the detonation wave velocity to the properties of the gases behind the detonation wave front. It is assumed that all chemical energy is released at the detonation front and the reaction zone has no thickness. This approximation allows the detonation wave to be considered as a self-sustained supersonic wave travelling through the explosive at constant velocity. Generally, shock waves in inert materials can be described on the basis of three equations of conservation of energy, momentum and mass across the shock front. These equations are also called jump conditions. They allow the determination of the shock velocity (U) in terms of the pressure (p), density (ρ) and particle velocity (u) variables. Though these jump conditions do apply in the CJ theory as well, an additional condition is needed to determine the

detonation wave velocity (D) because energy is released at the front of the detonation wave making it self-propagating.

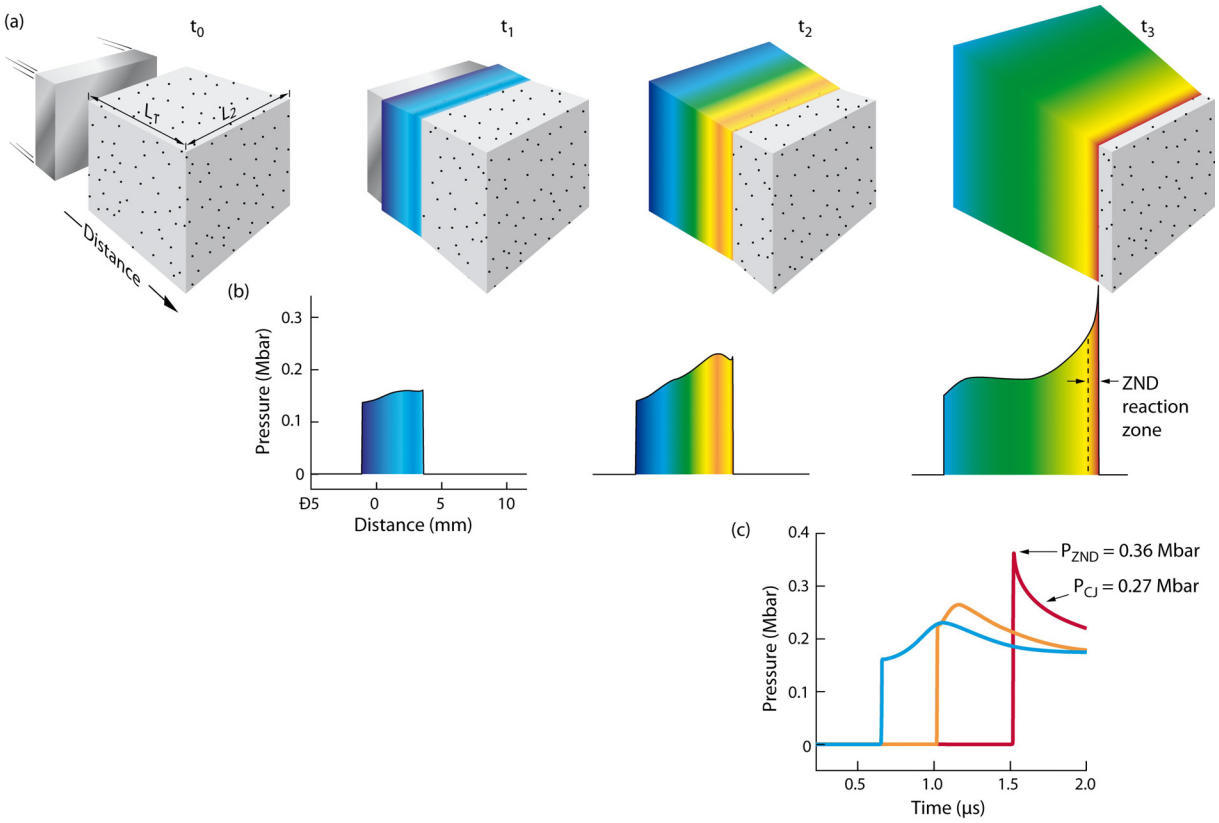

Figure 1.5. Initiation and Propagation of a Detonation Wave according to the model of Zel'dovic, Neuman and Döring (ZND). (a) A schematic 1-D (planar) experiment is shown at different times. In the experiment, the impact of a plate thrown on one face of a cube of explosive ($t = t_0$) produces a planar shock wave ($t = t_1$) that gradually accelerates ($t = t_2$) to a steady-state detonation ($t = t_3$) as the shock wave sweeps through the explosive and causes chemical energy to be released to the flow at a finite rate. (b) The corresponding pressure-vs-distance snapshots show the evolution of an essentially inert shock wave at $t = t_1$ growing into a classical 1-D ZND detonation structure at $t = t_3$, namely, a shock, or pressure, discontinuity at the ZND point followed by decreasing pressure through the reaction zone, ending at the CJ point, the pressure predicted by the CJ model (see text). (c) Pressure-vs-time plots for material particles originally at the shock front locations in (b) show the particle pressure (or velocity) histories. Only at the location of the right-most particle has a ZND detonation fully formed. [2] (Credit: Courtesy of Dr. J.B. Bdzil, LANL)

Combustion. Combustion of energetic materials designates any exothermic oxidation reaction, including, but not limited to those produced by introduction of atmospheric oxygen (see burning).

Deflagration. Deflagration (lat. de + flagrare = to burn) of propellants proceeds the same as normal burning and designates the process of very rapid burning without introduction of atmospheric oxygen but propagating at a velocity less than the speed of sound in that material. Due to the rate determining factors in the reaction being the rate of heat transfer into the propellant grain from the burning surface and the rate of decomposition of the propellant formulation, deflagration can result from having a fuel and oxidant in very close contact.

Deflagration to Detonation Transition. Deflagration can be considered to be an intermediate process between burning and detonation. As mentioned above (see Burning Rate), a large surface area of an energetic material can result into deflagration and the same is true for confined materials due to the burning reaction and the deflagration reaction being based on heat transfer. The velocity of the reaction is rising until it reaches the magnitude of the material's sound speed generating first shockwaves passing the material. A further acceleration to supersonic velocities yielding a detonation reaction depends on the type of material, its surface area and its confinement. [15] Hence, a burning reaction can be accelerated to a deflagration and by corresponding interference of shock waves further to a detonation reaction. The latter process is called deflagration-to-detonation transition (DDT). The detonation reaction is triggered by a shock wave. It occurs if enough of the explosive compound is compressed such that a chemical reaction can occur before it physically fragments and a shock wave is formed inside the sample. A shock wave moving at supersonic speed proceeds through the explosive causing further decomposition of the explosive material. Detonation designates the supersonic propagation of chemical reactions through an explosive. It can be rationalized as a shock wave moving through an explosive accompanied by chemical reactions. The shock compresses the material thus increasing its temperature to the point of ignition. The energy release of the chemical reactions taking

place in the ignited material behind the shock front support the shock propagation. This self-sustained detonation wave is different from a deflagration, which propagates at a subsonic speed and without a shock or any significant pressure change. If there is no shock wave, the reaction is called a deflagration. The major difference in the two reactions is the velocity of propagation of the reaction front. The shock wave has a velocity of the order of km s^{-1} instead of cm s^{-1} in the case of a deflagration. In the case of a detonation, the reaction rate is determined by the velocity of the shock wave, not by the rate of heat transfer.

Explosion. An Explosion (lat. explodere = to shatter) is a sudden expansion of matter accompanied by an increase of its volume. [16] Explosions may both be caused by explosive chemical or nuclear reactions and physical processes. Accordingly, the term explosion includes effects that follow rapid burning, detonation, as well as physical processes like the bursting of a vessel filled with compressed gas. The resulting effect of an explosion is a sudden expansion of gases or vapor, whether they were present before, or originated during the explosion process. A chemical explosion is accompanied by the formation of large amounts of gaseous decomposition products and liberation of heat during a very short time. The gaseous products (usually several hundred liters during microseconds) are heated to several thousands of degrees centigrade and can not expand instantaneously resulting in a sudden pressure rise ranging to several hundred of kbar during detonation reactions. Subsequently they expand and exert strong impact effects and shock waves to the surroundings.

Gap Test. In contrast to sensitivity towards impact, sensitivity of an explosive to shock is a very reproducible quantity. Shocks generated by a donor explosive can cause detonation in another explosive material. The strength of the shock wave required is a relative measure of the sensitivity of the material under test. In practice, a strong shock is produced and attenuated in an inert medium. The width of the medium that will allow detonation in 50 percent of the trials is reported as the test result. These tests are called gap tests. Gap test results are much more reliable data than impact test results, although there is

some dependence on the geometry of the test apparatus. Gap test have not been performed within the scope of this thesis.

Heat of Combustion. The heat of combustion is the amount of heat produced when a material is burned. This differs from the heat of detonation because the products formed are different. Generally, the products formed in combustion are at a lower energy level than the products formed during detonation. For example, carbon monoxide and carbon dioxide may be products of both detonation and combustion for a particular explosive. However, the detonation process might produce more carbon monoxide, while combustion might produce more carbon dioxide. Heat of combustion is usually measured for a new explosive for the determination of the heat of formation.

Heat of Detonation. The heat of detonation is considered to be the thermochemical energy produced during detonation and usable for the work to be done by the explosive. According to first principles – energy conservation – considerations, this quantity would seem to be a primary parameter of an explosive, upon which performance depends. Indeed it has been suggested [17] that some other detonation condition or parameter is as important as CJ pressure for the performance of explosives. Two explosives may serve as an example: TATB and NQ. In spite of their reasonably high calculated CJ pressure and measurements of detonation velocity and pressure they produce rather low performance. Kamlet [18] wondered whether, for some reason, *insensitive explosives were not reaching the infinite-medium steady-state condition. He also suggested that the trouble with NQ (poor performance) was the low Q (heat of detonation), and that no formulation very rich in NQ or other low-Q explosives would have high performance.* Two quantities are usually given for the heat of detonation, one with liquid water in the reaction products and one with gaseous water in the reaction products. The test used to determine these quantities uses a standard calorimeter. When the water is allowed to condense to liquid, the total heat produced by the detonation reaction is measured. The heat of detonation with gaseous water more accurately reflects the process of detonation in a non-laboratory setting. However, the results are less reproducible.

Heat of Fusion. The heat of fusion is the amount of heat necessary to transform (melt or fuse) a unit of solid into a liquid at the same temperature and standard pressure. This quantity is usually expressed in terms of calories per gram.

Heat of Sublimation. The heat of sublimation is the amount of heat necessary to convert a weight of solid directly into vapor in a constant temperature process. This quantity is usually expressed in calories per gram.

Heat of Vaporization. The heat of vaporization is the amount of heat necessary to convert a unit of liquid to vapor at the same temperature. This quantity is usually expressed in terms of calories per gram.

Oxygen Balance. The oxygen balance (OB) of the explosive is closely related to the power. The oxygen balance is the ratio of oxygen contained in the explosive material to the amount of oxygen required for complete oxidation of the explosive material. Explosive compositions with better oxygen balances are more powerful.

$$OB = (O - 2C - 0.5H) \cdot \frac{1600}{M}$$

Figure 1.6. OB: Oxygen balance [%] for a compound composed of the elements C/H/N/O to be oxidized completely to H_2O and CO_2. M: molecular weight of the compound.

Negative values of oxygen balance indicate that the explosive does not contain enough oxygen to convert each atom of carbon and hydrogen to CO_2 and H_2O during detonation, where no atmospheric oxygen is consumed. Most energetic materials are oxygen deficient resulting in lower heats of detonation compared to the condition of complete oxidation. In contrast, zero-balanced compounds contain exactly the amount of oxygen necessary for carbon and hydrogen to be oxidized to carbon dioxide and water. Examples are ethylene glycol dinitrate (EGDN, $C_2H_4N_2O_6$), azidoformamidinium dinitramide ($C_1H_4N_8O_4$), aminotetrazolium dinitramide ($C_1H_4N_8O_4$) [19] or bis-(2,2,2-trinitroethyl)-urea ($C_5H_6N_8O_{13}$). Compounds with positive values of oxygen balance contain excess oxygen and can serve as oxidizer components in energetic compositions.

Examples are ammonium perchlorate (AP, NH_4ClO_4 + 33.8), ammonium dinitramide (ADN, $N_4H_4O_4$ +25.8), ammonium nitrate (AN, $N_2H_4O_3$, +20) or hydrazinium nitroformate (HNF, $C_1H_5N_5O_6$, +13.1)

Performance. One of the driving forces for the development of any new energetic material is performance. Usually the discussion of new compounds includes a comparison of their 'performance' to the current highest energy density materials. The performance indicators used as a guide to the most promising materials are detonation velocity or detonation pressure in case of high explosives or values of the specific impulse in the case of propellants. However useful and apparent these indicators are, evaluation of performance is more complex and can lead to different results based on the intended use of the compound. There is no single indicator that allows judging the performance of either high explosive or propellants. For example, the effect of shaped charges is dependent on the composition of the product gases and the detonation energy, not solely on the detonation velocity. [20] As far as propellants are concerned, important criteria include the burning rate, burning rate exponent, temperature sensitivity and other parameters. Moreover, increased 'performance' in a compound will not necessarily yield increased available performance in a usable composition. Compositions containing any new material usually contain a binder to tune the mechanical properties and achieve a tolerable safety and comparisons of single performance indicators do not allow for the amount of binder required in different applications to obtain acceptable mechanical, processing or safety properties. [21] Promoting new compounds based on single performance parameters like detonation velocity or detonation pressure would miss those materials that might give similar performance when used in compositions to those compositions in use today with increased safety. Less performance in terms of the above mentioned indicators do not necessarily have to be a drawback in case the physical and safety properties allow for higher useable proportions in compositions. One example mentioned by Sanderson would be 'super-TNT', a compound that can be melt casted and used like TNT in neat form or melt cast with other high explosives. [21] Though its performance would intrinsically be less compared to HMX, it could lead to compositions of higher performance.

Power. The power of an explosive is the total energy available to do work and depends both on its energy density and its detonation wave speed. This is a different quantity than brisance. Two explosives may serve as example: ammonium nitrate and RDX. If a charge of each is placed beneath a rock, the ammonium nitrate might hurl the rock many meters but the RDX might pulverize the boulder into many fragments. The former quality is power whereas the latter quality is brisance. Power is measured by the Trauzl lead block test in which a sample of the explosive is detonated in a cavity in a lead block. The expansion of the cavity is a measure of the power of the explosive. The ballistic pendulum and ballistic mortar tests are also used to measure power. A heavy weight is accelerated by the detonation of an explosive. The swing of the pendulum or movement of the mortar's weight is a measure of the power of the explosive.

Prediction of Detonation Properties. The prediction of detonation properties (detonation pressure, velocity of detonation) from a given molecular structure and the known or estimated crystal density is of fundamental importance especially for the synthesis of new high-explosive compound and aided by the calculated properties a decision can be made whether it is worth the effort to attempt a new and complex synthesis. It has been found that estimates of detonation pressure and velocity are possible for C/H/N/O explosives by means of relatively simple empirical equations. These equations imply that the mechanical properties of the detonation depend only on the number of moles of detonation gases per unit weight of explosive, the average molecular weight of these gases, the chemical energy of the detonation reaction ($Q = -\Delta H^0$), and the loading density. [22]

(a) Detonation Pressure

$$P = K \rho_0^2 \Phi$$

Figure 1.7. P [kbar]; K: 15.58; ρ_0 [g cm^{-3}]; $\Phi = N M^{0.5} Q^{0.5}$; N [moles of gas per gram of explosive]; M [grams of gas per mole of gas]; Q [cal g^{-1}].

(b) Detonation Velocity

The detonation velocity is the rate at which the detonation reaction proceeds through an explosive. The velocity of the shock wave depends on the physical characteristics of the individual explosive material and its chemical homogeneity next to degree of confinement and geometric configuration of the charge. The more heterogeneous a material is, the slower is the reaction rate and the more energy is lost to maintain shock wave velocity. The velocity of detonation (VOD) depends on density due to the sound velocity of a material being depended on its density. Both chemical homogeneity and density have to be optimized to yield high detonation velocities.

$$D = A\,\Phi^{1/2}\,(1+B\,\rho_0)$$

Figure 1.8. D [m s^{-1}]; A: 1.01; B: 1.30; $\Phi = N\,M^{0.5}Q^{0.5}$; N [moles of gas per gram of explosive]; M [grams of gas per mole of gas]; Q [cal g^{-1}].

1.2 General Characteristics of the Trinitromethyl Group

The large oxygen content ($\Omega_{(CO2)}$ = +37%) and the reactive hydrogen atom in trinitromethane (nitroform) render this molecule to be very interesting for the preparation of high oxygen explosives (HOX). Trinitromethane has been known as early as 1857. [23] In contrast, reports of the chemistry of trinitromethyl compounds appeared rather late in the open literature. According to a review published by Noble, Borgardt and Reed, a program initiated by the Office of Naval Research (ONR) was initiated in 1947 *to investigate the nitroaliphatics for potential use as explosives and propellants.* [11] Portions of this work have appeared in patents, reviews and monographs when reports became gradually declassified in the early 1970s but often few or no information about synthetic procedures or physicochemical characteristics were given. Today, excellent reviews describing the chemistry of the trinitromethyl group are available summarizing the data on synthesis and properties of these polynitro compounds. [11, 24-25] The purpose of this introduction into the chemistry and characteristics of the trinitromethyl group is to summarize the most important general findings thus providing necessary and useful basic information intended to serve as a first navigation into the wide and complex area of polynitro chemistry.

Depending on the hybridization of the carbon atom carrying the three nitro groups two major groups of reactions can be differentiated. The first group refers to the chemistry of the trinitromethanide (nitroformate) ion whereas the second group involves the chemistry of the tetrahedral hybridized trinitromethyl group.

1.2.1 Tetranitromethane as Source to the Trinitromethanide Ion

Synthesis

An efficient and inexpensive method for the production of tetranitromethane or trinitromethane is a condition for its practical utility. Today, tetranitromethane is no longer commercially available though it has been produced in Germany during World War II on industrial scale utilizing the nitration of acetic anhydride (Fig. 1.9).[26-27]

Figure 1.9. Formation of tetranitromethane via nitration of acetic anhydride.

Approximately 10 tons of tetranitromethane were produced within a few weeks without regard to cost or yield but production stopped after the end of the war due to the high associated costs. In the 1950's this method was attempted on an industrial scale by the Nitroform Products Company (Newark, USA) but the entire plant was destroyed by an explosion in 1953.

Tetranitromethane can also be prepared from acetylene by the action of nitric acid in higher yields.[28] Acetylene is passed through a solution of mercuric nitrate containing solution of nitric acid resulting in trinitromethane (nitroform) as well as a mixture of carbon dioxide and nitrogen oxide. The nitrogen oxides can be recovered as nitric acid using an absorption tower. Finally, a nitric acid and sulfuric acid are added to the nitroform solution at elevated temperatures yielding in yields of 90% (based on nitric acid).[29]

Furthermore, tetranitromethane has also been prepared by nitrating nitroform,[23] from acetic anhydride by the action of diacetylorthonitric acid,[30] from iodopicrin and silver nitrite,[31] from acetyl nitrate by heating with acetic anhydride or glacial acetic acid,[32] from nitrobenzene by distilling with a mixture of nitric acid and fuming sulfuric acid,[33] by adding acetic anhydride to nitrogen pentoxide or a mixture of nitrogen pentoxide and nitrogen peroxide,[34] by the action of acetic anhydride on highly concentrated nitric acid,[35] from toluene by nitration,[36], from nitrobenzene and a mixture of nitric and fuming nitric acids,[37] and from acetylene and ethylene by the action of nitric acid in

the presence of a catalyst. [38] The nitration of 4,6-dihydroxypyrimidine in sulfuric acid has recently been found to yield trinitromethane as the sole product. [39]

Figure 1.10. Tetranitromethane as source to the trinitromethanide anion.

Uses

Due to its high oxygen balance ($\Omega_{(CO_2)}$ = +49.0%), tetranitromethane has been investigated as oxidizer but its freezing point of 13.8°C has precluded practical application. [40] Tetranitromethane can be used as nitrating agent both for aromatic [41] and aliphatic [42] nitro compounds and a valuable reagent for detection of double bonds. [43] The latter effect utilizes the inherent and strong yellow colour of charge transfer complexes arising from the interaction between the electron poor carbon atom of tetranitromethane and the electron rich double bonds.

Safety

CAUTION! The sensitivity of tetranitromethane strongly depends on its purity. Whereas pure tetranitromethane is difficult to initiate (initiation fails even when tetryl is used as detonator), small amounts of impurities yield extremely sensitive explosive mixtures that belong to the most brisant mixtures known. [44] A severe explosion accident happened in 1920 during a lecture experiment in which a mixture of toluene and tetranitromethane was burned at the chemical institute of the University of Münster (Germany) a severe explosion occurred. [45] It has been reported that of the thirty people affected by this explosion, ten lost their lifes and twenty people were severly injured. [46]

1.2.2 Trinitromethanide Ion as a Nucleophile

In principal, the reactions that can be utilized to synthesise compounds containing the trinitromethyl group include carbonyl condensation reactions, addition reactions, as well as alkylation reactions.

Carbonyl Condensation Reactions

The condensation reaction of an aldehyde and a polynitroalkane having an acidified α proton yielding a β-nitro substituted alcohol is referred to as Henry reaction. The Henry reaction between trinitromethane and formaldehyde affords good yields of 2,2,2-trinitroethanol. However, attempts to add trinitromethane to a variety of other aldehydes or ketones have been reported to yield no isolable products. [47] Though not isolable, formation of 1-alkyl-2,2,2-trinitroethanols was shown to occur in solution (see Table 1.2) and the extent of dissociation of these alcohols was found to increase in the order
Y = $-CH_2-$ < $-CH(CH_3)-$ < $(CH_2)_3C$ < $-C(CH_2)_2-$

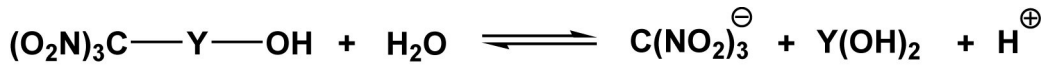

Figure 1.11. Dissociation of trinitromethylalcohols according to Hall *et al.* (see Table 1.2). the extent of dissociation of these alcohols was found to increase in the order Y = $-CH_2-$ < $-CH(CH_3)-$ < $-C(CH_2)_2-$

Table 1.2. Dissociation Constants determined by Hall in aqueous acid. [48]

Compound	K, M^{-1}
$(NO_2)_3C-CH_2-OH$	$7.80 \cdot 10^{-7}$
$(NO_2)_3C-CH(CH_3)-OH$	$2.80 \cdot 10^{-4}$
$(NO_2)_3C-C(CH_2)_2-OH$	a)

Notes. a) No detectable amount of alcohol was produced.

It was concluded that steric interactions between the substituent on the alpha carbon atom and the trinitromethyl group governs the position of the equilibrium. The reaction is acid catalyzed and reversed in base affording the salt of the nitro compound and formaldehyde.

The Mannich condensation reaction between a nitroalkane, an aldehyde and an amine is a very useful method for the preparation of β-nitro substituted alkylated amines.

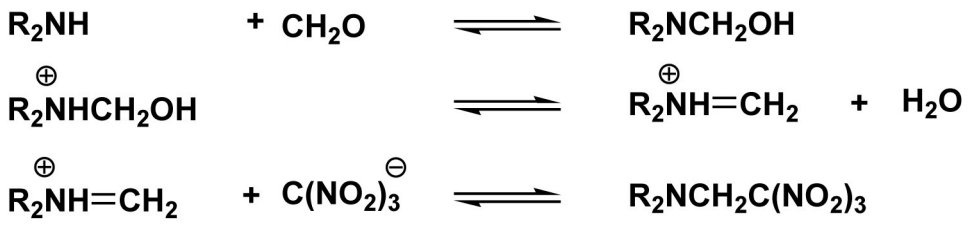

Figure 1.12. Steps involved in the Mannich reaction.

According to mechanistic studies, the rate controlling step involves the addition of the trinitromethanide anion to the cationic iminium intermediate previously formed from the condensation between the amine and the aldehyde. (49-50)

Though this reaction provides convenient access to a variety of Mannich bases from polynitroakylamines, examples reported in the literature suggest them to be only moderately thermally stable. This has been rationalized in terms of a facile path for the reversal of the Mannich equilibrium. (24)

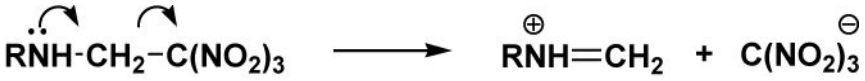

Figure 1.13. Reversal of the Mannich reaction.

The resonance stabilized trinitromethanide anion serves as a driving force for this reaction. However, it has been found that nitration of the Mannich bases to the corresponding nitramines (BTNNA, Bis-(2,2,2-trinitroethyl)-nitramine) or delocalization of the p electron pair of the nitrogen atom (BTU, Bis-(2,2,2-trinitroethyl)-urea) enhances the stability of these products. (51)

Addition Reactions

A wide variety of Michael systems have been utilized in Michael addition reactions with the trinitromethanide ion. Noble *et al.* has reviewed the various adducts that have been prepared. [11]

In principal, addition to a variety of α, β – unsaturated Michael systems of the general formula CH_2=CHY (Y = EWG) yields the corresponding 3-Y-1,1,1-trinitropropyl derivatives.

1,2-Addition reactions to unconjugated olefin systems have been reported using the mercury derivative of trinitromethane. Novikov and coworkers have extensively studied the reaction of mercury trinitromethanide with variours olefinic and active hydrogen substrates. [52] They found that it has a covalent structure in the solid state and dissociates in aqueous or alcoholic solutions:

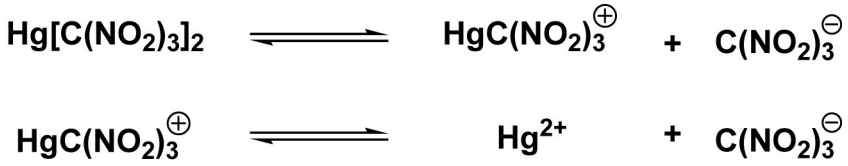

Figure 1.14. Dissociation of mercury trinitromethanide in aqueous or alcoholic solution.

They report that they found no evidence for the existence of the tautomeric form in which oxygen was bonded to mercury neither in solid state nor in solution – the same bonding situation has been observed in the related compound mercury fulminate only recently. [53-54] The synthetic utility of using the mercury route as a preparative tool in trinitromethyl chemistry is somewhat limited due to the lack of a suitable general method for the cleavage of the carbon-mercury bond in the trinitroalkyl mercury derivatives.

Alkylation Reactions

The nucleophilic displacement of halogen atoms from a saturated carbon by trinitromethanide is not a general synthetic strategy to obtain the corresponding carbon alkylated trinitromethyl compound. It has been reported that only simple primary alkyl iodides produced the desired derivatives whereas several other halide substrates including α-halogen acids, α-halogen esters, α-halogen ketones, α-halogen acetals and acetylenic halides yielded no carbon alkylation products though quantitative yields of the by product silver halide was observed together with the formation of a complex product mixture containing considerable amounts of unstable, red oils, which were assumed to be O-alkylation products. [55] The trinitromethanide ion is an ambident nucleophile and accordingly alkylation can either occur at the carbon or the oxygen atom. Assuming the alkylation taking place at the more electronegative oxygen atom, the formation of the carbon alkylated products would require subsequent rearrangement.

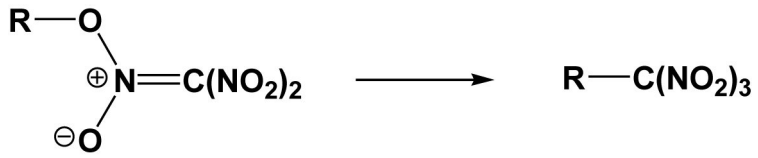

Figure 1.15. Formation of O-alkylated intermediate and subsequent rearrangement to the C-alkylated product.

Sterically demanding substituents certainly disfavour this rearrangement and products usually do not form. In contrast, the formation of carbon alkylation products in the case of simple primary alkyl halides or the formation of 1,1,1,6,6,6-hexanitro-3-hexyne from the reaction between 1,4-dibromo-2-butyne and silver trinitromethanide can be rationalized in terms of sterically less demanding substituents. [56]

1.2.3 Stepwise Construction of the Trinitromethyl Group

Another approach to trinitromethyl containing compounds involves the stepwise construction of the trinitromethyl group. A nitromethyl derivative is converted into a dinitromethyl derivative and finally nitrated to the trinitromethyl compound. In order to obtain the 1,1-dinitroalkane, a nitroalkane can be converted to the α chloronitroalkane using the ter Meer reaction [57] or, alternatively, an oxidative nitration technique reported by Kaplan and Shechter. [58]

However, according to Kaplan, there is no general route that allows for the further nitration to the corresponding trinitromethyl compounds. [24] Selected examples reported in the literature include:

a) Nitration in alkaline media using tetranitromethane: [59]

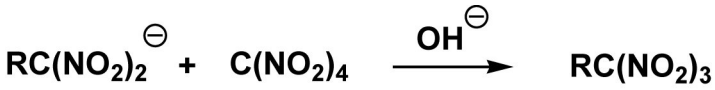

Figure 1.16. R = $C_6H_5CH_2CH_2$, $(CH_3)_2CH$, $(CH_3)_2CHCH_2$, $(CH_3)_3C$, CH_3CH_2, $CH_3CH_2CH_2$, $CH_3CH_2CH_2CH_2$.

b) Nitration of phenyl substituted alkaline earth metal salts of selected nitromethanes using dinitrogen tetroxide: [60]

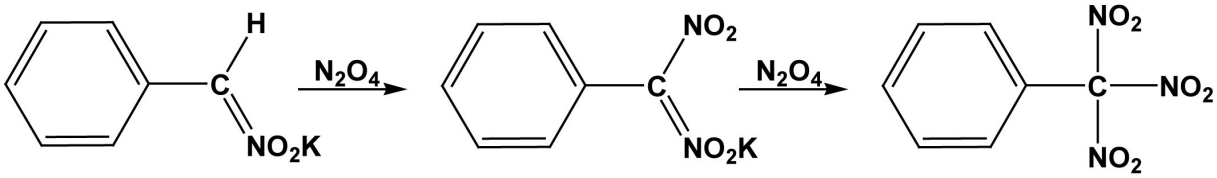

Figure 1.17. Stepwise nitration using dinitrogen tetroxide.

c) Destructive nitration of the carboxyl group to the trinitromethyl entity using a 4:3 mixture of sulfuric acid (ρ = 1.84 g cm^{-3}) and nitric acid (ρ = 1.5 g cm^{-3}): [61]

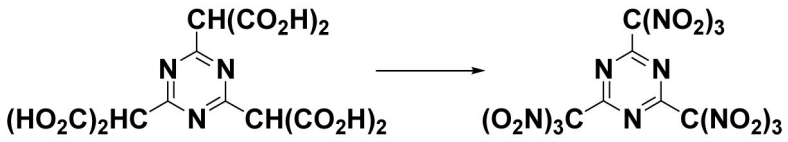

Figure 1.18. Synthesis of 2,4,6-Tris(trinitromethyl)-1,3,5-triazine. According to the reported properties the compound is unstable when exposed to air and displays a melting point of 90-91°C.

Further examples of nitration of dinitroalkanes or other intermediates include the formation of hexanitroethane from 1,1,2,2-tetranitroethane [62] or trinitroacetonitrile from cyanoacetic acid [63] as well as the formation of tetranitromethane from acetylene [28] or ketene [64].

1.2.4 Reactions of Trinitromethyl Compounds

As already pointed out by Kaplan, a diversity of chemical reactions can be employed not affecting the trinitromethyl group yielding a variety of valuable products. [24] For example, 4,4,4-trinitrobutyric acid can be converted to the acid chloride and subsequently to the corresponding isocyanate which in turn can undergo typical reactions including amine, urea and urethane formation (Fig. 1.19). [65]

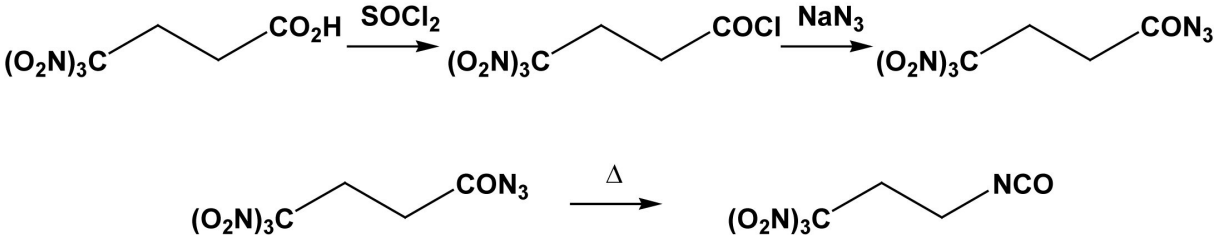

Figure 1.19. Stepwise formation of 4,4,4-trinitroisocyanate from 4,4,4-trinitrobutyric acid.

In addition, the acid chloride itself allows for a variety of other product, for example the formation of bis-(4,4,4-trinitrobutyryl)-peroxide (Fig. 1.20). [66]

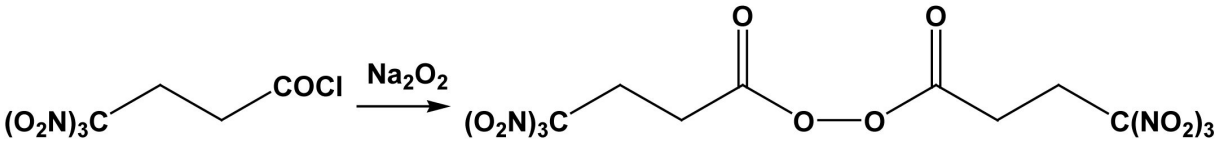

Figure 1.20. Formation of bis-(4,4,4-trinitrobutyryl)peroxide.

Instead of using the 4,4,4-trinitrobutyryl moiety ($C_4H_6N_3O_6$, $\Omega_{(CO2)}$ = -41.6%) for the development of oxygen rich energetic materials, we chose to introduce the trinitromethyl group using 2,2,2-trinitroethanol due to the positive oxygen balance value of the 2,2,2-trinitroethyl moiety ($C_2H_2N_3O_6$, $\Omega_{(CO2)}$ = +9.8%).
As pointed out earlier (see Table 1.2, page 38) and in contrast to the products arising from the reactions between a variety of aldehydes and ketones and trinitromethane, 2,2,2-trinitroethanol is an example of a stable condensation product. At the same time it displays a positive oxygen balance. It can readily be obtained in high yields and high purity from the Henry reaction between trinitromethane and formaldehyde, can be safely handled, stored and it can

conveniently and stoichiometrically be applied under ambient conditions. Other advantages of this group will be discussed in the appropriate sections of this thesis.

Unfortunately, much of the chemistry reported for the trinitrobutyryl or trinitropropyl groups is not applicable in case of the trinitroethyl group because of the specific electronic properties of the trinitromethyl group that are most pronounced in the case of the trinitroethyl group ($\sigma^* = 1.62$) and significantly limit the chemistry to introduce this group compared to the chemistry available in the case of the trinitropropyl group or trinitrobutyryl group. The chemistry of 2,2,2-trinitroethanol is different to that of other alcohols owing to the electron withdrawing inductive effect of the trinitromethyl group ($\sigma^* = 4.54$) decreasing the oxygen basicity of the hydroxyl group. The alcohol becomes acidic ($pKa = 6.1$) and at pH values greater than 6, the equilibrium lies in the direction of the trinitromethanide anion and formaldehyde. This dissociation under weakly acidic or basic conditions precludes the possibility of 2,2,2-trinitroethoxy derivatives through the use of nucleophilic displacement reactions utilizing the 2,2,2,-trinitroethoxide anion. Generally, attack of nucleophilic reagents like hydroxide on trinitroethyl compounds can take place at several sites:

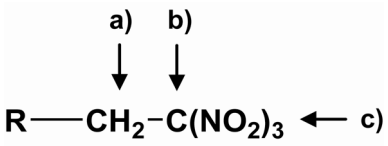

Figure 1.21. Possible sites for nucleophilic attack on the trinitroethyl moiety.

Proton removal (a)

As a consequence of the strong electron withdrawing properties of the trinitromethyl group, hydrogen atoms α to the trinitromethyl group are acidified subject to being removed yielding E_2-type base-catalyzed elimination of nitrous acid and subsequent further decomposition yielding dinitromethanide (Fig. 1.22). [67]

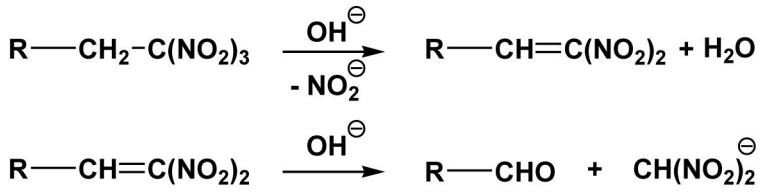

Figure 1.22. Proton removal and subsequent formation of dinitromethanide.

Next to base-catalyzed elimination of nitrous acid, there are at least two further modes of decomposition for the 2,2,2-trinitroethyl fragment. The first path involves removal of an acidic proton by base followed by intramolecular rearrangement of a nitro group of the trinitromethyl group via the resulting vicinal carbanion as reported in the degradation of 2,2,2-trinitroethyl chloride to 1,1,2,2-tetranitroethane. [68] The second path is the reversal of the Mannich reaction yielding trinitromethanide anion and the unsaturated counterpart. [24]

Nucleophilic attack on carbon (b)

Reactions of nucleophilic reagents at the carbon atom carrying the nitro groups has been reported indicating that the sterically crowded carbon atom can be accessed under certain conditions as reported in the formation of succinic acid from the reaction between 4,4,4-trinitrobutyric acid with hydroxide (Fig. 1.23) [69] or the formation of carbonate from the reaction between tetranitromethane with hydroxide (Fig. 1.24): [70]

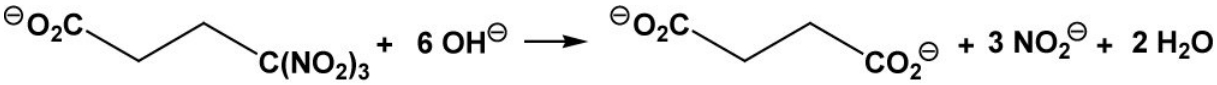

Figure 1.23. Formation of succinic acid from the reaction between 4,4,4-trinitrobutyric acid and hydroxide.

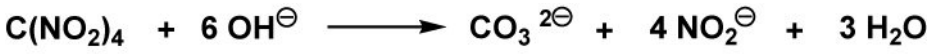

Figure 1.24. Carbonate formation from the reaction between tetranitromethane and hydroxide.

Displacement of nitrite (c)

Attack of the nitro group affords displacement of nitrite by hydroxide with reduction of the trinitromethyl group yielding 1,1-dinitroalkane anion and nitrate. A S_N2 or S_N2' mechanism has been suggested but no evidence was given whether the reaction takes place at nitrogen (S_N2) or oxygen (S_N2'). [67]

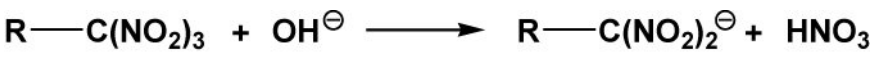

Figure 1.25. Displacement of nitrite.

There is no general preference for each of the above mentioned decomposition modes as they strongly depend on the reaction conditions. Products arising from these reactions may be complex mixtures arising from a combination of different decomposition reactions taking place.

1.3 Methods

Standard analytical methods that have been applied to characterize chemical compounds include elemental analysis next to spectroscopic methods like NMR spectroscopy, optical spectroscopy (UV-Vis) or vibrational spectroscopy (Infrared and Raman spectroscopy) as well as mass spectrometry, bomb calorimetry or X-ray diffraction and are mentioned in the appropriate chapters of this thesis. A few additional notes regarding single crystal X-ray diffraction are mentioned here due to the importance of this technique within the scope of this thesis. X-ray diffraction techniques have been developed that enable to extract information that goes beyond routine structure determination - provided the reliability of the data is high enough. In contrast to neutron diffraction where the nuclei are responsible for the diffraction, X-ray diffraction involves the internal and valence electrons of a molecule. In the case of the hydrogen atom the centre of gravity of the electron density does not coincide with the nucleus yielding systematically shorter bond distances. When judging the *quality* of a structure, it is useful to keep the following two criteria in mind: The first one has to do with the agreement between the observed structure factors (F_o) and the calculated ones (F_c). They should be of the same order of magnitude as the experimental accuracy to which the F_o's are found. The second criterion involves the reliability index (R). Usually more reliable results are obtained with lower R values. However, it can be important to keep in mind that the information derived using the R value is based on the extent to which the model chosen for the calculation of the structure fits to the experimental results. Calculated structure factors that match the observed ones are a necessary condition for a good crystallographic analysis but they are not a solely sufficient condition to avoid erroneous results with excellent R values.

In contrast to the standard analytical methods mentioned above, those methods with relevance to energetic materials research are briefly mentioned in this section to serve as a guide for the reader not familiar in the area of energetic materials research.

Safety Analysis

The great amount of energy delivered from energetic materials places a premium on all aspects of their safety including manufacture, handling, transportation and storage. Likewise, much of the high-explosives work involves determining the sensitivity of new materials to impact, friction, electrostatic discharge or heat prior to further handling to obtain their sensitivity characteristics.

Sensitivity. Various external stimuli can cause release of the energy contained in energetic materials. Knowing the response of individual energetic materials to specific stimuli like impact, shock, heat, friction or electric spark is important in terms of safety and in determining the suitability of a material for a specific application. However, sensitivity is anything but an absolute quantity and dependent on a variety of factors. Sensitivity reflects the ease of triggering a detonation which in turn depends on a complex interplay of a number of factors including, but not limited to molecular and crystal properties, physical conditions, the nature of the stimulus etc. [71-74] There are different types of machines and apparatus to measure the respond of an explosive to external stimuli and determine the corresponding value. This value, however, is always obtained for a sample in the particular environment of the test that was used. The criteria chosen for determining whether a test resulted in an explosion ('go') or failure ('no go') may vary between different laboratories and further depend on the operator to signify a 'go' result, often based on visual observation of smoke, flash or flame, crackling or sound of explosion. One consequence of this evaluation together with the complex interplay of factors affecting sensitivity is the difficulty or reproducibly quantifying sensitivity. Nevertheless, examination of the respond of a material to these external stimuli like electrostatic discharge (Electrostatic Sensitivity), friction (Friction Sensitivity) or impact (Impact Sensitivity) is very important to be able to make at least some estimates of the level of sensitivity and thus important information in terms of safety and handling of these substances as well as a qualitative comparison between them. Electrostatic sensitivity is an equally important quantity in terms of handling a compound under study compared to

friction or impact sensitivity. Some explosives can be detonated from the shock of a person charged with static electricity. The test procedures used to determine sensitivity are covered in Chapter 4. As far as safety is concerned, it is important to notice that sensitivity of most materials is not a fundamental and unalterable property. Sensitive materials can sometimes be made to behave acceptably insensitive (desensitization).

Impact Sensitivity. The initiation response of an explosive to the blow of a falling weight is called impact sensitivity. Impact sensitivity is generally reported as the corresponding impact energy in Joule, given by the product *mgh*, where m is the mass of the falling weight, g is the acceleration due to gravity and h is the height of the falling weight. As mentioned above, it is very difficult to obtain reproducible impact sensitivity values. They should therefore be regarded as, at best, qualitative indicators of relative impact sensitivities. [75] there are a variety of different machines for determining this value. They are different in detail, but they are technically essentially similar though test procedures and test data analyses may differ. Traditionally, explosives have been subjected to falling weights to measure impact sensitivity. Within the scope of this work a standardized BAM drophammer (Bundesanstalt für Materialprüfung) has been employed to measure the impact sensitivity. In this test, the substance is placed between two steel cylinders that are subject to being impacted by a falling weight. The sound produced serves as information whether an explosion or failure has occurred together with a visual inspection of the sample after each experiment. The value taken as *impact sensitivity* (in Joule) is defined as the product of the mass of the falling weight and the distance necessary to yield not more than one explosion out of six experiments.

There have been numerous attempts trying to relate impact sensitivity (usually within a given class of compounds) to various other parameters like the strengths of certain bonds, enthalpy of formation (Table 1.3) or decomposition temperature (Table 1.4):

Table 1.3. Impact sensitivity compared to enthalpy of formation. [76]

Compound	$\Delta_f H^0$	FI
1,2,4-Trinitrobenzene	-56	103
1,3,5-Trinitrobenzene	-38	109
2,4,6-Trinitroaniline	+22	111
2,3,4,6-Tetranitroaniline	-43	86
Pentanitroaniline	-339	36
2,3,4-Trinitrotoluene	-124	92
2,3,5-Trinitrotoluene	-86	101
2,4,6-Trinitrotoluene (TNT)	-74	114
3,4,5-Trinitrotoluene	-104	95
3,4,6-Trinitrotoluene	-93	102

Notes. Test method: Rotter Impact Test [77]; FI: Figure of Insensitiveness; FI (picric acid) = 100 by definition; $\Delta_f H^0$ / kJ mol^{-1}.

Table 1.3 is a summary of the impact sensitivity data of isomers of trinitrotoluene, polynitroanilines and trinitrobenzene. The stabilities of the aromatic compounds are generally higher as long as the nitro groups are not in adjacent positions on the ring. It appears to show a relation between the enthalpy of formation (enthalpy of destabilization) as one method of characterizing impact sensitivity.

Table 1.4. Impact sensitivity versus thermal stability. [Fehler! Textmarke nicht definiert.]

Compound	IS / cm	T / °C
Hexanitrobenzene (HNB)	15	165
2,4,6-Trinitrotoluene (TNT)	148	250
Picric Acid	191	260
Diaminotrinitrobenzene (DATB)	320	300
Triaminotrinitrobenzene (TATB)	> 320	340

Notes. Test method: Type 12 machine. The value given represents the result of 25 drops to give the height at which the propability of explosion is 50%. Setup: 40 mg of sample are placed on sandpaper between an anvil and a steel cylinder and a 2.5 kg weight is dropped from different heights. The temperature is given as the onset of exotherm.

The results of Table 1.4 suggest a dependence of impact sensitivity and thermal stability. The higher the thermal stability of an explosive, the less impact sensitive it appears to be. In addition, it has been observed, that impact sensitivity is temperature dependent (Table 1.5). [78]

Table 1.5. The impact sensitivity of TNT increases with increasing temperature.

Temperature / °C	Height / inches	Height / cm
-40	17	43.18
25	14	35.56
80	7	17.78
90	3	7.62
105	2*	5.08

Notes. Test method: Picatinny Arsenal apparatus [79], 2 kg weight; * five explosions in 20 trials.

Another contribution to the possible factors affecting impact sensitivities of energetic compounds has recently been reported. It has been suggested that there may be a link in terms of a crystal volume factor between the impact sensitivities of energetic compounds and the space available to their molecules in their crystal lattice. The authors suggested *'that the availabiltiy of more space enhances the molecule's ability to absorb and localize, vibrationally or translationally, the external energy coming from the impact.'* [75]

Additional approaches for the prediction of some aspects of safety that appear in the literature are listed in Table 1.6. Assistance for the targeted design of safe compounds based on predictive methods available today is however by far not well established as there is yet no complete approach to sensitivity at molecular level.

Table 1.6. Methods for the prediction of the sensitivity of energetic compounds. [21]

Method	Ref.	Function	Requirements	Comments
quantum mechanical structure property relatonships / QSPR	(80)	impact sensitivity	numerous predicted or measured parameters	empirical method for predicting any material characteristic using physical and chemical properties
ab initio / semi empricial molecular structure	(81)	bond lengths / strengths		useful indicators, but no direct correlation with any sensitivity properties
correlation to oxygen balance (Stine)	(82)	impact, shock, critical temperature	oxygen balance	does not account for anomalous behaviour caused by other chemical or mechanical properties
correlation to oxygen balance (Kamlet)	(83)	impact	oxygen balance	does not account for anomalous behaviour caused by other chemical or mechanical properties
correlation to bond length / charge distribution	(84)	impact	bond lengths, electrostatic surface potential	does not account for anomalous behaviour caused by other chemical or mechanical properties
statistical / neural network	(85)	impact	numerous predicted or measured parameters	mechanical influence on sensitivity is not taken into account
electronic structure / impact sensitivity correlation	(86)	impact	relative variation of polarity of 'trigger bond' on excitation from MO calculations	mechanical influence on sensitivity is not taken into account
electronic structure / impact sensitivity correlation	(87)	impact	HOMO and LUMO energies	correlated only for a limited number of compounds

A more general approach trying to relate impact sensitivity to molecular properties has also been suggested. Politzer & Murray reported a quantitative relationship of impact sensitivities for a number of nitroaromatics and nitroheterocycles to the degree of internal charge separation and the presence of strongly positive electrostatic potential (ESP) maxima on their molecular surfaces based on theoretical calculations of isolated molecules. [88] They have demonstrated that *'there is a link – not necessarily a causal relationship – between the anomalous imbalance in the molecular surface electrostatic potentials of energetic compounds and their impact sensitivities.'* [75] Rice & Hare have extended this idea and conclude that '*the level of sensitivity to impact is related to the degree of positive charge build-up over covalent bonds within the inner framework of these explosives*' [74] based on the idea that the C-NO_2 and N-NO_2 bonds associated with these

positive regions concomitantly become weaker. The unifying concept is based on the ideal that the breaking of a certain type of bond, a *trigger linkage*, is a key step in the decomposition process. Politzer & Murray have recently summarzied this as follows: *'Thus, to the extent that C-NO_2 and N-NO_2 bonds are trigger linkages in some energetic compounds, the link between the imbalance in their molecular surface potentials and impact sensitivity may be that the former reflects the electronic charge depletion that facilitates the breaking of these bonds.'* [75] In doing so, they also recognized the limitations imposed by the number of factors affecting impact sensitivity and the uncertainty associated with its measurement and stated that their goal, therefore, was not a precise structure/activity correlation but rather a better understanding of the factors and properties actually influencing sensitivity as opposed to relationships that are symptomatic or even coincidental. [75] Meanwhile it has been recommended to include the experimentally derived charge density distribution and derived ESP of high resolution X-ray diffraction experiments in future theoretical studies. Impact sensitivity is a bulk property and the ESP of isolated molecules in the gas phase neglect the effects of intermolecular interactions. In contrast, the ESP obtained from a diffraction experiment represents molecules as part of the crystal and therefore includes both these effects. [89]

A novel approach towards sensitivity of energetic compounds has been suggested very recently and outlining the relevance of kinetics of decomposition reactions on sensitivity. It has been reported that water displays catalytic behaviour in PETN (Pentaerythritol tetranitrate) reactions challenging the traditional view of water in high explosives chemistry which had previously only been considered to be one of the three major decomposition products next to carbon dioxide and molecular nitrogen. In contrast this recent study has demonstrated that water plays an active role in detonation chemistry and *'the kinetics of water formation may also contribute to high explosives sensitivity'*. [3]

Stability. Stability is the ability of energetic materials to retain, unaltered, such properties as detonation velocity and sensitivity after long periods of storage under adverse conditions. All energetic materials are unstable to some extent. The degree of instability varies greatly. Compatibility with other materials and long-term stability is expected for safety in handling and use as well as storage of the products. Whatever its performance, an energetic material will not be widely used unless it can be used in formulations with a reasonable life expectancy. The safe service life of an explosive is made up of the safe storage life, also referred to as the chemical shelf life and the so-called functional life. Shelf life covers the period of time during which the explosive can safely be stored and is limited by chemical ageing reactions. The functional life is the period of time where a safe use of the explosive and its functional requirements remain fulfilled. The functional life is limited both by (i) chemical ageing reactions of the explosive that may yield lower energy content or reactions with the binder that may change the mechanical properties and (ii) physical processes within the explosive like diffusion or phase changes. [90]

Picric acid may serve as an example. Though more powerful than TNT it was initially extensively used until it was found that it is incompatible with acid sensitive materials, particularly in the formation of sensitive metal salts. [91]

There are two types of reactions that have to be distinguished when considering the stability of energetic materials. [92] The first type of thermal decomposition can be described as chemical ageing and occurs at low temperatures or at room temperature. The second type refers to thermal decomposition with ignition of the material. Generally, thermal decomposition occurs when bonding forces within the corresponding molecules or ions are weaker compared to those between atoms of neighbouring units. An increase in temperature may result in bond redistribution and the formation of decomposition products. It has been estimated that activation energies of decomposition higher than 170 kJ mol^{-1} correspond to a chemical shelf life in the order of thousands of years at room temperature whereas values below 155 kJ mol^{-1} indicate limited stability and require further examination of the stability. [93] An estimation of the shelf life time of an energetic material based on the measurements of the activation energy has been reported by Klapötke *et al.* [94]

Thermal Stability. When heated, an explosive will begin to decompose exothermically. If a large enough sample is heated above its critical temperature, it can explode. The factors responsible to reach this critical temperature include the shape and size of the explosive sample, its thermal conductivity and its kinetics of decomposition. [95]

(a) Differential Scanning Calorimetry. A small-scale test for the thermal stability of energetic materials is differential scanning calorimetry (DSC). Typically two milligrams of sample are placed inside an aluminium container and heated inside a furnace purged with dry nitrogen against a reference. A temperature programme is run and the instrument records the difference in heat flow of the two compartments as a function of temperature. A positive deflection corresponds to an exothermic process and a negative deflection corresponds to an endothermic one. The use of DSC is not limited to the characterization of the thermal stability of energetic materials but additionally yields useful information:
Solids that do not exhibit the same high degree of ordering found in crystalline samples can be detected through the presence of a broad temperature range on melting. This is known as glass transition. Melting of a crystalline solid appears as a quite sharp peak in contrast. Information about the exothermic thermal decomposition includes the decomposition temperature, the width of the thermal reaction, the onset and offset temperatures of the peak and the enthalpy of the thermal decomposition corresponding to the peak area. A kinetic evaluation of data obtained at several heating rates (non-isothermal) allows for the estimation of the activation energy of decomposition.
(b) Isothermal Long Term Testing. This test is used to obtain information on thermal ageing properties at elevated temperatures. Within the scope of this work, a RADEX oven has been employed. [96] Typically, 100 mg of sample were placed inside a steel container and isothermally heated for 48 hours inside the RADEX oven at elevated temperatures up to 40°C below the thermal decomposition point of the sample obtained from DSC measurements. Any heat flow occurring during the measurement is recorded. Howerver, it is important to note that a RADEX measurement is not that sensitive as microcalorimetry and thermal ageing might have occurred although no heat flow has been

recorded in case the heat flow was too small and thermal decomposition occurred slowly. For this reason it is important to visually inspect the sample after a measurement and carry out additional analytical tests to be able to guarantee that no ageing has occurred. Those tests include DSC measurements to judge wether a change in decomposition of the material has occurred compared to the decomposition temperature of a sample that has not been heated using the RADEX oven as well as other standard analytical methods like NMR spectroscopy.

Chemical Compatibility. Next to thermal stability of the neat sample it is additionally possible to test chemical compatibility of the sample using differential scanning calorimetry (DSC). For this purpose selected compounds like nitroguanidine or methylammonium nitrate are added to the sample and the mixture heated. A subsequent comparison to the results obtained from the measurement of the neat sample allows drawing conclusions of any unfavourable interactions of the sample to the compounds added.

Classification. In order to obtain an interim hazard classification for the transport of dangerous goods standardized tests have to be carried out for substances prior to shipment according to the instructions as specificated in the technical bulletin *Department of Defense Ammunition and Explosives Hazard Classification Procedures.* [97] The test procedures (Table 1.7) include the results of impact sensitivity (UN 3a), friction sensitivity (UN 3b), thermal stability (UN 3c), small scale burning (UN 3d) and may additionally include a test of 'thermal stability for articles and packaged articles' (UN 4a) in case the test (UN 3c) fails as well as a 12 m free fall test (UN 4b) in case one of the tests (UN 3a, UN 3b, UN 3c) fails. Details of the procedures to these tests are documented in the appendix to this thesis (Chapter 4).

Table 1.7. UN hazard classification procedures for articles and substances.

	test	**conditions**	**+ (failure)**	**- (pass)**
UN 3a	impact sensitivity	5 tests, 50%	≤ 3.5 J	> 3.5 J
UN 3b	friction sensitivity	5 tests, 1 / 5	≤ 184 N, visible sparks, visible flame, audible expl., loud crackling noise	> 184
UN 3c	thermal stability	75°C, 48 h	visual: - color change, - explosion, - ignition, - weight loss (any more than H_2O) RADEX: self-heating > 3°C	
UN 3d	small scale burning	Kerosene-soaked sawdust, unconfined	explosion or detonation	
UN 4a	thermal stability for articles and packaged articles	75°C, 48 h	visual: - color change, - explosion, - ignition, - weight loss (any more than H_2O) RADEX: self-heating > 3°C	
UN 4b	free fall	12 m free fall	fire, explosion or detonation	

Chapter 2

2.1 Energetic Materials: Salts

2.1.1 Salts of Trinitromethane

Introduction

Energetic salts containing the nitroformate anion have been known for over a century [98], however, only one compound hydrazinium nitroformate (HNF) has gained practical application as high performing, halogen free oxidizer for advanced propellant formulations. It has been called a promising candidate for the replacement of ammonium perchlorate (AP) oxidizer and indeed HNF-based propellants show improved performance in terms of specific impulse over AP-based propellants due to the high oxygen content and only slightly negative heat of formation ($\Delta_f H^{\circ}_{(s)}$ = -94 cal g^{-1}). [99] Since the discovery of HNF in 1951, more than eighty publications [100] have appeared, showing that HNF is of continued interest. Recently, two derivatives of hydrazinium nitroformate (HNF), namely monomethylhydrazinium nitroformate (MMHNF) and dimethylhydrazinium nitroformate (DMHNF) were synthesised and suggested as being promising new high performance energetic materials. [101] In the course of our investigations into high energy density materials (HEDM), we recently focussed our attention on various nitroformate salts, in order to explore their potential as possible new ingredients for high performance, halogen-free propellant formulations, which would avoid the problematic formation of hydrogen chloride from the use of ammonium perchlorate as oxidizer in rocket propellant formulations (see page 125). The cations which were combined with the nitroformate anion in this work were potassium, ammonium, hydrazinium, melaminium, guanidinium, aminoguanidinium, diaminoguanidinium and triaminoguanidinium. Potassium nitroformate, [102] ammonium nitroformate, [98] hydrazinium nitroformate, [98] guanidinium nitroformate, [103] and melaminium nitroformate [104] have already

been mentioned in the literature. However, to the best of our knowledge, not all were characterized in the solid state using single crystal X-ray diffraction. In the course of our investigations we have obtained the solid state structures of potassium-, ammonium-, hydrazinium-, melaminium-, guanidinium-, aminoguanidinium-, diaminoguanidinium- and triaminoguanidinium nitroformate using single crystal X-ray diffraction. The salts containing the nitroformate anion which have been characterized using single crystal X-ray diffraction are described in references. [102, 105-120]

Synthesis and Characterization

The nitroformate salts were obtained in high yields as bright yellow solids (Fig. 2.1) either by the reaction of nitroform with the corresponding base in accordance with literature procedures (ANF, [98] MNF, [121] and HNF [122]) or, in the case of GNFH, AGNF, DAGNF and TAGNF, by a metathetical reaction of the potassium or silver salt of nitroform with the corresponding guanidinium chloride in acetonitrile according to a slightly modified procedure. [123]

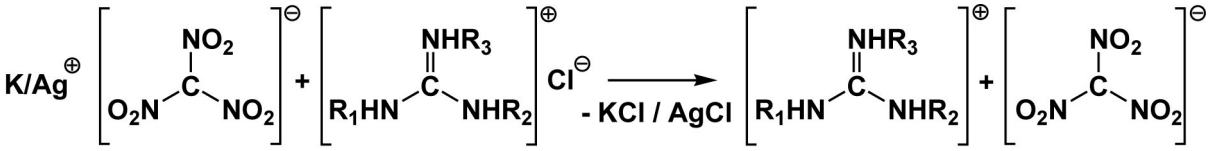

GNFH: $R_1 = R_2 = R_3 = H$
AGNF: $R_1 = NH_2, R_2 = R_3 = H$
DAGNF: $R_1 = R_2 = NH_2, R_3 = H$
TAGNF: $R_1 = R_2 = R_3 = NH_2$

Figure 2.1. Preparation of GNFH, AGNF, DAGNF and TAGNF.

Tetranitromethane, trinitromethane, the potassium salt of trinitromethane and the silver salt of trinitromethane are educts for the synthesis of the novel compounds and were synthesised first. Tetranitromethane was synthesised from acetic acid anhydride and concentrated nitric acid according to a literature procedure. Though it is known that sulfuryl chloride is a catalytically active component of this pernitration, a possible reaction

mechanism of the formation of tetranitromethane from acetic acid anhydride has never been reported to the best of our knowledge. In order to rationalize the formation of tetranitromethane the following mechanism is formally be proposed (Fig. 2.2).

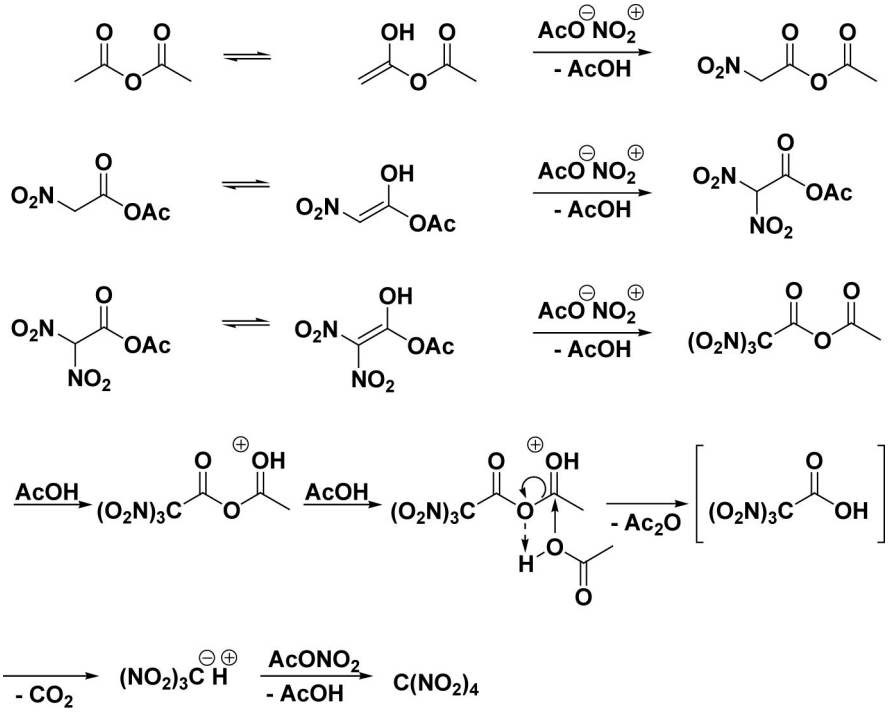

Figure 2.2. Proposed mechanism for the formation of tetranitromethane from acetic acid anhydride.

The nitroformate salts prepared were characterized in solution using ^{1}H, ^{13}C and $^{14/15}N$ NMR spectroscopy. The ^{13}C and $^{14/15}N$ spectra of the anion in all of the salts showed one signal at room temperature. A comparison of the obtained signals can be found in Table 2.1. The signals observed in the ^{13}C NMR spectra which correspond to the anion are in good agreement with those reported by A.A. Gakh *et al.* [124] for the cesium and the tetrabutylammonium salts of the nitroformate anion at 150.3 ppm and 151.6 ppm (both measured in [D_6]acetone), respectively. Differential Scanning Calorimetry (DSC) was used to determine the thermal stabilities of compounds ANF, MNF as well as GNFH, AGNF, DAGNF and TAGNF. Whereas ANF shows only one decomposition signal at 116°, MNF, GNFH, AGNF, DAGNF and TAGNF show melting points as well as subsequent decomposition points. The thermal stability increases within the series AGNF (71°C melting with decomp.) < DAGNF (80°C m.p. / 82°C decomp.) < TAGNF (84°C m.p. / 105°C decomp.) < GNFH (69°C m.p. / 113°C decomp.) < ANF (116°C decomp.) < MNF

(118°C m.p. / 143°C decomp.). Figure 2.3 shows the DSC spectra of AGNF, DAGNF and TAGNF at different heating rates:

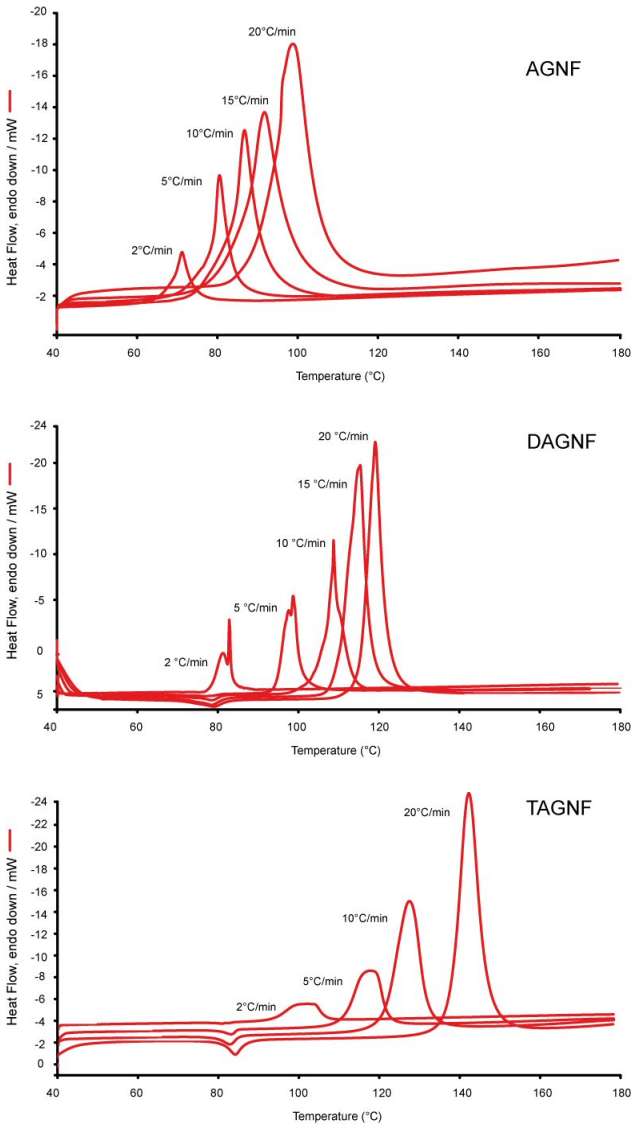

Figure 2.3. DSC spectra of AGNF, DAGNF and TAGNF. Each spectrum was recorded at different heating rates to illustrate the dependency of heating rate and decomposition temperature.

The spectra show the dependency of the decomposition temperatures on the heating rate. The decomposition temperatures of these three compounds cover a range of roughly 40°C when heated at a rate of 2°C min^{-1} compared to a rate of 20°C min^{-1}. Table 2.1 summarizes the analytical data of ANF, MNF, GNFH, AGNF, DAGNF and TAGNF.

Table 2.1. Selected Analytical Data for ANF, MNF, GNFH, AGNF, DAGNF and TAGNF.

Parameter	ANF	MNF	GNFH	AGNF	DAGNF	TAGNF
^{1}H NMR δ / ppm:	7.54 N***H***$_4^+$	7.6 C-N***H***$_2$	6.90 C-N***H***$_2$ 3.39 ***H***$_2$O	8.52 N***H***-NH$_2$ 6.94 C-N***H***$_2$ 4.28 NH-N***H***$_2$	8.50 N***H***-NH$_2$ 4.48 (C-N***H***$_2$, NH-N***H***$_2$)	9.79 N***H***-NH$_2$ 3.53 NH-N***H***$_2$
^{13}C NMR δ / ppm:	153.3 ***C***$(NO_2)_3^-$	159.9 R$_2$***C***-NH$_2^+$ 150.3 ***C***$(NO_2)_3^-$	158.0 ***C***$(NH_2)_3^+$ 150.3 ***C***$(NO_2)_3^-$	158.9 H$_2$N-NH=***C***$(NH_2)_2^+$ 150.3 ***C***$(NO_2)_3^-$	159.9 (H$_2$N-NH)$_2$***C***=NH$_2^+$ 150.4 ***C***$(NO_2)_3^-$	161.8 ***C***$(H_2N\text{-}NH)_3^+$ 150.6 ***C***$(NO_2)_3^-$
$^{14/15}$N NMR δ / ppm:	-364 ***N***H$_4^+$ -30 ***N***O$_2$	-29.9 ***N***O$_2$	-306 C-***N***H$_2$ -31 ***N***O$_2$	-326 NH-***N***H$_2$ -311 ***N***H-NH$_2$ -284 C-***N***H$_2$ -30 ***N***O$_2$	-328 NH-***N***H$_2$ -313 ***N***H-NH$_2$ -288 C-***N***H$_2$ -31 ***N***O$_2$	-348 NH-***N***H$_2$ -283 ***N***H-NH$_2$ -31 ***N***O$_2$
Raman/ cm^{-1}	1273 νs (NO$_2$) 871 δ (NO$_2$)	1257 νs (NO$_2$) 870 δ (NO$_2$)	1299 νs (NO$_2$) 868 δ (NO$_2$)	1277 νs (NO$_2$) 869 δ (NO$_2$)	1247 νs (NO$_2$) 873 δ (NO$_2$)	1385 νs (NO$_2$) 868 δ (NO$_2$)
Mass Spectrometry	18 (cation, FAB$^+$) 150 (anion, FAB$^-$)	127 (cation, FAB$^+$) 150 (anion, FAB$^-$)	60 (cation, FAB$^+$) 150 (anion, FAB$^-$)	75 (cation, FAB$^+$) 150 (anion, FAB$^-$)	90 (cation, FAB$^+$) 150 (anion, FAB$^-$)	105 (cation, FAB$^+$) 150 (anion, FAB$^-$)
DSC / °C (2°C/min)	116 (decomp.)	118 (m.p.) 143 (decomp.)	69 (m.p.) 113 (decomp.)	71 (decomp.)	80 (m.p.) 82 (decomp.)	84 (m.p.) 105 (decomp.)
Elemental Analysis / % (calc./found)	N (33.34 /) C (7.15 /) H (2.40 /)	N (45.48 / 44.59) C (17.33 / 17.72) H (2.55 / 2.81)	N (36.84 / 36.39) C (10.53 / 10.36) H (3.53 / 3.96)	N (43.55/ 42.84) C (10.67 / 10.83) H (3.13 / 3.22)	N (46.66 / 45.38) C (10.00 / 10.42) H (3.36 / 3.41)	N (49.41 / 48.75) C (9.41 / 10.08) H (3.56 / 3.32)

Crystal Structure Analysis

The influence of the many factors that affect the geometry of the nitroformate anion is complex and has been the subject to several publications. [123, 125-126] Previously reported data include the results of ab initio calculations [125-126] and single crystal X-ray diffraction studies. [102, 106-108, 112, 115, 119, 127-136] Competition between slow crystal growth and decomposition of the nitroformate moiety is a problem when trying to obtain single crystals of salts containing the nitroformate anion which are suitable for X-ray diffraction. Using Infrared and Raman spectroscopy, the decomposition of concentrated solutions of GNF, AGNF and DAGNF on standing at room temperature yielding the corresponding guanidinium nitrates could be observed. It is known that silver nitroformate solutions on standing decompose to form silver nitrate (Figure 2.4). [119]

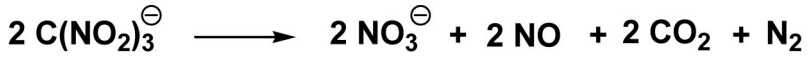

Figure 2.4. Decomposition of the trinitromethanide anion.

In much the same way, GNF, AGNF and DAGNF are expected to decompose with the formation of the corresponding guanidinium nitrates. However, a systematic study of the crystal structure was of interest to us in order to obtain reliable values for the density, cell volume and the number of formula units per unit cell, in order to be able to predict performance data for these energetic materials. Crystals suitable for X-ray diffraction were therefore measured as soon as they were obtained. Detailed structural parameters of all compounds determined using single crystal X-ray diffraction are provided in the appendix (Chapter 4).

Potassium Nitroformate (KNF)

In addition to the two previously described single crystal structures of KNF, [102, 119] it was possible to obtain a further third polymorph in this work on recrystallizing potassium nitroformate from acetone at room temperature. This polymorph of potassium nitroformate **1** crystallizes in the space group $P2_1/n$ (no.14) with four formula units per unit cell. The dihedral angles of the nitro groups relative to the central C-N_3 moiety are 23° (N_1, Fig. 2.5), 10° (N_2, Fig. 2.5) and 38° (N_3, Fig. 2.5). The density obtained from single crystal X-ray diffraction (2.325 g cm^{-3}) is significantly higher than the density of the two previously reported polymorphs that have densities of 2.216 g cm^{-3} [102] and 2.217 g cm^{-3}. [119]

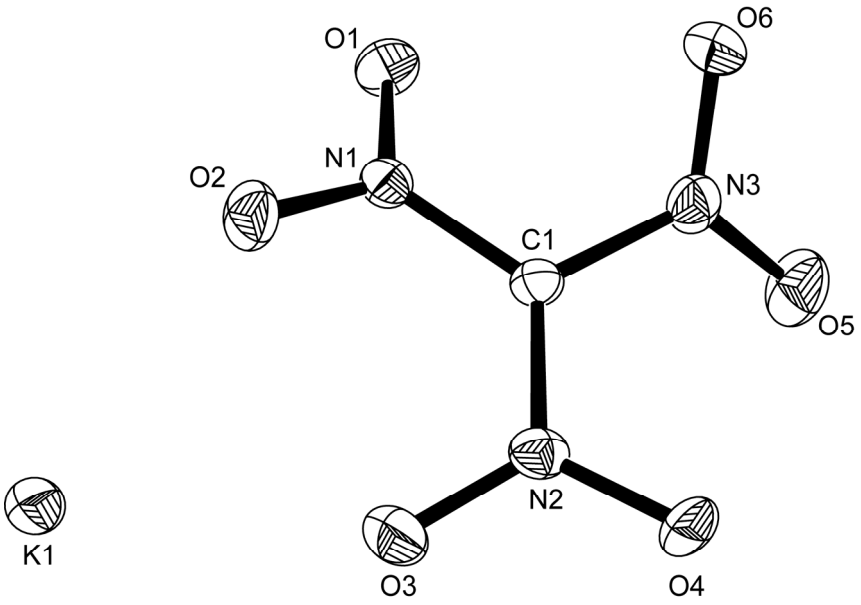

Figure 2.5. ORTEP representation of the molecular structure of potassium trinitromethanide in the crystalline state. Displacement ellipsoids are shown at the 50 % probability level.

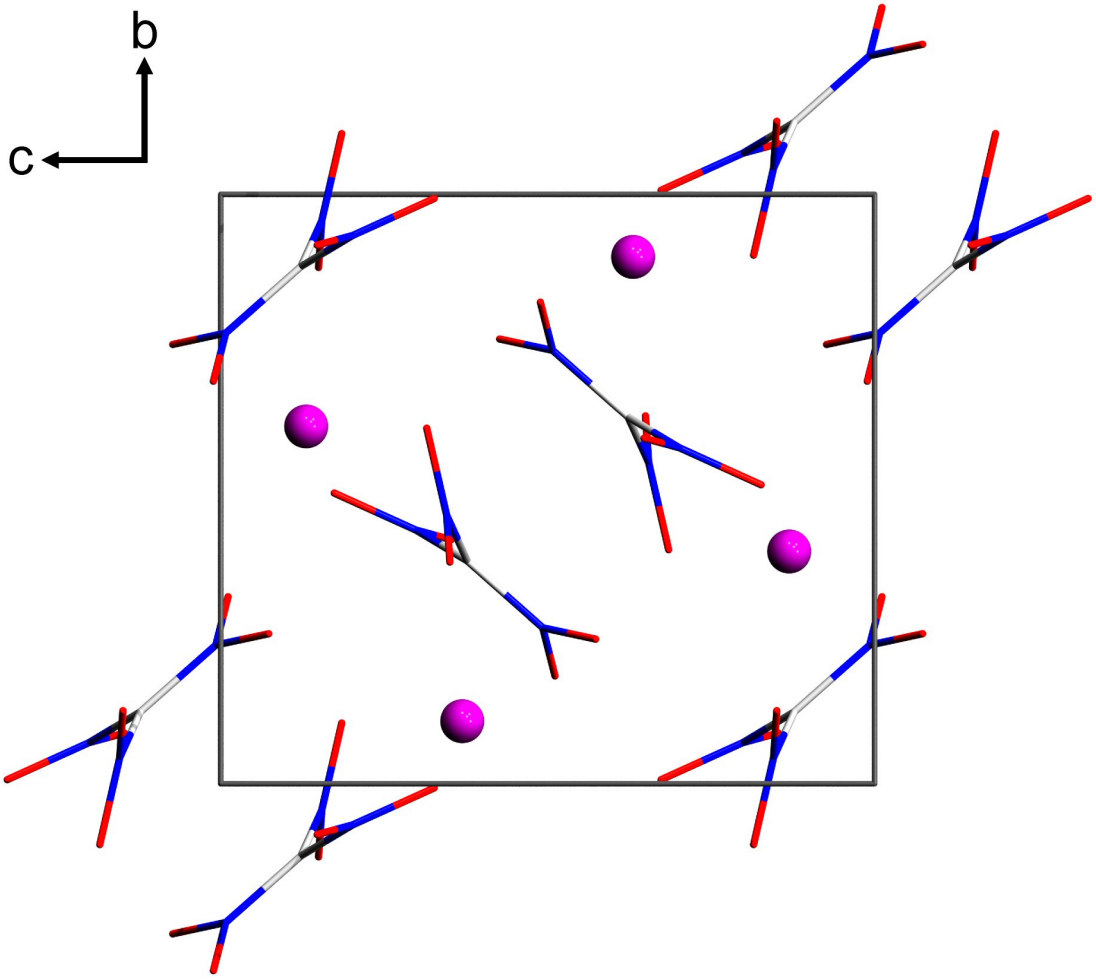

Figure 2.6. Unit cell of potassium trinitromethanide, viewed along the *c* axis.

Ammonium Nitroformate (ANF)

Although ANF has been known for a long time, [98] surprisingly no single crystal structure had been reported prior to our work. Crystals suitable for single crystal X-ray diffraction were obtained by recrystallization of ANF from propionitrile at room temperature. Ammonium nitroformate **2** crystallizes in the chiral tetragonal space group $P4_12_12$ (no.92) with four formula units per unit cell. The numbering of the atoms in Figure 2.7 indicates that the nitroformate anion lies on a special position having site symmetry along the C_1-N_1 bond which is part of a C_2 axis. The dihedral angles of the nitro groups relative to the central C-N_3 moiety are 57° (N_1, Fig. 2.7) and 1° (N_2, Fig. 2.7). The hydrogen atoms of the ammonium group are disordered, resulting in two

tetrahedra that are twisted against each other. In Figure 2.7 only one of the two tetrahedra is shown.

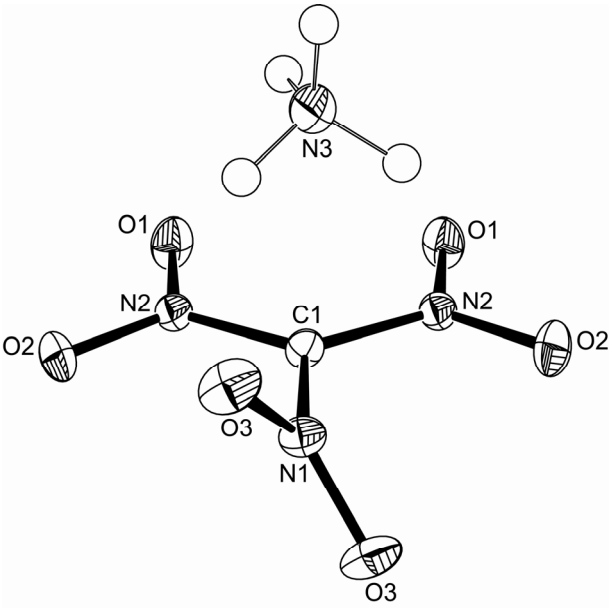

Figure 2.7. ORTEP representation of the molecular structure of ammonium trinitromethanide in the crystalline state. Displacement ellipsoids are shown at the 50 % probability level.

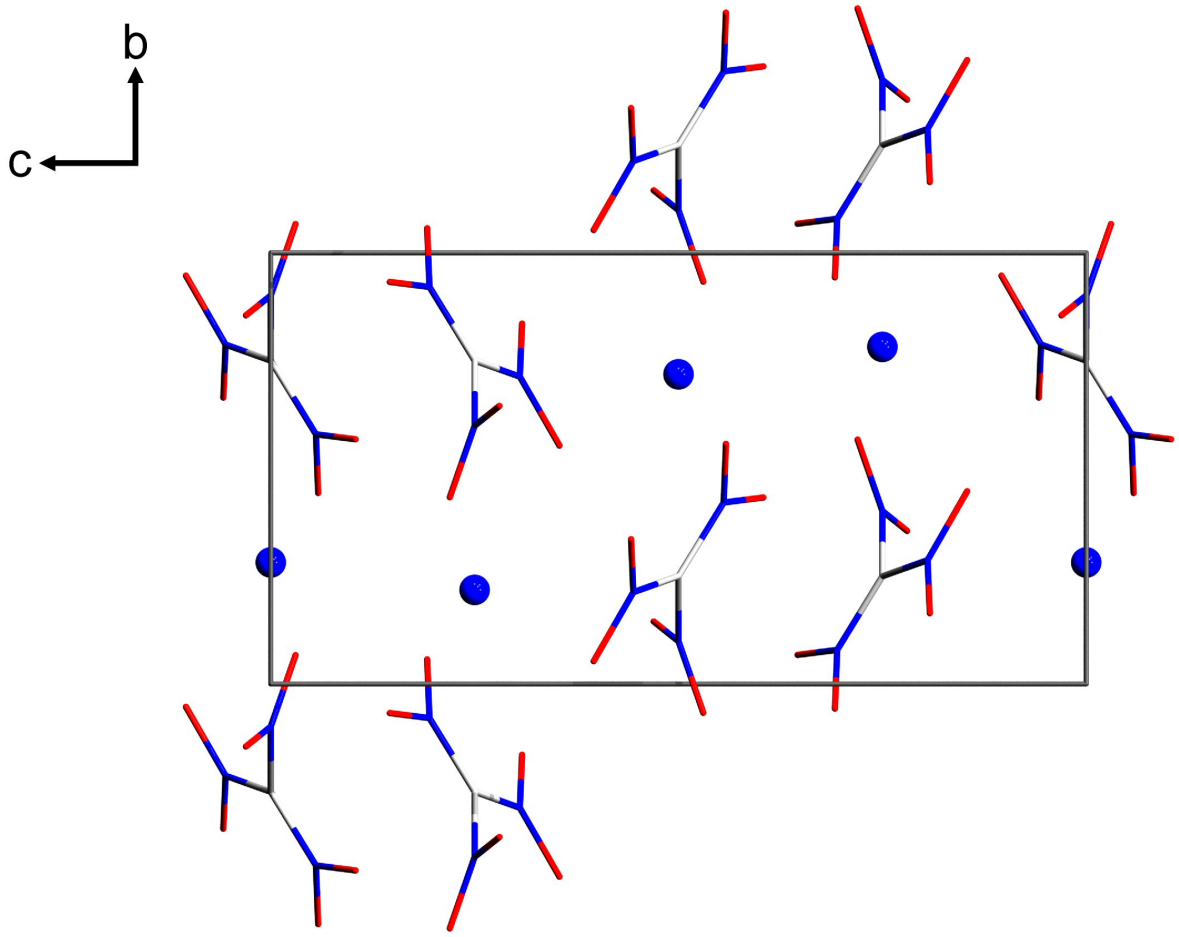

Figure 2.8. Unit cell of ammonium trinitromethanide, viewed along the *a* axis. The hydrogen atoms of the ammonium cation have been ommited for clarity.

Hydrazinium Nitroformate (HNF)

The single crystal structure of HNF was previously reported by Dickens in 1967, [137] and has been extensively studied. However, prior to this work, no further polymorph had been described. The reported calculated density obtained from single crystal X-ray diffraction has a value of 1.93 g cm^{-3}. [138] A second modification with a calculated density of 1.938 g cm^{-3} was now obtained on recrystallizing HNF from ethyl acetate at room temperature. Hydrazinium nitroformate ***3*** crystallizes in the space group $P2_1/n$ (no.14) with four formula units per unit cell. The structure reported by Dickens shows two crystallographically independent nitroformate anions with dihedral angles for the nitro groups of 41°, 7°, 8° for the first anion, and of 74°, 4° and 5° for the second anion. [137] The two corresponding hydrazinium cations are different and show staggered as well as eclipsed symmetry of the hydrogen atoms. The second modification, however, consists of only one ion pair whereby the nitro groups of the anion have dihedral angles relative to the central C-N_3 moiety of 10° (N_1, Fig. 2.9), 8° (N_2, Fig. 2.9) and 77° (N_3, Fig. 2.9), and the hydrogen atoms of the hydrazinium countercation show a staggered arrangement. The N-N distance in the hydrazine ion is 1.446(3) Å which is in good agreement with the values of the N-N distances of the hydrazine cations in the previously described polymorph (1.44 ± 0.02 Å and 1.42 ± 0.02 Å)

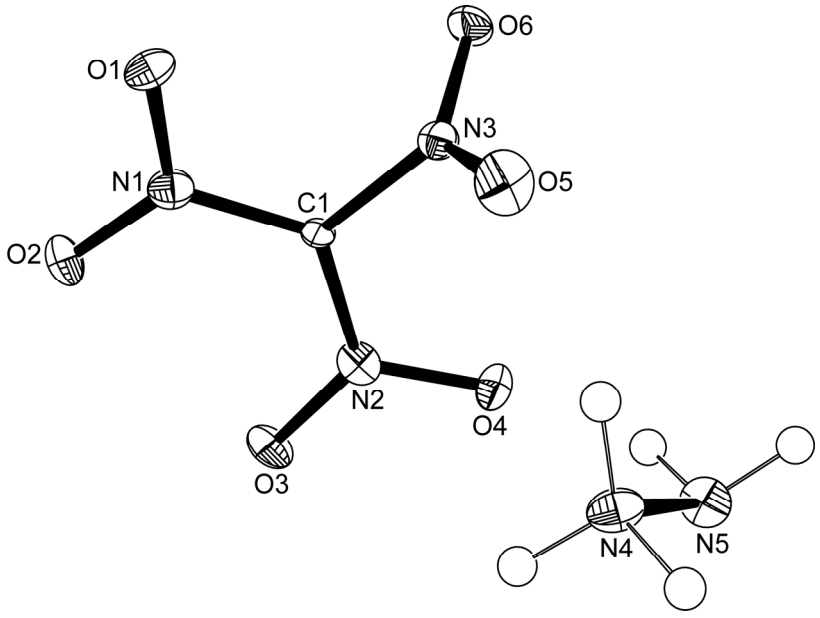

Figure 2.9. ORTEP representation of the molecular structure of hydrazinium trinitromethanide in the crystalline state. Displacement ellipsoids are shown at the 50 % probability level.

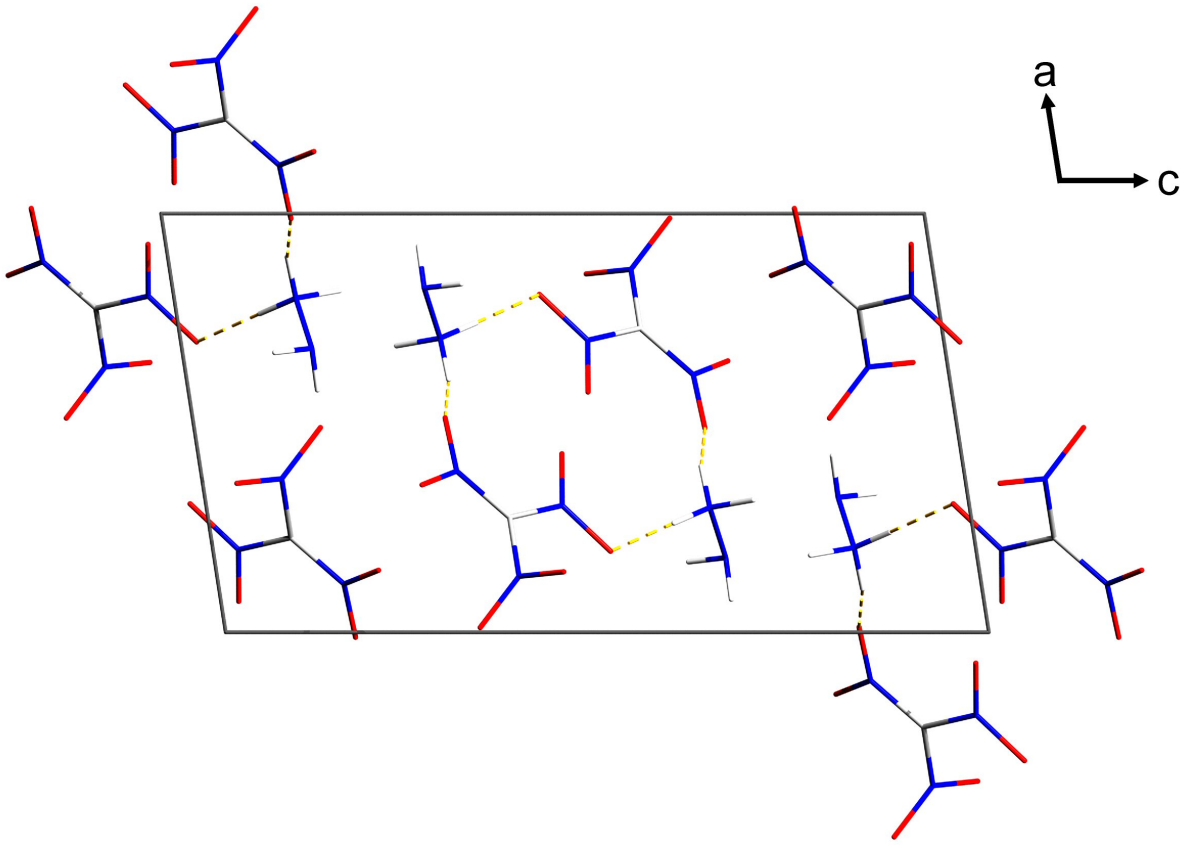

Figure 2.10. Unit cell of hydrazinium trinitromethanide, viewed along the *b* axis. Yellow dashed lines indicate hydrogen bonding.

Melaminium Nitroformate (MNF)

Although two and three-fold protonated melaminium salts are known, [139] the reaction between melamine and nitroform only afforded a 1:1 adduct. In the course of studying this reaction, however, several single crystal X-ray structures could be obtained. Two different modifications of MNF have been determined; a high density modification (MNF_{HD}) with a density of 1.914 g cm^{-3}, and a low density modification (MNF_{LD}) with a density of 1.771 g cm^{-3} (Figs. 2.11 and 2.13). The high density modification of MNF crystallizes in the space group $P2_1/n$ (no.14) with four formula units per unit cell, whereas the low density modification crystallizes in the chiral space group $P2_1$ (no.4) with two independent formula units.

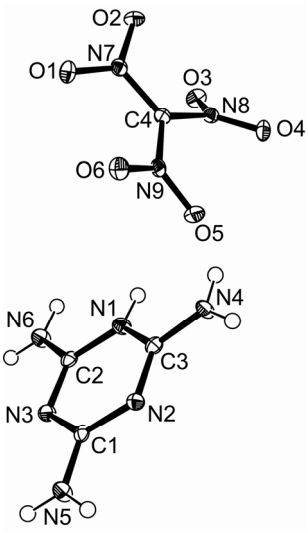

Figure 2.11. ORTEP representation of the molecular structure of melaminium trinitromethanide (high density modification) in the crystalline state. Displacement ellipsoids are shown at the 50 % probability level.

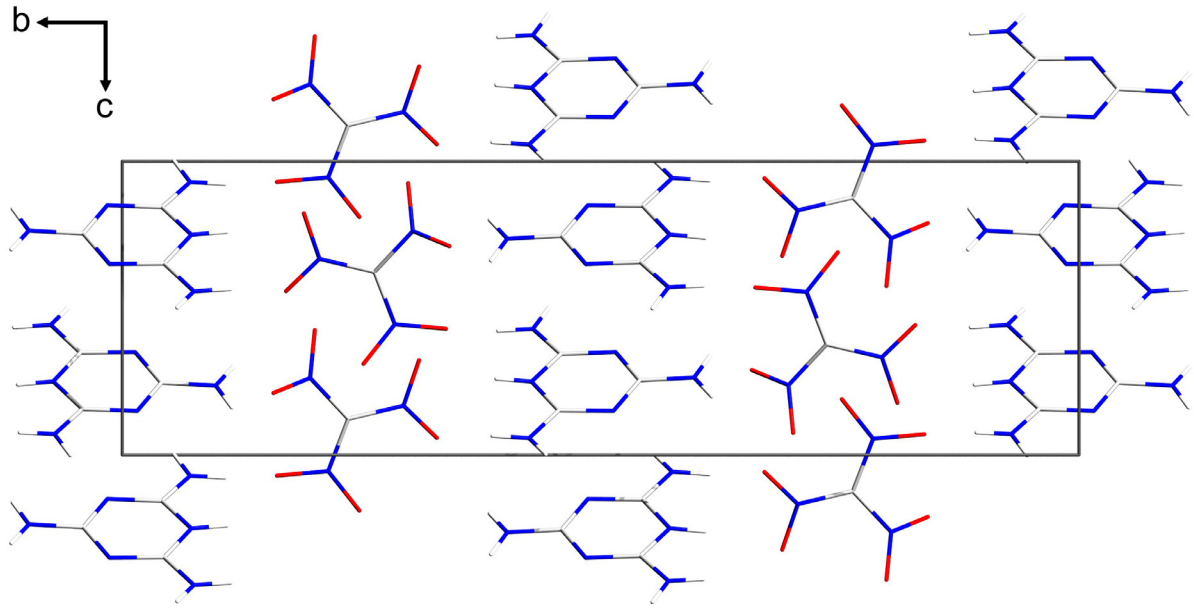

Figure 2.12. Unit cell of melaminium trinitromethanide (high density modification), viewed along the *a* axis.

The asymmetric unit of the high density modification consists of one formula unit whereas the asymmetric unit of the low density modification consists of two independent formula units. The nitroformate anion in the high density modification shows dihedral angles of the three nitro groups of 16° (N_7, Fig. 2.11), 41° (N_8, Fig. 2.11) and 8° (N_9, Fig. 2.11), whereas the dihedral angles of the nitro groups of the two crystallographically independent nitroformate anions of the low density modification are 51° (N_{13}, Fig. 2.13), 12° (N_{14}, Fig.

2.13) and 6° (N_{15}, Fig. 2.13) for the first anion and 81° (N_{16}, Fig. 2.13), 6° (N_{17}, Fig. 2.13) and 5° (N_{18}, Fig. 2.13) for the second anion.

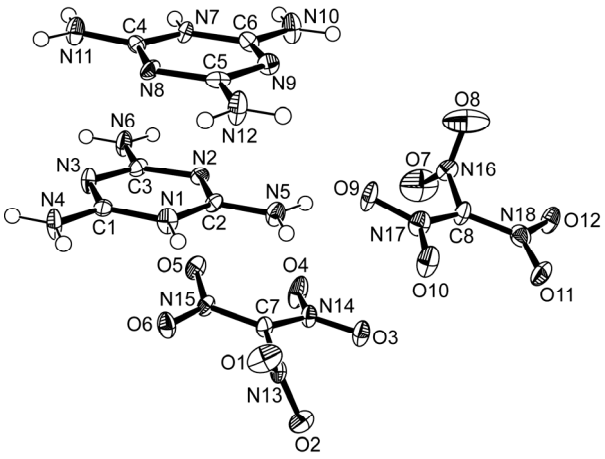

Figure 2.13. ORTEP representation of the molecular structure of melaminium trinitromethanide (low density modification) in the crystalline state. Displacement ellipsoids are shown at the 50 % probability level.

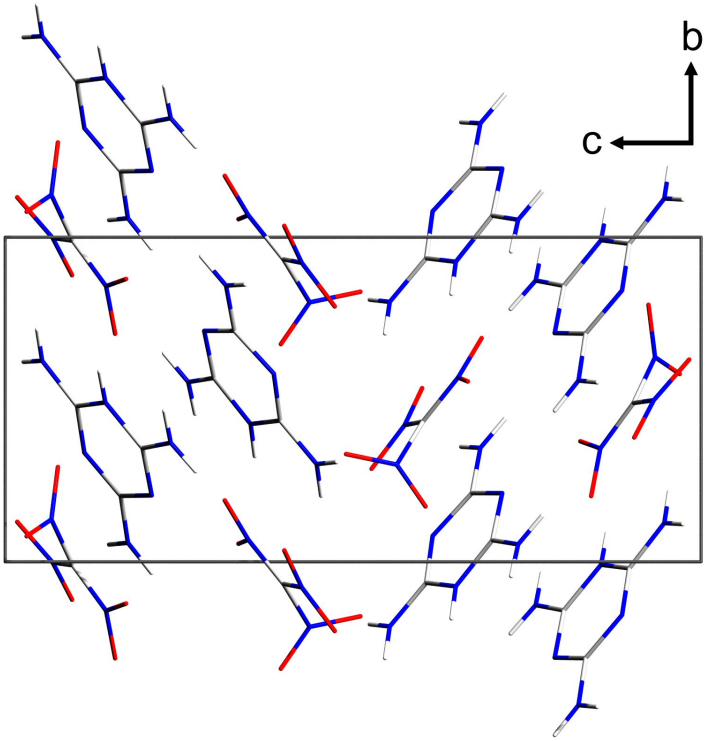

Figure 2.14. Unit cell of melaminium trinitromethanide (low density modification), viewed along the *a* axis.

In addition, two further structures of MNF could be obtained by recrystallizing MNF from either dimethylsulfoxide or methanol. The 1:1 co-crystal of MNF and DMSO crystallizes in the space group $P\bar{1}$ with two formula units per unit cell, whereas the 1:1 co-crystal of MNF and MeOH crystallizes in the space group $P2_1/c$ with four formula units per unit cell. The

asymmetric unit of MNF · MeOH (Fig. 2.15) consists of one formula unit whereas the asymmetric unit of MNF · DMSO (Fig. 2.17) consists of two independent formula units.

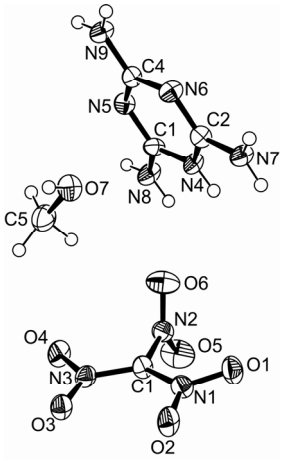

Figure 2.15. ORTEP representation of the molecular structure of melaminium trinitromethanide · methanol (1:1) in the crystalline state. Displacement ellipsoids are shown at the 50 % probability level.

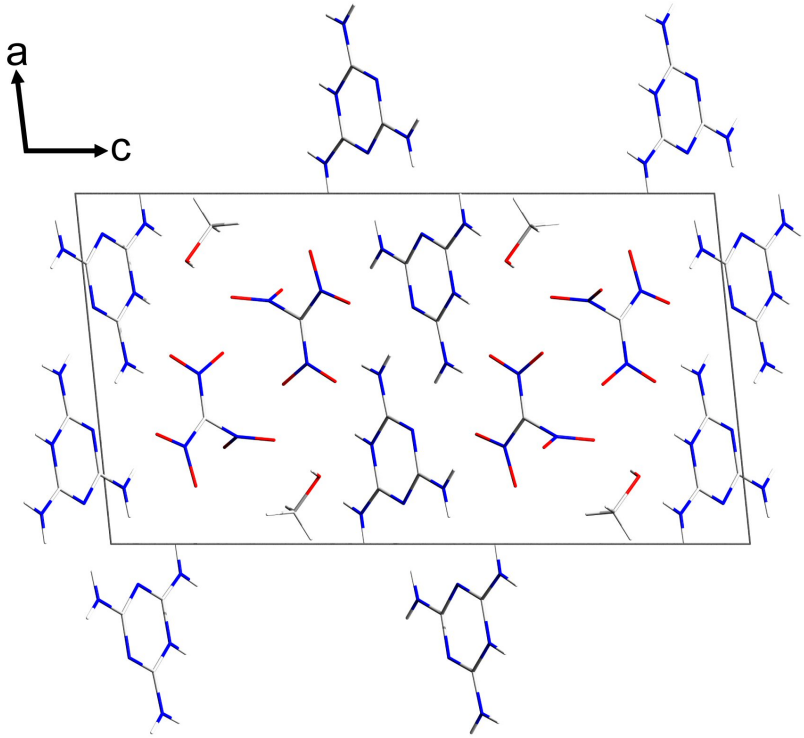

Figure 2.16. Unit cell of melaminium trinitromethanide · methanol (1:1), viewed along the *b* axis.

The nitroformate anion in MNF · MeOH shows dihedral angles for the three nitro groups of 4° (N_1, Fig. 2.15), 88° (N_2, Fig. 2.15) and 2° (N_3, Fig. 2.15), whereas the dihedral angles of the nitro groups of the two independent nitroformate anions in MNF · DMSO are 82° (N_{13}, Fig. 2.17), 9° (N_{14}, Fig.

2.17) and 7° (Fig. 2.17) for the first anion and 86° (N_{16}, Fig. 2.17), 3° (N_{17}, N_{18} Fig. 2.17) for the second anion.

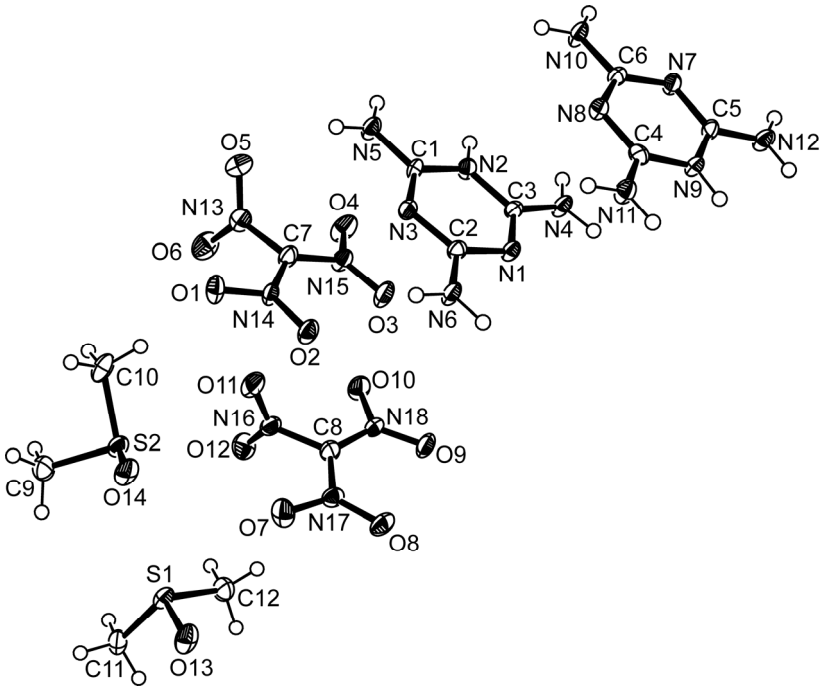

Figure 2.17. ORTEP representation of the molecular structure of melaminium trinitromethanide · dimethylsulfate (1:1) in the crystalline state. Displacement ellipsoids are shown at the 50 % probability level.

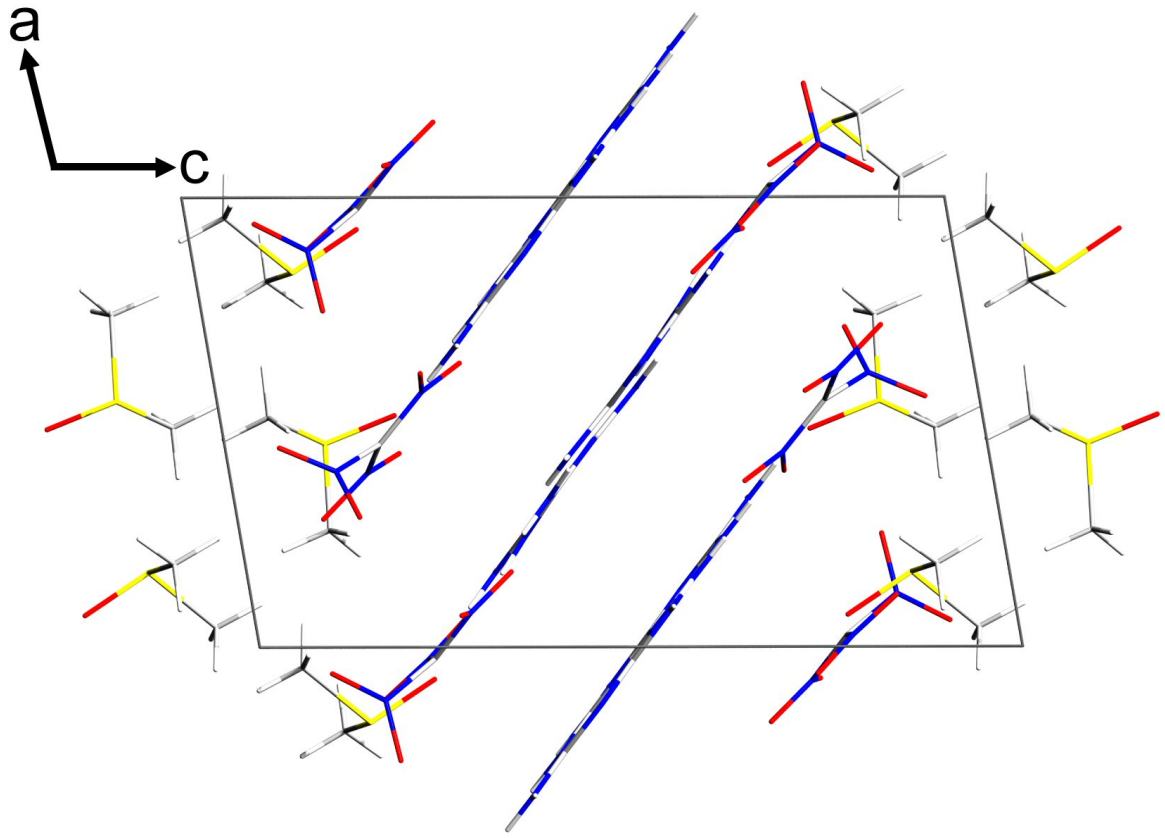

Figure 2.18. Unit cell of melaminium trinitromethanide · dimethylsulfate (1:1), viewed along the *b* axis.

Guanidinium Nitroformate Hydrate (GNFH)

The X-ray structure of guanidinium nitroformate hydrate (GNFH) consists of a two dimensional layer of guanidinium cations, nitroformate anions and water. The anion shows both the characteristic planar C-N_3 moiety and the typical conformation of the nitro groups, which has been previously described in the literature. [140] Two of the nitro groups (Fig. 2.19) are almost co-planar with ONCN torsion angles of 5°, whereas the third nitro group is twisted with a ONCN torsion angle of 81°. The C-N_3 moiety in the guanidinium cation is planar as expected, and the hydrogen atoms of the amino groups are slightly twisted out of plane with HNCN torsion angles of 1°, 3° and 9°.

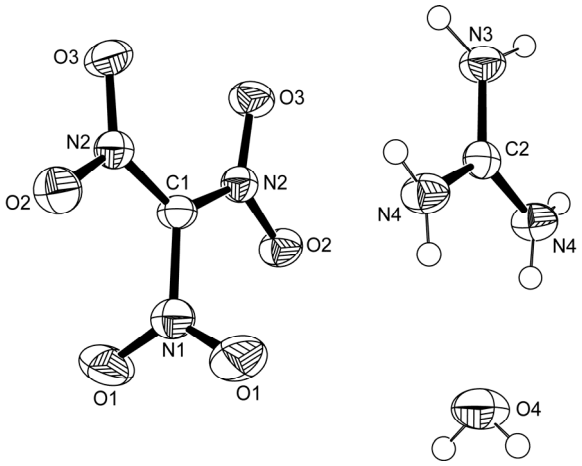

Figure 2.19. ORTEP representation of the molecular structure of guanidinium trinitromethanide · water (1:1) in the crystalline state. Displacement ellipsoids are shown at the 50 % probability level.

Two anions form hydrogen bonds with one *in-plane* nitro group towards two amino groups of the cation. The remaining hydrogen atoms of the guanidinium cation show hydrogen bonding to the neighboring water molecule. The third nitro group, which is almost perpendicular to the C-N_3 moiety, is not involved in the formation of hydrogen-bonds. Both planar nitro groups of the anion form a pair of chains with the guanidinium cation, which are interrupted by a chain of water (Fig. 2.20).

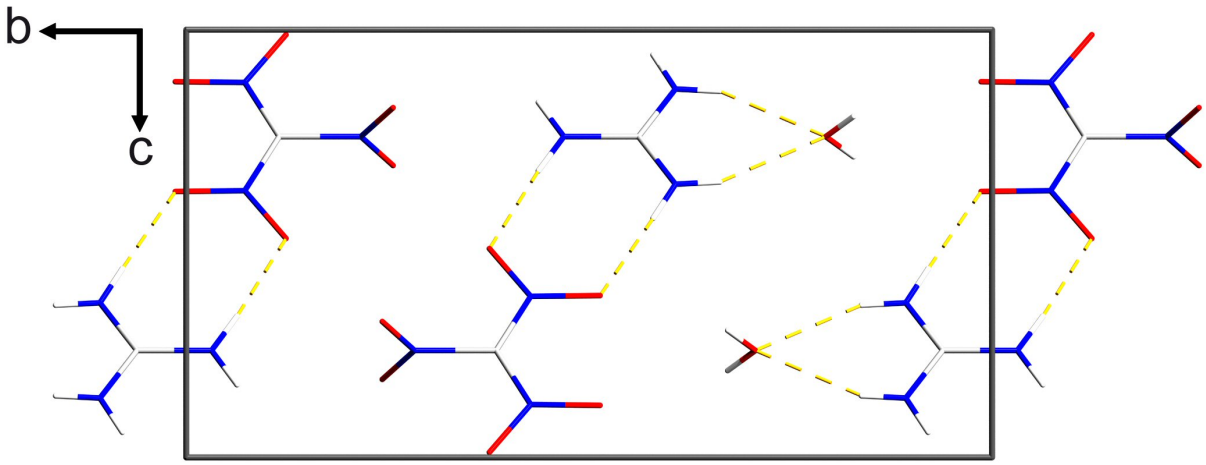

Figure 2.20. Unit cell of guanidinium trinitromethanide · water (1:1), viewed along the *a* axis.

Aminoguanidinium Nitroformate (AGNF)

Single crystals of aminoguanidinium nitroformate (AGNF) were obtained by recrystallizing AGNF from propionitrile at room temperature. Since the above mentioned competition between formation of single crystals and decomposition is a major issue in this case, crystals formed in the saturated solution were measured immediately. In contrast to the C_{2v} like orientation of the nitro groups found in GNFH, the nitro groups aminoguanidinium nitroformate are twisted in a propeller-like manner (Fig. 2.21) with dihedral angles of 25°, 17° and 36°.

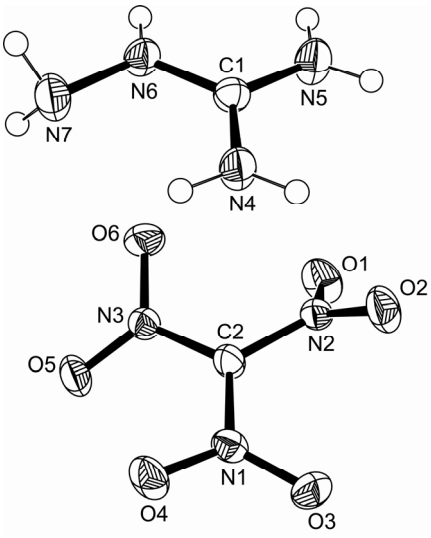

Figure 2.21. ORTEP representation of the molecular structure of aminoguanidinium trinitromethanide in the crystalline state. Displacement ellipsoids are shown at the 50 % probability level.

The b-c plane of the single crystal reveals an alternating, chessboard pattern of the anions and the cations (Fig. 2.22), whereas along the *a* axis the structure of AGNF is composed of chains of alternating cations and anions.

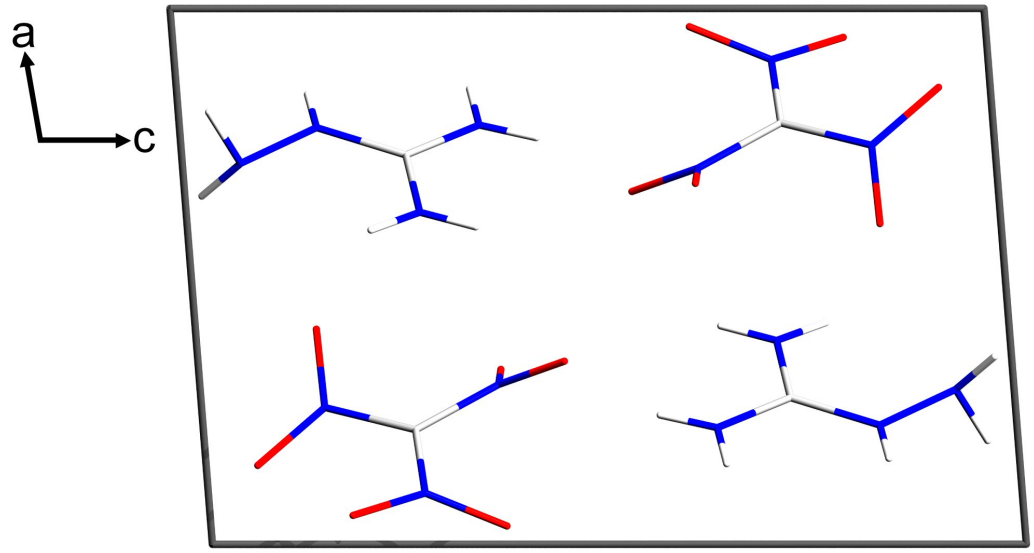

Figure 2.22. Unit cell of aminoguanidinium trinitromethanide, viewed along the *b* axis.

Diaminoguanidinium Nitroformate (DAGNF)

The solid state structure of diaminoguanidinium nitroformate (DAGNF) showed a further possible configuration for the nitroformate anion, whereby one nitro group lies nearly in plane (6°) with respect to the central C-N_3 moiety, and the other nitro groups are slightly twisted out of the plane (21° and 35°) (Fig. 2.23).

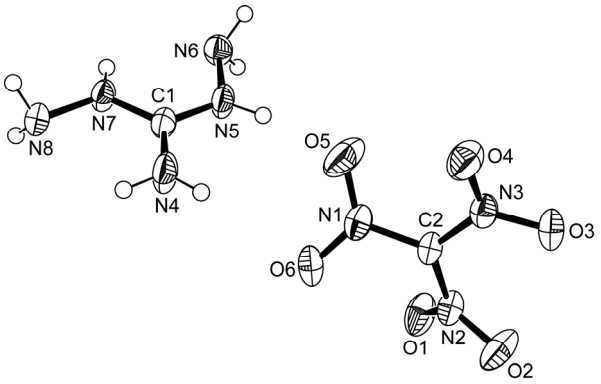

Figure 2.23. ORTEP representation of the molecular structure of diaminoguanidinium trinitromethanide in the crystalline state. Displacement ellipsoids are shown at the 50 % probability level.

In this structure, the view along the *b* axis of the unit cell (Fig. 2.24) reveals an alternating arrangement of layers of cations and the anions whereby the planes of the corresponding layers are perpendicular to each other.

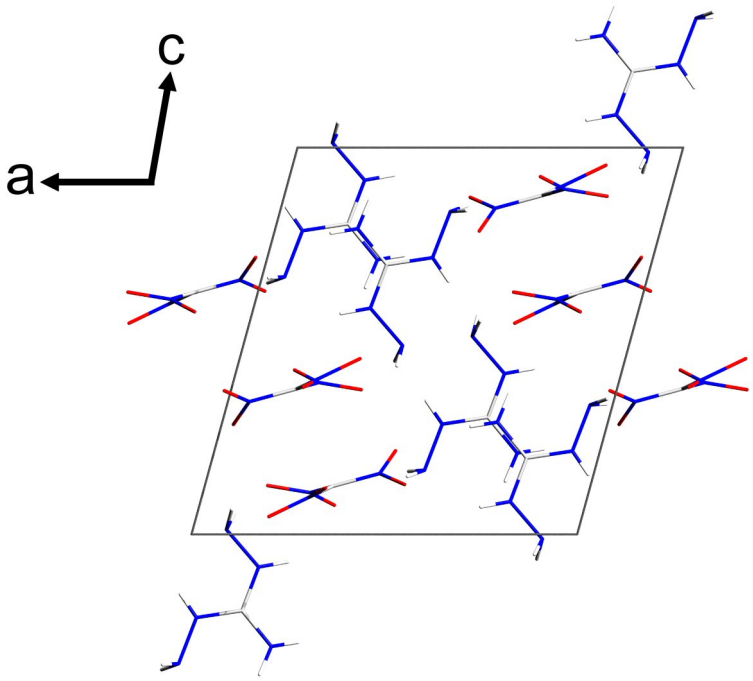

Figure 2.24. Unit cell of diaminoguanidinium trinitromethanide, viewed along the *b* axis.

Triaminoguanidinium Nitroformate (TAGNF)

In GNFH as well as AGNF both the anions and the cations lie in a common plane concerning the C-N_3 moieties, whereas triaminoguanidinium nitroformate (TAGNF) can be compared with DAGNF in that the C-N_3 moieties of the cation and the anion are perpendicular to each other (Fig. 2.25).

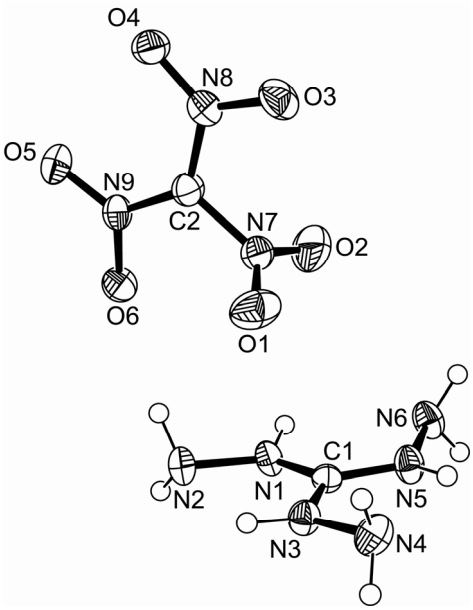

Figure 2.25. ORTEP representation of the molecular structure of triaminoguanidinium trinitromethanide in the crystalline state. Displacement ellipsoids are shown at the 50 % probability level.

The structure reveals the characteristic C_{2v} like conformation of the nitro groups of the nitroformate anion. Two of the nitro groups are almost co-planar with ONCN torsion angles of 4° and 1° respectively, whereas the third nitro group is twisted with a ONCN torsion angle of 86° (Fig. 2.25). The central C-N_3 moiety is planar, as was also observed for GNFH, AGNF and DAGNF. According to our calculations using Gaussian 03, [141] the calculated structure of the triaminoguanidinium cation is planar in the gas phase at the MP2 level of theory using a ccPVDZ basis set, whereas the amino groups of the X-ray structure are slightly twisted out of the plane with NCNN torsion angles of 10°, 9° and 7°.

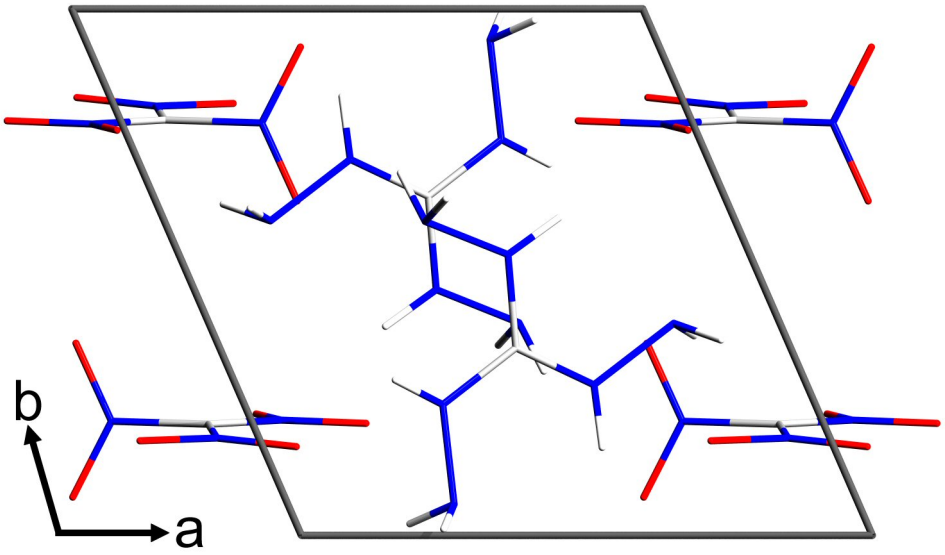

Figure 2.26. Unit cell of triaminoguanidinium trinitromethanide, viewed along the *c* axis.

Thermal Stability, Sensitivity and Performance Data

The sensitivity data of ANF, MNF, GNFH, AGNF, DAGNF and TAGNF were measured in order to establish safe handling procedures for these compounds. Two different instruments were used to determine the friction and impact sensitivity: the Bundesanstalt für Materialforschung und Prüfung (BAM) drop hammer (BAM fh (Fallhammer)) and friction tester (BAM ft). [142] GNFH was found to meet the United Nations (UN) recommendations for the transport of dangerous goods, with a friction sensitivity of greater than 360 N and an impact sensitivity of greater than 29.6 J. In contrast, great care should be taken when handling the other salts (Table 2.3) which are considerably more sensitive. The sensitivity data and the thermal behaviour of the series of guanidinium nitroformate salts appear to follow a general trend. The sensitivity towards friction and impact increases within the series AGNF < DAGNF < TAGNF, as does the thermal stability. GNFH is the least sensitive compound and also shows the highest decomposition point in the series of guanidinium nitroformate salts investigated. Hydrogen bonding between GNF and water stabilizes this compound. ANF, MNF, GNFH, AGNF, DAGNF and TAGNF showed no sensitivity towards electrostatic discharge.
Calorimetric measurements of the energies of combustion of nitro compounds present considerable difficulties because the compounds often explode on exposure to heat or mechanical shock. [143] The heats of combustion for nitro compounds are usually lower than for hydrocarbons, and the handling of larger quantities of such substances is dangerous because of the possible change from combustion to detonation. In addition, it is difficult to obtain accurate values for the enthalpy of formation since the accurate determination of the enthalpy of combustion effects the accuracy of the derived enthalpy of formation. The energies and heats of formation for ANF, HNF, MNF, GNF, AGNF, DAGNF and TAGNF were therefore calculated at the MP2 level of theory using an aug-cc-pVDZ basis set (Table 2.2). The values for the heat of formation obtained from our calculations can be compared with the previously reported values for ANF (-47.3 ± 0.2 kcal mol^{-1}), [144] HNF (-18.4 ± 0.3 kcal mol^{-1}), [144] and GNF (-50.9 ± 0.3 kcal mol^{-1}) [144] which were determined using both combustion calorimetry and reaction calorimetry. Although the previously

reported values for HNF and GNF appear to deviate from our calculated values, they are in good agreement, since according to our experimental results, GNF can only be obtained as a monohydrate, and the previously reported experimental value most probably corresponds to the hydrate GNFH, whereas our calculated value is for anhydrous GNF. The difference in the two values for HNF can be explained by the stoichiometric equation used for the combustion of the salts. The experimental value for the heat of formation of HNF is reported to be -18.4 kcal mol^{-1} assuming the physical state of the water being formed during combustion to be liquid whereas a value of +7.6 kcal mol^{-1} can be obtained assuming the physical state to be gaseous.

Table 2.2. Calculated energies and heats of formation.

	M	ρ	ΔH_L	ΔU_L	ΔH^0_f	ΔU^0_f
ANF	168.10	1.910	132.4	131.2	-35.9	-792
HNF	183.09	1.938	130.0	128.8	+0.8	+125.7
		1.930	129.8	128.6	+1.0	
		1.890	129.1	127.9	+1.7	
		1.860	128.5	127.3	+2.3	
MNF	277.20	1.914	116.2	115.0	-3.7	+42.4
GNF	210.10	1.695	121.2	120.0	-35.3	-597.4
AGNF	225.15	1.766	120.0	118.8	-9.5	-66.9
DAGNF	240.16	1.702	117.1	115.9	+19.4	+451.2
TAGNF	255.18	1.689	115.0	113.8	+59.1	+1085.4

Notes. M = molar mass / g mol^{-1}, ρ = density obtained from single crystal X-ray diffraction studies / g cm^{-3}, ΔH_L = lattice enthalpy / kcal mol^{-1}, ΔU_L = lattice energy / kcal mol^{-1}, ΔH^0_f = enthalpy of formation / kcal mol^{-1}, ΔU^0_f = energy of formation / kJ kg^{-1}

By applying the theoretical maximum density (TMD) values obtained from the crystal structure determination and the calculated energy of formation, the performance parameters of ANF, HNF, MNF, GNF, AGNF, DAGNF and TAGNF were calculated using the programme EXPLO5 (v. 5.02) [145-149] and are summarized in Table 2.3.

Table 2.3. Calculated performance data and experimental sensitivity data of ANF, HNF, MNF, GNF, AGNF, DAGNF, TAGNF and comparison with TNT and RDX.

	ρ	Ω	Q_v	V_0	T_{ex}	P	D	impact sensitivity	friction sensitivity
ANF	1.910	+19.0	-4328	800	3575	312	8532	3	96
HNF	1.938	+13.1	-5451	826	4085	380	9286	15 [150]	25 [150]
	1.930	+13.1	-5452	826	4057	368	9146		
	1.890	+13.1	-5447	826	4086	354	9028		
	1.860	+13.1	-5443	826	4107	344	8948		
MNF	1.914	-31.8	-4729	764	3579	329	8693	-	-
GNF	1.695	-7.6	-5250	853	4012	290	8558	30	> 360
AGNF	1.766	-10.7	-5617	854	4091	328	8877	10	144
DAGNF	1.702	-13.3	-5853	873	4209	317	8846	5	32
TAGNF	1.689	-15.7	-6274	885	4358	330	8982	2	20
TNT	1.64 [151]	-74	-5089	622	3741	202	7150	15 [151]	> 353 [151]
						210[a] [152]	6900[a] [151]		
RDX	1.80 [152]	-21.6	-6034	796	4334	340	8882	7.4 [153]	120 [153]
						347[a] [153]	8750[a] [153]		

Notes. a) experimental value, D = ρ / g cm^{-3} , Ω = oxygen balance / %, Q_v = heat of explosion / kJ kg, V_0 = volume of gaseous detonation products / L kg^{-1}, T_{ex} = explosion temperature / K, P = detonation pressure / kbar, D = speed of detonation / m s^{-1}, impact sensitivity / J, friction sensitivity / N.

A comparison of the calculated values of TNT and RDX with their corresponding experimental values is included in Table 2.3 and shows that the calculated values obtained using this method are in good agreement with the experimental values. The theoretically predicted values for the velocity of detonation and the detonation pressure for ANF, HNF, MNF, GNF, AGNF, DAGNF and TAGNF all lie within the range expected for high explosives such as RDX and are even superior compared to TNT, while at the same time releasing larger amounts of gaseous decomposition products and having a more favourable oxygen balance. Of all the compounds studied in this work, HNF has the highest predicted values for the detonation pressure (380 kbar) and the velocity of detonation (9286 m s^{-1}), whereas ANF shows the most positive oxygen balance with a value of +19%. Of the new compounds studied, TAGNF is not only thermally more stable in contrast to AGNF and DAGNF which decompose on standing at room temperature after several hours, it also shows the highest predicted values for the detonation pressure (330 kbar) the speed of detonation (8982 m s^{-1}). Furthermore, TAGNF is predicted to release the largest amount of gaseous detonation products (885 L kg^{-1}) and display the highest positive heat of formation (+59.1 kcal mol^{-1}).

Experimental

Caution!

Salts containing the nitroformate anion are energetic materials. Proper protective measures (safety glasses, face shields, leather coat, earthening (equipment and person), Kevlar™ gloves and ear plugs) should be used when handling these materials.

All reagents and solvents were used as received (Aldrich, Fluka) if not stated otherwise. Nitroform, potassium nitroformate and silver nitroformate were prepared according to literature procedures. [119] The thermal behaviour of the salts was investigated in a nitrogen atmosphere using differential scanning calorimetry (Perkin-Elmer Pyris 6 DSC or Linseis DSC PT-10) at heating rates of 2°C min^{-1}. ^{1}H, ^{13}C and $^{14/15}N$ NMR spectra were recorded using a Jeol Eclipse 270, Jeol EX 400 or Jeol Eclipse 400 instrument operating at 400 MHz (^{1}H), 100.6 MHz (^{13}C), 40.5 MHz (^{15}N) and 28.9 MHz (^{14}N). All chemical shifts are quoted in ppm relative to TMS (^{1}H, ^{13}C) or nitromethane (^{14}N). Infrared (IR) spectra were recorded using a Perkin-Elmer Spektrum One FT-IR (using KBr disks) or a Perkin-Elmer Spektrum BX FT-IR (pure substance) instrument. Raman spectra were measured using a Perkin Elmer Spektrum 2000R NIR FT-Raman instrument equipped with a Nd:YAG laser (1064 nm). Elemental analyses were performed with a Netsch Simultanous Thermal Analyser STA 429. Two different instruments were used to determine the friction and impact sensitivity: the Bundesanstalt für Materialforschung und Prüfung (BAM) drop hammer (BAM fh (Fallhammer)) and friction tester (BAM ft). [154] The initial electrostatic sensitivity was tested using a 20 kV Tesla-coil spark device. [155]

Tetranitromethane (TNM)

44 mL of 100% HNO_3 (1.08 mol) were filled into a three necked round bottom flask and cooled with an ice bath. To this, a solution of 50 mL acetic acid anhydride containing 0.4 mL of sulfuryl chloride was added dropwise within half an hour. The temperature of the reaction mixture was kept below 15°C. Subsequently, 50 mL of acetic acid anhydride containing 2 mL of sulfuryl chloride were added to the reaction mixture in the same way. The reaction flask containing a slight yellow solution was then protected from light with silver foil and left standing for seven days. Then the solution was put onto 100 mL of ice water in a separating funnel. Two layers formed, one yellow upper phase and one colourless phase at the bottom. The colourless phase was washed ten times with 10 mL of water and then with 20 mL of a water solution containing ten percent sodium carbonate affording pure tetranitromethane (Fig. 2.27).

Figure 2.27. Isolation of Tetranitromethane. The reaction mixture is poured onto ice water and separates as heavy phase (left picture). NMR pure tetranitromethane is obtained as a colourless liquid after several washings using sodium bicarbonate (right picuture).

44.3 g of TNM were obtained which corresponds to a yield of 83.7 % related to HNO_3. m.p.: 13.0 - 14.0°C; ^{13}C NMR (DMSO-d6) δ: 116.5 (C_q); ^{14}N NMR (DMSO-d6) δ: -48.3 (-NO_2, $\Delta\nu_{1/2}$ = 4.4Hz); $\tilde{\nu}$ (KBr, r.t.)[cm^{-1}]: Raman (250mW, protection shield, 50 scans, 2 cm^{-1}, r.t.) $\tilde{\nu}$ [cm^{-1}]: 1647 [$\nu_{as}(NO_2)$,(10)], 1615 [$\nu_{as}(NO_2)$,(10)], 1343 [ν_s (NO_2),(18)], 1276 [ν_s (NO_2),(12)], 998 (5), 862 [C-NO_2,

(100)], 801 [C-NO_2, (4)], 605 [$\delta_s(NO_2)$,(5)], 414 [δ_{C-N}, (18)], 358 [δ_{C-N}, (82)], 227 [δ_{C-N}, (11)], 197 [δ_{C-N} , (12)].

Potassium Nitroformate (KNF)

Potassium nitroformate was prepared according to the literature. [119] Potassium hydroxide (111mg, 2 mmol) and glycerol (183 mg, 2 mmol) was dissolved in 5 mL of water and stirred at ice bath temperature. To this solution, were added portion-wise over a period of ten minutes, 130 mg of tetranitromethane (0.66 mmol). The ice-bath was removed and the reaction mixture was allowed to warm up to room temperature and stirred for one hour. The precipitate was filtered off and washed with 2 mL of diethylether. The mother liquor was used again instead of the 5 mL of water used initially and the procedure was repeated. Crystals suitable for single X-ray crystallography were obtained by recrystallizing potassium nitroformate from nitromethane at room temperature and were measured immediately.
The yield was 180 mg (72%) of bright yellow KNF. m.p.: 83°C (decomp. with evolution of gas); ^{13}C NMR (DMSO-d6) δ: 150.8 ($C(NO_2)_3$); ^{14}N NMR (DMSO-d6) δ: -30.3 (-NO_2, $\Delta\nu_{1/2}$ = 22.3 Hz); Raman (100 mW, protection shield, 60 scans, 4cm^{-1}) $\tilde{\nu}$ [cm^{-1}]: 1508(5), 1466 (3), 1422 (6), 1394 (38), 1291 (34), 1272 (100), 1246 (21), 1168 (7), 873 (35), 794 (11), 719 (7), 465 (8), 442 (3), 283 (6), 257 (14), 155 (12), 113 (8); UV-VIS (Acetone): 349 nm (E=0.525); m/z (FAB-/NBA): 150 [$C(NO_2)_3^-$, vs], 62 [NO_3^-, w], 46 [NO_2^-, m]; Details of the single crystal X-ray diffraction experiment are listed in the appendix (Chapter 4).

Nitroform (NFM)

313 mg of KNF (1.66 mmol) were suspended in 2.5 mL of pentane and cooled with an ice bath. To this suspension 1 mL of concentrated sulfuric acid (98%) was given dropwise over a period of ten minutes. The sulfuric acid turned yellow at once. After two hours the color had disappeared and the sulfuric acid was extracted ten times with 2 mL of pentane. Alternatively, the potassium salt of trinitromethane can be acidifiend using gaseous hydrochloric acid (Fig.

2.28). In order to isolate the nitroform as a white solid, the collected pentane phases were treated with a current of nitrogen. Because of the heat of evaporation of pentane it was ensured that the precipitating white nitroform crystals would not liquefy and clean product was obtained.

Figure 2.28. Synthesis of trinitromethane from potassium nitroformate. Dry potassium nitroformate is suspended in pentane and acidified using gaseous hydrochloric acid (left picture) affording a colourless solution of trinitromethane in pentane after a few minutes. On passing a stream of nitrogen over the pentane solution, trinitromethane precipitates from the solution in high yield and purity (right picture).

The yield was 157.5 mg (63%); m.p.: 25.4°C ; ^{1}H NMR ($CDCl_3$) δ: 7.46 (s, 1H, *H*-C$(NO_2)_3$); ^{13}C NMR ($CDCl_3$) δ: 114.4 (sept., 1C, *J* 8.7 Hz, H-*C*$(NO_2)_3$); ^{14}N NMR (DMSO-d6) δ: -38.3 (-*N*O_2, $\Delta\nu_{1/2}$ = 7.2 Hz); $\tilde{\nu}$ (gas, -196°C defrost)[cm^{-1}]: 3063 [ν(CH)], 1618 [s, $\nu_{as}(NO_2)$], 1608 [s, $\nu_{as}(NO_2)$], 1303 [s, $\nu_s(NO_2)$ antiphase], 947 [w, ν(CN)], 845 [$\delta(NO_2)$ synphase], 779 [s, $\delta(NO_2)$ antiphase], 630 [w, $w(NO_2)$], 569 [w, $w(NO_2)$]; Raman (100 mW, protection shield, 40 scans, 0°C, 2 cm^{-1}) $\tilde{\nu}$ [cm^{-1}]: 3029 (25), 2758 (5), 1626 (49), 1611 (24), 1375 (50), 1327 (22), 1309 (36), 1243 (26), 950 (69), 943 (57), 840 (51), 774 (22), 628 (36), 574 (21), 405 (100), 375 (95), 237 (12), 204 (18), 121 (14); m/z (CI+, NH_3) 152 [(M+1)(0,6)], 105 [(M-NO_2)(0,07)], 46 [(NO_2)(100)], 30,0 [(NO)(32,6)].

Ammonium Nitroformate (ANF)

Ammonium nitroformate was prepared according to the literature. [98] Crystals suitable for X-ray diffraction were obtained by recrystallizing ANF from propionitrile at room temperature.
m.p.: 116 °C (onset, decomp., Linseis DSC); $\tilde{\nu}$ (pure substance, solid) [cm^{-1}]: 3222 (m), 1681 (w), 1533 (m), 1460 (m), 1415 (s), 1375 (s), 1247 (s), 1147 (s), 1006 (m), 926 (m), 869 (m), 823 (w), 788 (s), 735 (s), 689 (m); Raman (200 mW, 100 scans, 2 cm^{-1}, protection shield) $\tilde{\nu}$ [cm^{-1}]: 3172 (4), 2986 (7), 1610 (7), 1535 (6), 1515 (6), 1475 (10), 1380 (43), 1349 (19), 1310 (28), 1273 (72), 1225 (39), 1156 (36), 1138 (25), 871 (100), 859 (35), 791 (12), 727 (10), 466 (24), 443 (18), 415 (20), 396 (16), 375 (21), 275 (23); m/z (FAB$^+$, NBA): 18 [NH_4^+, w]; (FAB$^-$, NBA): 150 [($C(NO_2)_3^-$), vs]; ^{1}H NMR ([D$_6$]acetone) δ: 7.54 (NH_4^+, t); ^{13}C NMR ([D$_6$]acetone) δ: 153.3 ($C(NO_2)_3^-$); ^{14}N NMR ([D$_6$]acetone) δ: -30 (NO_2), -364 (NH_4^+); $C_1H_4N_4O_6$: calc.: N: 33.3 %, C: 7.2 %, H: 2.4 %; found: N: 33.5 %, C: 7.6 %, H: 2.7 %; Details of the single crystal X-ray diffraction experiment are listed in the appendix (Chapter 4).

Silver Nitroformate Hydrate (AgNFH)

258 mg of freshly prepared and moist silver oxide (1.11 mmol) were suspended in 5 mL of water and the suspension was filtered.
146 mg of nitroform (0.97 mmol) were dissolved in 5 mL of freshly distilled diethylether and cooled with an ice-bath. Freshly filtrated and moist silver oxide was then added to this solution while stirring vigorously. After fifteen minutes, the reaction mixture was filtered and the solvent removed affording bright yellow crystals. Single crystals suitable for X-ray structure determination were obtained by recrystallizing these crystals from water and were immediately measured. 185 mg of yellow silver nitroformate monohydrate were obtained (74% yield).
m.p.: 70°C (decomp. with evolution of gas); ^{13}C NMR (DMSO-D$_6$) δ: 150.4 ($C(NO_2)_3$); ^{14}N NMR (DMSO-D$_6$) δ: -29.9 (-NO_2, $\Delta\nu_{1/2}$ = 13.5 Hz); Raman (100 mW, protection shield, 100 scans, 4cm^{-1}) $\tilde{\nu}$ [cm^{-1}]: 1463 (14), 1379 (78), 1257

(87), 1153 (35), 878 (100), 791 (13), 722 (8), 473 (16), 455 (15), 420 (8), 280 (16), 166 (24); UV-VIS (Acetone): 349 nm (E=0.382); m/z (FAB$^-$, NBA): 150 [($C(NO_2)_3^-$), vs], 104 [($C(NO_2)_2^-$, w], 46 [(NO_2), w]; Details of the single crystal X-ray diffraction experiment are listed in the appendix (Chapter 4).

Hydrazinium Nitroformate (HNF)

Hydrazinium nitroformate was prepared according to the literature. [156] Crystals suitable for X-ray diffraction were obtained by recrystallizing HNF from ethyl acetate at room temperature. Details of the single crystal X-ray diffraction experiment are listed in the appendix (Chapter 4).

Melaminium Nitroformate (MNF)

Melaminium nitroformate was prepared according to the literature. [157] Crystals suitable for X-ray crystallography were obtained by recrystallizing MNF from acetone (high density modification and low density modification) dimethylsulfoxide (DMSO adduct) or methanol (methanol adduct) at room temperature.

m.p.: 118 °C (onset, Linseis DSC), 143 °C(onset, Linseis DSC); $\tilde{\nu}$ (pure solid substance) [cm^{-1}]: 3446 (w), 3367 (m), 3317 (m), 3149 (m), 2960 (m), 1712 (m), 1645 (s), 1613 (s), 1509 (s), 1467 (s), 1409 (s), 1367 (m), 1338 (m), 1263 (s), 1213 (s), 1124 (s), 995 (s), 976 (s), 869 (m), 792 (s), 773 (s), 744 (s), 732 (s), 688 (m); Raman (200 mW, 200 scans, 1 cm^{-1}) $\tilde{\nu}$ [cm^{-1}]: 3330 (6), 2989 (6), 1696 (8), 1650 (7), 1596 (8), 1557 (9), 1520 (18), 1504 (13), 1479 (13), 1410 (16), 1375 (48), 1257 (100), 1223 (68), 1156 (32), 1127 (45), 980 (13), 870 (96), 797 (22), 739 (8), 723 (12), 687 (61), 578 (16), 562 (26), 478 (18), 444 (13), 384 (15), 279 (23), 195 (14), 161 (13), 137 (14); ^{1}H NMR ([D$_6$]acetone) δ: 7.6 (s, NH_2); ^{13}C NMR ([D$_6$]acetone) δ: 159.9 (C_3, $H_7N_6^+$), 150.3 ($C(NO_2)_3^-$); ^{14}N NMR ([D$_6$]acetone) δ: -29.9 (NO_2); $C_4H_7N_9O_6$: calc.: N: 45.48 %, C: 17.33 %, H: 2.55 %; found: N: 44.59 %, C: 17.72 %, H: 2.81 %; Details of the single crystal X-ray diffraction experiment are listed in the appendix (Chapter 4).

Guanidinium nitroformate (GNF)

To an ice-cooled suspension of 108.3 mg of guanidinium chloride (1.1 mmol) in 6 mL freshly distilled acetonitrile, a solution of 222 mg silver nitroformate (0.8 mmol) dissolved in 7.6 mL of freshly distilled acetonitrile was added drop-wise over a period of 10 minutes. Silver chloride precipitated instantly. The reaction mixture was stirred for a further 2.5 hours. The reaction mixture was allowed to warm up to room temperature and was then stirred for further 2 hours. The precipitated silver chloride was then filtered off and washed with 4 mL of acetonitrile. In order to isolate GNFH, the solvent was first removed using a rotary evaporator affording a yellow, highly viscous liquid. The remaining solvent was removed using high vacuum. GNFH was obtained as a bright yellow solid.

m.p.: 69°C (PE DSC), 113°C (decomp., PE DSC); $\tilde{\nu}$ (KBr pellets) [cm^{-1}]: 3397 (m), 3280 (w), 3197 (w), 2917 (w), 2851 (w), 1662 (m), 1640 (m), 1513 (m), 1495 (m), 1421 (m), 1358 (w), 1272 (s), 1177 (m), 1144 (w), 976 (w), 866 (w), 794 (m), 733 (m), 515 (w); Raman (200 mW, 100 scans, 4 cm^{-1}, protection shield) $\tilde{\nu}$ [cm^{-1}]: 3287 (3), 1528 (11), 1470 (10), 1388 (63), 1299 (37), 1244 (35), 1155 (46), 1055 (12), 1013 (63), 868 (100), 789 (15), 728 (13), 533 (24), 472 (25), 442 (15), 252 (17); m/z (FAB$^+$, NBA): 213 [($C(NH_2)_3^+$ + NBA), s], 119 [($C(NH_2)_3^+$ + $HN{=}C(NH_2)_2$), m], 60 [($C(NH_2)_3^+$), vs]; (FAB$^-$, NBA): 360 [(2 $C(NO_2)_3^-$ + $C(NH_2)_3^+$), s], 303 [($C(NO_2)_3^-$ + NBA), m], 150 [($C(NO_2)_3^-$), vs], 104 [($C(NO_2)_2^-$), w]; ^{1}H NMR ([D_6]DMSO) δ: 6.90 (NH_2), 3.39 (H_2O); ^{13}C NMR ([D_6]DMSO) δ: 158.0 ($C(NH_2)_3^+$), 150.3 ($C(NO_2)_3^-$); ^{15}N NMR ([D_6]DMSO) δ: -31 (NO_2), -306 (NH_2); $C_2H_8N_6O_7$: calc.: N: 36.8 %, C: 10.5 %, H: 3.5 %; found: N: 36.4 %, C: 10.4 %, H: 3.9 %; Details of the single crystal X-ray diffraction experiment are listed in the appendix (Chapter 4).

Aminoguanidinium nitroformate (AGNF)

124.8 mg of aminoguanidinium chloride (1.1 mmol) were suspended in 3 mL of freshly distilled acetonitrile and cooled with an ice bath. To this suspension was added a solution of 222 mg silver nitroformate (0.8 mmol) in 7.6 mL freshly distilled acetonitrile drop-wise over a period of 10 min. After stirring the reaction mixture for a further 30 minutes, the ice bath was removed. The mixture was stirred for an additional 75 minutes and the silver chloride precipitate was filtered off. The solvent was removed using a rotary evaporator. After removal of the remaining acetonitrile from the highly viscous liquid using high vacuum, a bright yellow solid was obtained (Fig. 2.29)

Figure 2.29. Sample of bright yellow aminoguanidinium nitroformate.

m.p.: 71°C (decomp., PE DSC); $\tilde{\nu}$ (KBr pellets) [cm^{-1}]: 3447 (m), 3362 (m), 3297 (m), 2917 (w), 2846 (w), 2181 (w), 1657 (s), 1512 (s), 1495 (s), 1421 (m), 1272 (s), 1177 (s), 984 (w), 943 (w), 866 (w), 794 (m), 733 (m), 614 (w), 499 (w); Raman (100 mW, 20 scans, 2 cm^{-1}, protection shield) $\tilde{\nu}$ [cm^{-1}]: 3282 (1), 1487 (10), 1465 (6), 1380 (76), 1333 (10), 1277 (100), 1244 (56), 1197 (16), 1163 (17), 960 (10), 869 (93), 793 (13), 788 (13), 721 (11), 501 (19), 445 (15), 273 (18), 262 (16), 156 (12); m/z (FAB$^+$, NBA): 167 [(H_2N-HN=$C(NH_2)_2^+$ + NBA + H_2O), m], 149 [(H_2N-N=$C(NH_2)_2^+$ + H_2N-N=$C(NH_2)_2$),vs]; (FAB$^-$, NBA): 150 [($C(NO_2)_3^-$), vs]; ^{1}H NMR ([D_6]DMSO) δ: 8.52, 6.94, 4.28; ^{13}C NMR ([D_6]DMSO) δ: 158.9 ((H_2N-HN=*C*$(NH_2)_2^+$), 150.3 (*C*$(NO_2)_3^-$); ^{15}N NMR ([D_6]DMSO) δ: -30 (*N*O_2), -284 (C-*N*H_2), -311 (*N*H-NH_2), -326 (NH-*N*H_2); $C_2H_7N_7O_6$: calc.: N: 43.6 %, C: 10.7 %, H 3.1 %; found: N: 42.8 %, C: 10.8 %, 3.2 %; Details of the single crystal X-ray diffraction experiment are listed in the appendix (Chapter 4).

Diaminoguanidinium nitroformate (DAGNF)

A solution of 182 mg silver nitroformate (0.66 mmol) in 5 mL of acetonitrile was added dropwise over a period of 10 minutes to a suspension of 85.5 mg diaminoguanidinium chloride (0.69 mmol) in 2 mL of acetonitrile at 0°C. The reaction mixture was stirred for a further 40 minutes. The reaction mixture was then allowed to warm up to room temperature and was stirred for a further 2 hours. The silver chloride precipitate was filtered off and the solvent was removed using a rotary evaporator. The highly viscous yellow liquid was dried using high vacuum affording a bright yellow solid.
m.p.: 80°C (PE DSC), 82°C (decomp., PE DSC); $\tilde{\nu}$ (KBr pellets) [cm^{-1}]: 3432 (m), 3307 (s), 3247 (w), 2978 (w), 2554 (w), 2175 (w), 1682 (s), 1621 (m), 1512 (s), 1495 (s), 1421 (s), 1352 (w), 1270 (s), 1177 (s), 992 (m), 957 (m), 869 (w), 794 (s), 733 (s), 653 (w), 549 (w); Raman (200 mW, 100 scans, 4 cm^{-1}, protection shield) $\tilde{\nu}$ [cm^{-1}]: 3299 (3), 1379 (66), 1247 (100), 1184 (33), 1158 (25), 873 (81), 793 (12), 725 (9), 277 (19), 152 (14); m/z (FAB^+, NBA): 243 [$(H_2N{=}C(NH\text{-}NH_2)_2^+$ + NBA), w], 90.1 [$(H_2N{=}C(NH\text{-}NH_2)_2^+$, vs], 89.1 [$(HN{=}C(NH\text{-}NH_2)_2$, m]; m/z ($FAB^-$, NBA): 303 [$(C(NO_2)_3^-$ + NBA), w], 150 [$(C(NO_2)_3^-$), vs]; ^{1}H NMR ([D_6]DMSO) δ: 8.50 (N*H*-NH_2), 4.48 (C-NH_2, NH-NH_2); ^{13}C NMR ([D_6]DMSO) δ: 159.9 ($(H_2N\text{-}C(NH\text{-}NH_2)_2)^+$), 150.4 ($C(NO_2)_3^-$); ^{15}N NMR ([$D_6$]DMSO) δ: -31 ($NO_2$), -288 (C-$NH_2$), -313 ($NH\text{-}NH_2$), -328 (NH-$NH_2$); $C_2H_8N_8O_6$: calc.: N: 46.7, C: 10.0 %, H: 3.4 %; found: N: 45.4 %, C: 10.4%, H: 3.4 %; Details of the single crystal X-ray diffraction experiment are listed in the appendix (Chapter 4).

Triaminoguanidinium nitroformate (TAGNF)

To a suspension of 185 mg triaminoguanidinium chloride (1.33 mmol) in 2 mL of freshly distilled acetonitrile, a solution consisting of 363 mg (1.32 mmol) silver nitroformate and 10 mL of acetonitrile was added dropwise within a period of 10 minutes at 0°C. The reaction mixture was then stirred for a further 40 minutes. The solution was allowed to warm up to room temperature and stirred for a further 70 minutes.

After removing the precipitated silver chloride from the reaction mixture, the solution was concentrated using the rotary evaporator. A highly viscous yellow liquid was obtained. The remaining solvent was removed using high vacuum, whereby a bright yellow solid could be obtained.

m.p.: 84°C (PE DSC), 105°C (decomp., PE DSC); $\tilde{\nu}$ (KBr pellets) [cm^{-1}]: 3317 (m), 3210 (s), 1683 (m), 1614 (w), 1513 (s) 1421 (m), 1333 (w), 1276 (s), 1177 (s), 1127 (m), 951 (m), 871 (w), 793 (s), 733 (s), 638 (w), 603 (m), 483 (w); Raman (200 mW, 200 scans, 4 cm^{-1}, protection shield)$\tilde{\nu}$[cm^{-1}]: 3287 (6), 1648 (25), 1461 (16), 1437 (15), 1385 (71), 1331 (38), 1260 (27), 1153 (67), 868 (100), 789 (19), 735 (6), 470 (34), 430 (24), 152 (20);

m/z (FAB$^+$, NBA): 227 [(H_2N-N=C(NH-NH_2)$_2$ + (C(NH-NH_2)$_3^+$ + H_2O), w], 209 [(H_2N-N=C(NH-NH_2)$_2$ + (C(NH-NH_2)$_3^+$), w], 105 [(C(NH-NH_2)$_3^+$, vs]; ^{1}H NMR ([D_6]acetone) δ: 9.79 (C(N*H*-NH_2)$_3^+$), 3.53 (C(NH-N*H_2*)$_3^+$); ^{13}C NMR ([D_6]acetone) δ: 161.8 (*C*(NH-NH_2)$_3^+$), 150.6 (*C*(NO_2)$_3^-$); ^{15}N NMR ([D_6]acetone) δ: -31 (*C*(*N*O_2)$_3^-$), -283 (C(*N*H-NH_2)$_3^+$), -348 (C(NH-*N*H_2)$_3^+$); $C_2H_9N_9O_6$: calc.: N: 49.4 %, C: 9.4 %, H: 3.6 %; found: N: 47.8 %, C: 10.4 %, H: 3.3 %; Details of the single crystal X-ray diffraction experiment are listed in the appendix (Chapter 4).

2.1.2 Salts of Nitric Acid

Melaminium Dinitrate (MDN)

Introduction

Melamine (2,4,6-triamino-1,3,5-triazine) is a nitrogen-rich, planar compound which can form salts containing mono- or diprotonated melaminium cations. Melaminium nitrate was synthesised by Tanbug *et al.* and classified as a novel energetic material. [158] However, no sensitivity or performance data were reported. In the course of investigating oxygen-rich energetic materials, the earlier unknown nitrogen and oxygen-rich energetic salt melaminium dinitrate was readily obtained from the reaction between melamine and concentrated nitric acid. [159] The salt was characterized using vibrational spectroscopy (IR, Raman), multinuclear NMR spectroscopy and elemental analysis. The thermal behaviour of MDN was monitored using differential scanning as well as isothermal long term calorimetry. In addition, the impact, friction and electrostatic sensitivity data were measured. The crystal structure of MDN was determined using single crystal X-ray diffraction.

Sensitivity and Performance

The friction and impact sensitivities were measured with a BAM drop-hammer and a BAM friction tester. The friction sensitivity of this compound was determined as being greater than 350 N, and the impact sensitivity more than 30 J. The thermal long term stability was studied using a RADEX V5 Oven. Isothermal tempering of the substance showed that the substance is thermally stable for at least 48 hours at a temperature of 140°C

Table 2.4. Performance Data of MDN and comparison to TNT.

	MDN	TNT
sum formula	$C_3H_8N_8O_6$	$C_7H_5N_3O_6$
m.w. / g mol^{-1}	252.2	227.1
ρ / g cm^{-3}	1.852(2)	1.64 [160]
Δ_fH^0(s) / kcal mol^{-1}	-149.8	-13.27
Δ_fU^0(s) / kJ kg^{-1}	-2377.3	-175
Ω / %	-25.4	-74.0
Q / kJ kg^{-1}	2977	5064
T_{ex} / K	2562	3749
V_0 / L kg^{-1}	803	625
P_{CJ} / kbar	236	203
D / m s^{-1}	7723	7170

Although MDN has a favourable oxygen balance (Ω = -25.4) and a combined oxygen and nitrogen content of greater than 80%, it shows a remarkable thermodynamic stability ($T_{decomp.}$ = 330 °C). It was found to meet the United Nations (UN) recommendations for the transport of dangerous goods, with a friction sensitivity of greater than 360 N and an impact sensitivity of greater than 30 J. Excessive hydrogen bonding in the solid state not only stabilizes this compound but also results in a dense packing of the crystalline material leading to a remarkably high density (1.852 g cm^{-3}) and performance values exceeding the detonation pressure, the detonation velocity of TNT while at the same time producing a favourably larger amount of decomposition gases and lower explosion temperature. These properties render MDN to be an interesting material displaying potential for applications requiring insensitivity and thermal stability, for example for perforation and fracturing purposes for oilfield exploration (Table 2.4).

Crystal Structure Analysis

MDN at 200 K has monoclinic symmetry; space group $P2_1/c$ (no.14) The asymmetric unit contains one doubly protonated melaminium cation and two nitrate anions (Fig. 2.30).

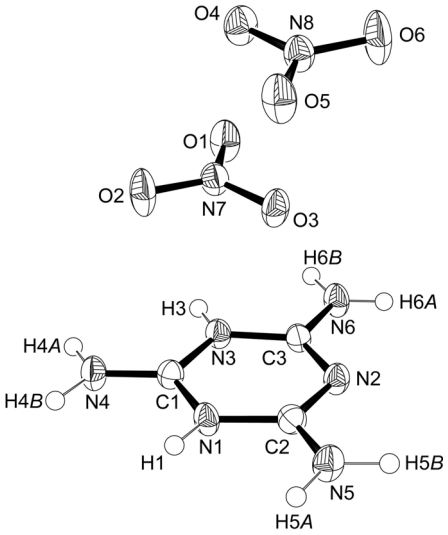

Figure 2.30. ORTEP representation of the molecular structure of melaminium dinitrate in the crystalline state. Displacement ellipsoids are shown at the 50 % probability level. Selected bond lengths [Å] and angles [°]: C_1-N_1 1.337(3), N_1-C_2 1.369(3), C_2-N_2 1.307(3), N_2-C_3 1.309(3), C_3-N_3 1.361(3), N_3-C_1 1.335(3), C_1-N_4 1.278(3), C_2-N_5 1.311(3), C_3-N_6 1.300(3), N_7-O_1 1.240(3), N_7-O_2 1.236(3), N_7-O_3 1.249(3), N_8-O_4 1.232(3), N_8-O_5 1.243(3), N_8-O_6 1.230(3), C_1-N_1-C_2 120.5(2), N_1-C_2-N_2 122.2(2), C_2-N_2-C_3 117.4(2), N_2-C_3-N_3 122.1(2), C_3-N_3-C_1 121.0(2), N_3-C_1-N_1 116.7(2), O_1-N_7-O_2 120.3(2), O_1-N_7-O_3 121.1(2), O_2-N_7-O_3 118.6(2), O_4-N_8-O_5 120.4(2), O_4-N_8-O_6 119.3(2), O_5-N_8-O_6 120.3(2).

The melaminium cation is essentially planar. Considering the plane defined by the three ring carbon atoms, the deviations from planarity of the ring nitrogen atoms are 0.025Å (N_1), 0.009Å (N_2) and -0.038Å (N_3) and the deviation of the exocyclic nitrogen atoms are 0.014Å (N_4), -0.053 Å (N_5) and 0.003Å (N_6). Compared to the corresponding deviations observed in melamine itself [161] where a slight boat configuration has been observed, the deviations from planarity in the case of the doubly protonated melaminium cation are likely to be due to packing effects in the solid state including hydrogen bonding. Protonation of the aromatic ring in melamine results in a redistribution of the π-electrons. The exocyclic C-NH_2 bonds (1.278(3)–1.311(3) Å) are considerably shorter compared to the parent neutral base (1.337(1)–1.362(4) Å) [161] and even shorter when compared to the monoprotonated melaminium cation (1.311(3)–

1.319(3) Å) [162] indicating an increase in bond order of these bonds on protonation. This is particularly the case for the imino-type exocyclic C-N bond arranged between the two protonated ring nitrogen atoms (d(C_1-N_4) = 1.278(3)Å). The deviation from D_{3h} symmetry is not only reflected in bond lengths. The angles within the six-membered ring become highly asymmetric on protonation. The endocyclic angles at the nitrogen atoms range from 117.4(2) to 121.0(2)° with the largest angle being associated opposite the imino-type exocyclic C-N bond. In contrast, the corresponding angles in melamine are essentially equal (114.3(2) – 114.7(1)°). Angle opening at the protonated sites has also been observed in other diprotonated melaminium cations like melaminium diperchlorate hydrate [163] and melamine-cyanuric acid hydrochloride. [164]

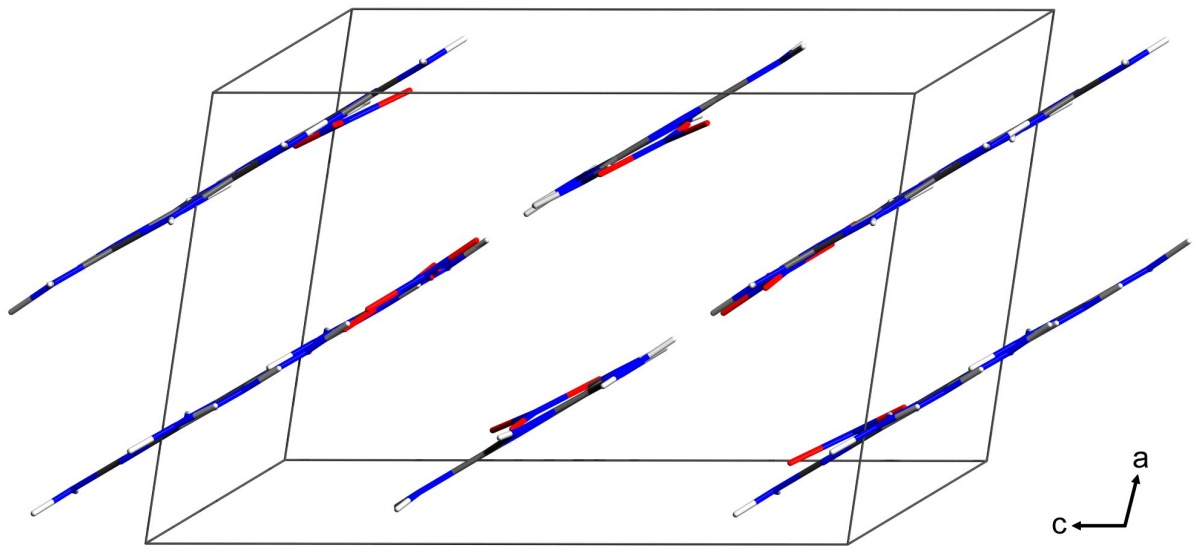

Figure 2.31. Unit cell of melaminium dinitrate, viewed along the *b* axis.

The doubly protonated melaminium cation and nitrate anions exhibit a layered structure (Figs. 2.31 and 2.32). The cations and anions in adjacent layers are stacked such that the cations are followed by anions and *vice versa*, rendering π-stacking interactions difficult. Nevertheless, the spacing between adjacent layers is as small as 334 pm. Within the planar two dimensional layers a tight hydrogen-bonding network is formed, with donor-acceptor distances ranging from 269 to 305 pm. The corresponding H···A contacts cover the range from

180 to 222 pm, thus demonstrating the remarkably efficient packing of the ions wihtin the planar sheets.

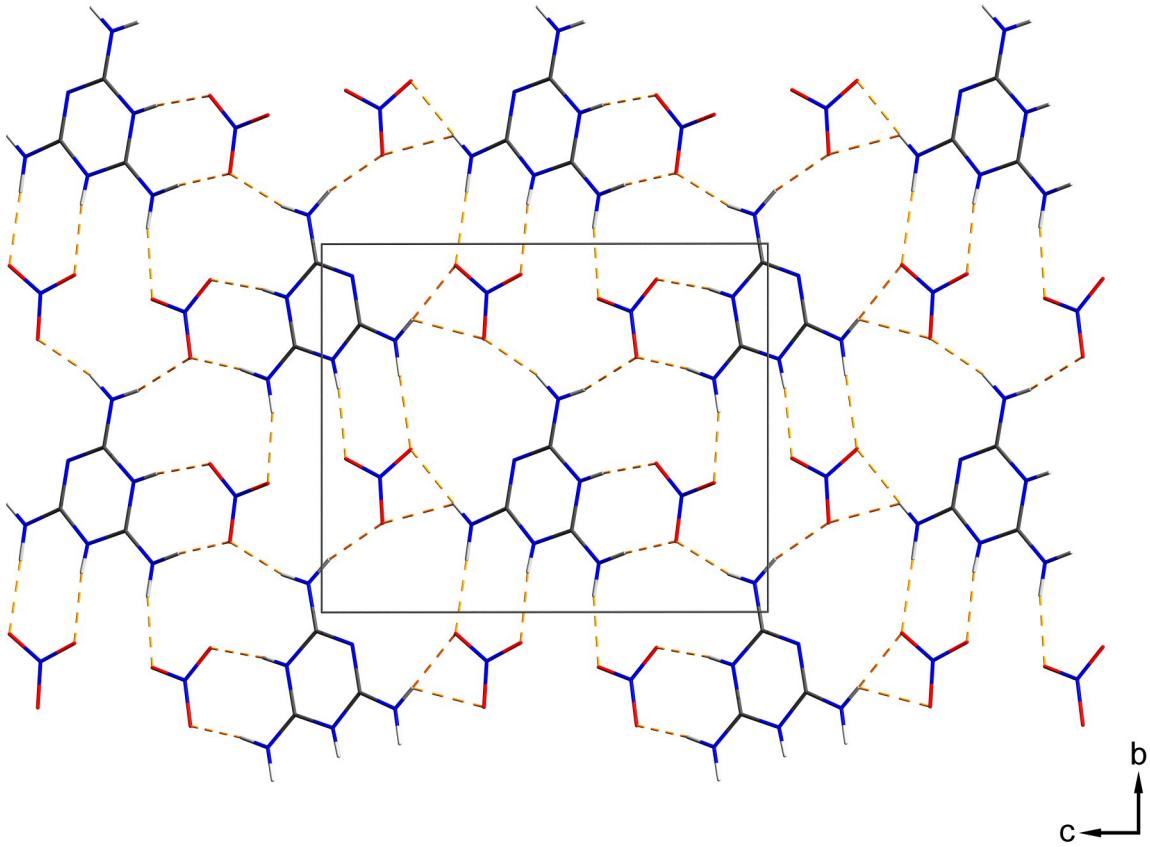

Figure 2.32. Representation of one layer of melaminium dinitrate. Yellow dashed lines indicate hyrogen bonding (N_1-H_1···O_1, N_3-H_3···O_6^{i}, N_4-H_{4A}···O_2^{ii}, N_4-H_{4B}···O_3, N_5-H_{5A}···O_2^{iii}, N_5-H_{5A}···O_3^{iii}, N_5-H_{5B}···O_4^{iv}, N_6-H_{6A}···O_4^{v}, N_6-H_{6A}···O_5^{v}, N_6-H_{6B}···O_5^{i}). (i) x, 1/2-y, 1/2+z, (ii) 1-x, -1/2+y, 1/2-z, (iii) 1-x, 1/2+y, 1/2-z, (iv) x, 3/2-y, 1/2+z, (v) -x, 1-y, 1-z.

Extensive two dimensional hydrogen bonding can be observed within a layer resulting in a significantly higher density compared to the monoprotonated melaminium nitrate species (1.85 g cm^{-3} compared to 1.70 g cm^{-3}).
Every hydrogen atom of the melaminium cation and every oxygen atom of the two nitrate anions is involved. Note that hydrogen bonding involving a non-protonated ring nitrogen atom does not occur.

Experimental

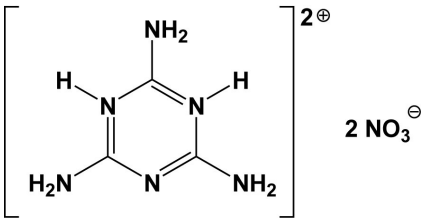

Nitric acid (7 mL, 0.1 mol, 65 %) was added drop wise to a hot aqueous solution (95 °C) of melamine (0.226 mg, 1 mmol in 5 mL H_2O). Subsequent cooling of the reaction mixture to room temperature afforded precipitation of colorless crystalline product in pure form containing single crystals suitable for X-ray diffraction analysis.

DSC (Linseis, 2 K min^{-1}): 330°C (decomp.); Radex (isothermal long term stability, 48h, 140°C): unchanged; ^{1}H NMR ([D_4]methanol) δ: 9.8 (s, 2H), 7.7 (s, 6H); ^{13}C NMR ([D_4]methanol) δ: 159.7; ^{14}N NMR ([D_4]methanol) δ: -11.6; IR (KBr) $\tilde{\nu}$ /cm^{-1}: 3425(s), 3294(m), 3130(s), 1683(s), 1644(m), 1618(m), 1574(w),1520(m), 1384(s), 1190(m), 1149(w), 1116(w), 1007(w), 981(w), 816(w), 769(w), 724(w), 696(w), 660(w), 584(w), 575(w); Raman (4 cm^{-1}) $\tilde{\nu}$ /cm^{-1}: 1052(100), 690(69), 556(21), 391(9), 372(9), 141(20); Calc. for $C_3H_8N_8O_6$: N (44.14%), C (14.29%), H (3.20%), found: N (44.16%), C (14.64%), H (3.24%); impact sensitivity: > 30 J, friction sensitivity: > 160 N; Details of the single crystal X-ray diffraction experiment are listed in the appendix (Chapter 4).

Guanidinium Nitrate : Azidoformamidinium Nitrate (1:1)

Single Crystals consisting of guanidinium nitrate and azidoformamidinium nitrate could be obtained as decomposition products from the reaction between silver trinitromethanide and azidoformamidinium chloride. Silver trinitromethanide was allowed to react with azidoformamidinium chloride in acetonitrile solution at room temperature. The isolation of the product of the reaction resulted in an exothermic decomposition reaction when the solvent was removed using the rotary evaporator. The decomposition was accompanied by gas release and a flash of light. The isolation was immediately stopped and the remaining liquid was put in the freezer affording single crystals suitable for X-ray diffraction.

Crystal Structure Analysis

The double salt guanidinium nitrate and azidoformamidinium nitrate at 100K has monoclinic symmetry, space group $P2_1/c$ (no. 14). The asymmetric is shown in Figure 2.33.

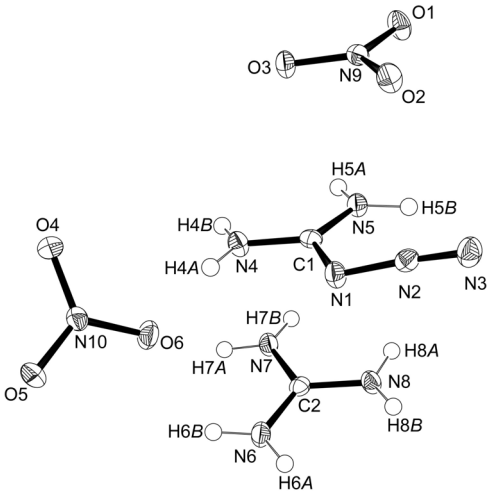

Figure 2.33. ORTEP representation of the molecular structure of guanidinium nitrate, azidoformamidinium nitrate (1:1) in the crystalline state. Displacement ellipsoids are shown at the 50 % probability level. Selected bond lengths [Å] and angles [°]: C_1-N_1 1.3937(15), N_1-N_2 1.2611(14), N_2-N_3 1.1158(14), C_1-N_4 1.3021(15), C_1-N_5 1.3171(15), C_2-N_6 1.3219(16), C_2-N_7 1.3247(15), C_2-N_8 1.3295(16), N_9-O_1 1.2436(12), N_9-O_2 1.2636(12), N_9-O_3 1.2520(12), N_{10}-O_4 1.2494(12), N_{10}-O_5 1.2504(12), N_{10}-O_6 1.2593(13), C_1-N_1-N_2 116.00(10), N_1-N_2-N_3 170.84(12), N_4-C_1-N_1 113.64(11), N_4-C_1-N_5 123.28(11), N_5-C_1-N_1 123.07(11), N_6-C_2-N_7 120.29(12), N_7-C_2-N_8 120.07(12), N_8-C_2-N_6 119.65(11), O_1-N_9-O_2 119.36(9), O_1-N_9-O_3 121.44(9), O_3-N_9-O_2 119.20(9), O_4-N_{10}-O_5 120.93(10), O_4-N_{10}-O_6 119.60(9), O_5-N_{10}-O_6 119.47(9).

Each of the guanidinium-type cations of the double salt guanidinium nitrate - azidoformamidinium nitrate (1:1) contains one carbon atom carrying three nitrogen containing substituents (guanidinium cation (II) / azidoformamidinium cation (III), Fig. 2.34). Further single crystal X-ray structural data within this are only available for the triazidocarbonium cation (IV, 2.34) [165] and the free base guanidin (I, 2.34) whose structure could be determined for the first time within the scope of this thesis (see page 213). A summary of bond lengths of each of the four types of is provided in Table 2.5.

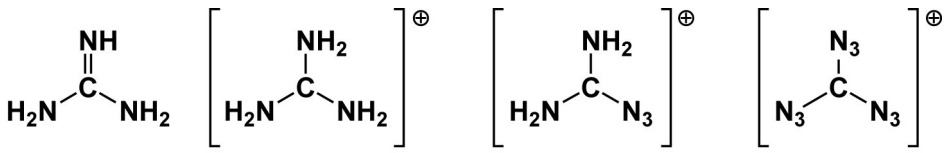

(I) (II) (III) (IV)

Figure 2.34. Types of guanidine-based motivs where single crystal structural data are available.

Table 2.5. Comparison of selected bond lengths of guanidine (I), guanidinium (II), azidoformamidinium (III) and triazidocarbenium (IV).

	d(C-NH) /Å	d(C-NH_2) /Å	d(C-N_3) /Å	d(N_α-N_β) /Å	d(N_β-N_α) /Å
(I) [a]	1.295(2) (C1-N1)	1.366(2) (C1-N2)	-	-	-
	-	1.355(2) (C1-N3)	-	-	-
(I) [b]	1.304(2) (C1-N1)	1.350(3) (C1-N2)	-	-	-
	-	1.359(3) (C1-N3)	-	-	-
	1.300(3) (C7-N8)	1.361(3) (C7-N9)	-	-	-
		1.361(3) (C7-N10)	-	-	-
(II) [c]	-	1.3219(16) (C2-N6)	-	-	-
	-	1.3247(15) (C2-N7)	-	-	-
	-	1.3295(16) (C2-N8)	-	-	-
(III) [d]	-	1.3021(15) (C1-N4)	1.3937(15) (C1-N1)	1.2611(14) (N1-N2)	1.1158(14) (N2-N3)
	-	1.3171(15) (C1-N5)	-	-	-
(III) [e]	-	1.302(4) (C1-N1)	1.393(4) (C1-N3)	1.265(4) (N3-N4)	1.110(4) (N4-N5)
	-	1.314(4) (C1-N2)	-	-	-
(IV) [f]	-	-	1.312(18) (C1-N1)	1.411(19) (N1-N2)	1.022(17) (N2-N3)
	-	-	1.358(18) (C1-N4)	1.361(19) (N4-N5)	1.069(16) (N5-N6)
	-	-	1.348(18) (C1-N7)	1.398(18) (N7-N8)	1.062(17) (N8-N9)

Notes. a) co-crystal of guanidine and 2-amino-4,6-dimethyl-1,3,5-triazine (1:1), b) co-crystal of guanidine and 2-amino-4,6-dimethyl-1,3,5-triazine (2:1), reference (166); c) guanidinium nitrate, this work, double salt; d) azidoformamidinium nitrate, this work, double salt; e) azidoformamidinium chloride, reference (167) f) triazidocarbonium hexachloroantimonate, reference (165).

The C-N bond lengths of the free base guanidine (I) are different and indicate substantial double bond character of the imino-type C-N bond (range: 1.295(2)Å – 1.304(2)Å) and single bond character of the two remaining amino-type C-N bonds (range: 1.350(3)Å – 1.366(2)Å). In contrast, the C-N bond length of the guanidinium cation (II) in the double salt are all of comparable size (range: 1.3219(16)Å – 1.3295(16)Å) indicating Y-aromaticity [168] with delocalisation of π electron density affording a formal bond order of 1.33 of each C-N bond and agree well to typical bond lengths of guanidinium cations. It has been mentioned that the azide groups of triazidocarbonium (IV) display unusual bond lengths compared to other covalently bonded azides. Müller and Bärnighausen [165] have reported the structure of triazidocarbonium-hexachloroantimonate and assigned single bond character to the N_α-N_β nitrogen bonds (range: 1.361(19)Å – 1.411(19)Å) and triple bond character to the N_β-N_γ bonds (range: 1.022(17)Å – 1.069(16)Å), in marked contrast to the values observed in other covalently bonded azides like methyl azide (d(N_α-N_β) = 1.24Å corresponding to double bond character) [169]. They also concluded that delocalisation of π electron density towards the electrophilic carbon atom was evenly distributed across the three C-N bonds in the guanidinium cation and the triazidocarbonium cation due to the fact that the corresponding bonds in each molecule were of comparable size and significantly shorter compared to a formal C-N single bond (1.47Å). Though the CN_3 moiety of the azidoformamidinium cation has the same planar geometry as the CN_3 moieties of the guanidinium and the triazidocarbonium cations, the C-N bond lenghts differ. The bond between the carbon atom and the N_α atom of the azide group (1.3937(15)Å) is significantly longer compared to the bond lengths of the carbon atom to the nitrogen atoms of the NH_2 groups (1.3021(15) Å, 1.3171(15)Å) indicating only weak interaction between the π systems of the guanyl-moiety, $(H_2N)_2$-C, and the π systems of the azide group. Compared to the unusual bond length of the azide group observed in the triazidocarbonium cation, the bond lengths of the azide group of the azidoformamidinium cation have typical values compared to other covalent azides like methyl azide. These geometrical data of the azidoformamidinium cation present in the double salt agree well to those reported for azidoformamidinium chloride. [170] The

extended structure of the double salt of guanidinium nitrate and azidoformamidinium nitrate is shown in Figure 2.35.

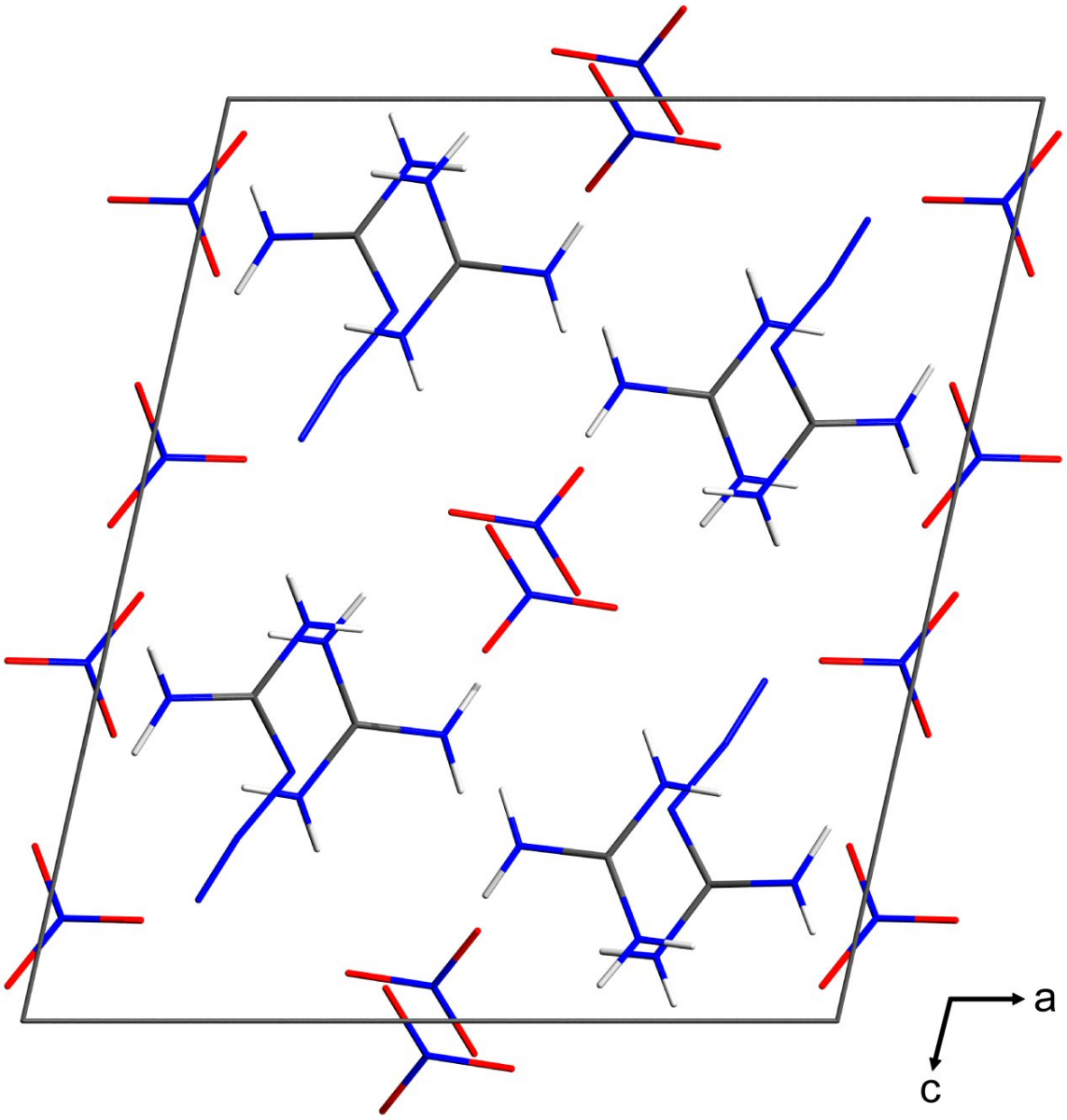

Figure 2.35. Unit cell of guanidinium nitrate, azidoformamidinium nitrate (1:1), viewed along the *b* axis.

The structure is mainly governed by a complex hydrogen bond network. Every hydrogen atom of both the guanidinium and the azidoformamidinium cations is involved in intermolecular N–H···O hydrogen bonding between those cations and the nitrate anions (Table 2.6). Of interest, the azide group is not involved in N–H···N hydrogen bonding.

Table 2.6. Intermolecular hydrogen bonding of the double salt guanidinium nitrate and azidoformamidinium nitrate.

D–H···A	D–H / Å	H··· A / Å	D···A / Å	D–H···A / °
N_4–H_{4A}···O_6	0.852(15)	1.960(15)	2.8081(15)	173.8(13)
N_4–H_{4B}···$O_1^{(i)}$	0.834(14)	2.072(14)	2.9057(14)	179.8(19)
N_5–H_{5A}···$O_3^{(i)}$	0.854(13)	2.097(13)	2.9504(14)	176.8(11)
N_5–H_{5B}···O_2	0.927(15)	1.976(15)	2.8822(14)	165.4(13)
N_6–H_{6A}···$O_6^{(ii)}$	0.869(15)	2.039(15)	2.8728(14)	160.3(13)
N_6–H_{6B}···$O_4^{(iii)}$	0.868(16)	2.055(15)	2.8995(14)	164.2(13)
N_7–H_{7A}···$O_4^{(iv)}$	0.862(16)	2.412(15)	3.1614(14)	145.7(13)
N_7–H_{7A}···$O_5^{(iii)}$	0.862(16)	2.505(15)	3.1378(14)	131.0(12)
N_7–H_{7B}···$O_3^{(v)}$	0.824(14)	2.242(14)	3.0518(15)	167.6(13)
N_8–H_{8A}···$O_2^{(v)}$	0.808(14)	2.220(14)	3.0033(15)	163.3(13)
N_8–H_{8B}···$O_5^{(ii)}$	0.865(16)	2.154(15)	3.0113(14)	171.3(13)

Notes. Symmetry code: (i) x,1/2-y,-1/2+z, (ii) 1-x,-1/2+y,1/2-z, (iii) 1-x,1-y,-z, (iv) x,-1+y,z, (v) -x,-1/2+y,1/2-z.

Experimental

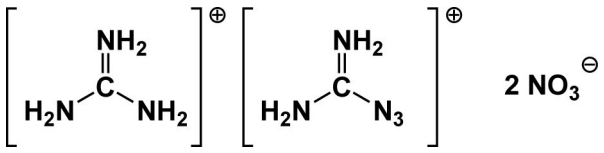

Single Crystals consisting of guanidinium nitrate and azidoformamidinium nitrate could be obtained as decomposition products from the reaction between silver trinitromethanide and azidoformamidinium chloride. Silver trinitromethanide was allowed to react with azidoformamidinium chloride in acetonitrile solution at room temperature. The isolation of the product of the reaction resulted in an exothermic decomposition reaction when the solvent was removed using the rotary evaporator. The decomposition was accompanied by gas release and a flash of light. The isolation was immediately stopped and the remaining liquid was put in the freezer affording single crystals suitable for X-ray diffraction.

Details of the single crystal X-ray diffraction experiment are listed in the appendix (Chapter 4).

2.1.3 Salts of Diaminopicric Acid

Introduction

Bellamy *et al.* have recently investigated a variety of salts of 3,5-diaminopicric acid. [171] Amongst the compounds the series of guanidinium salts showed particularly promising thermal stability and sensitivity data. The compounds were characterized using multinuclear NMR spectroscopy, IR spectroscopy, differential scanning calorimetry, thermogravimetry, scanning electron microscopy and CHN elemental analysis. Their heats of combustion were measured using bomb calorimetry in order to calculate their heats of formation. We have now determined the structures of guanidinium 3,5-diaminopicrate (GDAP), aminoguanidinium 3,5-diaminopicrate (AGDAP), diaminoguanidinium 3,5-diaminopicrate (DAGDAP) and triaminoguanidinium 3,5-diaminopicrate (TAGDAP) in the solid state using single crystal X-ray diffraction as a preliminary step in an investigation of the relationships between crystal density and explosive performance parameters.

Sensitivity and Performance

The detonation rate and detonation pressure values of GDAP, AGDAP, DAGDAP and TAGDAP have been reported according to the Rothstein and Petersen method. Based on the calculated densities from our crystal structure analysis and using the programme EXPLO5 (v. 5.02), we carried out performance calculations in order to predict the performance properties of of GDAP, AGDAP, DAGDAP and TAGDAP. A comparison of the results obtained using the two different methods is summarized in Table 2.7. A comparison of the calculated values of TNT with the corresponding experimental values shows that the calculated values obtained using this method are in good agreement with the experimental analogues.

Table 2.7. Sensitivity and Performance Data of GDAP, AGDAP, DAGDAP, TAGDAP and comparison to TNT.

parameter	GDAP	AGDAP	DAGDAP	TAGDAP	TNT
$T_{dec.}$, DSC / °C [a]	331	231	202	197	-
F of I [b]	> 130	> 130	100	30	-
ρ / g cm^{-3}	1.84	1.76	1.79	1.77	1.64 [151]
D / m s^{-1} [c]	7737	7874	7998	8113	6900 [151]
P / kbar [c]	266	279	290	301	210 [172]
D / m s^{-1} [d]	7852	7614	7859	8140	7150
P / kbar [d]	255	231	252	274	202
Q / kJ kg^{-1} [d]	3983	3922	4294	4899	5089
V_0 / L kg^{-1} [d]	716	735	750	764	622
T_{ex} / °C [d]	3010	2983	3132	3443	3741

Notes. [a] 10°C min^{-1} [b] Figure of Insensitiveness (Rotter Impact Test, RDX = 80) [c] exp. value, according to Rothstein and Petersen (ref. 149) [d] according to EXPLO5, D = velocity of detonation, P = detonation pressure, Q = heat of explosion, V_0 = volume of gaseous detonation products, T_{ex} = explosion temperature.

The theoretically predicted values for the velocity of detonation and the detonation pressure of the four 3,5-diaminopicrate salts all lie within the range expected for high explosives and are superior compared to TNT. TAGDAP has the highest predicted values for the detonation pressure (274 kbar) and the velocity of detonation (8140 m s^{-1}) while at the same time showing the highest sensitivity towards impact (F of I = 30) indicating a potential use as initiator. In contrast, GDAP and AGDAP display a remarkable insensitivity towards impact (F of I > 130) and possess high decomposition temperatures.

Crystal Structure Analysis

Though the structure of picric acid and many structural reports containing salts thereof have been well documented, there are no structural reports containing the 3,5-diaminopicrate anion. In fact, only the structure of the parent compound, 3,5-diamino-2,4,6-trinitrophenol has been reported [173] rendering the four structures of guanidinium 3,5-diaminopicrate (GDAP), aminoguanidinium 3,5-diaminopicrate (AGDAP), diaminoguanidinium 3,5-diaminopicrate (DAGDAP) as well as triaminoguanidinium 3,5-diaminopicrate (TAGDAP) to be first examples of a crystallographic characterization of the 3,5-diaminopicrate anion.

Before the structural features of the 3,5-diaminopicrate anion will be discussed, a brief summary of general features that have been observed and explored by various authors is given. [174] Compared to benzene, the benzene ring of various nitroanilines exhibits characteristic distortions due to substitution of a hydrogen atom by both nitro- and amino-groups. The angle having C-NH_2 as vertex is smaller than 120°, whereas the corresponding angles with C-NO_2 are greater than 120°. There seems to be a correlation between the C-N bond distances and the values of the adjacent C-C bond lengths of the phenyl ring in aromatic amines and various interpretations of the ring deformation have been made [175-177] based on (1) intramolecular nonbonded interactions; [178-180] (2) coulombic interaction between formally charged atoms; [175] (3) hybridization effects at the carbon atom to which the substituent is bonded; [181-182] and (4) valence-shell electron-pair repulsion. [183-188] Accordingly, the overall deformation of the phenyl ring due to the presence of an electron-attracting (nitro) substitutent consists of a shortening of the adjacent C-C bonds, an increase in the endocyclic bond angle opposite to the functional group and a minor decrease in the two adjacent endocyclic angles. The reverse is true for an electron-donating (amino) substituent. The presence of *ortho* and *meta* derivatives seems not to be rationalizable due to a multiplication of the various effects.

A comparison of selected structural parameters of the 3,5-diaminopicrate anion in the structures of the series of guanidinium 3,5-diaminopicrates can be found

in Table 2.8. A comprehensive summary of the crystallographic details can be found in the appendix (Chapter 4).

Table 2.8. Comparison of selected structural parameters of the 3,5-diaminopicrate anion (DAP), taken from the corresponding crystal structures of GDAP, AGDAP, DAGDAP and TAGDAP.

	GDAP	AGDAP	DAGDAP	TAGDAP
d (C_1-C_2) / Å	1.448(3)	1.455(5)	1.445(5)	1.452(3)
d (C_2-C_3) / Å	1.429(4)	1.443(5)	1.419(5)	1.413(3)
d (C_3-C_4) / Å	1.447(3)	1.451(5)	1.458(5)	1.455(2)
d (C_4-C_5) / Å	1.447(3) [a)]	1.454(5)	1.442(5)	1.450(3)
d (C_5-C_6) / Å	1.429(4) [a)]	1.417(5)	1.422(5)	1.420(2)
d (C_6-C_1) / Å	1.448(3) [a)]	1.435(5)	1.452(5)	1.449(2)
d (C_1-O_1) / Å	1.224(5)	1.249(4)	1.257(4)	1.239(2)
d (C_2-N_1) / Å	1.411(3)	1.405(5)	1.422(5)	1.426(2)
d (C_3-N_2) / Å	1.322(3)	1.313(5)	1.326(5)	1.331(2)
d (C_4-N_3) / Å	1.409(4)	1.414(5)	1.416(5)	1.402(2)
d (C_5-N_4) / Å	1.322(3) [a)]	1.320(5)	1.330(5)	1.320(2)
d (C_6-N_5) / Å	1.411(3) [a)]	1.426(4)	1.416(5)	1.415(2)
d (O_1-ring $_{plane}$) / Å	0.117 [b)]	0.304 [c)]	0.522 [c)]	0.322 [c)]
δ (O_1-C_1-C_2-C_3) / °	177.99(18)	168.0(4)	-160.1(4)	167.53(18)
δ (O_1-C_1-C_6-C_5) / °	177.99(18) [a)]	-166.5(4)	161.4(4)	-166.40(18)
δ (O_1-C_1-C_2-N_1) / °	-2.3(3)	-10.5(6)	16.7(6)	-14.3(3)
δ (O_1-C_1-C_6-N_5) / °	-2.3(3) [a)]	13.4(6)	-16.8(6)	16.5(3)

Notes. a) generated by symmetry. b) mean plane as defined by the atoms C_2, C_3, and C_4. c) mean plane as defined by the atoms C_2, C_4, and C_6.

The comparison of C-C bond lengths shows that they are generally longer (range: 1.413(3) Å - 1.458(5) Å) than the 1.392 Å C-C distance in benzene [189] because of amino group substitutions at C_3 and C_5. The general finding mentioned above, that angles having C-NH_2 as vertex are smaller than 120°, whereas the corresponding angles with C-NO_2 are greater than 120° is true in the case of the 3,5-diaminopicrate anion as it is true in the case of the 3,5-diamino-2,4,6-trinitrophenol or 1,3,5-triamino-2,4,6-trinitrobenzene [190]. It has been reported for 3,5-diamino-2,4,6-trinitrophenol that the most obvious relationship would be the one between the C-N distance and the corresponding C-NO_2 out-of-plane rotation with larger amounts of C=N character yielding smaller torsion angles. [191] By comparison, it is difficult to judge whether the same effect is present in the anionic species as well. Contrary to the case of neutral 3,5-diamino-2,4,6-trinitrophenol where a coplanar orientation of the hydroxyl group and the benzene ring has been reported, the phenolic oxygen

atom of the 3,5-diaminopicrate anion shows a deviation from the benzene ring plane. This deviation is smallest in the case of the guanidinium 3,5-diaminopicrate and increases as do the torsion angles of the nitro groups at the C_2 and C_4 positions. Moreover, strong intermolecular hydrogen bonding is present in all four compounds yielding noticeably higher densities (TAGDAP: 1.770 g cm^{-3}, AGDAP: 1.755 g cm^{-3}, DAGDAP: 1.786 g cm^{-3}, GDAP: 1.842 g cm^{-3}) significantly higher compared to the average value of 1.3 to 1.4 g cm^{-3} usually observed for compounds composed only of the elements carbon, hydrogen, oxygen and nitrogen.

Guanidinium 3,5-Diaminopicrate (GDAP)

Guanidinium 3,5-diaminopicrate at 200K has monoclinic symmetry, space group *C2/c*. The asymmetric unit consists of half of the guanidinium cation and half of the 3,5-diaminopicrate anion (Fig. 2.36).

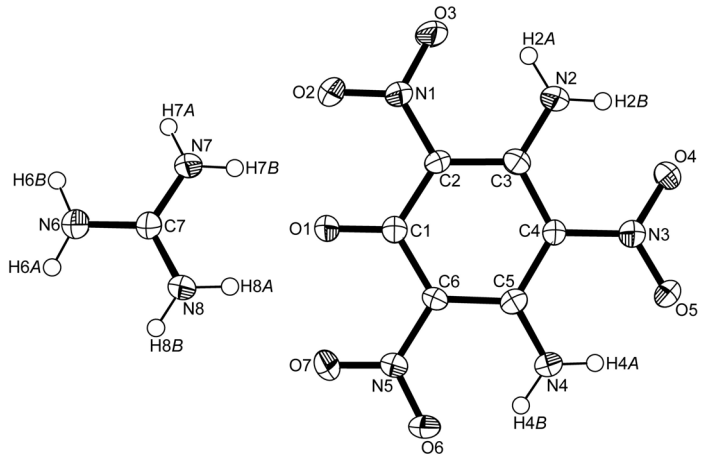

Figure 2.36. ORTEP representation of the molecular structure of guanidinium 3,5-diamino-picrate in the crystalline state. Displacement ellipsoids are shown at the 50 % probability level. Only one half of each the guanidinium cation as well as the 3,5-diamino-picrate anion constitute the asymmetric unit. The N_6, C_7, O_1, C_1, C_4, and N_3 atoms are part of a mirror plane wich is oriented orthoghonal to the plane of the guanidinium cation and the 3,5-diaminopicric anion and the sheet of this paper. Selected bond lengths [Å] and angles [°]: cation: C_7-N_6 1.323(5), C_7-N_7 1.322(3), N_6-C_7-N_7 119.95(17) anion: C_1-C_2 1.448(3), C_2-C_3 1.429(4), C_3-C_4 1.447(3), C_1-O_1 1.224(5), C_2-N_1 1.411(3), N_1-O_2 1.214(3), N_1-O_3 1.239(3), C_3-N_2 1.322(3), C_4-N_3 1.409(4), N_3-O_4 1.251(2), O_1-C_1-C_2 121.53(16), C_1-C_2-C_3 122.6(2), C_2-C_3-C_4 118.1(2), C_3-C_4-N_3 119.25(15), O_1-C_1-C_2-C_3 177.99(18), O_1-C_1-C_2-N_1 -2.3(3).

The extended structure of GDAP displays a complex hydrogen bond network (Table 2.9) yielding a high crystal density of 1.8422(8) g cm^{-3}.

Table 2.9. Hydrogen bonding of guanidinium 3,5-diaminopicrate.

D–H···A	type	D–H / Å	H···A / Å	D···A / Å	D–H···A / °
N_2–H_{2A}···O_3	intra	0.90(4)	1.82(4)	2.524(3)	134(4)
N_2–H_{2B}···O_4	intra	0.86(4)	1.85(4)	2.511(3)	132(3)
N_6–H_{6B}···$O_3^{(i)}$	inter	0.89(4)	2.37(4)	3.189(3)	154(3)
N_6–H_{6B}···$O_4^{(ii)}$	inter	0.89(4)	2.45(4)	3.019(4)	122(3)
N_7–H_{7A}···$O_2^{(i)}$	inter	0.87(4)	2.27(4)	3.113(4)	162(4)
N_7–H_{7A}···$O_3^{(i)}$	inter	0.87(4)	2.52(4)	3.288(4)	147(3)
N_7–H_{7B}···$O_1^{(iii)}$	inter	0.86(4)	2.03(4)	2.811(4)	151(3)
N_7–H_{7B}···$O_2^{(iv)}$	inter	0.86(4)	2.26(4)	2.963(3)	139(3)

Notes. Symmetry code: (i) x,-y,-1/2+z, (ii) 1/2-x,-1/2+y,1/2-z, (iii) 1/2+x,1/2+y,z, (iv) 1/2-x,1/2+y,1/2-z.

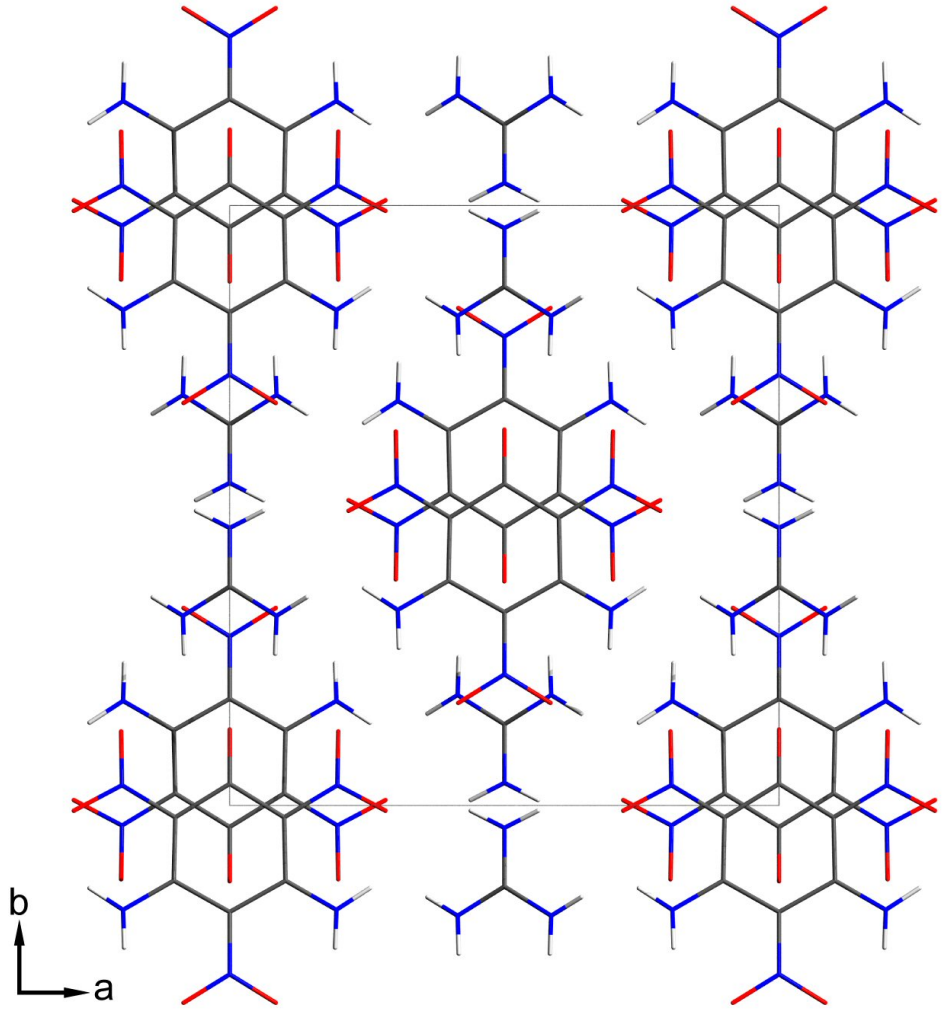

Figure 2.37. Unit cell of guanidinium 3,5-diaminopicrate, viewed along the *c* axis.

Aminoguanidinium 3,5-Diaminopicrate (AGDAP)

Aminoguanidinium 3,5-diaminopicrate at 200K has monoclinic symmetry, space group $P2_1/c$. The asymmetric unit consists of one aminoguanidinium cation and one 3,5-diaminopicrate anion (Fig. 2.38).

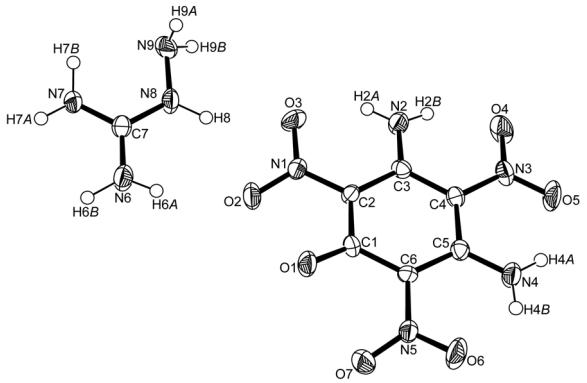

Figure 2.38. ORTEP representation of the molecular structure of aminoguanidinium 3,5-diaminopicrate in the crystalline state. Displacement ellipsoids are shown at the 50 % probability level. Selected bond lengths [Å] and angles [°]: cation: C_7-N_6 1.321(5), C_7-N_7 1.306(5), C_7-N_8 1.343(5), N_8-N_9 1.412(5), N_6-C_7-N_7 120.6(4), N_6-C_7-N_8 119.3(4), N_7-C_7-N_8 120.1(4), C_7-N_8-N_9 117.3(3) anion: C_1-C_2 1.455(5), C_2-C_3 1.443(5), C_3-C_4 1.451(5), C_1-O_1 1.249(4), C_2-N_1 1.405(5), N_1-O_2 1.246(4), N_1-O_3 1.250(4), C_3-N_2 1.313(5), C_4-N_3 1.414(5), N_3-O_4 1.249(4), O_1-C_1-C_2 121.6(3), C_1-C_2-C_3 122.1(3), C_2-C_3-C_4 118.0(3), C_3-C_4-N_3 119.1(3), O_1-C_1-C_2-C_3 168.0(4), O_1-C_1-C_2-N_1 -10.5(6), O_1-C_1-C_6-C_5 -166.5(4), O_1-C_1-C_6-N_5 13.4(6).

Table 2.10. Hydrogen bonding of aminoguanidinium 3,5-diaminopicrate.

D–H···A	type	D–H / Å	H···A / Å	D···A / Å	D–H···A / °
N_2–H_{2A}···O_3	intra	0.83(5)	1.88(5)	2.552(5)	137(3)
N_2–H_{2B}···O_4	intra	0.82(4)	1.84(4)	2.504(5)	137(3)
N_4–H_{4A}···O_5	intra	0.86(5)	1.84(5)	2.517(5)	135(5)
N_4–H_{4B}···O_6	intra	0.88(4)	1.90(4)	2.548(5)	128(3)
N_4–H_{4A}···$O_5^{(i)}$	inter	0.86(5)	2.44(5)	3.096(5)	134(4)
N_6–H_{6A}···$O_2^{(ii)}$	inter	0.84(5)	2.24(5)	3.042(5)	161(4)
N_6–H_{6B}···$O_1^{(iii)}$	inter	0.96(4)	1.97(5)	2.817(5)	146(3)
N_6–H_{6B}···$O_2^{(iii)}$	inter	0.96(4)	2.27(4)	3.039(5)	136(3)
N_7–H_{7A}···$O_1^{(iii)}$	inter	0.90(4)	2.01(4)	2.805(5)	146(4)
N_7–H_{7A}···$O_7^{(iii)}$	inter	0.90(4)	2.16(4)	2.875(4)	136(3)
N_7–H_{7B}···$O_6^{(iv)}$	inter	0.97(6)	2.18(5)	3.133(5)	170(4)
N_8–H_8···$O_2^{(ii)}$	inter	0.97(5)	2.33(5)	3.180(5)	146(4)
N_8–H_8···$O_3^{(ii)}$	inter	0.97(5)	2.09(5)	3.007(5)	157(4)
N_8–H_8···$N_1^{(ii)}$	inter	0.97(5)	2.58(5)	3.546(5)	174(5)
N_9–H_{9A}···$N_8^{(v)}$	inter	0.94(7)	2.45(6)	3.302(6)	152(5)
N_9–H_{9B}···$O_4^{(vi)}$	inter	0.88(4)	2.21(4)	3.047(5)	158(4)

Notes. Symmetry code: (i) 1-x,1-y,-z, (ii) -1+x,y,z, (iii) 2-x,-y,-z, (iv) x,1/2-y,1/2+z, (v) 1-x,1/2+y,1/2-z, (vi)1-x,-1/2+y,1/2-z.

The extended structure of AGDAP displays a complex hydrogen bond network (Table 2.10) yielding a crystal density of 1.7555(4) g cm^{-3}.

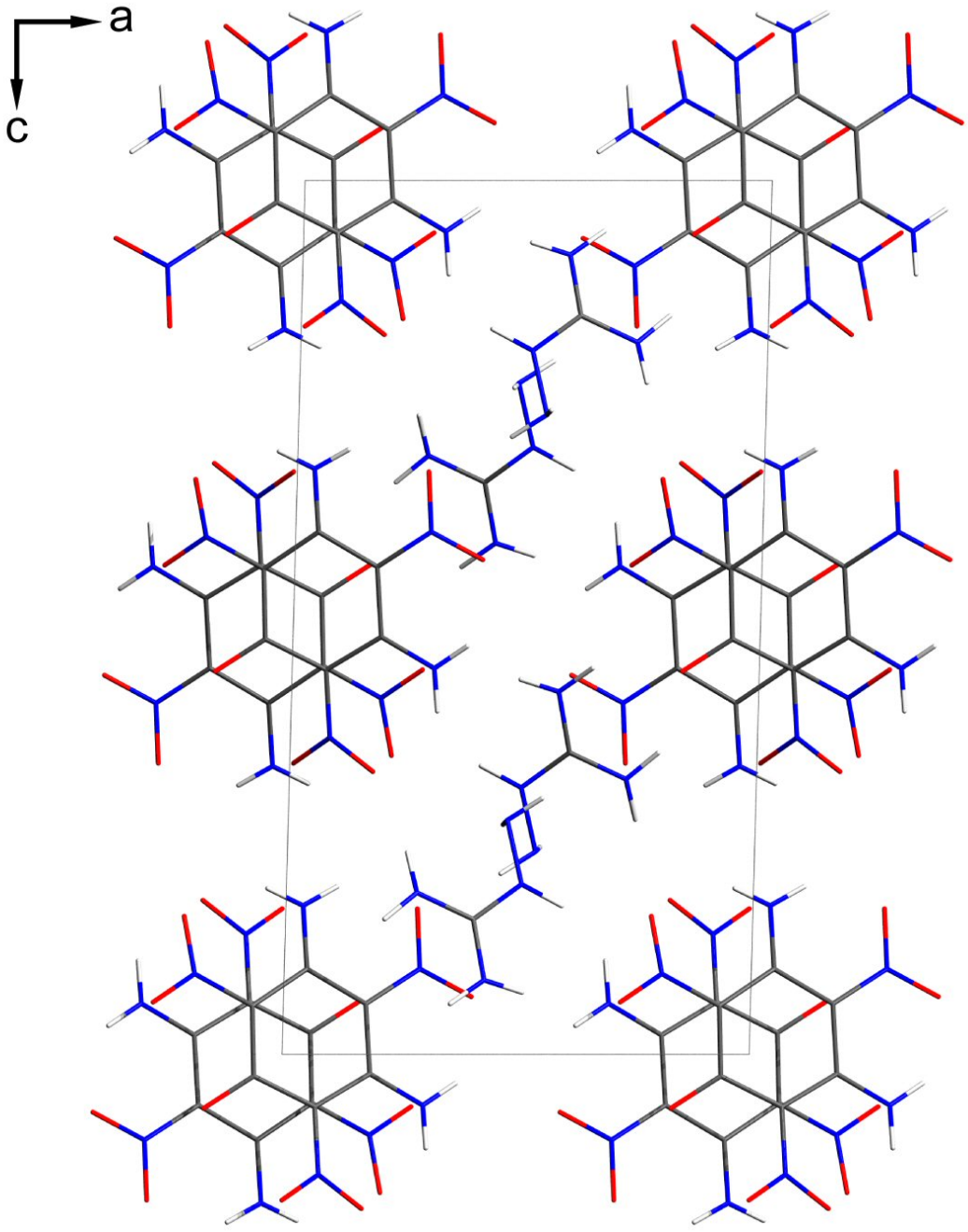

Figure 2.39. Unit cell of aminoguanidinium 3,5-diaminopicrate, viewed along the *b* axis.

Diaminoguanidinium 3,5-Diaminopicrate (DAGDAP)

Diaminoguanidinium 3,5-diaminopicrate at 200K has monoclinic symmetry, space group $P2_1/n$. The asymmetric unit consists of one diaminoguanidinium cation and one 3,5-diaminopicrate anion (Fig. 2.40).

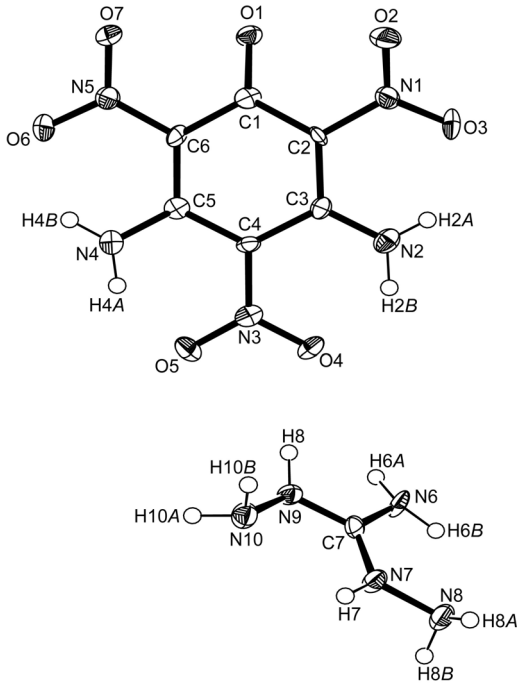

Figure 2.40. ORTEP representation of the molecular structure of diaminoguanidinium 3,5-diaminopicrate in the crystalline state. Displacement ellipsoids are shown at the 50 % probability level. Selected bond lengths [Å] and angles [°]: cation: C_7-N_6 1.331(6), C_7-N_7 1.313(5), C_7-N_9 1.333(5), N_7-N_8 1.418(5), N_9-N_{10} 1.425(5), N_6-C_7-N_7 120.8(4), N_6-C_7-N_9 118.7(4), N_7-C_7-N_9 120.6(4), C_7-N_7-N_8 119.4(4), C_7-N_9-N_{10} 117.7(4) anion: C_1-C_2 1.445(5), C_2-C_3 1.419(5), C_3-C_4 1.458(5), C_1-O_1 1.257(4), C_2-N_1 1.422(5), N_1-O_2 1.245(4), N_1-O_3 1.260(4), C_3-N_2 1.326(5), C_4-N_3 1.416(5), N_3-O_4 1.261(4), O_1-C_1-C_2 120.7(4), C_1-C_2-C_3 122.5(4), C_2-C_3-C_4 117.6(4), C_3-C_4-N_3 119.3(4), O_1-C_1-C_2-C_3 -160.1(4), O_1-C_1-C_2-N_1 16.7(6), O_1-C_1-C_6-C_5 161.4(4), O_1-C_1-C_6-N_5 -16.8(6).

Table 2.11. Hydrogen bonding of diaminoguanidinium 3,5-diaminopicrate.

D–H···A	type	D–H / Å	H···A / Å	D···A / Å	D–H···A / °
N_2–H_{2A}···O_3	intra	0.83(6)	1.93(6)	2.556(5)	131(5)
N_2–H_{2A}···$O_7^{(i)}$	inter	0.83(6)	2.49(6)	3.043(6)	125(5)
N_2–H_{2B}···O_4	intra	0.93(4)	1.82(4)	2.500(5)	128(4)
N_2–H_{2B}···$O_6^{(i)}$	inter	0.93(4)	2.26(4)	2.978(5)	134(4)
N_4–H_{4A}···O_5	intra	0.85(6)	1.78(6)	2.511(5)	143(6)
N_4–H_{4B}···O_6	intra	0.86(4)	1.86(4)	2.540(5)	135(4)
N_6–H_{6A}···O_1	inter	0.88(4)	2.00(4)	2.851(5)	162(4)
N_6–H_{6A}···O_7	inter	0.88(4)	2.53(5)	3.134(6)	126(4)
N_6–H_{6B}···$O_3^{(ii)}$	inter	0.88(4)	2.43(4)	3.170(6)	142(3)
N_7–H_7···$N_{10}^{(iii)}$	inter	0.91(3)	2.22(3)	2.986(6)	142(2)
N_9–H_8···O_1	inter	0.88(6)	2.48(5)	3.077(5)	126(4)
N_9–H_8···$O_4^{(iv)}$	inter	0.88(6)	2.19(6)	2.945(5)	144(5)
N_8–H_{8A}···$O_5^{(v)}$	inter	0.87(5)	2.48(4)	3.101(6)	129(4)
N_8–H_{8A}···$O_3^{(vi)}$	inter	0.87(5)	2.59(5)	3.313(6)	142(4)
N_8–H_{8B}···$O_1^{(vii)}$	inter	0.87(4)	2.36(4)	3.186(6)	160(4)
N_8–H_{8B}···$O_2^{(vii)}$	inter	0.87(4)	2.37(4)	2.932(5)	123(4)
N_{10}–H_{10A}···$O_3^{(viii)}$	inter	0.93(6)	2.41(6)	3.118(6)	133(4)
N_{10}–H_{10B}···$O_1^{(ix)}$	inter	0.88(5)	2.28(5)	3.085(5)	151(5)
N_{10}–H_{10B}···$O_7^{(ix)}$	inter	0.88(5)	2.45(6)	3.116(6)	132(5)

Notes. Symmetry code: (i) -1/2+x,3/2-y,-1/2+z,(ii) 1/2+x,3/2-y,1/2+z, (iii) -x,-y,1-z, (iv) -x,1-y,-z , (v) 1/2-x,-1/2+y,1/2-z, (vi) 1/2+x,1/2-y,1/2+z, (vii) -x,1-y,1-z (viii -1/2-x,-1/2+y,1/2-z , (ix) x,-1+y,z.

The extended structure of DAGDAP displays a complex hydrogen bond network (Table 2.11) yielding a high crystal density of 1.7856(17) g cm^{-3}.

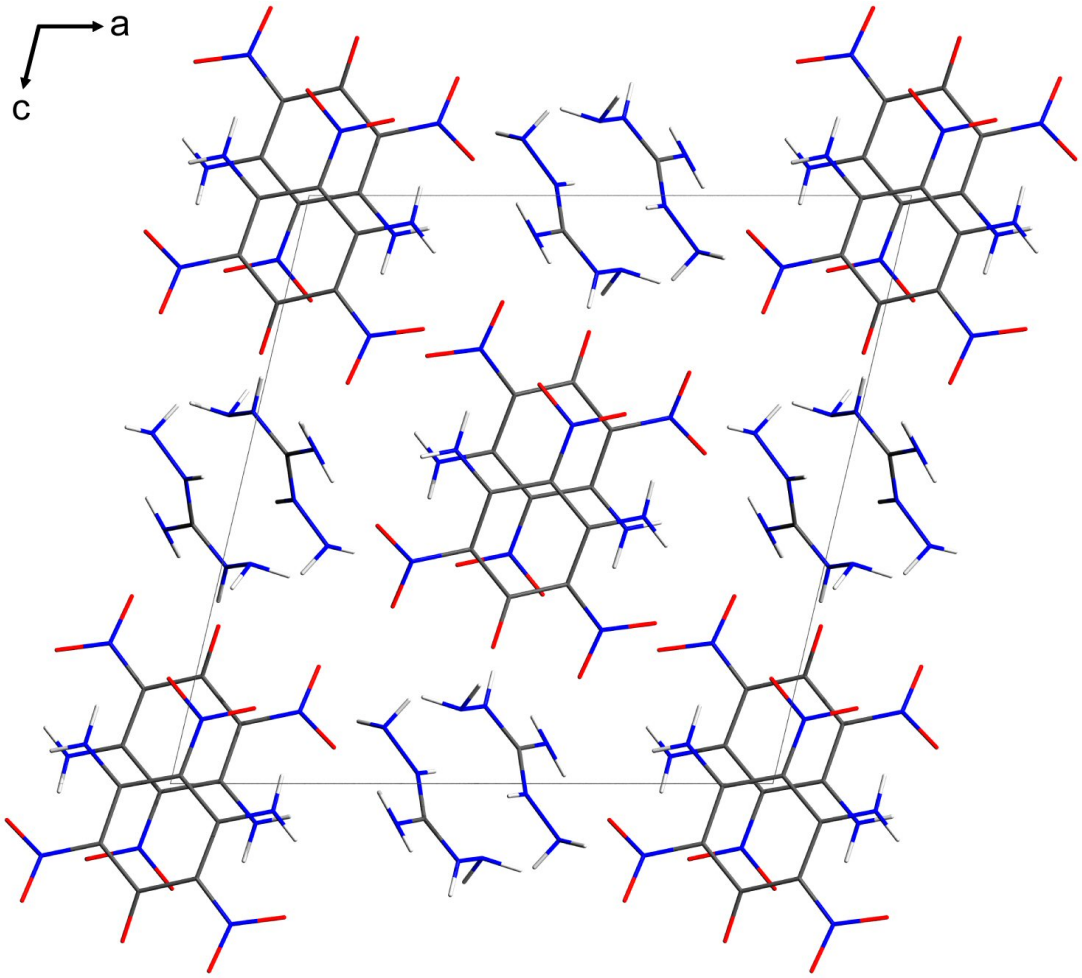

Figure 2.41. Unit cell of diaminoguanidinium 3,5-diaminopicrate, viewed along the *b* axis.

Triaminoguanidinium 3,5-Diaminopicrate hydrate (TAGDAP · H_2O)

Triaminoguanidinium 3,5-diaminopicrate monohydrate at 100K has monoclinic symmetry, space group $P2_1/n$. The asymmetric unit consists of one diaminoguanidinium cation and one 3,5-diaminopicrate anion (Fig. 2.42).

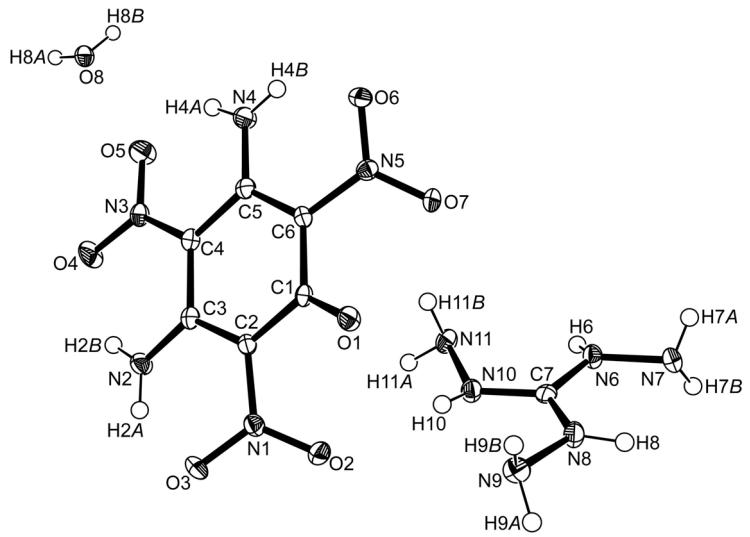

Figure 2.42. ORTEP representation of the molecular structure of triaminoguanidinium 3,5-diaminopicrate hydrate in the crystalline state. Displacement ellipsoids are shown at the 50 % probability level. Selected bond lengths [Å] and angles [°]: cation: C_7-N_6 1.331(6), C_7-N_8 1.313(5), C_7-N_{10} 1.333(5), N_6-N_7 1.418(5), N_8-N_9 1.425(5), N10-N11, N_6-C_7-N_8 120.8(4), N_6-C_7-N_{10} 118.7(4), N_8-C_7-N_{10} 120.6(4), C_7-N_6-N_7 119.4(4), C_7-N_8-N_9 117.7(4), C_7-N_{10}-N_{11} anion: C_1-C_2 1.452(3), C_2-C_3 1.413(3), C_3-C_4 1.455(2), C_1-O_1 1.239(2), C_2-N_1 1.426(2), N_1-O_2 1.2386(19), N_1-O_3 1.248(2), C_3-N_2 1.331(2), C_4-N_3 1.402(2), N_3-O_4 1.252(2), O_1-C_1-C_2 122.55(16), C_1-C_2-C_3 124.24(16), C_2-C_3-C_4 117.68(16), C_3-C_4-N_3 119.50(16), O_1-C_1-C_2-C_3 167.53(18), O_1-C_1-C_2-N_1 -14.3(3), O_1-C_1-C_6-C_5 -166.40(18), O_1-C_1-C_6-N_5 16.5(3).

Table 2.12. Hydrogen bonding of triaminoguanidinium 3,5-diaminopicrate, hydrate.

D–H···A	type	D–H / Å	H···A / Å	D···A / Å	D–H···A / °
N_2–H_{2A}···O_3	intra	0.88(2)	1.92(2)	2.609(2)	133.7(19)
N_2–H_{2A}···$O_7^{(i)}$	inter	0.88(2)	2.40(2)	2.984(2)	124.3(18)
N_2–H_{2B}···O_4	intra	0.84(3)	1.84(3)	2.520(2)	137(2)
N_2–H_{2B}···$O_6^{(i)}$	inter	0.84(3)	2.41(2)	2.958(2)	124(2)
N_4–H_{4A}···O_5	intra	0.86(2)	1.82(2)	2.518(2)	138.0(19)
N_4–H_{4A}···$O_8^{(ii)}$	inter	0.86(2)	2.50(2)	3.040(3)	121.5(16)
N_4–H_{4B}···O_6	Intra	0.86(2)	1.89(3)	2.585(2)	137(2)
N_4–H_{4B}···$N_{11}^{(iii)}$	Inter	0.86(2)	2.53(2)	3.187(3)	134(2)
N_6–H_6···$O_8^{(iv)}$	Inter	0.90(2)	2.04(2)	2.858(2)	151(2)
N_7–H_{7B}···$O_2^{(v)}$	Inter	0.89(2)	2.38(2)	2.943(2)	121.2(16)
N_7–H_{7B}···$O_3^{(v)}$	Inter	0.89(2)	2.52(2)	3.305(2)	147.5(18)
N_8–H_8···$O_5^{(vi)}$	Inter	0.86(3)	2.21(3)	3.031(2)	160(2)
O_8–H_{8A}···O_1	Intra	0.87(3)	1.95(3)	2.795(2)	163(3)
O_8–H_{8A}···O_7	Intra	0.87(3)	2.41(3)	2.974(2)	123(2)
O_8–H_{8B}···$N_7^{(vii)}$	Inter	0.85(3)	2.57(3)	3.078(2)	119(2)
N_9–H_{9A}···$O_1^{(viii)}$	Inter	0.90(2)	2.33(2)	3.072(2)	140.6(18)
N_9–H_{9B}···O_8	Intra	0.91(3)	2.49(2)	3.098(2)	124.2(19)
N_9–H_{9B}···$O_2^{(viii)}$	Inter	0.91(3)	2.36(3)	3.047(2)	132.1(18)
N_{10}–H_{10}···O_1	Intra	0.80(2)	2.50(2)	3.045(2)	127(2)
N_{10}–H_{10}···O_2	Intra	0.80(2)	2.30(2)	2.945(2)	139(2)
N_{11}–H_{11A}···$O_4^{(ix)}$	Inter	0.90(2)	2.18(2)	3.020(2)	155(2)
N_{11}–H_{11A}···O_4	Intra	0.90(2)	2.28(2)	3.122(2)	155(2)

Notes. Symmetry code: (i) -1/2+x,3/2-y,-1/2+z, (ii) 1/2-x,1/2+y,1/2-z, (iii) 1/2-x,-1/2+y,1/2-z, (iv) x,1+y,z, (v) 1-x,2-y,-z, (vi) 1+x,y,z, (vii) 3/2-x,-1/2+y,1/2-z, (viii) 1-x,1-y,-z, (ix) -x,2-y,-z.

The extended structure of TAGDAP displays a complex hydrogen bond network (Table 2.12) yielding a high crystal density of 1.7704(1) g cm^{-3}.

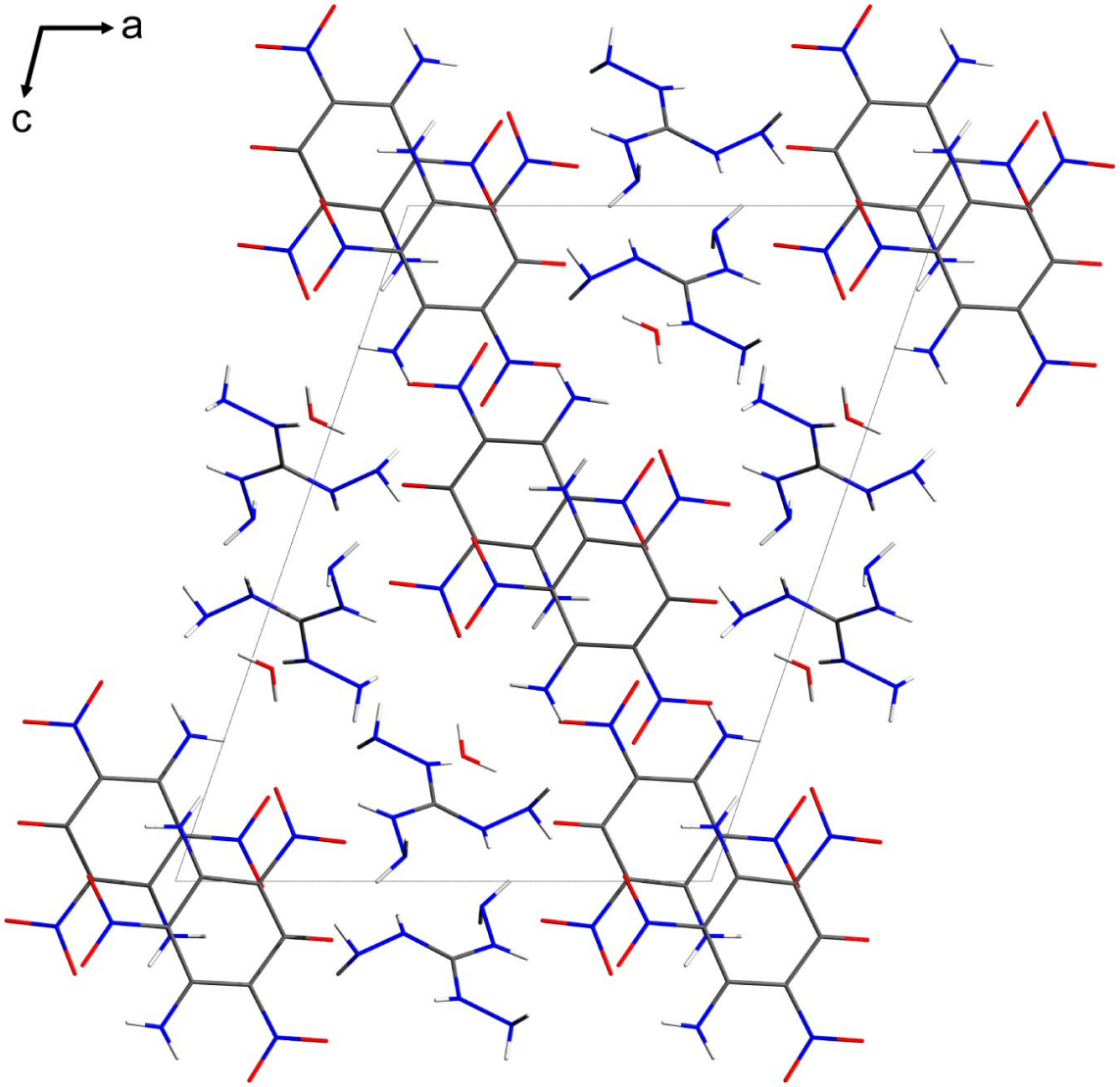

Figure 2.43. Unit cell of triaminoguanidinium 3,5-diaminopicrate hydrate, viewed along the *b* axis.

Experimental

Samples of GDAP, AGDAP, DAGDAP and TAGDAP were provided by Dr. Anthony J. Bellamy from Cranfield University, UK. Single crystals suitable for X-ray diffraction were obtained from dissolving the compounds in hot water and subsequent cooling to room temperature. Details of the single crystal X-ray diffraction experiment are listed in the appendix (Chapter 4).

2.1.4 Salts of Hydrochloric Acid

3,6-Diamino-1,2,4,5-tetrahydro-tetrazinium dichloride

3,6-diamino-1,2,4,5-tetrazine is a starting material for the synthesis of bis-(2,2,2-trinitroethyl)-3,6-diamino-1,2,4,5-tetrazine (BTAT) and was synthesised from the condensation of diaminoguanidinium hydrochloride with 2,4-pentanedione, followed by oxidation of the resulting dihydrotetrazine with sodium perborate (see section 2.2). [192] Two pathways have been found for the preparation and isolation of BTAT. According to the first pathway, BTAT can be obtained on reaction of a solution of 3,6-diaminotetrazine in concentrated hydrochloric acid (37%) at a temperature of 70°C with stoichiometric amounts of trinitroethanol. The product precipitates from the solution and can be obtained in high purity on simple filtration. However, we observed that the yields of this approach are quite low.

The reason for the low yields can now be rationalized in terms of formation of the previously unkown compound 3,6-diamino-1,2,4,5-tetrahydro-1,2,4,5-tetrazinium dichloride (Fig. 2.44).

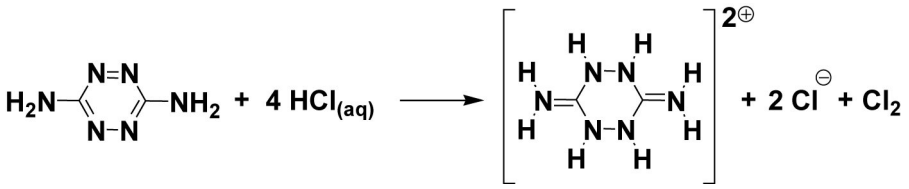

Fig. 2.44. Synthesis of 3,6-diamino-1,2,4,5-tetrahydro-tetrazinium dichloride from the reaction between 3,6-diamino-1,2,4,5-tetrazine and hydrochloric acid.

The compound becomes reoxidized to the corresponding 3,6-diamino-1,2,4,5-tetrazine educt on contact with air already at ambient conditions within a few minutes. However, it was possible to determine the structure of the the tetrahydrotetrazinium dichloride using single crystal X-ray diffraction.

Attempts to facilitate the formation of BTAT taking advantage of the higher reactivity of the amino groups present in this salt compared to the less reactive amino groups present in 3,6-diamino-1,2,4,5-tetrazine were unsuccessful so far due to the fact that oxidation of the tetrahydrotetrazinium salt on contact with trinitroethanol is preferred over the formation of BTAT.

Crystal Structure Analysis

Of the three possible tetrazine isomers (1,2,3,4-tetrazines, 1,2,3,5-tetrazines, 1,2,4,5-tetrazines), the class of 1,2,4,5-tetrazines appears to be the best-known. [193] Two important Lewis type structures of the parent compound (**1**) can be drawn (Fig. 2.45, 1a, 1b).

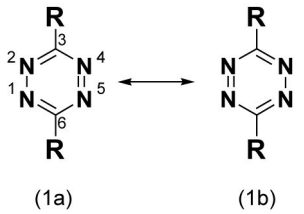

Figure 2.45. Lewis type structures of the 1,2,4,5-tetrazine ring system.

In addition to the aromatic tetrazine system (**1**), dihydro-1,2,4,5-tetrazines, tetrahydro-1,2,4,5-tetrazines, and hexahydro-1,2,4,5-tetrazines have been reported (Fig. 2.46). X-ray diffraction has revealed the dihydro derivatives to be best described as the 1,4-dihydro isomers (**2**). The corresponding 1,2-dihydro- and 1,6-dihydro isomers (***3***) and (**4**) are very rare. [193] Though tetrahydro- and hexahydro-tetrazines (**5**, **7**) have been reported, no X-ray crystallographic analysis of a dicationic tetrahydro-1,2,4,5-tetrazine (**6**) has been published so far to our knowledge. A similar structural motiv displays 1,4-dihydro-1,2,4,5-tetrazine-3,6(2*H*,5*H*)-dione, the tautomer of 3,6-dihydroxy-1,4-dihydro-1,2,4,5-tetrazine (p-urazine) from which tetraalkyl derivatives have been reported. [194]

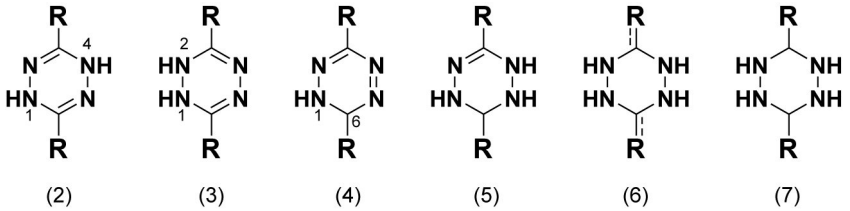

Figure. 2.46. Dihydro-, tetrahydro- and hexahydro derivatives of the 1,2,4,5-tetrazine ring system.

It appears that 3,6-diamino-1,2,4,5-tetrahydro-1,2,4,5-tetrazinium dichloride, which can formally be viewed as a dimer of guanidinium chloride, represents the first example of a dicationic 1,2,4,5-tetrahydro-1,2,4,5-tetrazine ring system. 3,6-diamino-1,2,4,5-tetrahydro-1,2,4,5-tetrazinium dichloride at 100K

has triclinic symmetry, space group *P*-1 (no.2). The asymmetric unit is shown in Figure 2.47.

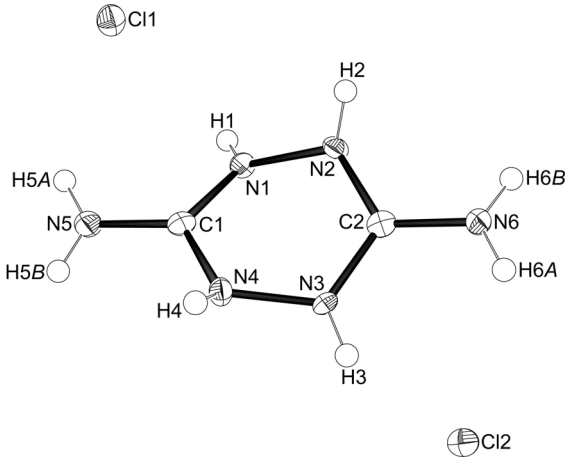

Figure 2.47. ORTEP representation of the molecular structure of 3,6-diamino-1,2,4,5-tetrahydro-1,2,4,5-tetrazinium dichloride in the crystalline state. Displacement ellipsoids are shown at the 50 % probability level. Selected bond lengths [Å] and angles [°]: N_1-N_2 1.402(2), N_2-C_2 1.326(2), C_2-N_3 1.348(2), N_3-N_4 1.405(2), N_4-C_1 1.326(2), C_1-N_1 1.346(2), C_1-N_5 1.311(3), C_2-N_6 1.307(3), N_4-C_1-N_5 123.13(18), N_5-C_1-N_1 119.98(17), N_4-C_1-N_1 116.78(17), C_1-N_1-N_2 115.92(15), N_1-N_2-C_2 119.58(15), N_2-C_2-N_6 122.27(17), N_6-C_2-N_3 121.15(17), N_2-C_2-N_3 116.57(17), C_2-N_3-N_4 116.16(15), N_3-N_4-C_1 119.78(16), N_5-C_1-N_4-N_3 162.05(19), N_5-C_1-N_1-N_2 163.51(18), N_6-C_2-N_3-N_4 168.52(18), N_6-C_2-N_2-N_1 156.85(18), C_1-N_4-C_3-N_2 34.88(24), C_1-N_1-N_2-C_2 37.32(23).

Boeyens mentioned that there was no generally accepted nomenclature or symbolic formalism to distinguish between the many conformations of six-membered rings and introduced a new formalism. [195] The established terminology for the classical forms (chair, boat, half-chair, twist-boat) are retained and rendered more precisely. According to this ring conformational analysis, the tetrazine ring of 3,6-diamino-1,2,4,5-tetrahydro-1,2,4,5-tetrazinium dichloride displays a twist-boat conformation (Fig. 2.48) of $^2T_4$ type (puckering amplitude (Q) = 0.3771(15) Å, θ = 88.5(2)°, φ = 218.6(2)°).

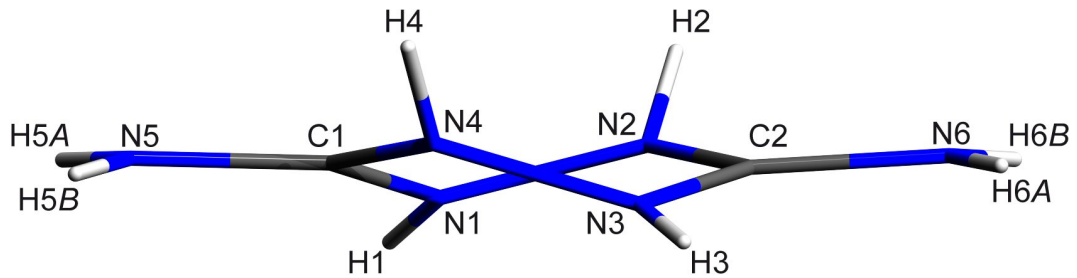

Figure 2.48. Representation of the molecular structure of 3,6-diamino-1,2,4,5-tetrahydro-1,2,4,5-tetrazinium dichloride in the crystalline state. According to the ring conformational analysis formalism suggested by Boeyens, the ring system displays a $^2T_4$ type twist form. [195]

A comparison of bond length and angles of 3,6-diamino-1,2,4,5-tetrahydro-1,2,4,5-tetrazinium dichloride to other di- or tetrahydro-derivatives of 3,6-diamino-1,2,4,5-tetrazine is not possible because of a lack of structural data of the latter compounds. The exocyclic C-N bonds are shorter (1.307(3)Å, 1.311(3) Å) compared to the corresponding C-N bond length of 3,6-diamino-1,2,4,5-tetrazine (1.332(1)Å) indicating substantial double bond character. This notion is supported by the fact that the carbon atoms lie well in the plane spread through the three adjacent nitrogen atoms. The four endocyclic C-N bonds can be grouped pairwise. The C_1-N_4 bond as well as the C_2-N_2 (1.326(2) bond both have a value of 1.326(2)Å and belong to the first set of pairs whereas the C_1-N_1 bond (1.346(2)Å) and the C_2-N_3 bond (1.348(2)Å) form the second set of pairs with significantly longer bonds. The double bond character indicated by the shorter C-N bond length is again supported by the planar geometry of the N_4 and N_2 nitrogen atoms as indicated by the angle sum of 360° around these atoms. Complementary, the longer bond length values of the C_1-N_1 and C_2-N_3 bonds are accompanied by a pyramidal hybridization of the corresponding nitrogen atoms N_1 and N_3 affording a angle sum of 351.2(2)° around each of the two nitrogen atoms. Though the tetrazine ring of 3,6-diamino-1,2,4,5-tetrahydro-1,2,4,5-tetrazinium dichloride is part of a dication, the two N-N bonds are significantly longer (1.402(2)Å, 1.405(2)Å) than the corresponding N-N bonds of the aromatic 3,6-diamino-1,2,4,5-tetrazine (1.314(2)Å, 1.328(2)Å) and of comparable length to the N-N bond length observed in the two similar compounds tetrahydro-1,2,4,5-tetramehtyl-1,2,4,5-tetrazine-3,6-dione (1.411(2)Å, 1.414(2)Å) [194] and tetrahydro-1,2,4,5-tetramehtyl-1,2,4,5-tetrazine-3,6-dithione (1.413(2)Å, 1.418(2)Å) [194]. The comparison with the two aforementioned compounds reveals and is limited to a similar twist-boat conformation of the tetrazine ring. Further comparisons of bond distances, bond angles or the extended structures seem little reasonable because the latter compounds contain 1,2,4,5-tetramethyl-1,2,4,5-tetrazine rings in contrast to the 1,2,4,5-tetrahydro-1,2,4,5-tetrazine ring present in 3,6-diamino-1,2,4,5-tetrahydro-1,2,4,5-tetrazinium dichloride with all the necessary electronic and steric effects on those values.

The extended structure of 3,6-diamino-1,2,4,5-tetrahydro-1,2,4,5-tetrazinium dichloride (Figs. 2.49 and 2.50) displays extensive hydrogen bonding with all the N-H groups participating in N–H···Cl hydrogen bonding (Table 2.13).

.

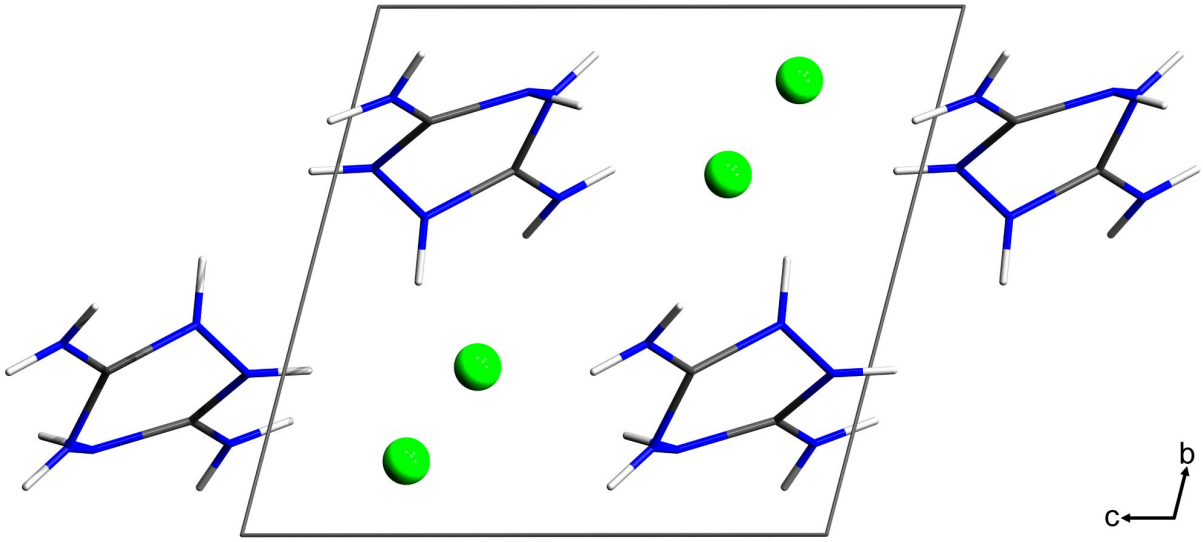

Figure 2.49. Unit cell of 3,6-diamino-1,2,4,5-tetrahydro-1,2,4,5-tetrazinium dichloride, viewed along the *a* axis.

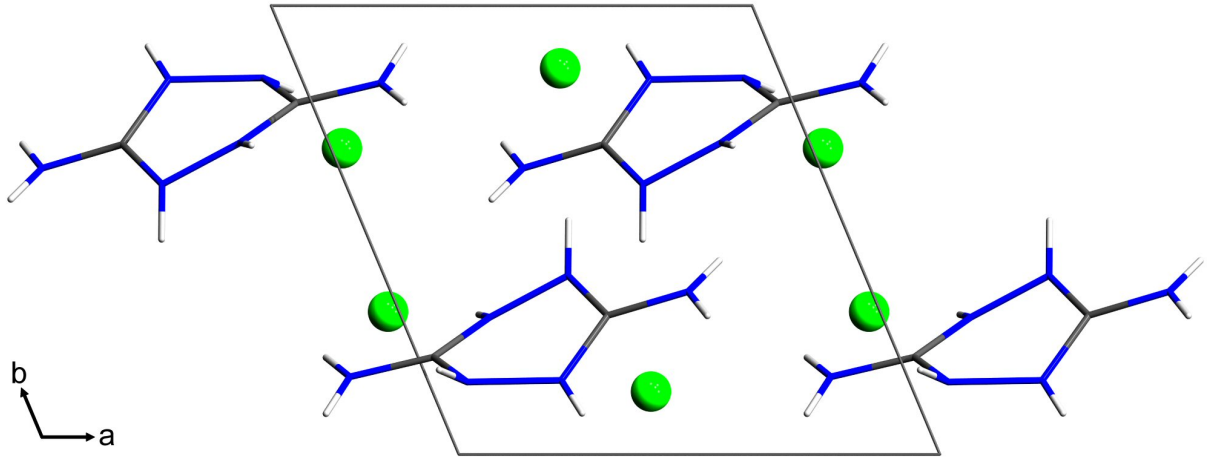

Figure 2.50. Unit cell of 3,6-diamino-1,2,4,5-tetrahydro-1,2,4,5-tetrazinium dichloride, viewed along the *c* axis.

Table 2.13. Intermolecular hydrogen bonding of 3,6-diamino-1,2,4,5-tetrahydro-tetrazinium dichloride.

D–H···A	D–H / Å	H···A / Å	D···A / Å	D–H···A / °
N_1–H_1···Cl_2 (i)	0.83(2)	2.25(2)	3.0838(14)	176(2)
N_2–H_2···Cl_1 (ii)	0.78(2)	2.38(2)	3.1135(14)	157(2)
N_3–H_3···Cl_1 (iii)	0.84(2)	2.31(2)	3.1359(14)	167(2)
N_4–H_4···Cl_2	0.776(18)	2.68(2)	3.2438(14)	131.5(17)
N_5–H_{5A}···Cl_1 (i)	0.80(2)	2.65(2)	3.2331(15)	132(2)
N_5–H_{5B}···Cl_1 (iv)	0.82(2)	2.41(2)	3.2055(15)	164(2)
N_6–H_{6A}···Cl_2 (v)	0.87(2)	2.63(2)	3.2691(15)	131.9(19)
N_6–H_{6A}···Cl_1 (ii)	0.87(2)	2.77(2)	3.4439(15)	135.3(19)
N_6–H_{6B}···Cl_1 (vi)	0.77(2)	2.46(2)	3.2201(15)	170(2)

Notes. Symmetry code: (i) 1-x,1-y,1-z; (ii) -x,1-y,-z; (iii) -x,1-y,1-z; (iv) 1+x,y,z; (v) -1+x,y,-1+z; (vi) -x,-y,1-z.

Experimental

3,6-diamino-1,2,4,5-tetrazine (0.5 g, 4.5 mmol) was dissolved in concentrated hydrochloric acid (500 mL). 2,2,2-Trinitroethanol (2.42 g, 13.4 mmol) was added and the solution heated to 100°C over a period of three hours using reflux conditions. During the reaction the initially red colour of the solution disappeared. Removal of the solvent afforded crystalline 3,6-diamino-1,2,4,5-tetrahydro-tetrazinium dichloride as colourless solid. Details of the single crystal X-ray diffraction experiment are listed in the appendix (Chapter 4).

2.1.5 Salts of Perchloric Acid

1-Methyl-5-(N-methyl)-aminotetrazolium Perchlorate

The formation of 1-methyl-5-(N-methyl)-aminotetrazolium perchlorate has been observed recently on treatment of 1-methyl-5-(1-methyl-2-(2,2,2-trinitroethyl)hydrazinyl)-1*H*-tetrazole with perchloric acid. This product has not been synthesised on purpose and was obtained by coincidence.
As stated earlier (see page 59) the use of the perchlorate anion is an issue of concern predominantly in the United States due to contamination of drinking water supplies owing to its solubility and non-reactivity. The perchlorate anion is problematic because it is known to affect the function of the thyroid gland in mammals and its toxicity primarily results from the fact that it inhibits thyroid hormone output with all the negative consequences on normal physical and mental development or foetal and infant neuropsychological development just to name a few. [196] Today, great efforts are undertaken to replace energetic materials that contain this moiety as an oxidizing component, preferentially in propellants. Perchlorate does not occur naturally in the environment and its presence as an environmental contaminant mainly results from the use of ammonium perchlorate as an energetic booster or oxidant in solid rocket fuels. A prominent example where such a replacement would be highly desirable can be found in the use of ammonium perchlorate as component in solid state boosters of the Ariane 5 rocket, frequently used for space missions.
Though only small quantities of 1-methyl-5-(N-methyl)-aminotetrazolium perchlorate were obtained as a side product of this reaction, it was possible to proof the existence of this previously unknown compound using single crystal X-ray diffraction.

Crystal Structure Analysis

1-Methyl-5-(N-methyl)-aminotetrazolium perchlorate crystallizes in the orthorhombic space group $P2_12_12_1$ (no. 19) with four moieties in the unit cell. The asymmetric unit consist of one moiety (Fig. 2.51).

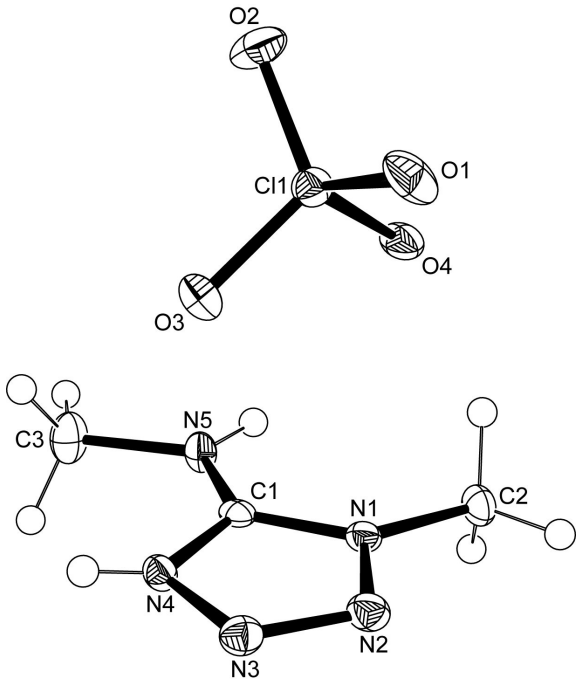

Figure 2.51. ORTEP representation of the molecular structure of 1-Methyl-5-(N-methyl)-aminotetrazolium perchlorate in the crystalline state. The thermal ellipsoids are shown at the 50 % probability level. Selected bond lengths [Å]: C_1-N_1 1.344(4), N_1-N_2 1.359(3), N_2-N_3 1.274(3), N_3-N_4 1.362(3), N_4-C_1 1.333(4), C_1-N_5 1.315(4), N_5-C_3 1.463(4), N_1-C_2 1.452(3), O_1-Cl_1 1.450(2), O_2-Cl_1 1.4478(19), O_3-Cl_1 1.448(2), O_4-Cl_1 1.5563(19).

The bond length and bond angles of the cation as well as the anion show typical values commonly observed for tetrazolate cations and the perchlorate anion in other structures. The extended structure is shown in Figure 2.52. The two N-H functionalities of the 1-methyl-5-(N-methyl)-aminotetrazolium cation are involved in N-H(cation)···O(anion) hydrogen bonding yielding an alternating, wavelike pattern of cations and anions along the crystallographic c axis (Fig. 2.52). The crystal density is only moderate (1.6408(1) g cm-3) rendering a possible use of this potential energetic material not only unlikely due to the general concerns regarding the perchlorate anion mentioned above but also due to the low performance characteristics that have to be expected as a consequence of the rather low value of the crystal density.

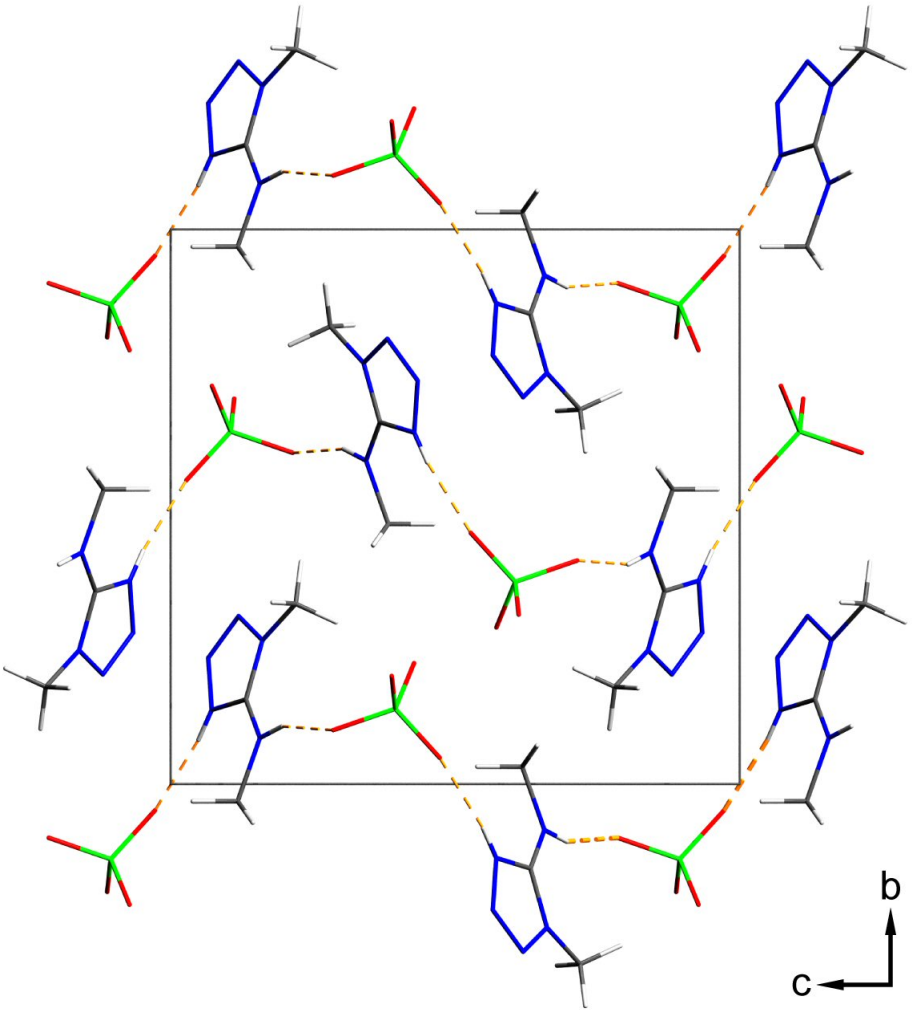

Figure 2.52. Unit cell of 1-Methyl-5-(N-methyl)-aminotetrazolium perchlorate, viewed along the *a* axis (left) and *c* axis (right). Yellow dashed lines indicate hyrogen bonding (N_4-H_4···O_2^{i}, N_5-H_5···O_3^{ii}). (i) 1/2-x,1-y,-1/2+z, (ii) 1+x,y,z.

Experimental

The formation of 1-methyl-5-(N-methyl)-aminotetrazolium perchlorate has been observed as decomposition product from treatment of 1-methyl-5-(1-methyl-2-(2,2,2-trinitroethyl)hydrazinyl)-1H-tetrazole with perchloric acid at ambient conditions and letting stand the reaction mixture for several weeks at ambient conditions. Though only small quantities of 1-methyl-5-(N-methyl)-aminotetrazolium perchlorate were obtained as a side product of this reaction, it was possible to proof the existence of this previously unknown compound using single crystal X-ray diffraction. Details of the single crystal X-ray diffraction experiment are listed in the appendix (Chapter 4).

2.2 Energetic Materials: Molecules

Molecules Containing the Trinitroethyl Functionality

Introduction

The development and testing of energetic materials is an exciting and challenging area of chemistry both as far as applied and fundamental aspects are concerned. Considering the many applications of non nuclear energetic materials as explosives or propellants, it is important to discover new representatives having significant advantages over compounds currently used not only for military but also for civilian purpose because of environmental considerations and safety requirements while at the same time securing high performance. A new generation energetic material has to meet several standards in order to become widely accepted.

Next to performance properties, the desired criteria are insensitivity towards destructive stimuli like electrostatic discharge, heat, friction and impact to ensure safe handling procedures and enhance controllability of kinetic energy release as well as low water solubility and hydrolytic stability to protect the ground, longevity- and compatibility questions and furthermore criteria addressing highest priority ecological toxicity requirements. The *Strategic Environmental Research and Development Program* (SERDP) and the *Environmental Security Technology Certification Program* (ESTCP) are the United States of America *Department of Defence's* (DoD) and *Department of Energy* (DOE) environmental technology programs supporting such progress ever since having been established in the late eighties of the twentieth century.

Traditional representatives of high oxygen explosives (HOX) have been reported in public literature as research reports initiated by the *Office of Naval Research* (ONR) became declassified in the early seventies of the twentieth century; however, relevant data were published mainly in the patent literature, often without giving information about synthetic procedures or specifying the physicochemical characteristics of the compounds obtained. [11] Some of the most promising materials initially considered were polynitroaliphatic

compounds containing the dinitromethyl, fluorodinitromethyl and trinitromethyl groups. [197] Among them, the trinitroethyl compounds were found to have the most favourable heats of detonation and oxygen balance values. However, thermal stability was reported to be generally limited to 150°C when solid and 100°C when molten reversing further investigation into trinitroethyl substituted compounds. [13]

We have now investigated compounds mentioned in the literature and we have developed and tested novel compounds with the trinitroethyl functionality in order to explore its potential for the design of next generation energetic materials trying to enhance the thermal stability of this class of compounds and finding the molecule offering the best trade-off between energy capability and thermal stability. In the course of the global emerging interest in high-energetic, dense materials (HEDM) [198] we are currently developing new energetic materials preferentially containing both high oxygen and nitrogen content with the trinitroethyl group contributing to a positive oxygen balance value. Oxygen balance (OB) is defined as the ratio of the oxygen content of a compound to the total oxygen required for the complete oxidation of all carbon, hydrogen and other elements that can be oxidised to form CO_2, H_2O, etc and is used to classify energetic materials as either oxygen deficient or oxygen rich.

Most energetic materials are oxygen deficient. In contrast, this new class of compounds contains sufficient amounts of oxygen and releases energy not only from oxidation of the carbon back bone but also from the liberation of dinitrogen. Nitrogen is unique amongst all other elements of the periodic table in so far that the bond energy per two-electron bond increases from a single over a double to a triple bond resulting in dinitrogen being more stable than any other nitrogen species. [10] Here we report the synthesis, characterization and the energetic properties of compounds belonging to this new class of energetic materials and we are investigating structure property relationships of the trinitroethyl group affecting the density.

Higher performance of a high explosive material crucially depends on density next to other critical parameters responsible for the effectiveness like the energy of the decomposition reactions, the number of moles and the molecular weight of the gaseous products. The velocity of detonation increases linearly

with density and the detonation pressure increases to the density squared. [22] In view of the high densities reported for trinitroethyl substituted compounds it seemed desirable to study the effect of this group on crystal density. In turn, all the compounds have been structurally characterized using single crystal x-ray analysis as a preliminary step in an investigation of the relationships between structure and crystal density.

Synthesis and thermal stability

The chemistry of 2,2,2-trinitroethanol is different to that of other alcohols owing to the electron withdrawing inductive effect of the trinitromethyl group ($\sigma^* = 4.54$) [199] decreasing the oxygen basicity of the hydroxyl group. The alcohol becomes acidic ($pK_a = 6.1$) and at pH values greater than 6, the equilibrium lies in the direction of the trinitromethanide anion and formaldehyde. [200] Due to the equilibrium position of the reaction forming trinitroethanol being dependent on the pH value, two pathways are possible for the Mannich reaction to occur with either the trinitromethane or trinitroethanol as the active hydrogen component. To study the behaviour of various heterocyclic amines in the Mannich reaction, we prepared a variety of amines of the tetrazole series and screen their properties in order to be able to judge which compounds would show promising properties in terms of fulfilling the desired criteria a new energetic material has to meet (see Table 1.1, page 15). We were interested in determining the possibility of condensing these amines with formaldehyde and trinitromethane or directly with 2,2,2-trinitroethanol and establishing the conditions of this reaction (Fig. 2.53).

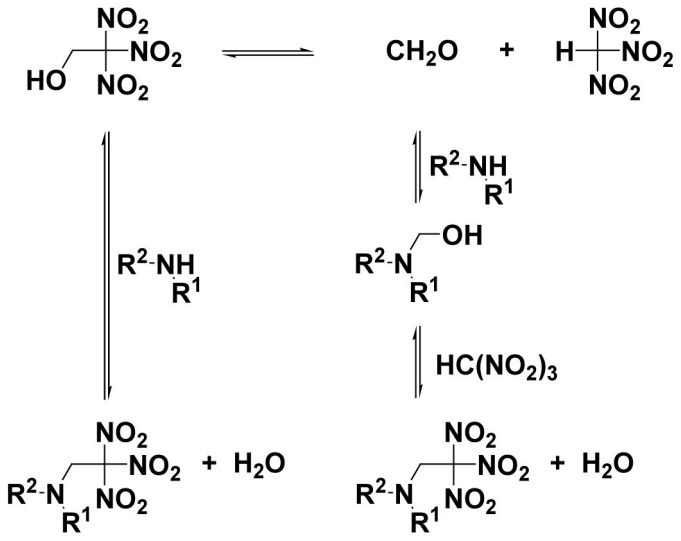

Figure 2.53. Condensation of the amine can either occur directly with the alcohol or via the stepwise reaction with formaldehyde and trinitromethane.

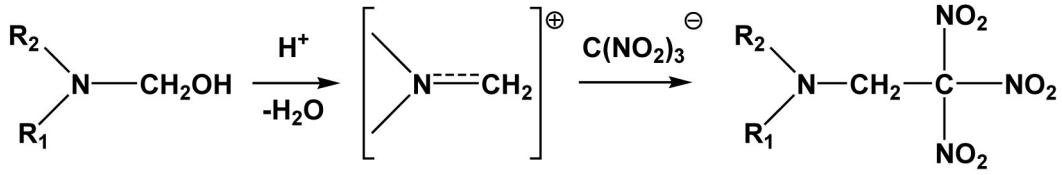

Figure 2.54. The two step reaction involves the condensation between the amine and formaldehyde yielding an intermediate iminium-type cation and subsequent product formation after reaction with trinitromethanide.

The screening revealed that triazol or tetrazol derivatives carrying a hydrazine group were most readily converted into the corresponding condensation products already at room temperature and within a few minutes. In detail, 1-methyl-1-(1*H*-tetrazol-5-yl)hydrazine, 1-methyl-1-(1-methyl-1*H*-tetrazol-5-yl)hydrazine, 2-(5-(1-methyl-hydrazinyl)-1*H*-tetrazol-1-yl)ethanol and 1-amino-2,5-hydroxymethyltriazine underwent this reaction and gave the corresponding products 5-(1-methyl-2-(2,2,2-trinitroethyl)hydrazinyl)-1*H*-tetrazol (MTHT), 1-methyl-5-(1-methyl-2-(2,2,2-trinitroethyl)hydrazinyl)-1*H*-tetrazol (MMTHT), 2-(5-(1-methyl-2-(2,2,2-trinitroethyl)hydrazinyl)-1*H*-tetrazol-1-yl)ethanol (MTHTE) and 2-(5-(1-methyl-2-(2,2,2-trinitroethyl)hydrazinyl)-1*H*-tetrazol-1-yl)ethanol (MTHTE). However, the reversal of the Mannich reaction was most developed in these hydrazine-type compounds as well.

The equilibria in organic solvents were shifted towards the educts preventing accurate NMR analysis. In addition, the thermal stabilities were very low. MTHT showed the highest thermal stability (100°C), followed by MMTHT (82.5°C) as well as MTHTE and THMT that already decomposed at room temperature. The basic character of the nitrogen atom carrying the trinitroethyl moiety obviously prevents practical application of these compounds as energetic materials. In order to stabilize trinitroethyl Mannich bases that contain a free NH fragment effectively, a nitro group can be introduced to reduce the electron density of the amine nitrogen atom as a result of conjugation between the free electron pair of the amine nitrogen and the nitro group. As mentioned above, MTHT showed the highest thermal stability of this series of trinitroethylamines and was exemplarily chosen for this purpose. However, nitration of MTHT with various nitrating agents (mixtures of nitric acid with acetic acid and trifluoroacetic anhydrides, sulfuric acid, nitronium fluoroborate in acetonitrile) led to the formation of (E)-1-methyl-1-(1*H*-tetrazol-5-yl)-2-(2,2,2-trinitroethylidene)hydrazine (MTTH) instead of the desired nitramine (Fig. 2.55).

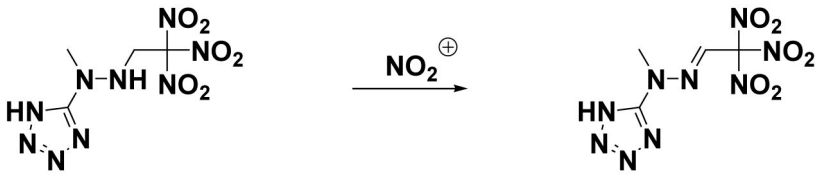

Figure 2.55. Formation of (E)-1-methyl-1-(1*H*-tetrazol-5-yl)-2-(2,2,2-trinitroethylidene)-hydrazine, MTTH.

MTTH is a rare example of a compound containing the trinitroethaniminyl moiety. A SciFinder Database enquiry revealed that there were only three entries mentioning molecules containing this fragment. [201-203] To our knowledge, MTTH represents the first example of a structurally characterized molecule containing this trinitroethylidene moiety. The crystal structure could be determined and is discussed in more detail later in this chapter. It is interesting to note that hydrazone formation was preferred over nitramine formation even though such a mild and non-oxidizing nitrating agent as nitronium tetrafluoroborate was used. A possible rational would be the presence of the nitramine as an intermediate product (Fig. 2.56).

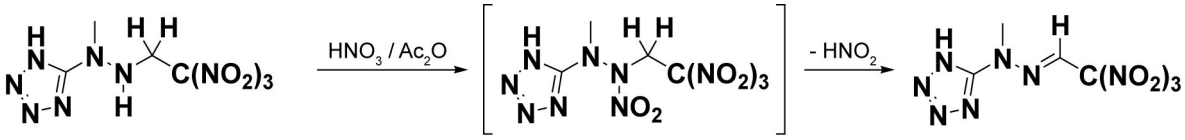

Fig. 2.60. A possible rationale for the formation of MTTH includes intermediate nitramine formation with subsequent elimination of HNO_2.

Indeed, it has been suggested that hydrazone formation could thermodynamically be favoured compared to nitramine formation. [203]

Another possibility to decrease the basicity of the amine would be disubstitution with two trinitroethyl moieties. However, the only example where double condensation occurs seems to be ammonia itself yielding bis-(2,2,2-trinitroethyl)amine (BTNA). BTNA was first synthesised by Schenck [204] who reported the reaction of 2,2,2-trinitroethanol even with only one equivalent of ammonia yielding BTNA instead of 2,2,2-trinitroethylamine. N-trinitroethyl compounds are generally base sensitive compounds with the methylene hydrogen atoms being acidified due to the electron withdrawing effect of the trinitromethyl group facilitating the reversal of the Mannich equilibrium involving the unshared *p* electron pair on the nitrogen atom yielding the methylene immonium ion and trinitromethanide anion.

This effect is decreased in the novel compounds N^1-(2,2,2-trinitroethyl)-1*H*-tetrazole-1,5-diamine (TTD) and N^1,N^5-bis(2,2,2-trinitroethyl)-1*H*-tetrazole-1,5-diamine (BTTD) where the sp^3-type electron pair is deactivated as a consequence of the electron withdrawing, inductive properties of the tetrazole unit. TTD and BTTD combine both the advantages of the tetrazole, as well as the trinitroethyl moiety. The tetrazole unit with its high nitrogen content together with its endothermic character [205] is remarkably thermally stable [206] and the trinitroethyl fragment contributes to a positive oxygen balance. The formation of TTD from the Mannich condensation between diaminotetrazole and trinitroethanol in water at ambient conditions can be accelerated when applying ultrasound. The product precipitates as a white solid and can be obtained in high yield and purity by simple filtration. On heating the neat sample using the DSC we observe a shift of the decomposition signal starting from 125.6°C (5 K min^{-1}) to 146.5°C (1 K min^{-1}) (Fig. 2.61).

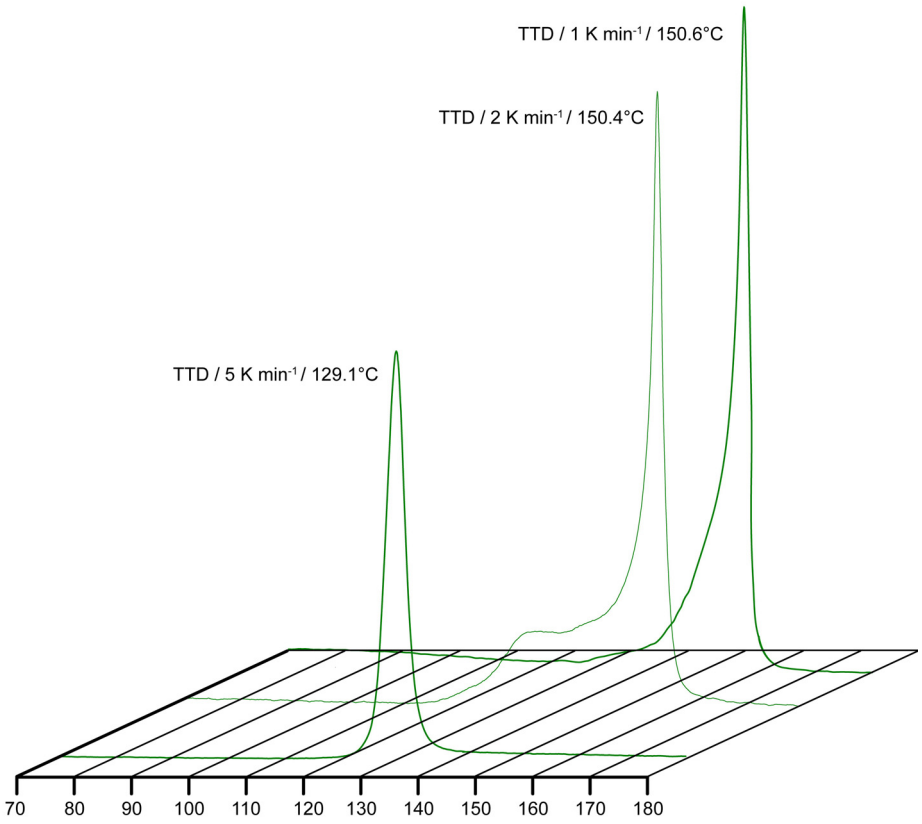

Figure 2.61. DSC plot of TTD at heat rates β = 5 K min $^{-1}$, β = 2 K min $^{-1}$ and β = 1 K min $^{-1}$ (up = exo).

Thermal rearrangement of substituted 5-aminotetrazoles is known to be a classic example of the Dimroth rearrangement and Moderhack *et al.* reported this reaction also to occur in case of substituted 1,5-diaminotetrazoles (Fig. 2.62). [207]

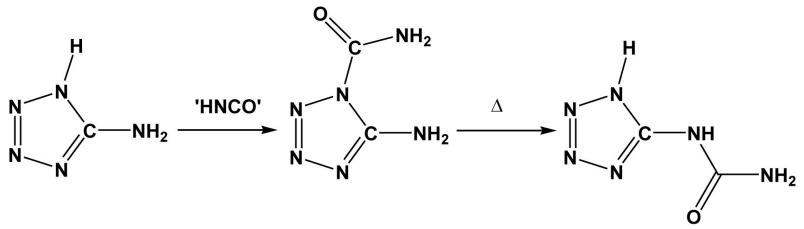

Figure 2.62. Thermal rearrangement of 5-amino-1H-tetrazole-1-carboxamide to 1-(1*H*-tetrazol-5-yl)urea.

In analogy we suppose the signal appearing in the DSC measurement at higher temperature to belong to 1-(1*H*-tetrazol-5-yl)-2-(2,2,2-trinitroethyl)-hydrazine or its open-ring tautomer azido-(2-(2,2,2-trinitroethyl)-hydrazinyl)-methanamine (Fig. 2.63).

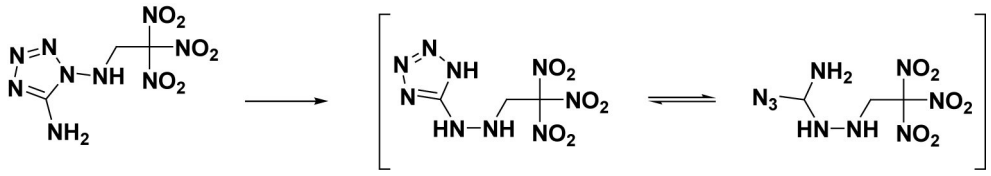

Figure 2.63. Thermal rearrangement of TTD.

The results of the isothermal long term experiment (85°C, 48h) show no decomposition or thermal rearrangement of TTD whereas the same experiment run at 120°C afforded an explosion of the sample with destruction of equipment. Isolation of this compound failed because of its extreme sensitivity and no further attempts were made to prove the existence of 1-(1*H*-tetrazol-5-yl)-2-(2,2,2-trinitroethyl)-hydrazine or its open-ring tautomer azido-(2-(2,2,2-trinitroethyl)-hydrazinyl)-methanamine as a consequence.

Bis-(2,2,2-trinitroethyl)-3,6-diaminotetrazine (BTAT), has been mentioned in the literature to be a potentially promising energetic molecule according to theoretical calculations predicting its heat of formation [208] and velocity of detonation. [209] Experimental evidence for this substance is scarce. In detail, only the UV/VIS absorption bands have experimentally been determined in a study where this material has been used for time resolved optical UV/Vis spectroscopy but no other experimental data or synthesis were reported in this work. [210] Instead, Jeff Bottaro and Rob Schmidt from SRI international were given credit for providing samples of this material. Of interest, we mention that there is a structural report of the similar compound 3,6-bis(2-fluoro-2,2-dinitroethylamino)-1,2,4,5-tetrazine. [211] No experimental data of this compound or synthetic protocols for this compound were provided in this work. Instead, Robert Schmitt of SRI international, Palo Alto, California was given credit in the experimental section for having synthesised this compound. Experimental evidence of BTAT available at the time of writing this thesis were limited to UV-Vis spectra. No other data or synthetic protocols were available to our knowledge.

Here we present a synthetic pathway of 3,6-(2,2,2-trinitroethylamino)-1,2,4,5-tetrazine (BTAT) and its detailed characterization. We find that the reversal Mannich reaction mentioned above is most effectively cancelled in this compound due to the unshared *p* electron pair at the sp^2-type nitrogen atom

being delocalized over the tetrazine ring system. The lack of reactivity of this amino group present in the starting material (3,6-diaminotetrazine) prevents it from reacting with 2,2,2-trinitroethanol even at drastic conditions when being heated solvent free. However, we find that condensation occurs with the aid of a Lewis acid or strong mineral acids (see section 2.14, page 119).

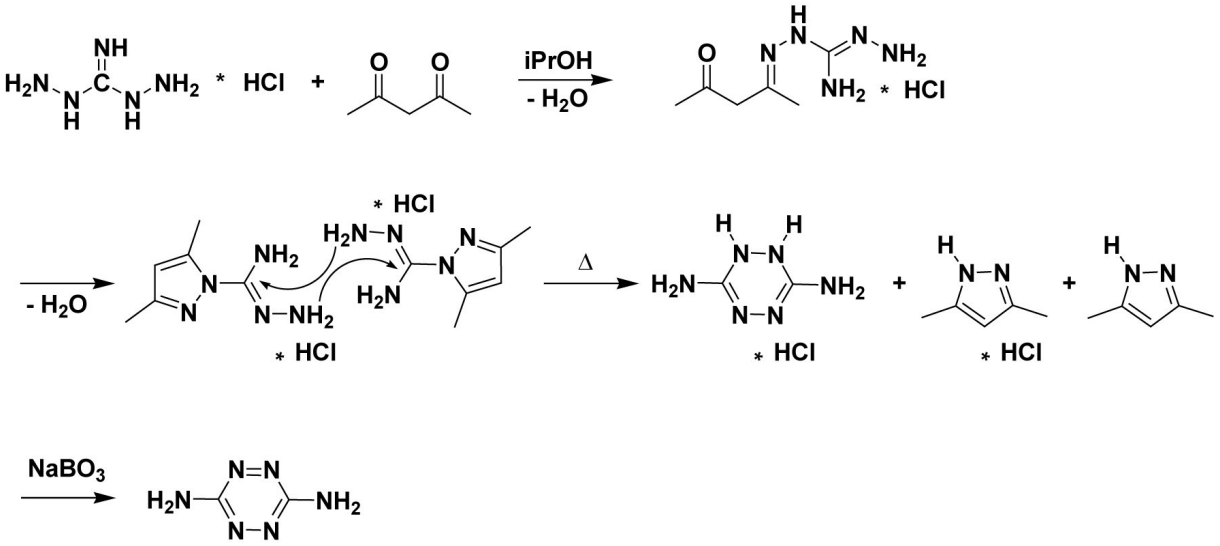

Figure 2.64. Mechanism for the formation of 3.6-diamino-1,2,4,5-tetrazine from diaminoguanidinium hydrochloride and acetylacetone according to Coburn *et al.* [212]

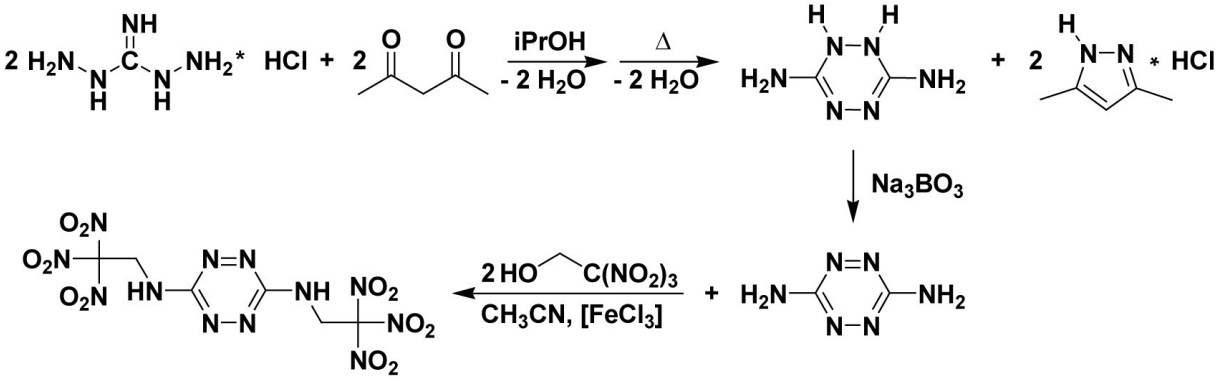

Figure 2.65. Iron-(III)-chloride aided, three step synthesis of BTAT starting from diaminoguanidinium hydrochloride, 2,4-pentanedione and 2,2,2-trinitroethanol.

The ultraviolet spectrum shows that the π→π* (tetrazine) band appears in the UV region at 240.5 nm. Two additional transitions are present in the visible region at 413.5 and 507.5 nm. The thermal stability of BTAT is enhanced compared to TTD with decomposition starting at 184°C (DSC, 5K min^{-1}). BTAT is chemically stable at a temperature of 140°C for at least 48h (Fig. 2.66).

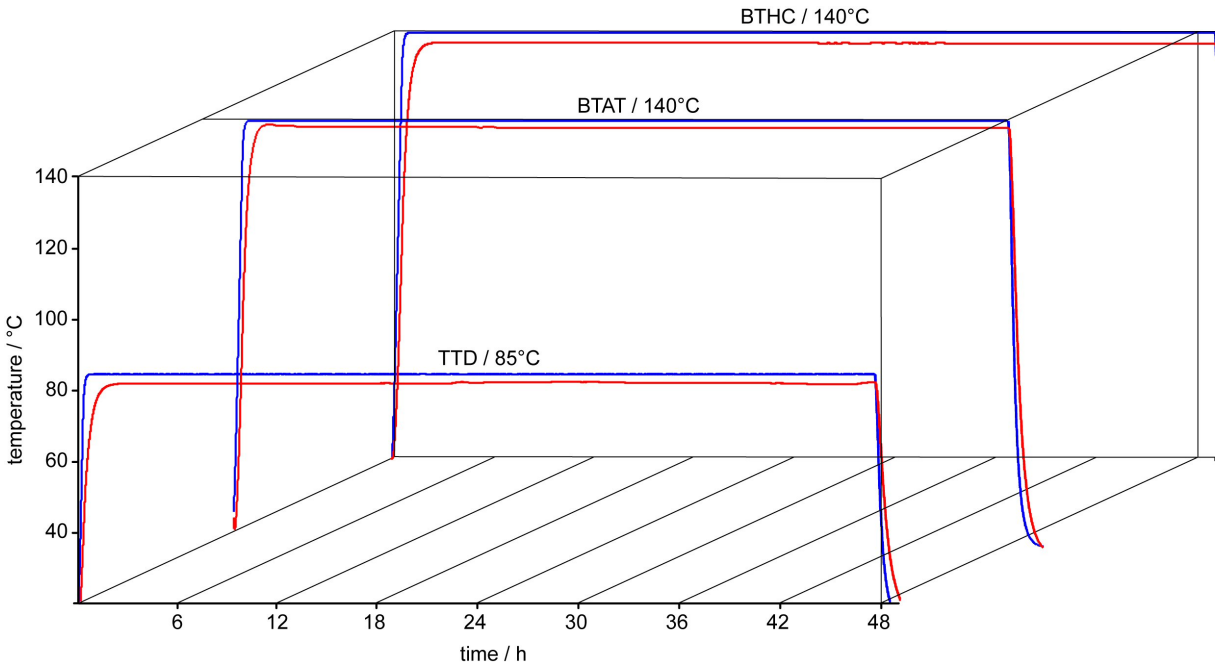

Figure 2.66. Isothermal long term experiment (48h) of N^1-(2,2,2-trinitroethyl)-1*H*-tetrazole-1,5-diamine (TTD), bis(2,2,2-trinitroethyl)-3,6-diaminotetrazine (BTAT) and bis-(2,2,2-trinitroethyl)-hydrazodicarboxylate (BTHC). Color: sample (red), oven (blue). Decomposition did not occur rendering TTD, BTAT and BTHC long term stable at ambient as well as at elevated temperatures.

Other compounds that can be related to BTAT in terms of having a similar composition include 2,4,6-(2,2,2-trinitroethylamino)-triazine (TTAT) and 2,2,4,4,6,6-(2,2,2-trinitroethylamino)-triazine (HTAT). Formal comparison of BTAT and TTAT shows that the six membered ring of the latter compound (TTAT) consists of a six-membered ring containing three nitrogen atoms, three carbon atoms and three N-trinitroethyl functionalities, BTAT contains a six-membered ring containing four ring nitrogen atoms, two carbon atoms and two exocyclic N-trinitroethyl moieties. 2,4,6-(2,2,2-trinitroethylamino)-1,3,5-triazine (TTAT) has been mentioned in only two publications. [213-214] The reported properties include infrared as well as NMR spectroscopic data next to elemental analysis and a melting point of 55-57°C. [214] Two synthetic routes towards the preparation of 2,2,4,4,6,6-(2,2,2-trinitroethylamino)-triazine (HTAT) have been reported and shown to be unsuccessful: a) replacement of the chlorine atoms of cyanuric chloride by bis-(2,2,2-trinitroethyl)amine in the presence of pyridine as well as b) reaction of cyanamide with two equivalents of 2,2,2-trinitroethanol to give bis-(2,2,2-trinitroethyl)cyanamide, followed by

trimerization of the latter. [215] In order to study whether the thermal stability could further be enhanced we also developed compounds where we take advantage of the unshared p electron pair of nitrogen trying to impact thermal stability through oxygen-balance neutral introduction of conjugation affording carbamates from the reaction between 2,2,2-trinitroethylchloroformate and a nitrogen nucleophile. 2,2,2-trinitroethyl-azidoformate (TAF) was obtained from the reaction of 2,2,2-trinitroethylchloroformate and trimethylsilylazide as shown in Figure 2.67.

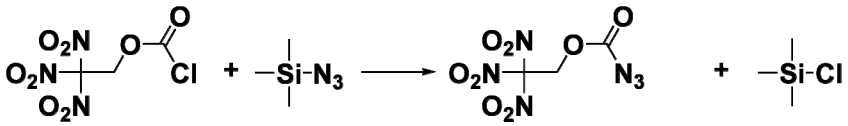

Figure 2.67. Synthsis of TAF.

The DSC diagram of TAF shows that melting of the white solid occurs at 27.5°C (onset). A second endothermic signal (96.2°C onset) corresponds to boiling with subsequent decomposition (130.4°C onset / 158.4°C max). A second exothermic signal appears (191.6°C onset / 205.6°C max) possibly originating from 2,2,2-trinitroethylcarbamate formed during pyrolysis of TAF in analogy to the azide pyrolysis of ethyl azidoformate where elimination of molecular N_2 has been reported to occur on thermal decomposition. [216] 2,2,2-trinitroethylcarbamate represents the most simple carbamate carrying the trinitroethyl moiety. Formally, bis-(2,2,2-trinitroethyl)-hydrazodicarboxylate (BTHC) can be considered as a dimer of 2,2,2-trinitroethylcarbamate and was obtained according to Figure 2.68.

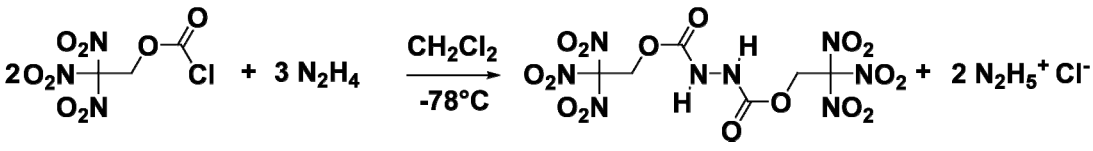

Figure 2.68. Synthesis of BTHC.

In order to prevent facile dissociation of the base sensitive trinitroethyl moiety we chose to apply kinetic control and to avoid an excess of nucleophile. Under these conditions, even strong bases like hydrazine can be reacted. The NMR spectra of dissolved single crystals of BTHC and ethyl acetate (1:1) are shown in Figures 2.69 – 2.71.

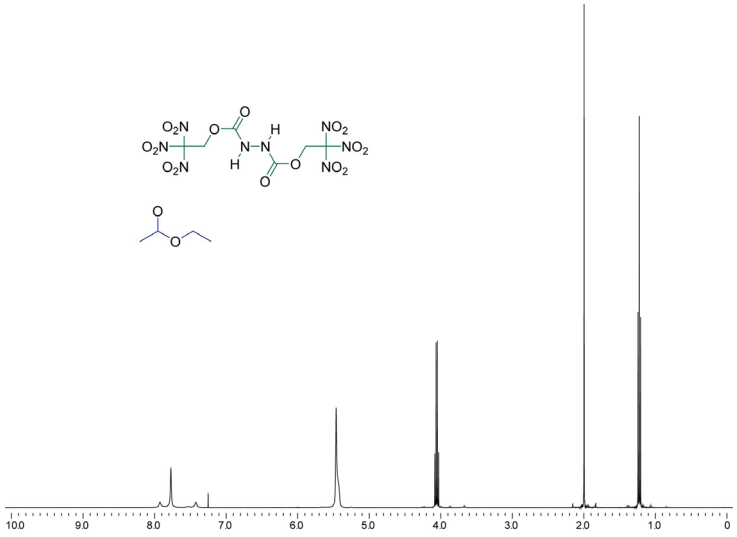

Figure 2.69. ^{1}H NMR Spectrum of BTHC / EtOAc (1:1). ([D3]chloroform) δ: 5.46 (2H, s, -CH_2-), 7.4 – 7.9 (2H, s, -NH-).

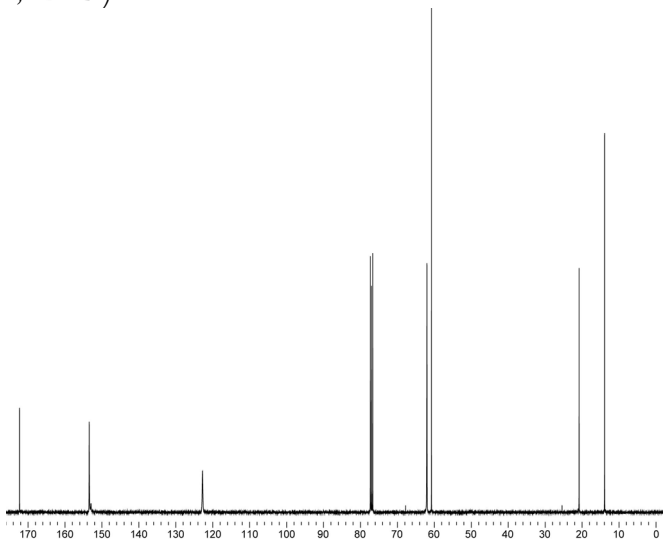

Figure 2.70. ^{13}C NMR Spectrum of BTHC / EtOAc (1:1). ([D3]chloroform) δ: 62.0 (s, -CH_2-), 122.7 (bs, -$C(NO_2)_3$), 153.4 (s, -O_2C-).

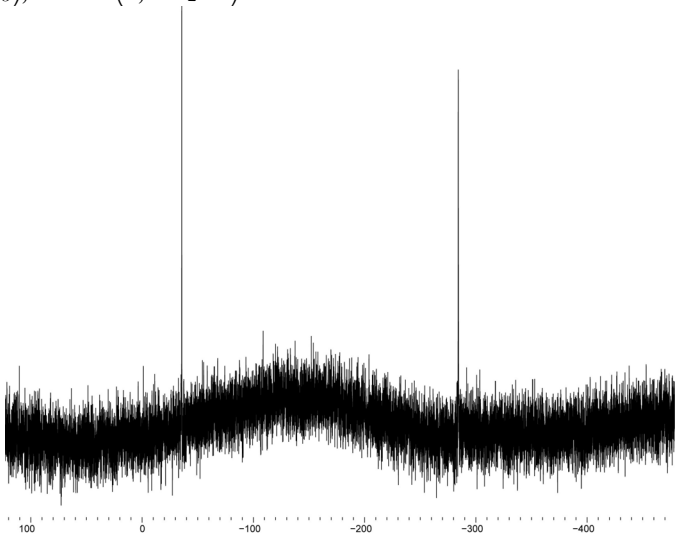

Figure 2.71. ^{15}N NMR Spectrum of BTHC / EtOAc (1:1). ([D3]chloroform) δ (nitromethane): -35.6 (s, -NO_2), 284.0 (s, -NH-).

The pure substance (BTHC) is a glass-like, amorphous solid at room temperature rather softening than melting in the vicinity of greater 80°C as can be depicted from the DSC plot (Fig. 2.72). The DSC measurement was run at a rate (β) of 5 K min^{-1} displaying an onset of decomposition as high as 188.3°C. The property of having a reasonable low melting point together with a liquid range of greater than 100°C renders this material as a promising candidate for use as melt-castable explosive.

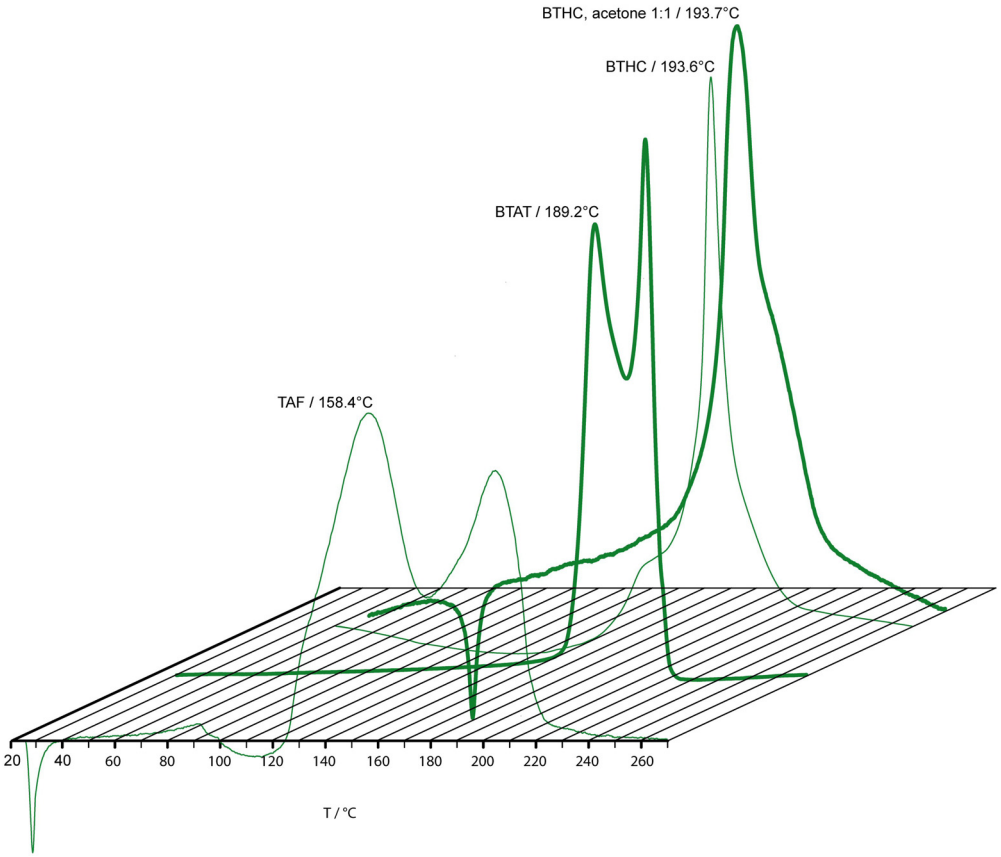

Figure 2.72. DSC plot of TAF (decomp. onset: 130.4°C), BTAT (decomp. onset: 184°C), BTHC (decomp. onset: 188.3°C) and BTHC/acetone (decomp. onset: 185.4°C) 1:1 (β = 5 K min^{-1}, exo = up). The temperatures of the first exothermic maxima are given.

The isothermal long term test (48 h) of BTHC has been carried out at 120°C and 140°C with no evidence of decomposition or change in decomposition point. The chemical long term stabilities of BTHC and BTAT at 140°C are exceptionally high for this class of trinitroethyl containing compounds. The decomposition rates in the liquid state or in solution are usually up to 50 – 100 times faster than at corresponding temperatures in the solid state. [217-219] This

can be considered as a consequence of the atoms involved in the decomposition reactions being relatively immobile in the solid state hindering chemical reactions to take place and facilitating atom-to-atom recombination reactions in contrast to the liquid state. [13] Considering this fact, the stability of liquid BTHC can be considered excellent. A possible rationale for this could be that on comparing different molecules, additional rotational modes can effectively act as enthalpy sink with more energy being required to break bonds. In contrast, restriction of rotational modes due to steric effects or the rigid body of a molecule can lead to energy redistribution within the molecule with more energy going into the vibrational modes eventually leading to bond homolysis.

Heat of Formation

Calorimetric measurements of the energies of combustion of nitro compounds present considerable difficulties [220] because the compounds often explode on exposure to heat or mechanical shock. The heats of combustion for nitro compounds are usually lower than for hydrocarbons, and the handling of larger quantities of such substances is dangerous because of the possible change from combustion to detonation. In addition, it is difficult to obtain accurate values for the enthalpy of formation since the accurate determination of the energy of combustion effects the accuracy of the derived enthalpy of formation. In order to obtain highly accurate energy values, we first calculated the absolute gas phase enthalpies (*H*) at 298.15K using a modification of the Complete Basis Set (CBS) method of Peterson and co-workers. The CBS models make use of the asymptotic convergence of pair natural orbital expressions to extrapolate correlation energies from calculations using a finite basis set to the estimated complete basis set limit. [221] CBS-4 starts with a HF/3-21G(d) geometry optimization in order to compute the zero-point vibrational energy. Then a large basis set SCF calculation is performed yielding a base energy corrected through a second order MP2/6-31+G calculation with a CBS extrapolation. Higher-order contributions are estimated using a MP4(SDQ)/6-31G calculation. An empirical correction is then used to treat spin contamination effects. [222] In this study we applied the modified CBS-4M method (M referring to the use of minimal population localization) which is a re-parameterized

version of the original CBS-4 method. [223] The determination of the gas phase heats of formation was accomplished by using the method of atomization energies (Fig. 2.73). [224]

$$\Delta_f H^\circ(M_{(g)}, 298) = H^\circ(M_{(g)}, 298) - \sum_{atoms} H^\circ(A_{(g)}, 298) + \sum_{atoms} \Delta_f H^\circ(A_{(g)}, 298)$$

Fig. 2.73. Notes. M refers to molecule, A refers to atoms, and 298.15 K is denoted as 298 for clarity.

Finally, sublimation enthalpies were estimated according to Trouton's rule (Fig. 2.74) and subtracted from the gas phase enthalpies of formation in order to obtain the solid state heat of formation values. [225]

$$\Delta_{sub}H°(M_{(s)}, 298)\ [\text{J mol}^{-1}] = 188 \cdot T_m \qquad [\text{K}]$$

Figure 2.74. Estimation of the heat of sublimation.

The values obtained for the heat of formation obtained from our calculations can be compared with the previously reported values for ethanol (EtOH), 2,2,2-trinitroethanol (TNE), 2,4,6-trinitrotoluene (TNT) and cyclotrimethylenetrinitramine (RDX) as well as cyclotetramethylenetetranitramine (HMX) and hexanitrohexaazaisowurtzitane (HNIW / CL-20) which were determined using both precision combustion calorimetry and reaction calorimetry (Table 2.14).

Table 2.14. Comparison of experimentally determined and calculated heat of formation.

Δ_fH^0 / kcal mol^{-1}	CBS-4M	experimental a)
EtOH	-58.0 (g)	-56.1 ± 0.1 (g) [226]
TNE	-47.0 (g) / -62.5 (s)	-62.3 ± 0.7 (s) [227]
TNT	2.21 (g)	5.8 ± 0.8 (g) [228]
RDX	41.6 (g)	45.9 (g) [229]
HMX	30.1 (s)	24.6 ± 0.7 [230]
CL-20	96.7 (s)	102.9 (s) ± 3.1 [231]

The differences between the experimentally determined and the calculated $\Delta_fH°$ values do not exceed a range of 5 kcal mol^{-1} rendering this method valid for the estimation of the heats of formation (Table 2.15). Hence, the calculated

values for those compounds where no experimental data exist should be reliable estimates. High heat of formation is a critical parameter for the performance properties of a high explosive and most of the energy derived in modern HEDM stems not only from oxidation of the carbon backbone as in traditional energetic materials but also from ring or cage strain and from their very high positive heat of formation. Tetrazoles are the most promising heterocycles amongst five-membered rings with four nitrogen atoms in the ring displaying high heats of formation due to an increasing positive trend in heat of formation with increasing number of nitrogen moving from imidazole ($\Delta_f H^0$, + 58.5 kJ mol^{-1}) to 1,2,4-triazole ($\Delta_f H^0$, + 109.0 kJ mol^{-1}) to tetrazole ($\Delta_f H^0$, + 237.2 kJ mol^{-1}). [232] As far as six-membered nitrogen containing heterocycles are concerned, tetrazines display the highest heat of formation with four nitrogen atoms in the ring. The standard heat of formation of 1,2,4,5-tetrazine has been calculated to be as high as 489.9 kJ mol^{-1}. [233] In accordance, the tetrazole and tetrazine based compounds TTD, BTTD and BTAT display the highest values for the heat of formation of the compounds presented in this work (Table 2.15).

Table 2.15. Composition, oxygen balance and calculated heat of formation.

	i	formula	Σ (O, N)	N	O	Ω	$\Delta_f H^{0}_{(g)}$ [a]	$\Delta_f H^{0}_{(s)}$
BTHC	3, 4	$C_6H_6N_8O_{16}$	82.50	25.12	57.38	+3.6	-610.18	-671.27
BTC	24	$C_5H_4N_6O_{15}$	83.48	21.65	61.83	+12.4	-508.08	-581.05
TNE	8	$C_2H_3N_3O_7$	85.07	23.21	61.86	+13.3	-196.78	-261.57
BTNA	10	$C_4H_5N_7O_{12}$	84.16	28.57	55.59	+7.0	-5.34	-77.77
TAF	9	$C_3H_2N_6O_8$	84.78	33.60	51.18	+6.4	-1.55	-58.07
BTAT	15	$C_6H_6N_{12}O_{12}$	82.18	38.36	43.82	-10.9	+422.00	+336.11
TTD	7	$C_3H_5N_9O_6$	84.39	47.91	36.48	-15.2	+430.51	+355.54
BTTD	17	$C_5H_6N_{12}O_{12}$	84.49	39.44	45.05	-3.8	+435.66	+360.69
TNT		$C_7H_5N_3O_6$	60.76	18.50	42.26	-74.0	+9.27	-57.27
RDX		$C_3H_6N_6O_6$	81.06	37.84	43.22	-21.6	+174.2	+84.50
HMX		$C_4H_8N_8O_8$	81.06	37.84	43.22	-21.6	+230.57	+126.20

Notes. *i* = index used to reference individual compounds, see Chart 1. M = molar mass / g mol^{-1}, ρ = calculated density obtained from single crystal X-ray diffraction studies / g cm^{-3}, Σ (O, N) = sum combined oxygen and nitrogen content / %, Ω = oxygen balance / %, $\Delta_f H^0$ = calculated enthalpy of formation / kJ mol^{-1}.

Tables 2.15 and 2.16 contain the heat of formation and performance data of two molecules where we previously reported the crystal structures with 2,2,2-trinitroethanol (TNE) [234] representing the most simple trinitroethyl

substituted compound as well as bis(2,2,2-trinitroethyl)carbonate (BTC) [235] displaying the highest crystal density amongst all trinitroethyl substituted compounds as well as the heat of formation and performance data of standard explosives such as 2,4,6-trinitrotoluene (TNT), 1,3,4-trinitro-1,3,5-triazacyclohexane (RDX) and 1,3,5,7-tetranitro-1,3,5,7-tetraazacyclooctane (HMX) for comparison.

Sensitivity and Performance

In order to establish safe handling procedures the sensitivity data of the new compounds towards mechanical destructive stimuli like impact or friction and electrostatic discharge have been measured. The sensitivity can be used to classify them as primary or secondary explosives. Whereas primary explosives explode readily from light to modest mechanical stimuli or application of heat, some secondary explosives or simply high explosives need a high energy impulse like the shock of a detonation in order to initiate detonation and will simply burn in small enough quantities. According to BAM (Bundesanstalt für Materialprüfung), a compound can be classified as being insensitive (impact energy > 40 J / friction force > 360 N), less sensitive (impact energy ≥ 35 J / friction force = 360 N), sensitive (impact energy ≥ 4 J / friction force < 360 N to > 80 N), very sensitive (impact energy ≤ 3 J / friction force ≤ 80 N) and extremely sensitive (impact energy ≤ 3 J / friction force ≤ 10 N). Of all the compounds tested, the following order of sensitivity including the standard explosives TNT, RDX, HMX and CL-20 arises: CL-20 (very sensitive, 4 J / 48N) [236] > TTD (sensitive, < 30 J / 40 N) > HMX (sensitive, 7.4 J / < 120 N); [236] RDX (sensitive, 7.4 J / 120 N); [236] BTAT (sensitive, 7J / > 160 N) > TNT (sensitive, 15 J / 353 N) [236] > BTNA (sensitive, 15 J / > 360 N) > BTHC (insensitive, > 100 J / > 360 N). By applying the calculated density values obtained from the crystal structure determination and the calculated energy of formation, the performance parameters of TTD, BTTD, BTAT, TAF and BTHC as well as 2,2,2-trinitroethanol (TNE), bis-(2,2,2-trinitroethyl)-amine (BTNA) and bis-(2,2,2-trinitroethyl)-carbonate (BTC) were calculated using the software EXPLO5 (v. 5.02) [237-241] and are summarized in Table 2.16. The software is based on the chemical equilibrium, steady-state model of detonation

and uses the Becker-Kistiakowsky-Wilson's equation of state (BKWN EOS) for gaseous detonation products.

Table 2.16. Selection of calculated performance properties and comparison to TNT, RDX and HMX.

	ρ	$\Delta_f U^0$	Q_{CJ}	V_0	T_{ex}	P_{CJ}	D
BTHC calc.	1.8	-1421	5333	682	4376	284	8188
TNE calc.	1.839	-1355	4875	712	4041	285	8180
TAF calc.	1.853	-153	5353	675	4549	303	8359
BTC calc.	1.975	-1417	4792	665	4068	317	8396
BTNA calc.	1.881	-138	6010	705	4733	343	8815
TTD calc.	1.831	+1443	6018	788	4650	370	9194
BTTD calc.	1.897	+932	6479	739	5009	388	9323
BTAT calc.	1.886	+852	6135	743	4867	389	9261
TNT calc.	1.64	-175	5064	625	3749	203	7170
TNT exp.	1.64 [242]	-	-	-	-	210 [a) 242]	6950 [a) 242]
RDX calc.	1.80	+280	5875	797	4290	338	8894
RDX exp.	1.80 [242]	-	-	-	-	347 [a) 242]	8750 [a) 242]
HMX calc.	1.89	+526	6169	791	4385	384	9288
HMX exp.	1.89 [242]	-	-	-	-	390 [a) 242]	9110 [a) 242]

Notes. a) experimental value, ρ = calculated density obtained from single crystal X-ray diffraction studies / g cm^{-3}, $\Delta_f U^0$ = energy of formation / kJ kg^{-1}, Ω = oxygen balance / %, Q_{CJ} = heat of explosion / kJ kg^{-1}, V_0 = volume of gaseous detonation products / L kg^{-1}, T_{ex} = explosion temperature / K, P_{CJ} = detonation pressure / kbar, D = velocity of detonation / m s^{-1}.

Figure 2.75. Small scale burning test (UN 3d) of BTAT as part of the interim hazard classification (IHC) procedure. An unconfined plastic transportcontainer filled with BTAT (2g) was placed in kerosene-soaked sawdust which was subsequently ignited. The picture in the middle shows deflagration of the substance indicating a pass of this test due to failure of explosion or detonation.

A comparison of the calculated values of 2,4,6-trinitrotoluene (TNT), 1,3,4-trinitro-1,3,5-triazacyclohexane (RDX) and 1,3,5,7-tetranitro-1,3,5,7-tetraazacyclooctane (HMX) based on the calculated (CBS-4M) solid state heat of formation to their corresponding experimental values is included in Table 2.16 and shows that the calculated values obtained using this method are in good agreement with the corresponding experimental values. TNT can be considered as first generation explosive, whereas the nitramine-type explosives RDX and HMX belong to the second generation and are standard explosives for most military applications today. The theoretically predicted performance values for TNE, BTC, BTNA, TTD, BTTD, BTAT, TAF and BTHC all lie within the range expected for high explosives while at the same time displaying a much more favourable oxygen balance compared to TNT, RDX and HMX. Oxygen balance values near or greater zero are highly desirable in order to reduce toxic fume gases like carbon monoxide. [236] The combined oxygen and nitrogen content of TNE, BTNA, BTC, TTD, BTTD, BTAT, TAF and BTHC all lie within 82.2% to 85.1% with oxygen balance values ranging from -15.2% to +13.3%. Of all the compounds studied in this work, TTD, BTTD and BTAT show the highest predicted values for the velocity of detonation (BTTD: 9323 m s^{-1} / BTAT: 9261 m s^{-1}/ TTD: 9194 m s^{-1}), detonation pressure (BTAT: 389 kbar / BTTD: 388 kbar / TTD: 370 kbar) and heat of explosion (BTTD: 6479 kJ kg^{-1} / BTAT: 6135 kJ kg^{-1} / TTD: 6018 kJ kg^{-1}) displaying performance values superior to RDX and comparable to HMX.

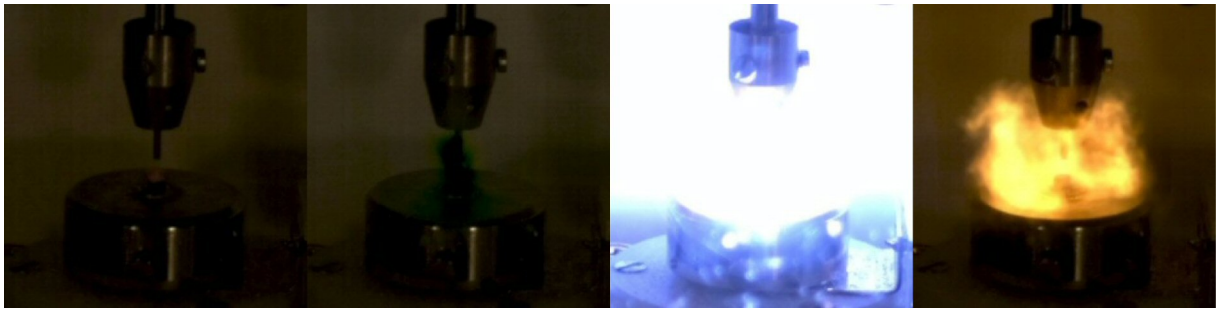

Figure 2.76. High Speed Video Images (4000 frames per second) of the electrostatic ignition of BTAT and subsequent explosive decomposition. The four pictures show the unreacted sample, ignition of the sample by electrostatic discharge accompanied by formation of dark coloured gases, detonation accompanied by a flash of light and burning of the hot decomposition gases (from left to right).

Figure 2.77 displays the pictures of a Steel Sleeve test (Koenen test) on TTD. This is indicative for the respond to thermal shock and performance of a compound under confinement according to *German law of explosives* as well as the *United Nation Recommendations on the Transport of Dangerous Goods.* [243] A steel core [d] (Fig. 2.77) filled with 25 mL of compound gets locked using a perforated disk [b] with variable whole width using screw threads [a] + [c]. The sample is then placed into the test setup where four *Bunsen* burners simultaneously heat it up to five minutes. Subsequently, large amounts of liberated gaseous decomposition products arise. The whole diameter of the perforated disk where no destruction of the steel assembly occurs is called the limiting diameter. This diameter has been found to be 6 mm for TNT, and 8 mm for RDX and HMX. In case the steel sleeve is ruptured into three or more pieces the test is evaluated as explosion. A whole width of 10 mm was used in this test (Fig. 2.77) and the steel tube was fragmented into powder-like pieces. Furthermore, the screw threads [a] + [c] were also broken into pieces rendering TTD as sensitive compound with a critical diameter of greater 10mm (Type H). The explosion was recorded using a high speed camera at 3500 frames per second and found to take place within less than 0.5 milliseconds according to two frames with the first frame showing ignition and the second frame (picture B, Fig. 2.77) revealing that no visible metal pieces are present any longer.

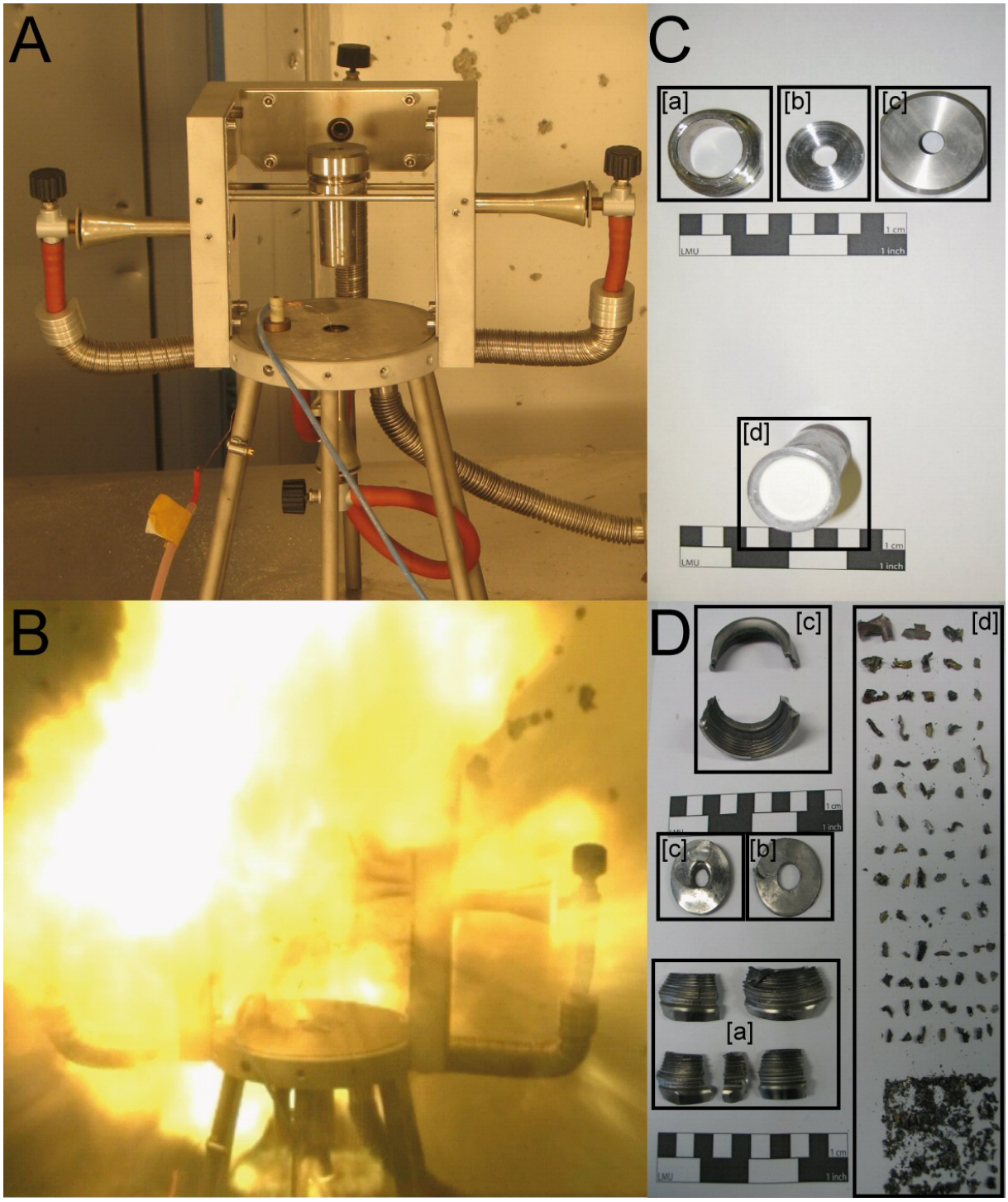

Figure 2.77. Steel Sleeve test (Koenen) of TTD (10mm). A: Setup, B: High Speed Image (3500 fs^{-1}) of the detonation, C: Steel sleeve assembly before the test: [a] + [c] screw thread, [b] perforated disk (10mm whole width), [d] steel core, filled with TTD, D: Steel sleeve residues.

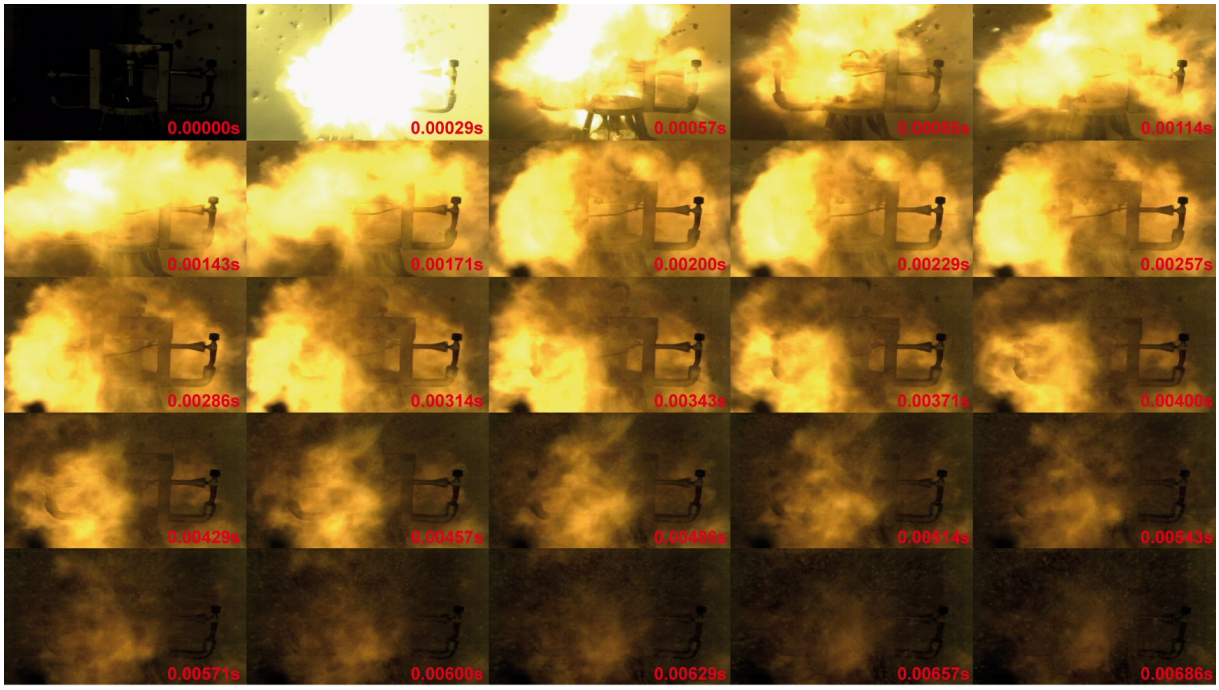

Figure 2.78. Series of high speed images (3500 fs^{-1}) of the Koenen Test of TTD.

Crystal Structure Analysis

Due to density being one of the most important parameters specifying detonation properties we determined solid state molecular and crystal structures in order to investigate the relationships between structure and crystal density. In order to evaluate the significance of the trinitroethyl group for the design of novel compounds displaying superior high energy density, intermolecular interactions of this moiety were of particular interest. The close approach of oxygen atoms with intermolecular oxygen···oxygen distances substantially less than 3.04Å, the sum of the *van der Waals* radii for O (1.52Å) [244] were chosen as manifestations of dipolar nitro group interactions and were investigated in analogy to those discussed in the structure determinations of 2,2,2-trinitroethanol [234] and bis-(2,2,2-trinitroethyl)-carbonate [235]. The attractive nitro group interaction is supposed to be both of dispersive as well as electrostatic nature. Nitrogen···oxygen distances less than 3.27Å were investigated to that effect. The value of 3.27Å was chosen as the sum of the *van der Waals* radii of nitrogen and oxygen [244] plus a tolerance value of 0.2 Å.

2,2,2-Trinitroethanol (TNE)

The structure of 2,2,2-trinitroethanol, $C_2H_3N_3O_7$, at 100 (2) K has monoclinic ($P2_1/c$) symmetry with eight formula units in the unit cell whereby the asymmetric unit consists of two molecules. The compound is of interest with respect to energetic materials. The structure displays intramolecular O—H···O as well as intermolecular O—H···O and C—H···O hydrogen bonding, directed four-membered OH···OH···OH rings and dipolar nitro group interactions that account for the high density of 1.839 g cm^3. 2,2,2-Trinitroethanol with three nitro groups bonded to the same carbon atom is a valuable intermediate in the preparation of energetic materials. However, the structure of TNE in the solid state has not been investigated. Only a hypothesis about intramolecular as well as intermolecular hydrogen bonding, based on IR spectroscopy data, has been made. [245] Our X-ray investigation shows intra- as well as intermolecular O—H···O hydrogen bonding next to non-classical C—H···O hydrogen bonding. The asymmetric unit of TNE (Fig. 2.79) consists of two crystallographically independent trinitroethanol molecules.

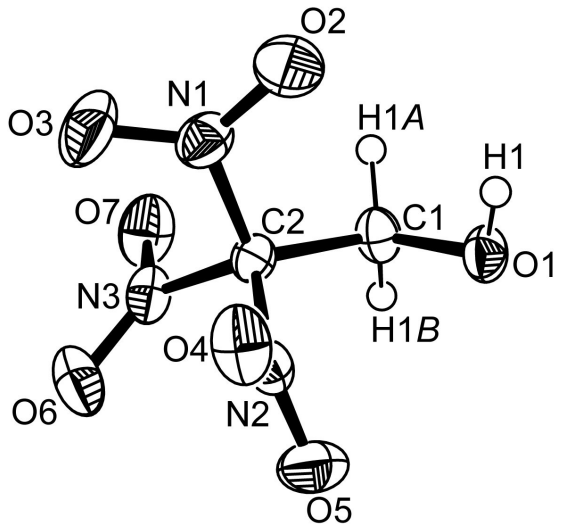

Figure 2.79. ORTEP representation of the molecular structure of 2,2,2-Trinitroethanol in the crystalline state. Only one of the two molecules of the asymmetric unit is shown. Displacement ellipsoids are shown at the 50 % probability level. Selected bond lengths [Å] and angles [°]: C_1-C_2 1.5352(19), C_1-O_1 1.4050(17), C_2-N_1 1.5197(18), C_2-N_2 1.5155(17), C_2-N_3 1.5159(17), N_1-O_2 1.2094(18), N_1-O_3 1.2130(18), O_2-N_1-O_3 126.98(14), N_1-C_2-N_2 106.24(11), N_1-C_2-N_3 105.90(10), N_2-C_2-N_3 108.43(10), N_1-C_2-C_1 113.42(12), C_2-C_1-O_1 110.77(11), N_2-C_2-C_1-O_1 -34.29(16).

These two moieties display a very similar molecular geometry with a propeller-type orientation of the nitro groups (D_3) bonded to the β carbon atom. In both molecules the conformation of the substituents of the α- as well as the β carbon atom is found to be staggered and intramolecular O—H···O hydrogen bonding does occur (O_1—H_1···O_3, O_8—H_8···O_{13}). The length of the C-N bonds joining the three nitro groups to the β carbon atom (range 1.5150 ± 0.0018 Å - 1.5197 ± 0.0018 Å) are significantly longer than the normal C-N bond distance of 1.47 Å [246] as was already observed in the determination of the crystal structure of *N*,*N*'-bis-(2,2,2-trinitroethyl)-urea [247]. A comparison of the geometrical trends for the bonding of the three nitro groups to one carbon atom in TNE with those in *N*,*N*'-bis-(2,2,2-trinitroethyl)-urea reported by Lind again shows good agreement taking into account that the measurement of Lind was undertaken at 296 K whereas our experiment was run at 100 K. The independent N-C-N bond angles are less (range 105.90 (0.10)° - 108.43 (0.10)°) than the tetrahedral value whereas the corresponding N-C-C bond angles are greater (range 110.18 (0.11)° - 113.42 (0.12)°) than the tetrahedral value. The three independent nitro groups of each TNE molecule are identical in structure within the limits of error and display common geometry parameters like N-O distances (range 1.2079 (0.0018)Å - 1.2181 (0.0018) Å), O-N-O bond angles (range 126.96 (0.14)° - 127.91 (0.15)°) and O-N-C bond angles (range 113.63 (0.12)° - 118.64 (0.12)°). In turn, the arrangement of the C-N and N-O bonds is coplanar with the sums of the three bond angles around one nitrogen atom being 360° within the limits of error.

The extended structure of TNE involves secondary interactions in terms of intermolecular O—H···O hydrogen bonding, intermolecular C—H···O hydrogen bonding as well as dipolar nitro group interactions. The circular O—H···O hydrogen bonding between the hydroxyl groups of four trinitroethanol molecules results in four-membered homodromic rings (O_1—H_1···O_8—H_8···O_1—H_1···O_8—H_8). The structure that can be observed along the crystallographic *a* axis shows a stacking of these rings. Every ring is surrounded by four neighbouring rings whereby two of the four molecules of trinitroethanol that form such a ring interconnect the central ring to the surrounding rings via C_3—H_{3B}···O_{14} hydrogen bonding (Fig. 2.80).

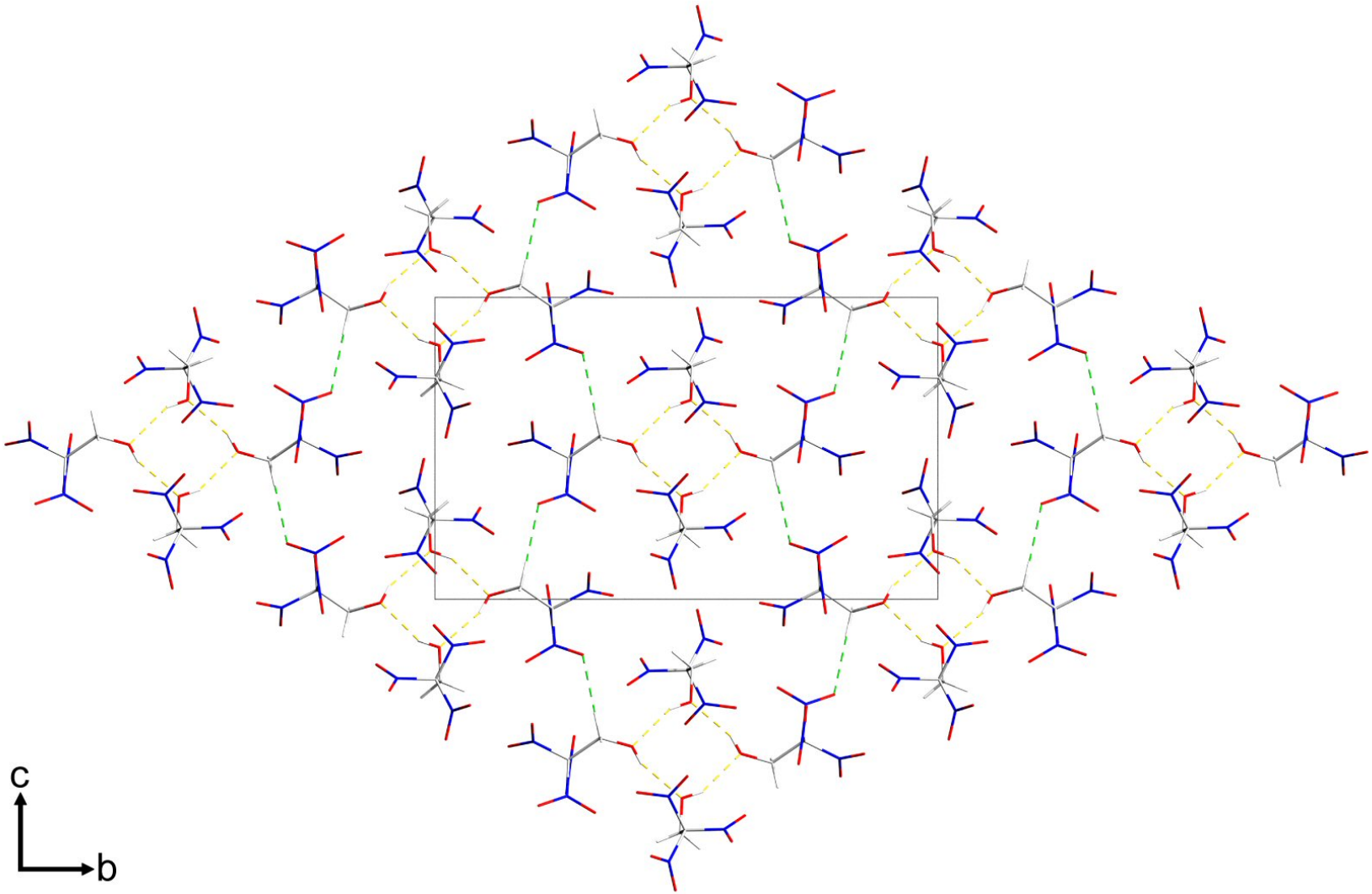

Figure 2.80. Unit cell packing of 2,2,2-Trinitroethanol, viewed along the *a* axis. Yellow dashed lines indicate intermolecular hydrogen bonding (O_1-H_1···O_8, O_8-H_8···O_1^{i}) Green dashed lines indicate intermolecular hydrogen bonding of the acidified methylene type hydrogen atoms of the trinitroethyl moiety (C_3-H_{3B}···O_{14}^{ii}); Symmetry code: (i) –x+2, -y+1, -z+1; (ii) x, -y+1/2, -z+1/2.

Additional contacts: Intramolecular hydrogen bonds: O_1-H_1···O_3 and O_8-H_8···O_{13}.The close approach of oxygen atoms found in the extended structure of TNE suggest the possibility of dipolar nitro group interactions in analogy to a variety of non-covalent interactions such as halogen···$O_{(nitro)}$ [248], halogen···O=C [249] and carbonyl interactions [250]. Short intermolecular oxygen···oxygen distances with values substantially less than 3.04Å, the sum of the van der Waals radii for O (1.52Å) [244], were investigated to that effect. Dipolar nitro group interactions were accepted for nitrogen···oxygen contacts less than 3.17Å. The value of 3.17Å was chosen as the sum of the van der Waals radii of nitrogen and oxygen plus a tolerance value of 0.1 Å. [244] Given these values, two dipolar nitro group contacts were identified. Those two interactions were found for the $N_2O_4O_5$ nitro group interacting with the $N_5O_{11}O_{12}$ nitro group in one case and with itself in the other leading to oxygen···oxygen distances with values of 2.8519 (18) Å (O_5···O_{12}) and 2.8251 (15) Å (O_4···O_4). The correspondig values for the nitrogen···oxygen contacts are 3.1184 (17) Å (O_5···N_5) and 3.1234 (16) Å (O_4···N_2). Figure 2.81 displays the symmetric interaction of the two $N_2O_4O_5$ nitro groups.

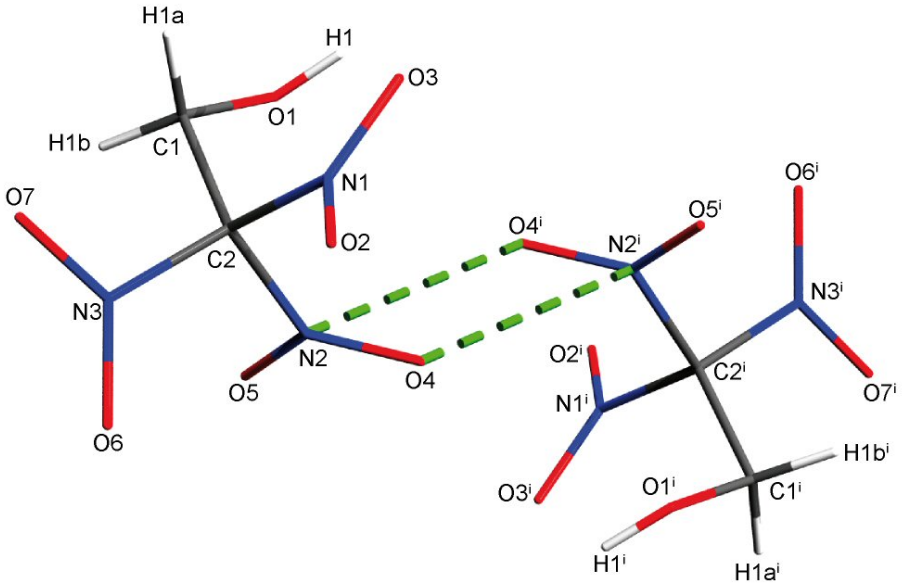

Figure 2.81. Example of dipolar nitro group interaction in trinitroethanol. The interaction between the N_2 and the O_4 atoms [d(O···N^i) = 3.1234 (16) Å, symmetry code i = -x+1, -y+1, -z+1] obviously brings the O atoms into close proximity. [234]

Bis-(2,2,2-trinitroethyl)-amine (BTNA)

BTNA is a high oxygen explosive (oxygen balance Ω = +7.0) and a valuable intermediate in the preparation of energetic materials. However, the structure had not been reported previously. The structure of BTNA at 200 K displays orthorhombic symmetry, space group P*bca* (no.61). The asymmetric unit consists of one bis-(2,2,2-trinitroethyl)-amine molecule (Fig. 2.82).

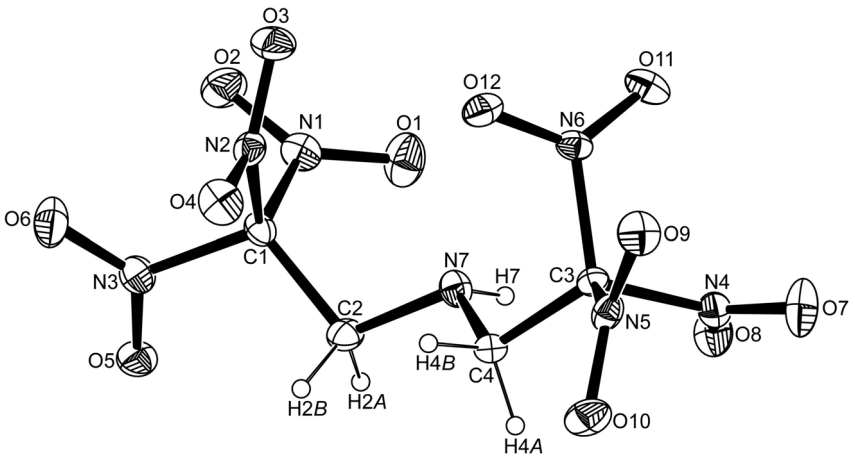

Figure 2.82. ORTEP representation of the molecular structure of BTNA in the crystalline state (right picture). Displacement ellipsoids are shown at the 50 % probability level. Selected bond lengths [Å] and angles [°]: C_1-N_1 1.524(2), N_1-O_1 1.206(2), N_1-O_2 1.215(2), C_1-C_2 1.521(2), C_2-N_7 1.457(2), O_1-N_1-O_2 127.31(16), N_1-C_1-N_2 107.57(12), N_1-C_1-C_2 114.24 (14), C_1-C_2-N_7 109.28(13), C_2-N_7-C_4 113.54(14).

The two trinitroethyl moieties display a very similar molecular geometry with a propeller-type orientation of the nitro groups bonded to the β carbon atom. In both moieties the conformation of the substituents of the α- as well as the β carbon atom is found to be staggered. The length of the C-N bonds joining the three nitro groups to the β carbon atom (range 1.513 (2) Å - 1.530 (2) Å) are significantly longer than the C-N bond distances joining the trinitroethyl moieties to the secondary amine that lie in the normal range of 1.47 Å [246] as observed in the determination of the crystal structures of 2,2,2-trinitroethanol, [234] bis(2,2,2-trinitroethyl)carbonate, [235] and *N*,*N*'-bis-(2,2,2-trinitroethyl)urea. [247] The independent N-C-N bond angles of the trinitromethyl group are less (range 104.9 (1)° - 108.2 (1)°) than the tetrahedral value whereas the corresponding N-C-C bond angles are close to or greater (range 109.5 (1)° -

114.2 (1)°) than the tetrahedral value. The six independent nitro groups of each molecule are identical in structure within the limits of error and display common geometry parameters. In turn, the arrangement of the C-N and N-O bonds is coplanar with the sums of the three bond angles around one nitrogen atom being 360° within the limits of error. The extended structure of BTNA involves secondary interactions in terms of intermolecular C—H···O hydrogen bonding as well as dipolar nitro group interactions. The amine proton is involved in one intermolecular N—H···O hydrogen bond (N_7-H_7···O_{10}, symmetry code: x-1/2, -y+1/2, -z+1) and two intramolecular hydrogen bonds (N_7-H_7···O_1 and N_7-H_7···O_8). Figure 2.83 displays the unit cell packing of BTNA together with trinitroethyl mediated intermolecular interactions. A color code was chosen in order to more clearly reveal the packing mode of the crystal structure of BTNA when comparing the two different views of the unit cell in Figure 2.83 with grey denoting all the molecules the unit cell is comprised of whereas the colors blue, orange, red and light blue were used in order to highlight the underlying packing motiv. The wave like pattern present in the view along the crystallographic *b* axis turns out to be comprised of molecules of two different layers when looking at the structure along the crystallographic *a* axis. The view along the crystallographic *b* axis reveals two dipolar nitro group interactions (green dashed lines) connecting the molecules along the crystallographic *a* and *c* axis (left picture). Intermolecular C—H···O hydrogen bonding (yellow dashed lines) between two BTNA molecules results in two membered, infinite chains oriented along the crystallographic *b* axis (right picture).

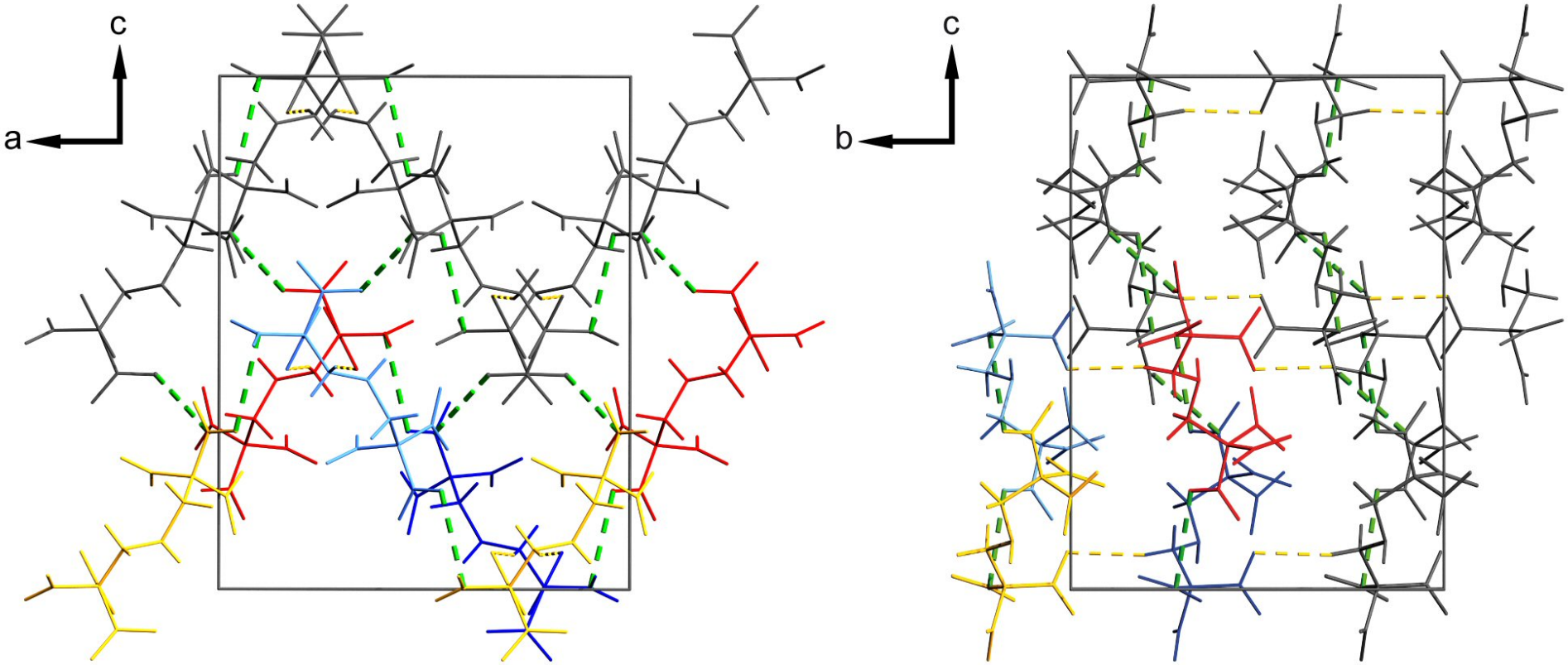

Figure 2.83. Unit cell packing of BTNA. Yellow dashed lines indicate trinitroethyl mediated intermolecular hydrogen bonding (C_4-H_{4A}···O_{12}^{i}). Green dashed lines indicate dipolar nitro group interactions. Two dipolar nitro group interactions were found with the $N_3/O_5/O_6$ nitro group interacting with the $N_4/O_7/O_8$ nitro group (contact distances: 3.174(2) Å [N_3···O_8^{ii}]; 3.039(2) Å [O_6···O_8^{ii}]) and the $N_5/O_9/O_{10}$ nitro group (contact distance: 3.1468(2) Å [N_5···O_5^{iii}]; Symmetry code: (i) 3/2-x, 1/2+y, z; (ii) x, 1/2-y, -1/2+z; (iii) 1/2+x, y , 1/2-z.

N^1-(2,2,2-trinitroethyl)-1*H*-tetrazole-1,5-diamine (TTD)

The structure of TTD at 100K has orthorhobic symmetry, space group $Pna2_1$. The asymmetric unit consists of one molecule (Fig. 2.84).

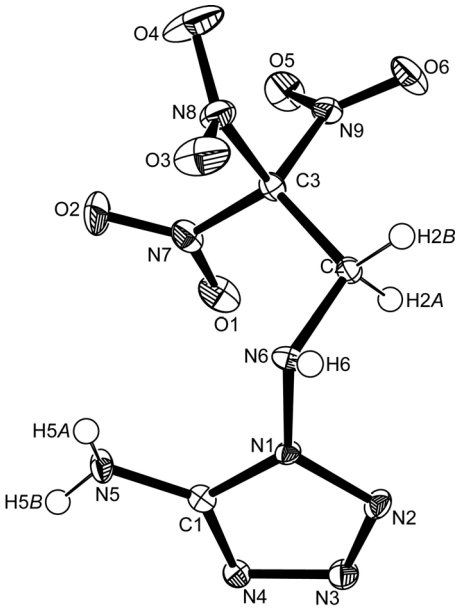

Figure 2.84. ORTEP representation of the molecular structure of TTD in the crystalline state. Displacement ellipsoids are shown at the 50 % probability level. Selected bond lengths [Å] and angles [°]: C_3-N_9 1.525(3), N_9-O_6 1.221(3), N_9-O_5 1.207(3), C_3-C_2 1.522(3), C_2-N_6 1.459(3), N_1-N_6 1.386(2), N_1-C_1 1.352(3), N_1-N_2 1.369(3), N_2-N_3 1.286(3), N_3-N_4 1.380(3), C_1-N_4 1.325(3), C_1-N_5 1.333(3), O_5-N_9-O_6 127.5(2), N_9-C_3-N_8 104.81(17) , N_9-C_3-C_2 112.27(19), C_3-C_2-N_6 109.98(17), C_2-N_6-N_1 114.47(17), N_6-N_1-N_2 124.05(18), N_6-N_1-C_1 126.29(19), N_1-C_1-N_5 124.14(19).

The geometry parameters of the trinitroethyl group of the TTD molecule agree well with the aforementioned details in the discussion of the BTNA molecule. Furthermore, the tetrazole unit displays common structural bond length and angles compared to 1,5-diamino-1*H*-1,2,3,4-tetrazole with the 5-amino group being conjugated with the π-system of the tetrazole ring and the 1-amino group being sp^3-hybridized and nonconjugated. The molecular packing reveals four types of secondary interactions in terms of $N_{(amino)}$—H···$N_{(tetrazole)}$ hydrogen bonding, C—H···$N_{(tetrazole)}$ hydrogen bonding, C—H···O hydrogen bonding and dipolar nitro group interactions resulting in a strong three dimensional network with each the tetrazole rings and the trinitromethyl moieties packed in chains along the *b* axis and alternating along the *a* axis (Fig. 2.85).

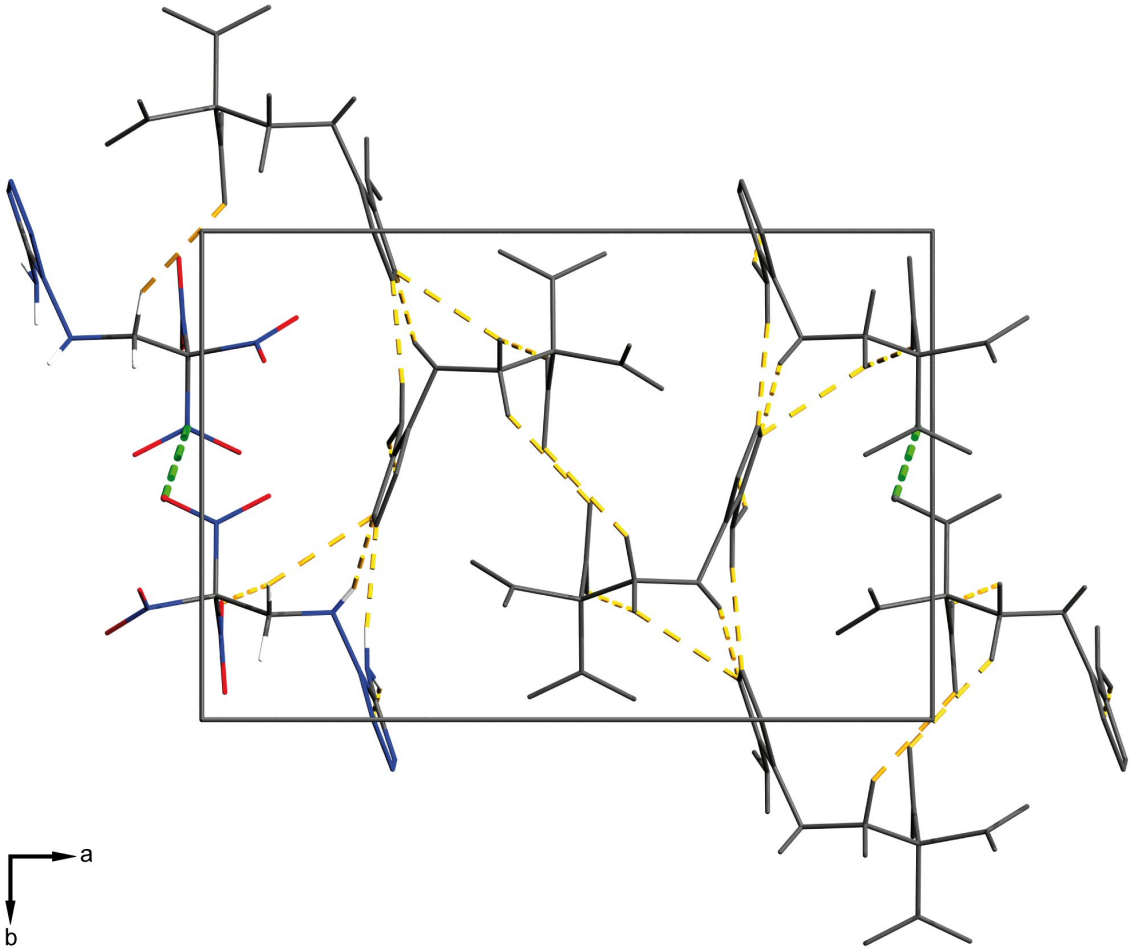

Figure 2.85. Unit cell packing of TTD, viewed along the *c* axis. Yellow dashed lines indicate intermolecular hydrogen bonding (N_5-H_{5A}···N_3^{i}, N_5-H_{5B}···N_2^{ii}, N_6-H_6···N_4^{iii}, C_2-H_{2A}···N_4^{iii}, C_2-H_{2A}···O_2^{iv}, C_2-H_{2B}···O_1^{v}). Green dashed lines indicate dipolar nitro group interactions. One dipolar nitro group interaction was found between two $N_8/O_3/O_4$ nitro groups (contact distances: 3.270(3) Å [N_8···O_3^{vi}]; 3.051(3) Å [O_3···O_4^{vii}]); Symmetry code: (i) 3/2-x, 1/2+y, 1/2+z, (ii) x, y, 1+z, (iii) 3/2-x, 1/2+y, -1/2+z, (iv) x, y, -1+z, (v) 2-x, -y, -1/2+z, (vi) 2-x, 1-y, -1/2+z, (vii) 2-x, 1-y, 1/2+z.

N^1,N^5-Bis-(2,2,2-trinitroethyl)-1*H*-tetrazole-1,5-diamine (BTTD)

The structure of BTTD at 100K has monoclinic symmetry, space group $P2_1/c$. The asymmetric unit consists of one molecule (Fig. 2.86).

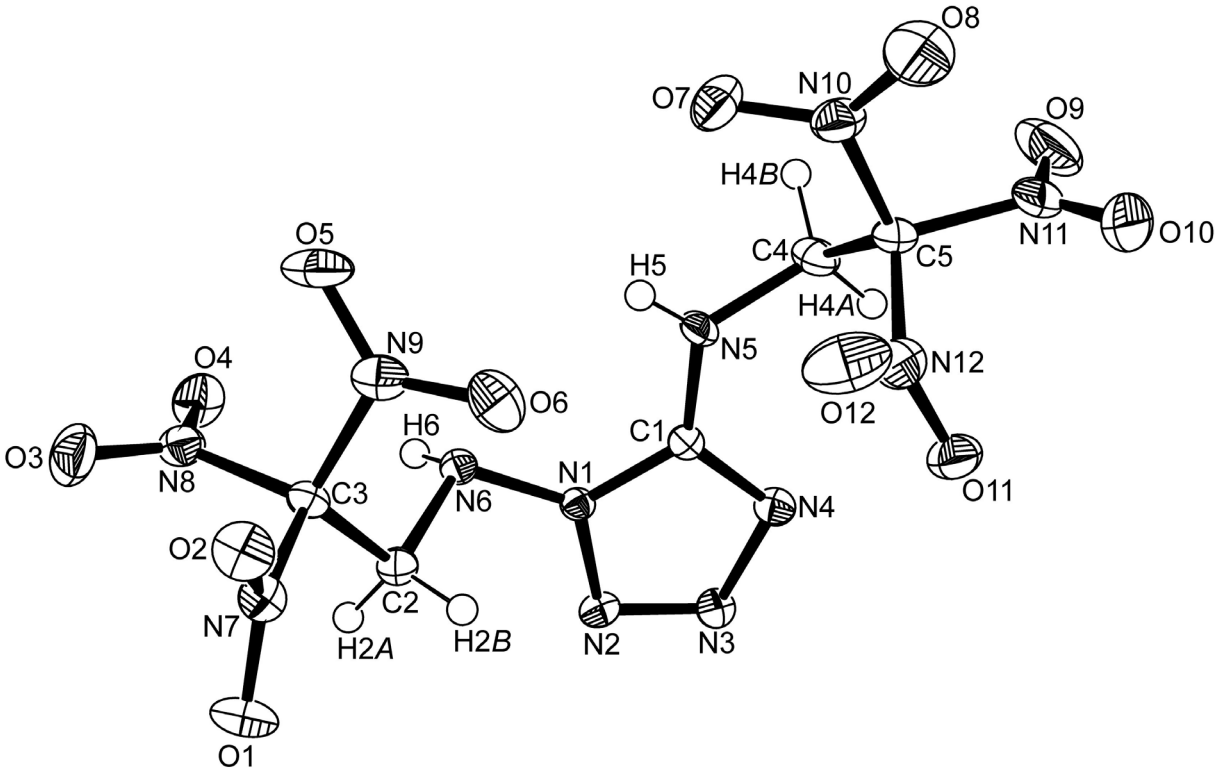

Figure 2.86. ORTEP representation of the molecular structure of BTTD in the crystalline state. Displacement ellipsoids are shown at the 50 % probability level. Selected bond lengths [Å] and angles [°]:C_3-N_9 1.523(5), N_9-O_6 1.214(5), N_9-O_5 1.217(4), C_3-C_2 1.516(5), C_2-N_6 1.469(5), N_1-N_6 1.392(4), N_1-C_1 1.333(5), N_1-N_2 1.369(4), N_2-N_3 1.291(4), N_3-N_4 1.372(4), C_1-N_4 1.322(4), C_1-N_5 1.359(4), N_5-C_4 1.441(5), C_4-C_5 1.522(6), C_5-N_{11} 1.537(5), N_{11}-O_9 1.207(4), N_{11}-O_{10} 1.211(5), O_5-N_9-O_6 127.7(4), N_9-C_3-N_8 106.7(3), N_9-C_3-C_2 111.7(3), C_3-C_2-N_6 109.1(3), C_2-N_6-N_1 111.5(3), N_6-N_1-N_2 124.6(3), N_6-N_1-C_1 126.6(3), N_1-C_1-N_5 123.8(3), C_1-N_5-C_4 119.3(3), N_5-C_4-C_5 111.3(4), C_4-C_5-N_{11} 113.0(3) , N_{11}-C_5-N_{12} 106.3(3), O_9-N_{11}-O_{10}.

The presence of the second trinitroethyl group in the BTTD molecule does not noticeably change either the bond length and angles of the trinitroethyl group or the tetrazole ring compared to TTD and 1,5-diamino-1*H*-1,2,3,4-tetrazole. The 5-amino group remains sp^2 hybridized as indicated by the angles around the N_5 atom being close to 120°. The orientation of the N_5-C_4 bond and the C_1-N_1 bond are *trans* relative to the C_1-N_5 bond directing the N_5 trinitroethyl group into the less sterically demanding position. The 1-amino group remains sp^3 hybridized with the H_6 atom and the C_2 atom being located on different sides of the tetrazole plane and the angles around the N_6 atom being close to the tetrahedral angle. Two BTTD molecules form dimers interconnected with

$N_{(amino)}$—H···$N_{(tetrazole)}$ hydrogen bonding and C—H···$N_{(tetrazole)}$ hydrogen bonding resulting in a stacking of the tetrazole rings along the *b* axis. The $N_7/O_1/O_2$ nitro group interacts with the $N_8/O_3/O_4$ nitro group (contact distances: 2.869(4) Å [N_7···O_3]; 2.908(4) Å [O_2···O_3], 2.927(4) Å [O_1···O_4], symmetry code as in Fig. 2.87) and the $N_9/O_5/O_6$ nitro group interacts with the $N_{11}/O_9/O_{10}$ nitro group (contact distances: 2.896(5) Å [N_{11}···O_5]; 3.041(4) Å [O_5···O_9], symmetry code as in Fig. 2.87). These two dipolar nitro group interactions interconnect one pair of dimers with four surrounding pairs of dimers.

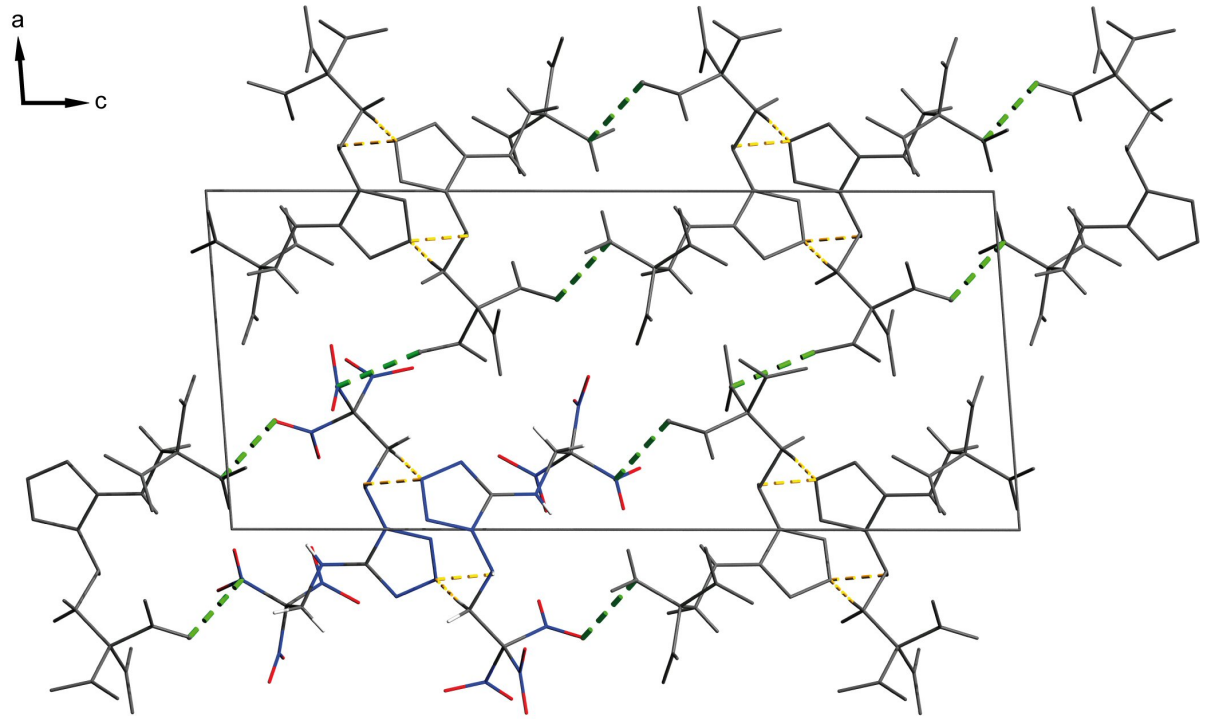

Figure 2.87. Unit cell packing of BTTD, viewed along the *b* axis. Yellow dashed lines indicate hydrogen bonding (N_6-H_6···N_3^{i}, C_2-H_{2B}···N_3^{ii}). Green dashed lines indicate dipolar nitro group interactions. Two dipolar nitro group interactions were found with the $N_7/O_1/O_2$ nitro group interacting with the $N_8/O_3/O_4$ nitro group (contact distances: 2.869(4) Å [N_7···O_3^{iii}]; 2.908(4) Å [O_2···O_3^{iii}], 2.927(4) Å [O_1···O_4^{iv}]) and the $N_9/O_5/O_6$ nitro group interacting with the $N_{11}/O_9/O_{10}$ nitro group (contact distances: 2.896(5) Å [N_{11}···O_5^{v}]; 3.041(4) Å [O_5···O_9^{v}]. Symmetry code: (i) 2-x, 1/2+y, 1/2-z; (ii) 2-x, -1/2+y, z; (iii) 1-x, 1/2+y, 1/2-z; (iv) x, 1+y, z; (v) 2-x, -y, 1-z.

(E)-1-methyl-1-(1*H*-tetrazol-5-yl)-2-(2,2,2-trinitroethylidene)hydrazine (MTTH)

The structure of MTTH at 100K has orthorhombic symmetry, space group *Pbca* (no. 61). The asymmetric unit consists of one molecule (Fig. 2.88).

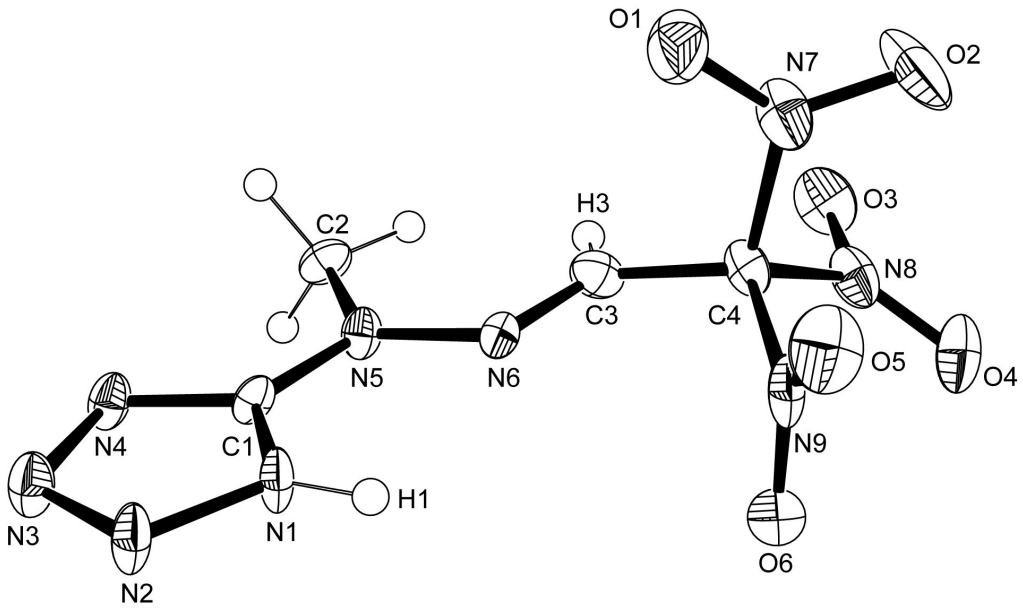

Figure 2.88. ORTEP representation of the molecular structure of (E)-1-methyl-1-(1*H*-tetrazol-5-yl)-2-(2,2,2-trinitroethylidene)hydrazine (MTTH) in the crystalline state. Displacement ellipsoids are shown at the 50 % probability level. Selected bond lengths [Å] and angles [°]: N_1-C_1 1.320(6), N_1-N_2 1.357(6), N_2-N_3 1.290(6), N_3-N_4 1.363(6), N_4-C_1 1.315(6), C_1-N_5 1.369(6), N_5-C_2 1.460(6), N_5-N_6 1.355(6), N_6-C_3 1.255(7), C_3-C_4 1.475(8), C_4-N_8 1.516(7), N_8-O_3 1.221(6), N_8-O_4 1.219(6), N_1-C_1-N_5 124.8(5), C_1-N_5-C_2 121.4(4), C_1-N_5-N_6 114.5(4), N_5-N_6-C_3 119.4(5), N_6-C_3-C_4 117.6(6), C_3-C_4-N_8 113.4(5), N_1-C_1-N_5-N_6 -6.1(7), N_1-C_1-N_5-C_2 179.0(5), C_1-N_5-N_6-C_3 -177.1(5), N_5-N_6-C_3-C_4 175.3(4).

MTTH is a rare example of a compound containing the trinitroethaniminyl moiety. Currently there are only eight entries in the SciFinder Database and only three of those entries contain experimental evidence for molecules containing this fragment and the structure determination was based on elemental analysis and spectral characteristics. [251-253] To our knowledge, MTTH represents the first example of a structurally characterized molecule containing this trinitroethylidene moiety. Bond length and angles of the tetrazole ring show no noticeable differences compared to other tetrazole containing molecules and neither do the geometrical parameter of the trinitromethyl group. The value of the N_5-N_6 bond length of the hydrazine

group is shorter (1.355(6) Å) compared to free hydrazine (1.46 Å) [254] due to mesomerism between the sp^2-type N_6 nitrogen atom and the sp^2-type C_3 carbon and is in fair accordance with the N-N bond length reported for diethyl 1,2-hydrazinedicarboxylate (1.385 Å) [255] and diisopropyl hydrazocarboxylate molecule (1.381(2) Å). [256] With the exception of the C_2 methyl hydrogen atoms and the three nitro groups of the trinitromethyl group, the whole molecule is planar within a few degrees. The torsional angles are given in the caption of Figure 2.89. The value of the C_3-C_4 carbon bond (1.475(8)Å) is significantly shorter compared to a standard carbon single bond (1.54Å) [257] or the corresponding bond distances of the trinitroethyl group (2,2,2-trinitroethanol (1.5352(19)Å), MMTHT (1.5109(19)Å)) reflecting the higher s-character of the C_3 carbon atom of the trinitroethylidene moiety.

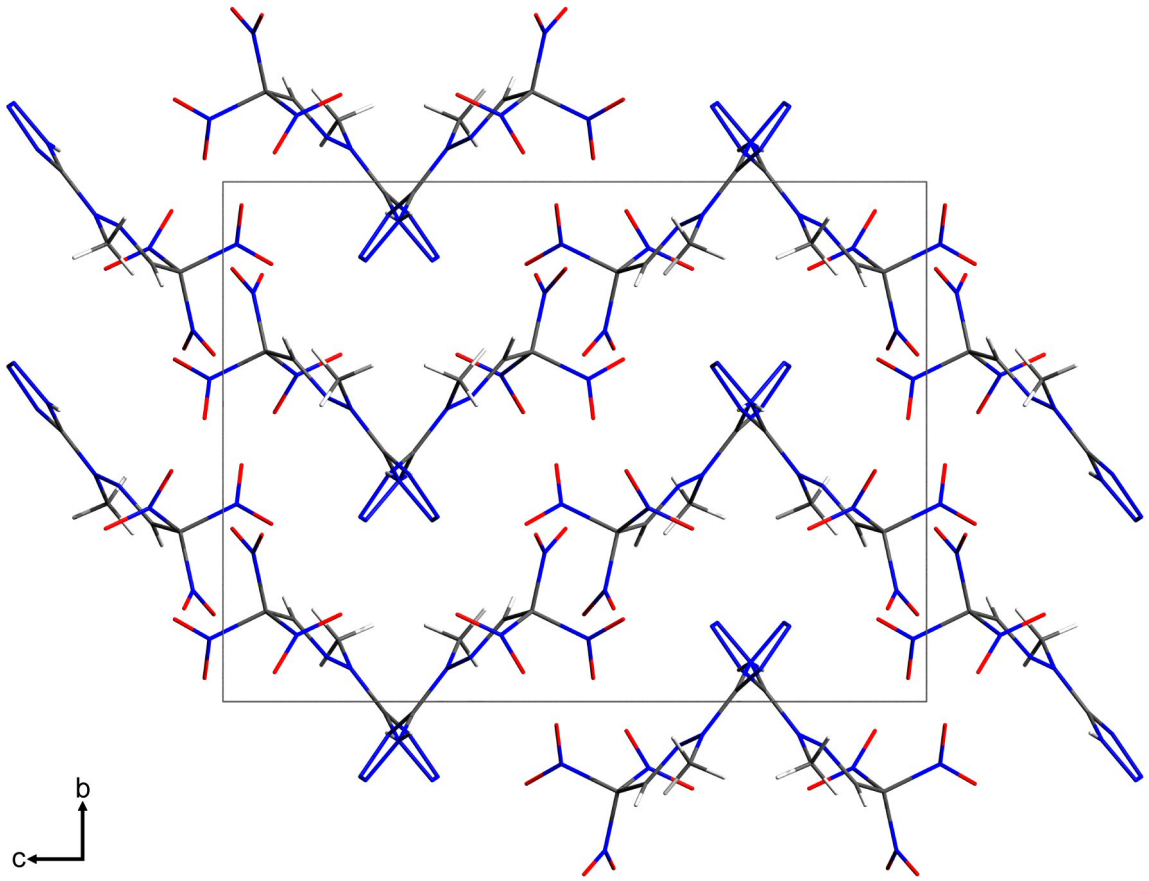

Figure 2.89. (E)-1-methyl-1-(1*H*-tetrazol-5-yl)-2-(2,2,2-trinitroethylidene)hydrazine (MTTH), viewed along the *b* axis, viewed along the *a* axis.

The extended structure of MTTH displays intermolecular N_1-H_1···$N_{4,ring}$ hydrogen bonding that mainly governs the molecular packing of the compound (Figs. 2.90 and 2.91), a characteristic feature of N-H substituted tetrazoles as has exemplarily shown by Goddard *et al.* for the parent compound (α-tetrazole). (258)

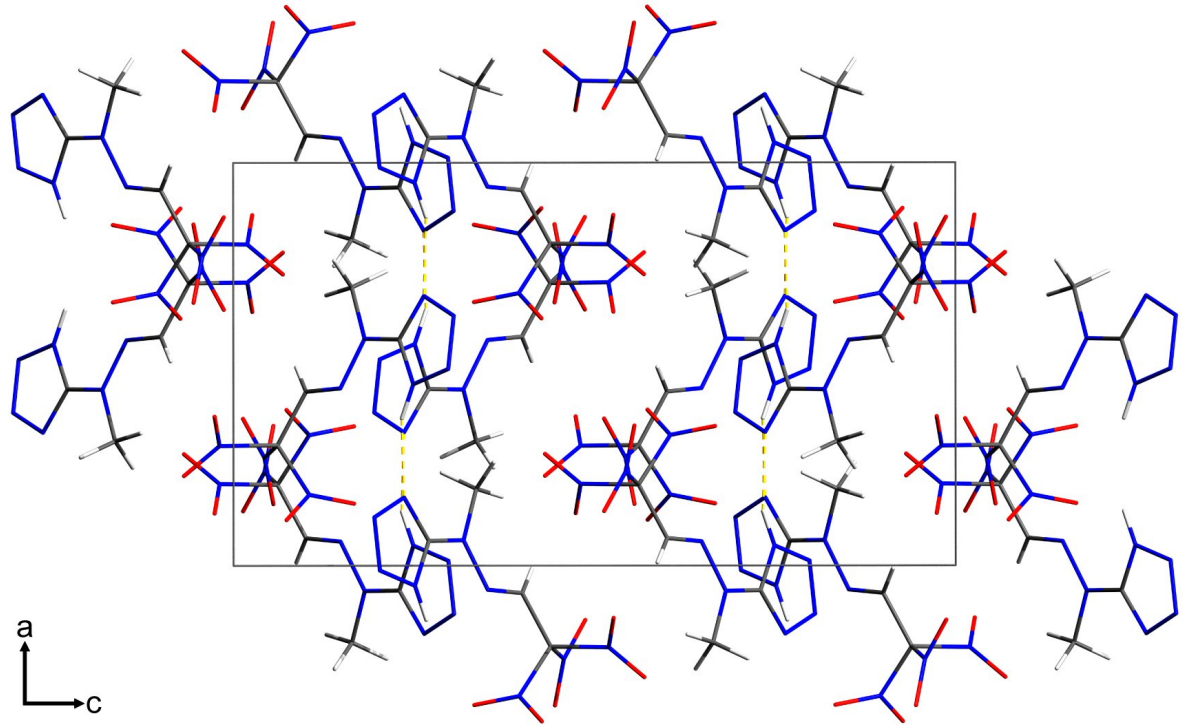

Figure 2.90. Unit cell packing of (E)-1-methyl-1-(1*H*-tetrazol-5-yl)-2-(2,2,2-trinitroethylidene)hydrazine (MTTH), viewed along the *b* axis. Yellow dashed lines indicate intermolecular hydrogen bonding (N_1-H_1···N_4^i); Symmetry code: (i) 1/2+x, y, 1/2-z.

Due to the presence of the trinitroethylidene moiety, the characteristic hydrogen bonding of the acidified methylene-type hydrogen atoms of trinitroethyl substituted compounds is no longer possible in this compound yielding a crystal density of 1.69 g cm^{-3}. Moreover, the remaining hydrogen atom is not involved in intermolecular hydrogen bonding. However, we observe interaction of a nitro group and the π electrons of the tetrazole ring (Fig. 2.91).

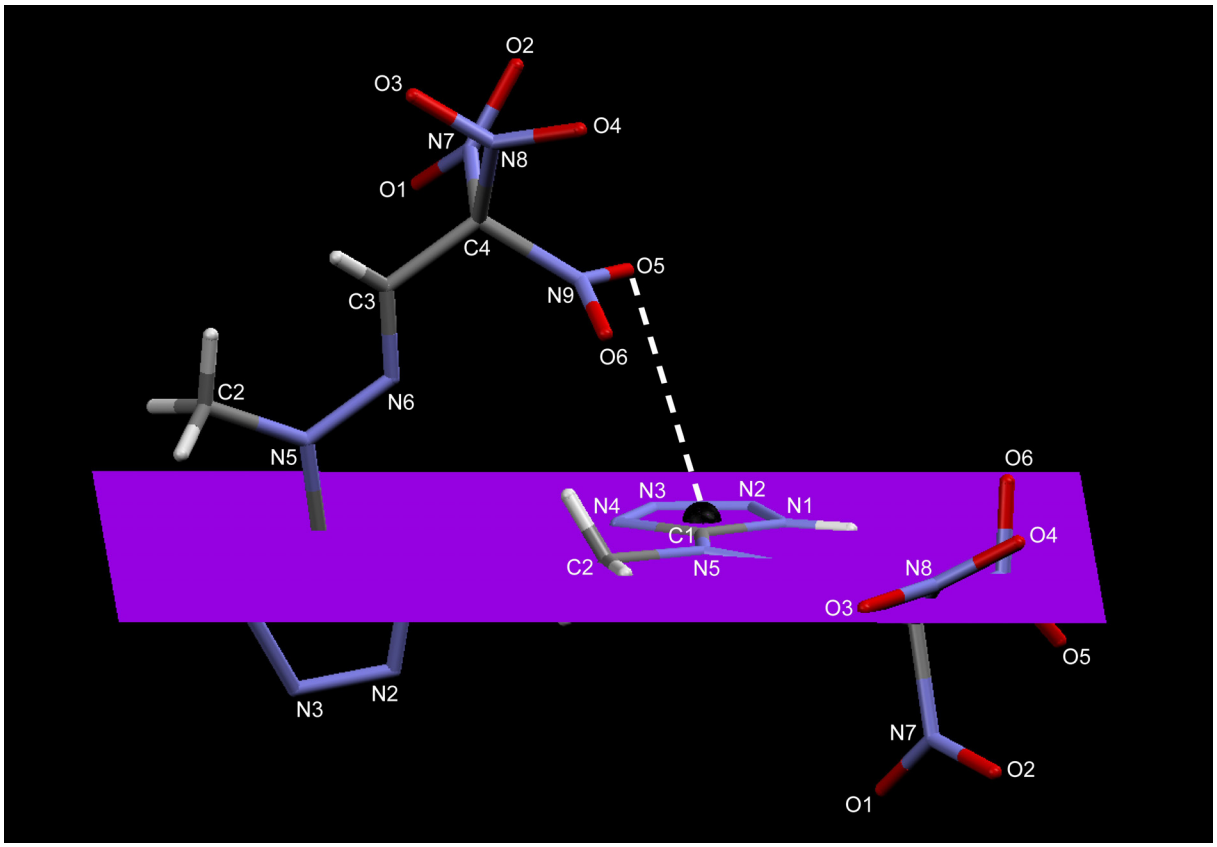

Figure 2.91. N_9-O_5···Centre of Gravity(C_g, π ring) Interaction. Distance O_5···C_g (π-Ring): 3.372(6) Å, O_5···plane$_{(\text{perpendicular projecton of } O5)}$: 3.222 Å, angle γ ($C_g$- O_5-plane$_{(\text{perpendicular projecton of } O6)}$: 17.13°.

1-methyl-5-(1-methyl-2-(2,2,2-trinitroethyl)hydrazinyl)-1*H*-tetrazole (MMTHT)

The structure of MMTHT at 100K has triclinic symmetry, space group P-1 (no. 2). The asymmetric unit consists of one molecule (Fig. 2.92).

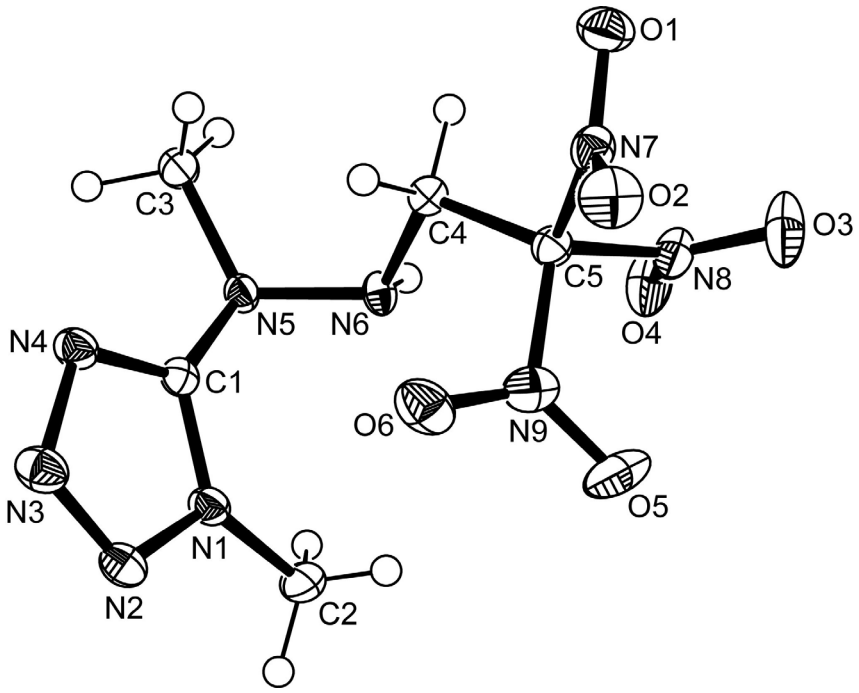

Figure 2.92. ORTEP representation of the molecular structure of 1-methyl-5-(1-methyl-2-(2,2,2-trinitroethyl)hydrazinyl)-1*H*-tetrazole (MMTHT) in the crystalline state. Displacement ellipsoids are shown at the 50 % probability level. Selected bond lengths [Å] and angles [°]: C_1-N_1 1.3425(18), N_1-N_2 1.3527(16), N_2-N_3 1.2888(17), N_3-N_4 1.3620(15), C_1-N_5 1.3782(16), N_5-N_6 1.4311(16), N_6-C_4 1.4616(18), C_4-C_5 1.5109(19), C_5-N_9 1.5162(18), N_9-O_6 1.2154(16), N_9-O_5 1.2158(17), N_1-C_2 1.4538(20), N_5-C_3 1.4663(19), C_1-N_5-N_6 111.5(1), C_1-N_5-C_3 115.5(1), C_3-N_5-N_6 117.0(1), N_5-N_6-C_4 112.5(1), N_5-N_6-H_6 103.6(1), H_6-N_6-C_4 112.4(1), C_1-N_5-N_6-C_4 -88.0(1).

Of interest, the structure of MMTHT may be compared to the previous structure, MTTH. The two structures are quite similar in terms of molecular connectivity but differ in the substitution of the N_1 ring nitrogen and C_4 carbon atoms as well as in the hybridization of the N_6 nitrogen and C_4 carbon atoms. The N_1 ring nitrogen atom of MMTHT carries a methyl group in contrast to the hydrogen atom of MTTH, the C_4 carbon atom of MMTHT has two hydrogen atoms compared to only one hydrogen atom in MTTH and the N_6 nitrogen atom of the hydrazine group and the C_4 carbon atom of MMTHT are

sp^3 hybridized in contrast to the sp^2-type hybridization observed in MTTH. As a consequence, the hydrazine group of MMTHT no longer has a planar geometry but the typical gauche conformation characteristic for hydrazine (Fig. 2.93).

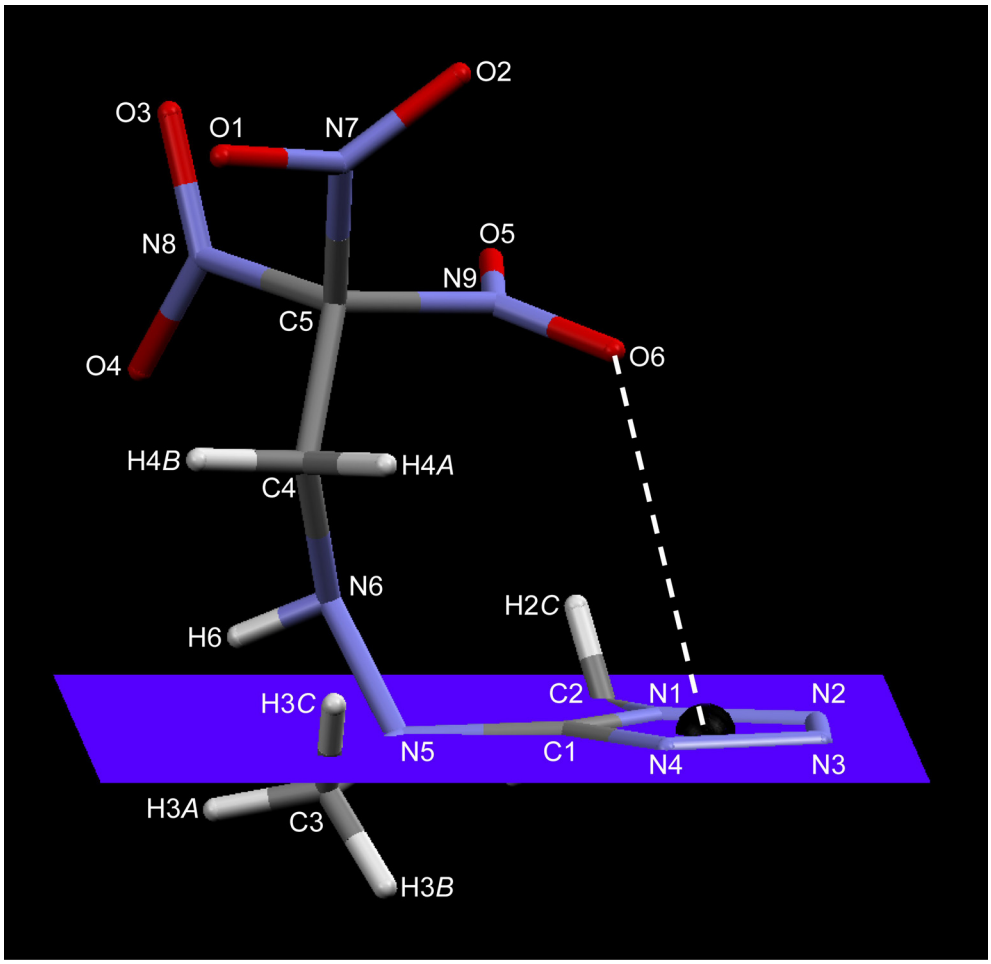

Figure 2.93. N_9-O_6···Centre of Gravity(C_g, π ring) Interaction. Distance O_6···C_g (π-Ring): 3.268(2) Å, O_6···plane$_{(\text{perpendicular projecton of } O6)}$: 3.055 Å, angle γ ($C_g$- O_6-plane$_{(\text{perpendicular projecton of } O6)}$): 20.83°.

The N_5-N_6 bond length of the hydrazine group of MMTHT (1.4311(16) Å) closely resembles that of free hydrazine (1.46 Å) [254]. The gauche conformation of the hydrazine group is stabilized by intramolecular nitro group - π-Ring interaction.

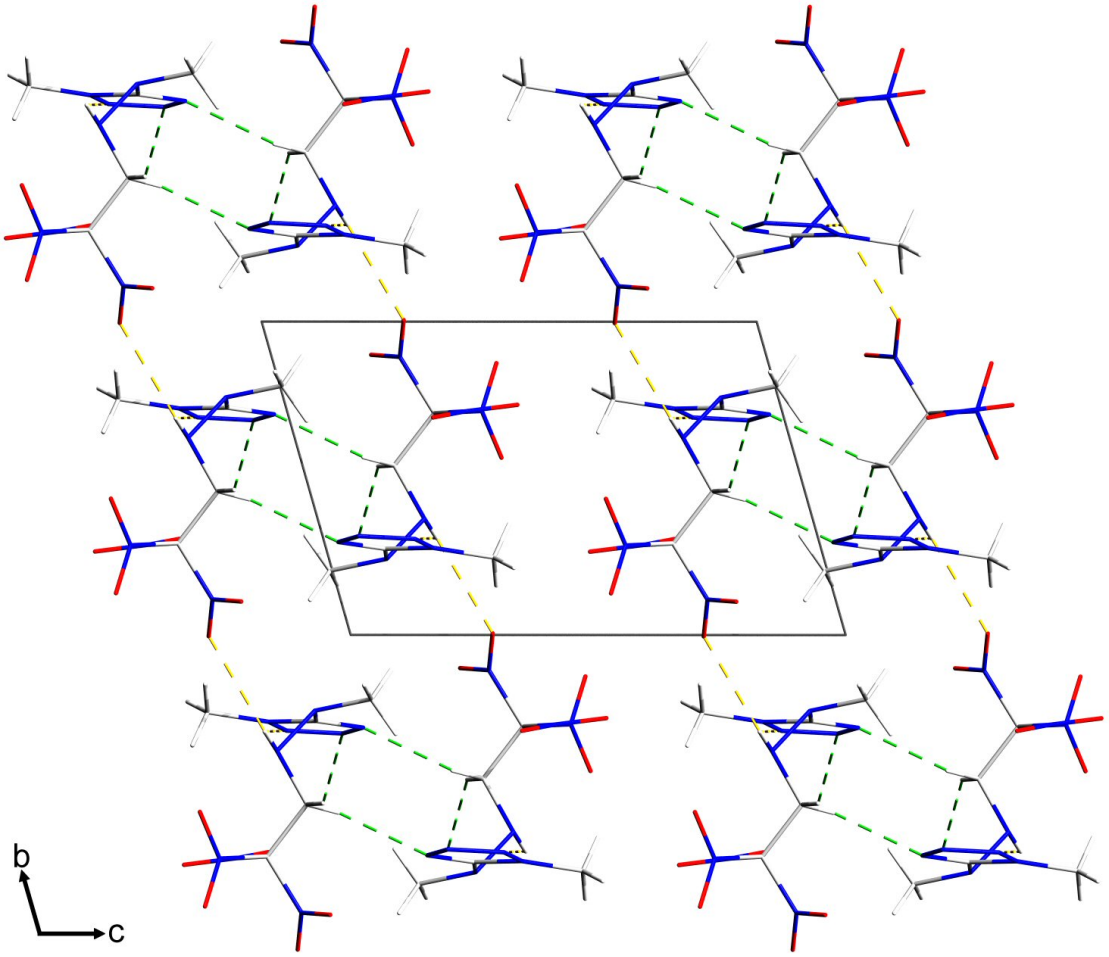

Figure 2.94. Unit cell packing of 1-methyl-5-(1-methyl-2-(2,2,2-trinitroethyl)hydrazinyl)-1H-tetrazole (MMTHT), viewed along the *a* axis. Yellow dashed lines indicate intermolecular hydrogen bonding (N_6-H_6···O_2^{i}, N_6-H_6···N_2^{ii}). Green dashed lines indicate intermolecular hydrogen bonding of the acidified methylene type hydrogen atoms of the trinitroethyl moiety (C_4-H_{4A}···N_4^{iii}, C_4-H_{4B}···N_3^{ii}); Symmetry code: (i) x, -1+y, z; (ii) 1+x, 1+y, z; (iii) 1-x, 1-y, -z.

The extended structure of MMTHT is shown in Figure 2.94. The acidified methylene-type hydrogen atoms are involved in intermolecular hydrogen bonding yielding a pair of dimers running along the crystallographic *a* axis (C_4-H_{4A}···N_4, C_4-H_{4B}···N_3, Fig. 2.94). Due to the presence of the methyl groups, the characteristic intermolecular N-H···N_{ring} hydrogen bonding frequently observed in tetrazole compounds cannot occur. However, the hydrazinic-type hydrogen atom H_6 is involved in a bifurcated hydrogen bond (N_6-H_6···O_2, N_6-H_6···N_2, Fig. 2.94) towards both the tetrazole ring and one nitro group interconnecting the pairs of dimers formed due to C-H···N hydrogen bonding and mentioned above. Compared to MTTH (1.69 g cm^{-3}), the crystal density of MMTHT (1.63 g cm^{-3}) is slightly lower although – a tribute to the two bulky methyl groups present in MMTHT.

2-(5-(1-methyl-2-(2,2,2-trinitroethyl)hydrazinyl)-1*H*-tetrazol-1-yl)ethanol (MTHTE)

The structure of MTHTE at 100K has monoclinic symmetry, space group $P2_1/c$ (no. 14). The asymmetric unit consists of one molecule (Fig. 2.95).

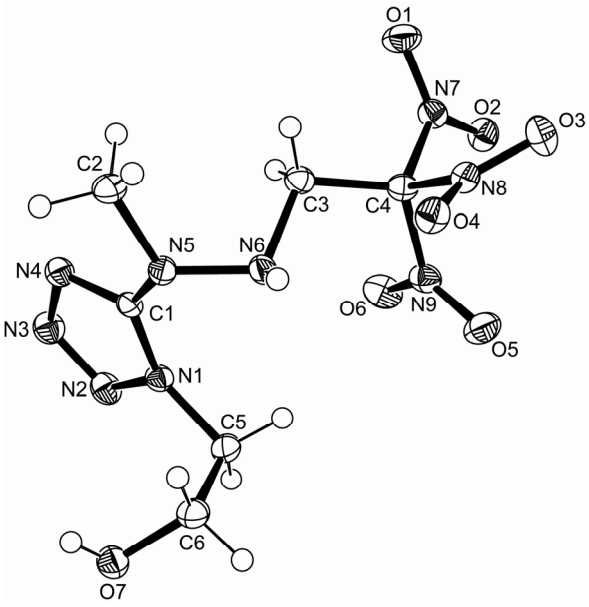

Figure 2.95. ORTEP representation of the molecular structure of 2-(5-(1-methyl-2-(2,2,2-trinitroethyl)hydrazinyl)-1H-tetrazol-1-yl)ethanol (MTHTE) in the crystalline state. Displacement ellipsoids are shown at the 50 % probability level. Selected bond lengths [Å] and angles [°]: C_1-N_1 1.3476(15), N_1-N_2 1.3567(14), N_2-N_3 1.2838(15), N_3-N_4 1.3685(15), N_4-C_1 1.3240(15), N_1-C_5 1.4723(16), C_5-C_6 1.5118(19), C_6-O_7 1.4195(15), C_1-N_5 1.3720(15), N_5-C_2 1.4662(15), N_5-N_6 1.4232(14), N_6-C_3 1.4713(16), C_3-C_4 1.5113(17), C_4-N_8 1.5223(15), N_8-O_3 1.2157(13), N_8-O_4 1.2178(13), N_1-C_1-N_5 126.47(11), C_1-N_5-C_2 116.18(10), C_1-N_5-N_6 114.68(9), N_5-N_6-C_3 110.79(9), N_6-C_3-C_4 110.08(10), C_3-C_4-N_8 112.41(10), C_1-N_5-N_6-C_3 92.93(12), C_2-N_5-N_6-C_3 -49.10(14), N_5-C_1-N_1-N_2 174.27(11), N_5-C_1-N_1-C_5 4.9(2), C_6-C_5-N_1-C_1 69.05(16), C_6-C_5-N_1-N_2 -99.28(13), N_4-C_1-N_5-N_6 -141.91(12), N_1-C_1-N_5-N_6 43.89(16), N_4-C_1-N_5-C_2 0.68(17), N_1-C_1-N_5-C_2 -173.52(12).

The presence of the hydroxyethyl group in MTHTE compared to the methyl group present in MMTHT does not noticeably change the values of bond lengths or bond angles. The gauche conformation of the hydrazine group is retained and the hydrazinic-type H_6 hydrogen atom is involved in a bifurcated hydrogen bond yielding one intramolecular hydrogen bond (N_6-H_6···O_4) and one intermolecular hydrogen bond (N_6-H_6···O_2, Fig. 2.96).

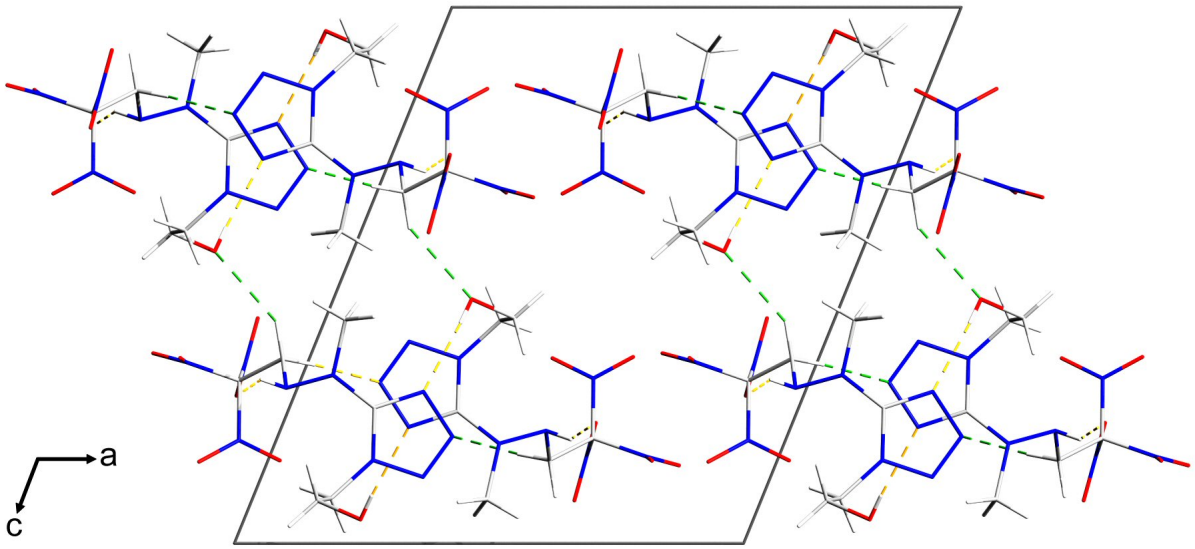

Figure 2.96. Unit cell packing of 2-(5-(1-methyl-2-(2,2,2-trinitroethyl)hydrazinyl)-1H-tetrazol-1-yl)ethanol (MTHTE), viewed along the *b* axis. Yellow dashed lines indicate intermolecular hydrogen bonding (N_6-H_6···O_2^{i}, O_7-H_7···N_4^{ii}). Green dashed lines indicate intermolecular hydrogen bonding of the acidified methylene type hydrogen atoms of the trinitroethyl moiety (C_3-H_{3A}···O_7^{iii}, C_3-H_{3B}···N_3^{iv}); Symmetry code: (i) x, -1+y, z; (ii) 3/2-x,-1/2+y,1/2-z; (iii) -1/2+x,3/2-y,-1/2+z; (iv) 3/2-x,1/2+y,1/2-z.

Additional intermolecular contacts include hydrogen bonding of the hydroxyl group to a ring nitrogen atom (O_7-H_7···N_4, Fig. 2.96) as well as a non-covalent dipolar interaction between the oxygen atom of the hydroxyl group and the nitrogen atom of a nitro group of a neighbouring molecule as indicated by the distance between these two atoms which is shorter than the sum of the van der Waals radii of these atoms (d(vdW) =3.07 Å, d(O_7···N_8) = 2.96 Å). The characteristic hydrogen bonding of the acidified methylene-type hydrogen atoms of the trinitroethyl moiety can be observed and both of the hydrogen atoms are involved in intermolecular contacts. The first hydrogen atom is part of a bond to the hydroxyl oxygen atom (C_3-H_{3A}···O_7, Fig. 2.96) and the second hydrogen atom forms a bond to a ring nitrogen atom (C_3-H_{3B}···N_3, Fig. 2.96) yielding a crystal density of 1.63 g cm^{-3}. By comparison, the values of MMTHT and MTHTE have the same crystal density values indicating that the additional bonding interactions of the hydroxyethyl group (MTHTE) compared to the methyl group (MMTHT) are counterbalanced by its sterically more demanding nature.

1-(^{4}N-2,2,2-trinitroethyl)-2,5-Hydroxymethyltriazine (THMT)

The structure of THMT at 100K has monoclinic symmetry, space group $P2_1/n$ (no. 14). The asymmetric unit consists of one molecule (Fig. 2.97).

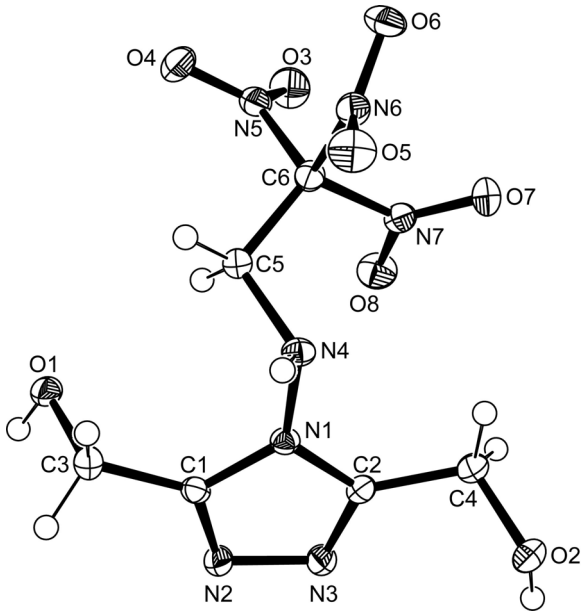

Figure 2.97. ORTEP representation of the molecular structure of 1-(^{4}N-2,2,2-trinitroethyl)-2,5-hydroxymethyltriazine (THMT) in the crystalline state. Displacement ellipsoids are shown at the 50 % probability level. Selected bond lengths [Å] and angles [°]: C_1-N_2 1.3082(18), N_2-N_3 1.3946(17), N_3-C_2 1.3051(18), C_2-N_1 1.3686(18), C_1-N1 1.3702(18), C_1-C_3 1.488(2), C_3-O_1 1.4298(18), C_2-C_4 1.494(2), C_4-O_2 1.4238(18), N_1-N_4 1.4050(16), N_4-C_5 1.4618(19), C_5-C_6 1.516(2), C_6-N_5 1.5158(19), N_5-O_3 1.2163(15), N_5-O_4 1.2147(16), O_1-C_3 C_1 110.50(12), C_2-C_4-O_2 110.96(12), N_1-N_4-C_5 112.71(12), N_4-C_5-C_6 109.77(12), C_5-C_6-N_5 111.01(12), N_1-C_1-C_3-O_1 90.96(18), N_2-C_1-C_3-O_1 -87.46(18), N_3-C_2-C_4-O_2 -58.9(2), N_1-C_2-C_4-O_2 115.07(15), C_2-N_1-N_4-C_5 120.40(15), C_1-N_1-N_4-C_5 -56.99(18), C_6-C_5-N_4-N_1 -120.43(13), N_4-C_5-C_6-N_5 165.54(12).

The presence of the triazole ring compared to 1,5-diamino-1*H*-1,2,3,4-tetrazole in TTD or BTTD does not noticeably change either the bond length and angles of the trinitroethyl group or the hydrazinic group. The hydrazinic-type amino group remains sp^3 hybridized with the H_4 atom and the C_5 atom being located on different sides of the triazole plane and the angles around the N_4 atom being close to the tetrahedral angle (Fig. 2.97). The orientation of the C_4-O_2 bond is pointing in the opposite direction relative to the C_3-O_1 bond directing the C_4-O_2 hydroxymethyl group into the less sterically demanding position. This geometry is stabilized by intramolecular hydrogen bonds (C_4-H_{4A}···N_4 and C_5-H_{5A}···O_1, Fig. 2.98).

The extended structure of THMT reveals both intermolecular non-covalent dipolar interactions and intermolecular hydrogen bonding.

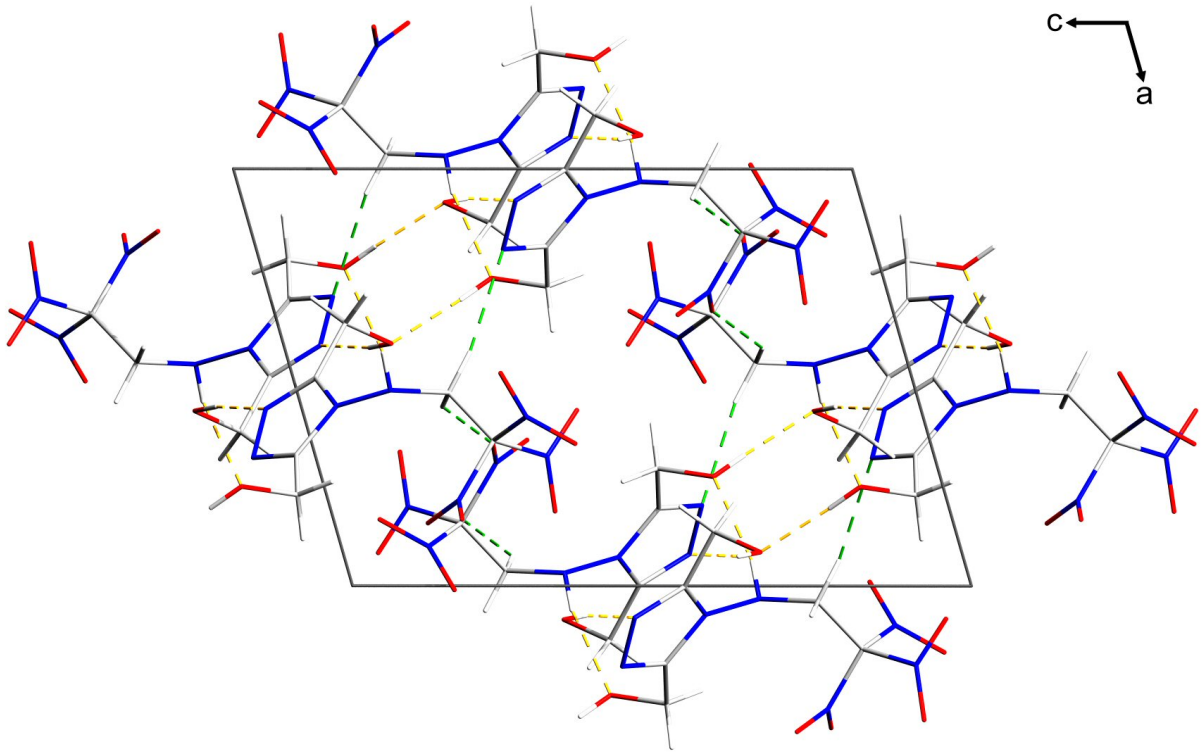

Figure 2.98. Unit cell packing of 1-(⁴N-2,2,2-Trinitroethyl)-2,5-hydroxymethyltriazine (THMT), viewed along the *b* axis. Yellow dashed lines indicate intermolecular hydrogen bonding (O_1-H_1···N_2^{i}, O_2-H_2···O_1^{ii}, N_4-H_4···O_2^{iii}). Green dashed lines indicate intermolecular hydrogen bonding of the acidified methylene type hydrogen atoms of the trinitroethyl moiety (C_5-H_{5A}···O_7^{iv}, C_5-H_{5B}···N_3^{V}); Symmetry code: (i) -x,1-y,1-z, z; (ii) 1/2+x,1/2-y,1/2+z; (iii) -x,-y,1-z; (iv) 1/2-x,1/2+y,1/2-z; (v) -1/2+x,1/2-y,-1/2+z.

Intramolecular hydrogen bonding includes contacts between a hydroxyl group and a ring nitrogen atom (O_1-H_1···N_2, Fig. 2.98), two hydroxyl groups (O_2-H_2···O_1, Fig. 2.98), the hydrazinic-type hydrogen atom and a hydroxyl group (N_4-H_4···O_2, Fig. 2.98) as well as hydrogen bonds of the acidified methylene-type protons characteristic for the trinitroethyl group (C_5-H_{5A}···O_7, C_5-H_{5B}···N_3, Fig. 2.98). Additionally, a non-covalent dipolar interaction between the O_3 oxygen atom of one nitro group and the N_2 ring nitrogen atom of a neighbouring molecule is present as indicated by the distance between these two atoms which is shorter than the sum of the van der Waals radii of these atoms (d(vdW) =3.07 Å, d(O_3···N_2) = 2.93 Å) yielding a crystal density of 1.71 g cm^{-3}.

N^3,N^6-bis-(2,2,2-trinitroethyl)-1,2,4,5-tetrazine-3,6-diamine (BTAT)

The structure of BTAT at 100K has orthorhombic symmetry, space group *Pna*2_1. The asymmetric unit consists of one molecule (Fig. 2.99).

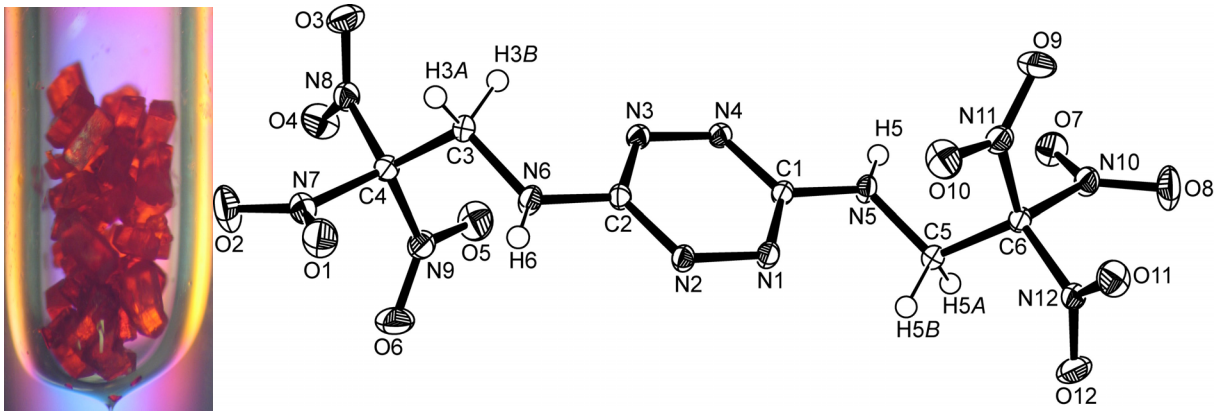

Figure 2.99. Photographic picture of single crystals of BTAT (left picture). ORTEP representation of the molecular structure of BTAT in the crystalline state (right picture). Displacement ellipsoids are shown at the 50 % probability level. Selected bond lengths [Å] and angles [°]: C_1-N_1 1.337(2), N_1-N_2 1.320(2), N_2-C_2 1.349(2), C_2-N_3 1.344(2), N_3-N_4 1.3179(19), N_4-C_1 1.355(2), C_1-N_5 1.370(2), N_5-C_5 1.433(2), C_5-C_6 1.537(2), C_6-N_{10} 1.529(2), N_{10}-O_7 1.211(2), N_{10}-O_8 1.215(2), C_2-N_6 1.365(2), N_6-C_3 1.441(2), C_3-C_4 1.530(2), C_4-N_7 1.531(2), N_7-O_1 1.213(2), N_7-O_2 1.220(2), C_1-N_5-C_5 120.15(15), N_5-C_5-C_6 112.69(14), C_5-C_6-N_{10} 112.67(14), N_{10}-C_6-N_{12} 105.53(13), O_7-N_{10}-O_8 127.98(16), N_3-C_2-N_6 118.14(15), C_2-N_6-C_3 120.35(14), N_6-C_3-C_4 112.33(14), C_3-C_4-N_7 112.67(14), N_7-C_4-N_8 105.87(13), O_1-N_7-O_2 127.64(17), N_1-C_1-N_4 124.78(15), C_1-N_4-N_3 116.87(14), N_4-N_3-C_2 118.32(14), N_3-C_2-N_2 124.64(15), C_2-N_2-N_1 117.06(14), N_2-N_1-C_1 118.32(14).

The planar geometry reported for 3,6-diamino-1,2,3,4-tetrazine [259] is retained in the structure of BTAT. The two trinitroethyl groups bonded to the sp^2-type amino nitrogen atoms are oriented *trans* to each other and are located on different sides of the tetrazine plane. Bond length and angles of the trinitroethyl group display no distinctive features compared to the structures of BTNA, TTD or BTTD and neither do the geometric parameters of the tetrazine moiety compared to the values of 3,6-diamino-1,2,3,4-tetrazine. The unit cell of solid BTAT consists of pairs of dimers of BTAT molecules connected through $N_{(amino)}$—H···$N_{(tetrazine)}$ hydrogen bonding. In turn, these pairs of dimers are interconnected with each other through dipolar nitro group interactions yielding a two dimensional chain of BTAT molecules running along the axis. The chains are connected through C—H···O hydrogen bonding along the *c* axis yielding a high crystal density of 1.89 g cm^{-3} (Fig. 2.100).

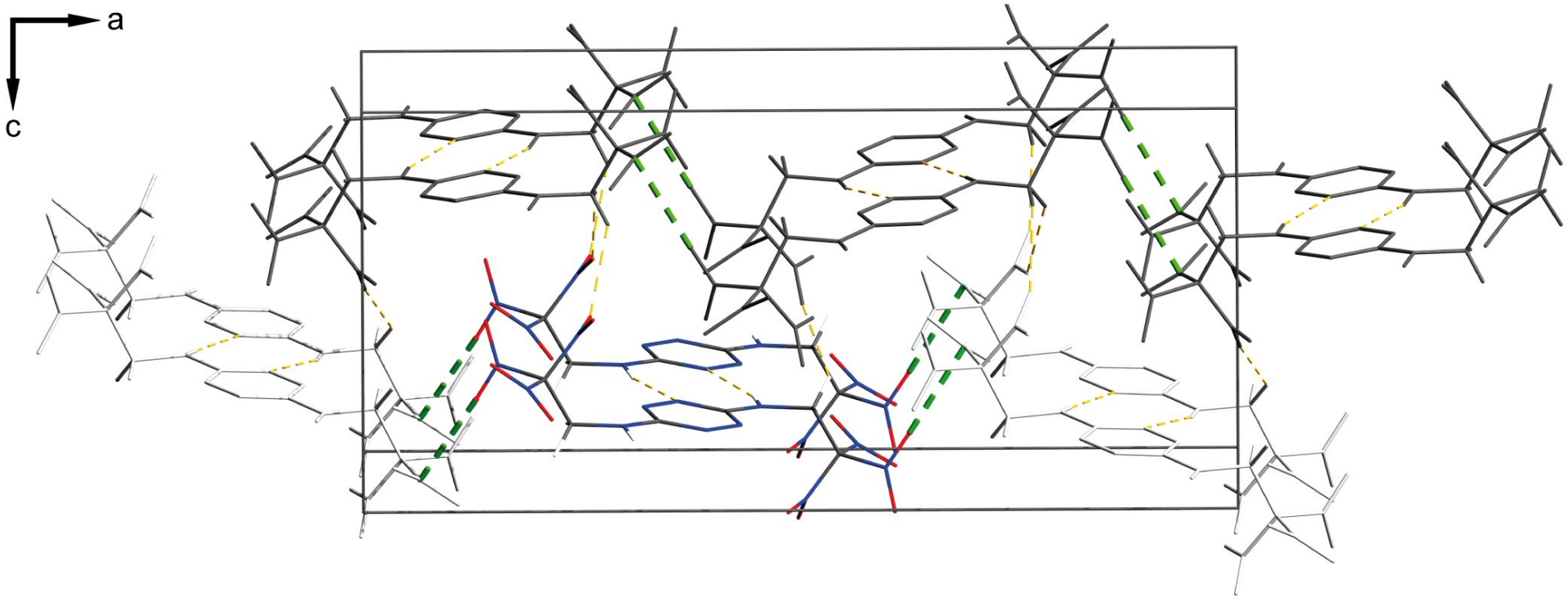

Figure 2.100. Unit cell packing of BTAT, viewed along the *b* axis. Yellow dashed lines indicate hydrogen bonding (N_5-H_5···N_2^{i}, N_6-H_6···N_4^{ii}, C_3-H_{3B}···O_6^{iii}, C_5-H_{5A}···O_9^{iv}, C_3-H_{3A}···O_5^{v}). Green dashed lines indicate dipolar nitro group interactions. Two dipolar nitro group interactions were found with the $N_8/O_3/O_4$ nitro group interacting with the $N_{10}/O_7/O_8$ nitro group (contact distances: 2.965(2) Å [O_3···N_{10}^{vi}]; 2.900(2) Å [O_8···O_7^{vi}]) and the $N_{12}/O_{11}/O_{12}$ nitro group interacting with the $N_7/O_1/O_2$ nitro group (contact distances: 2.859(2) Å [O_{12}···N_7^{vii}]; 2.857(2) Å [O_{12}···O_1^{vii}]. Symmetry code: (i) x, -1+y, z; (ii) x, 1+y, z; (iii) 1/2-x, y-1/2 , 1/2+z; (iv) -x, -y, z-1/2 ; (v) 1/2-x, 1/2+y, 1/2+z; (vi) 1/2+x, 1/2-y, z; (vii) -1/2+x, 3/2-y, z.

S-Ethyl-2,2,2-trinitroethyl-thioformate

S-Ethyl-2,2,2-trinitroethyl-thioformate at ambient conditions is a liquid. Crystals suitable for X-ray diffraction could be obtained on cooling the liquid to 5°C in the fridge (Fig. 2.101).

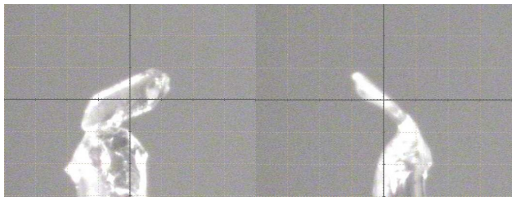

Figure X. Photographic pictures of crystalline S-Ethyl-2,2,2-trinitroethyl-thioformate. The two pictures show a crystal mounted on the tip of a glass fiber during alignment in the centre of the X-ray beam of the Oxford Xcalibur3 CCD diffractometer.

However the crystals proved to consist of two slightly twisted, thin plates resulting in pseudo-merohedral twinning. However, subsequent twin refinement using the Software CrysAlisPro from Oxford Diffraction Ltd. resulted in a dataset suitable for structure solution and refinement. The structure of S-ethyl-2,2,2-trinitroethyl-thioformate at 100K has triclinic symmetry, space group *P*-1 (no. 2). The asymmetric unit consists of one molecule (Fig. 2.102).

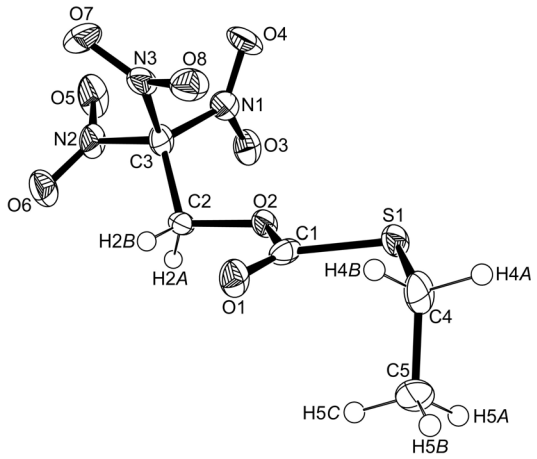

Figure XX. ORTEP representation of the molecular structure of S-ethyl-2,2,2-trinitroethyl-thioformate in the crystalline state. The two molecules of the asymmetric unit show very similar geometric paramters and only one molecule is shown for clarity. Displacement ellipsoids are shown at the 50 % probability level. Selected bond lengths [Å] and angles [°]: O_6-N_2 1.2167 (21), N_2-C_3 1.5202 (27), C_3-C_2 1.5109 (29), C_2-O_2 1.4264 (25), O_2-C_1 1.3737 (25), C_1-O_1 1.1964 (23), C_1-S_1 1.7443 (23), S_1-C_4 1.8082 (22), C_4-C_5 1.5111 (31), O_6-N_2-O_5 127.76(19), O_6-N_2-C_3 114.20(18), N_2-C_3-N_3 106.95(17), N_2-C_3-N_1 107.14(16), N_3-C_3-N_1 107.28(16), N_1-C_3-C_2 111.23(18), C_3-C_2-O_2 107.69(17), O_2-C_1-O_1 124.4(2), O_2-C_1-S_1 107.09(15), O_1-C_1-S_1 128.52(18), C_1-S_1-C_4 99.67(11), S_1-C_4-C_5 114.05(16), C_3-C_2-O_2-C_1 -124.56(19), C_2-O_2-C_1-O_1 -2.4(3), S_1-C_1-O_2-C_2 178.54(14), O_1-C_1-S_1-C_4 -1.4(2), C_1-S_1-C_4-C_5 -78.05(18).

The conformation of thiocarbonate moiety well reflects the *s-cis-s-cis* conformation of the carbonate moiety observed in the structure determination of bis-(2,2,2-trinitroethyl)carbonate (see page 177) and is governed by a variety of intramolecular interactions (Fig. 2.103).

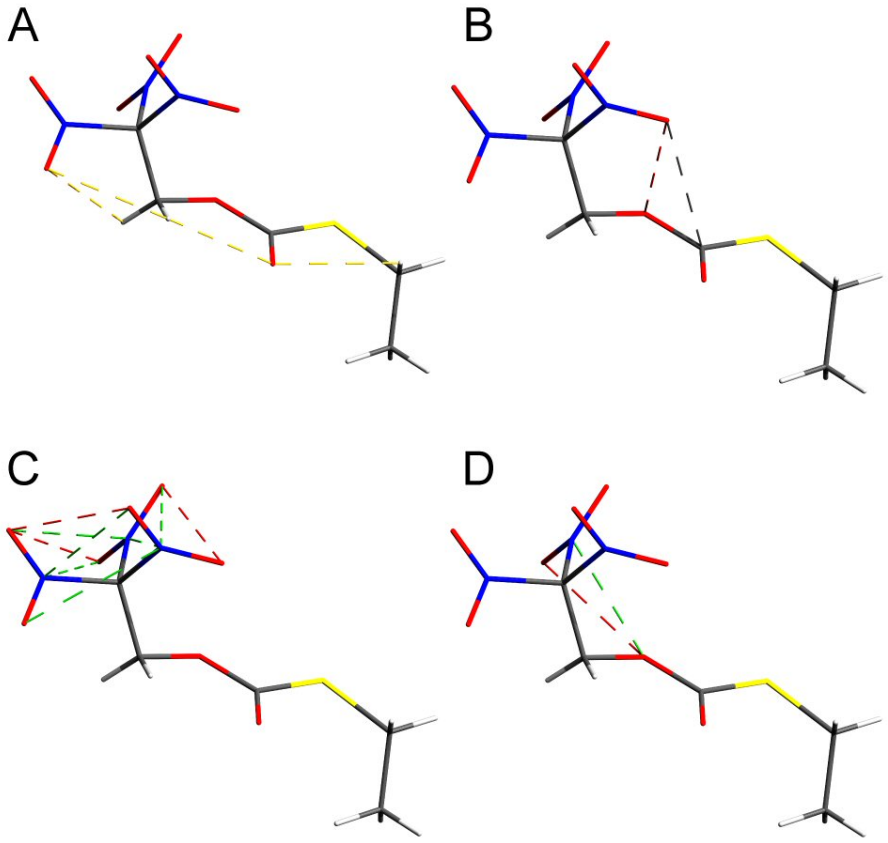

Figure 2.103. Intramolecular short contacts in S-ethyl-2,2,2-trinitroethyl-thioformate. A) Orange dashed lines indicate hydrogen bonding of acidifiend methylene-type hydrogen atoms: C_2-H_{2B}···O_6, C_2-H_{2A}···O_6, C_2-H_{2B}···O_1, C_4-H_{4B}···O_1) B) The green dashed line indicates a short distance between the carbonate carbon atom and one oxygen atom of the nitro group: C_1-O_8 (3.099(3)Å < 3.22Å$_{(vdW)}$ – 0.12Å) The red dashed line indicates the accompanying short distance between two oxygen atoms: O_2-O_3 (2.895(2)Å < 3.04Å $_{(vdW)}$ – 0.14Å) C) Green dashed lines indicate short distances between a nitrogen atom of one nitro group and an oxygen atom of a neighbouring nitro group: N_1-O_5 (2.599(3)Å << 3.07Å – 0.47Å); N_1-O_8 (3.034(2)Å < 3.07Å – 0.04Å); N_2-O_3 (2.875(2)Å < 3.07Å – 0.19Å); N_2-O_7 (2.580(3)Å << 3.07Å – 0.49Å); N_3-O_4 (2.565(2)Å << 3.07Å – 0.50Å); N_3-O_6 (3.011(3)Å < 3.07Å – 0.06Å). Red dashed lines indicate the accompanying short oxygen / oxygen distances between oxygen atoms of neighbouring nitro groups: O_3-O_5 (2.873(2)Å < 3.04Å – 0.17Å); O_4-O_8 (2.970(2)Å < 3.04Å – 0.07Å); O_5-O_7 (3.022(2)Å < 3.04Å – 0.02Å) D) The green dashed line indicates a short distance between the nitrogen atom of this nitro group and the oxygen atom of the carbonate moiety: O_2-N_1 (2.663(3)Å << 3.07Å – 0.41Å) The red dashed line indicates the accompanying short oxygen / oxygen distance between the oxygen atom of the nitro group and the oxygen atom of the carbonate moiety: O_2-O_3 (2.895(2)Å < 3.04Å – 0.14Å).

The extended structure is shown in Figure 2.104 and reveals that the characteristic intermolecular hydrogen bonding of the acidified methylene type protons of the trinitroethyl group is present in the solid state next to non-covalent dipolar interactions including nitro group carbonyl and nitro group sulfur interactions affording a crystal density of 1.69 g cm^{-3}.

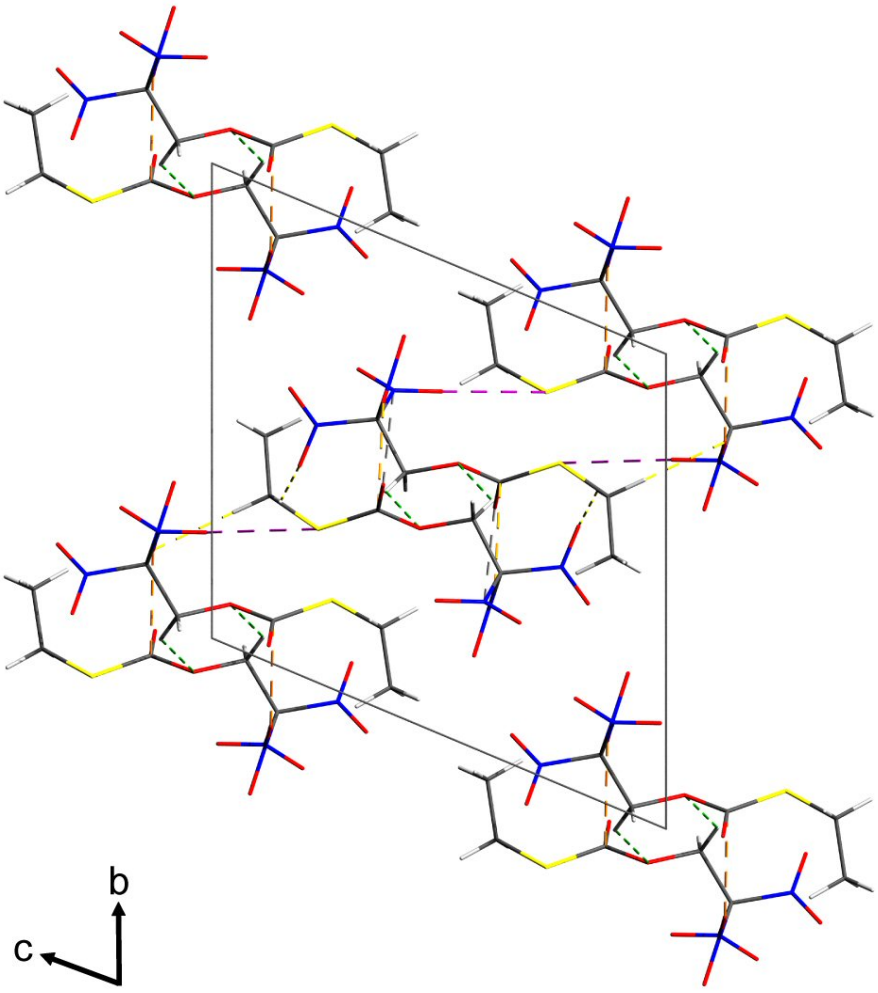

Figure 2.104. Unit cell packing of S-ethyl-2,2,2-trinitroethyl-thioformate, viewed along the *a* axis. Green dashed lines indicate intermolecular hydrogen bonding of the acidified methylene type hydrogen atoms of the trinitroethyl moiety (C_2-H_{2A}···O_2^{i}, C_7-H_{7A}···O_{10}^{ii}, C_7-H_{7B}···O_9^{iii}); Symmetry code: (i) 1-x, 2-y, -z; (ii) 1-x, 1-y, -z; (iii) 1-x, 1-y, 1-z. The orange dashed line indicates intermolecular short distances between the carbonate carbon atom and one oxygen atom of a nitro group: C_1-O_3 (3.046(3)Å < 3.22Å – 0.17Å); C_6-O_{12} (3.128(3)Å < 3.22Å – 0.09Å). The grey dashed line indicates intermolecular short distances between the carbonyl oxygen atom and a nitrogen atom of a nitro group: O_9-N_6 (2.955(3)Å < 3.07Å – 0.12Å). The pink dashed lines indicate intermolecular short distances between a sulfur atom and an oxygen atom of a nitro group: O_{15}-S_1 (3.1154(17)Å << 3.32Å – 0.20Å); O_8-S_2 (3.3052(18)Å < 3.32Å – 0.01Å).

Bis-(2,2,2-trinitroethyl)carbonate (BTC)

The structure of bis-(2,2,2-trinitroethyl)carbonate (BTC), $C_5H_4N_6O_{15}$, at 100K has orthorhombic (*Pbca*) symmetry. The asymmetric unit consists of one molecule (Fig. 2.105).

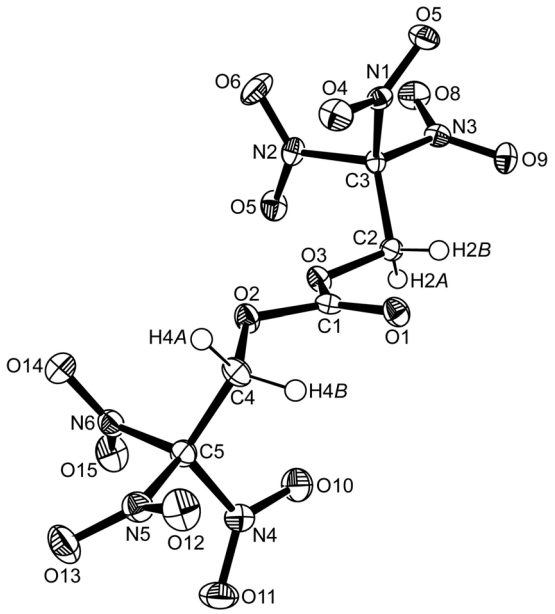

Figure 2.105. ORTEP representation of the molecular structure of bis-(2,2,2-trinitroethyl)carbonate in the crystalline state. Displacement ellipsoids are shown at the 50 % probability level. Selected bond lengths [Å] and angles [°]: C_1-O_1 1.1915(12), C_1-O_2 1.3451(12), C_1-O_3 1.3399(12), C_2-O_3 1.4255(12), C_3-N_1 1.5238(13), C_3-N_2 1.5214(13), C_3-N_3 1.5201(13), C_4-O_2 1.4294(13), C_5-N_4 1.5262(14), C_5-N_5 1.5131(13), C_5-N_6 1.5271(13), O_1-C_1-O_3 127.57(10), O_1-C_1-O_2 126.98(9), O_3-C_1-O_2 105.46(8), O_3-C_2-C_3 107.83(8), C_2-C_3-N_3 110.72(8), C_2-C_3-N_2 112.73(8), N_3-C_3-N_2 107.22(8), C_2-C_3-N_1 113.01(8), N_3-C_3-N_1 106.17(8), N_2-C_3-N_1 106.59(8), N_5-C_5-C_4 112.25(8), N_5-C_5-N_4 107.55(8), C_4-C_5-N_4 113.26(8), N_5-C_5-N_6 107.57(8), C_4-C_5-N_6 109.88(8), N_4-C_5-N_6 105.99(8), C_1-O_2-C_4 116.48(8), C_1-O_3-C_2 116.39(8), O_1-C_1-O_2-C_4 17.35(15), O_3-C_1-O_2-C_4 -162.59(8), C_5-C_4-O_2-C_1 118.99(9), O_1-C_1-O_3-C_2 9.22(15), O_2-C_1-O_3-C_2 -170.84(8), C_3-C_2-O_3-C_1 117.22(9).

The structure displays *s-cis-s-cis* conformation of the carbonate group, intra as well as intermolecular C—H···O hydrogen bonding and dipolar nitro group interactions that account for its exceptionally high density of 1.975 g·cm^{-3}, which is significantly higher than the reported value of 1.88 g·cm^{-3}. [260]. As a consequence of the relationship between structure and crystal density this polymorph contains available oxygen in amounts even superior to liquid oxygen. The geometry in both trinitroethyl moieties is very similar with a propeller-type orientation of the nitro groups (C_3) bonded to the β-C atoms and the conformation of the substituents of the α- and β-C atoms being staggered. Bond lengths of the trinitroethyl units show unusual values in that the C-N

bonds joining the three nitro groups to the β-C atom are significantly longer than the normal C-N bond distance of 1.47Å [246], the N-C-N bond angles are smaller than the tetrahedral value whereas the corresponding N-C-C angles are greater as was similarily observed in the structure determinations of bis-(2,2,2-trinitroethyl)urea [247] and 2,2,2-trinitroethanol [234]. Early investigations into the structural properties of BTC using IR spectroscopy could not settle the question what molecular geometry the carbonate adopts with *s-cis-s-cis*, *s-cis-s-trans* or *s-trans-s-trans* conformations being all possible for organic carbonates. [261] Our X-ray investigation shows that intramolecular C—H···O hydrogen bonding (C_2-H_{2B}···O_1 and C_4-H_{4B}···O_1) does occur unambiguously demonstrating the *s-cis-s-cis* conformation. Bond lengths and angles of the carbonate moiety may be considered normal in comparison to the Cambridge Structural Database results. [262] The extended structure of BTC involves secondary interactions in terms of intermolecular C—H···O hydrogen bonding (C_4-H_{4B}···O_9^{i} and C_2-H_{2B}···O_1^{i}, symmetry code as in Fig. 2.106). The resulting bifurcated hydrogen bonding is displayed in Figure. 2.106.

Short intermolecular O···O distances with values substantially less than 3.04 Å, the sum of the van der Waals radii for O (1.52 Å) [244] are observed as a consequence of non covalent dipolar nitro-group interactions. Dipolar nitro-group interactions were accepted for N···O contacts shorter than 3.17Å. This value was chosen as the sum of the van der Waals radii of nitrogen and oxygen plus a tolerance value of 0.1 Å. Given these values, three dipolar nitro-group contacts were identified. These interactions were found for the $N_1/O_4/O_5$ nitro group interacting with the $N_6/O_{14}/O_{15}$ nitro group as well as with the $N_2/O_6/O_7$ and the $N_3/O_8/O_9$ nitro groups and finally for the $N_6/O_{14}/O_{15}$ nitro group interacting with the $N_4/O_{10}/O_{11}$ nitro group and the $N_5/O_{12}/O_{13}$ nitro group, leading to O···O distances of 2.8317 (11)Å [O_4···O_7^{ii}; symmetry code: (ii) -x + 3/2, y - 1/2, z], 2.8626 (12)Å [O_5···O_{14}^{iii}; symmetry code: (iii) -x + 3/2, -y, z-1/2] and 2.8381 (12)Å [O_{14}···O_{12}^{iiii}; symmetry code: (iiii) x + 1/2, y, -z + 3/2]. The corresponding values for the N···O contacts are 3.0125 (11)Å [O_4···N_3^{ii}], 2.9935 (12)Å [O_5···N_6^{iii}] and 3.1045 (12) Å [O_{14}···N_4^{iiii}].

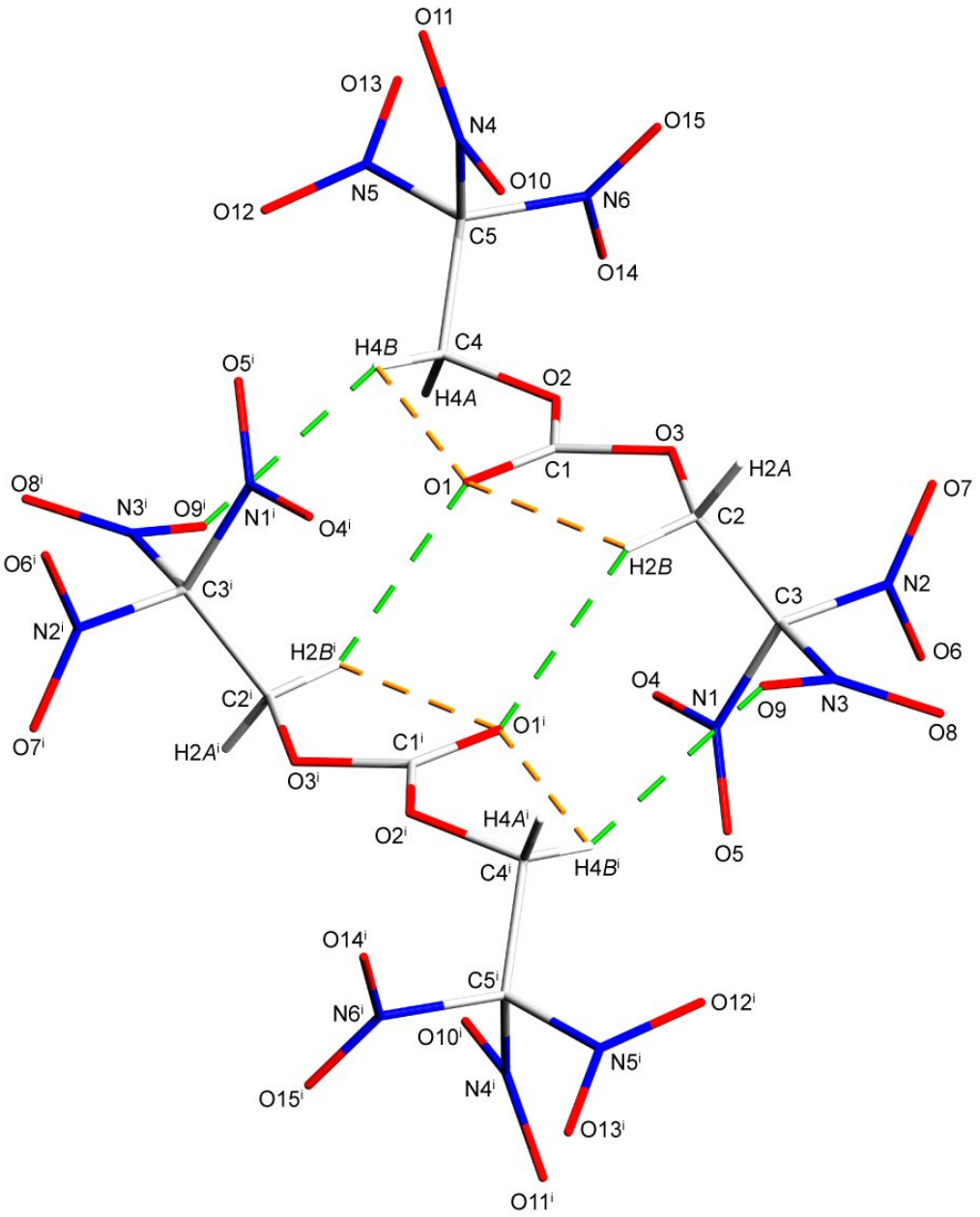

Figure 2.106. A centrosymmetric dimer containing two bis-(2,2,2-trinitroethyl)carbonate molecules. The bifurcated hydrogen bonding is indicated by dashed lines. Green dashed lines indicate intermolecular hydrogen bonding of the acidified methylene type hydrogen atoms of the trinitroethyl moiety (C_2-H_{2B}···O_1^i). Yellow dashed lines indicate intramolecular hydrogen bonding of the acidified methylene type hydrogen atoms of the trinitroethyl moiety (C_2-H_{2B}···O_1, C_4-H_{4B}···O_1). Symmetry code: (i) –x+1, -y, -z+1.

The high oxygen content of BTC, together with the intermolecular contacts (dipolar nitro-group interactions and hydrogen bonding) yield a high-crystal-density polymorph that displays an oxygen content of 1.221 Mg m^{-3}, higher than the value of liquid oxygen at 90 K that corresponds to 1.140 Mg m^{-3} [263].

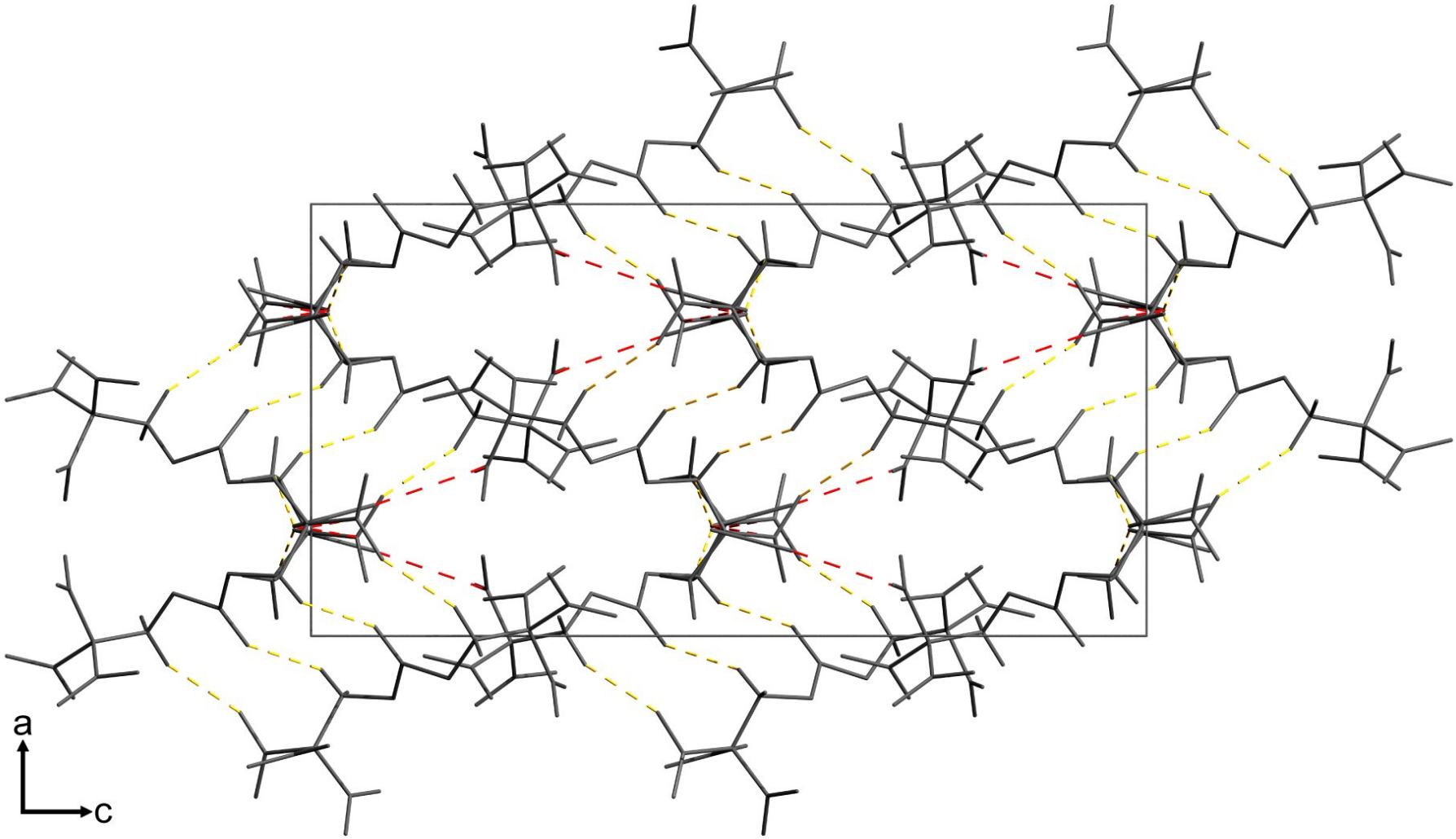

Figure 2.107. Unit cell packing of bis-(2,2,2-trinitroethyl)carbonate, viewed along the *b* axis. Yellow dashed lines indicate intermolecular hydrogen bonding. Red dashed lines indicate intermolecular dipolar nitro group interactions ($N_3 \cdots O_4$, $N_6 \cdots O_5$).

2,2,2-Trinitroethyl-azidoformate (TAF)

The structure of TAF at 100K has monoclinic symmetry, space group $P2_1/c$ (no. 14). The asymmetric unit consists of two molecules (Fig. 2.108).

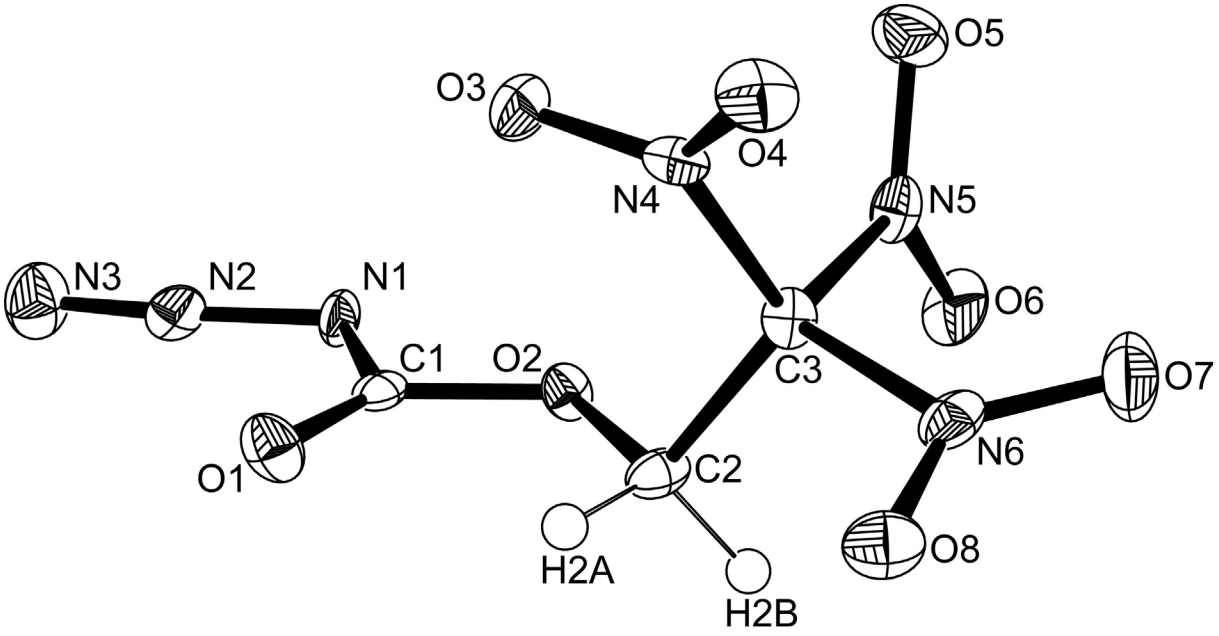

Figure 2.108. ORTEP representation of the molecular structure of TAF in the crystalline state. The two molecules of the asymmetric unit show very similar geometric paramters and only one molecule is shown for clarity. Displacement ellipsoids are shown at the 50 % probability level. Selected bond lengths [Å] and angles [°]: N_3-N_2 1.115(5), N_2-N_1 1.266(5), N_1-C_1 1.397(5), C_1-O_1 1.199(5), C_1-O_2 1.345(5), O_2-C_2 1.426(5), C_2-C_3 1.513(6), C_3-N_5 1.532(5), N_5-O_5 1.212(4), N_5-O_6 1.219(4), N_3-N_2-N_1 173.5(4), N_2-N_1-C_1 110.1(3), N_1-C_1-O_1 128.0(4), N_1-C_1-O_2 106.4(3), C_1-O_2-C_2 115.7(3), O_2-C_2-C_3 106.8(3), C_2-C_3-N_5 113.1(4), N_5-C_3-N_6 105.8(3), O_5-N_5-O_6 127.9(4).

The trinitroethyl group displays common bond length and angles compared to the structures discussed earlier in this work. The N_α—N_β / N_β—N_γ bond lengths as well as the N_α—N_β—N_γ angles are in good agreement with other covalently bound azides. [264] With *s-cis-s-cis*, *s-cis-s-trans* or *s-trans-s-trans* conformations being all possible for the azidoformate moiety, our X-ray investigation shows that intramolecular C—H···O hydrogen bonding (C_2—H_{2A}···O_1, symmetry code as in Fig. 2.109) does occur unambiguously demonstrating the *s-cis-s-cis* conformation. Bond lengths and angles of the carbonate moiety may be considered normal in comparison to the Cambridge Structural Database results. [265] Secondary interactions include C—

H···O$_{(carbonyl)}$ and C—H···N$_{(azide)}$ hydrogen bonding as well as dipolar nitro group interactions. A view along the *a* axis (Fig. 2.109) reveals that the C—H···O$_{(carbonyl)}$ hydrogen bonding results in dimers being aligned in a chessboard like way with one sort of dimers (e.g. length axis of the molecule aligned horizontally) belonging to one kind of possible fields (e.g. black) and the other sort of dimers (e.g. length axis of the molecule aligned vertically) belonging to the other kind of field (e.g. white).

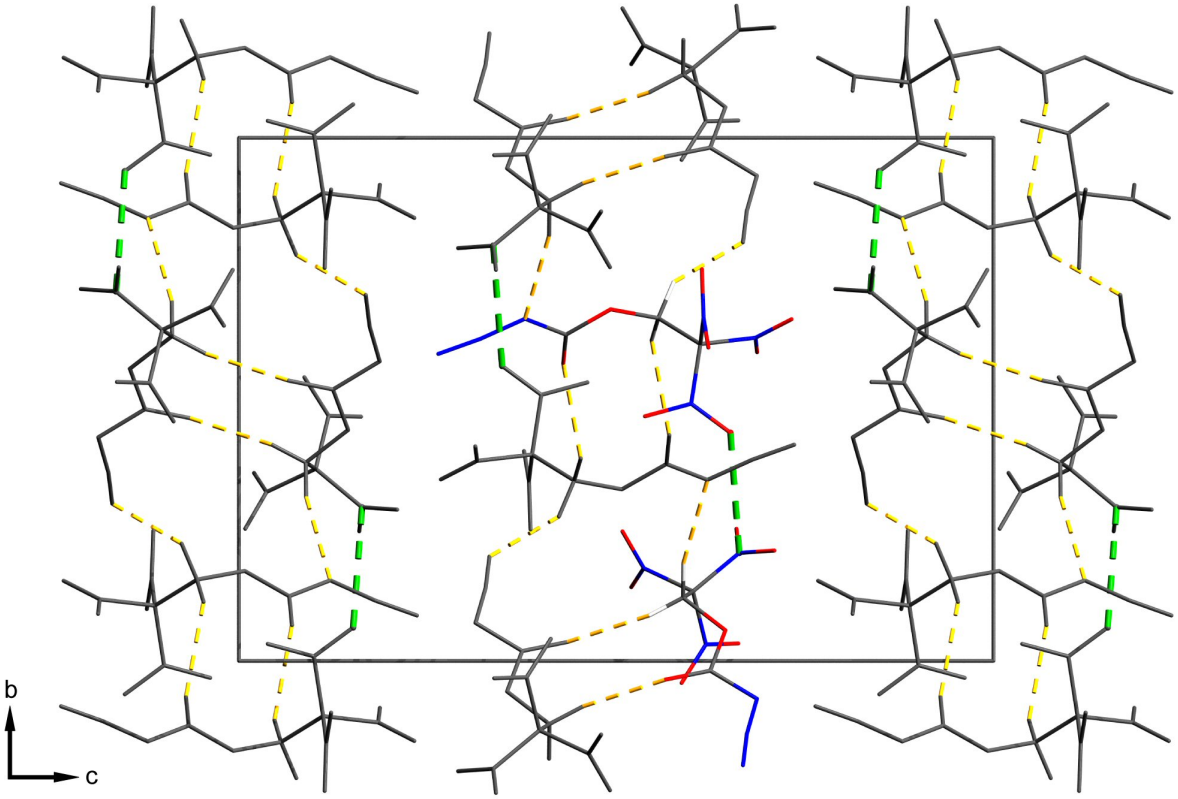

Figure 2.109. Unit cell packing of TAF, viewed along the *a* axis. Yellow dashed lines indicate intermolecular hydrogen bonding (C_2-H_{2A}···O_1^{i}, C_2-H_{2B}···N_7, C_5-H_{5A}···N_3^{ii}, C_5-H_{5B}···O_9^{iii}). Green dashed lines indicate dipolar nitro group interactions. One dipolar nitro group interaction was found with the $N_5/O_5/O_6$ nitro group interacting with the $N_{12}/O_{15}/O_{16}$ nitro group (contact distances: 3.082(5) Å [N_5···O_{15}^{iv}]; 2.966(4) Å [O_6···O_{15}^{iv}]); Symmetry code: (i) 1-x, 2-y, 1-z; (ii) 2-x, 2-y, 1-z; (iii) 2-x, 1-y, 1-z, (iv) 1-x, 1-y, 1-z.

Bis-(2,2,2-trinitroethyl)-hydrazodicarboxylate (BTHC)

Pure BTHC solidifies as a glass-like amorphous solid. However, two solvents were found to combine with BTHC to form stoichiometric crystal inclusion complexes. In both co-crystals the host : guest ratio equals 1:1 for the acetone as well as the ethyl acetate complex (BTHCa / BTHCe).

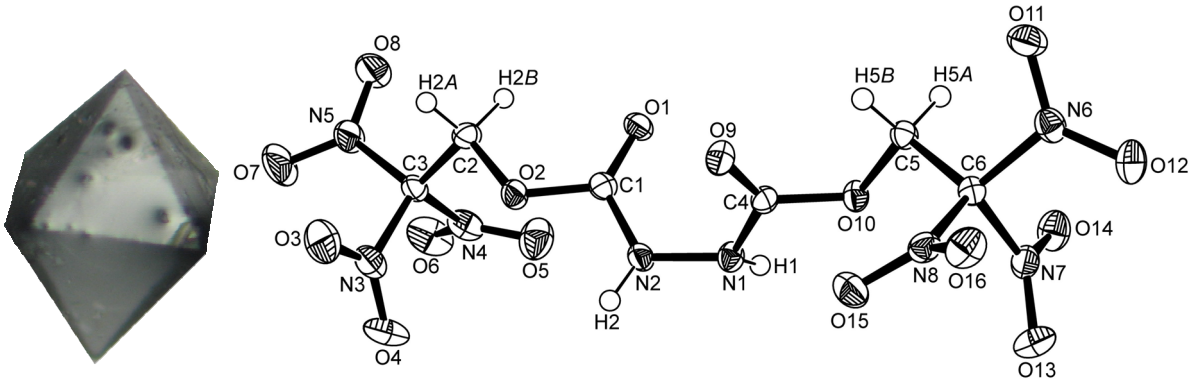

Figure 2.110. Photographic picture of a single crystal of the 1:1 co-crystal of BTHC and ethyl acetate (left picture). ORTEP representation of the molecular structure of BTHC in the 1:1 co-crystal of BTHC and ethyl acetate (right picture). Displacement ellipsoids are shown at the 50 % probability level. Selected bond lengths [Å] and angles [°]: O_7-N_5 1.2124(17), N_5-O_8 1.2079(18), N_5-C_3 1.5291(19), C_3-C_2 1.507(2), C_2-O_2 1.427(2), O_2-C_1 1.3603(19), C_1-O_1 1.2040(18), C_1-N_2 1.345(2), N_2-N_1 1.3779(19), N_1-C_4 1.360(2), C_4-O_9 1.2001(18), C_4-O_{10} 1.3641(18), O_{10}-C_5 1.4265(18), C_5-C_6 1.519(2), C_6-N_7 1.523(2), N_7-O_{13} 1.2117(17), N_7-O_{14} 1.2131(16), O_7-N_5-O_8 126.53(13), N_5-C_3-N_3 108.00(11), N_5-C_3-C_2 113.90(13), C_3-C_2-O_2 104.55(12), C_2-O_2-C_1 114.11(12), O_2-C_1-O_1 124.12(14), O_2-C_1-N_2 108.70(13), O_1-C_1-N_2 127.18(14), C_1-N_2-N_1-C_4 70.93(18), C_1-N_2-N_1 119.47(13), N_2-N_1-C_4 117.32(13), N_1-C_4-O_9 126.31(14), N_1-C_4-O_{10} 108.66(12), O_9-C_4-O_{10} 125.03(14), C_4-O_{10}-C_5 115.87(11), O_{10}-C_5-C_6 108.45(12), C_5-C_6-N_7 111.43(12), N_7-C_6-N_8 106.10(12), O_{13}-N_7-O_{14} 127.60(13).

Each of these mixed crystals crystallise in the space group *P*-1. Compared to the 2,2,2-trinitroethylformyl moiety present in the structure of 2,2,2-trinitroethylazidoformate, the geometric parameters of this group present in the BTHC molecule of the two co-crystals show no significant differences. Figure 2.110 exemplarily displays one BTHC molecule of the co-crystal of BTHC with ethyl acetate. The values of the N_1-N_2 bond length of the hydrazine group are shorter (1.3779(19) Å / BTHCe and 1.3790(14) Å / BTHCa) compared to free hydrazine (1.46 Å) [254] due to mesomerism between the nitrogen, carbon and carbonyl oxygen atoms and are in fair accordance with the N-N bond length reported for diethyl 1,2-hydrazinedicarboxylate

(1.385 Å) [255] and diisopropyl hydrazocarboxylate molecule (1.381(2) Å). [266] Bond lengths and angles of the carbonate moiety agree well to the results of a comparison with Cambridge Structural Database entries. [267] Intramolecular C—H···$O_{(carbonyl)}$ hydrogen bonding is present in BTHCe and BTHCa favouring the the s-cis-s-cis conformation of the carbamate group.

The C_1-N_2-N_1-C_4 torsion angle of BTHCe (70.93(18)°) slightly differs from the corresponding angle in BTHCa (67.80(14)°) due to secondary N—H···O(carbonyl) hydrogen bonding of the hydrazine hydrogen atoms and the carbonyl oxygen atom of the ethyl acetate or acetone molecule present in the co-crystals. Intermolecular C—H···$O_{(nitro)}$ as well as C—H···$O_{(carbonyl)}$ hydrogen bonding and dipolar nitro group interactions are present between two BTHC molecules in the structures of BTHCe and BTHCa resulting in the formation of BTHC dimers in both cases. These dimers are interconnected through N—H···$O_{(carbonyl)}$ hydrogen bonding of the hydrazine hydrogen atom of a BTHC molecule and the carbonyl oxygen atom of acetone in the case of BTHCa or ethyl acetate in the case of BTHCe yielding alternating pairs of BTHC host and acetone or ethyl acetate guest molecules stacked along the b axis (BTHCa) and a axis (BTHCe) (Fig. 2.111). A comparison of the extended structures of BTHCe and BTHCa reveals that the same types of interactions are present in both mixed crystals between the BTHC molecules and the acetyl groups of acetone and ethyl acetate. A remarkable fact mirrored in the very similar cell axes and angles of the single crystals. Details of the structure determinations are listed in the appendix (Chapter 4).

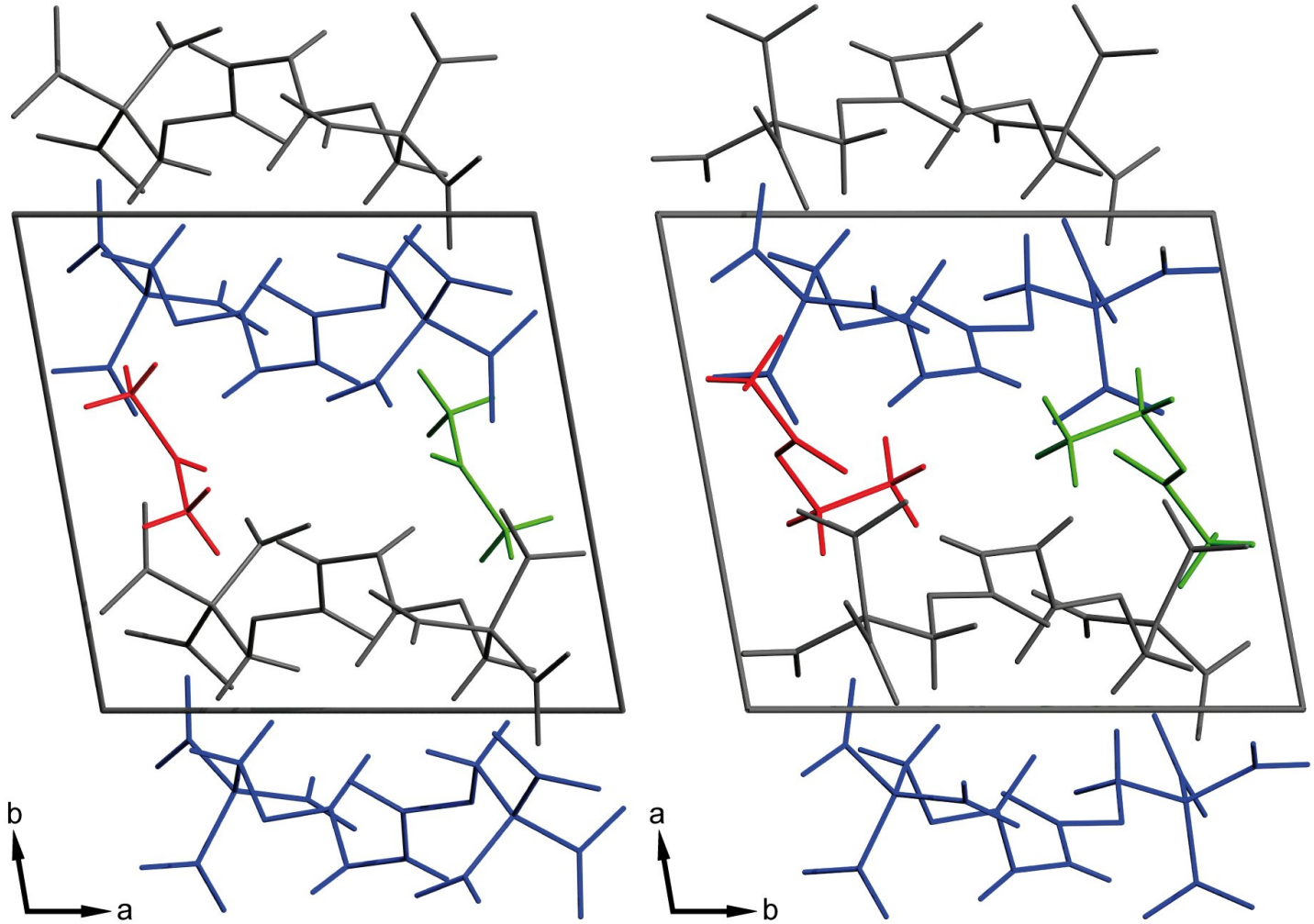

Figure 2.111. Comparison of the unit cells of BTHC/acetone 1:1 (left) and BTHC/ethyl acetate 1:1 (right).

Structural Relationships and the Concept of Higher Densities

The number of crystal structures carrying the trinitroethyl group and published by us [234-235, 268] is nine with the number of different molecules being eight. A search of the Cambridge Structural Database (CSD version 5.29, November 2007) resulted in fifteen entries considering compounds carrying the trinitroethyl moiety. The number of different molecules amongst these entries is thirteen with three entries (refcodes NOETNA, NOETNA01, NOETNA02) describing polymorphs of the same molecule (bis-(2,2,2-trinitroethyl)-nitramine / BTNNA). One structure (N-nitro-N-(2,2,2-trinitroethyl)-guanidine) has been reported without having been deposited at the CCDC resulting in a total of only twenty two different molecules where crystal structure data have been reported. A summary of all structures is displayed in Figure 2.112. The corresponding names of the molecules are given and assigned a crystal index number, used to reference individual molecules in the figures and tables.

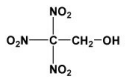

(9) 2,2,2-trinitroethanol

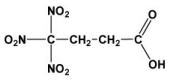

(2) 4,4,4-trinitrobutanoic acid

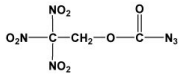

(10) 2,2,2-trinitroethyl-azidoformate

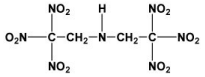

(11) bis(2,2,2-trinitroethyl)amine

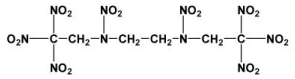

(14) 1,1,1,3,6,8,8,8-octanitro-3,6-diaza-octane

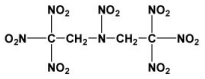

(20,23,24) bis(2,2,2-trinitroethyl)nitramine

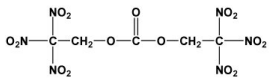

(25) bis(2,2,2-trinitroethyl)carbonate

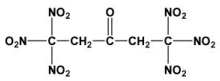

(17) 1,1,1,5,5,5-hexanitropentan-3-one

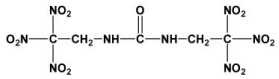

(12) bis(2,2,2-trinitroethyl)urea

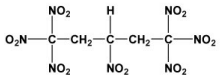

(19) 1,1,1,3,5,5,5-heptanitropentane

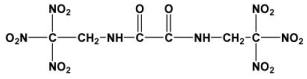

(7) bis(2,2,2-trinitroethyl)oxamide

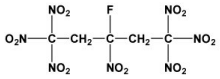

(15) 3-fluoro-1,1,1,3,5,5,5-heptanitropentane

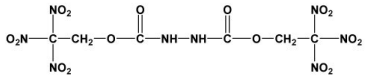

(3,4) bis(2,2,2-trinitroethyl)-hydrazodicarboxylate

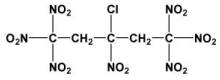

(21) 3-chloro-1,1,1,3,5,5,5-heptanitropentane

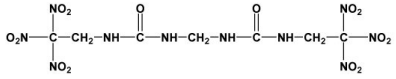

(5) methylene di(N-(2,2,2-trinitroethyl)urea)

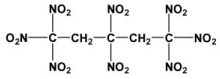

(22) 1,1,1,3,3,5,5,5-octanitropentane

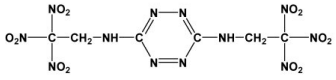

(16) N^3, N^6-bis(2,2,2-trinitroethyl)-1,2,4,5-tetrazine-3,6-diamine

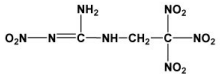

(6) N-nitro-N'-(2,2,2-trinitroethyl)-guanidine

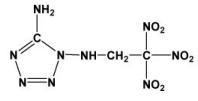

(8) N^1-(2,2,2-trinitroethyl)-1H-tetrazole-1,5-diamine

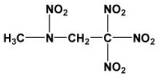

(13) 1,1,1,3-tetranitro-3-azabutane

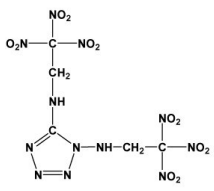

(18) N^1,N^5-bis(2,2,2-trinitroethyl)-1H-tetrazole-1,5-diamine

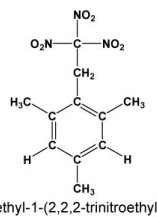

(1) 2,4,6-trimethyl-1-(2,2,2-trinitroethyl)benzene

Figure 2.112. Summary of available trinitroethyl compounds deposited at the CCDC.

In addition, Table 2.16 includes the corresponding crystal *refcode* used in the *Cambridge Structural Database* [269] together with the reported densities.

Table 2.16. Comprehensive summary of crystal structures containing the trinitroethyl moiety. The index I assigned to the compounds is related to increasing crystal density.

I	compound	refcode	$R_{1\ (I>2\sigma)}$	T / K	ρ / g cm^{-3}	ref.
1	2,4,6-trimethyl-1-(2,2,2-trinitroethyl)-benzene	TUMBAE	0.0742	158	1.473	[270]
2	4,4,4-trinitrobutanoic acid	NABMIM	0.0612	298	1.621	[271]
3	Bis-(2,2,2-trinitroethyl)-hydrazodicarboxylate / EtOAc	**)	0.0361	100	1.675	*)
4	Bis-(2,2,2-trinitroethyl)-hydrazodicarboxylate / acetone	**)	0.0366	100	1.691	*)
5	methylene-di(N-(2,2,2-trinitroethyl)-urea)	QQQAUY	-	298	1.699	[247]
6	*N*-nitro-*N'*-(2,2,2-trinitroethyl)-guanidine	***)	0.063	295	1.758	[272]
7	Bis-(2,2,2-trinitroethyl)-oxamide	BINSUM	0.032	298	1.798	[273]
8	N^1-(2,2,2-trinitroethyl)-1*H*-tetrazole-1,5-diamine	**)	0.0354	100	1.831	*)
9	2,2,2-trinitroethanol	DIKXEB	0.0370	100	1.839	[234]
10	2,2,2-trinitroethyl-azidoformate	**)	0.0830	100	1.852	*)
11	Bis-(2,2,2-trinitroethyl)-amine	**)	0.0392	200	1.857	*)
12	Bis-(2,2,2-trinitroethyl)-urea	NOEURA	0.054	298	1.861	[247]
13	1,1,1,3-tetranitro-3-azabutane	**)	0.0558	100	1.862	[274]
14	1,1,1,3,6,8,8,8-octanitro-3,6-diaza-octane	DILFUZ	0.032	298	1.876	[275]
15	3-fluoro-1,1,1,3,5,5,5-heptanitropentane	CUVXUM	0.057	298	1.884	[276]
16	N^3,N^6-bis(2,2,2-trinitroethyl)-1,2,4,5-tetrazine-3,6-diamine	**)	0.0269	100	1.886	*)
17	1,1,1,5,5,5-hexanitropentan-3-one	SINMUX	0.089	110	1.897	[277]
18	N^1,N^5-bis(2,2,2-trinitroethyl)-1*H*-tetrazole-1,5-diamine	**)	0.0844	100	1.897	*)
19	1,1,1,3,5,5,5-heptanitropentane	CUVXUG	0.068	298	1.908	[276]
20	Bis-(2,2,2-trinitroethyl)-nitramine	NOETNA	0.055	298	1.919	[278]
21	3-chloro-1,1,1,3,5,5,5-heptanitropentane	CUVYAT	0.043	298	1.924	[276]
22	1,1,1,3,3,5,5,5-octanitropentane	CEYDUF	0.054	100	1.94	[279]
23	Bis-(2,2,2-trinitroethyl)-nitramine	NOETNA02	0.105	298	1.953	[280]
24	Bis-(2,2,2-trinitroethyl)-nitramine	NOETNA01	0.058	298	1.955	[279]
25	Bis-(2,2,2-trinitroethyl)-carbonate	DIWHIB	0.0270	100	1.975	[235]

Notes. *) this work. **) this structure has yet to be allocated a refcode. ***) this structure has not been deposited at the CCDC.

The density values can be split into two groups: The first group shows densities in a range of 1.4 – 1.8 g cm^{-3} and the second group summarizes those crystals with densities in a range of 1.8 – 2.0 g cm^{-3} (Fig. 2.113).

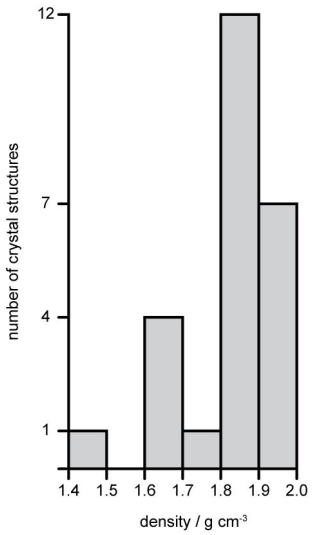

Figure 2.113. Number of crystal structures related to density range.

A comparison with organic crystals containing atoms no heavier than oxygen (range 1.1 – 1.3 g cm $^{-3}$) [281] reveals that the molecules of the first group have higher densities although consisting of sterically unfavourable molecular frameworks (Table 2.16, entries 1, 2 and 5) or co-crystals (Table 2.16, entries 3 and 4). The molecules of the second group display exceptionally high densities. The seven structures discussed in this work display hydrogen bonding of the methylene-type protons and dipolar nitro group interactions of the trinitroethyl moiety contributing to their high densities. We recently reported the crystal structures of **9** (2,2,2-trinitroethanol, ρ = 1.839 g cm^{-3}) and ***25*** (bis(2,2,2-trinitroethyl)carbonate, ρ = 1.975 g cm^{-3}) and showed the same trinitroethyl assisted intermolecular interactions to be present in these two compounds. The results of a survey towards dipolar nitro group interactions of all compounds where structural coordinates are available, is given in Table 2.17. According to this listing of interatomic oxygen···oxygen and oxygen···nitrogen distances dipolar nitro group interactions are present in all twenty two entries. Contact details are given for nitro groups of trinitroethyl groups interacting with each other.

Table 2.17. Summary of short intermolecular nitrogen/oxygen and corresponding oxygen distances of compounds 1 – 25. Only nitro groups being part of the trinitroethyl substituent have been considered. The intermolecular interactions are limited to those less than the sum of the *van der Waals* radii ($\sum(vdW_{N,O})$ = 3.07 Å, $\sum(vdW_{O,O})$ = 3.04 Å) plus a tolerance value of 0.2 Å.

I	nitro interaction between	N/O contact	d(N···O) / Å	Δ / vdW	O/O contact	d(O···O) / Å	Δ / vdW
1	$N_4/O_7/O_8$ and $N_2/O_3/O_4$	$N_4\cdots O_3$	3.025(6)	-0.04	$O_3\cdots O_8$	3.047(6)	0.01
2	$N_3/O_7/O_8$ and $N_2/O_5/O_6$	$N_3\cdots O_6$	2.966(6)	-0.10	$O_6\cdots O_7$	3.011(7)	-0.03
3	$N_3/O_3/O_4$ and $N_7/O_{13}/O_{14}$	$N_3\cdots O_{13}$	3.196(2)	0.13	$O_3\cdots O_{14}$	2.985(2)	-0.06
					$O_3\cdots O_{14}$	3.170(2)	0.13
					$O_3\cdots O_{13}$	3.118(2)	0.08
					$O_4\cdots O_{13}$	3.021(2)	-0.02
	$N_4/O_5/O_6$ and $N_5/O_7/O_8$	$N_4\cdots O_7$	3.259(2)	0.19	$O_6\cdots O_7$	2.991(2)	-0.05
					$O_7\cdots O_7$	2.971(2)	-0.07
	$N_7/O_{13}/O_{14}$ and $N_3/O_3/O_4$	$N_7\cdots O_3$	3.251(2)	0.18	$O_{14}\cdots O_3$	2.985(2)	-0.06
4	$N_6/O_{11}/O_{12}$ and $N_6/O_{11}/O_{12}$	$N_6\cdots O_{11}$	3.225(2)	0.16	$O_{11}\cdots O_{12}$	3.087(2)	0.05
6	$N_3/O_5/O_6$ and $N_3/O_5/O_6$	*)	-	-	$O_6\cdots O_6$	2.823	-0.22
7	$N_3/O_4/O_5$ and $N_4/O_6/O_7$	$N_3\cdots O_6$	2.9506	-0.12	$O_6\cdots O_5$	3.0210	-0.02
8	$N_8/O_3/O_4$ and $N_8/O_3/O_4$	$N_8\cdots O_3$	3.270(3)	0.20	$O_3\cdots O_4$	3.051(3)	0.01
9	$N_2/O_4/O_5$ and $N_2/O_4/O_5$	$N_2\cdots O_4$	3.123(2)	0.05	$O_4\cdots O_4$	2.825(2)	-0.21
	$N_2/O_4/O_5$ and $N_5/O_{11}/O_{12}$	$N_5\cdots O_5$	3.118(2)	0.05	$O_5\cdots O_{12}$	2.852(2)	-0.19
10	$N_5/O_5/O_6$ and $N_{12}/O_{15}/O_{16}$	$N_5\cdots O_{15}$	3.082(5)	0.01	$O_6\cdots O_{15}$	2.966(4)	-0.07
11	$N_3/O_5/O_6$ and $N_4/O_7/O_8$	$N_3\cdots O_8$	3.174(2)	0.10	$O_6\cdots O_8$	3.039(2)	
	$N_3/O_5/O_6$ and $N_5/O_9/O_{10}$	$N_5\cdots O_5$	3.147(2)	0.08	-	-	-
12	$N_2/O_2/O_3$ and $N_3/O_4/O_5$	$N_2\cdots O_5$	3.1647	0.09	$O_2\cdots O_4$	3.1632	0.12
					$O_3\cdots O_5$	3.2100	0.17
	$N_3/O_4/O_5$ and $N_4/O_6/O_7$	$N_3\cdots O_6$	3.2421	0.17	$O_4\cdots O_6$	3.0480	0.01
					$O_4\cdots O_7$	2.9010	-0.14
					$O_5\cdots O_6$	3.1179	0.08
	$N_4/O_6/O_7$ and $N_2/O_2/O_3$	$N_4\cdots O_3$	3.2385	0.17	$O_6\cdots O_2$	2.9963	-0.04
13	$N_3/O_3/O_4$ and $N_5/O_7/O_8$	$N_3\cdots O_8$	3.254(5)	0.18	$O_3\cdots O_8$	2.837(5)	-0.20
	N3/O3/O4 and N3/O3/O4	$N_3\cdots O_3$	3.247(5)	0.18			
14	*)	-	-	-	-	-	-
15	$N_5/O_9/O_{10}$ and $N_1/O_1/O_2$	$N_5\cdots O_2$	3.250(6)	0.18	$O_2\cdots O_{10}$	3.215(8)	0.17
16	$N_7/O_1/O_2$ and $N_{12}/O_{11}/O_{12}$	$N_7\cdots O_{12}$	2.859(2)	-0.21	$O_{12}\cdots O_1$	2.857(2)	-0.18
	$N_8/O_3/O_4$ and $N_{10}/O_7/O_8$	$N_{10}\cdots O_3$	2.965(2)	-0.11	$O_3\cdots O_7$	2.900(2)	-0.14
18	$N_7/O_1/O_2$ and $N_8/O_3/O_4$	$N_7\cdots O_3$	2.869(4)	-0.20	$O_2\cdots O_3$	2.908(4)	-0.13
					$O_1\cdots O_4$	2.927(4)	-0.11
	$N_9/O_5/O_6$ and $N_{11}/O_9/O_{10}$	$N_{11}\cdots O_5$	2.896(5)	-0.17	$O_5\cdots O_9$	3.041(4)	0.00
19	$N_5/O_9/O_{10}$ and $N_6/O_{11}/O_{12}$	$N_5\cdots O_{12}$	3.154(3)	0.08	$O_9\cdots O_{11}$	3.150(3)	0.11
					$O_{10}\cdots O_{11}$	3.208(3)	0.17
					$O_{10}\cdots O_{12}$	3.136(3)	0.10

					$O_{11}\cdots O_{12}$	3.116(3)	0.08
20	$N_5/O_3/O_4$ and $N_6/O_9/O_{10}$	$N_5\cdots O_{10}$	3.2167	0.15	$O_3\cdots O_{10}$	3.1049	0.06
					$O_4\cdots O_{10}$	2.9503	-0.09
21	$N_2/O_3/O_4$ and $N_3/O_5/O_6$	$N_2\cdots O_5$	3.1623	0.09	$O_4\cdots O_5$	2.8822	-0.16
					$O_4\cdots O_5$	3.1153	0.08
	$N_2/O_3/O_4$ and $N_6/O_{11}/O_{12}$	$N_2\cdots O_{12}$	3.0535	-0.02	$O_3\cdots O_{11}$	3.1834	0.14
	$N_7/O_{13}/O_{14}$ and $N_1/O_1/O_2$	$N_7\cdots O_1$	3.1174	0.05	$O_1\cdots O_{13}$	3.2207	0.18
	$N_7/O_{13}/O_{14}$ and $N_1/O_1/O_2$	$N_7\cdots O_2$	3.2469	0.18			
22	$N_3/O_5/O_6$ and $N_8/O_{15}/O_{16}$	$N_3\cdots O_{16}$	3.2622	0.19	$O_5\cdots O_{16}$	3.1066	0.07
					$O_6\cdots O_{16}$	3.0431	0.00
	$N_7/O_{13}/O_{14}$ and $N_8/O_{15}/O_{16}$	$N_7\cdots O_{15}$	3.2530	0.18	$O_{14}\cdots O_{15}$	3.1836	0.14
	$N_8/O_{15}/O_{16}$ and $N_4/O_7/O_8$	$N_8\cdots O_7$	3.2575	0.19	-	-	-
23	*)	-	-	-	-	-	-
24	*)	-	-	-	-	-	-
25	$N_1/O_4/O_5$ and $N_2/O_6/O_7$	$N_1\cdots O_6$	3.259(1)	0.19	$O_4\cdots O_7$	2.832(1)	-0.21
					$O_5\cdots O_6$	2.957(1)	-0.08
	$N_1/O_4/O_5$ and $N_3/O_8/O_9$	$N_3\cdots O_4$	3.013 (1)	-0.06	$O_4\cdots O_8$	3.093(1)	0.05
					$O_5\cdots O_9$	3.122(1)	0.08
	$N_1/O_4/O_5$ and $N_6/O_{14}/O_{15}$	$N_6\cdots O_5$	2.994 (1)	-0.08	$O_5\cdots O_{14}$	2.863(1)	-0.18
					$O_5\cdots O_{15}$	2.942(1)	-0.10
	$N_4/O_{10}/O_{11}$ and $N_6/O_{14}/O_{15}$	$N_4\cdots O_{14}$	3.105(1)	0.03	-	-	-
	-	-	-	-	$O_{12}\cdots O_{14}$	2.838(1)	-0.20

Notes. Indices 5 and 17 refer to refcodes QQQAUY and SINMUX. Structural coordinates are missing, only the cell parameters are given. *) Dipolar nitro group interactions are present between nitro groups of the trinitroethyl substituent and the nitramine moiety. Structural coordinates referring to index 6 are not available; values were taken from reference 273.

Four entries (6,14,23,24) display dipolar nitro group interactions between nitro groups of the trinitroethyl moiety and aliphatic nitro groups (14) or nitramine type nitro groups (6, 23 and 24) not included in the table. Nineteen out of the twenty structures display short oxygen···oxygen distances considering a value of 3.14 Å and thereof fourteen structures contain distances with values even less than the sum of the *van der Waals radius* (3.04 Å) indicating that the close approach of oxygen atoms due to dipolar nitro group interactions can commonly be observed in structures containing the trinitroethyl group. The occurrence of C—H···A hydrogen bonding was observed in the crystal structures of 2,2,2-trinitroethanol and bis-(2,2,2-trinitroethyl)carbonate. Here we present a comprehensive list of this kind of hydrogen bonding (Table 2.18).

Table 2.18. Summary of methylene-type C—H···A hydrogen bonding of the trinitroethyl group in compounds 1-25.

I	D—H···A	D—H	H···A	D···A	D—H···A	*i*
1	-	-	-	-	-	-
2	-	-	-	-	-	-
3	C_2—H_{2A}···$O_{12(nitro)}^{i}$	0.92(2)	2.54(2)	3.428(2)	162.8(18)	x,y,-1+z
	C_2—H_{2B}···$O_{1(carbonyl)}^{i}$	0.91(2)	2.49(2)	3.237(3)	138.6(15)	-x,1-y,1-z
	C_5—H_{5B}···$O_{9(carbonyl)}^{i}$	0.90(2)	2.383(18)	3.1437(19)	142.6(17)	-x,1-y,2-z
4	C_2—H_{2B}···$O_{1(carbonyl)}^{i}$	0.991(17)	2.354(18)	3.112(2)	132.7(13)	1-x,2-y,2-z
	C_5—H_{5B}···$O_{9(carbonyl)}^{i}$	0.952(17)	2.355(15)	3.1350(17)	138.9(13)	1-x,2-y,1-z
6	*)					
7	C_2—H_3···$O_{1(carbonyl)}^{i}$	0.96	2.37	3.229(2)	150	1-x,-y,1-z
8	C_2—H_{2A}···$O_{2(nitro)}^{i}$	0.99	2.57	3.452(3)	149	2-x,-y,-1/2+z
	C_2—H_{2A}···$N_{4(ring)}^{i}$	0.99	2.62	3.225(3)	119	3/2-x,1/2+y,-1/2+z
	C_2—H_{2B}···$O_{1(nitro)}^{i}$	0.99	2.57	3.452(3)	149	2-x,-y,-1/2+z
9	C_3—H_{3B}···$O_{14(nitro)}^{i}$	0.953(17)	2.385(17)	3.3304(19)	171.0(13)	
10	C_2—H_{2A}···$O_{1(carbonyl)}^{i}$	0.95(6)	2.44(5)	3.263(5)	144(4)	1-x,2-y,1-z
	C_2—H_{2B}···$N_{7(azide)}$	0.95(5)	2.49(5)	3.417(6)	165(3)	
	C_5—H_{5A}···$N_{3(azide)}^{i}$	1.00(4)	2.54(4)	3.360(6)	139(3)	2-x,2-y,1-z
	C_5—H_{5B}···$O_{9(carbonyl)}^{i}$	0.97(5)	2.56(5)	3.361(6)	141(4)	2-x,1-y,1-z
11	C_4—H_{4A}···$O_{12(nitro)}^{i}$	0.93(2)	2.52(2)	3.432(2)	167.6(17)	3/2-x,1/2+y,z
12	C_2—H_1···$O_{3(nitro)}^{i}$	1.08	2.38	3.3560	150	x,y,1+z
13	C_2—H_{2A}···$O_{1(nitro)}^{i}$	0.99	2.37	3.319(5)	160	-1+x,y,z
	C_2—H_{2B}···$O_{2(nitro)}^{i}$	0.99	2.37	3.344(5)	169	-x,1/2+y,1/2-z
14	C_2—H_1···$O_{7(nitro)}^{i}$	0.93	2.55	3.4015	152	1+x,y,z
	C_3—H_3···$O_{8B*(nitro)}^{i}$	0.91	2.59	3.4952	176	1+x,y,z
15	C_2—H_3···$O_{13(nitro)}^{i}$	0.99	2.41	3.1129	128	-x,1-y,1/2+z
	C_2—H_4···$O_{7(nitro)}^{i}$	0.97	2.55	3.3528	140	x,-1+y,z
16	C_3-H_{3A}···$O_{5(nitro)}^{i}$	0.99	2.58	3.421(2)	142	1/2-x,1/2+y,1/2+z
	C_3-H_{3B}···$O_{6(nitro)}^{i}$	0.99	2.42	3.155(2)	130	1/2-x,-1/2+y,1/2+z
	C_5-H_{5A}···$O_{9(nitro)}^{i}$	0.99	2.40	3.188(2)	136	-x,-y,-1/2+z
18	C_2-H_{2B}···$N_{3(ring)}^{i}$	0.92(4)	2.57(4)	3.480(5)	171(3)	2-x, -1/2+y, z
19	**)					
20	*)					
21	C_2—H_3···$O_{1(carbonyl)}^{i}$	0.96	2.37	3.2292	150	1-x,-y,1-z
22	C_4—H_3···$O_{1(nitro)}^{i}$	0.98	2.40	3.3273	157	x,1+y,z
	C_4—H_4···$O_{8(nitro)}^{i}$	0.93	2.56	3.4791	174	1/2-x,-y,-1/2+z
23	C_1—H_2···$O_{8(nitro)}^{i}$	1.08	2.52	3.4991	151	-1/2-x,-1/2+y,1/2-z
	C_3—H_4···$O_{2(nitro)}^{i}$	0.84	2.45	3.2261	154	1/2-x,-1/2+y,1/2-z
24	*)					
25	C_2—H_{2B}···$O_{1(nitro)}^{i}$	0.923(13)	2.448(12)	3.2598(13)	146.7(10)	-x+1,-y,-z+1
	C_4—H_{4B}···$O_{9(nitro)}^{i}$	0.966(13)	2.651(13)	3.4532(13)	140.7(9)	-x+1,-y,-z+1

Notes. Indices 5 and 17 refer to refcodes QQQAUY and SINMUX. Structural coordinates are missing, only the cell parameters are given. *) no hydrogen atom coordinates available. **) 19: C_3—H_5···$O_{1(nitro)}$ hydrogen bond between a non trinitroethyl hydrogen atom and an oxygen atom of a trinitroethyl nitro group.

Of all the structures listed in Table 2.16 were hydrogen atom positions were available, C—H···A hydrogen bonding of the methylene-type hydrogen atoms of the trinitroethyl group was observed in seventeen out of twenty structures rendering C—H···A hydrogen bonding as another important intermolecular feature of the trinitroethyl functionality supporting higher densities.

Conclusion

Based on the crystal structures reported in this work and available in the literature, we find that trinitroethyl mediated intermolecular interactions like dipolar nitro group interactions and hydrogen bonding of the acidified methylene-type protons govern mainly the molecular packing of these compounds yielding high-crystal-density polymorphs with promising explosive performance parameters. Five new highly explosive compounds are introduced belonging to a new class of energetic materials preferentially containing both high-nitrogen and high-oxygen content. TTD, BTTD and BTAT display superior performance properties to RDX with BTAT at the same time being less sensitive and displaying a better oxygen balance value yielding smokeless combustion and less toxic fumes on decomposition. The compounds are water insoluble in contrast to energetic salts, a prerequisite to protect the ground and one important environmental advantage amongst the qualification criteria for new HEDM. It is shown that temperature stability can be higher than 140°C for solid and liquid compounds carrying the trinitroethyl moiety not only as far as decomposition temperatures but also as far as chemical long term stabilities are concerned. BTAT and BTHC are shown to be the molecules offering the best trade-off between energy capability and thermal stability. Next to its excellent thermal stability as well as its positive oxygen balance value, BTHC displays the rare and desirable property of being a solid with a reasonable low melting point and a liquid range of greater than 100°C while at the same time being insensitive according to BAM standards rendering a possible use as safe

melt-castable explosive. The tendency of conglomerate crystallization of BTHC is a further important point allowing for the specific design of its performance as well as sensitivity properties.

Experimental

CAUTION: The compounds described in this work are potential explosives, which may be subject to accidental initiation by such environmental stimuli as impact, friction, heat, or electrostatic discharge. Appropriate precautions and proper protective measures (safety glasses, face shields, leather coat, grounding (equipment and person), Kevlar™ gloves and ear plugs) should be taken and used when handling these materials. To avoid difficulties with the sensitivity of these compounds only millimolar amounts should be handled with care. Calculations. All calculations were carried out using the Gaussian G03W (revision B.03) program package. [282]

Materials. All reagents and solvents were used as received (Acros, Aldrich, Fluka) if not stated otherwise.

Instrumentation and Measurement. Electronic absorption spectra were acquired by using a Varian CARY 50 Conc UV-visible spectrophotometer in quartz cuvettes. ^{1}H, ^{13}C and $^{14/15}N$ NMR spectra were recorded using a Jeol Eclipse 270, Jeol EX 400 or Jeol Eclipse 400 instrument operating at 400 MHz (^{1}H), 100.6 MHz (^{13}C), 40.5 MHz (^{15}N) and 28.9 MHz (^{14}N). All chemical shifts are quoted in ppm relative to TMS (^{1}H, ^{13}C) or nitromethane (^{14}N / ^{15}N). Infrared (IR) spectra were recorded using a Perkin-Elmer Spektrum One FT-IR (using KBr disks) or a Perkin-Elmer Spektrum BX FT-IR (pure substance) instrument. Raman spectra were measured using a Perkin Elmer Spektrum 2000R NIR FT-Raman instrument equipped with a Nd:YAG laser (1064 nm). Elemental analyses were performed with a Netsch Simultanous Thermal Analyser STA 429. The thermal behaviour of the salts was investigated in a nitrogen atmosphere using differential scanning calorimetry (Linseis DSC PT-10) at heating rates (β) of 5 K min^{-1} and a nitrogen flow of 5 L h^{-1}. Typically, 2 mg of substance were measured inside a pressed aluminium container equipped with a hole (0.1 mm) for the gas release. Isothermal long term experiments were performed using a Systag TSC (isothermal safety calorimeter) station.

Ultrasound was applied using a Bandelin Sonorex RK 510 ultrasonic bath. The single crystal X-ray diffraction data were collected using an Oxford Xcalibur3 diffractometer equipped with a Kappa CCD detector. The Mo*Kα* radiation (λ = 0.71073 Å) was generated from a Spellman generator (50 kV, 40 mA) and focussed using a graphite collimator. The data collection was undertaken using the CrysAlis CCD software [283] and data reduction was performed using the CrysAlis RED software. [284] The structures were solved using SIR-92 [285] and refined using SHELXL-97 [286] implemented in the program package WinGX [287] and finally checked using PLATON. [288] The impact sensitivity tests were carried out according to STANAG 4489 [289] modified according to instruction [290] using a BAM (Bundesanstalt für Materialprüfung) drophammer. The friction sensitivity tests were carried out according to STANAG 4487 [291] modified according to instruction [292] using the BAM friction tester. The particle size was determined using a DIN 4188 testing sieve (Retsch). The respond to thermal shock and performance was tested using a Koenen steel sleeve apparatus. [293] The electrostatic sensitivity tests were carried out using an electric spark tester ESD 2010EN (OZM Research) operating with the 'Winspark 1.15 software package'. High speed images were recorded using a Visario G2 high-speed camera (Speed Cam Visario G2, Weinberger Deutschland GmbH, Erlangen, Germany).

2,2,2-Trinitroethanol (TNE)

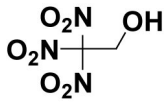

Trinitroethanol [294] was prepared from the reaction of trinitromethane with formaldehyde. [295] The crude product can be distilled (Caution: potential risk of explosion!). Suitable conditions for distillation have been found to be: pressure: 36 mbar / oil bath temperature: 135°C / trinitroethanol fraction temperature: 115°C, or: pressure: 22 mbar / oil bath temperature: 127°C / trinitroethanol fraction temperature: 112°C. Multinuclear NMR spectroscopy data confirm the structure of the compound:
^{1}H NMR ([D$_6$]acetone) δ(ppm): 5.17 (2H, d, ^{3}J=5.6 Hz), 6.32 (1H, t, ^{3}J= 5.6 Hz); ^{13}C NMR ([D$_6$]acetone) δ(ppm): 63.1 (d, -*C*H$_2$), 127.5 (bs, -*C*(NO$_2$)$_3$); ^{14}N NMR ([D$_6$]acetone) δ(ppm, nitromethane): -30.8 (-*N*O$_2$); impact sensitivity (50%, 2.5 kg weight) [296]: 11cm (pure crystals), 22cm (monohydrate), 25cm (wet with CCl_4), 86-101cm (crude oil); m.p. 73.5-74°C, sublimes easily under reduced pressure. The crystal growth was accomplished by sublimation of the solid at 298 K applying static low pressure (0.1 mbar), yielding colourless single crystals of rectangular habitus. Details of the single crystal X-ray diffraction experiment are listed in the appendix (Chapter 4).

Bis-(2,2,2-trinitroethyl)-amine (BTNA)

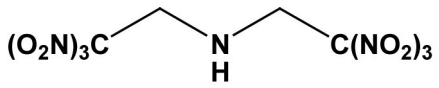

a) Though Murray and Sauer claim [297] that the condensation of nitroform with hexamethylenetetramine would afford bis-(2,2,2-trinitroethyl)amine we were not successful using this strategy or confirm it.
Potassium nitroformate (0.8849g, 4.47 mmol) were suspended in water (1 mL) and hydrochloric acid was added (1 M) until the pH value of one was achieved. Hexamethylenetetramine (0.1026g, 0.731 mmol) was dissolved in water (1 mL)

and slowly added to the solution of potassium nitroformate using a syringe while stirring the reaction mixture at 20°C (water bath). In order to keep the pH value below one, a further amount of hydrochloric acid (1M, 2.5 mL) was added in small portions. The reaction mixture was allowed to stir at room temperature for twelve hours. The yellow precipitate formed was filtered and identified as potassium nitroformate using Raman spectroscopy. The solution was evaporated and the yellow solid shown to be potassium nitroformate according to the intensities obtained from Raman spectroscopy.

b) Bis-(2,2,2-trinitroethyl)amine was successfully prepared from the reaction of trinitroethanol with ammonium acetate. [298] 2,2,2-trinitroethanol (2.5 g, 1.38 mmol) is dissolved in water (1 mL). To this is added a solution of ammonium acetate (0.525 g, 0.68 mmol) dissolved in water (4 mL) at room temperature. The solution turned orange after a few seconds and a white precipitate formed on stirring the solution at room temperature after five minutes. Stirring was continued for further 30 minutes. The precipitate was filtered and washed with cold water (3 times, each 2 mL). The white solid obtained was air dried (oven, 40°C, 30 min). The crystal growth was accomplished by storing a saturated carbontetrachloride solution in the refrigerator (7°C), yielding colorless single crystals of needle like habit.

DSC (Linseis, 5 K min^{-1}): 112.1°C (onset, decomp.); IR (KBr disk) $\tilde{\nu}$ /cm^{-1}: 3406 (w), 3370 (m), 2987 (w), 2946 (w), 2894 (w), 1582 (vs), 1478 (s), 1442 (s), 1431 (m), 1408 (w), 1397 (w), 1376 (m), 1350 (w), 1339 (w), 1307 (vs), 1298 (vs), 1258 (s), 1243 (m), 1156 (m), 1133 (m), 1089 (m), 1059 (w), 1049 (m), 1020 (w), 1008 (w), 883 (m), 873 (m), 854 (s), 803 (vs), 791 (vs), 781 (vs), 751 (w), 740 (m), 712 (w), 660 (m), 642 (s); Raman (1 cm^{-1}) $\tilde{\nu}$ /cm^{-1}: 3011 (8), 2982(13), 2949(24), 1607(27), 1445 (20), 1431 (11), 1398 (16), 1377 (15), 1354 (43), 1311 (41), 1260 (8), 859 (100), 809 (8), 782 (8), 663 (8), 644 (10), 562 (9), 536 (11), 423 (47), 397 (50), 376 (90), 299 (19), 280 (22), 213 (24); MS (DEI, 70eV): 343 [m^+], HRMS: Calc. for BTNA: 342.9996 found: 342.9970 (-2.6 mmu); impact sensitivity: 15 J (1/6, explosion), friction sensitivity: greater 360 N; Details of the single crystal X-ray diffraction experiment are listed in the appendix (Chapter 4).

5-(1-Methyl-2-(2,2,2-trinitroethyl)hydrazinyl)-1H-tetrazole (MTHT)

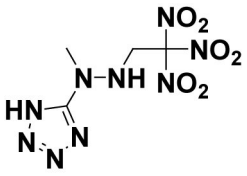

1-Methyl-1-(1*H*-tetrazol-5-yl)hydrazine (0.114 g, 1 mmol) was dissolved in water (200 mL) at ambient temperature. A solution of 2,2,2-trinitroethanol (0.200 mg, 1.1 mmol) in water (50 mL) was added and the reaction mixture was exposed to ultrasound at ambient temperature for ten minutes affording a white solid to precipitate. The reaction mixture was stirred for another two hours. The precipitate was filtered, washed with water (two times, 50 mL) and dried using a desiccator (P_4O_{10}).

Raman (100 mW, 100 scans, protection shield, 1 cm^{-1}) $\tilde{\nu}$ /cm^{-1}: 3287 (39), 2996 (21), 2948 (43), 2826 (14), 1627 (34), 1605 (42), 1464 (24), 1450 (23), 1413 (38), 1403 (41), 1349 (48), 1303 (41), 1285 (36), 1228 (19), 1114 (25), 1086 (38), 1063 (25), 1038 (28), 998 (25), 971 (30), 856 (100), 800 (17), 779 (15), 740 (15), 656 (23), 629 (19), 541 (21), 449 (31), 404 (72), 372 (75), 312 (28), 255 (30), 202 (29), 187 (30); IR (pure solid substance) $\tilde{\nu}$ /cm^{-1}: 3286 (w), 2992 (w), 2946 (w), 2890 (w), 2736 (w), 1774 (w), 1582 (vs), 1475 (w), 1410 (w), 1386 (w), 1348 (w), 1298 (s), 1225 (m), 1162 (w), 1126 (w), 1061 (m), 1035 (m), 992 (w), 964 (w), 876 (w), 854 (w), 834 (w), 796 (vs), 776 (s), 738 (m), 709 (w), 690 (w), 655 (w); $T_{decomp.}$(Büchi melting point apparatus, 5°/min): 98°C (colour change from initally white to yellow), 100°C (deflagration).

(E)-1-Methyl-1-(1*H*-tetrazol-5-yl)-2-(2,2,2-trinitroethylidene)hydrazine (MTTH)

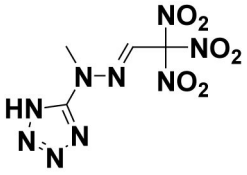

Details of the single crystal X-ray diffraction experiment are listed in the appendix (Chapter 4).

1-Methyl-5-(1-methyl-2-(2,2,2-trinitroethyl)hydrazinyl)-1*H*-tetrazole (MMTHT)

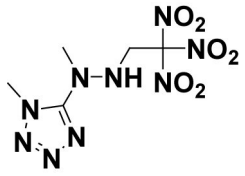

1-Methyl-1-(1-methyl-1*H*-tetrazol-5-yl)hydrazine (0.128 g, 1 mmol) was dissolved in water (200 mL) at ambient temperature. A solution of 2,2,2-trinitroethanol (0.200 mg, 1.1 mmol) in water (50 mL) was added and the reaction mixture was exposed to ultrasound at ambient temperature for ten minutes affording a white solid to precipitate. The reaction mixture was stirred for another two hours. The precipitate was filtered, washed with water (two times, 50 mL) and dried using a desiccator (P_4O_{10}).

IR (pure solid substance between KBr plates) $\tilde{\nu}$ /cm^{-1}: 3342 (m), 2974 (w), 2941 (w), 2903 (w), 1610 (m), 1571 (vs), 1474 (s), 1458 (m), 1430 (m), 1419 (m), 1405 (w), 1391 (w), 1354 (w), 1308 (s), 1298 (s), 1265 (w), 1235 (w), 1202 (w), 1143 (m), 1122 (w), 1107 (w), 1045 (w), 879 (w), 858 (w), 821 (m), 797 (vs), 770 (s), 755 (m), 717 (w), 663 (w); $T_{decomp.}$: 82.5°C (onset, 2°C/min, Linseis DSC); $T_{decomp.}$(Büchi melting point apparatus, 5°/min): 82°C (colour change from initially white to yellow), 87°C (melting with decomp.) $C_5H_9N_9O_6$: calc.: N (43,3%), C (20,6%), H (3,1%), found: N (43,1%), C (20,9%), H (3,3%); impact sensitivity (powder): > 30J, impact sensitivity (single crystals): > 30J, friction sensitivity: 108N (visible flame, no sound), $\Delta U_{comb.}$ (exp.): 2936 cal/g, Ω: -46.7%, Q_v (calc.): -6368 kJ/kg, T_{ex} (calc.): 4404 K, P_D (calc.): 277 kbar, V_D (calc.): 8307 m/s, V_0 (calc.): 783 L/kg. Details of the single crystal X-ray diffraction experiment are listed in the appendix (Chapter 4).

2-(5-(1-Methyl-2-(2,2,2-trinitroethyl)hydrazinyl)-1*H*-tetrazol-1-yl)ethanol (MTHTE)

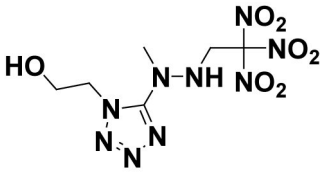

2-(5-(1-Methyl-hydrazinyl)-1H-tetrazol-1-yl)ethanol (0.158 g, 1 mmol) was dissolved in water (200 mL) at ambient temperature. A solution of 2,2,2-trinitroethanol (0.200 mg, 1.1 mmol) in water (50 mL) was added and the reaction mixture was exposed to ultrasound at ambient temperature for ten minutes affording a white solid to precipitate. The reaction mixture was stirred for another two hours. The precipitate was filtered, washed with water (two times, 50 mL) and dried using a desiccator (P_4O_{10}).
Details of the single crystal X-ray diffraction experiment are listed in the appendix (Chapter 4).

1-(^{4}N-2,2,2-Trinitroethyl)-2,5-hydroxymethyltriazine (THMT)

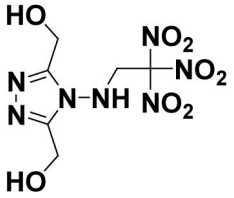

1-Amino-2,5-hydroxymethyltriazine (0.144 g, 1 mmol) was dissolved in water (200 mL) at ambient temperature. A solution of 2,2,2-trinitroethanol (0.200 mg, 1.1 mmol) in water (50 mL) was added and the reaction mixture was exposed to ultrasound at ambient temperature for ten minutes affording a white solid to precipitate. The reaction mixture was stirred for another two hours. The precipitate was filtered, washed with water (two times, 50 mL) and dried using a desiccator (P_4O_{10}).
Details of the single crystal X-ray diffraction experiment are listed in the appendix (Chapter 4).

N^1-(2,2,2-Trinitroethyl)-1*H*-tetrazole-1,5-diamine (TTD)

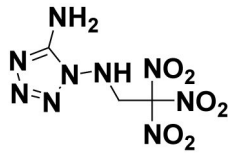

2,2,2-Trinitroethanol is a starting material for the synthesis of TTD and was synthesised from the condensation of formaldehyde and trinitromethane. [295] 1,5-Diaminotetrazole (0.100 g, 1 mmol) was dissolved in water (200 mL) at ambient temperature. A solution of 2,2,2-trinitroethanol (0.200 mg, 1.1 mmol) in water (50 mL) was added and the reaction mixture was exposed to ultrasound at ambient temperature for ten minutes affording a white solid to precipitate. The reaction mixture was stirred for another two hours. The precipitate was filtered, washed with water (two times, 50 mL) and dried using a desiccator (P_4O_{10}).

DSC (Linseis, 5 K min^{-1}): exo (125.6°C, onset / 129.1°C, max / 131.9°C, offset); T_{dec}(Büchi melting point apparatus, 10°/min): 156°C-157°C (explosion); isothermal long term stability (48 h, 85°C): unchanged; isothermal long term stability (isoperibol steps, temperature was held constant every 20°C for one hour): explosion at 100°C; ^{1}H NMR ([D_6]acetone) δ: 5.33 (2H, -CH_2-, d, ^3J = 6.1 Hz) 6.09 (2H, s, -NH_2), 7.55 (1H, -NH-, t, ^3J = 6.1 Hz); ^{13}C NMR ([D_6]acetone) δ: 52.4 (s, -CH_2-), 126.6 (bs, -$C(NO_2)_3$), 153.5 (s, C_{ring}); IR (KBr) $\tilde{\nu}$ /cm^{-1}: 3414 (vs), 3311 (s), 3173 (vs), 3001 (m), 2955 (m), 1651 (vs), 1610 (vs), 1585 (vs), 1494 (s), 1459 (w), 1414 (s), 1381 (w), 1347 (w), 1321 (vs), 1302 (vs), 1136 (m), 1120 (m), 1081 (m), 1040 (w), 989 (w), 907 (w), 855 (w), 835 (w), 806 (vs), 774 (m), 739 (w), 715 (w), 673 (w), 648 (m), 582 (w), 546 (w), 459 (w); Raman (4 cm^{-1}) $\tilde{\nu}$ /cm^{-1}: 3172 (19), 3001 (23), 2987 (59), 2958 (41), 1652 (37), 1612 (42), 1585 (25), 1495 (33), 1463 (31), 1416 (42), 1381 (34), 1349 (50), 1323 (81), 1305 (43), 1278 (29), 1141 (24), 1116 (29), 1080 (23), 1041 (30), 1003 (18), 991 (21), 909 (18), 857 (100), 808 (38), 780 (95), 736 (14), 675 (20), 643 (20), 543 (19), 519 (23), 460 (26), 416 (57), 400 (58), 375 (100), 335 (61), 305 (32), 264 (42), 225 (32), 207 (42), 172 (46); MS (DCI+, isobutane): 264 [m+H]; Calc for $C_3H_5N_9O_6$: N (47.9%), C (13.7%), H (1.9%), found: N (47.5%), C (13.9%), H

(2.0%); impact sensitivity: < 30 J (decomposition), friction sensitivity: 40 N (explosion), electrostatic spark sensitivity (particle size 0.08 – 0.16 mm): < 0.1 J (explosion); Koenen Test: > 10 mm; Details of the single crystal X-ray diffraction experiment are listed in the appendix (Chapter 4).

N^1,N^5-Bis-(2,2,2-trinitroethyl)-1*H*-tetrazole-1,5-diamine (BTTD)

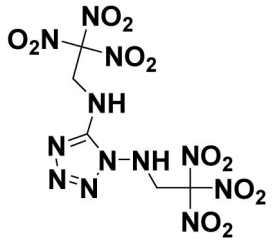

TTD (0.158 g, 0.6 mmol) was dissolved in concentrated hydrochloric acid (50 mL). To the stirred solution was added 2,2,2-trinitroethanol (0.254 g, 1.4 mmol) at room temperature. The colorless solution was heated to 50°C for one hour and extracted using dichloromethane. The collected organic fractions were dried using magnesium sulfate, filtered and concentrated using a rotary evaporator.

DSC (Linseis, 5 K min^{-1}): exo (126.6°C, onset / 132.0°C, max / 137.4°C, offset); MS (DCI+, isobutane): 427 [m+H]; Calc. for $C_5H_6N_{12}O_{12}$: N (39.4%), C (14.1%), H (1.4%), found: N (39.0%), C (14.2%), H (1.5%); Details of the single crystal X-ray diffraction experiment are listed in the appendix (Chapter 4).

N^3,N^6-Bis-(2,2,2-trinitroethyl)-1,2,4,5-tetrazine-3,6-diamine (BTAT)

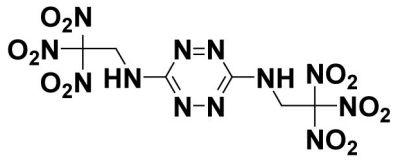

3,6-Diamino-1,2,4,5-tetrazine is a starting material for the synthesis of BTAT and was synthesised from the condensation of diaminoguanidinium hydrochloride with 2,4-pentanedione, followed by oxidation of the resulting dihydrotetrazine with sodium perborate. [299] Two pathways have been found for the preparation and isolation of BTAT. Method a) According to the first pathway, BTAT can be obtained on treating a solution of 3,6-diaminotetrazine in concentrated hydrochloric acid (37%) at a temperature of 70°C. The product precipitates from the solution and can be obtained in high purity on simple filtration. We observed that the yields of this approach are quite low (see section 2.1.4, page 119). Method b) 3,6-diamino-1,2,4,5-tetrazine (0.067 g, 0.6 mmol) was suspended in acetonitrile (100 mL) at room temperature. A solution of iron-(III)-chloride (0.100 g, 0.6 mmol) dissolved in nitromethane (5 mL) was added. 2,2,2-trinitroethanol (0.253 g, 1.4 mmol) was subsequently added and the reaction stirred for four hours at room temperature. The reaction mixture was then treated with hydrochloric acid (2M, 100 mL) and extracted three times using dichloromethane (100 mL). The collected organic phases were dried using magnesium sulfate, filtered and concentrated using a rotary evaporator affording a red solid containing BTAT of rather low purity.
Method c) 3,6-diaminotetrazine (2,2g) was suspended in acetonitrile (200 mL). Trinitroethanol (9g) and subsequently a solution of iron-(III)-chloride (12g) dissolved in nitromethane (75mL) were added yielding a clear solution of all of the components. The reaction was allowed to stir at ambient conditions for 10h. The reaction mixture was concentrated using a rotary evaporator (60°C, 90mbar) affording a sticky, nearly solid dark residue. Subsequently, the following steps were involved in the work up procedure:

1) The residue was dissolved in acetonitrile (20 mL) and filtered to remove unreacted starting material (3,6-diamino-1,2,4,5-tetrazine, 200mg).

2) Hydrochloric acid (2M, 2L) was added to the filtrate to precipitate the BTAT from solution and keep the iron complex in solution. It takes several hours for the product to precipitate (bright orange colour). The picture on the right was taken after one day.

3) The orange precipitate is filtered yielding crude product.

4) The crude product is dissolved in a small amount of acetonitrile and the undissolved iron complex is removed by filtration.

7) Hydrochloric acid (2M) is added to precipitate the BTAT from solution. Finally, the product is filtered and washed with water yielding BTAT as bright orange powder of high purity.

DSC (Linseis, 5 K min^{-1}): decomposition, 1st exo (183.7°C, onset / 189.2°C, max / 197.8°C, offset), 2nd exo (201.4°C, onset / 208.4°C, max / 214.2, offset); isothermal long term stability (48h, 140°C): no decomposition; ^{1}H NMR ([D_6]acetone) δ: 7.88 (1H, -NH-, t, ^{3}J = 6 Hz), 5.61 (2H, -CH_2- d, ^{3}J = 6 Hz) ^{13}C NMR ([D_6]acetone) δ: 44.8 (s, -CH_2-), 125.6 (bs, -$C(NO_2)_3$), 160.6 (s, C_{ring}); ^{14}N NMR ([D_6]acetone) δ (nitromethane): -253.7 (bs, -NH-), -31.2 (s, -NO_2), 109.9 (bs, N_{ring}); IR (KBr pellet) $\tilde{\nu}$ /cm^{-1}: 3285(m), 3013(w), 2963(w), 2890(w), 1612(vs), 1580(vs), 1531(vs), 1441(s), 1416(m), 1386(w), 1356(w), 1313(s), 1264(m), 1135(w), 1116(w), 1069(w), 1051(s), 1002(w), 941(m), 890(w), 854(w), 816(m), 790(m), 772(w), 723(w), 640(w), 575(w), 541(w), 496(w); Raman (4 cm^{-1}) $\tilde{\nu}$ /cm^{-1}: 3289(7), 3006(4), 2965(17), 1896(6), 1607(14), 1556(19), 1509(27), 1421(13), 1385(29), 1357(27), 1306(19), 1292(13), 1130(5), 1058(4), 1002(6), 895(39), 857(73), 806(8), 784(5), 768(4), 680(6), 645(10), 602(6), 532(9), 519(7), 423(19), 393(21), 375(26), 333(7), 300(17), 219(11), 205(13), 95(4); UV-vis (CH_3CN) (λ_{max}, nm): 240.5 nm, 413.5 nm, 507.5 nm; MS (DEI+): 438 [m, 13.5%], 392 [m - NO_2, 1.4%], 346 [m - 2 NO_2, 1.5%], 300 [m - 3 NO_3, 2.0%],

206 [N≡C–NH–CH_2–$C(NO_2)_3$, 21.9%], 149 [$C(NO_2)_3$, 8.2%], 46 [NO_2, 25.8%]; Calc. for $C_6H_6N_{12}O_{12}$: N (38.4), C (16.5%), H (1.4%), found: N (37.7%), C (17.1%), H (1.5%); impact sensitivity: 7 J (decomp.) , friction sensitivity: between 160 N (no decomp.) and 168 N (decomp.), electrostatic spark sensitivity (particle size 0.08 – 0.16 mm): 0.2 J (decomp.); Details of the single crystal X-ray diffraction experiment are listed in the appendix (Chapter 4).

Tris-(2,2,2-trinitroethyl)borate (TTB)

A mixture of 1g (5.5 mmol) 2,2,2-trinitroethanol and 4.8 g (32.8 mmol) of triethyl borate was heated to 95°C over a period of four hours under inert reflux conditions. Ethanol was removed under reduced pressure affording a white solid. The substance shows a green flame colour.

DSC (Linseis, 5 K min^{-1}): 1st endo (153.3°C onset / 160.9°C min / 164.8 offset), 2nd endo (175.7°C onset / 178.7°C min / 181.4 offset), 3rd endo (210.0 onset / 211.2 min / 214.9 offset); T_{melt}(Büchi melting point apparatus, 5°/min): 175-176°C ; ^{1}H NMR ([D_3]acetonitrile) δ: 5.18 (2H, s, -CH_2-); ^{13}C NMR ([D_3]acetonitrile) δ: 62.4 (s, -CH_2-), 124.1 (bs, -$C(NO_2)_3$); ^{15}N NMR ([D_3]acetonitrile) δ (nitromethane): -33.8 (s, -NO_2); ^{11}B NMR ([D_3]acetonitrile) δ: 16.7; MS (DEI+): 503 [m, 1%].

S-Ethyl-2,2,2-trinitroethyl-thioformate

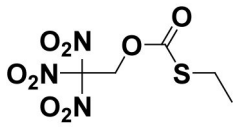

Ethyl chlorothioformate (Acros, ρ (20°C) = 1.195 g mL^{-1}, 5g, 40 mmol) is added to a stirred solution of 2,2,2-trinitroethanol (7.24g, 40 mmol) in dichloromethane (15 mL), followed by the addition of a solution of iron(III)chloride in nitromethane (1.4g $FeCl_3$, 4mL CH_3NO_2). A vigorous reaction with evolution of hydrogen chloride begins immediately and is essentially complete within a few minutes. To insure complete reaction, stirring is continued for 30 minutes at ambient temperature. The reaction mixture is taken up in additional dichloromethane (50mL) and washed consecutively with dilute hydrochloric acid (2M, 100mL) and water (3x100mL). The organic phase is dried using magnesium sulfate, filtered and the solvent removed in vacuo yielding essentially pure product.

Figure 2.114. Trinitroethanol (left picture), colourless solution of trinitroethanol and ethyl chlorothioformate (second left picture). A vigorous reaction starts immediately after the addition of iron(III)chloride (picuture in the middle). The formation of hydrogen chloride can be monitored using indicator paper (right picture).

IR (KBr disk) $\tilde{\nu}$ /cm^{-1}: 2964 (s), 2932 (m), 2878 (m), 2641 (w), 2592 (w), 1723 (vs), 1599 (vs), 1440 (s), 1379 (s), 1298 (vs), 1118 (vs), 1088 (vs), 1059 (s), 1032 (m), 970 (m), 881 (w), 852 (m), 817 (m), 795 (vs), 776 (s), 758 (w), 739 (w), 720 (w), 658 (m), 545 (m); Raman (200 mW, 100 scans, protection shield, 4 cm^{-1}) **$\tilde{\nu}$ /cm^{-1}:** 2980 (60), 2939 (92), 2878 (41), 1727 (37), 1613 (40), 1451 (40), 1419 (37), 1381 (43), 1350 (49), 1302 (43), 1055 (34), 1032 (33), 890 (29), 857 (75), 795 (25), 706 (36), 684 (33), 668 (42), 658 (42), 636 (31), 550 (30), 509 (38), 401 (49), 373 (70), 271 (53). Details of the single crystal X-ray diffraction experiment are listed in the appendix (Chapter 4).

2,2,2-Trinitroethyl-chloroformate

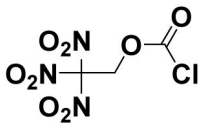

A solution of S-ethyl-2,2,2-trinitroethyl-thioformate (40mmol) in 1,2-dichloroethane (50mL, b.p. 83°C) and sulfuryl chloride (20mL, b.p. 68-70°C) is heated to reflux for six hours and then allowed to cool. The more volatile components are removed using a rotary evaporator and the residue is distilled through a short-path vigreux column (Caution: potential risk of explosion!). Suitable conditions for distillation have been found to be: pressure: $2.8 \cdot 10^{-2}$ mbar (dynamic vacuum) / oil bath temperature: 70°C / S-ethyl-2,2,2-trinitroethyl-thioformate fraction temperature: 45°C, or: pressure: 22 mbar / oil bath temperature: 127°C / trinitroethanol fraction temperature: 112°C.

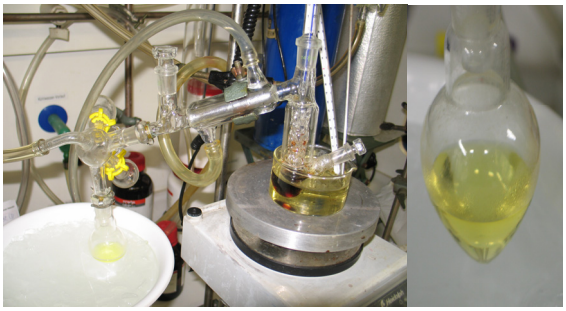

Figure 2.115. Destillation of S-ethyl-2,2,2-trinitroethyl-thioformate (left picture) and pure product (right picture).

IR (KBr disk) $\tilde{\nu}$ /cm^{-1}: 3022 (w), 2971 (w), 2893 (w), 2642 (w), 2593 (w), 1784 (vs), 1598 (vs), 1438 (s), 1383 (m), 1347 (m), 1297 (vs), 1147 (vs), 1091 (vs), 1034 (w), 979 (m), 890 (w), 853 (s), 827 (m), 798 (vs), 779 (vs), 721 (s), 677 (vs), 644 (m), 609 (w), 548 (s), 496 (w) ; Raman (200 mW, 100 scans, protection shield, 4 cm^{-1}) $\tilde{\nu}$ /cm^{-1}: 3021 (11), 2972 (35), 1785 (13), 1615 (26), 1439 (14), 1301 (32), 1168 (7), 1092 (8), 1033 (25), 982 (4), 892 (21), 856 (100), 828 (8), 800 (14), 778 (8), 724 (5), 644 (8), 549 (12), 501 (57), 463 (11), 399 (51), 373 (86), 336 (15), 284 (48), 233 (29), 197 (29).

Bis-(2,2,2-trinitroethyl)-carbonate (BTC)

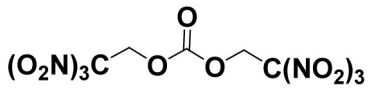

Bis-(2,2,2-trinitroethyl)-carbonate (Hill, 1956) was prepared from the reaction of trinitroethanol with phosgene (Hall, 1968). The crystal growth was accomplished by concentration of a saturated $CHCl_3$ solution at ambient temperature, yielding colourless single crystals.
The following experimental data are available in the literature: [300-301] m.p. 115°C, impact sensitivity (50%, NOL app., 2.5 kg, 16cm): 4 J; Details of the single crystal X-ray diffraction experiment are listed in the appendix (Chapter 4).

2,2,2-Trinitroethyl-azidoformate (TAF)

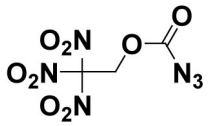

2,2,2-Trinitroethyl-chloroformate is a starting material for the synthesis of TAF and was synthesised according to literature procedure. [302] Trimethylsilyazide (0.524 g, 4.55 mmol) was dissolved in acetonitrile (10 mL). 2,2,2-Trinitroethyl-chloroformate (0.499 g, 2.05 mmol) dissolved in acetonitrile (1 mL) was added to this solution drop wise at room temperature and kept under a constant stream of nitrogen. The color of the solution changed from colorless to orange and got turbid after a few minutes with the formation of a precipitate. The reaction was allowed to stir for further twelve hours. The solvent was then removed using a high vacuum line affording orange oil together with precipitate. Pure TAF was obtained as a white solid on sublimation of the reaction residue using a cold finger (-78°C).
DSC (Linseis, 5 K min^{-1}): 1st endo (27.5°C, onset / 29.9°C, min / 32.3°C, offset), 2nd endo (96.2°C, onset / 118.4°C, min / 129.2°C, offset), 1st exo (130.4°C, onset / 158.4°C, max / 174.5°C, offset), 2nd exo (191.6°C, onset / 205.6°C, max

/ 218.6, offset); ^{1}H NMR ([D$_6$]acetone) δ: 5.96 (2H, s, -CH$_2$-); ^{13}C NMR ([D$_6$]acetone) δ: 63.7 (s, -CH$_2$-), 123.9 (bs, -C(NO$_2$)$_3$), 156.1 (s, O$_2$CN$_3$); ^{15}N NMR ([D$_6$]acetone) δ (nitromethane): -34.7 (s, -NO$_2$), -141.1 (s, N$_{beta}$), -148.2 (s, N$_{gamma}$), -266.9 (s, N$_{alpha}$); IR (KBr disk) $\tilde{\nu}$ /cm^{-1}: 3018 (vs), 2971 (vs), 2893 (s), 2651 (w), 2601 (w), 2399 (w), 2190 (vs), 1751 (s), 1598 (s), 1442 (s), 1386 (s), 1354 (s), 1297 (s), 1236 (s), 1186 (s), 1099 (m), 1049 (m), 1007 (m), 941 (m), 879 (m), 855 (m), 806 (m), 783 (m), 742 (m), 708 (w); Raman (4 cm^{-1}) $\tilde{\nu}$ /cm^{-1}: 2974 (36), 2170 (11), 1615 (38), 1384 (29), 1357 (43), 1304 (44), 1099 (15), 1009 (22), 942 (27), 894 (19), 857 (83), 734 (21), 531 (20), 408 (61), 375 (73), 292 (53), 256 (41); MS (DEI+): 250 [m, 1.7%], 204 [m - NO$_2$, 2%], 164 [m - O$_2$C-N$_3$, 100%], 158 [m - 2 NO$_2$, 19.8%], 118 [m - (O$_2$C-N$_3$, 2 NO$_2$), 100%], 70 [N$_3$CO, 10.5%], 44 [CO$_2$, 3.8%]; Calc. for C$_3$H$_2$N$_6$O$_8$: C (14.4 %), H (0.8 %), N (33.6 %), found: C (14.7 %), H (1.0 %), N (32.5 %) ; Details of the single crystal X-ray diffraction experiment are listed in the appendix (Chapter 4).

Bis-(2,2,2-trinitroethyl)-hydrazodicarboxylate (BTHC)

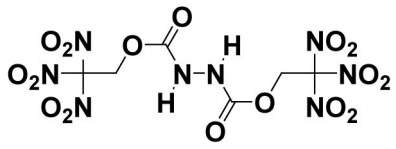

2,2,2-Trinitroethylchloroformate (4.00 g, 18.7 mmol) was dissolved in dichloromethane (20 mL). The solution was cooled to -78°C. To this was added 23.92 g of a solution of hydrazine in THF (1 molar, density 0.89 g/mL). A white precipitate formed. The reaction mixture was allowed to warm to 0°C over a period of one hour. Cold water (0°C) was added (20 mL) and the solution extracted with diethyl ether (5x, each 50 mL). The collected organic phases were dried using magnesium sulfate, filtered and concentrated using a rotary evaporator. The density of the pure substance was estimated to be 1.8 g cm^{-3} according to weighing several samples of different volume. Solidified BTHC was dissolved in acetone or ethyl acetate affording single crystals on standing at room temperature.

DSC (Linseis, 5 K min^{-1}): exo (188.3°C, onset / 193.6°C, max / 201.7°C, offset); Isothermal long term stability (RADEX, 48h, 140°C): no decomposition; impact sensitivity: greater 100 J, friction sensitivity: greater 360 N.

BTHC / acetone 1:1

DSC (Linseis, 5 K min^{-1}): BTHC acetone (1:1): endo (87.1°C, onset / 89.8°C, min / 92.6°C, offset), exo (185.4°C, onset / 193.7°C, max / 206.4°C, offset); ^{1}H NMR ([D_6]acetone) δ: 5.79 (2H, s, -CH_2-); ^{13}C NMR ([D_6]acetone) δ: 66.2 (s, -CH_2-), 128.7 (bs, -$C(NO_2)_3$), 158.2 (s, -O_2C-); MS (DEI+, acetone): 446 [m, 7.4%], 400 [m - NO_2, 0.6%], 266 [m – O-CH_2-$C(NO_2)_3$, 2.5%], 46 [NO_2, 62.5%], 30 [NO, 100%]; Details of the single crystal X-ray diffraction experiment are listed in the appendix (Chapter 4).

BTHC / ethyl acetate 1:1

DSC (Linseis, 5 K min^{-1}): BTHC ethyl acetate (1:1): endo (51.5°C, onset / 55.7°C, min / 59.2°C, offset), exo (188.6°C, onset / 193.6°C, max / 207.3°C, offset); ^{1}H NMR ([D_3]chloroform) δ: 5.46 (2H, s, -CH_2-), 7.77 (2H, s, -NH-); ^{13}C NMR ([D_3]chloroform) δ: 62.0 (s, -CH_2-), 122.7 (bs, -$C(NO_2)_3$), 153.4 (s, -O_2C-); ^{15}N NMR ([D_3]chloroform) δ (nitromethane): -35.6 (s, -NO_2), 284.0 (s, -NH-); IR (KBr disk) $\tilde{\nu}$ /cm^{-1}: 3416 (bs, w), 3020 (w), 2973 (w), 2900 (w), 1789 (m), 1762 (m), 1693 (m), 1603 (vs), 1529 (w), 1497 (w), 1439 (w), 1384 (w), 1302 (s), 1273 (m), 1207 (s), 1116 (m), 1093 (m), 1047 (w), 879 (w), 856 (w), 805 (m), 785 (m), 753 (w), 647 (bs, w), 614 (w), 542 (w), 467 (w); Details of the single crystal X-ray diffraction experiment are listed in the appendix (Chapter 4).

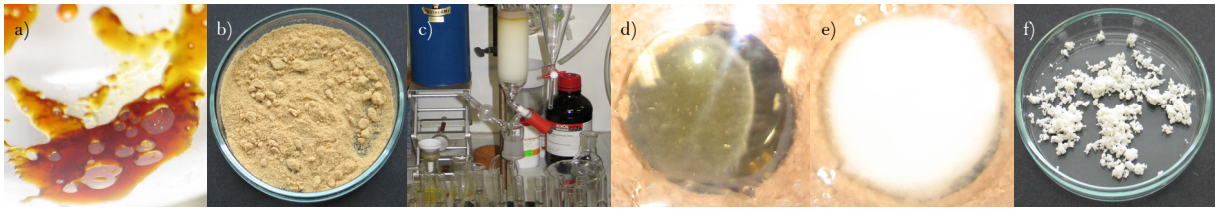

Figure 2.116. a+b) crude reaction product c) column chromatography d) pure, glass-like prodcut e+f) co-crystallization with ethyl acetate to yield a white solid.

2.3 Precursor Molecules for the Synthesis of Energetic Materials

2.3.1 Guanidine

Introduction

Guanidinium nitroformate was of interest to us not only because of its potentially promising energetic properties but also because the covalent form can formally be considered as saturated analogue to 1,1-dinitro-2,2-diamino-ethene [303-304] (FOX-7), one of the most promising novel novel and insensitive energetic materials. [305] Of interest, 1,1,1-triamino-2,2,2-trinitroethane can be described as a hexasubstituted push-pull ethane where the electron distribution is influenced by or even switched between two extreme cases due to solvent molecules or change of physical state resulting in ionic (guanidinium nitroformate, GNF) and covalent (triaminotrinitroethane, TTE) bond-strech isomers (Fig. 2.117). [306-308]

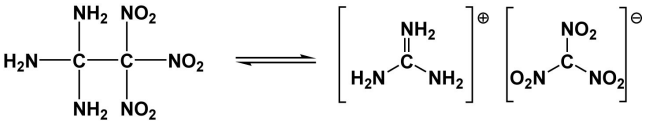

Figure 2.117. Bond stretch isomerism can formally occur in the substance composed of guanidine and trinitromethyl giving rise to 1,1,1-triamino-2,2,2-trinitroethane or its ionic form, guanidinium trinitromethanide.

Hence, we were interested in investigating whether guanidinium nitroformate can exist in ionic or respectively and its corresponding covalent form (1,1,1-triamino-2,2,2-trinitroethane, TTE). Our experimental data on GNFH (see Chapter 2.1.1) show that the hydrated guanidinium nitroformate exists in the ionic form both in solution and the solid state. However, the presence of water undoubtedly affects the stability of the salt as can be depicted by comparison of the sensitivity and thermal stability data of GNFH and the corresponding homologous guanidinium nitroformate salts where GNFH has been found to show the lowest sensitivity as well as highest thermal stability data. However, the possibility of a covalently-bonded isomer does occur either in an anhydrous state or other solvents not stabilizing the ionic form.

Synthesis

Guanidine was prepared from the acid base reaction between guanidinium chloride and sodium methanolate in dry methanole (Fig. 2.118).

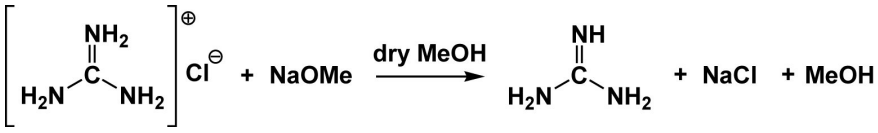

Figure 2.118. Synthesis of guanidine from guanidinium chloride and sodium methanolate.

In order to synthesise the anhydrous compound, we tested another approach utilizing the reaction between the free base guanidine and trinitromethane (Fig. 2.119).

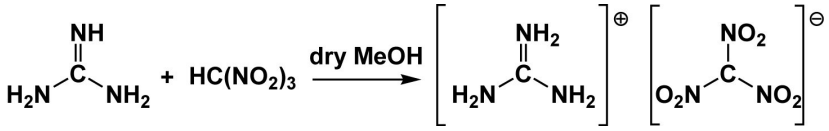

Figure 2.119. Synthesis of anhydrous guanidinium nitroformate from guanidine and trinitromethane.

A stoichiometric amount of dry trinitromethane was subsequently added affording a yellow solution. As mentioned earlier, the yellow colour is characteristic for the nitroformate anion indicating that the compound formed in methanolic solution was ionic. By comparison, the Raman spectrum of the yellow solid obtained after removal of methanol was shown to be identical with guanidinium nitroformate hydrate except for the signals of water suggesting that anhydrous guanidinium nitroformate exists in its ionic form. Furthermore, we were able to proof that the educt used was indeed the free base guanidine as evidenced by the successful growth of single crystals and its subsequent structure determination. Only very recently, density functional theory calculations of both the ionic guanidinium nitroformate as well as the covalent form 1,1,1-triamino-2,2,2-trinitroethane have been reported. According to these calculations, guanidinium nitroformate has been found to be 85 kJ mol^{-1} more stable than 1,1,1-triamino-2,2,2-trinitromethane. [309]

Crystal Structure Analysis

Due to the high basicity, guanidine (aminoformamidine) was considered to be the strongest neutral organic base (pK_a = 13.6) [310] until *proton sponges* [311-312] were synthesised. The question of its molecular structure and the reason for its exceptional properties inspired several controversial theoretical works [313-322] since an experimentally determined structure for guanidine was not available. To our knowledge, only a few neutral derivatives of guanidines containing sterically demanding organic substituents have been structurally characterized using single-crystal X-ray diffraction. Rare examples describe 1,1,3,3-tetrasubstituted [323-324] as well as 1,2,3-trisubstituted [325] guanidine derivatives acting as ligands in transition metal complexes. Here we report crystal structures containing the unsubstituted free base guanidine and 2-amino-4,6-dimethyl-1,3,5-triazine. Single crystals consisting of guanidine and 2-amino-4,6-dimethyl-1,3,5-triazine were obtained when acetonitrile was allowed to slowly diffuse into a methanolic solution of guanidine. The presence of 2-amino-4,6-dimethyl-1,3,5-triazine in the crystal structures of the 1:1 co-crystal as well as the 2:1 co-crystal corresponds to and confirms the formation of substituted 2-amino-triazines from aliphatic nitriles and guanidine in the presence of alkoholates. [326]

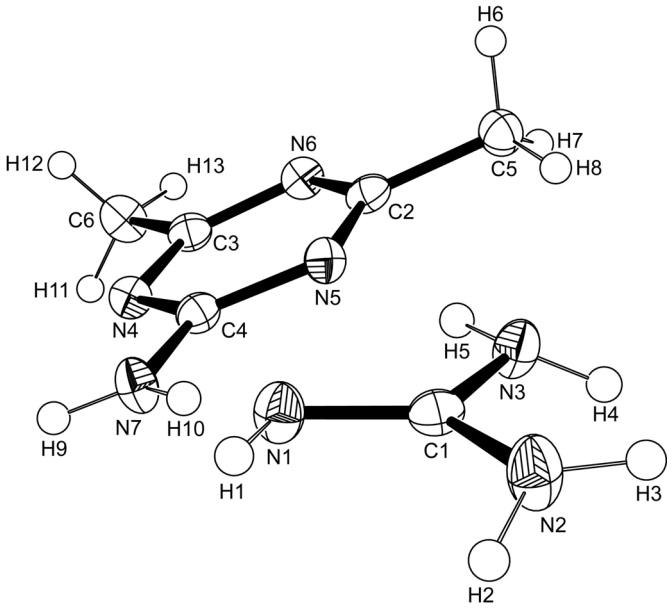

Figure 2.120. Ortep representation of the structure of 2-amino-4,6-dimethyl-1,3,5-triazine · guanidine. The thermal ellipsoids are shown at the 50 % probability level.

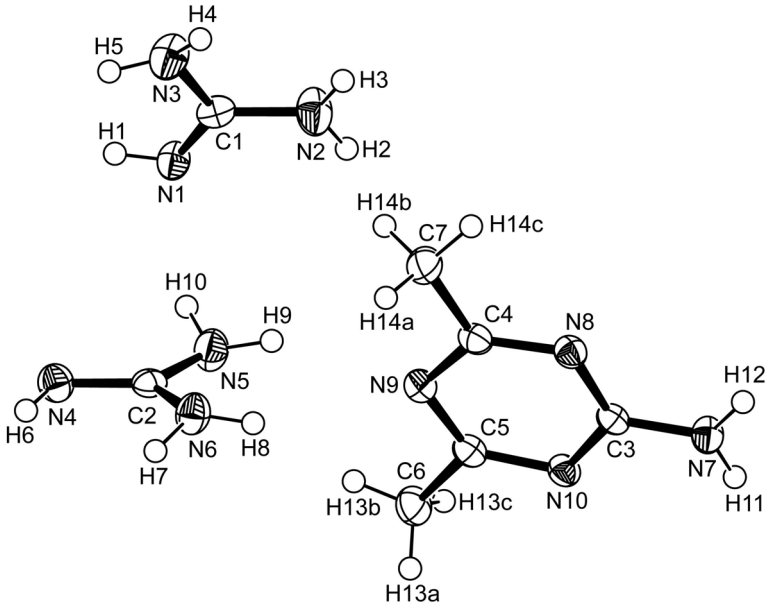

Figure 2.121. Ortep representation of the structure of 2-amino-4,6-dimethyl-1,3,5-triazine · 2 guanidine. The thermal ellipsoids are shown at the 50 % probability level.

A comparison of 2-amino-4,6-dimethyl-1,3,5-triazine in the crystal structures (Figs. 2.120, 2.121) with the earlier reported crystal structure of the pure compound [327] reveals the same planar triazine ring and a similar packing with the formation of dimers due to hydrogen bonding between the two terminal amino groups and two ring nitrogen atoms (Figs. 2.122, 2.123).

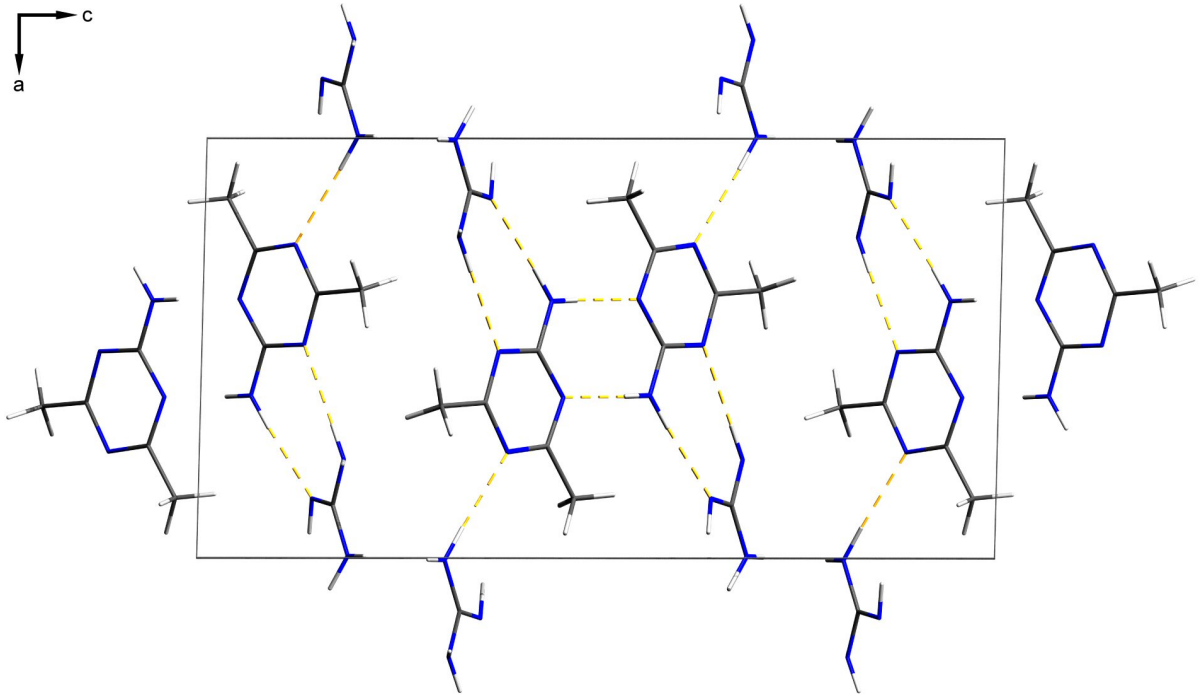

Figure 2.122. Representation of the unit cell of guanidine and 2-amino-4,6-dimethyl-1,3,5-triazine (1:1) along the *b* axis. Dashed lines indicate hydrogen bonding.

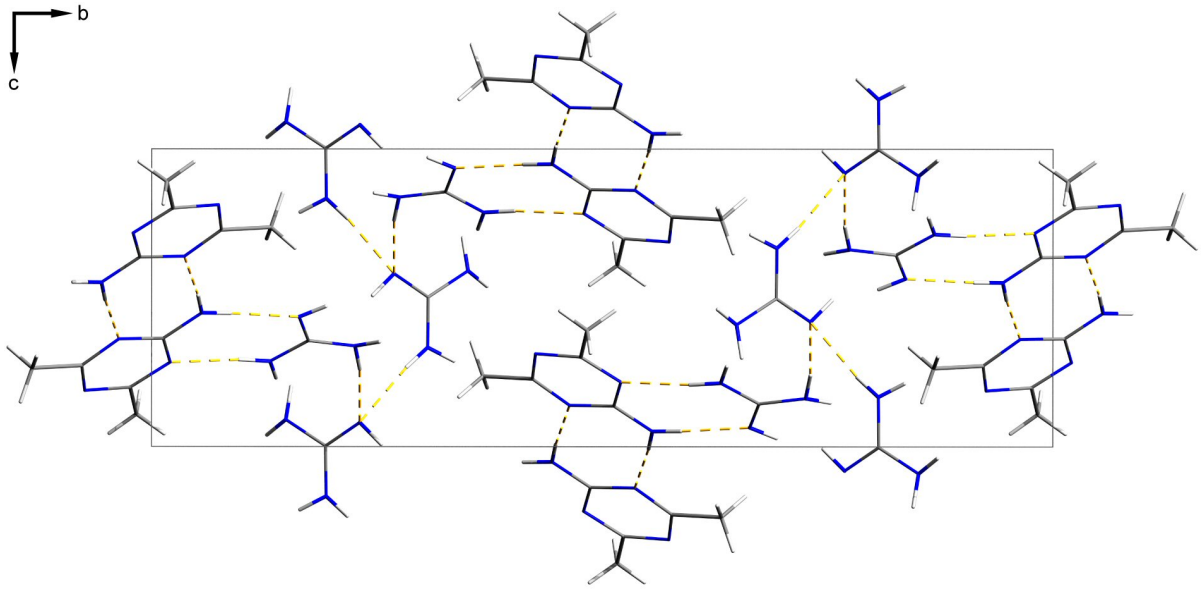

Figure 2.123. Representation of the unit cell of guanidine and 2-amino-4,6-dimethyl-1,3,5-triazine (2:1) along the *a* axis. Dashed lines indicate hydrogen bonding.

The N-H···N distance reported for the pure substance (3.070(4) Å) is in good agreement with our finding (2.978 Å (1:1 co-crystal) / 3.006 Å (2:1 co-crystal)). The C-NH_2 and C-NH hydrogen atoms of the guanidine molecules were directly located in the crystallographic study using difference *Fourier* maps. The attachment to the imino nitrogen atoms of the guanidine is further confirmed by the observation that the C-NH bonds between the central guanidine carbon atom and the attached nitrogen atoms [range 1.295(2) Å – 1.304(2) Å] are significantly shorter than the remaining C-NH_2 bonds to these carbons [range 1.350(3) Å – 1.366(2) Å]. A summary of selected bond lengths and angles is given in Table 2.19.

Table 2.19. Selected bond lengths and angles of the guanidine molecule.

structure	1:1 (G : ADMT)		2:1 (G : ADMT)			
guanidine	#1		#2		#3	
d / Å	C_1-N_1	1.295(2)	C_1-N_1	1.304 (2)	C_7-N_8	1.300 (3)
	C_1-N_2	1.366 (2)	C_1-N_2	1.350 (3)	C_7-N_{10}	1.361 (3)
	C_1-N_3	1.355 (2)	C_1-N_3	1.359 (3)	C_7-N_9	1.359 (3)
angle / °	N_1-C_1-N_2	124 (0)	N_1-C_1-N_3	125 (0)	N_8-C_7-N_9	125 (0)
	N_1-C_1-N_3	120 (0)	N_1-C_1-N_2	120 (0)	N_8-C_7-N_{10}	120 (0)
	N_2-C_1-N_3	116 (0)	N_2-C_1-N_3	115 (0)	N_{10}-C_7-N_9	115 (0)
	C_1-N_1-H_1	110 (1)	C_1-N_1-H_1	109 (1)	C_7-N_8-H_8	110 (1)
✝ / °	N_2	356 (4)	N_2	359 (5)	N_{10}	348 (5)
	N_3	351 (3)	N_3	350 (6)	N_9	353 (5)

✝ Degree of planarity given as the angle sum around the nitrogen atom of the corresponding amino group $\Sigma_{CNH,CNH,HNH}$.

The central carbon atom of the guanidine molecule in structures of the 1:1 and 2:1 co-crystals of guanidine and 2-amino-4,6-dimethyl-1,3,5-triazine forms one plane with the three surrounding nitrogen atoms (Σ_{NCN} = 360 °). In contrast, the two amino groups of guanidine show a pyramidal geometry confirming a theoretical study published by Frenking *et al.* [328] where a nonplanar geometry of the guanidine molecule with strongly pyramidal NH_2 groups was predicted at the *MP2* level of theory using a *6-31G(d)* basis set. In addition, our experimentally determined bond lengths agree well with the calculated ones of the theoretical study where values of 1.284 Å, 1.396 Å and 1.400 Å (*MP2/6-31G(d)*) were proposed. The deviations of the experimentally obtained values for the structure of guanidine in the solid state compared to the calculated equilibrium gas phase data are surprisingly small. Although the environment of the guanidine molecules in the two crystal structures is different and hydrogen bonding between guanidine itself as well as guanidine and 2-amino-4,6-dimethyl-1,3,5-triazine does occur (Table 2.20), a comparison of the three observed guanidine molecules shows that the interatomic distances and angles (Table 2.19) are in excellent agreement and are not noticeably influenced by packing effects of the crystal. The obtained geometrical data of the free base guanidine thus provide reliable experimental evidence for the nature of the molecular structure of guanidine for the first time.

Table 2.20. Hydrogen bonding in the crystal structures of guanidine (G) and 2-amino-4,6-dimethyl-1,3,5-triazine (ADMT) (1:1 and 2:1).

structure	D-H··A	d (D-H) / Å	d (H··A) / Å	d (D··A) / Å	< DHA
1:1 (G:ADMT)	N_3-H_{3B}··N_5	0.908(15)	2.202(16)	3.1100(16)	178.7(13)
	N_2-H_{2A}··N_6^{i}	0.927(18)	2.177(19)	3.1021(17)	175.7(15)
	N_7-H_{7A}··N_4^{ii}	0.856(15)	2.122(16)	2.9777(17)	177.6(12)
	N_7-H_{7B}··N_1	0.915(15)	2.018(16)	2.9273(16)	172.50(13)
2:1 (G:ADMT)	N_2-H_{2A}··N_4^{iii}	0.89(3)	2.17(3)	3.052(3)	170(2)
	N_3-H_{3A}··N_8^{iv}	0.88(3)	2.17(3)	3.041(3)	171(2)
	N_9-H_{9A}··N_8^{v}	0.93(2)	2.11(3)	3.030(3)	170.2(18)
	N_7-H_{7A}··N_1^{iii}	0.88(2)	2.05(2)	2.934(3)	178(2)
	N_7-H_{7B}··N_6^{vi}	0.93(2)	2.08(2)	3.006(2)	176.7(19)

Notes. Symmetry codes: (i) x+1, y, z, (ii) –x+1, -y, -z, (iii) –x+2, -y, -z, (iv) x+1, y, z, (v) x, -y+1/2, z+1/2, (vi) –x+3, -y, -z+1.

Experimental

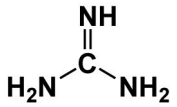

Guanidine was prepared by adding a THF solution of guanidinium chloride (16.7 mmol, 24 mL) to a THF solution of sodium methanolate (16.8 mmol, 24 mL) using standard *Schlenk* techniques. Acetonitrile was allowed to slowly diffuse into the solution until crystals suitable for X-ray diffraction formed at 4°C (guanidine and 2-amino-4,6-dimethyl-1,3,5-triazine, 1:1) or 25°C (guanidine and 2-amino-4,6-dimethyl-1,3,5-triazine, 2:1). Details of the single crystal X-ray diffraction experiment are listed in the appendix (Chapter 4).

Anhydrous GNF was obtained for the first time by reacting the free guanidinium base with nitroform in dry methanol. A yellow solution was obtained indicating the presence of the trinitromethanide anion. After evaporation of the methanol a yellow solid was obtained. The Raman spectrum of this substance closely resembles that of the monohydrate of GNF. Hence, the anhydrous GNF obtained exist as ionic species rather than the covalent isomer.

Raman (r.t.): $\tilde{\nu}$ = 2987(13), 1528(15), 1469(14), 1388(76), 1298(46), 1244(44), 1156(54), 1014(56), 867(100), 790(18), 729(14), 533(25), 473(30), 442(20), 253(24), 164(25).

Silylated 1,5-Diamino-1*H*-tetrazole derivatives

Introduction

Tetrazoles have manifold and highly diverse applications in chemistry. As far as energetic materials are concerned, they represent important building blocks for the synthesis of novel energetic materials. Of the many excellent reviews about tetrazoles, the work of Ostrovskii *et al.* [329] as well as the work of Benson *et al.* [330] is particularly noteworthy. Recent results and developments obtained in our laboratories at LMU Munich are documented in the dissertations of Hammerl [331], Weigand [332] and Stierstorfer [333] and references cited therein. As mentioned earlier, high heat of formation is a critical parameter for the performance properties of a high explosive and most of the energy derived in modern HEDM stems not only from oxidation of the carbon backbone as in traditional energetic materials but also from ring or cage strain and from their very high positive heat of formation. Tetrazoles are the most promising heterocycles amongst five-membered rings with four nitrogen atoms in the ring displaying high heats of formation due to an increasing positive trend in heat of formation with increasing number of nitrogen. Among the advantages of tetrazole based explosive and propellants we mention the large amount of gaseous decomposition products preferentially containing environmentally- as well as (eco)-toxicologically benign dinitrogen, a significant advantage in order to meet one of the major goals of contemporary research on next generation energetic materials. We were interested in synthesizing derivatives of 1,5-diamino-1*H*-tetrazole (DAT) that would give access to novel synthetic routes for the preparation of functionalized derivatives of this high nitrogen containing (84.0 %) compound. Two examples of such derivatives have already been mentioned in Chapter 2.2.1, N^1-(2,2,2-trinitroethyl)-1*H*-tetrazole-1,5-diamine (TTD) as well as N^1,N^5-bis-(2,2,2-trinitroethyl)-1*H*-tetrazole-1,5-diamine (BTTD) and were shown to have superior performance properties approaching or even exceeding those of RDX. However, they were lacking sufficient thermal stability and thus, an increase in this property would be highly desirable. We have shown that it is possible to keep the advantages of the trinitroethyl group and improve the thermal stability of the class of N-

trinitroethyl substituted compounds by oxygen balance neutral introduction of carbon dioxide, manifested in terms of the carbamate functionality. [269]
However, due to solubility properties of DAT, reactions were restricted to highly polar solvents like DMF, methanol or hot water precluding the possibility to perform reactions in common organic solvents. To overcome this drawback we decided to reduce the polarity of the DAT molecule by replacing the amino hydrogen atoms with silyl groups. In addition, this approach was chosen due to the benefit of higher reactivity of the functionalized amino groups towards electrophiles. The stabilization of the tetrazole ring system towards ring opening, commonly observed in the case of electron poor tetrazole derivatives, through the use of the electron donating properties of the trimethylsilyl substituens [334] was another advantage of this strategy. Interesting target molecules that would be readily at hand given that the corresponding trimethylsilyl protected DAT derivatives were available are shown in Figure 2.124.

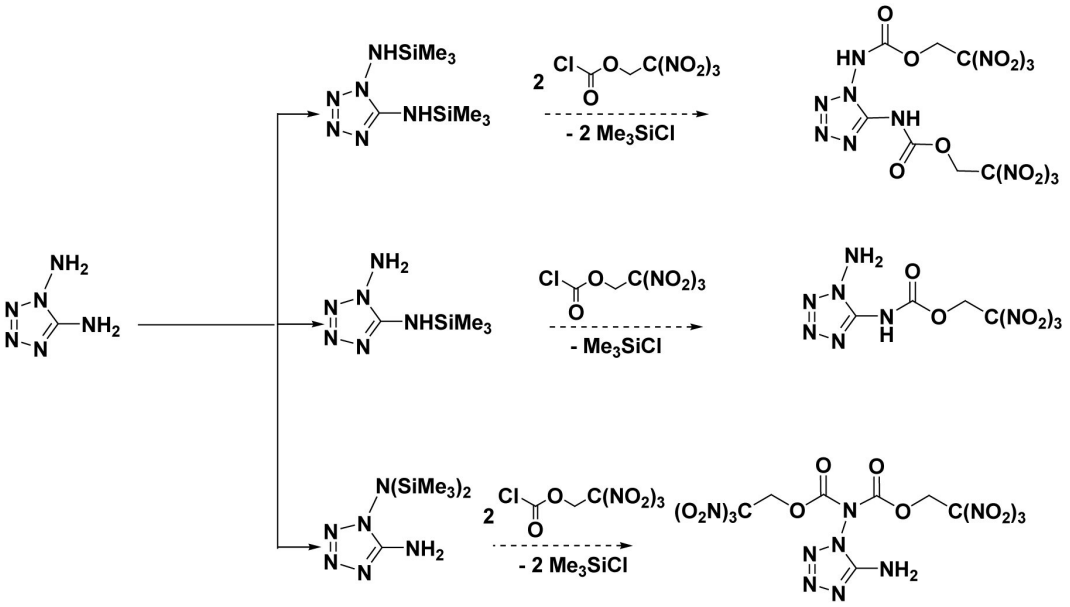

Figure 2.124. Silylated target derivatives of DAT and examples of possible subsequent functionalization.

The possible target molecules as shown in Figure 2.124 would be expected to display performance properties comparable to TTD and BTTD while at the same time having higher thermal stabilities through the aid of the carbamate junction between the trinitroethyl- and the tetrazol moiety. Here we present the synthesis and characterization of the previously unknown silylated

derivatives of 1,5-diamino-1*H*-tetrazole including NMR- and vibrational spectroscopy, mass spectrometry and single crystal X-ray diffractometry. Structural optimizations of the isolated molecules in the gas phase and frequency analyses were also performed as a preliminary step for the assignment of vibrational frequencies.

Synthesis

Different methods have been reported for the silylation of amines in the literature. [335-341] Due to the fact, that DAT bears two amino groups, each exhibiting different chemical behaviour, selective monosilylation of each group is not a straightforward reaction. According to the literature, the following three silylation strategies are frequently employed:

1. Direct silylation using trimethylsilyl chloride (TMSCl) in presence of a base. [342-343]

2. Deprotonation of the amino group using *n*-buthyllithium and subsequent reaction with TMSCl. [344]

3. Silylation using hexamethyldisilazane (HMDS) in presence of Lewis acids. [345-346]

Among the reaction conditions applied, direct reaction of DAT with TMSCl using THF as solvent and applying reflux conditions proofed to be succesfull and yielded the doubly silylated product N^1,N^5-bis-(trimethylsilyl)-1,5-diamino-1*H*-tetrazole (1,5-BTMSD, Fig. 2.125).

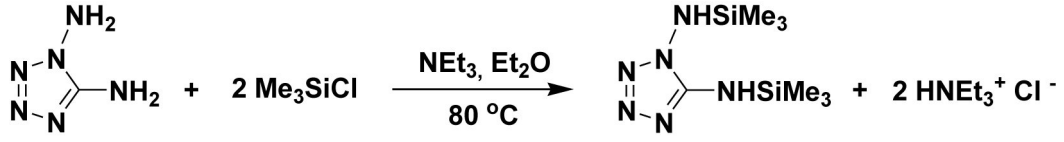

Figure 2.125. Synthesis of N^1,N^5-bis-(trimethylsilyl)-1,5-diamino-1*H*-tetrazole (1,5-BTMSD) from the reaction between DAT and TMSCL.

However, due to difficulties during the work up and the low purity of the product obtained other reaction pathways were tested. Formally, selective deprotonation using *n*-butyllithium and subsequent reaction with trimethylsiylchloride with variation of the temperature and the quantity of base used was applied to selectively silylate the two different amino groups but proved to lead to similar results compared to the first method mentioned above. Instead, the most successful strategy for the preparation of 1,5-BTMSD proved to be the reaction using HMDS (Fig. 2.126).

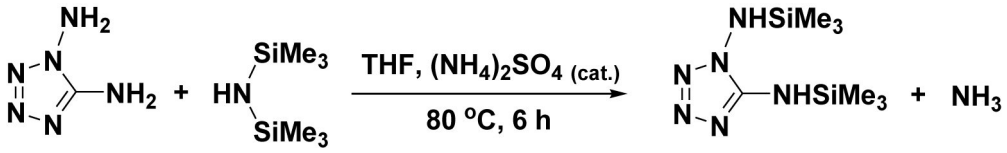

Scheme 2.126. Synthesis of N^1,N^5-bis-(trimethylsilyl)-1,5-diamino-1*H*-tetrazole (1,5-BTMSD) from the reaction between DAT and HMDS.

Silyl transfer reactions using HMDS are frequently used, e.g. in carbohydrate chemistry for alcohol protection. It has been suggested that the most probable mechanism of these reactions includes a concerted transfer of formal Me_3Si^+ and H^+ fragment between the non-silylated amino group and HMDS with the thermodynamic driving force of this reaction being the evolution of gaseous ammonia and while at the same time shifting the equilibrium in favour of the products. [347] We observed that silylation using HMDS always ended up at the stage of monosilylation of each amino group suggesting that the acidity of the remaining silylamino-proton to be not high enough for a second silylation step. Thus, this strategy offers the advantage of simple reaction control. The reaction is accompanied by release of ammonia (as indicated using indicator paper at the gas outlet) and can simply be monitored, indicated both by the stop of ammonia release and a clear solution having formed since unreacted DAT is only very slightly soluble in the THF solvent. We observed that 1,5 - BTMSD is quite sensitive towards air and moisture. On contact with air, the solution gets turbid and crystallization is hindered.

We found that reaction between 1,5-BTMSD and acetone at room temperature readily results in the formation of N^1-(propan-2-ylidene)1,5-diamino-1*H*-tetrazole (1-PYD).

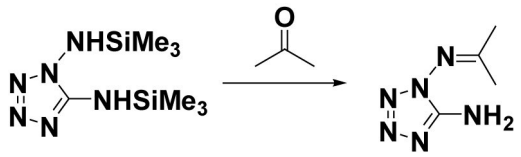

Figure 2.127. Synthesis of N^1-(propan-2-ylidene)-1,5-diamino-1H-tetrazole, (1-PYD)

However, the trimetylsilylamino group at the N5-position does not react to the corresponding Schiff base, but is converted into a $-NH_2$ group, possibly due to the presence of traces of water in the acetone.

In order to increase the selectivity of the silylation reaction and achieve monosilylation of only one amino group we chose to apply kinetic control (Fig. 2.128). Since heating proved to be necessary for the silylation reaction to take place in case HMDS was used as TMS-transfer reagent, other silylation agents were tested. The use of TMSCl in presence of triethylamine at 0 °C proved to be successful.

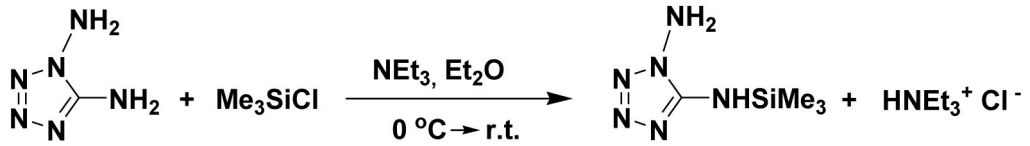

Figure 2.128. Synthesis of N^5-(trimethylsilyl)-1,5-diamino-1*H*-tetrazole (5-TMSD) from the reaction between DAT and TMSCL.

According to the general assumption that higher nucleophilicity should lead to the kinetic product, the hydrazine-type amino group was expected to display a higher reactivity compared to the conjugated sp^2-type amino group. (348) Instead, the silylated amino group was found to be not the hydrazinic-type nitrogen, but the sp^2-type amino group conjugated to the aromatic ring.

Whereas all the silylated products mentioned so far already showed the desired solubility characteristics described in the introduction, N^1,N^1,N^5-

tris(trimethylsilyl)-1,5-diamino-1*H*-tetrazole (1,1,5-TTMSD) was of further interest to us because of the possibility of double functionalization of a single nitrogen atom and additionally should display increased stability towards air, moisture and alcohols compared to the monosilylated amines. [349] Several strategies have been reported for the preparation of doubly silylated amines. Deprotonation using n-butyl lithium and subsequent reaction with trimethylsilylchloride proved to be succesfull only in a few cases. [350-352] Another method utilizes the transfer of a trimethylsilyl group to an amide, fo r example the reaction between N-methyl-N-trimethylsilylacetamide and diethyltrimethylsilylamine. [353-354] Taking advantage of the very good leaving group properties of the triflate group, we found that the reaction between trimethylsilyl triflate and the monosilylamine of 1,5-BTMSD in the presence of a base (Fig. 2.129) worked best in our case after having tested several other methods.

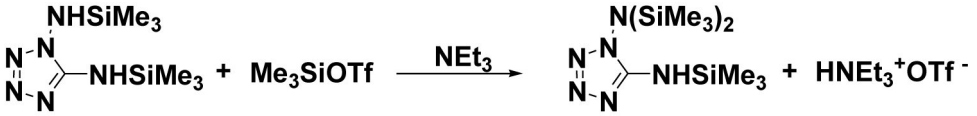

Figure 2.129. Synthesis of N^1,N^1,N^5-tris(trimethylsilyl)-1,5-diamino-1*H*-tetrazole (1,1,5-TTMSD) from the reaction between 1,5-BTMSD and TMSOTF.

It was essential to add the base (dry triethylamine) after the addition of the trimethylsilyl triflate in order to avoid silylation of triethylamine. Further silylation yielding N^1,N^1,N^5,N^5-tetrakis(trimethylsilyl)-1,5-diamino-1*H*-tetrazole did not occur using this strategy.

Crystal Structure Analysis

Though silylated derivatives of heterocycles are generally important reagents in chemical synthesis, information about the structural chemistry of silyltetrazoles is scarce. Table 2.21 summarizes selected geometrical data obtained from the determination of the crystal structures of N^5-trimethylsilyl-1,5-diamino-1*H*-tetrazole (5-TMSD), N^1,N^5-bis-(trimethylsilyl)-1,5-diamino-1*H*-tetrazole (1,5-BTMSD), N^1,N^1-bis-(trimethylsilyl)-1,5-diamino-1*H*-tetrazole (1,1-BTMSD) and N^1,N^1,N^5-tris-(trimethylsilyl)-1,5-diamino-1*H*-tetrazole (1,1,5-TTMSD) and a comparison to 1,5-diamino-1*H*-tetrazole (DAT) as well as 5-(Trimethylsilyl)amino-1*H*-tetrazole (5-TAT).

Table 2.21. Selected geometrical data of the series of silylated 1,5-diamino-1*H*-tetrazol derivatives and comparison to DAT as well as 5-TAT.

d / Å	5-TAT [a]	DAT [b]	5-TMSD	1,5-BTMSD	1,1-BTMSD	1,1,5-TTMSD
C_1-N_1	-	1.345(1)	1.41(3)	1.3460(18)	1.346(7)	1.354(2)
N_1-N_2	-	1.363(1)	1.35(2)	1.3753(1)	1.366(6)	1.371(2)
N_2-N_3	-	1.279(1)	1.272(19)	1.2924(18)	1.293(6)	1.292(2)
N_3-N_4	-	1.367(1)	1.37(2)	1.3647(18)	1.377(7)	1.372(2)
N_4-C_1	-	1.327(1)	1.35(4)	1.3379(19)	1.332(7)	1.332(2)
C_1-N_5	1.346(4)	1.334(1)	1.29(3)	1.3495(19)	1.331(8)	1.351(3)
N_1-N_6	-	1.383(1)	1.36(3)	1.3836(17)	1.392(6)	1.403(2)
N_5-Si	1.760(3)	-	1.75(2)	1.7631(13)	-	1.7456(19)
N_6-Si_1	-	-	-	1.7600(13)	1.780(5)	1.7750(17)
N_6-Si_2	-	-	-	-	1.766(5)	1.7745(17)

Notes. 5-TAT = 5-(Trimethylsilyl)amino-1H-tetrazole. a) ref. (355) b) ref. (356)

The comparison of the data of the compounds listed in Table 2.21 shows that the tetrazole ring is planar within the limits of error in all the structures. The bond length values of the endocyclic bonds are consistent with those observed previously for 1-mono- and 1,5-disubstituted tetrazoles. The exocyclic C_1-N_5 bonds of the silylated derivatives display no significant deviations compared to the value of DAT and the 5-amino groups are coplanar to the tetrazole plane indicating a conjugation of the π system and the tetrazole ring. Similar to the N_5 nitrogen atom, the N_6 nitrogen atom also lies in the tetrazole ring plane. However, the lone pair of the N_6 nitrogen atom is not conjugated with the π

system of the tetrazole ring indicated by the positions of the substituents bonded to this atom being located on different sides of the tetrazol ring plane. The N_5-Si distances show no significant deviation from the typical value of a nitrogen silicon single bond with values in the range of 1.75 - 1.76 Å. In contrast, the N_6-Si distances in the compounds carrying two trimethylsilyl groups at the N_6 nitrogen atom are longer (1.78 Å). The involvement of the p-orbital of the N_6 nitrogen atom in terms of p → σ* (Si-C) hyperconjugation might serve as a possible rationale. This interpretation is supported by the planar geometry of the N_6 nitrogen atom in contrast to the commonly observed sp^3-type hybridization of this amino group. The extended structures of the silylated derivatives of DAT display interesting structural features and are subject to a more detailed discussion in the following sections.

N^5-Trimethylsilyl-1,5-diamino-1*H*-tetrazole (5-TMSD)

N^5-trimethylsilyl-1,5-diamino-1*H*-tetrazole (5-TMSD) crystallizes in the monoclinic space group $P2_1/c$ (no. 14) with four molecules in the unit cell. The asymmetric unit is comprised of one molecule (Fig. 2.130).

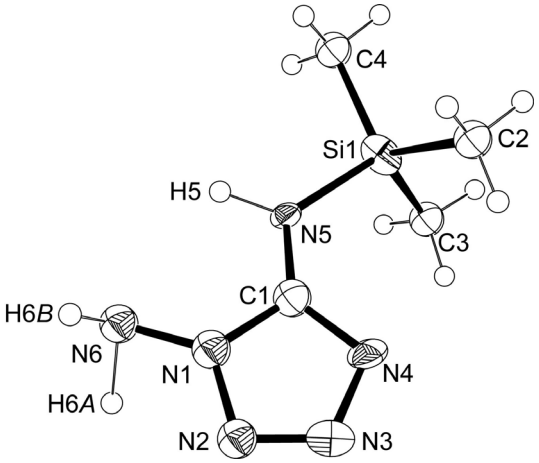

Figure 2.130. ORTEP representation of the molecular structure of N^5-trimethylsilyl-1,5-diamino-1*H*-tetrazole (5-TMSD) in the crystalline state. Displacement ellipsoids are shown at the 50 % probability level. Selected bond lengths [Å] and angles [°]: C_1-N_1 1.41(3), N_1-N_2 1.35(2), N_2-N_3 1.272(19), N_3-N_4 1.37(2), N_4-C_1 1.35(4), N_1-N_6 1.36(3), C_1-N_5 1.29(3), N_5-Si_1 1.75(2), Si_1-C_2 1.838(15), Si_1-C_3 1.868(15), Si_1-C_4 1.819(16), C_1-N_5-Si_1 122(2), N_1-C_1-N_5-Si_1 175.4(13), N_4-C_1-N_5-Si_1 5(4).

The single crystals were of rather small size giving rise to only a weak diffraction pattern precluding the possibility of an independent refinement of the hydrogen atoms and a detailed discussion of the intermolecular contacts. Of interest, we mention that due to the overall bond precision of this structure being lower by one digit compared to the other silylated structures mentioned in this chapter, a comparision of the bond length and angles is only possible within the error margins.

N^1,N^5-Bis-(trimethylsilyl)-1,5-diamino-1*H*-tetrazole (1,5-BTMSD)

1,5-BTMSD crystallizes in the monoclinic space group $P\,2_1/n$. An Ortep representatin of the asymetric unit of 1,5-BTMSD in the solid state is shown in Fig. 2.131.

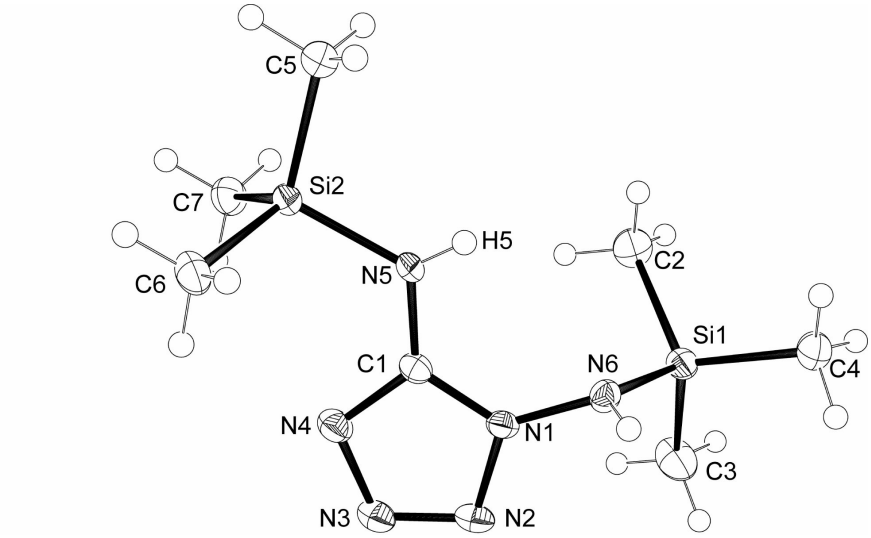

Figure 2.131. ORTEP representation of the molecular structure of N^1,N^5-bis-(trimethylsilyl)-1,5-diamino-1*H*-tetrazole (1,5-BTMSD) in the crystalline state. Displacement ellipsoids are shown at the 50 % probability level. Selected bond lengths [Å] and angles [°]: C_1-N_1 1.3460(18), N_1-N_2 1.3753(17), N_2-N_3 1.2924(18), N_3-N_4 1.3647(18), N_4-C_1 1.3379(19), C_1-N_5 1.3495(19), N_5-Si_2 1.7631(13), Si_2-C_5 1.8499(18), Si_2-C_6 1.8564(16), Si_2-C_7 1.8576(17), N_1-N_6 1.3836(17), N_6-Si_1 1.7600(13), Si_1-C_2 1.8512(18), Si_1-C_3 1.8624(18), Si_1-C_4 1.8513(18), C_1-N_5-Si_2 122.54(11), N_1-N_6-Si_1 119.92(9), N_1-C_1-N_5-Si_2 177.15(10), N_4-C_1-N_5-Si_2 -4.15(19), C_1-N_1-N_6-Si_1 106.84(13), N_2-N_1-N_6-Si_1 -77.20(15).

The structure of the two amino groups of 1,5-BTMSD, each substituted with one trimethylsilyl group, is comparable to the geometry of the two amino groups of 1,5-diamino-1*H*-tetrazole [360]: one amino group (N_6) displays a trigonal pyramidal coordination whereas the other amino group (N_5) shows a planar, sp^2-type coordination sphere. Accordingly, the trimethylsilyl group at the N_6 nitrogen atom is almost orthogonal to the plane of the aromatic ring (torsion angle C_1-N_1-N_6-Si_1 = -106.84(13)°), while the other one is nearly coplanar (torsion angle N_1-C_1-N_5-Si_2 = 177.15(10)°) indicating that conjugation of the electron pair at the N_5 nitrogen atom with the π-system of the tetrazol ring. The extended structural motif in the crystal is comprised of

infinite ribbons, each consisting of two antiparallel planar chains of 1,5-BTMSD molecules. The chains are oriented parallel to the crystallographic *b* axis and interconnected by hydrogen bonding (Table 2.22).

Table 2.22. Intermolecular hydrogen bonding of N^1,N^5-bis-(trimethylsilyl)-1,5-diamino-1*H*-tetrazole (1,5-BTMSD).

D–H···A	D–H / Å	H··· A / Å	D···A / Å	D–H···A / °
N_6–H_6···$N_2^{(i)}$	0.793 (17)	2.600 (17)	3.2317 (18)	137.8 (16)
N_6–H_6··· $N_3^{(i)}$	0.793 (17)	2.600 (17)	3.3485 (19)	158.1 (16)
N_5–H_5···$N_3^{(ii)}$	0.767 (19)	2.69 (2)	3.4353 (19)	164.7 (17)

Notes. Symmetry code: (i) −x, 2−y, 1−z; (ii) x, y−1, z.

Every chain is planar and contains the aromatic rings of the 1,5-BTMSD molecules that gave rise to it. Inside every chain, the molecules are held together via intermolecular hydrogen bonding (N_5–H_5···N_3, Table 2.22). The chains again are interconnected through intermolecular hydrogen bonding (N_6–H_6···N_2, N_6–H_6···N_3, Table 2.22) yielding two dimensional bands consisting of two antiparallel oriented chains of 1,5-BTMSD molecules (Figs. 2.132, 2.133).

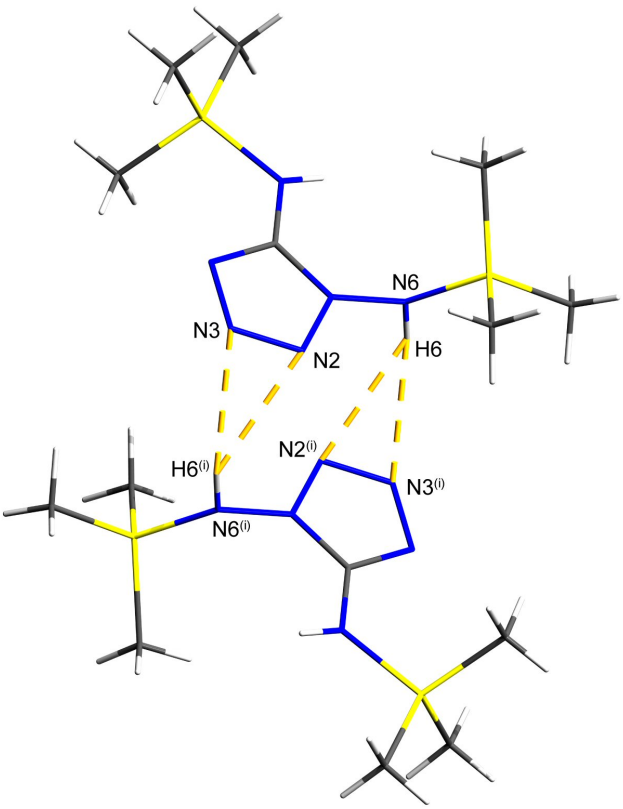

Figure 2.132. Intermolecular hydrogen bonding motiv interconnectiong two 1,5-BTMSD molecules to a pair of dimers.

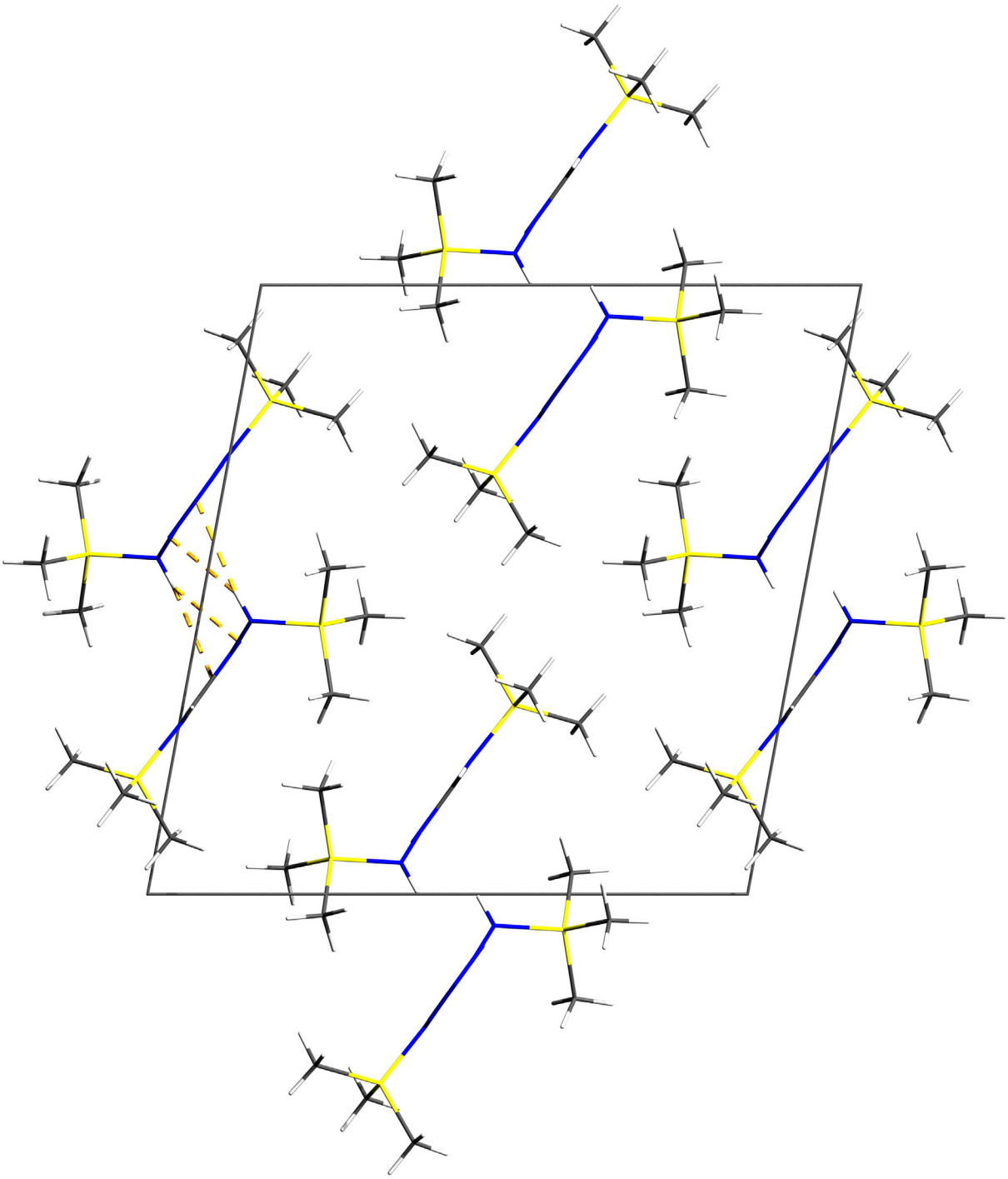

Figure 2.133. View along the *b* axis of the crystal structure of 1,5-BTMSD. Hydrogen bonding is indicated by yellow dashed lines and is shown for only one pair of 1,5-BTMSD molecules.

N^1-(Propan-2-ylidene)-1,5-diamino-1*H*-tetrazole (1-PYD)

N^1-(Propan-2-ylidene)-1,5-diamino-1*H*-tetrazole (1-PYD) crystallizes in the monoclinic space group $P2_1/c$ (no. 14) with four molecules in the unit cell. The asymmetric unit is comprised of one molecule. The molecular structure of the asymmetric unit is shown in Figure 2.134.

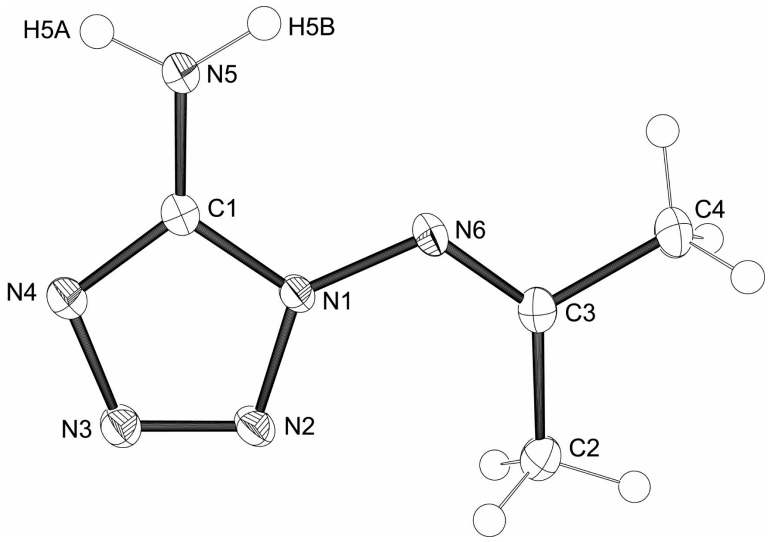

Figure 2.134. ORTEP representation of the molecular structure of N^1-(propan-2-ylidene)-1,5-diamino-1*H*-tetrazole (1-PYD) in the crystalline state. Displacement ellipsoids are shown at the 50 % probability level. Selected bond lengths [Å] and angles [°]: C_1-N_1 1.3561(11), N_1-N_2 1.3799(9), N_2-N_3 1.2889(10), N_3-N_4 1.3674(10), N_4-C_1 1.3309(11), C_1-N_5 1.3289(11), N_1-N_6 1.3854(9), N_6-C_3 1.2866(11), C_3-C_2 1.4970(13), C_3-C_4 1.4928(12), N_1-N_6-C_3 120.84(7), C_1-N_1-N_6-C_3 176.40(8), N_2-N_1-N_6-C_3 -2.07(13).

The propan-2-ylidene substitutent is oriented coplanar to the rest of the molecule. In fact, all the non-hydrogen atoms of this molecule rest in one plane (torsion angle C_1-N_1-N_6-C_3 = 176.40(8)°). This finding, as well as the angle of 120.84(7)° indicates a sp^2-type hybridization of the N_6 nitrogen atom. Intermolecular hydrogen bonding is present in the crystal giving rise to a pair of dimers of 1-PYD molecules (Table 2.23, Fig. 2.135).

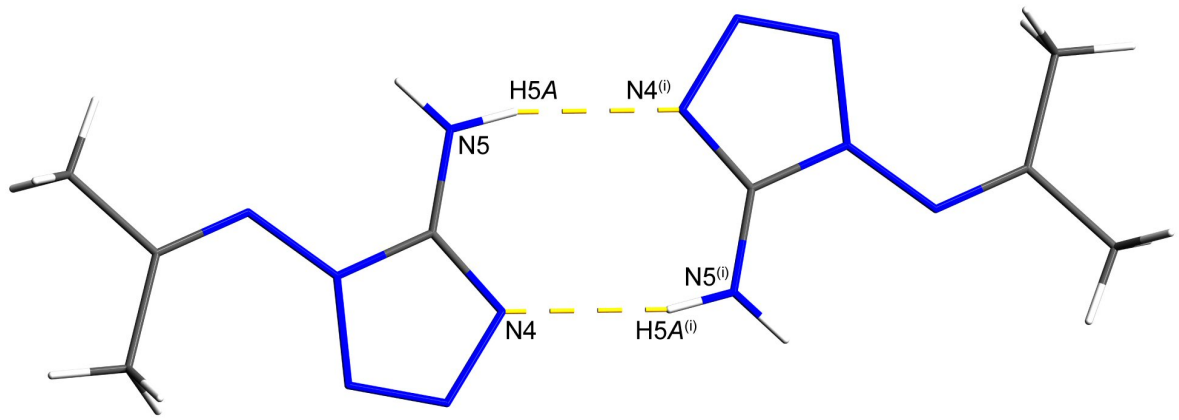

Figure 2.135. Pair of dimers of 1-PYD molecules. Hydrogen bonding is indicated by yellow dashed lines. (N_5–H_{5A}···$N_4^{(i)}$ and $N_5^{(i)}$–$H_{5A}^{(i)}$···N_4; (i) 1–x, 1–y, –z).

Table 2.23. Intermolecular hydrogen bonding of N^1-(propan-2-ylidene)-1,5-diamino-1*H*-tetrazole (1-PYD).

D–H···A	D–H / Å	H··· A / Å	D···A / Å	D–H···A / °
N_5–H_{5A}···$N_4^{(i)}$	0.850(13)	2.150(12)	2.9817(11)	165.9(11)
N_5–H_{5B}··· $N_3^{(ii)}$	0.891(13)	2.195(13)	3.0572(11)	162.7(10)

Notes. Symmetry code: (i) 1–x, 1–y, –z; (ii) x, 1/2-y, –1/2+z.

Additional hydrogen bonding ($N_{5,amino}$–H_{5B}···$N_{3,Ring}$; Table 2.23) is present interconnecting a pair of dimers to surrounding pairs resulting in three dimensional hydrogen bonded network (Figs. 2.136, 2.137).

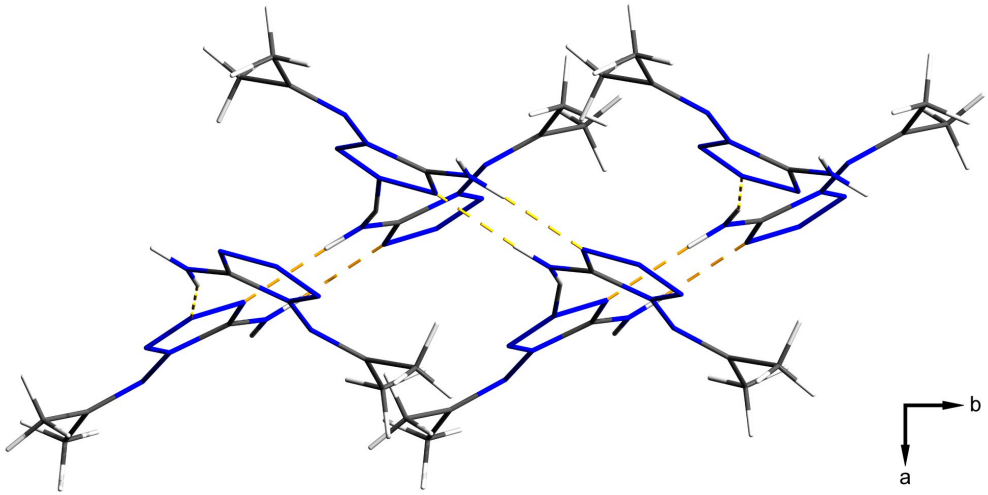

Figure 2.136. Representation of the three-dimensional hydrogen bonding network of 1-PYD.

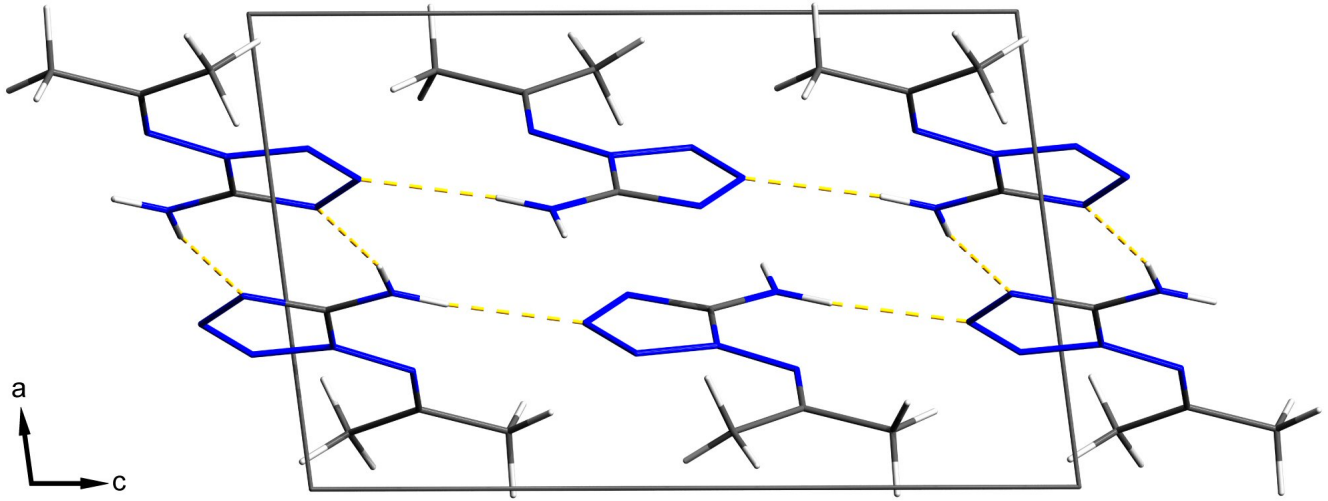

Figure 2.137. Unit cell representations of 1-PYD, viewed along the crystallographic *b* axis.

N^1,N^1-Bis(trimethylsilyl)-1,5-diamino-1*H*-tetrazole (1,1-BTMSD)

1,1-BTMSD crystallizes in the monoclinic space group $P2_1/c$ (no. 14) with four molecules in the unit cell. The asymmetric unit is comprised of one molecule. The molecular structure of the asymmetric unit is shown in Figure 2.138.

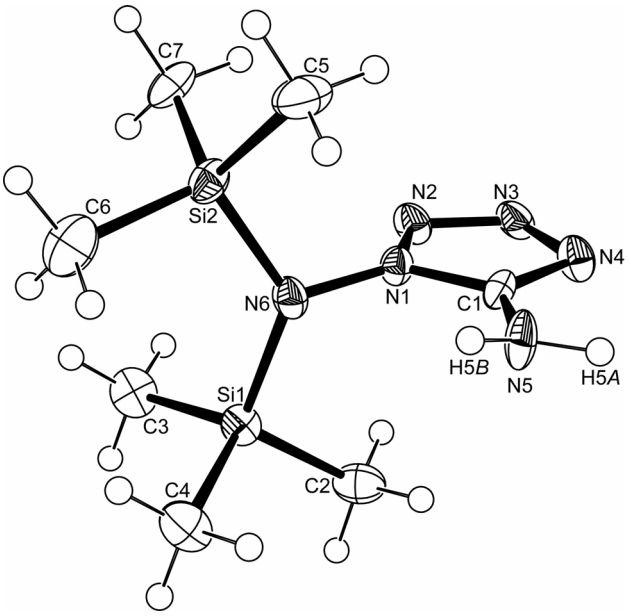

Figure 2.138. ORTEP representation of the molecular structure of N^1,N^1-bis(trimethylsilyl)-1,5-diamino-1*H*-tetrazole (1,1-BTMSD) in the crystalline state. Displacement ellipsoids are shown at the 50 % probability level. Selected bond lengths [Å] and angles [°]: C_1-N_1 1.346(7), N_1-N_2 1.366(6), N_2-N_3 1.293(6), N_3-N_4 1.377(7), N_4-C_1 1.332(7), C_1-N_5 1.331(8), N_1-N_6 1.392(6), N_6-Si_1 1.780(5), Si_1-C_2 1.854(6), Si_1-C_3 1.851(7), Si_1-C_4 1.847(6), N_6-Si_2 1.766(5), Si_2-C_5 1.849(7), Si_2-C_6 1.853(7), Si_2-C_7 1.861(6), N_1-N_6-Si_1 114.3(4), N_1-N_6-Si_2 113.4(4), C_1-N_1-N_6-Si_1 -92.4(6), N_2-N_1-N_6-Si_1 75.9(6), C_1-N_1-N_6-Si_2 106.3(6), N_2-N_1-N_6-Si_2 -85.5(6).

The compound exhibits an interesting pattern of intermolecular hydrogen bonding (Table 2.24, Figs. 2.139, 2.140).

Table 2.24. Intermolecular hydrogen bonding of N^1,N^1-bis(trimethylsilyl)-1,5-diamino-1*H*-tetrazole (1,1-BTMSD).

D–H···A	D–H / Å	H··· A / Å	D···A / Å	D–H···A / °
N_5–H_{5A}···$N_4^{(i)}$	0.91(7)	2.11(7)	3.004(9)	170(7)
N_5–H_{5B}···$N_3^{(ii)}$	0.80(6)	2.39(6)	3.107(9)	151(5)

Notes. Symmetry code: (i) 1−x, 1−y, −z; 1+x, y z.

According to graph set analysis, the predominant structural hydrogen bonding motif can be described at the unitary level as antidromic N_1= C_1^1 (5) $R_2^2(4)$ motifs or at the secondary level as ring motiv: $N_2 = R_4^4(10)$.

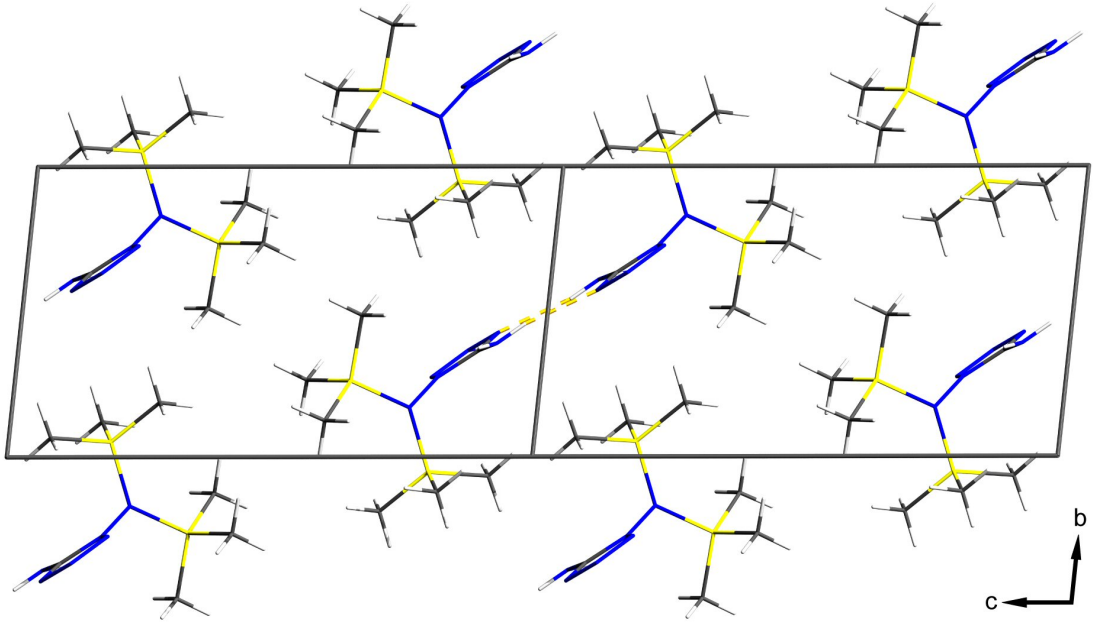

Figure 2.139. Unit cell representation of two adjacent cells of 1,1,- BTMSD, viewed along the a axis. The hydrogen bonding pattern shown in Figure X is indicated by yellow dashed lines.

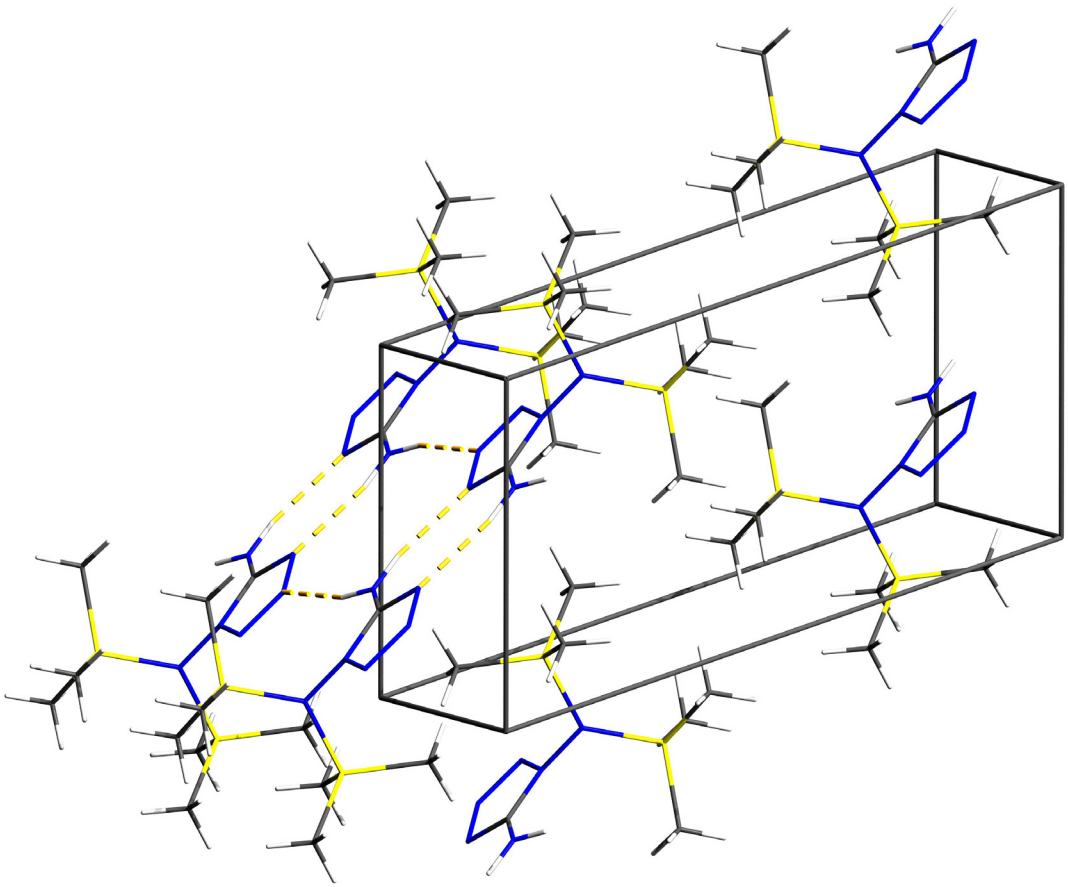

Figure 2.140. Unit cell representation of 1,1,-BTMSD, together with a perspective view of the intermolecular hydrogen bonding motif ($R_4^4(10)$).

N^1,N^1,N^5-Tris(trimethylsilyl)-1,5-diamino-1*H*-tetrazole (1,1,5-TTMSD)

N^1,N^1,N^5-tris-(trimethylsilyl)-1,5-diamino-1*H*-tetrazole crystallizes in the monoclinic space group $P2_1/c$ (no. 14) with four molecules in the unit cell. The asymmetric unit is comprised of one molecule. The molecular structure of the asymmetric unit is shown in Figure 2.141.

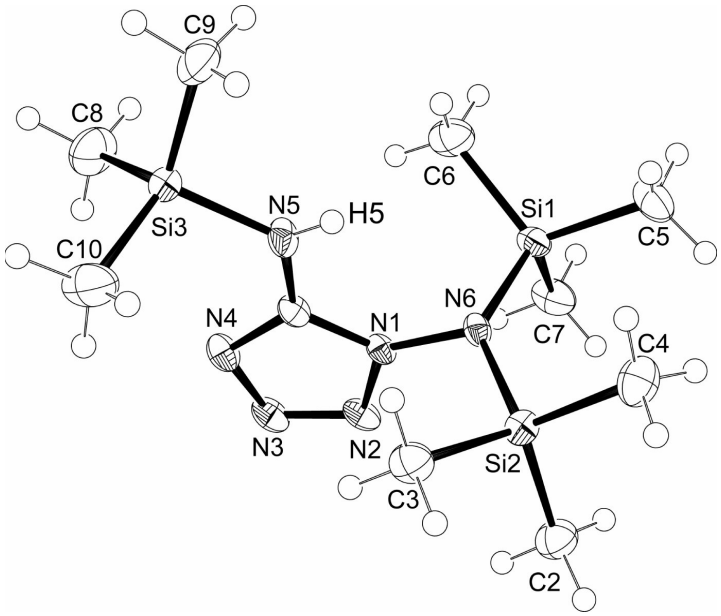

Figure 2.141. ORTEP representation of the molecular structure of N^1,N^1,N^5-tris(trimethylsilyl)-1,5-diamino-1*H*-tetrazole (1,1,5-TTMSD) in the crystalline state. Displacement ellipsoids are shown at the 50 % probability level. Selected bond lengths [Å] and angles [°]: C_1-N_1 1.354(2), N_1-N_2 1.371(2), N_2-N_3 1.292(2), N_3-N_4 1.372(2), N_4-C_1 1.332(2), C_1-N_5 1.351(3), N_5-Si_3 1.7456(19), Si_3-C_8 1.853(2), Si_3-C_9 1.858(2), Si_3-C_{10} 1.846(2), N_1-N_6 1.403(2), N_6-Si_1 1.7750(17), Si_1-C_5 1.856(2), Si_1-C_6 1.867(2), Si_1-C_7 1.861(2), N_6-Si_2 1.7745(17), Si_2-C_2 1.859(2), Si_2-C_3 1.861(2), Si_2-C_4 1.855(2), C_1-N_5-Si_3 126.09(15), N_1-N_6-Si_1 111.32(12), N_1-N_6-Si_2 111.09(12), N_1-C_1-N_5-Si_3 178.43(15), N_4-C_1-N_5-Si_3 -2.4(3), C_1-N_1-N_6-Si_1 -97.9(2), N_2-N_1-N_6-Si_1 77.63(18), C_1-N_1-N_6-Si_2 98.52(19), N_2-N_1-N_6-Si_2 -85.96(18).

The two sterically demanding trimethylsilyl groups attached to the N_6 nitrogen atom result in an almost planar geometry in marked contrast to the pseudo-tetrahedral geometry commonly observed for this hydrazinic-type nitrogen atom. In detail, the angle sum around the N_6 nitrogen atom has a value of 357° (Si_1-N_6-Si_2: 135 °, Si_1-N_6-N_1 and Si_2-N_6-N_1: 111 °) resulting in a deviation of the position of the N_6 nitrogen atom from the Si_1-Si_2-N_1 plane of 0.16 Å.

Compared to the structure of 1,5-BTMSD, this compound has only limited possibilities for the formation of hydrogen bonds yielding a less dense packing and a lower density (1,1,5-TTMSD: 1.0861(1) g cm^{-3}, 1,5-BTMSD: 1.1702(1) g cm^{-3}. The hydrogen bonding pattern is presented in Table 2.25 and Figure 2.142. In fact, there is only a single hydrogen bond between the proton of the amino group and the N_3 ring nitrogen atom of a neighboring molecule.

Table 2.25. Intermolecular hydrogen bonding of N^1,N^1,N^5-tris-(trimethylsilyl)-1,5-diamino-1*H*-tetrazole (1,1,5-TTMSD).

D–H···A	D–H / Å	H··· A / Å	D···A / Å	D–H···A / °
N_5–H_5···$N_3^{(i)}$	0.74(2)	2.26(2)	2.969(2)	162(2)

Notes. (i) x, 1/2–y, –1/2+z.

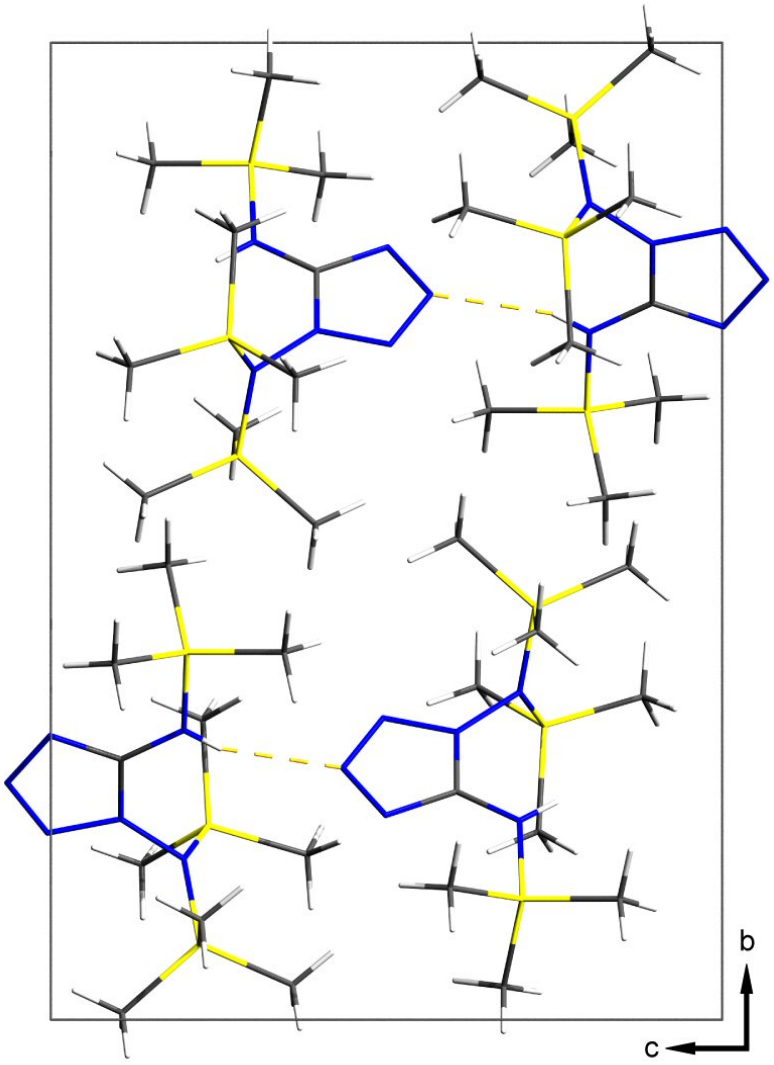

Figure 2.142. Unit cell representation of the structure of 1,1,5-TTMSD, viewed along the a axis. Intermolecular hydrogen bonding is indicated by yellow dashed lines.

Conclusion

The attempts to synthesise the different singly and multiply silylated diaminotetrazoles lead to five new molecules, which have been characterized. Next to the acetone adduct 1-PYD, 5-TMSD represents a single silylated species whereas 1,1-BTMSD and 1,5-BTMSD represent doubly silylated. Furthermore, 1,1,5-TTMSD could be synthesised representing a triple silylated species.
The synthetic conditions, especially towards 1,5-BTMSD were optimized with respect of the purity and yield of product.
The initially promising strategy involving deprotonation using *n*-BuLi, did not lead to good synthetic results due to problems with the workup of the products. The preparation of the silylated compounds opens new possibilities for the functionalization of diaminotetrazole. In this way the DAT unit could be used in terms of a synthon and be reacted with a large spectrum of electrophiles as already mentioned in the introduction. Other silylated compounds of interest would include 1-TMSD as well as the persilylated compound N^1,N^1,N^5,N^5-tetrakis(trimethylsilyl)-1,5-diamino-1*H*-tetrazole. In terms of retrosynthesis, double silylation of a nitrogen atom converts it into a (d,d) (double donor) centre giving rise to further interesting reactions like ring closures, possibly leading to new fused heterocycles.

Experimental

All reagents were of p.a. purity and were used as received from Aldrich, Fluka or Merck (if not stated otherwise). THF and diethyl ether were dried and freshly distilled prior to use. ^{1}H, ^{13}C, ^{15}N and ^{29}Si NMR spectra were measured on a Jeol Eclipse 270, Jeol EX 400 or Jeol Eclipse 400 instrument. Infrared spectra were measured in KBr pellets using a Perkin-Elmer Spectrum One FT-IR instrument equipped with CsI windows. Raman spectra were measured on a Perkin Elmer Spectrum 2000R NIR FT-Raman instrument (Nd:YAG laser, 1064 nm, laser power 200 – 400 mW). Mass spectra were recorded on a JEOL

MStation JMS 700 instrument. Differential scanning calorimetry measurements were performed using a Perkin ElmerPyris 6 DSC instrument.
The reactions were generally performed using standard Schlenk techniques (if not stated otherwise). The reaction flasks, stirring bars and condensers were heated three times using of a heat gun *in vacuo* ($2.5 \cdot 10^{-2}$ mbar) and vented with nitrogen before being loaded with reagents. Solids were added over the neck of the flask in a counterflow of dry nitrogen, liquids were added using a syringe.
Single crystal X-ray diffraction data for all compounds were collected using an Xcalibur3 CCD diffractometer from Oxford Diffraction equipped with a graphite monochromator affording Mo-K_α radiation (λ = 0.71073 Å). The structures were solved with direct methods using the program SHELXS 97 and refined using the program SHELXL 97.

1,5-Diamino-1H-tetrazole (DAT)

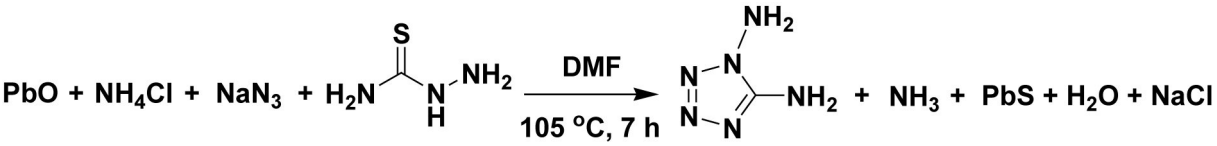

1,5-Diamino-1*H*-tetrazole (DAT) was synthesised according to a modified literature procedure. [357] DMF (350mL) was filled into a 500 mL two-necked, round-bottomed flask equipped with a reflux condenser, a large magnetic stirring bar and a glass stopper. Lead(II) oxide (89.2 g, 0.400 mol, 2.0 eq) and ammonium chloride (21.3 g, 0.400 mol; 2.0 eq) were added. After the mixture had been stirred at room temperature for 30 min., thiosemicarbazide (18.0 g, 0.2 mol; 1.0 eq) was added and the reaction mixture heated to 90 °C. Subsequently, sodium azide (21.3 g, 0.4 mol, 2.0 eq) was added in small portions over a period of 10 minutes. The reaction mixture was stirred at 105 °C for 7 h.
The hot mixture was filtered off using a Büchner funnel with two layers of filter paper. The reddish filtrate was evaporated until dryness (Caution!) and the solid residue dissolved in hot water (80 mL). The hot solution was filtered through Celite and allowed to cool down to room temperature over night. The crystalline material obtained was filtered off and washed using ice water.

Concentration of the mother liquor to half of its volume yielded additional product. The crude product was recrystallized in water. After filtration, the purified product was washed three times using both cold ethyl acetate and subsequently cold diethyl ether. Colorless crystals (9.91 g; 197.5 mmol; yield 50.1%) were obtained and later shown to be DAT.
Caution: Explosive lead(II) azide ($Pb(N_3)_2$) is formed as a side product during the reaction. The black precipitate obtained after the filtration of the reaction mixture should be kept wet and finally be destroyed by putting it into a water solution of sodium nitrite (5%) subsequent acidification with hydrochloric acid (1M).

^{1}H NMR (400 MHz, [D_6]-DMSO, 25 °C): δ = 6.35 (2H; NH_2), 6.38 ppm (2H; NH_2); ^{13}C NMR (100 MHz, [D_6]-DMSO, 25°C): δ = 155.00 ppm; ^{15}N NMR (40.55 MHz, [D_6]-DMSO, 25°C): δ = −338.8 (N_6), −315.2 (N_5), −167.8 (N_1), −97.5 (N_4), −20.8 (N_2), 5.5 (N_3); IR (KBr disk) $\tilde{\nu}$ /cm^{-1}: 3324 (vs), 3237 (s), 3154 (s), 1656 (vs), 1578 (m), 1487 (w), 1329 (vs), 1109 (s), 1077 (m), 1002 (m), 933 (m), 746 (w), 700 (w), 608 (m); Raman (200 mW) $\tilde{\nu}$ /cm^{-1}: 3243 (6), 3244 (11), 1671 (9), 1623 (6) 1547 (20), 1497 (6), 1329 (15), 1307 (19), 106 (16), 1079 (12), 792 (100), 698 (15), 323 (26), 231 (13).

N^1,N^5-Bis(trimethylsilyl)-1,5-diamino-1H-tetrazole (1,5-BTMSD)

a) Hexamethyldisilazane route

All procedures were carried out using Schlenk techniques. DAT (0.500 g, 5.00 mmol, 1.0 eq) and ammonium sulfate (0.10 g, 0.75 mmol, 0.15 eq) were placed inside a dry Schlenk flask (100 mL), equipped with a reflux condenser and bubble counter. Dry THF (15 mL) was added by means of a syringe and the suspension was stirred at room temperature. HMDS (2,42 g, 15.0 mmol, 3.0 eq) was added slowly to this mixture using a syringe and the temperature was raised to 80 °C. The reaction mixture was stirred at this temperature for 6 h until no ammonia evolved any longer at the outlet of the bubble counter (indicator paper) and the solids in the reaction mixture were almost completely dissolved. The hot reaction mixture was filtered into another Schlenk flask using a Schlenk frit (pore size 3) and the solvent removed *in vacuo*. The colorless solid residue was then dissolved in hot and dry THF (30 mL), filtered. The volume of the solvent was slowly reduced (*in vacuo*) affording prismatic colorless single crystals that were later shown to be 1,5-BTMSD (0.971 g, 80% yield). The product can alternatively be purified by sublimation at 100 °C in static vacuum ($2.5 \cdot 10^{-2}$ mbar) and using a cold finger cooled with liquid nitrogen.

^{1}H NMR (400 MHz, $CDCl_3$, 25°C): δ = 0.08 (s, 9H, $Si(CH_3)_3$), 0.22 (s, 9H, $Si(CH_3)_3$), 4.25 (s, 1H, NH), 4.82 ppm (s, 1H, NH); ^{13}C NMR (100 MHz, $CDCl_3$, 25°C): δ = – 1.23 ($Si(CH_3)_3$), – 0.83 ($Si(CH_3)_3$), 154.53 ppm (tetrazole C); ^{15}N NMR (40.55 MHz, $CDCl_3$, 25°C): δ = –332.6 (d, $J(^{29}Si\text{-}^{15}N)$ = 82.2 Hz, N_6), –313.4 (d, $J(^{29}Si\text{-}^{15}N)$ = 81.3 Hz, N_5), –164.1 (s, N_1), – -97.5 (s, N_4), –20.2 (s, N_2), –6.8 ppm (s, N_3); ^{29}Si NMR (79.5 MHz, $CDCl_3$, 25°C, INEPT, 9H, J = 6.5 Hz): δ = 10.57, 15.82 ppm; IR (for an assignment of the vibrations, see Appendix, KBr disk) $\tilde{\nu}$ /cm^{-1}: 3334 (vs), 2903 (vs), 2557 (m), 2411 (m), 1656 (vs), 1585 (vs), 1483 (s), 1428 (vs), 1378 (vs), 1352 (vs), 1289 (vs), 1250 (vs), 1209 (vs), 1102 (vs), 987 (vs), 877 (vs), 848 (vs), 760 (vs), 715 (s), 696 (s), 650

(s), 616 (s), 585 (m), 494 (w); Raman (for an assignment of the vibrations, see Appendix (Chapter 4); 200 mW) $\tilde{\nu}$ /cm^{-1}: 3328 (16), 2964 (41), 2904 (50), 1587 (20), 1485 (6), 1419 (14), 1289 (21), 1264 (6), 1209 (14), 1103 (17), 988 (5), 896 (6), 856 (12), 840 (12), 698 (14), 625 (100), 522 (13), 375 (10), 341 (11), 315 (20), 263 (22), 194 (20); m.p. (DSC, T_{onset}, 2 °C/min) 90.1 °C, 231.3 °C decomp.; MS (DEI+, $CHCl_3$): m/z = 244.3 [M^+], 171.2 [$M^+ - Me_3Si^-$], 98.08 [$M^+ - 2\ Me_3Si^-$], 146.2, 115.2, 73.2 [$SiMe_3^+$], 45.2, 43.1; Details of the single crystal X-ray diffraction experiment are listed in the appendix (Chapter 4).

b) Chlorotrimethylsilane route

DAT (100 mg, 0.100 mmol, 1.00 eq) and diethyl ether (1 mL) were placed inside a dry Schlenk flask (50 mL) and sealed with a septum. TMSCl (119 mg) was added dropwise through the septum using a syringe. The mixture was stirred for 30 minutes at room temperature. The septum was replaced with a reflux condenser and triethylamine (111 mg, dried over 3 Å molecular sieve) was added over a period of five minutes and the temperature of the reaction mixture was raised to 80 °C. Diethylether (1 mL) was added after three hours. The heating was stopped after a total of 6 hours. The reaction mixture was filtered using a Schlenk frit, the flask washed with pentane (two times 2 mL) and the filtrate was evaporated to dryness. The solid residue was recrystallized from pentane and cooled to -20 °C. The resulting white amorphous precipitate was identified as 1,5-BTMSD using raman spectroscopy and mass spectrometry. The product obtained was of lower purity compared to the product obtained from the HMDS procedure.

N^5-Trimethylsilyl-1,5-diamino-1H-tetrazole (5-TMSD)

DAT (100 mg, 0.100 mmol, 1.00 eq) and diethyl ether (1 mL) were placed inside a dry Schlenk flask (50 mL) and sealed with a septum. Using a syringe, TMSCl (119 mg) was added dropwise through the septum. The mixture was stirred for 30 minutes at 0 °C. Then 111 mg of triethylamine (dried over 3 Å molecular sieve) were added over 5 min and the reaction mixture was heated up

to 80 °C. After 3 hours, further diethyl ether (1 mL) was added. The heating was stopped after 6 hours. The reaction mixture was filtered of using a Schlenk frit, the flask was washed with two times with 2 mL pentane and the filtrate was evaporated *in vacuo*. The solid residue was dissolved in excess of pentane (30 mL) and the solvent was slowly removed *in vacuo*. Thereby colorless needles of the product were formed (101 mg; 0.563 mmol; 58%). The structure was determined by single crystal x-ray diffraction.

IR (KBr disk) $\tilde{\nu}$ /cm^{-1}: 3436 (vs), 2960 (w), 1646 (s), 1586 (vs), 1383 (m), 1289 (m), 1254 (s), 1209 (m), 1102 (m), 1102 (m), 995 (m), 988 (w), 875 (s), 849 (s), 760 (w), 651 (w), 579 (w); Raman (400 mW, 25 °C, 100 scans) $\tilde{\nu}$ /cm^{-1}: 3328 (16), 2963 (34), 2903 (57), 1586 (23), 1413 (22), 1290 (34), 1210 (25), 1104 (30), 838 (24), 792 (28), 698 (29), 653 (28), 625 (89), 520 (26), 494 (32), 316 (31), 264 (37). Details of the single crystal X-ray diffraction experiment are listed in the appendix (Chapter 4).

1,1-Bis(trimethylsilyl)-1,5-diamino-1H-tetrazole (1,1-BTMSD)

Inside a dry 100 mL Schlenk flask, equipped with a reflux condenser and a bubble counter, were placed 0.500 g (5.00 mmol; 1.00 eq) of DAT and 0.100 g (0.75 mmol; 0.15 eq) ammonium sulfate. Dry THF (15 mL) was added and the suspension was stirred at room temperature. HMDS (2.421 g, 15.00 mmol, 3.00 eq) was added slowly to this mixture and the temperature was increased to 120 °C. The reaction mixture was stirred at this temperature for 12 h until the evolution of ammonia could no longer be detected as indicated by indicator paper at the outlet of the bubble counter and the solids in the reaction mixture had almost completely dissolved. Slow evaporation of the solvent at ambient conditions yielded a white precipitate containing single crystals (colorless needles) suitable for X-ray diffraction

IR (KBr disk) $\tilde{\nu}$ /cm^{-1}: 3408 (s), 3307 (m), 3241 (m), 3179 (m), 2959 (m), 1645 (vs), 1579 (m), 1416 (w), 1309 (m), 1097 (m), 979 (w), 933 (vs), 886 (vs), 847 (vs), 760 (w), 690 (w), 625 (w), 524 (w); Raman (400 mW, 25 °C, 100 scans) $\tilde{\nu}$ /cm^{-1}: 3148 (8), 2904 (75), 1646 (21), 1452 (19), 1413 (15), 1310 (16), 1102

(12), 1051 (10), 982 (10), 833 (12), 769 (20), 745 (22), 964 (17), 646 (100), 426 (29), 361 (20), 290 (15), 251 (23); MS (DEI+, $CHCl_3$): *m/z* = 244.2 [M^+], 174.2 [$M^+ - Me_3Si^-$], 174.2, 146.2, 130.1, 115.2, 100.1 [$M - Me_3Si\cdot+2H]^+$, 73.2 [$SiMe_3^+$], 45.1; Details of the single crystal X-ray diffraction experiment are listed in the appendix (Chapter 4).

N^1-(Propan-2-ylidene)-1,5-diamino-1H-tetrazole (1-PYD)

1,5-BTMSD (200 mg, 0.818 mmol) were placed inside a dry Schlenk flask (50 mL), equipped with a septum and magnetic stirring bar. By using a syringe, dry acetone ([D_6]acetone, 2 mL, 1.43 g, 24.5 mmol, 30 eq) was added and the reaction mixture was stirred at room temperature for 6 h. The slightly turbid solution was filtered and the filtrate slowly evaporated affording colorless prismatic crystals (95.1 mg; 0.679 mmol; 83%).

($C_4H_2D_6N_6$): ^{1}H NMR (400 MHz, [D_6]acetone) δ:, 25°C): δ = 0.08 (s, 9H, $Si(CH_3)_3$), 0.22 (s, 9H, $Si(CH_3)_3$), 4.25 (s, 1H, NH), 4.82 ppm (s, 1H, NH); ^{13}C NMR (100 MHz, [D_6]acetone): δ = 29.6 (septet, $J(^{13}C\text{-}D)$=19.3 Hz, C_2, C_4), 132.6 (C_1), 205.8 ppm (C_3); MS (DEI+, $CHCl_3$): *m/z* = 146.3 [M^+], 62.3, 48.2, 28.2 [N_2^+]; Details of the single crystal X-ray diffraction experiment are listed in the appendix (Chapter 4).

N^1,N^1,N^5-Tris(trimethylsilyl)- 1,5-diamino-1H-tetrazole (1,1,5-TTMSD)

1,5-BTMSD (312 mg, 1.28 mmol, 1.00 eq) and triethylamine (freshly distilled, 260 mg, 2.57 mmol, 2.00 eq) were added to a dry Schlenk flask (25 mL), equipped with a reflux condenser, bubble counter and a stirring bar by means of a syringe over the stopcock of the flask. The suspension was stirred at room temperature and subsequently trimethylsilyl triflate (569 mg, 2.57 mmol, 2.00 eq) was added dropwise. A pale reddish coloured solution was obtained and the reaction mixture was stirred for further 8 h at 80 °C. Colorless crystals precipitated from the solution already after approximately three hours.
The reaction was cooled to room temperature, and freshly distilled diethyl ether (10 mL) were added affording a sepparation into two phases: a lower, red

coloured oily phase, containing mainly triethylammonium triflate, and an upper colorless phase, containing the product. The phases were separated (by means of a Pasteur pipette) and the lower phase was washed three times with 5 mL of ether. The ether solutions were combined and collected inside a dry Schlenk flask put under a nitrogen atmosphere. The volume of the solvent was reduced by fifty percent and the solution was cooled to 0 °C. The product crystallized over night in form of colorless prismatic crystals. The yield was 320 mg (0.823 mmol; 64%).

^{1}H NMR (400 MHz, [D_6]benzene, 25°C): δ = 0.29 (s, 18H, ($Si(CH_3)_3)_2$), 0.12 ppm (s, 9H, $Si(CH_3)_3$); ^{13}C NMR (100 MHz, [D_6]benzene, 25°C): δ = 1.15, 1.79; ^{29}Si NMR (79.5 MHz, [D_6]benzene, 25°C, INEPT, 9H, J = 6.5 Hz): δ = 7.59, − 21.35 ppm; IR (for an assignment of the vibrations, see Appendix, KBr disk) $\tilde{\nu}$ /cm^{-1}: 3410 (s), 3237 (m), 3181 (s), 2958 (m), 2903 (w), 1645 (s), 1580 (s), 1477 (w), 1454 (w), 1440 (w), 1347 (w), 1309 (w), 1298 (m), 1256 (vs), 1204 (m), 1165 (m), 1097 (m), 1031 (m), 982 (w), 936 (s), 884 (s), 840 (vs), 759 (m), 690 (w). 638 (m), 576 (w), 525 (w); Raman (for an assignment of the vibrations, see Appendix, 400 mW, 25°C, 100 scans) $\tilde{\nu}$ /cm^{-1}: 2962 (50), 2902 (100), 1645 (5), 1580 (9), 1452 (10), 1413 (15), 1299 (11), 1205 (8), 1105 (11), 1034 (6), 983 (7), 899 (5), 759 (11), 692 (19), 644 (49), 621 (32), 531 (14), 425 (21), 358 (19), 290 (14), 210 (25); MS (DCI+, isobutane): m/z = 317.2 $[M+H]^+$, 245.3 $[M - Me_3Si^{\cdot} + 2\ H]^+$, 173.2 $[M - 2Me_3Si^{\cdot} + 3H]^+$, 102.2, 57.2, 34.2; Details of the single crystal X-ray diffraction experiment are listed in the appendix (Chapter 4).

Reaction of 1,5-BTMSD with n-Buthyllithium and TMSCl

A dry Schlenk flask (100 mL) was charged with 1,5-BTMSD (255 mg, 1.04 mmol, 1.00 eq) using a dry box. The substance was dissolved in dry THF (15 mL) and the solution was cooled to −70 °C. By means of a syringe, a 0.707 M solution of a 0.707 M *n*-BuLi in hexanes (1.48 mL, 1.04 mmol, 1.00 eq) was added over a period of 10 minutes whith stirring of the reaction mixture. The reaction mixture was taken out of the cooling bath, warmed up to room temperature and stirred for additional 2 h. The solution was cooled again (−70 °C) and TMSCl (113 mg) was added over a period of five minutes with a syringe during which the reaction mixture turned yellow. The reaction mixture was stirred overnight under an atmosphere of nitrogen at room temperature. Then THF (20 mL) was added, the mixture was heated to 40 °C and filtered using a Schlenk frit, and the solvent was removed. Mass spectrometry of the solid residue revealed both the presence of 1,1,5,5-TTMSD [$C_{13}H_{36}N_6Si_4$] and 1,1,5,-TTMSD [$C_{10}H_{28}N_6Si_3$] according to the signals having a *m/z* of 388.2 and 316.17. No attempt was made to purify the product and optimize the procedure.

Raman (400 mW, 25 °C, 100 scans) $\tilde{\nu}$ /cm^{-1}: 2951 (65), 2893 (100), 1368 (45), 1283 (55), 1223 (60), 1105 (45), 997 (25), 961 (35), 675 (25), 615 (75), 321 (40), 210 (35). MS (DEI+): selected *m/z*: 388.2, 316.17.

2.3.3 Pyridazines

Introduction

Halogenated pyridazines have been synthesised as possible precursor molecules for the synthesis of novel energetic matierials like the elusive 3,4,5,6-tetraazido-1,2-pyridazine molecule. Next to our interest into the energetic properties of this compound pyridazines decorated with azide groups are interesting model compounds to study possible pyridazine azide cyclisation reactions.

Azide groups α-substituted to annular N-atoms in aromatic compounds are subject to tautomeric conversion to a tetrazole ring. [358] The potential energy surface on which this type of reaction takes place in solution has recently been investigated experimentally and theoretically. [359-360] It has been established for a series of 2,4-diazidopyrimidines and 4,6-diazidopyrimidines that the azido-tetrazole tautomerism is strongly solvent and temperature dependent and that the azide-azide and azide-tetrazole forms are energetically more favourable than the tetrazole-tetrazole form. [361] In the crystalline state, 3,6-diazidopyridazine has been found to exist in the azide-tetrazole form (Fig. 2.142). [362-363]

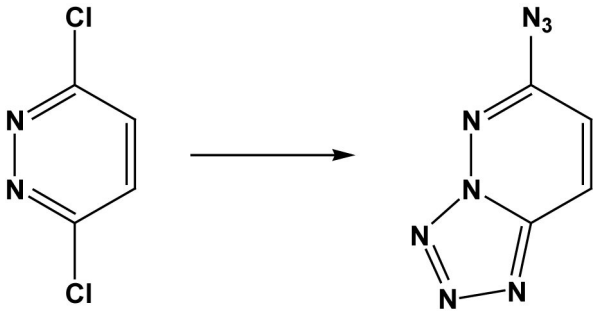

Figure 2.143. Formation of 6-azidotetrazolo-[1,5-b]pyridazine upon treatment of 3,6-dichloropyridazine wit sodium azide in a sealed tube with an ethanol-water solvent (90°C, 3h). [364]

In 2004, Allan *et al.* reported a study [365] investigating the reaction between 4-methyl-3,5,6-tribromopydridazine and sodium azide. They reported the formation of 4-methyl-3,5,6-triazidopyridazine as intermediate and subsequent cyclisation to one of the two possible bicyclic tetrazolo[1,5-b]pyridazine products. They stated that this product was thermally unstable and nitrogen

was liberated on heating this compound giving rise to 5-amino-3-diazido-4-methyl-tetrazolo[1,5-b]pydridazine. Finally they succeeded in determining the crystal structure of 3,5-diazido-4-methyl[1,5-b]tetrazolopyridazine confirming theoretical predictions that compound exists in the bicyclic (tetrazol-pyridazine) rather than the tricyclic (tetrazol-pyridazine-tetrazol) form. However, their attempts to grow single crystals resulted in 'twinned or otherwise unsuitable crystals that were prone to decomposition' and synchrotron radiation had to be used to measure the very small crystals. The data obtained were sufficient as a structural proof but they mentioned that 'due to the highly mosaic nature of the crystal the data is not of sufficient quality to give precise structural parameter'. We have synthesised both 3,4,6-trichloropyridazine and 3,4,5,6-trichloropyridazine from 3,6-dichloropyridazine in order to subsequently substitute the chlorine atoms with azide and study these products. In accordance with the well established behaviour that nitrogen para to the site of nucleophilic attack is activating in perhalogenated heteroaromatic systems we were only able to substitute the chlorine atom at the 4-position yielding 3,6-dichloro-4-azidopyridazine. A more comprehensive study of the regioselectivity of the reactions between tetrachloropyridazine and a variety of aliphatic nitrogen nucleophiles has only recently been reported confirming our finding of the regioselectivity. [366] The reported 'violently explosive' nature of 6-azidotetrazolo-[1,5-b]pyridazine together with its low thermal stability ($T_{dec.}$ = 128-129°C) [367] rendered it unlikely to obtain a material of sufficient stability to fulfil the qualification criteria for a novel energetic material (Table 1.1, page 15) and no further efforts were undertaken to overcome the difficulties experienced in obtaining a higher degree of azide substitution at this time.

However, due to the importance of 3,4,6-trichloropyridazine and 3,4,5,6-tetrachloropyridazine as educts in organic chemistry, their exceptional biological activity we investigated the solid state structures using single crystal X-ray diffraction because structural data of these two very simple compounds in the solid state were unkown.

Biological Activity

Especially the chloro derivatives we have synthesised are synthetically valuable precursor molecules in organic synthesis and display remarkable biological activities. The trihalopyridazines are excellent herbicides and insecticides, but are less bacterically against S-aureus than the tetrahalopyridazines. The tetrahalopyridazines are excellent pre- and post-emergent herbicides and they also possess exceptional fungicidal and bactericidal properties. From the reported data [368] it is apparent that 3,4,6-trichloropyridazine and 3,4,5,6-tetrachloropyridazine are unique in their extremely broad spectrum of biological activity in that they are as effective or more effective than the reference standards, even though in some instances the concentration was much lower than the reference standard against which the pyridazines were tested. Of interest, we mention that 3,4,6-trichloropyridazine has been reported to be not only toxic and an irritant, but also a strong contact allergen to humans and special care has to be taken when working with this substances. [369]

Crystal Structure Analysis

3,4,6-Trichloropyridazine (3,4,6-TCP)

The structure of 3,4,6-Trichloropyridazine at 100K has orthorhombic symmetry, space group *Pbca* (no. 61). The asymmetric unit consists of one molecule (Fig. 2.144).

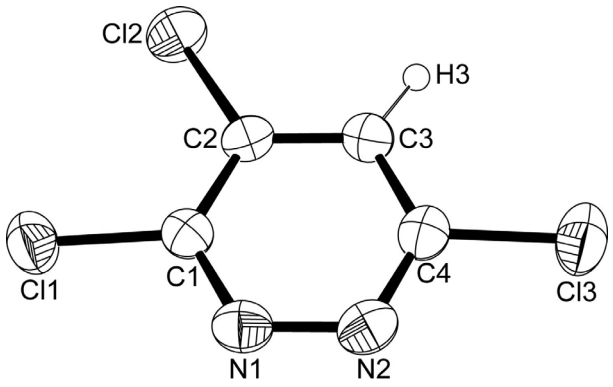

Figure 2.144. ORTEP representation of the molecular structure of 3,4,6,-trichlorpyridazine in the crystalline state. The thermal ellipsoids are shown at the 50 % probability level. Selected bond lengths [Å] and angles [°]:N_1-N_2 1.350(2), N_1-C_1 1.317(2), C_1-C_2 1.399(3), C_2-C_3 1.370(3), C_3-C_4 1.392(3), C_4-N_2 1.312(3), C_1-Cl_1 1.7205(18), C_2-Cl_2 1.7058(18), C_4-Cl_3 1.7274(19), N_1-C_1-Cl_1 115.50(14), Cl_1-C_1-C_2 121.06(13), C_1-C_2-Cl_2 121.66(13), Cl_2-C_2-C_3 121.34(14), C_3-C_4-Cl_3 119.50(14), Cl_3-C_4-N_2 115.37(14).

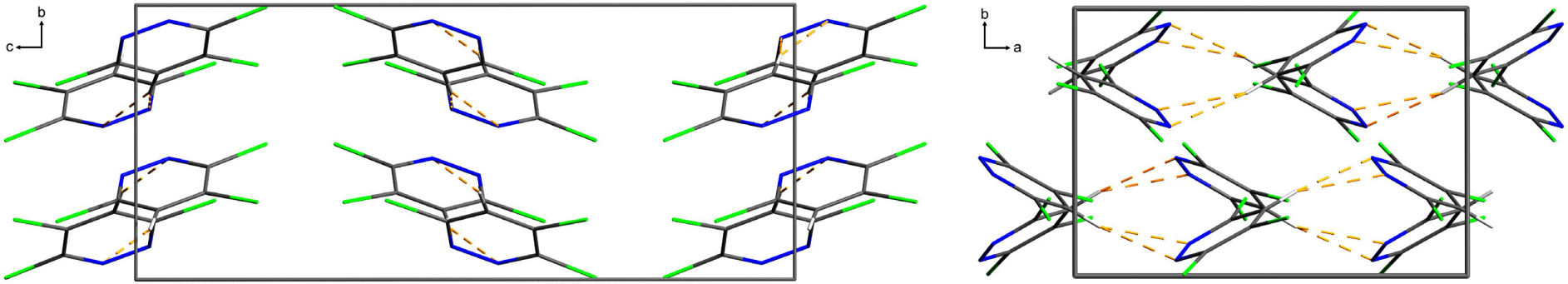

Figure 2.145. Unit cell of 3,4,6-trichlorpyridazine, viewed along the *a* axis (left) and *c* axis (right). Yellow dashed lines indicate hyrogen bonding (C_3-H_3···N_1^i , C_3-H_3···N_2^i). (i) 1/2+x,1/2-y,-z.

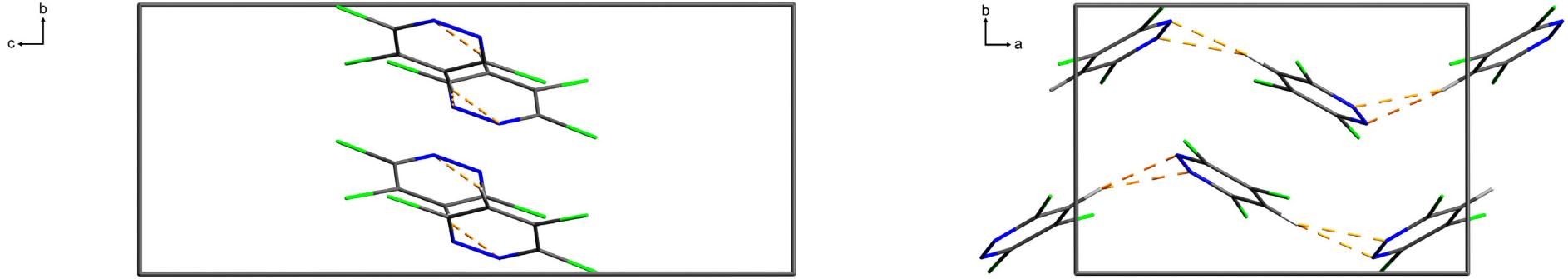

Figure 2.146. Detail of the unit cell of 3,4,6-trichlorpyridazine, viewed along the *a* axis (left) and *c* axis (right). Yellow dashed lines indicate hyrogen bonding (C_3-H_3···N_1^i , C_3-H_3···N_2^i). (i) 1/2+x,1/2-y,-z.

3,4,5,6-Tetrachloropyridazine (3,4,5,6-TCP)

The structure of 3,4,5,6-Tetrachloropyridazine at 100K has tetragonal symmetry, space group $P4_12_12$ (no. 92). The asymmetric unit consists of two molecules (Fig. 2.147).

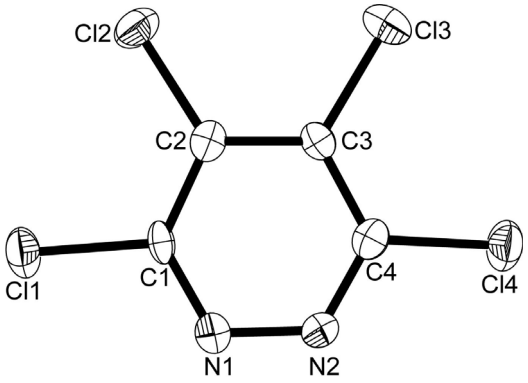

Figure 2.147. ORTEP representation of the molecular structure of 3,4,5,6-tetrachlorpyridazine in the crystalline state. The thermal ellipsoids are shown at the 50 % probability level. Selected bond lengths [Å] and angles [°]: N_1-N_2 1.347(8), N_1-C_1 1.314(10), C_1-C_2 1.410(10), C_2-C_3 1.385(10), C_3-C_4 1.407(10), C_4-N_2 1.317(10), C_1-Cl_1 1.739(7), C_2-Cl_2 1.691(8), C_3-Cl_3 1.719(7), C_4-Cl_4 1.709(8), N_1-C_1-Cl_1 115.2(6), Cl_1-C_1-C_2 118.9(6), C_1-C_2-Cl_2 123.1(6), Cl_2-C_2-C_3 122.2(6), C_2-C_3-Cl_3 120.6(6), Cl_3-C_3-C_4 121.3(6), C_3-C_4-Cl_4 121.0(6), Cl_4-C_4-N_2 116.3(6).

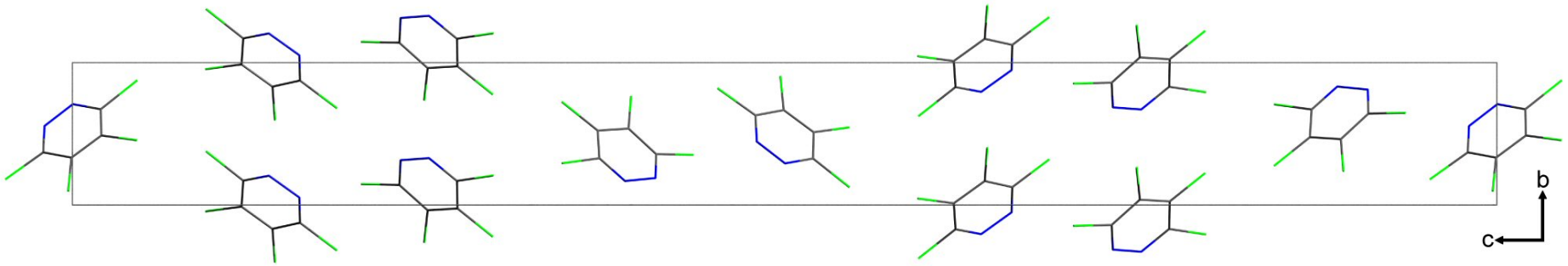

Figure 2.148. Unit cell of 3,4,5,6-tetrachlorpyridazine, viewed along h,k,l = 1, 0, 0. Colour code: carbon (grey), nitrogen (blue), chlorine (green).

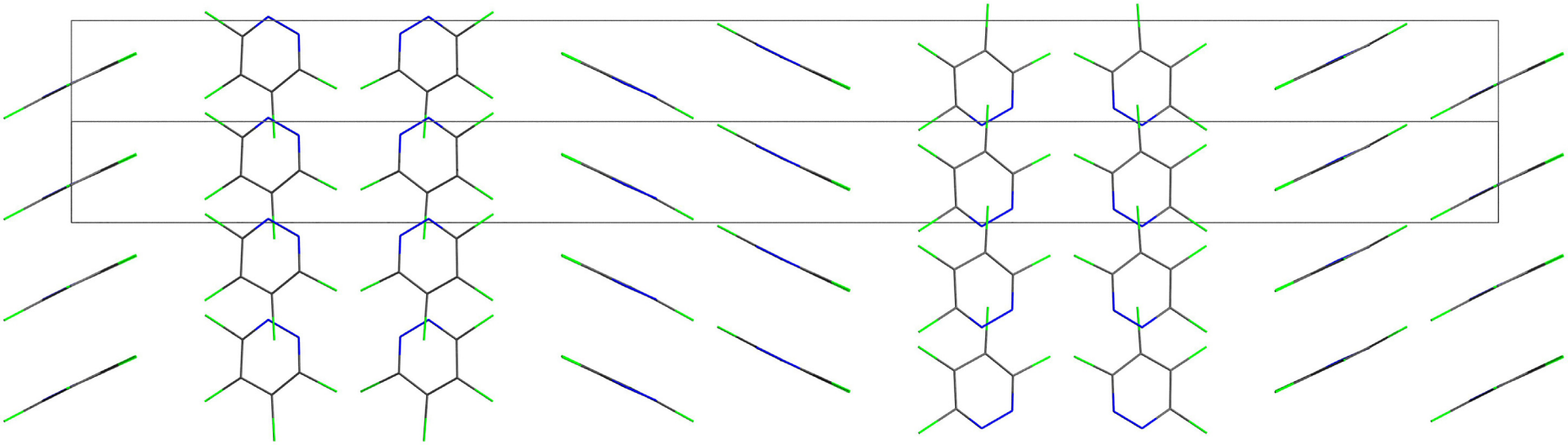

Figure 2.149. 2x2x2 super cell of 3,4,5,6-tetrachlorpyridazine, viewed along h,k,l = 1, -1, 0.

4-Azido-3,6-dichloropyridazine (4A-3,6-DCP)

The structure of 4-Azido-3,6-dichloropyridazine at 100K has orthorhombic symmetry, space group $P2_12_12_1$ (no. 19). The asymmetric unit consists of one molecule (Fig. 2.150).

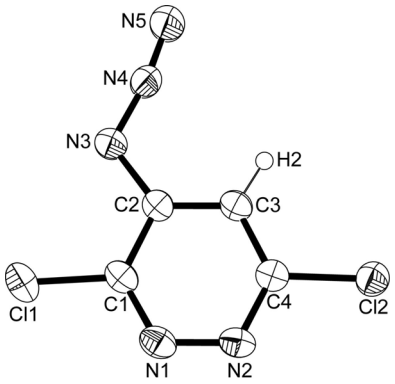

Figure 2.150. ORTEP representation of the molecular structure of 4-azido-3,6-dichloropyridazine in the crystalline state. The thermal ellipsoids are shown at the 50 % probability level. Selected bond lengths [Å] and angles [°]:N_1-N_2 1.361(3), N_1-C_1 1.310(4), C_1-C_2 1.415(4), C_2-C_3 1.372(4), C_3-C_4 1.389(4), C_4-N_2 1.318(4), C_1-Cl_1 1.728(3), C_2-N_3 1.403(4), N_3-N_4 1.272(4), N_4-N_5 1.107(4), C_4-Cl_2 1.727(3), N_1-C_1-Cl_1 116.0(2), Cl_1-C_1-C_2 119.4(2), C_1-C_2-N_3 117.0(3), N_3-C_2-C_3 127.2(3), C_2-N_3-N_4 113.3(2), N_3-N_4-N_5 170.7(3), C_3-C_4-Cl_2 118.8(2), Cl_2-C_4-N_2 115.4(2).

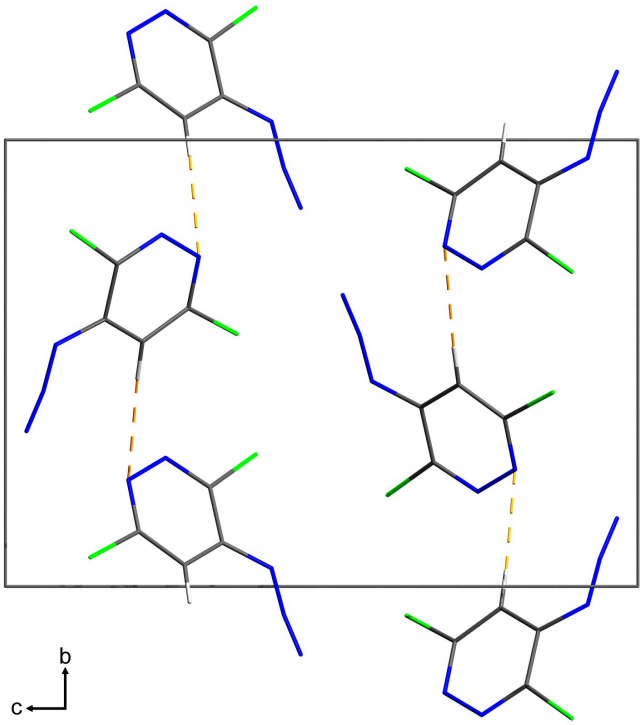

Figure 2.151. Unit cell of 4-azido-3,6-dichloropyridazine, viewed along the *a* axis. Yellow dashed lines indicate hyrogen bonding (C_3-H_3···N_2^i). (i) 2-x,-1/2+y,1/2-z.

4,6-Dichloro-3(2)H-pyridazinone

The structure of 4,6-dichloro-3(2)H-pyridazinone at 100K has monoclinic symmetry, space group $P2_1/n$ (no. 14). The asymmetric unit consists of one molecule (Fig. 2.152).

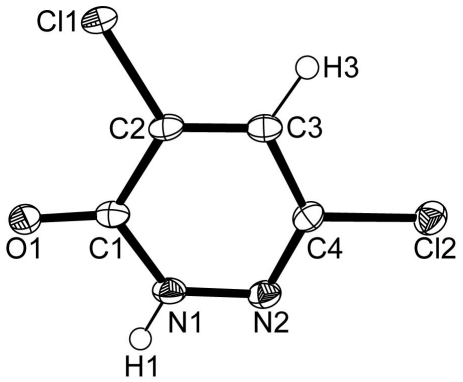

Figure 2.152. ORTEP representation of the molecular structure of 4,6-dichloro-3(2)H-pyridazinone in the crystalline state. The thermal ellipsoids are shown at the 50 % probability level. Selected bond lengths [Å] and angles [°]: N_1-N_2 1.352(2), N_1-C_1 1.368(2), C_1-C_2 1.457(2), C_2-C_3 1.345(2), C_3-C_4 1.423(2), C_4-N_2 1.292(2), C_1-O_1 1.233(2), C_2-Cl_1 1.7130(17), C_4-Cl_2 1.7310(17), N_1-C_1-O_1 121.39(15), O_1-C_1-C_2 125.39(15), C_1-C_2-Cl_1 117.01(13), Cl_1-C_2-C_3 122.03(13), C_3-C_4-Cl_2 118.22(13), Cl_2-C_4-N_2 116.22(12).

Due to the possibility of tautomerism, this compound can either exist as hydroxysubstituted pyridazine or as oxo-dihydropyridazine (Fig. 2.153).

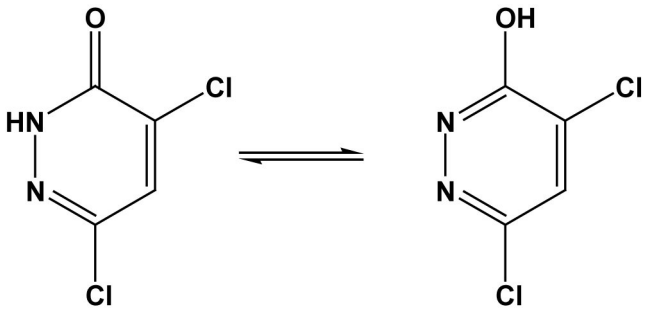

Figure 2.153. Possible tautomerism of 4,6-dichloro-3(2)H-pyridazinone.

The X-ray structure unabigously shows the oxo-dihydropyrdidazine tautomer to be the preferred motiv in the solid state.

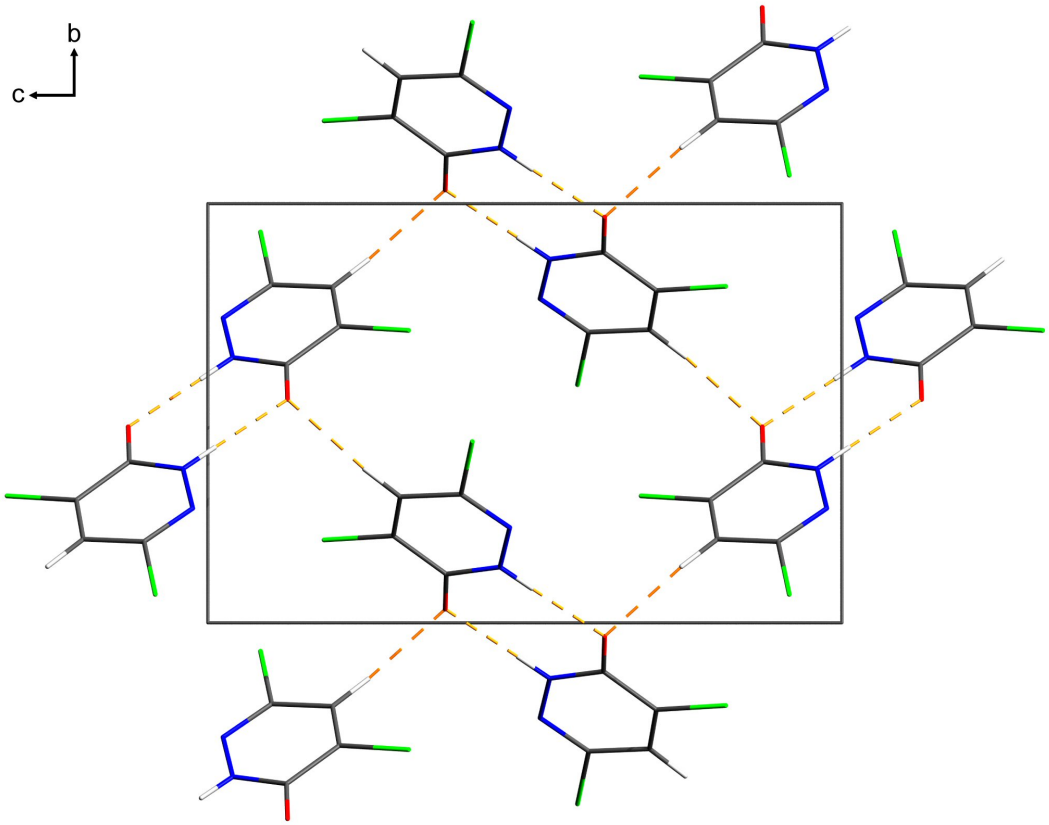

Figure 2.154. Unit cell of 4,6-dichloro-3(2)H-pyridazinone, viewed along the *a* axis. Yellow dashed lines indicate hyrogen bonding (N_1-H_1···O_1^i, C_3-H_3···O_1^i). (i) -x,1-y,-z, (ii) 1/2-x,-1/2+y,1/2-z.

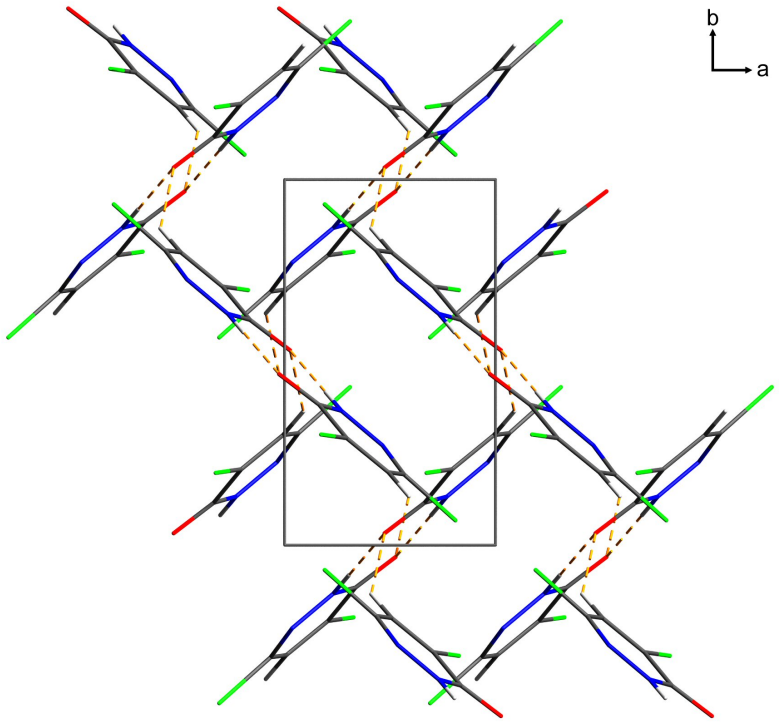

Figure 2.155. Unit cell of 4,6-dichloro-3(2)H-pyridazinone, viewed along the *c* axis. Yellow dashed lines indicate hyrogen bonding (N_1-H_1···O_1^i, C_3-H_3···O_1^i). (i) -x,1-y,-z, (ii) 1/2-x,-1/2+y,1/2-z.

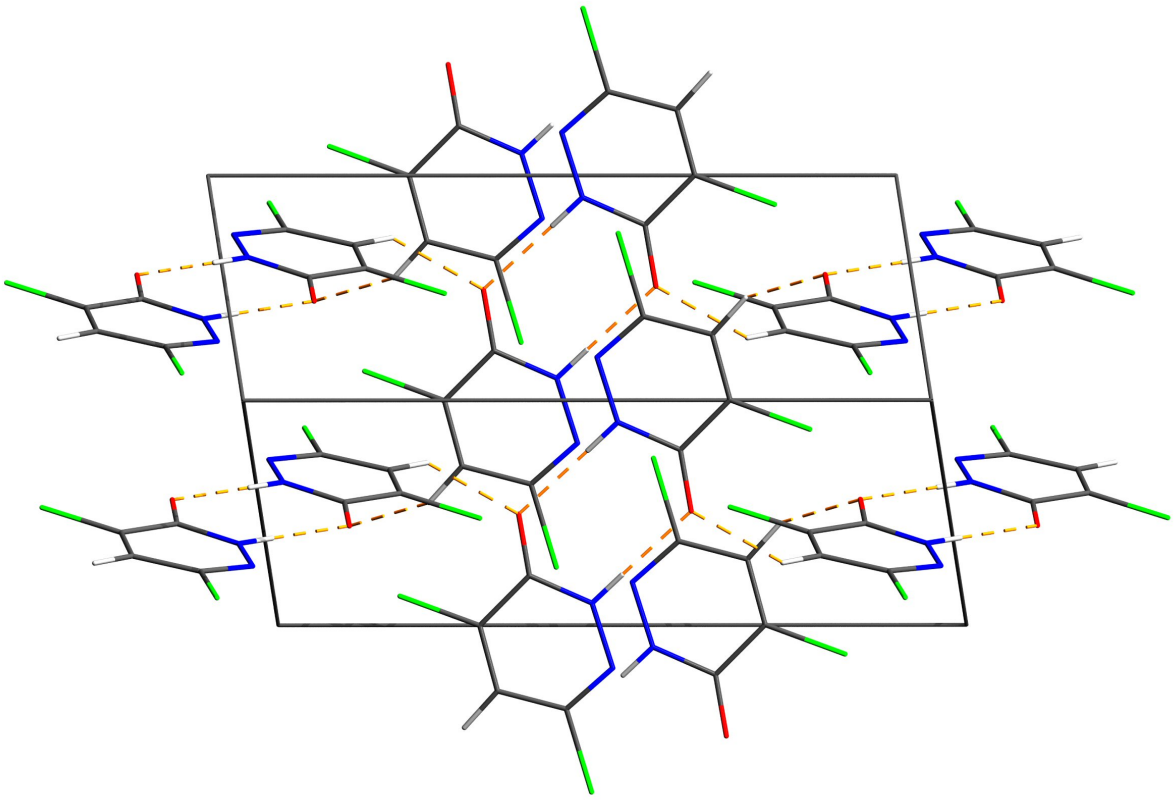

Figure 2.156. Unit cell of 4,6-dichloro-3(2)H-pyridazinone, viewed along h,k,l = -2.66, 7.63, 1.22. Yellow dashed lines indicate hyrogen bonding (N_1-H_1···O_1^i, C_3-H_3···O_1^i). (i) -x,1-y,-z, (ii) 1/2-x,-1/2+y,1/2-z.

Experimental

Synthesis of 3,4,6-Trichloropyridazine

Caution: Trichloropyridazine is a very strong contact allergen.

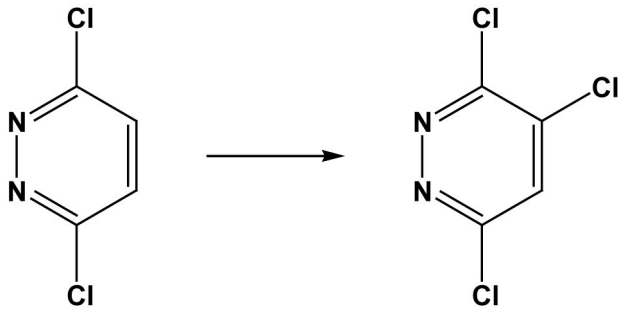

Dichloropyridazine (15g) together with PCl_5 (100g) were placed under inert conditions in a sealed steel cylinder (1000mL, swagelok). The cylinder was evacuated and heated for 20h up to 285°C using a heating tape. Afterwards, the container was washed with ice water and diethylether several times. The diethylether fractions were dried over magnesium sulphate and concentrated affording the crude product. Recrystallization from methanol afforded single crystals suitable for X-ray diffraction.

Raman (1 cm^{-1}) $\tilde{\nu}$ /cm^{-1}: 3094(w), 1533(w), 1498(w), 1475(w), 1289(w), 1186(m), 1086(w), 1045(w), 854(w), 685(m), 509(w), 467(w), 405(s), 347(vs), 215(w), 197(m), 186(w); m.p. 57 – 58°C (lit., 58 -59°C) [370]; Details of the single crystal X-ray diffraction experiment are listed in the appendix (Chapter 4).

Synthesis of 3,4,5,6-Tetrachloropyridazine

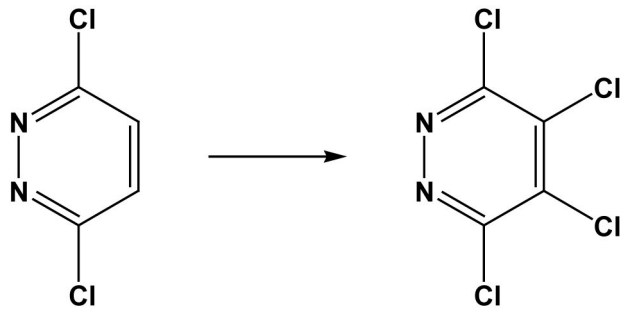

Though tetrachloropyridazine had previously been prepared from dichloromaleic anhydride, [371] we chose to prepare it using a slight modification from the reaction between commercially available 3,6-dichloropyridazine and phosphorus pentachloride at elevated temperature and pressure. [372]

Dichloropyridazine (15g) together with PCl_5 (100g) were placed under inert conditions in a sealed steel cylinder (1000mL, swagelok). The cylinder was evacuated and heated for 48h up to 360°C using a heating tape. Afterwards, the container was washed with ice water and diethylether several times. The diethylether fractions were dried over magnesium sulphate and concentrated affording the crude product. Recrystallization from methanol afforded light brown coloured single crystals suitable for X-ray diffraction.

^{13}C NMR ([D_6]acetone) δ: 155.2 (C_1,C_4), 138.2 (C_2,C_3); ^{15}N NMR ([D_6]acetone) δ (nitromethane): 4.5 (N_1,N_2); IR (KBr disk) $\tilde{\nu}$ /cm^{-1}: 1505, 1480, 1360, 1290, 1200, 1120, 1090, 890, 800, 630; Raman (1 cm^{-1}) $\tilde{\nu}$ /cm^{-1}: 1495(w), 1475(w), 1186(vs), 1085(w), 874(w), 617(w), 516(w), 500(w), 405(w), 348(s), 215(w); m.p. 86 – 88°C (lit., 85 - 86°C) [373] ; Details of the single crystal X-ray diffraction experiment are listed in the appendix (Chapter 4).

Synthesis of 4-azido-3,6-dichloropyridazine

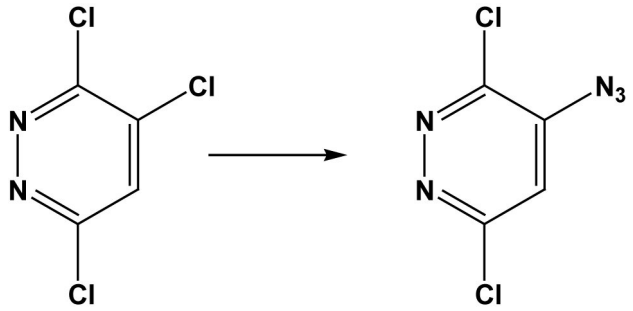

To a solution of 3,4,6-Trichloropyridazine (226 mg, 1,23 mmol) in a mixed solvent (6 mL THF and 3 mL DMSO) at room temperature was added sodium azide (480 mg, 7,38 mmol). NaN_3 was initially almost completely soluble but soon after the addition, a white precipitate was formed. The reaction mixture became coloured (orange) about 10 min after addition. It was stirred at room temperature for 12 h. Volatile solvent was removed under reduced pressure. The crude reaction mixture was taken up in ethyl acetate (90 mL), washed in turn with water (3 x 10 mL), dried over anhydrous Na_2SO_4 and concentrated under reduced pressure until dryness. Purification by chromatography (5% ethyl acetate / 95% hexane) and subsequent crystallisation afforded the potentially explosive compound as a solid. An analytical sample of this compound was prepared by recrystallisation from ethyl acetate and hexane yielding single crystals suitable for X-ray diffraction. Details of the single crystal X-ray diffraction experiment are listed in the appendix (Chapter 4).

Synthesis of 4,6-Dichloro-3(2)H-pyridazinone

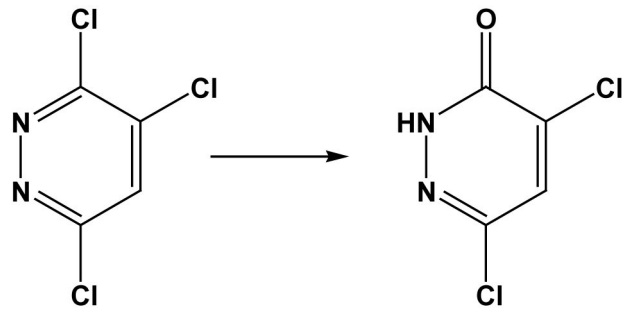

4,6-Dichloro-3(2)H-pyridazinone was obtained over a period of several weeks from the reaction between 3,4,6-trichloropyridazine and moisture of the air at room temperature. m.p., lit., [374] 170 -172°C. Details of the single crystal X-ray diffraction experiment are listed in the appendix (Chapter 4).

2.4 Molecules containing pseudohalide functionalities

2.4.1 Mercury Fulminate (MF)

Introduction

The alchemists in the 17th century, among them *Cornelius Drebbel* (1572-1634) and *Johann Kunckel von Löwenstein* (1630-1703) have known that mixtures of "spiritus vini" with mercury and silver in "aqua fortis" could explode. [375-380] The English chemist *Edward Howard* (1774-1816) [375-376] succeeded in 1799 (in the beginning of the "Scientific Chemistry") to isolate mercury fulminate by treating a solution of mercury in nitric acid with ethanol. *Howard's* report [387] in 1800 on the preparation and properties was a sensation within the scientific world. [380, 386] *Howard* originally planned to synthesise hydrochloric acid which at that time was regarded as a combination of oxygen, hydrogen and a hypothetical element "murium". As oxygen source *Howard* used nitric acid, and for hydrogen he took ethanol together with a metal (Hg) to give a metal chloride. To his surprise a violent detonation occurred when he tried to liberate hydrogen chloride from the greyish-white product by reaction with concentrated sulfuric acid.

From 1820 until 1855 *Justus von Liebig* (1803-1873) was fascinated by the chemistry of mercury and silver fulminates. [383] In 1824 *Liebig* and *Gay-Lussac* succeeded in analyzing silver fulminate as AgCNO. [384] This master piece of chemical work together with *Wöhler's* silver cyanate (AgNCO) led to the concept of isomerism. *Scholl* [385] and *Nef* [386] formulated fulminic acid as oxime of carbon monoxide and *Lothar Wöhler* [387] proved the monomeric nature of the fulminate ion $C{\equiv}N\text{-}O^-$.

Besides *Justus von Liebig* and *Joseph Louis Gay-Lussac* many famous chemists [388] were engaged in the chemistry of mercury and silver fulminate: *Friedrich Wöhler*, *Jöns Jakob Berzelius*, *August Kekulé*, *Louis-Jacques Thenard*, *Claude-Louis Berthollet*, *Pierre Berthelot*, [389] *Heinrich Wieland*, [390-391] *Linus Pauling*, *Rolf Huisgen*. [392] *Berthelot* [393] reported a very exact analysis of $Hg(CNO)_2$ and studied its explosive properties ($Hg(CNO)_2 \rightarrow Hg + 2CO + N_2$). *Wieland*

offered - after his own important contributions to the chemistry of fulminic acid - a widely accepted interpretation for Howard's formation of mercury fulminate from mercury, nitric acid and ethanol. [394]

Mercury fulminate was widely used as primary explosive for nearly a hundred years. In the beginning of the 20th century the annual production of mercury fulminate only in Germany was about 100 000 kg per year. [380, 395] *A. Nobel* used this energetic compound as a component in his recent developed metal blasting cap detonator to initiate dynamite. [380, 396] The wide application of dynamite was only possible when the use of $Hg(CNO)_2$ as primary explosive guaranteed a safe ignition. [400] For this purpose it is now replaced by lead azide which is more stable on storage. [397]

To our knowledge a detailed X-ray crystal structure determination of mercury fulminate has not been carried out. *Miles* reported a good method for the crystallization of mercury fulminate and performed also first investigations on the crystal structure of mercury fulminate with single crystals already in 1931. [398] He correctly derived the holohedric crystal class and also the lattice parameters (a = 5.48, b = 7.71, c = 10.43 Å, V = 441 $Å^3$), But atomic positions of the constituent atoms were not given.

About twenty years later, *Suzuki* performed a single crystal investigation on mercury fulminate. [399] He could set Hg atoms correctly in the positions of a face centred lattice with a total of only 49 reflections, indexed using the cell parameters given by Miles. [400] However, due to the wrong space group, the positions of the C, N and O atoms could not be located and a bent CNO-Hg-ONC structure was proposed as it was generally assumed at that time.

Within the last decades, two results of X-ray powder investigations have also been published. The first was presented by the *International Centre for Diffraction Data* (ICCD) as powder diffraction file 00-002-0287 for mercury fulminate, $HgC_2N_2O_2$, determined with *CuKα* radiation (λ = 1.540598 Å). It contained 22 d-values for non-indexed reflections. [401] These data were obtained from Canadian Industries Limited as private communication. The lattice parameters obtained by this d-values were calculated by least squares fit and correspond to a = 5.398(5), c = 10.214(4) and c = 7.630(10) Å. The result of the second X-ray powder investigation on mercury fulminate was published 1981 by Brown and Swallowe. [402] In this case, *NiKα* radiation was used (λ =

1.6592 Å) with longer wave length in comparison to that with Cu radiation. The precision of the obtained values is lower in this case since mercury fulminate strongly absorbs X-ray radiation. As a consequence, the obtained lattice parameters calculated by least squares fit show higher standard deviations (a = 5.44(3), b = 10.38(4), c = 7.75(5) Å).

Here we report the results of the X-ray investigations of single crystals as well as powders of $Hg(CNO)_2$. The single crystal investigation reveals - as expected - almost linear O-N-C-Hg-C-N-O bonds, similar to those in mercury cyanide NC-Hg-CN. [403] *Liebig* already recognized the close analogy between metal fulminates and metal cyanides. [404-405] In analogy, the correct structure for fulminic acid is H-C≡N-O [383, 406-407] and not C≡N-OH. Furthermore, the fulminate ligand forms transition metal complexes that are very similar to those of cyanide. [408-409] The X-ray structure determination of two polymorphic forms of silver fulminate revealed very interesting structures containing CNO bridges and three centred Ag-C-Ag bonds in hexameric units or infinite chains. [410] The structures of the metal complexes $[(Ph_3P)_2Pt(CNO)_2]$, [411] $[Ph_3PAuCNO]$, [412] $[Au(CNO)_2]^-$, [413] $[M(CNO)_4]^{2-}$ (M = Ni, Pt, Zn), [414] $[Hg(CNO)_4]^{2-}$ [415] as well as $[Co(CNO)_6]^{3-}$ [416] with almost linear M-C≡N-O bonds were determined using X-ray diffraction. Density functional theory (DFT) calculations for these fulminato complexes are in good agreement with the observed structural parameters. [417] In contrast, a recent DFT calculation predicts bent CNO-Hg-ONC units, [418] a structure which is still present in the literature to our surprise.

X-ray Powder Diffraction

An X-ray powder investigation of the micro crystalline $Hg(CNO)_2$ was performed on a *Huber G644 Guinier Diffractometer* using *MoKα1* radiation (λ = 0.7093 Å, quartz monochro-mator). The angle calibration of the diffractometer was performed using electronic grade germanium (a = 5.6575 Å). In the 2θ-range 1000 data points were collected with a counting time of 100 seconds for each increment (0.04°) between 6 and 46°.

The *Gunier* diffractogram was analysed by the *Rietveld* technique using the program *FullProf*. [419] The diffractogram was refined by profile matching [420] in the space group *Cmce* with reliability indices R = 6.36 % and R_{wp} = 8.91 %. The corresponding lattice parameters are a = 5.470(3), b = 10.376(5) and c = 7.700(4) Å at 295 K. Using the positional parameters derived by the single crystal investigation and applying soft distance constraints for Hg-C, C-N and N-O (2.03, 1.14, 1.25 Å), the *Guinier* diffractogram could be refined to R = 8.91 % and R_{wp} = 11.70 %. The *Rietveld* plot for the refinement is shown in Figure 2.157. The crystallographic data for the powder investigation at room temperature are summarized in Table 2.26.

Table 2.26. Crystallographic Data for $Hg(CNO)_2$ obtained by X-Ray Powder Investigation at 295 K with Mo-Kα1 radiation.

temperature / K	295
a / Å	5.470(3)
b / Å	10.376(5)
c / Å	7.700(4)
volume / Å ^{3}	437.0(3)
Hg (x,y,z)	0/0/0
C (x,y,z)	0/0.818(3)/0.095(3)
N (x,y,z)	0/0.711(3)/0.123(3)
O (x,y,z)	0/0.593(3)/0.149(3)
R	0.0868
R_{wp}	0.114
R_{Bragg}	0.151

Notes. Standard deviation in parentheses.

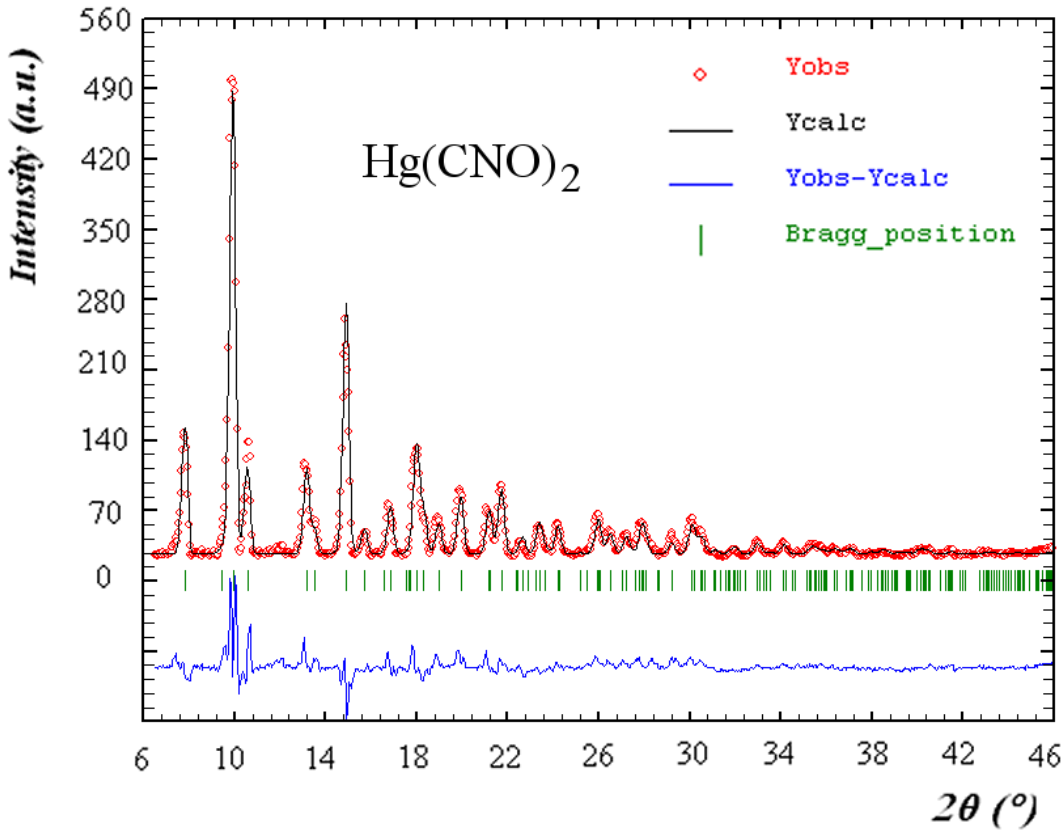

Figure 2.157. *Rietveld* plot of the *Guinier* diffractogram for Mercury Fulminate obtained at 295 K using $MoK_{\alpha 1}$ radiation in the 2-theta-range from 6-46 °.

The analysis of the *Guinier* powder data by applying the *Rietveld* technique does not allow for a decision whether the fulminate group is bonded via C-Hg-C or O-Hg-O due to the small scattering contribution of the light non-metal atoms in comparison to mercury. The scattering contribution of the atoms at small diffraction angles is related to the squares of their total electron numbers: 80^2 (one mercury) : $2 \cdot 6^2$ (two carbon atoms) : $2 \cdot 7^2$ (two nitrogen atoms) : $2 \cdot 8^2$ (two oxygen atoms) = 6400 : 72 : 98 : 128 ≈ 100 : 1.1 : 1.5 : 2.0. In comparison to mercury, the scattering contribution of the C-, N- and O-atoms in mercury fulminate lies between 1 and 2%. The nitrogen atoms in $Hg_2(N_3)_2$ next to mercury could not be located for the same reason by Meyer *et al.* [421] A reliable decision between C-Hg-C and O-Hg-O bonding in mercury fulminate can be made on the basis of precise single crystal X-ray diffraction data. The reliability indices R_1 / wR_2 [$I > 2\sigma(I)$] for C-Hg-C bonding are 0.0111 / 0.0241 in comparison to those obtained when O-Hg-O bonding is assumed (R_1 / wR_2 [$I > 2\sigma(I)$] 0.0362 / 0.0576).

Single Crystal X-ray Diffraction

A single crystal of mercury fulminate (0.05 X 0.05 X 0.01 mm) was measured using an *Oxford Xcalibur3 CCD* single crystal diffractometer from *Oxford Diffraction* (*MoKα* radiation, graphite monochromator, λ = 0.71073 Å). The temperature (100 K) of the single crystal was maintained using a *Cryojet Controller* from *Oxford Diffraction*. The conditions limiting possible reflections were hkl: h + k = 2n, h0l: l = 2n, hk0: h = 2n and yielding the space group *Cmce* (No.64, former space group *Cmca*). The derived centre of symmetry of this space group is in agreement with morphological studies of *Miles*. [422] A total of 4428 data were collected in the 2-Theta range up to 55.0° according to a reflection range from -6 < h < 6, -13 < k < 13, -9 < l < 9. The data were corrected for absorption. After merging, 257 unique reflections with a redundancy of seventeen remained resulting in an reliability index R_{int} = 4.18%. The structure was solved using *SHELXS-97* [423] and refined using *SHELXL-97*. [290] A summary of the crystallographic data for mercury fulminate obtained by the single crystal investigation is shown in the appendix (Chapter 4). The positional parameters and the thermal displacement parameters are listed in Table 2.27.

Table 2.27. Atomic Coordinates and Thermal Displacement Parameters (Å)^2 for $Hg(CNO)_2$ at100 K obtained from a Single-Crystal Investigation.

atom	Hg	C	N	O
x/a	0	0	0	0
y/b	0	0.8186 (6)	0.7109 (5)	0.5932 (4)
z/c	0	0.0951 (8)	0.1210 (6)	0.1481 (6)
U_{11}	0.0148 (1)	0.0126 (3)	0.0122 (2)	0.0245 (2)
U_{22}	0.0141 (1)	0.0213 (3)	0.0263 (3)	0.0193 (2)
U_{33}	0.0209 (2)	0.0220 (3)	0.0144 (2)	0.0299 (2)
U_{23}	-0.0032 (3)	0.0013 (2)	0.0040 (2)	0.0104 (2)
U_{13}	0	0	0	0
U_{12}	0	0	0	0
U_{eq}	0.0166 (1)	0.0187 (1)	0.0176 (1)	0.0246 (9)

Notes. Standard deviation in parentheses.

Crystal Structure Analysis

Mercury fulminate at 100K has orthorhombic symmetry, space group C*mce* (no.64). The asymmetric unit consists of half a mercury atom and one fulminate group. From the results of this structural investigation it is obvious that crystals of mercury fulminate consist of discrete monomeric molecules ONC-Hg-CNO which are C-Hg-C bonded. One discrete mercury fulminate molecule is shown in Figure 2.158. The bond lengths (Å) and bond angles (°) are given in the figure caption.

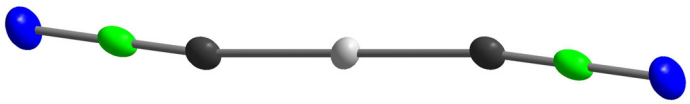

Figure 2.158. Representation of one mercury fulminate molecule with bond lengths (Å) and bond angles (°). The anisotropic thermal displacement parameters are shown at the 50% probability level. Selected bond lengths [Å] and angles [°]: Hg-C 2.029(6), C-N 1.143(8), N-O 1.248(6), C-Hg-C 180.0(2), Hg-C-N 169.1(5), C-N-O 179.7(6).

The fulminate group CNO consists of a short carbon-nitrogen and a longer nitrogen-oxygen bond. The carbon-nitrogen bond length is 1.143(8) Å. This refers to a triple bond, since the tabulated bond length C≡N is 1.11 Å and that for C=N is 1.22 Å. [424] The nitrogen-oxygen bond with a value of 1.248(6) Å is remarkably longer. Here the tabulated bond length for N=O is 1.17 Å and that for N-O is 1.45 Å. [429] Within the limitations of error, the atomic arrangement of the bonds C-N-O and C-Hg-C in the fulminate group is linear (179.7(6) °) and (180.0(2) °). However, the angle N-C-Hg (169.1(5) °) deviates from linearity by eleven degrees. The distances and angles of the $Hg(CNO)_2$ molecules are in the same range as for other metal fulminates. [416, 418, 420, 425-428]

Table 2.28. Bond lengths (Å) and angles (°) in mercury fulminates and cyanides

	Hg-C	C≡N	N-O	Hg-C≡N	C≡N-O	C-Hg-C
$Hg(CNO)_2$	2.029	1.143	1.248	169.1	179.7	180.0
$[Hg(CNO)_4]^{2-}$ [420]	2.16	1.13	1.25	170	178	102-118
	2.21	1.14	1.26	172	179	
$Hg(CN)_2$ [403]	2.015	1.137	-	177.0	-	175
$[Hg(CN)_4]^{2-}$ [429]	2.17	1.14	-	178	-	108
	2.19					111

A very similar structure has been determined for the linear isoelectronic gold complex $[Au(CNO)_2]^-$. [418] Of interest is the comparison of the linear $Hg(CNO)_2$ with the tetrahedral $[Hg(CNO)_4]^{2-}$. [420] As with the mercury cyanides [408, 435] (Table 2.28) the Hg-carbon distance in the neutral linear compounds are considerably shorter than in the tetrahedral complexes which is certainly due to a larger contribution of the 6s orbital in the Hg-C bonds. [430] Remarkably, the Hg-C and C≡N bond lengths in the mercury fulminates and cyanides are very similar (Table 2.28). In conclusion, the formula O-N≡C-Hg-C≡N-O well describes the bonding in the mercury fulminates.

Figure 2.159 shows a view along [010] on the structure of mercury fulminate.

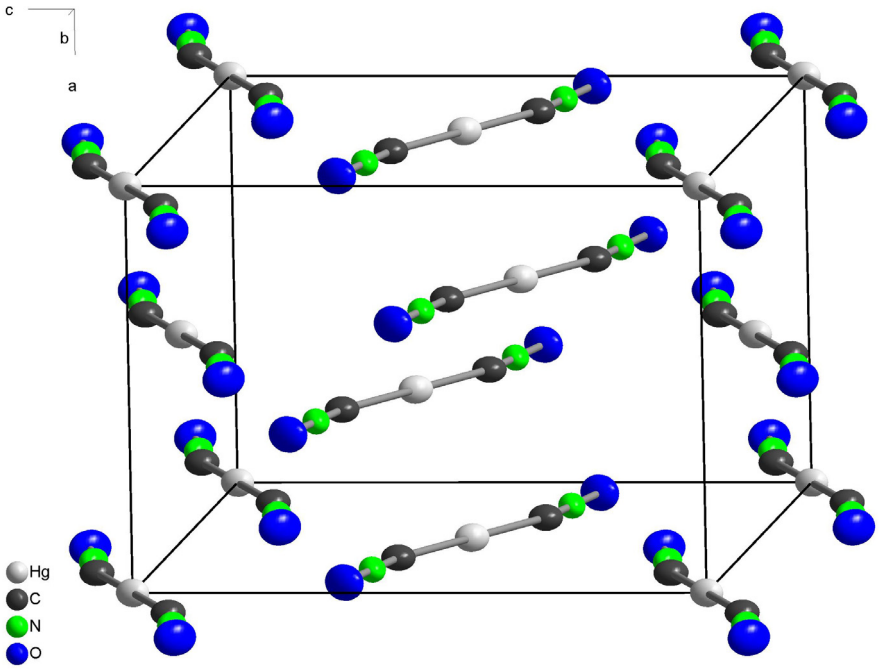

Figure 2.159. Representation of the unit cell of mercury fulminate along [010]. The anisotropic thermal displacement parameters are shown at the 50% probability level.

The mercury atoms have the positions of a face-centred lattice at (0,0,0), (0,0.5,0.5), (0.5,0.5,0) and (0.5,0,0.5) arranging the discrete mercury fulminate molecules at layers with x = 0 and x = 0.5 in the b-c-plane. Figure 2.160 shows planar layers of mercury fulminate molecules lying at x = 0 and x = 0.5 along [010].

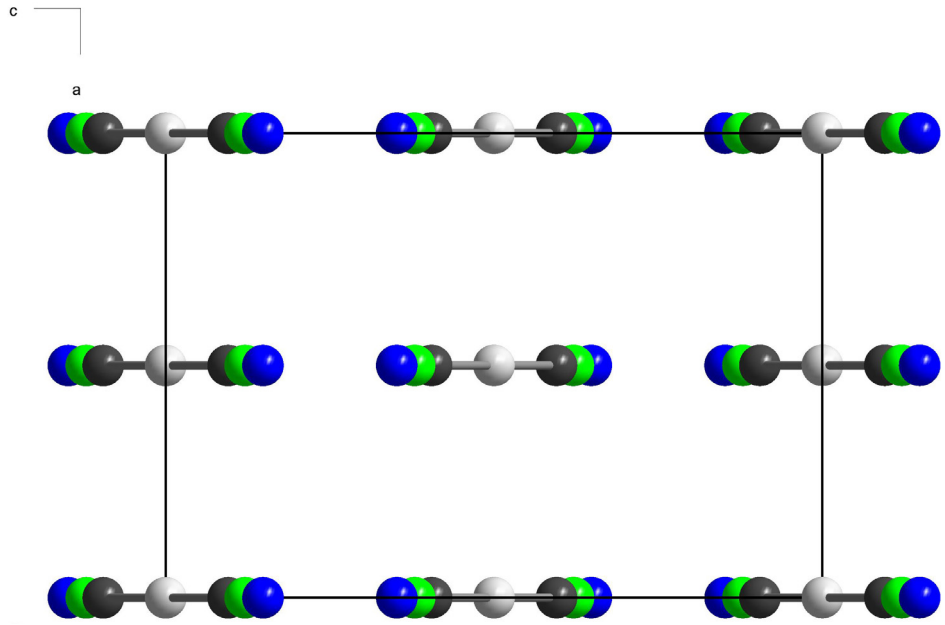

Figure 2.160. Planar layers of mercury fulminate molecules at x = 0 and x = 0.5. The anisotropic thermal displacement parameters are shown at the 50 % probability level.

In order to achieve a higher space filling, the fulminate molecules in the layers at x = 0 and x = 0.5 are rotated against each other by an angle of 41.5°. Figure 2.161 shows one layer with five discrete monomeric molecules. However, such an arrangement also leads to two mercury-oxygen contacts at 2.833(4) Å. The tabulated *van-der-Waals* radii for mercury and also for oxygen are 1.5 Å [431] leading to a *van-der-Waals* distance of about 3.0 Å. The measured Hg-O distance of 2.83 Å is slightly shorter than the *van-der-Waals* distance indicating some weak interactions. Similar contacts appear in the corresponding cyanide $Hg(CN)_2$ with mercury-nitrogen distances of 2.742 (3) Å. [408]

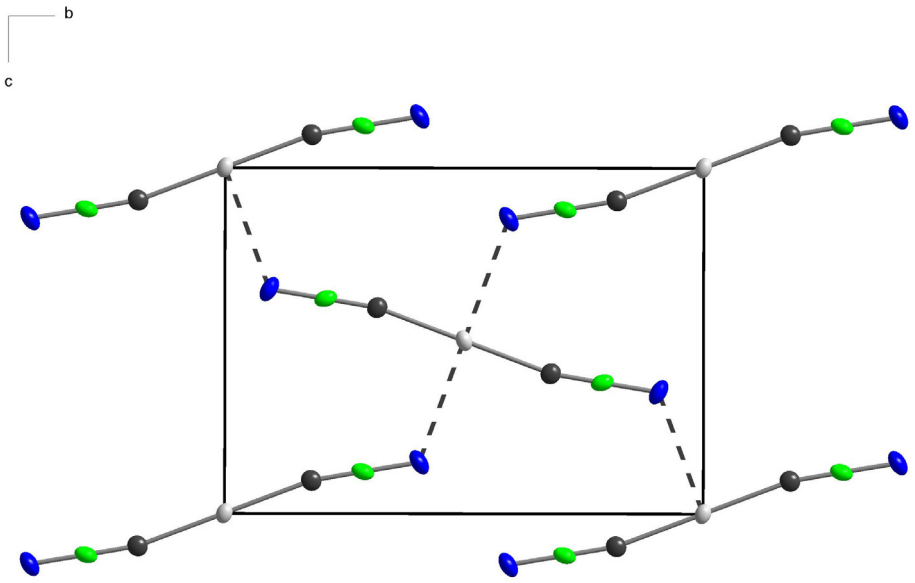

Figure 2.161. View along [100] on one layer of mercury fulminate molecules. In this orientation, two oxygen atoms form interatomic distances Hg···O of 2.833(4) Å, smaller than the calculated *van-der-Waals* distance of 3.0 Å. The anisotropic thermal displacement parameters are shown at the 50% probability level.

Considering the two surrounding layers, four additional mercury-oxygen contacts with distances of 3.06 Å are present. This results in six Hg···O distances. There are also six Hg-N distances (four times at 3.59 Å and two times at 3.62 Å). These twelve atoms centred by a mercury atom build up a distorted polyhedron with four atoms at the top, four atoms in the middle and four atoms at the bottom. If these four atoms were arranged symmetrically as parallel squares one would obtain a cuboctahedron. The real polyhedron is far away from this situation, however. Figure 2.162 shows the distorted polyhedron around one mercury atom and the two fulminate groups.

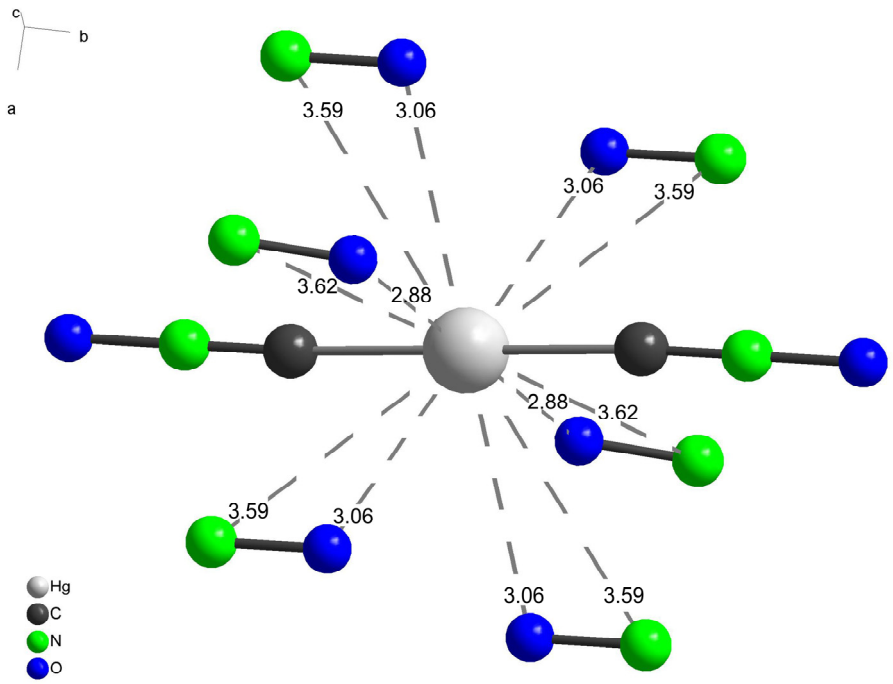

Figure 2.162. Distorted polyhedron built up by six oxygen and six nitrogen atoms. The two chemically bonded fulminate groups are also shown. The distances to the central Hg atom are given in Å. The anisotropic thermal displacement parameters are shown at the 50 % probability level.

It is interesting to compare the crystal structure of mercury fulminate $Hg(CNO)_2$ with that of mercury azide (with the analogous formula) $Hg(NNN)_2$. Both the fulminate and the azide anion are linear and contain 16 valence electrons resulting in one negative charge. The crystal structure of mercury azide was determined by Müller in 1973. [432] $Hg(N_3)_2$ crystallizes with four molecules per unit-cell as does the mercury fulminate. Both structures are not isotypic. $Hg(N_3)_2$ crystallizes in the non-centrosymmetric space group $Pca2_1$, $Hg(CNO)_2$ in the centrosymmetric space group *Cmce*. However, the unit-cell volume of the azide is V = 421.1(3) Å^3, [438] whereas that of the fulminate equals to 437.6 Å^3 at room temperature. As a consequence, the azide is packed more densely (4%) compared to the fulminate. But the most striking difference is the bonding angle of the azide group to the mercury atom which is due to the totally different hybridization of the atom directly bonded to the mercury atom (C: sp / N: sp^3). According to this, an oxygen bonded fulminate would lead to a bent M-O-N≡C group similar as in the corresponding azide $Hg(N_3)_2$. There are two crystallographic different azide groups in $Hg(N_3)_2$ with N-N-Hg angles of 111(2) and 120(2)°. [438] In $Hg(CNO)_2$ the two fulminate groups are

crystallographic identical and have bond angles N-C-Hg of 169.1(5)°. In addition, the atomic arrangement of N-N-N group in the the azide anions deviate with bond angles of 171(3) and 176(2) from linearity. This is also true for the atomic arrangement N-Hg-N with a bond angle of 175(1)°. Quite a puzzle are the Hg-N bond distances of the two crystallographically different azide groups. One Hg-N distance is 2.04(2) whereas the other is 2.14(2) Å. [438]
In summary, the molecular and crystal structure of the historically important mercury fulminate has been solved, more than 200 years after its discovery.

Experimental

Synthesis. $Hg(CNO)_2$ was synthesised by dissolving mercury (1g) in nitric acid (12g, ρ = 1.4 g cm^{-3}) and adding ethanol (11g) to this solution in two portions. [433] It is important to add the first half of ethanol before the red brown gases have disappeared. *Caution*: Mercury fulminate is sensitive to impact and friction and is easily detonated by sparks and flames. Before use it should be stored under water and with exclusion of light.
Powder Preparation. For X-ray powder experiments freshly prepared microcrystalline mercury fulminate was used. After drying on filter paper, a *Lindemann* capillary (d = 0.5 mm) was carefully filled in order to prevent grinding. Single Crystal Preparation. Single crystals of sufficient quality for the structure determination were obtained from aqueous ammonia / ethanol solutions (1:1:1) [434] and dried on filter paper with the exclusion of light. Small crystals of rhombic habitus with well-developed faces were selected under a polarization microscope and then cooled to 100 K using a *Cryojet Controller* of an *Oxford Xcalibur3 CCD* single crystal diffractometer from *Oxford Diffraction*. Details of the single crystal X-ray diffraction experiment are listed in the appendix (Chapter 4).

2.4.2 Hexaazidocyclotriphosphazene (P_3N_{21})

Introduction

Compounds which are composed of only the elements phosphorus and nitrogen can exist either as molecular species or as three dimensional polymeric solids. Examples of known solid state compounds include the structurally well characterised phases of the binary compound P_3N_5, which were reported by Schnick *et al.* [435] In contrast, none of the binary PN molecules described in the literature, namely P_4N_4, [436] $P(N_3)_3$, [437] $P(N_3)_5$, [438] $[PN(N_3)_2]_3$ [439-441] or the ionic compound $(N_5)P(N_3)_6$ [442] have been structurally characterised. The difficulties in the isolation and handling of these compounds have been shown by Christe *et al.* for $(N_5)P(N_3)_6$ to arise from their highly endothermic character, as well as their extremely low barriers towards an often uncontrollable explosive decomposition. [443–445, 448] Here we report the single crystal X-ray structure of the P_3N_{21} molecule and thereby the first example of a structurally characterised binary P-N molecule.

Synthesis

Although the synthesis of this compound was first reported over 50 years ago through the reaction of hexachlorophosphazene with sodium azide, [445] compound (**1**) was only characterised using elemental analysis, [445] vibrational [446-447] and NMR spectroscopy. [447] The experimental difficulties involved in the structural characterisation of this compound are a consequence of the high energy content of P_3N_{21}, for which our calculated enthalpy of formation corresponds to 89.0 kcal/mol. In order to obtain as pure a product as possible, a new synthetic strategy was chosen for the introduction of the N_3 group using Trimethylsilylazide (Fig. 2.163), whereby under the reaction conditions used, the trimethylsilylchloride side-product formed in the reaction was continuously removed form the reaction equilibrium. In addition, due to its volatility the excess trimethylsilylazide could be easily removed from the reaction mixture.

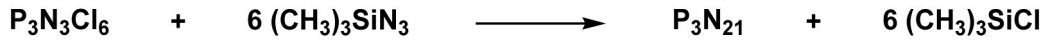

Figure 2.163. Synthesis of P_3N_{21}.

Characterization

After purification of the product using sublimation, compound (**1**) was obtained in high purity. The observation of only one signal in the ^{31}P NMR spectrum at δ = 13.6 ppm ($\Delta\nu_{1/2}$ = 10 Hz) and the absence of further phosphorus signals indicated that complete chloride-azide exchange had occurred. The ^{14}N and ^{15}N NMR Spectra are shown in Figure 2.164.

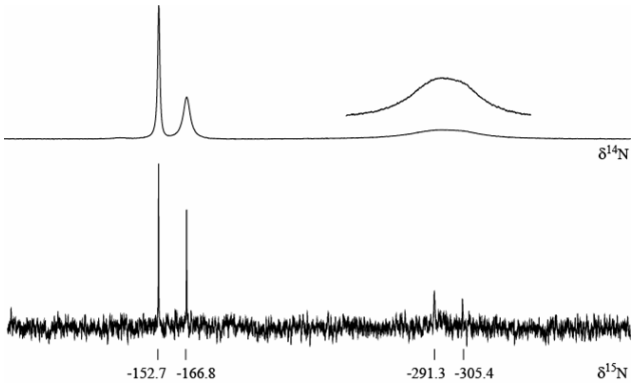

Figure 2.164. ^{14}N (top) and ^{15}N (bottom) NMR spectra of P_3N_{21} in C_6D_6. In addition, the broadened signal at δ = -300 ppm in the ^{14}N NMR spectrum is shown enlarged.

The ^{15}N NMR signal at δ = -305.4 ppm was assigned to the ring nitrogen atom after comparison with the chemical shift of the hexasubstituted cyclotriphosphazatriene. [446] The ^{15}N signals of the covalent azide group were assigned according to the typical chemical shifts reported for covalent azides [264] δ = -152.7 (N_β), -166.8 (N_γ) and -291.3 (N_α) ppm. In the ^{14}N NMR spectrum, a broadened peak at -300 ppm is observed for the ring nitrogen atom and the N_α atom. The experimentally obtained Raman and Infrared spectra are shown in Figure 2.165, and a comparison with the calculated (unscaled) vibrational frequencies is given in Table 2.29.

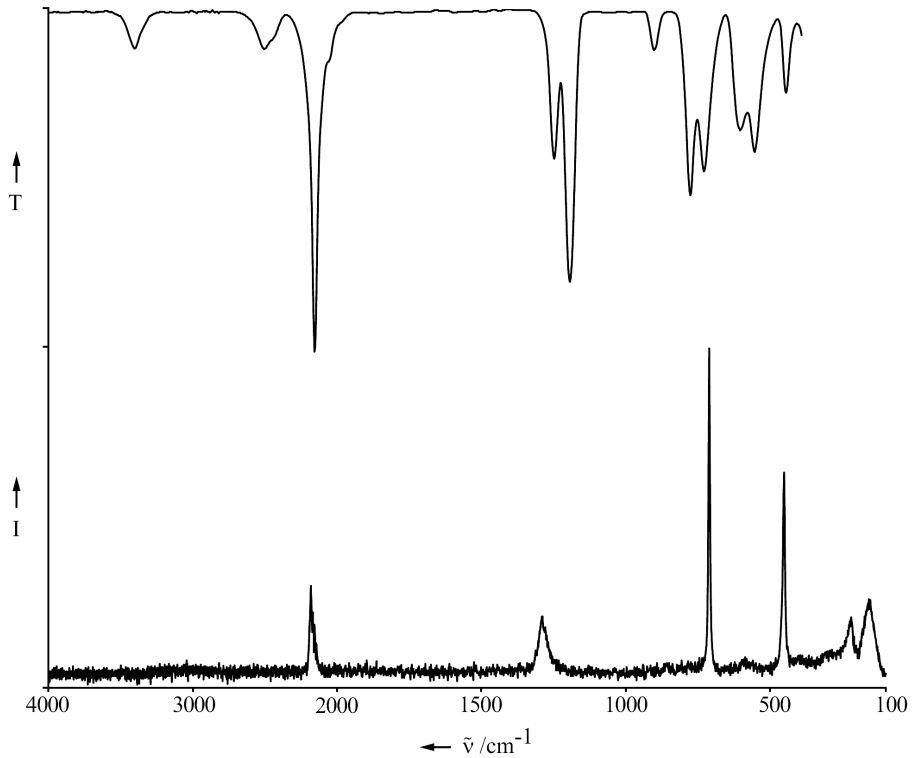

Figure 2.165. IR (top) and Raman (bottom) spectra of P_3N_{21}.

If standard scaling factors are applied for both methods [447] (BLYP/6-31G(d): 0.9940 / B3LYP/6-31G(d): 0.9613), good agreement between the calculated and experimental values is obtained. The vibrational frequencies observed for the liquid phase were assigned by comparison with the frequencies calculated for the molecule in C_1 symmetry, in contrast to the previously reported values in the literature [446-447] which were assigned on the basis of D_{3h} symmetry for the molecule.

Table 2.29. Comparison of the experimentally observed and theoretically calculated (C_1 point group) vibrational frequencies [cm^{-1}] and intensities[a].

Assignment	Experiment		Theory	
	IR	Raman	BLYP	B3LYP
$\nu_{as}N_3 + \nu_sN_3$	3406 (w)			
$2\nu_sN_3$	2511 (w)			
$\nu_{as}N_3$	2162 (vs)	2181 [26]	2189 (128) [196]	2318 (172)
			2181 (701) [30]	2308 (1016)
			2180 (567) [72]	2306 (624)
			2178 (940) [50]	2304 (1101)
			2175 (303) [25]	2303 (251)
			2173 (83) [8]	2300 (37)
ν_sN_3		1291 [21]	1275 (13) [51]	
			1257 (22) [18]	
ν_sN_3	1256 (s)		1268 (175) [1]	1336 (191)
			1265 (99) [6]	1333 (103)
			1258 (661) [3]	1324 (848)
ν_{as} $(PN)_{Ring}$	1201 (vs)		1149 (1536) [1]	1220 (1793)
			1114 (1069) [2]	1185 (1191)
ν_{as} $(PN)_{Ring}$	910 (w)		1048 (88) [0]	1120 (96)
δN_3	786 (m)		727 (421) [0]	779 (517)
δN_3	739 (m)		679 (175) [0]	729 (232)
			672 (191) [1]	721 (239)
$\delta_{bend}(PN)_{Ring}$		712 [100]	638 (1) [63]	
$\delta_{wag}(PN)_{Ring}$, δN_3	614 (m)		582 (222) [1]	617 (222)
$\delta_{rock}(PN)_{Ring}$, δN_3	564 (m)		562 (11) [15]	567 (137)
			533 (148) [0]	558 (99)
			526 (116) [1]	
$\delta_{bend}(NPN)$	456 (w)	454 [63]	410 (0) [47]	
		220 [21]	298 (2) [1]	
$\delta_{twist}(NPN)$		160 [26]	215 (1) [11]	

[a] The intensities of the calculated IR and Raman spectra are given in km mol^{-1} and $Å^4$ amu^{-1} respectively. The IR frequencies which were calculated using the B3LYP method to have very low intensities are not given.

Crystal Structure Analysis

The structure of P_3N_{21} at 100K has triclinic symmetry, space group space group $P\bar{1}$. The asymmetric unit consists of one molecules (Fig. 2.166).

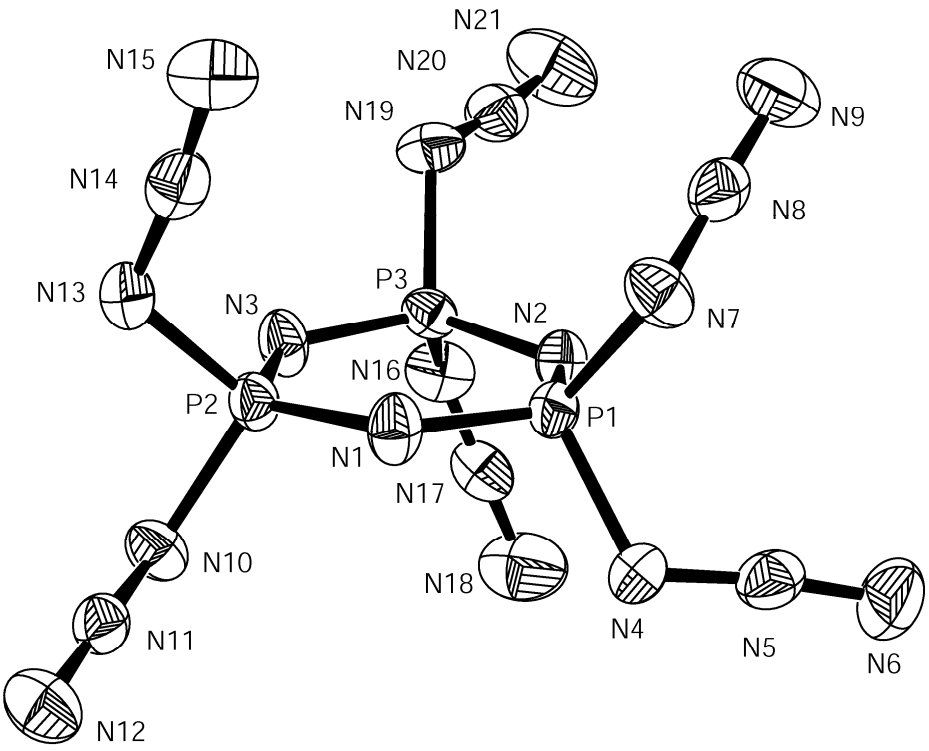

Figure 2.166. ORTEP representation of the molecular structure of P_3N_{21} in the crystalline state. The thermal ellipsoids are shown at the 50 % probability level. Selected bond lengths [Å] and angles [°]: P_1-N_1 1.558(2), P_1-N_2 1.576(2), P_1-N_4 1.666(2), P_1-N_7 1.671(2), N_4-N_5 1.218(3), N_5-N_6 1.117(3), N_7-N_8 1.203(3), N_8-N_9 1.114(3), N_1-P_1-N_2 118.2(1), P_1-N_1-P_2 122.1(1), N_4-N_5-N_6 173.4(3), N_7-N_8-N_9 173.5(3), P_1-N_4-N_5 117.7(2), P_1-N_7-N_8 119.2(2), N_4-P_1-N_7 102.2(1), N_1-P_1-N_4 104.5(1), N_2-P_1-N_4 111.9(1), N_1-P_1-N_7 108.9(1), N_2-P_1-N_7 109.8(1).

The calculated lowest energy conformation for free P_3N_{21} in the gas phase corresponds to that observed in the solid state using single crystal X-ray diffraction, whereby a similar arrangement of the azide groups and the C_1 point group are observed. The three azide groups (N_4-N_5-N_6, N_{10}-N_{11}-N_{12}, N_{19}-N_{20}-N_{21}) in Figure 2.166 are arranged in an almost parallel orientation with respect to the ring. In contrast, the other three azide groups (N_7-N_8-N_9, N_{13}-N_{14}-N_{15}, N_{16}-N_{17}-N_{18}) are oriented in a perpendicular manner with respect to the ring, just like in the calculated gas phase structure. The N_α-N_β/N_β-N_γ bond lengths as well as the N_α-N_β-N_γ angles are in good agreement with other covalently bound azides. [264] The six membered ring in P_3N_{21} is nearly planar and shows

good agreement with the values previously reported for the $(NPCl_2)_3$ starting material, [448] whereby both show a slight chair conformation. The PNP / NPN angles (120.8(2) - 122.9(2) ° / 117.0(2) - 118.2(1) °) as well as the PN-distances (1.556(2) - 1.576(2) Å) correspond well with the average values of 121.4 / 118.4° and 1.58 Å reported for $(NPCl_2)_3$. In addition, the N_α-P-N_α angles (99.2(1) – 102.2(1) °) correspond well with the Cl-P-Cl angles of 102° are also similar. However, the P-N_α distances (1.67 Å) are significantly shorter than the corresponding P-Cl distances (1.97 Å). The P-N_α-N_β angles are all approximately 120° and suggest the presence of sp^2-hybrided N_α nitrogen atoms.

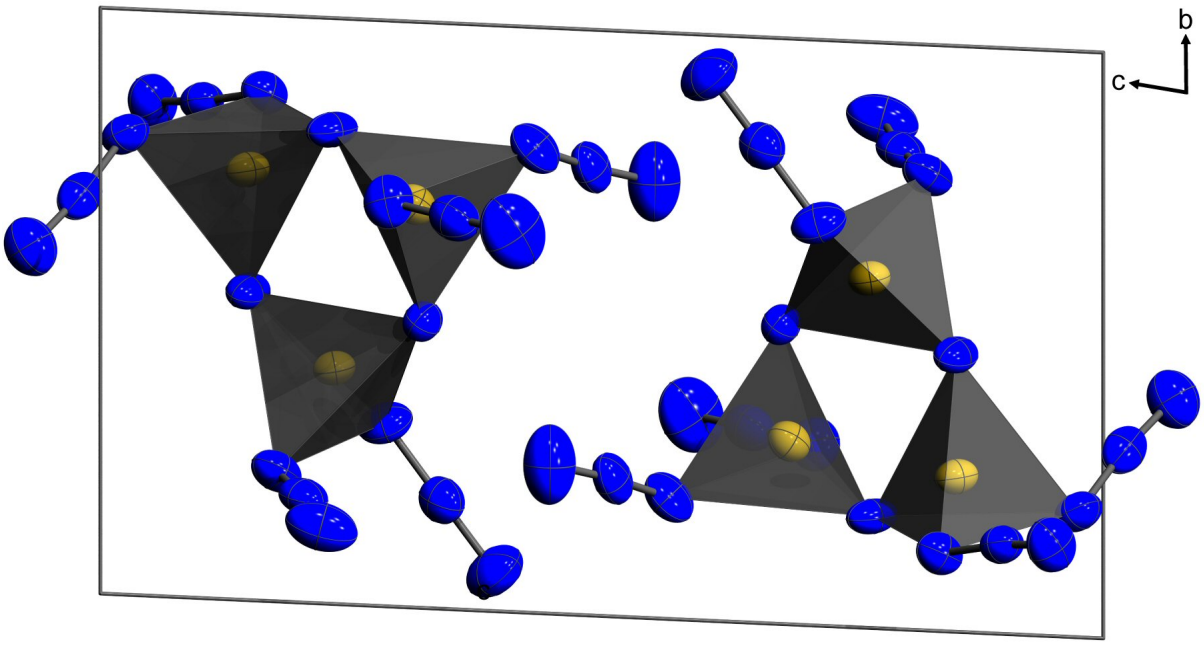

Figure 2.167. Unit cell of P_3N_{21}, viewed along the *a* axis.

The structure of a single P_3N_{21} molecule can be regarded as three membered ring built up of three corner-sharing PN_4 tetrahedra and each of the two remaining corners of a single tetrahedron being decorated with azide groups (Fig. 2.167).

The structure of P_3N_{21} contains a unique structural motiv (Figs. 2.168, 2.169): Covalently bonded nitrogen atoms are surrounded by each other as far as intermolecular distances are concerned rendering it possible to obtain an experimental estimate for the value of the van der Waals radius of a nitrogen atom.

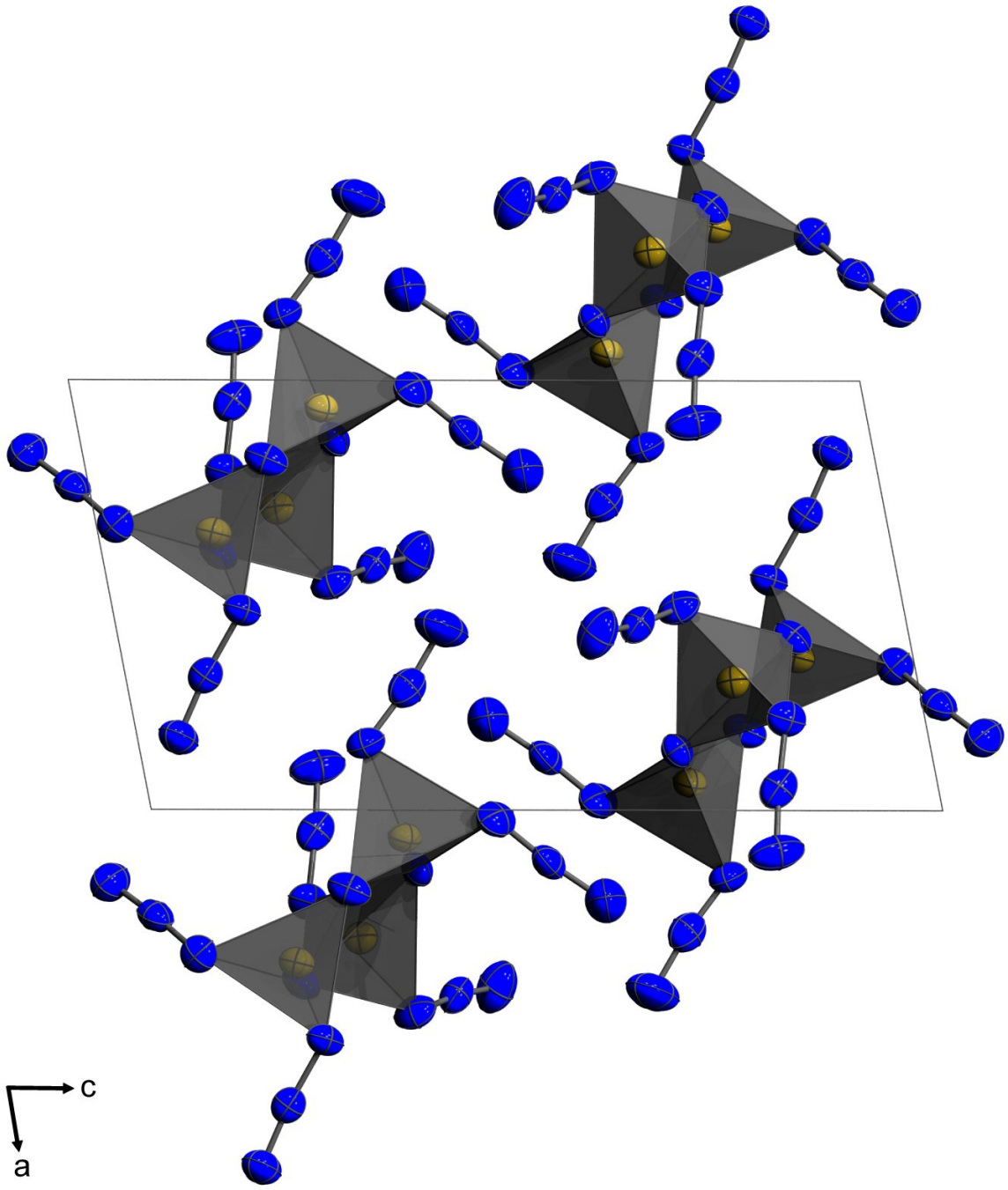

Figure 2.168. Unit cell of P_3N_{21}, viewed along the *b* axis.

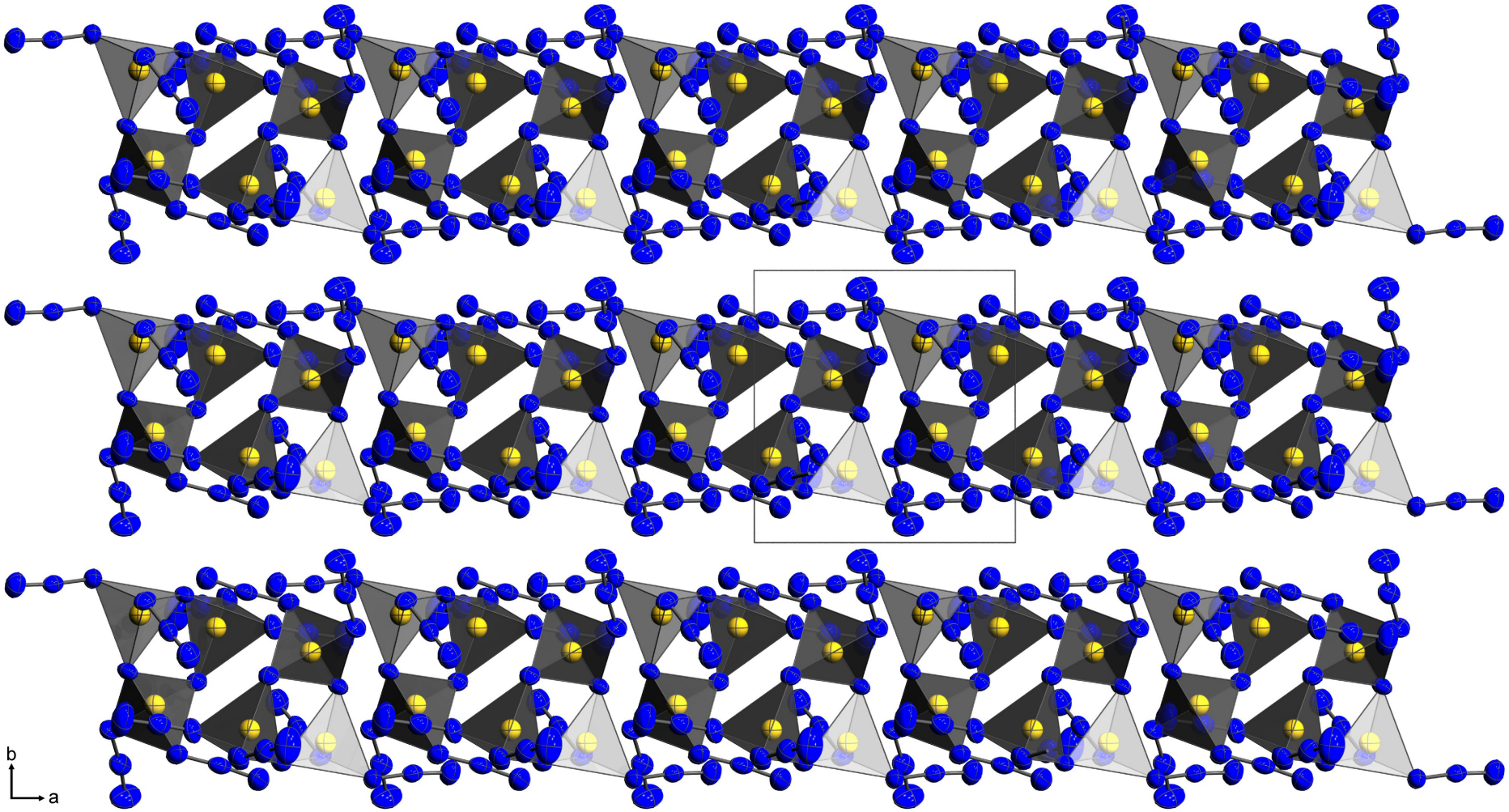

Figure 2.169. Unit cell of P_3N_{21}, viewed along the *c* axis.

Thermal stability and sensitivity

Furthermore, P_3N_{21} could also be identified using high resolution mass spectrometry, which showed in addition, that the compound can be transferred into the gas phase without decomposition. Two signals were observed in the mass spectrum, whereby the first mass peak corresponds to the molecular peak and the second peak corresponds to a species where one azide group had been removed from the P_3N_{21} molecule. The thermal stability of P_3N_{21} was investigated using DSC (*Differential Scanning Calorimetry*). Using a heat rate of 2°C min^{-1} resulted in the explosive decomposition of the compound at an onset temperature of 220°C. This relatively high decomposition temperature is in contrast to the very high impact sensitivity which gives a value of < 1J at room temperature. The substance is extremely impact sensitive. Direct heating in the flame also results in an explosive decomposition of the compound with an explosive sound and flash of light.

Experimental

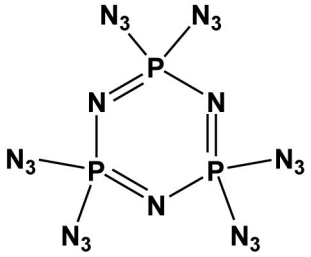

Caution! Phosphorus azides are highly endothermic compounds, and exhibit explosive decomposition under various conditions! Trimeric Phosphorusnitride diazide is extremely impact sensitive. Due to the high energy content of trimeric Phosphorus nitride diazide, explosions can cause substantial damage, even when quantities of 1 mmol are used. [445] The use of suitable protective clothing, in particular a face shield, ear protectors, a bullet proof vest, arm protectors and gloves made from Kevlar®, as well as protection from electrostatic charge using appropriate shoes is mandatory. **Ignoring these safety precautions can result in serious injuries!**

$P_3N_3Cl_6$ and TMS-N_3 were purchased from Aldrich. Propionitrile was dried over P_4O_{10} and distilled prior to use. Raman spectra were measured using a Perkin Elmer Spectrum 2000R NIR FT-Raman instrument (Nd:YAG Laser (1064 nm)). The Infrared spectra (IR) were recorded using a Perkin-Elmer Spektrum One FT-IR instrument. The ^{31}P, ^{15}N and ^{14}N NMR Spectra were obtained using a Jeol EX 400 NMR spectrometer operating at 28.9 MHz (^{14}N), 40.6 MHz (^{15}N) and 162.0 MHz (^{31}P), and the chemical shifts are given in ppm relative to nitromethane ($^{14/15}N$) and 85% phosphoric acid (^{31}P). The mass spectra were measured using a Jeol MStation JMS-700 mass spectrometer. The decomposition temperature was determined using a Pyris 6 DSC instrument. The values for the impact sensitivity of the substance at room temperature were determined using a BAM-drop hammer (Bundesanstalt für Materialforschung und Prüfung). Computational methods: BLYP and B3LYP density functional theory (DFT) calculations were used. Calculation of the geometry, IR and Raman spectra employing the 6-31G(d) Basis sets were achieved using the Gaussian programme. [81]

Preparation of P_3N_{21}: 224 mg (0.644 mmol) trimeric phosphorus nitride dichloride were added to a flamed out Schlenk flask under Argon, and dissolved in 20 mL of anhydrous Propionitrile at room temperature. Trimethylsilylazide (893 mg (7.750 mmol)) was added drop-wise to the stirred solution under a nitrogen purge. A blubberer was connected to the flask and a slow stream of nitrogen gas was passed continuously through the apparatus. The colourless solution was warmed to 60°C, and stirred for three hours at this temperature. Finally, the pale yellow solution was stirred for 19 hours at room temperature. The reaction mixture was subsequently concentrated using the rotary evaporator (30°C, 50 mbar) and the remaining solvent removed under vacuum using a Schlenk line ($1 \cdot 10^{-3}$ mbar, room temperature, several minutes). The pale yellow liquid that was obtained was purified using sublimation ($1 \cdot 10^{-3}$ mbar, 130°C oil bath temperature, -86°C cold finger temperature) and the product was obtained as a colourless liquid. Single crystals of P_3N_{21} were obtained via the controlled warming and cooling of the solid/liquid substance around its melting point. Repeated cooling of the substance to -78.5°C with dry ice and warming to -17°C in a cold room was monitored under a microscope, until

crystals formed. As soon as a liquid phase formed, the substance was re-cooled using dry ice. Handling of the single crystals requires great care !

Raman (liq., r.t.): s. Tab. 2.29. IR (Nujol, KBr, background subtracted): Tab. 2.29. ^{31}P NMR (C_6D_6, 25°C): δ = 13.6 ppm ($\Delta\nu_{1/2}$ = 10 Hz); ^{15}N NMR (C_6D_6, 25°C): δ = -152.7 (N_β), -166.8 (N_γ), -291.3 (N_α), -305.4 (N_{Ring}). ^{14}N NMR (C_6D_6, 25°C): δ = -152.7 (N_β, $\Delta\nu_{1/2}$ = 34 Hz), -166.8 (N_γ, $\Delta\nu_{1/2}$ = 115 Hz), -300 (N_α/ N_{Ring}, $\Delta\nu_{1/2}$ = 950 Hz). MS (DEI, 70eV): 387 [m^+, 30%], 345 [m-N_3^+, 100%]; MS (HR): calculated for P_3N_{21}: 386.9858, found: 386.9851 (-0.7 mmu). DSC (2°/min): 220°C (decomposition). Impact sensitivity: < 1J; Details of the single crystal X-ray diffraction experiment are listed in the appendix (Chapter 4).

2.4.3 Trinitromethanes

Trinitromethane (Nitroform, NFM)

The potential of the trinitromethyl group, $C(NO_2)_3$, as a component of energetic compounds has long been recognized. [13, 449-451] The parent molecule can be viewed as being trinitromethane, $HC(NO_2)_3$ (also called nitroform), which can be prepared by the reaction of acetylene with nitric acid. [457] It has a high crystal density (1.806 g cm^{-3}) and a low melting point (25 °C). [133] Though the presence of three nitro groups attached at one carbon atom might render this compound a priori to be an effective explosive, nitroform has found no use as an explosive. It has been reported to be very difficult to initiate, display poor performance characteristics and a low brisance. [452] Furthermore it's high acidity is connected with many disadvantages like its solubility in water contributing to make it hygroscopic and rendering it unsuitable for practical application as explosive. Finally, it displays unsatisfactory thermal stability yielding considerable (5-10%) decomposition even at such low temperatures as 30°C. However, trinitromethane can be used to prepare various compounds of energetic interest, like derivatives of 2,2,2-trinitroethanol, which can be obtained from the reaction between trinitromethane and formaldehyde and it displays some interesting academic aspects. [453] The three strongly electron-attracting NO_2 groups make the hydrogen very acidic (although not as much as might be anticipated); the experimental pK_a is 0.1 [457]. This should promote *aci* tautomerization, which involves the transfer of the proton to one of the nitro oxygens (Figs. 2.170, 2.171).

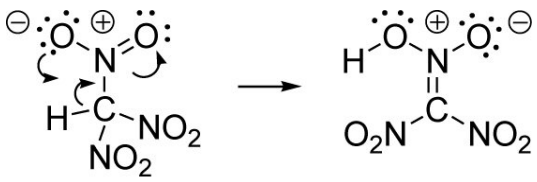

Figure 2.170. Formation of aci-trinitromethane.

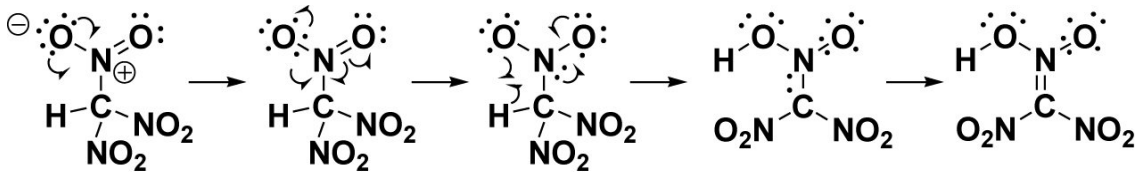

Figure 2.171. Proposed mechanism for the formation of aci-trinitromethane. The author of this thesis is indebted to and thanks both Prof. Dr. Thomas M. Klapötke and Dr. Harcourt for working out and kindly providing this scheme.

It is well known that some nitro derivatives containing the C-NO_2 linkage can undergo intramolecular transfer of a hydrogen to one of the nitro oxygens, forming an *aci* tautomer. [454-456] These *aci* tautomers are called nitronic acids; their pK_a values are usually between 2 and 6. They are quite reactive, and are important intermediates in organic synthesis, e.g. the Nef reaction. However they are often rather unstable, with half-lives measured in hours and days.

In the area of energetic materials, *aci* tautomerization is of particular importance because it is a possible early step in decomposition processes that are involved in detonation. [73, 457-458] For example, in developing their oxygen balance correlations for the impact sensitivities of energetic compounds, Kamlet and Adolph found it necessary to treat separately the nitroaromatics with a C-H on an alkyl group *ortho* to an NO_2. [459] Such compounds may be decomposing via *aci* tautomerization. The corresponding nitronate anion, has also been implicated in decompositions. [460-461]

This point has recently been addressed by us computationally in terms of reaction force analysis. [462] In the case of trinitromethane we found that rupture of a C-NO_2 bond in the ground state is energetically less demanding than overcoming the activation barrier to *aci*-trinitromethane; the respective ΔE(298 K) are 37 and 45 kcal mol^{-1}. Thus C-NO_2 homolysis may be the preferred first step in decomposition. To our knowledge, *aci*-trinitromethane has not been isolated, although there are reports that it may have been obtained but is quite unstable. [463-465]

Trinitromethanol

Whereas trinitroethanol is widely used in synthesis [269] and is well-characterized crystallographically [234], trinitromethanol is not known, as far as we are aware. Using reaction force analysis, we have recently analyzed trinitromethanol computationally. For trinitromethanol, we found the NO_2 groups in ground-state not to be in the propeller-like arrangement in contrast to trinitromethane. In trinitromethanol, one of them, e.g. NO_aO_b, was found to be nearly coplanar with the C-O-H portion of the molecule, while the other two were found to be approximately perpendicular to each other. This permits O-H···O_a hydrogen bonding as indicated by a H···O_a distance of 1.922 Å as opposed to the sum of the van der Waals radii (2.72 Å). [244] It is to O_a that the hydrogen will migrate. However, according to our gas phase calculations the result will not be an *aci* tautomer. Instead, they are indicative for trinitromethanol breaking up into a weakly-bound complex of $(O_2N)_2C{=}O$ and HO_aNO_b (Fig. 2.172), which is lower in energy by only 0.4 kcal mol^{-1} relative to the separate molecules.

Figure 2.172. Decompositon of the elusive trinitromethanol into dinitromethanone and nitrous acid.

This fragmentation has a very low activation barrier (10 kcal mol^{-1}). This barrier is less than the dissociation energy of the C-NO_aO_b bond alone (30 kcal mol^{-1}) since a new bond, O_a-H is being formed and the C-O bond is being converted into a double bond rendering it plausible why trinitromethanol is not known as far as we know.

Chlorotrinitromethane

Introduction

Describing interactions of atoms and atomic groups in molecules is a fundamental chemical challenge. Any compound showing deviations from normal geometric parameters is useful for critically assessing the strengths and failings of chemical bond models used to explain experimental results and thus helps aiding their further development. [466] In addition, current computer simulations of molecular systems are limited by and require reliable experimental data for the accurate description of the energies of interacting molecules and forces between them. [467] A better understanding of molecular interactions has recently been shown to be important for the manipulation of molecular recognition processes involving halogen bonding [468-469] and the design of specific material properties. [269] One class of compounds displaying remarkable inter- as well as intramolecular effects encompasses molecules having the trinitromethyl group, with three nitro groups bonded to one carbon atom. Consisting of elements of Groups IV, V and VI, the properties of the trinitromethyl group are comparable to those of a Group VII element; early studies describing the chemical properties of α-halogen derivatives of trinitromethane have demonstrated the potential of the uncharged trinitromethyl moiety to behave as a pseudohalogen. [470] Today, experimental evidence supporting this notion include the description of pseudointerhalogen compounds like azidotrinitromethane [471-472] and cyanotrinitromethane [473] along with the series of α-halogen derivatives of trinitromethane [474] and its dimer hexanitroethane. [475] Structural data for the halogen derivatives of trinitromethane have been limited to theoretical calculations [476-479] and spectroscopic analyses. [480-481] However, the determination of the equilibrium structure of a polyatomic molecule using only spectroscopic information becomes increasingly difficult with the number of atoms. [482-483] The difficulties in the case of chlorotrinitromethane were discussed by Sadova *et al.* [487] Reliable structural data for α-halogen-substituted trinitromethane molecules in the solid state did not exist at the beginning of this work. An attempted X-ray structure determination has been reported for iodotrinitromethane, $IC(NO_2)_3$.

[106] While this was the only representative amongst the halogen derivatives of trinitromethane retaining the crystalline state under standard conditions, the structure determination of iodotrinitromethane suffered from decomposition of several different single crystals exposed to the X-ray beam, considerably affecting the quality of the experimental data and precluding the possibility of a refinement of the individual parameters of the light atoms, resulting in a considerable scatter of the bond lengths. In regard to the trinitromethyl group as a pseudohalogen, chlorotrinitromethane holds a unique position amongst the halogen derivatives of trinitromethane. The question arises as to which halogen atom is most closely related to the $C(NO_2)_3$ group. Whereas the charges of the bromine and iodine atoms in the respective analogues are reported to be positive, [476, 484] there are contradictory estimates of the charge of the chlorine in chlorotrinitromethane, as being positive [476, 485] or negative. [106, 486] Experimental efforts to clarify this question were not successful, with neither positive nor negative mass spectra giving rise to parent ions even at low electron energies. [487] Another interesting point is that the structure of gaseous **1** derived from electron diffraction revealed the carbon-chlorine bond length (1.712 Å) to be the shortest yet found for a tetrahedral carbon. [486] In view of these findings, it seemed desirable to investigate single crystals of chlorotrinitromethane in order to obtain reliable geometrical data for the solid state.

Crystal Structure Analysis

Chlorotrinitromethane crystallizes in the monoclinic space group $P2_1/c$ with the asymmetric unit (Fig. 2.173a) consisting of one formula unit. The detailed structural parameters are given in the appendix (Chapter 4).

The lengths of the C-N bonds joining the three nitro groups to the carbon atom [1.538 (2) Å - 1.544 (2) Å] are significantly greater than the normal C-N bond distance of 1.47 Å. [246] The independent N-C-N bond angles of the trinitromethyl group are smaller [105.96(11)° – 106.83(10)°] than the tetrahedral value whereas the corresponding N-C-Cl bond angles are larger [112.32 (10)° - 112.73 (10)°]. The three independent nitro groups of each molecule are identical in structure within the limits of error and display common geometry parameters; the C-N and N-O bonds within each group are coplanar, with the sum of the three bond angles around the nitrogen being 360°. A propeller-like orientation of the nitro groups is observed, which minimizes repulsions between the oxygens on neighboring ones and which also allows for favourable intramolecular interactions. Figure 2.173b shows short intergroup nitrogen···oxygen distances, substantially less than the sum of the *van der Waals* radii of nitrogen and oxygen (3.07Å), [244] suggesting attractive interactions, presumably dispersive as well as electrostatic in nature. The oxygen atoms (O_2, O_4, O_6) that form close contacts to their neighbouring nitrogens (N_1, N_2, N_3) lie beneath the plane defined by these nitrogens, on the side opposite to the chlorine (Fig. 2.173b). The other three oxygen atoms (O_1, O_3, O_5) are located on the other side of this plane and display exceptionally short distances to the chlorine atom, with values substantially less than the sum of the *van der Waals* radii of oxygen and chlorine (3.27Å), [244] indicative of attractive interactions between these oxygens and the chlorine (Fig. 2.173b). As mentioned earlier, the carbon-chlorine bond length of 1.6944 (14) Å is exceptionally short and will be discussed in more detail in the following section.

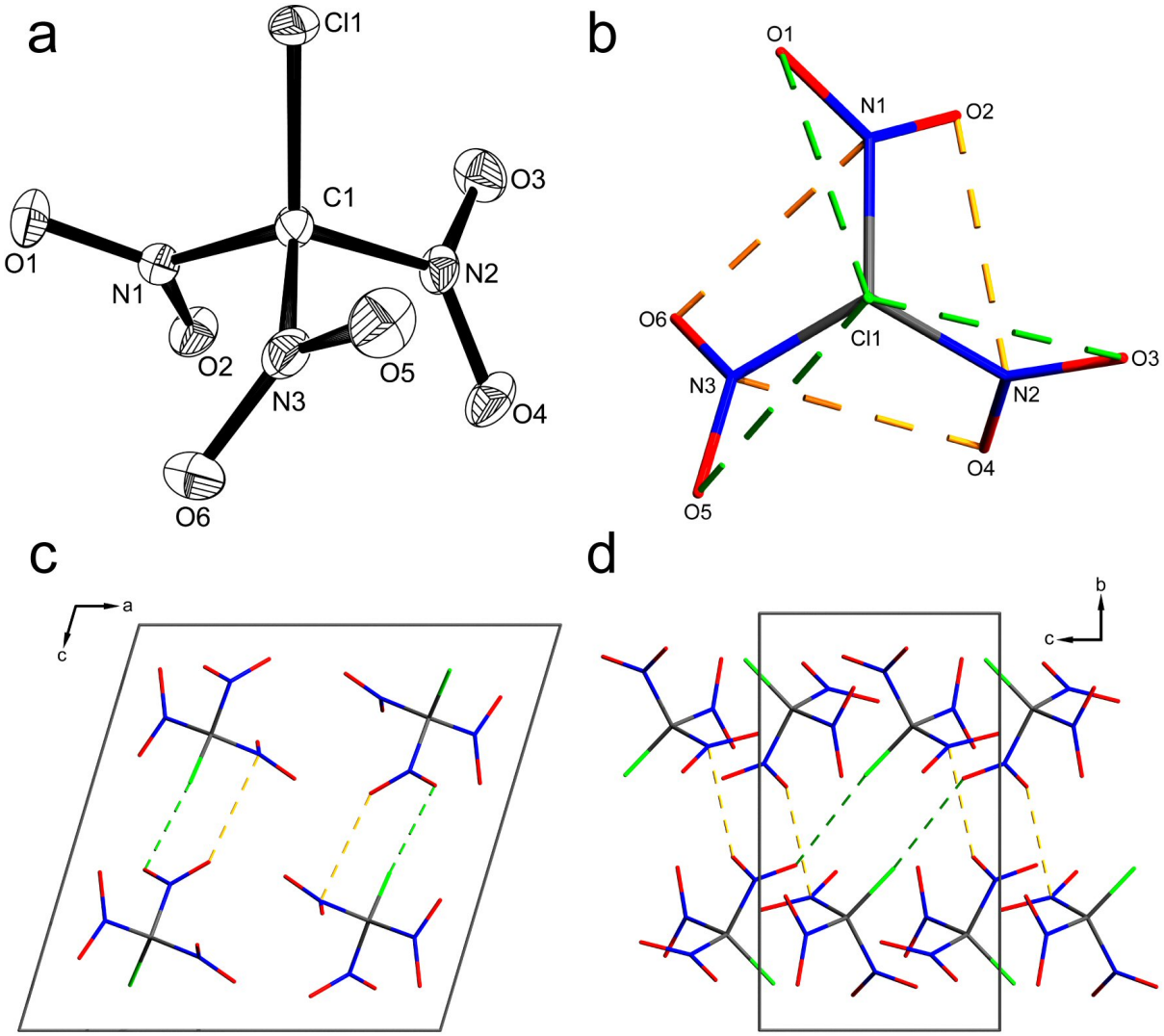

Figure 2.173. (a) ORTEP representation of the molecular structure of **1** in the crystalline state. The thermal ellipsoids are shown at the 50 % probability level. Selected bond lengths [Å] and angles [°]: C-Cl 1.6944(14), C-N_1 1.543(2), N_1-O_1 1.2135(18), N_1-O_2 1.2107(17), N_2-O_3 1.2048(19), N_2-O_4 1.2158(19), N_3-O_5 1.2088(18), N_3-O_6 1.2148(19), O_1-N_1-C_1 115.52(12), O_2-N_1-C_1 116.21(12), O_3-N_2-C_1 116.17(13), O_4-N_2-C_1 115.38(13), O_5-N_3-C_1 115.28(13), O_6-N_3-C_1 116.09(12), Cl-C-N_1 112.32(10), N_1-C-N_2 105.96(11), O_1-N_1-O_2 128.25(14), Cl-C-N_1-O_1 -46.58(16), Cl-C-N_1-O_2 134.90(12). (b) View of chlorotrinitromethane along the chlorine carbon axis. Dashed lines indicate short intramolecular nitrogen···oxygen (yellow) as well as chlorine···oxygen (green) distances: contact distances are d(N_1···O_6) = 2.5713(19) Å, d(N_2···O_2) = 2.547(2) Å, d(N_3···O_4) = 2.5540(16) Å, d(O_1···Cl) = 2.9388(12) Å, d(O_3···Cl) = 2.8973(12) Å, d(O_5···Cl) = 2.9025(13) Å. (c) Unit cell packing of chlorotrinitromethane along the crystallographic *b* axis and *a* axis (d). Green dashed lines indicate short intermolecular chlorine···oxygen distances while yellow dashed lines indicate short intermolecular nitrogen···oxygen distances: d(Cl···O_3^{i}) = 2.9489(12)Å, d(N_3···O_4^{ii}) = 2.9794(17)Å ; symmetry code: (i) x,3/2-y,1/2+z, (ii) x,1/2-y,1/2+z.

The crystal structure of chlorotrinitromethane consists of infinite one-dimensional chains parallel to the crystallographic *c* axis and running in opposite directions along the crystallographic *a*- and *b*-axes. Intermolecular chlorine···oxygen and nitrogen···oxygen distances with values substantially less than the sums of the *van der Waals* radii of chlorine / oxygen (3.27Å) [244] and nitrogen / oxygen (3.07Å) [244] suggest attractive interactions (Fig. 2.173c & Fig. 2.173d). Relative to the average conformation of monomeric chlorotrinitromethane in the gas phase, where C_3 symmetry was assumed for refinement of the electron diffraction data, [486] the crystal structure monomer displays lower C_1 symmetry. The nitro groups have a propeller-like orientation with torsion angles of 37.4°, 41.6° and 45.9°. Compared to the average gas phase torsion angles obtained from electron diffraction (49°) and ab initio calculations carried out in this study (42°), the torsion angle of 37.4° observed in the crystal structure reflects the intermolecular interactions in which the particular nitro group is involved. These secondary interactions result in a high crystal density of 2.0856(1) g cm^{-3}, an increase of more than 20% compared to the density of 1.66 g cm^{-3} reported [488-489] for liquid chlorotrinitromethane. A further comparison of the individual parameters obtained from single crystal X-ray analysis, electron diffraction and ab initio calculations is provided in Table 2.30.

Table 2.30. Comparison of selected bond lengths and angles of **1** obtained from single crystal X-ray diffraction of the solid, and from gas phase electron diffraction and ab initio calculations. [a]

	XRD	ED [486]	MP2/ccpVDZ[b]
d(C-Cl)	1.6944(14)	1.712 (4)	1.7205
d(N_1-O_1)	1.2135(18)	1.213 (1)	1.2261
d(N_1-O_2)	1.2107(17)	1.213 (1)	1.2221
d(N_2-O_3)	1.2048(19)	1.213 (1)	1.2261
d(N_2-O_4)	1.2158(19)	1.213 (1)	1.2221
d(N_3-O_5)	1.2088(18)	1.213 (1)	1.2261
d(N_3-O_6)	1.2148(19)	1.213 (1)	1.2221
d(C-N_1)	1.543(2)	1.513 (3)	1.5414
d(C-N_2)	1.5439(19)	1.513 (3)	1.5414
d(C-N_3)	1.538(2)	1.513 (3)	1.5414
ω (Cl-C-N_1)	112.32(10)	112.1 (0.5)	112.0
ω (Cl-C-N_2)	112.73(10)	112.1 (0.5)	112.0
ω (Cl-C-N_3)	112.53(10)	112.1 (0.5)	112.0
ω (N_1-C-N_2)	105.96(11)	-	106.8
ω (N_1-C-N_3)	106.83(11)	-	106.8
ω (N_2-C-N_3)	105.96(11)	-	106.8
ω (Cl_1-C_1-N_1-O_1)	-46.58(16)	-	-43.3
ω (Cl_1-C_1-N_1-O_2)	134.90(12)	-	139.0
φ (1st nitro group)	45.9	49	42.1
φ (Cl_1-C_1-N_2-O_3)	-37.72(17)	-	-43.3
φ (Cl_1-C_1-N_2-O_4)	143.00(12)	-	139.0
φ (2nd nitro group)	37.4	49	42.1
φ (Cl_1-C_1-N_3-O_5)	-42.34(15)	-	-43.3
φ (Cl_1-C_1-N_3-O_6)	139.23(12)	-	139.0
φ (3rd nitro group)	41.6	49	42.1

[a] d = distance / Å, ω = angle / °, φ = torsion angle / °. [b] this work.

The Carbon-Chlorine Bond Length

A Cambridge Structural Database search was carried out to provide a reference for evaluating the observed carbon-chlorine bond length of 1.6944(14) Å. The search produced 575 hits for comparable bonds in other molecules with chlorines attached to tetra-coordinated, tetrahedral carbons (Fig. 2.174). The shape of the bond length distribution may be compared to the asymmetric shape of the bond energy profile commonly used to describe the relationship between the potential energy and the distance between two covalently-bonded atoms where distortions to longer distances are energetically less demanding than those to equivalently shorter ones, resulting in longer bonds appearing more frequently than shorter ones. Examination of the bond length values in Figure 2.174 clearly reveals that the observed carbon-chlorine bond length in chlorotrinitromethane is exceptionally short.

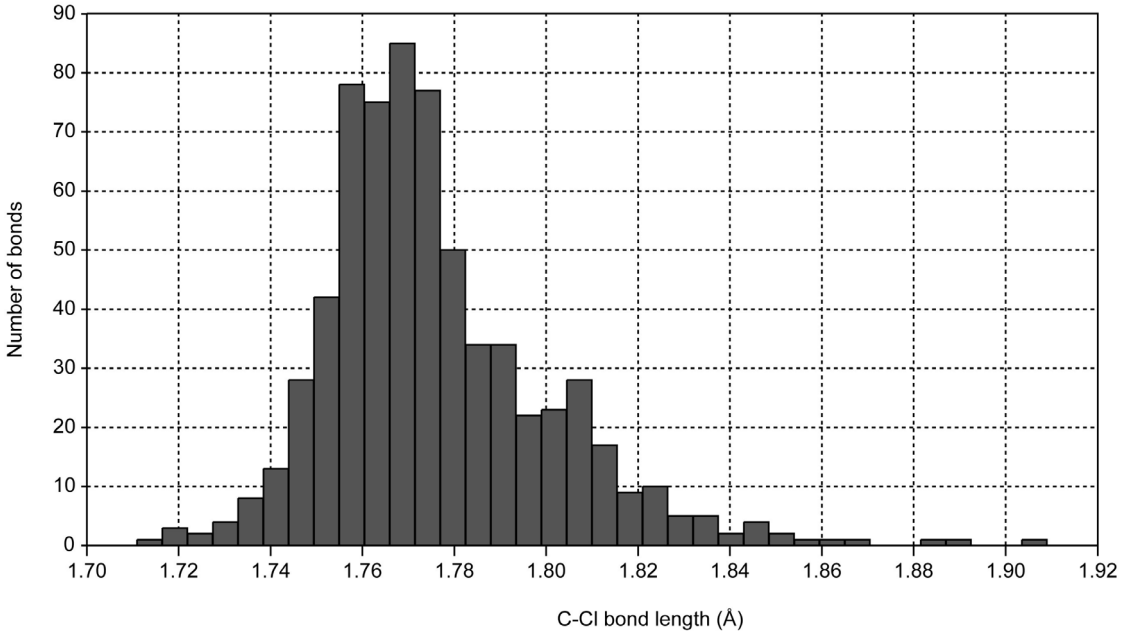

Figure 2.174. C-Cl bond length distribution for chlorine atoms attached to four-coordinate carbon atoms in a tetrahedral environment from 575 hits (Cambridge Structural Database). Shortest: 1.716 Å; longest: 1.906 Å; median: 1.771 Å.

As a first step in seeking to understand the reasons for the short carbon-chlorine bond length in chlorotrinitromethane, a natural bond orbital analysis (NBO) [490, 491] was carried out for an isolated chlorotrinitromethane molecule in the gas phase (Table 2.31). The results reveal a slight positive charge on the

chlorine atom, tetrahedral hybridization of the carbon, averaging $sp^{3.0}$, and a non-polar carbon-chlorine bond. Thus, the bond shortening can not be explained in terms of a higher *s* character of the carbon atom.

Table 2.31. Results of the NBO analysis of chlorotrinitromethane.[a]

atom	NBO charge	bond	hybridization	occupancy
Cl	+0.149	C-Cl	Cl: $sp^{4.56}d^{0.06}$	Cl: 49.5 %
C	+0.395	C-Cl	C: $sp^{2.62}d^{0.02}$	C: 50.5 %
N_1, N_2, N_3	+0.576	C-N_1	C: $sp^{3.12}d^{0.02}$	
O_1, O_3, O_5	- 0.380	C-N_2	C: $sp^{3.12}d^{0.02}$	
O_2, O_4, O_6	- 0.377	C-N_3	C: $sp^{3.12}d^{0.02}$	
			ø (C): $sp^{2.99}$	

[a]MP2/cc-pVDZ, (C_3 symmetry).

A possible resonance interpretation of the bond shortening in the carbon-chlorine bond involves hyperconjugation yielding the classical valence bond description (Fig. 2.175):

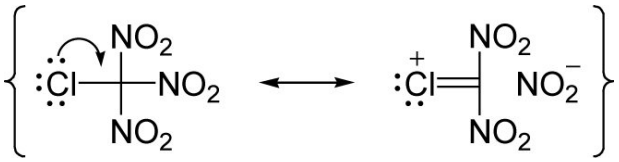

Figure 2.175. Valence bond descripton of chlorotrinitromethane.

The construction of an increased valence resonance structure (Fig. 2.176) allows for a better agreement to the NBO results compared to the Lewis structures of Figure 2.175. [492] It accounts for the observed elongation of the carbon nitrogen bonds as well as the sp^3 hybridization of the carbon atom.

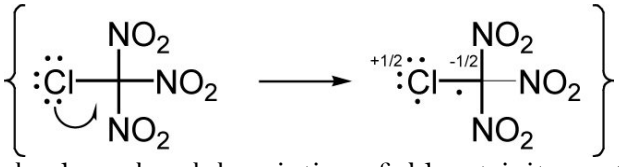

Figure 2.176. Increased valence bond description of chlorotrinitromethane.

However it should follow from these valence bond descriptions that other chloromethanes with strongly electron-withdrawing substituents, such as Cl-$C(CN)_3$ and Cl-CF_3, should also have anomalously short C-Cl bonds provided that the hybridization of the central carbon atom as well as the contributions of hyperconjugation are comparable. Although these conditions are fulfilled

according to the results of the NBO analyses for these molecules (Table 2.32), a comparison of the carbon chlorine bond length values in Table 2.33 shows that a similar bond shortening is not observed in Cl-C(CN)$_3$ or Cl-CF$_3$.

Table 2.32. Comparison of the NBO analysis results of chlorotrinitromethane, chlorotricyanomethane and chlorotrifluoromethane.

molecule	atom	NBO charge	bond	hybridization	occupancy	energy
Cl-C(NO$_2$)$_3$	Cl	+0.149	C-Cl	Cl: $sp^{4.56}d^{0.06}$	Cl: 49.5 %	52.9 [a]
	C	+0.395	C-Cl	C: $sp^{2.62}d^{0.02}$	C: 50.5 %	
	N$_1$, N$_2$, N$_3$	+0.576	C-N$_1$	C: $sp^{3.12}d^{0.02}$		
	O$_1$, O$_3$, O$_5$	- 0.380	C-N$_2$	C: $sp^{3.12}d^{0.02}$		
	O$_2$, O$_4$, O$_6$	- 0.377	C-N$_3$	C: $sp^{3.12}d^{0.02}$		
				ø (C): $sp^{2.99}$		
Cl-C(CN)$_3$	Cl	+0.067	C$_1$-Cl	Cl: $sp^{6}d^{0.06}$	Cl: 49.8 %	18.3 [b]
	C$_1$	- 0.245	C$_1$-Cl	C$_1$: $sp^{4.33}d^{0.02}$	C: 50.2%	
	C$_2$, C$_3$, C$_4$	+0.314	C$_1$-C$_2$	C$_1$: $sp^{2.68}d^{0.01}$		
	N$_1$, N$_2$, N$_3$	- 0.255	C$_1$-C$_3$	C$_1$: $sp^{2.68}d^{0.01}$		
			C$_1$-C$_4$	C$_1$: $sp^{2.68}d^{0.01}$		
				ø (C$_1$): $sp^{3.09}$		
Cl-CF$_3$	Cl	- 0.046	C-Cl	Cl: $sp^{5.17}d^{0.07}$	Cl: 55.6 %	39.8 [c]
	C	+1.276	C-Cl	C: $sp^{2.73}d^{0.03}$	C: 44.4 %	
	F$_1$, F$_2$, F$_3$	- 0.410	C-F$_1$	C: $sp^{3.05}d^{0.03}$		
			C-F$_2$	C: $sp^{3.05}d^{0.03}$		
			C-F$_3$	C: $sp^{3.05}d^{0.03}$		
				ø (C): $sp^{2.97}$		

Sum of intramolecular donor-acceptor interactions: a) LP (Cl) → σ*(C$_1$-N$_{1,2,3}$) / kcal mol^{-1} b) LP (Cl) → σ*(C$_1$-C$_{2,3,4}$) / kcal mol^{-1} c) LP (Cl) → σ*(C$_1$-F$_{1,2,3}$) / kcal mol^{-1}. MP2/cc-pVDZ.

Table 2.33. Comparison of carbon chlorine bond lengths in related molecules.[a]

molecule	method	temp. / K	d(C-Cl) / Å	state	reference
Cl-C(NO$_2$)$_3$	X-ray	100	1.6944(14)	solid	this work
	ED	318	1.712 (4)	gas	(486)
	Calc.		1.721	gas	(482), B3LYP/6-311+G(d,p)
	Calc.		1.708	gas	(482), MP2/6-31G(d,p)
	Calc.		1.720	gas	this work, MP2/ccPVDZ
	Calc.		1.713	gas	this work, B3PW91/6-31G(d,p)
Cl-C(CN)$_3$	X-ray	r.t.	1.78(1)	solid	(493)
	Calc.		1.809	gas	this work, MP2/ccPVDZ
	Calc.		1.818	gas	this work, B3PW91/6-31G(d,p)
Cl-CF$_3$	Calc.		1.765	gas	this work, MP2/ccPVDZ
	Calc		1.772	gas	this work, B3PW91/6-31G(d,p)

[a] X-ray = X-ray diffraction, ED = electron diffraction, Calc. = calculated value.

Although contributing, it follows that hyperconjugation seems not to be the dominant effect for the observed bond shortening in chlorotrinitromethane. Several approaches to the concept of short bonds may be taken, [494] or to bond length in general. In 1941, Schomaker and Stevenson proposed a relationship between the length of a covalent bond and the covalent radii, as well as electronegativities of the atoms. [495] In the approximation that permits polyatomic groups to be regarded as pseudo-atoms, the corresponding group electronegativities (χ_G) may be considered. These share the intrinsic problems associated with assigning electronegativities to atoms, [496] but help to understand the effects of substituents on the reactivity and physical properties of molecules. However, reliable electronegativity data for the trinitromethyl group do not exist at present. To explain the influence of substituents on molecular properties, another possibility is the linear free energy relationship approach, first demonstrated in the 1930s by Hammet for the dissociation of substituted benzoic acids. [497-498] Its alkyl counterpart was kinetically derived by Taft in the 1950s. [499] Hine and Bailey reported the Taft polar constant for the trinitromethyl group ($\sigma^* = 4.54$) to be the largest determined for any electrically neutral group. [199] A classic interpretation of σ^* is that it represents the electron-donating or -withdrawing power of a substituent. [500] The same perception is held for the electronegativity of a group, which indicates a possible correlation between χ_G and σ^*. Indeed, it was reported [501] that such a relationship exists and it was concluded 'that σ^* does represent some kind of electronegativity of a group with a steric component. [506] Assuming a positively charged chlorine atom because of the electron-withdrawing properties of the trinitromethyl group, it seems reasonable that the short intramolecular Cl···O_1, Cl···O_3 and Cl···O_5 distances observed in chlorotrinitromethane can be attributed to electrostatic attractions between the chlorine and these oxygen atoms. To gain further insight into the roles of such interactions in this molecule, we studied its electrostatic potential.

Molecular Electrostatic Potential Analysis

V(**r**), the electrostatic potential that is created at any point **r** by a molecule's nuclei and electrons, is given in Figure 2.177,

$$V(\mathbf{r}) = \sum_A \frac{Z_A}{|\mathbf{R}_A - \mathbf{r}|} - \int \frac{\rho(\mathbf{r}')d\mathbf{r}'}{|\mathbf{r}' - \mathbf{r}|}$$

Figure 2.177. V(r) is the electrostatic potential at any point r, Z_A is the charge on nucleus A, located at $\mathbf{R}_A$, and $\rho(\mathbf{r})$ is the electronic density function.

in which Z_A is the charge on nucleus A, located at $\mathbf{R}_A$, and $\rho(\mathbf{r})$ is the electronic density function. $V(\mathbf{r})$ is a physical observable, which can be determined experimentally [502-503] as well as computationally. Our interest is in $V(\mathbf{r})$ on the molecule's surface, which we take to be the 0.001 electrons bohr^{-3} contour of $\rho(\mathbf{r})$, as suggested by Bader *et al.* [504]. $V(\mathbf{r})$ computed on this surface is designated $V_S(\mathbf{r})$, and its most positive (maximum) and most negative (minimum) values as $V_{S,max}$ and $V_{S,min}$.

An interesting and important feature of $V_S(\mathbf{r})$ for many molecules containing Group IV – VII atoms is the presence of a localized region of positive potential on the extension of one or more of the covalent bonds to that atom. [505, 506] This is known as a positive σ-hole. [507] It develops when an orbital on that atom is involved in forming a covalent bond resulting in an electron deficiency in the outer (noninvolved) lobe of that orbital. Positive σ-holes can interact electrostatically with negative sites on other molecules (e.g. the lone pairs of Lewis bases) to form noncovalent bonds that are often similar in strength to hydrogen bonds. [508] These σ-hole bonding interactions are highly directional, since they are along the extensions of the covalent bonds that gave rise to the σ-holes.

Experimental indications of such interactions were found already quite some time ago, spectroscopically [509] and crystallographically, [510-511] and they are becoming increasingly important in molecular biology [512] and in materials science. [269, 474-475] When the σ-hole is on a Group VII atom, the interaction is often called "halogen bonding". [474-475, 513, 518] The maximum potential $V_{S,max}$ associated with a σ-hole increases with the polarizability of the Group IV – VII atom and with the electron-attracting power of the remainder of the molecule.

Accordingly, positive σ-holes are less likely to be found on the lightest (least polarizable) atoms in Groups IV – VII (i.e. C, N, O and F), although they do develop if the remainder of the molecule is sufficiently electron-withdrawing.[412] Chlorotrinitromethane illustrates well the importance of both inter- and intramolecular nonbonded interactions. Figure 2.173 shows that there are several of each type, the origins of which can be understood by examining the electrostatic potential on the molecule's surface. Four views of this are in Figure 2.178, and its most positive and most negative values (the $V_{S,max}$ and $V_{S,min}$) are listed in Table 2.34 along with the key inter- and intramolecular close contacts.

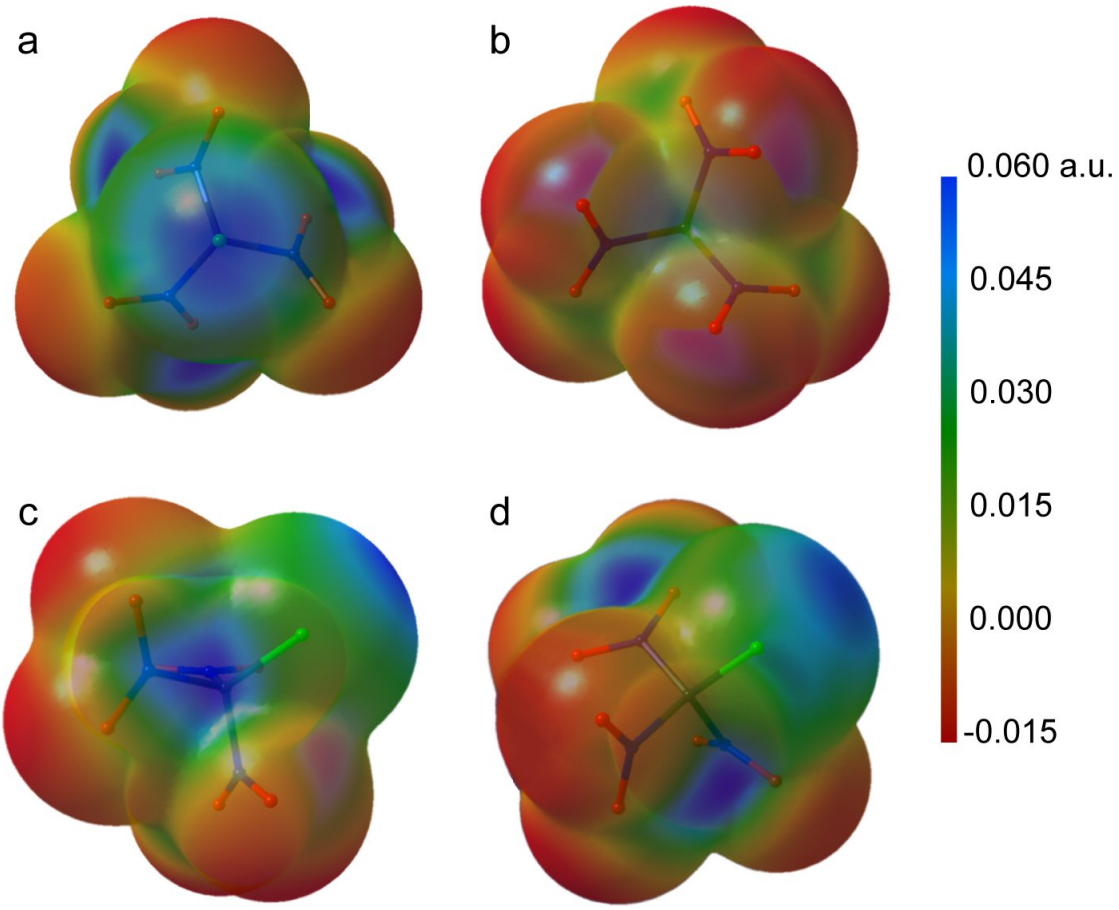

Figure 2.178. The molecular electrostatic potential of $Cl{-}C(NO_2)_3$ (in kcal mol^{-1}) computed on the 0.001 electrons $bohr^{-3}$ isodensity surface, with chlorine facing the reader (a), facing away from the reader (b) and pointing to the top right (c, d). The colors form a continuum from most positive, blue (greater than or equal to 30 kcal mol^{-1}), to most negative, red (equal to or more negative than -9.4 kcal mol^{-1}), with blue, light blue and green increasingly less positive, and yellow and red as negative. Note the strongly positive σ-hole on the chlorine surface (blue), on the extension of the C–Cl bond, and the weak one (green) on the carbon (middle of top right view) on the extension of the Cl–C bond. Color bars giving the continuum scales in atomic units are given to aid the reader (1 atomic unit = 627.5 kcal mol^{-1}).

Table 2.34. Inter- and intramolecular close contacts in chlorotrinitromethane, determined crystallographically, and most positive and negative values of electrostatic potential on molecular surface, $V_{S,max}$ and $V_{S,min}$, obtained from B3PW91/6-31G(d,p) calculations. Numbering of atoms is as in Figure 2.173. Sums of van der Waals radii: Cl···O: 3.27 Å, N···O: 3.07 Å.

Intermolecular close contacts / Å [a]	Intramolecular close contacts / Å [b]	$V_{S,max}$/kcal mol^{-1}	$V_{S,min}$/kcal mol^{-1}
Cl···O_{odd}: 2.9489	Cl···O_1: 2.9388	Cl: 35.5 (σ-hole)	O_1: −11.6
	Cl···O_3: 2.8973	C: 11.3 (σ-hole)	O_3: −11.6
	Cl···O_5: 2.9025	N: 36.2, 11.9	O_5: −11.6
N···O_{even}: 2.9794	N_1···O_6: 2.5713	N: 36.0, 11.8	O_6: −12.4
	N_2···O_2: 2.547	N: 35.9, 11.9	O_2: −12.4
	N_3···O_4: 2.5540		O_4: −12.4

Notes. [a] Figure 2.173c-d. [b] Figure 2.173b.

Regarding the question of the charge on the chlorine, mentioned in the introduction, we find the chlorine surface to be entirely positive (Fig. 2.178), in marked contrast to the chlorine in, e.g., methyl chloride, which is entirely negative. (513) Specifically, there are four strong positive sites shown in blue, on the chlorine and on the outer side of each nitrogen, all having $V_{S,max}$ of about 36 kcal mol^{-1}. The one on the chlorine is a positive σ-hole, on the extension of the C–Cl bond. These four positive regions participate in the intermolecular nonbonded interactions seen in Fig. 2.173c-d, each of which is with a negative site on the outer side of an oxygen atom on a neighboring molecule. The Cl···O intermolecular interactions are with the sites having $V_{S,min}$ of −11.6 kcal mol^{-1}, the N···O are with the $V_{S,min}$ of −12.4 kcal mol^{-1}. It is known that a σ-hole interaction R–X···B (B = Lewis base) is likely to affect the R–X bond, sometimes making it longer, with a lower vibration frequency (red shift), other times shortening it and increasing the vibration frequency (blue shift). (514, 515) Accordingly, we examined whether an intermolecular Cl···O σ-hole bond could be responsible for the anomalously short C–Cl bond. A B3PW91/6-31G(d,p) gas phase optimization of the geometry of the $[ClC(NO_2)_3]_2$ dimer formed by a Cl···O σ-hole interaction showed only a very small blue shift of the C–Cl bond, corresponding to a bond shortening of 0.002Å. A comparison of the calculated (B3PW91/6-31G(d,p)) C–Cl stretching frequency of methyl chloride (743.9 cm^{-1}) and chlorotrinitromethane (1041.8 cm^{-1}) shows that the trinitromethyl group causes a substantial increase (~ 300 cm^{-1}) indicating bond shortening of

the isolated molecule in the gas phase. This result together with the small difference between the experimentally determined gas phase and solid state values of the C–Cl bond (Table 2.33) indicates that the primary factor causing the observed shortening is most likely intramolecular. It was already pointed out that while the chlorine $V_{S,max}$ is on its outermost side, the entire surface of the chlorine is *positive* (Fig. 2.178). The propeller-like orientation of the nitro groups in **1** puts three of the oxygens (O_1, O_3 and O_5) close to the chlorine (Fig. 2.173); the Cl···O separations are about 2.90 Å and the Cl–C–N–O dihedral angles average 42° (Table 2.30). Thus the electrostatic attractions between the negative potentials on the inner sides of these oxygens (Fig. 2.178) and the positive chlorine are presumably the cause of the unusual shortening of the C–Cl bond.These Cl···O attractions would of course be maximized if the nitro groups were exactly coplanar with the C–Cl bond. We carried out a B3PW91/6-31G(d,p) calculation in which we forced this to be the case. The Cl···O separations decrease by 0.15 Å compared to the optimized geometry and the C–Cl bond is indeed shortened 0.013 Å. However this constrained structure is less stable by 6 kcal mol^{-1} than the optimized one, because it eliminates the intramolecular close contacts between the nitrogens and O_2, O_4 and O_6. These reflect electrostatic interactions between the respectively positive and negative inner sides of the nitrogens and these oxygens (Fig. 2.173b). The relevant nitrogen $V_{S,max}$ are only 12 kcal mol^{-1}, compared to their other $V_{S,max}$ of 36 kcal mol^{-1}, because they have been partially neutralized due to the proximity of the oxygens; for the analogous reason, inner-side $V_{S,min}$ of these oxygens cannot even be identified. With the observed structure being in equilibrium where the forces are balanced and the potential energy is minimized, our findings are in support of an intramolecular electrostatic attraction between the positively charged chlorine atom and the negatively charged oxygen atoms (O_1, O_3, O_5). Together with their axial symmetry around the C–Cl bond, these interactions are reflected in the anomalously short character of this bond.

Of interest, the data of Levchenkov *et al.* show a comparable shortening of the C–F and C–Br bonds in $F–C(NO_2)_3$ and $Br–C(NO_2)_3$. [482] Our calculated B3PW91/6-31G(d,p) electrostatic potentials on the molecular surfaces of

fluoro- and bromotrinitromethane show the surfaces of the halogen atoms to be entirely positive (Figs. 2.179, 2.180), just like the chlorine in Cl–$C(NO_2)_3$.

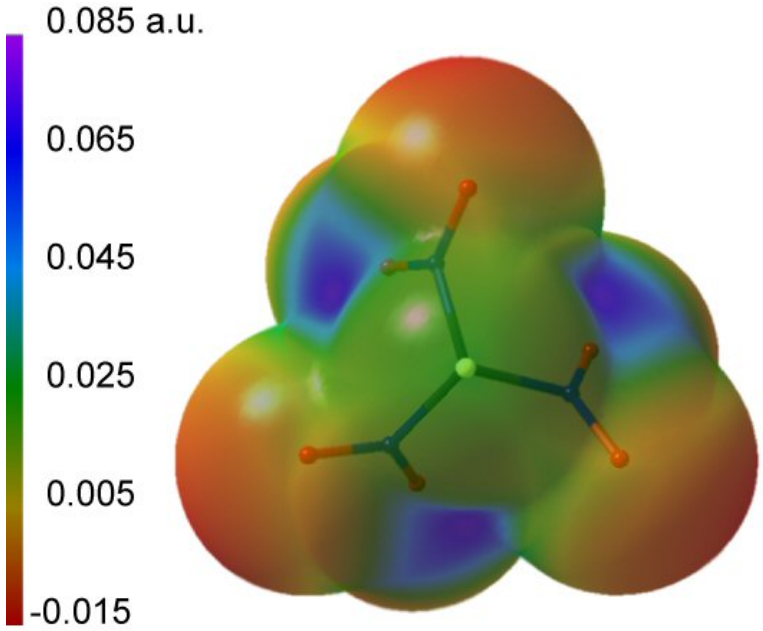

Figure 2.179. Computed electrostatic potential on the molecular surface of F–$C(NO_2)_3$. The fluorine atom is facing the viewer. The color ranges of the electrostatic potential, in kcal mol^{-1}, form a continuum from royal blue (more positive than 14) to red (more negative than -10). The surface of the fluorine is completely positive, with the most positive value on the extension of the C–F bond ($V_{S,max}$ = 15 kcal mol^{-1}).

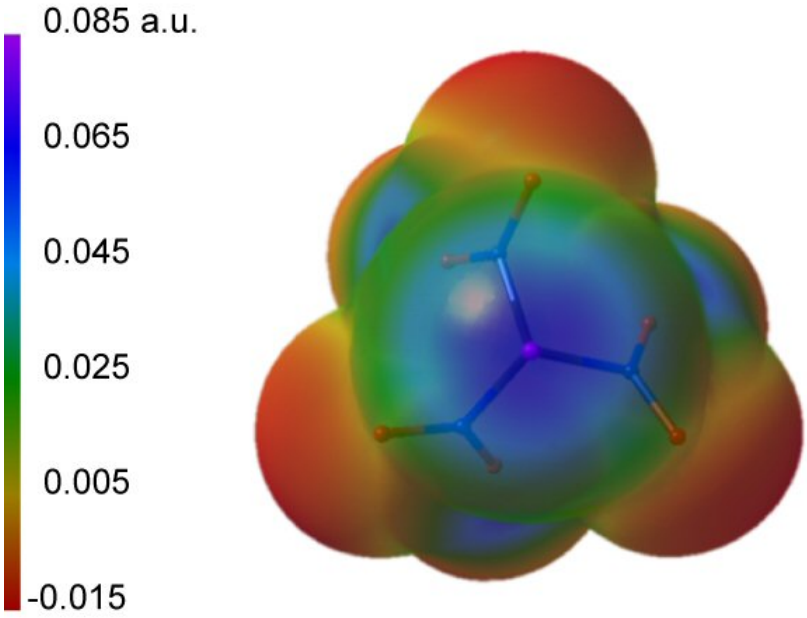

Figure 2.180. Computed electrostatic potential on the molecular surface of Br–$C(NO_2)_3$. The bromine atom is facing the viewer. The color ranges of the electrostatic potential, in kcal mol^{-1}, form a continuum from royal blue (more positive than 14) to red (more negative than -10). The surface of the bromine is completely positive, with the most positive value on the extension of the C–Br bond ($V_{S,max}$ = 43 kcal mol^{-1}).

A quantitative measure of the very strong electron-withdrawing power of the three NO_2 groups can be obtained by comparing the corresponding Taft polar constants (σ*), which are 4.54 [516-517] for the $C(NO_2)_3$ group *vs* 3.19 [523] for fluorine, 2.94 [523] for chlorine and 2.80 [523] for bromine. It seems likely, therefore, that the predicted [482] short F–C and Br–C bond lengths in $F–C(NO_2)_3$ and $Br–C(NO_2)_3$ can also be explained in terms of attractive electrostatic interactions, F···O and Br···O.

Chloromethanes – Concluding Remarks

The preceding discussion of the chlorotrinitromethane molecule has emphasized the striking effects that intramolecular interactions involving NO_2 groups can have upon molecular structures and properties. More recently, Macaveiu, Murray and Politzer examined this view in more detail computationally. [518] Chloromethane, $Cl\text{-}CH_3$, was selected as a reference molecule and the consequences of progressively introducing nitro groups were examined. For comparison, the corresponding cyano and fluoro derivatives were also included yielding a total of ten molecules that were included in this study: $Cl\text{-}CH_3$, $Cl\text{-}CH_n(NO_2)_{3-n}$, $Cl\text{-}CH_n(CN)_{3-n}$ and $Cl\text{-}CH_nF_{3-n}$, (n = 0, 1 and 2). The focus of this study has been not only upon the molecular geometries but also the accompanying changes in the strengths of the carbon-chlorine bonds. The detailed procedure and findings of the latter can be found in the original article. [524] Here we present a summary of significant findings in regard to the potential of the nitro group in stabilizing intramolecular contacts. As pointed out earlier, a significant feature of trinitromethane is the orientation of the NO_2 groups. Electron diffraction [486], rotational spectral analysis [519] and X-ray diffraction [133] have successively shown that they are in a propeller-like arrangement (Figure 2.181); the angle by which the nitro groups are rotated out of the respective H-C-N planes was found to be 44° crystallographically [133] and 42° computationally [459].

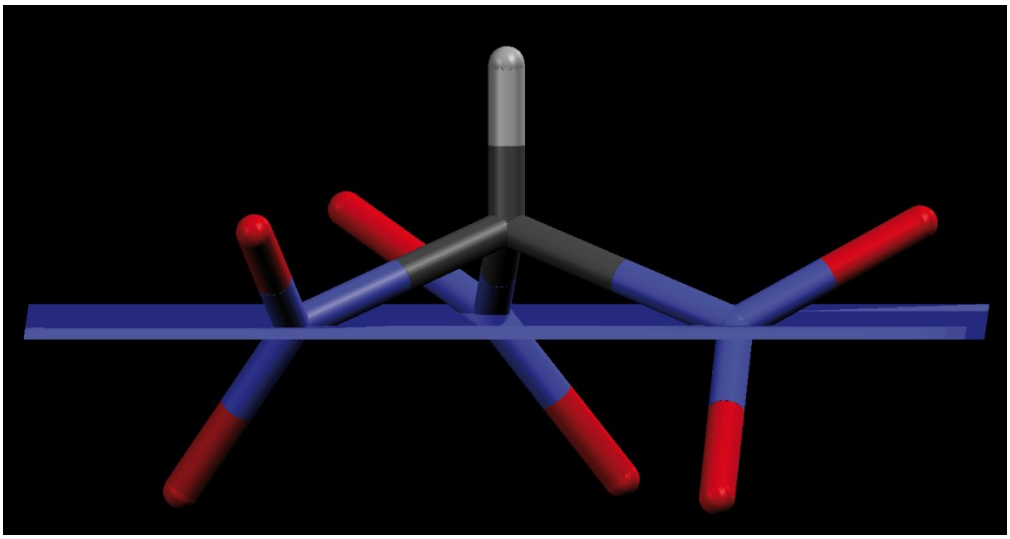

Figure 2.181. Structure of trinitromethane, optimized using the density functional B3PW91 procedure at the 6-311G(3d,2p) level, displaying a propeller-type arrangement of the nitro groups.

Figure 2.181 shows that the oxygens and the nitrogens are in three distinct planes, with the one containing the nitrogens being between the other two. This propeller-like structure is found for the trinitromethyl group in other molecules containing this group as well, and has been attributed to intramolecular electrostatic interactions between neighbouring nitrogen- and oxygen atoms involving the oxygens in the lowest plane (Fig. 2.181). [234, 520] In the case of the chlorotrinitromethane molecule it was concluded that the anomalous shortening of the carbon chlorine bond was due to intramolecular interactions between the chlorine atom and the oxygens in the upper (closer) plane after a detailed analysis of its molecular electrostatic potential. [526] In the present series of molecules, molecular electrostatic surface potential considerations revealed the chlorine in chloromethane to be entirely negative ($V_{S,min}$ = −16.6 kcal mol^{-1}) and progressively becoming less negative as fluorines were introduced with a positive $V_{S,max}$ appearing on the surface of the chlorine along the extension of the C-Cl bond already in chlorofluoromethane (+3.8 kcal mol^{-1}), becoming stronger in chlorodifluoromethane (+8.9 kcal mol^{-1}) and chlorotrifluoromethane (+16.3 kcal mol^{-1}). In the fluorine series, therefore, the chlorine was shown to have both positive and negative regions on its surface. The same was found also to be the case for chlorocyanomethane, but in the other cyano systems and in all of the nitro derivatives, the chlorine was shown to have no $V_{S,min}$ and its surface to be essentially totally positive.

Its $V_{S,max}$ was found to increase as cyano and especially nitro groups were added, to a high of +35.5 kcal mol^{-1} in chlorotrinitromethane. It was suggested that the electrostatic attraction between this very positive chlorine and the three negative upper oxygens contributed to the short carbon chlorine bond in chlorotrinitromethane. The most notable interactions were found to be the 1,4-contacts Cl···O and the N···O, which are well below the sums of the respective van der Waals radii. By comparison between the nitro derivatives and the other molecules, a key structural feature is the torsional possibilities available only to the nitro groups. In chloronitromethane, the nitro group was found to be in the Cl-C-N plane (Fig. 2.182). Chlorodinitromethane was found to have one nitro group coplanar with the Cl-C-N plane and the other rotated out of the corresponding plane by 70°. The propeller-type arrangement of the nitro groups in chlorotrinitromethane mentioned earlier and found in the crystal was confirmed with all three nitro groups rotated out of their respective Cl-C-N planes by 42° (Fig. 2.182). These conformations reflect and are stabilized by favourable intramolecular electrostatic interactions.

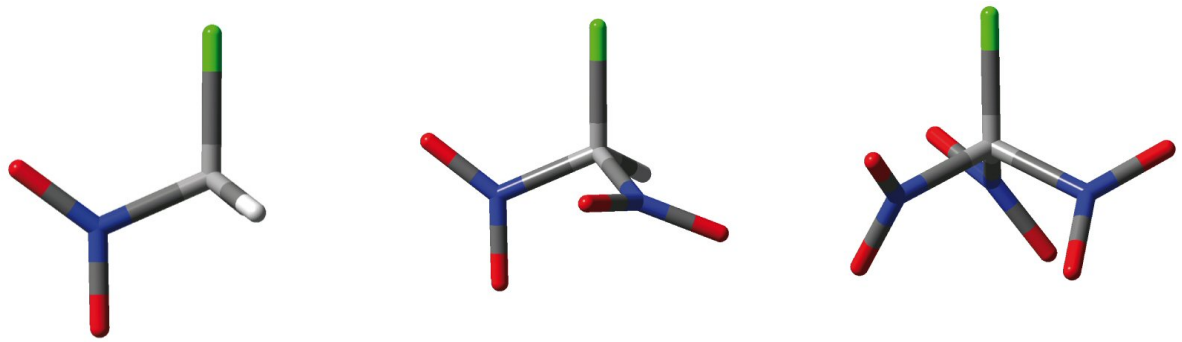

Figure 2.182. Structure of chloronitromethanes, optimized using the density functional B3PW91 procedure at the 6-311G(3d,2p) level. Chlorodinitromethane has one nitro group coplanar with the Cl-C-N plane (left), chlorodinitromethane has one nitro group is coplanar with the Cl-C-N plane and the other rotated out of the corresponding plane by 70° (middle) and chlorotrinitromethane displays a propeller-type arrangement of the nitro groups, rotated out of their respective Cl-C-N planes by 42° (right). The conformation of the molecules reflects N···O, Cl···O and H···O attractive interactions, as well as O···O repulsions.

A closer inspection of these interactions within the series of chloronitromethanes now yields additional support for the interpretation of carbon chlorine bond shortening due to electrostatic attraction between Cl···O, since an increase of the carbon chlorine bond length in chlorodinitromethane

and chloronitromethane was observed as the chlorine become less positive and was interacting with only one oxygen in each case. Further evidence was provided by rotating the nitro group in chloronitromethane out of its equilibrium position coplanar with the carbon chlorine bond. A change of the Cl-C-N-O dihedral angle from 0° to 90° was shown to successively cause an increase of the Cl···O separation and a subsequent lengthening of the carbon chlorine bond length from 1.744 Å (0°) to 1.758 Å (90°). Forcing the Cl-C-N-O dihedral angles in chlorotrinitromethane to be 0° was shoen to also decrease the Cl···O distances and further shortened the C-Cl bond. However the molecular energy *increased*, because of the unfavourable effect upon the interactions between the nitro groups. Obviously, the propeller-type arrangement of the nitro groups in chlorotrinitromethane has two favourable consequences:

(1) It promotes the attractive interactions between the nitrogens and the neighboring lower oxygens.
(2) It increases the O···O separations and hence diminishes repulsions between the lower oxygens on different nitro groups.

In the case of the cyano series, comparable interactions between the chlorines and the cyano nitrogens cannot take place because the latter are constrained by the C-C≡N linearity to be relatively far from the chlorines. The Cl···N distances were found to be 3.63 Å in Cl-C$(CN)_3$, considerably more than the sum of their van der Waals radii of 3.25 Å. In the fluoro series, the approximately 2.5 Å Cl···F separations were shown to be governed primarily by the Cl-C-F bond angles. Though the distances were found to be less than the sum of their van der Waals radii, they were not taken into account because in this case 1,3 contacts have to be considered and they are intrinsically governed by distances less than the sum of the van der Waals radii and cannot be called indicative for attractive interactions. Furthermore, the surface potentials supported the notion that no significant Cl···F attraction was present. In view of these findings, we suggest that the nitro group can play a unique role in intramolecular interactions.

This uniqueness comes from not one but a combination of factors:

(1) It includes three centers of charge, one positive (the nitrogen) and two negative (the oxygens).
(2) It is one of the most strongly electron-withdrawing groups, meaning that it can create an additional positive center or centers.
(3) It has rotational options that allow it to maximize the possibilities for favourable electrostatic interactions and minimize unfavourable ones. The effects of these factors multiply when a molecule contains more than one nitro group in close proximity.

As a consequence, only the chloronitromethanes have the unusual feature that intramolecular nonbonded Cl···O interactions are actually reinforcing covalent C-Cl bonds. This leads to the C-Cl bond energies being higher than expected, although they do decrease as additional nitro groups are introduced, as anticipated. Since the C-Cl bond lengths decrease in the same direction, we see that the chloronitromethanes (and Cl-CH_3) do not show the common inverse relationship between bond energy and bond length.

Experimental

All calculations were carried out using the Gaussian G03W (revision B.03, NBO version 5.G) program package. The molecular electrostatic potentials were visualized using the program *MOLISO*. [521] Cambridge Structural Database (CSD version 5.29 (November 2007), search criteria: angle around the carbon atom 109.5° ± 3° and substitution pattern of the carbon atom with at least two substituents not being hydrogen / deuterium. Methylene chloride, chloroform and tetracarbonchloride containing structures were excluded in those cases where the corresponding molecules are part of the structure as solvent molecules in order to make sure that no structures are included within the histogram containing disordered solvent molecules frequently obtained in these mixed crystals. Not included are furthermore structures containing disorder, R value greater ten percent, errors, polymeric compounds, ions and those structures where three dimensional coordinates are not available as well as powder structures.Instrumentation and Measurement. ^{13}C and ^{15}N NMR spectra were recorded using a Jeol EX 400 instrument operating at 100.6 MHz (^{13}C) and 40.5 MHz (^{15}N). All chemical shifts are quoted in ppm relative to TMS (^{13}C) or nitromethane (^{15}N). The single crystal X-ray diffraction data were collected using an Oxford Xcalibur3 diffractometer equipped with a Kappa CCD detector. The Mo$K_{\alpha 1}$ radiation (λ = 0.71073 Å) was generated from a Spellman generator (50 kV, 40 mA) and focussed using a graphite collimator. The data collection was undertaken using the CrysAlis CCD software and data reduction was performed using the CrysAlis RED software. The structures were solved using SIR-92 and refined using SHELXL-97 implemented in the program package WinGX and finally checked using PLATON. Chlorotrinitromethane was prepared from the reaction between trinitromethane and concentrated hydrochloric acid. [522] ^{13}C NMR (C_6D_6, 25°C) δ: 126.5 (bs, -$C(NO_2)_3$); ^{15}N NMR (C_6D_6, 25°C) δ (nitromethane): -36.2 (s, -NO_2). Single crystals of **1** were obtained on cooling the liquid to -30°C. A cold room tempered at -17°C was used to select suitable crystals for X-ray analysis in order to prevent thermal decomposition. Details of the single crystal X-ray diffraction experiment are listed in the appendix (Chapter 4).

Chapter 3

Summary

Today, the traditional procedure for formulating new energetic materials is largely guided by intuition, experience and testing, relying foremost on trial and error. In turn, a better understanding of the basic principles and relationships which are necessary to predict the properties of an energetic material are highly desirable in order to be able to more rationally design novel compounds with tailored properties and facilitate the development of next generation energetic materials. However, exploiting these possibilities requires an understanding of the properties of the individual molecules, their interaction amongst each other and to surrounding matter as well as an understanding of kinetic energy release and dynamics of initiation and decomposition processes. This *bottom-up* approach to energetic materials would allow for a more fundamental understanding of the evolution of properties with the size of the system as well as an understanding of the effects of the interaction of matter at different molecular-length scales with external stimuli, and finally a detailed understanding of the functionalities of matter at molecular-length scales. In this context, the scope of this thesis was defined by two major issues:

1. Gaining a deeper understanding of the basic principles of structure and matter as key to a more rational design process and the directed synthesis of novel compounds with tailored properties.

2. Development of a molecule with potential to replace RDX (hexahydro-1,3,5-trinitro-1,3,5-triazine), which is the most important highest energy explosive produced on a large scale.

In order to shed light on the question how performance arises from molecular parameters, an in-depth investigation of the trinitroethyl functionality (-CH_2-$C(NO_2)_3$) - chosen as model system - was conducted. The scope of this approach

covers both qualitative and a quantitative aspects. Various novel compounds carrying this moiety were synthesised, fully structurally characterized and screened for potential use as energetic materials. A closer analysis of these results and related molecules containing this fragment and available in the open literature revealed a key result of this thesis:
Based on the crystal structures reported in this work and available in the literature, we find that trinitroethyl mediated intermolecular interactions like dipolar nitro group interactions and hydrogen bonding of the acidified methylene-type protons govern mainly the molecular packing of these compounds yielding high-crystal-density polymorphs with promising explosive performance parameters. Whereas compounds based on the elements carbon, hydrogen, nitrogen and oxygen usually display density values in the range of 1.3 g cm^{-3} to 1.4 g cm^{-3}, compounds based on the same elements and containing the trinitroethyl functionality display density values of 1.8 g cm^{-3} on average and approaching 2 g cm^{-3}. This result is useful because two very important performance properties of an energetic material are directly related to density: the velocity of detonation is proportional to the density and the detonation pressure is proportional to the density squared.

• Taking advantage of the above mentioned concept of obtaining higher densities through the use of the trinitroethyl functionality, it was possible to synthesise BTAT (**B**is-(2,2,2-**T**rinitroethyl)-3,6-di**A**mino-1,2,4,5-**T**etrazine, sum formula $C_6H_6N_{12}O_{12}$), which represents a structural isomer of CL-20 (sum formula $C_6H_6N_{12}O_{12}$). While BTAT is less difficult to synthesise compared to CL-20, its performance characteristic is superiour to RDX by 15% and it displays a better oxygen balance value (BTAT: -10.9%, RDX: -21.6%) yielding smokeless combustion and less toxic fumes on decompositon. The compound is water insoluble in contrast to energetic salts, a prerequisite to protect the ground and one important environmental advantage amongst the qualification criteria for new HEDM. Increased performance and the results of initial safety characteristics render BTAT to be a suitable candidate in the process of replacing RDX subject to further investigations currently being carried out together with our collaboration partners.

• As far as thermal stability of trinitroethyl-derivatives is concerned, it was generally assumed that the decomposition temperatures of molecules carrying this functionality was generally limited to 150°C for solid compounds and 100°C for liquid compounds. In contrast, we were able to show that not only decomposition temperatures can be significantly higher but also thermal long term stabilities (140°C / 48h) showed no evidence of decomposition both in the case of solid and liquid compounds. BTAT and BTHC are shown to be the molecules offering the best trade-off between energy capability and thermal stability. Next to its excellent thermal stability as well as its positive oxygen balance value of +3.6%, BTHC displays the rare and desirable property of being a solid with a reasonable low melting point and a liquid range of greater than 100°C while at the same time being insensitive according to BAM standards rendering a possible use as safe melt-castable explosive. The tendency of conglomerate crystallization of BTHC is a further important point allowing for the specific design of its performance as well as sensitivity properties.

• The synthetic approaches towards novel engergetic materials preferentially containing the tetrazole moiety were often restricted to polar solvents like water or methanol due to the solubility behaviour of this nitrogen rich heterocycle. Within this thesis we have developed a series of tetrazole derivatives which are readily soluble in standard organic solvents and may serve as valuable educts for the manyfold chemical reactions possible in these solvents to overcome this former drawback.

• Of all the ionic energetic materials containing the trinitromethanide anion, only one compound hydrazinium nitroformate (HNF) has gained practical application as ingredient of propellant formulations so far. We have found a novel polymorph of HNF displaying a higher density compared to the previously reported one and we have investigated a series of novel compounds containing the trinitromethanide anion. Amongst these compounds, triaminoguanidinium nitroformate (TAGNF) was predicted to display superior performance characteristics in terms of detonation pressure, velocity of detonation and the highest positive heat of formation. Furthermore TAGNF

has been predicted to release the largest amount of gaseous decomposition products within the series of all known trinitromethanide salts rendering a possible use as high performance, halogen-free ingredient of propellant formulations that would avoid the problematic formation of hydrogen chloride from the use of ammonium perchlorate frequently used today. Furthermore, its water solubility would allow using concentrated solutions of it while at the same time reducing its sensitivity characteristics.

Our investigations in developing a more fundamental understanding of the evolution of properties with the size of the system - from molecular to macroscopic scale – was often based on structure determination in the solid state using single crystal X-ray diffraction. Aside from the results and conceptual advances mentioned above, it was possible to shed 'light' on a variety of other questions and determine the structures of several interesting compounds including:

• The structure of Mercury fulminate ($Hg(CNO)_2$), a historically important compound that allowed Alfred Nobel to establish the safe use of Dynamite could finally be revealed more than 300 years after it's first synthesis and it was established that the fulminate group is bonded to the mercury atom via the carbon atom.

• The structure of the free base guanidine ($C_1N_3H_5$) could be determined. Guanidine was considered to be the strongest organic and neutral base until the so-called proton sponges were developed. It could be demonstrated that its structure, which was subject to a long standing and controversial discussion is in fact not completely planar in contrast to its protonated form, the guanidinium cation, rendering Y-aromaticity to be the cause for its basic behaviour.

• The structure of hexaazidocylotriphosphazen (P_3N_{21}) could be determined representing the first structural characterisation of a binary molecule composed only of the elements phosphorus and nitrogen. The presence of covalently bonded nitrogen atoms being surrounded by covalently bonded

nitrogen atoms in this structure is a rare example and permits a very accurate experimental estimate for the size of the *van der Waals* radius of a nitrogen atom.

• The structure determination of the pseudo-interhalogencompound chlorotrinitromethane revealed an exceptionally short carbon-chlorine bond and led to the investigation of its possible cause using a concerted approach based on single crystal X-ray diffraction techniques and theoretical investigations of the molecular electrostatic potential. We observed that electrostatic interactions between neighbouring atoms to atoms of that bond are useful to clarify the cause of the tight bond. This in turn led to further studies that have shown how intra- and intermolecular interactions can significantly affect not only bond length but also properties including structure, acidity or tautomerisation behaviour.

• The structure of 3,6-diamino-1,2,4,5-tetrazinium chloride could be determined representing a novel energetic dication and the first example of a 1,2,4,5-tetrahydro-1,2,4,5-tetrazinium heterocyclic ring system.

• The structure of (E)-1-methyl-1-(1*H*-tetrazol-5-yl)-2-(2,2,2-trinitroethylidene)-hydrazine could be determined. The 2,2,2-trinitroethylidene moiety has only very rarely been mentioned in the literature and this structure determination represents the first structural proof for its existence. The use of this moiety in energetic materials research would enable compounds with better oxygen balance values compared to the corresponding 2,2,2-trinitroethyl derivatives while possibly retaining the favourable intermolecular interactions of the 2,2,2-trinitroethyl moiety contributing to higher densities.

Chapter 4

Appendix

4.1 Abbreviations

1,1-BTMSD	N^1,N^1-bis(trimethylsilyl)-1,5-diamino-1H-tetrazole
1,5-BTMSD	N^1,N^5-bis(trimethylsilyl)-1,5-diamino-1H-tetrazole
1-PYD	N^1-(propan-2-ylidene)-1,5-diamino-1H-tetrazole
5-TMSD	N^5-trimethylsilyl-1,5-diamino-1H-tetrazole
1,1,5-TTMSD	N^1,N^1,N^5-tris(trimethylsilyl)- 1,5-diamino-1H-tetrazole
ADN	Ammonium Dinitramide
ANFO	Ammonium Nitrate Fuel Oil
AN	Ammonium Nitrate
AP	Ammonium Perchlorate
DAT	1,5-diamino-1*H*-tetrazole
DATB	Diaminotrinitrobenzene
DMF	*N*,*N*-Dimethylformamide
DMSO	Dimethylsulfoxide
BAM	Bundesanstalt für Materialprüfung
BTAT	N^3, N^6-Bis(2,2,2-trinitroethyl)-1,2,4,5-tetrazine-3,6-diamine
BTC	Bis(2,2,2-trinitroethyl)carbonate
BTHC	Bis(2,2,2-trinitroethyl)-hydrazodicarboxylate
BTNA	Bis(2,2,2-trinitroethyl)amine
BTTD	N^1, N^5-Bis(2,2,2-trinitroethyl)-1H-tetrazole-1,5-diamine
CCDC	Cambridge Crystallographic Data Center
CJ	Chapman-Jouget
CL-20	2,4,6,8,10,12-hexanitrohexaazaisowurtzitane
CSD	Cambridge Structural Database
DDT	Deflagration to Detonation Reaction
DOD	Department of Defence

DOE	Department of Energy
DSC	Differential Scanning Calorimetry
ED	Electron Diffration
EGDN	Ethylene Glycol Dinitrate
ESD	Electrostatic Spark Discharge
ESP	Electrostatic Surface Potential
ESTCP	Environmental Security Technology Certification Program
FI	Figure of Insesitiveness
FIZ	Fachinformationszentrum Karlsruhe
FS	Friction Sensitivity
GAP	Glycidyl Azide Polymer
HE	High Explosive
HEDO	High Energy Dense Oxizider
HEDM	High Energy Dense Material
HMDS	Hexamethyldisilazane
HMX	Hexahydro-1,3,5,7-tetranitro-1,3,5,7-tetrazocene / Cyclotetramethylene-1,3,5,7-tetranitramine, 1,3,5,7-tetranitro-1,3,5,7-tetraazacyclooctane / Octogen
HNB	Hexanitrobenzene
HNF	Hydrazinium Nitroformate
HOX	High Oxygen Explosive
HTPB	Hydroxyl Terminated Polybutadiene
IHC	Insensitive Hazard Classification
IR	Infrared Spectroscopy
IS	Impact Sensitivity
LE	Low order Explosive
MF	Mercury Fulminate
MMTHT	1-Methyl-5-(1-methyl-2-(2,2,2-trinitroethyl)hydrazinyl)-1H-tetrazole
MP	Melting Point
MTHT	5-(1-Methyl-2-(2,2,2-trinitroethyl)hydrazinyl)-1H-tetrazole
MTHTE	2-(5-(1-Methyl-2-(2,2,2-trinitroethyl)hydrazinyl)-1H-tetrazol-1-yl)ethanol
MTTH	(E)-1-methyl-1-(1*H*-tetrazol-5-yl)-

	2-(2,2,2-trinitroethylidene)-hydrazine
NF	Nitroformate (Trinitromethanide)
NFM	Nitroform (Trinitromethane)
NMR	Nuclear Magnetic Resonance Spectroscopy
NQ	Nitroguanidine
OB	Oxygen Balance
ONR	Office of Naval Research
PETN	Pentaerythritol tetranitrate
PPM	Parts Per Million
RDX	Research Department Explosive, Hexahydro-1,3,5-trinitro-1,3,5-triazine, Cyclotrimethylenetrinitramine, Cyclonite, Hexahydro-1,3,5-trinitro-1,3,5-triazine
SERDP	Strategic Environmental Research and Development Program
STANAG	Standardisation Agreement of NATO/PfP
TAF	2,2,2-Trinitroethyl-azidoformate
TATB	Triaminotrinitrobenze
TCF	2,2,2-Trinitroethyl-chloroformate
THF	Tetrahydrofurane
THMT	1-(^{4}N-2,2,2-Trinitroethyl)-2,5-hydroxymethyltriazine
TMSCl	Trimethylsilylchloride / Chlorotimethylsilane
TNE	2,2,2-Trinitroethanol
TNM	Tetranitromethane
TNT	2,4,6-Trinitrotoluene
TTAT	2,4,6-(2,2,2-trinitroethylamino)-1,3,5-triazine
TTB	Tris-(2,2,2-trinitroethyl)-borate
TTD	N^{1}-(2,2,2-Trinitroethyl)-1H-tetrazole-1,5-diamine
TTE	1,1,1-Triamino-2,2,2-trinitroethane
VOD	Velocity of Detonation
XRD	X-ray Diffraction

Arbeitsanleitung

Vorsichtsmaßnahmen bei Arbeiten mit Explosivstoffen

1. Von größter Wichtigkeit ist absolut sauberes Arbeiten, vergleichbar den Arbeiten bei quantitativen Bestimmungen.
2. Direkte Sonnen- und starke Lichteinstrahlungen vermeiden.
3. Niemals ungeschultes Personal mit Initialsprengstoffen arbeiten lassen; niemals alleine arbeiten, nur mit zweiter, erfahrener Person.
4. Niemals größere Mengen (>250 mg) als Reinsubstanz in einem Ansatz isolieren oder manipulieren.
5. Niemals große Mengen (1-2 g ist schon eine sehr große Menge) von Initialsprengstoff trocken aufbewahren, sondern mit Wasser bedecken. Nicht in Glas-, sondern in Gefäßen aus elektrisch leitfähigem Material.
6. Keine Kleidung aus synthetischen Kunstfasern tragen, besonders keinen Arbeitskittel aus diesem Material.
7. Tragen Sie Spezialschuhe mit elektrisch leitfähiger Sohle. Der beste Schutz ist, barfuß in den Räumen zu gehen, in denen mit Initialsprengstoffen gearbeitet wird.
8. Alle Geräte, Tische, Böden müssen geerdet oder mit leitfähigem Gummi verkleidet sein.
9. Bei Manipulationen wie Sieben, Um- oder Einfüllen und Mischen von trockenem Initialsprengstoff sollte niemand sich gleichzeitig in demselben Raum aufhalten. Eine Bedienung der Geräte von geschützter Stelle aus, wenn möglich automatisch, ist erforderlich.
10. Zur Handhabung größerer Mengen eines sekundären hochenergetischen Materials ist ein mechanischer Manipulator zu verwenden (für primäre EM s. 4, 5).
11. Alle Räume, mit Ausnahme des Trockenraumes, sollten durch Befeuchtungsanlagen auf min. 70 % rel. Luftfeuchtigkeit gehalten werden.
12. Den sichersten Schutz bietet das Arbeiten in feuchtem Medium, d.h. z. B. Nasssieben und Nassmischen.
13. Alle zur Arbeit verwandten Geräte gründlich abspülen und die Spülwässer und Sprengstoffreste durch übliche chemische Zersetzungsreaktionen ungefährlich machen.
14. Die Lagerung von >500 mg eines sekundären EM hat in speziellen Containern in F90 Schränken oder im Lagerraum für Explosivstoffe zu erfolgen.

Verhütung von Unfällen

Wir möchten nochmals darauf hinweisen, dass bei irgendwie gefährlichen Versuchen sowie auch bei Arbeiten im Hochvakuum auf jeden Fall eine Schutzbrille und ein Vollvisiergesichtshelm zu tragen ist. Beim Arbeiten mit explosiven Materialien sind die allgemeinen Schutzmaßnahmen besonders zu beachten:

a) **Brille**
b) **Vollvisiergesichtsschutz**
c) **Durchführung der Reaktionen hinter Schutzgitter (Käfige) oder hinter einer Glasblende**
d) **Handschuhe (Kevlar mit Stahlverstärkung)**
e) **Ohrenschutz**
f) **Ledermantel, geschlossen**
g) **Erdung**

Die beste Vorsichtsmaßnahme ist nach wie vor, nur sehr kleine Mengen gefährlicher Substanzen einzusetzen. Bei Versuchen mit trockenen sehr explosiven Aziden, Tetra- und Pentazol sowie Nitroverbindungen soll die verwendete Menge keinesfalls mehr als 200 mg betragen.

Bei Explosionsgefahr sollen entweder ein Drahtgitter oder Schutzblenden aus bruchsicherem Glas verwendet werden. Bei Berührung explosiver Stoffe mit dem Hornspatel ist besondere Vorsicht geboten, da der Spatel elektrostatisch aufgeladen sein kann. Nach Erfahrungen ist es hier zweckmäßig, den Hornspatel vorher mit einem antielektrostatischen Tuch abzureiben bzw. einen Spatel aus leitfähigem Kunststoff zu verwenden.
Auf die Laborordnung für chemische Laboratorien und die TRGS 451 wird besonders hingewiesen.

Nichtbefolgung wird in jedem Fall disziplinarisch verfolgt !

München, den 29. September 2003

Prof. Dr. Th. M. Klapötke

New safety regulations for the research group of Professor Klapötke effective from December 18th 2006 - in addition to the general sefety regulations (Arbeitsanweisung Sept. 29th 2003), laboratory chemical safety guide, and all topics covered in the group seminar on Monday, October 23rd, 2006

Chemical laboratory work is only permitted during the usual work hours (**9.00 a.m. – 6.00 p.m.**)

No reaction without filled in and signed **reaction authorization and safety form**.

Handling of any energetic materials by AC-III students is not permitted.

Handling of primary explosives (or sensitive secondary explosives, e.g. PETN, TATP etc.) by AC-F students is not permitted.

Handling of less sensitive energetic materials (not primary explosives, e.g. aminotetrazole) by AC-F students is only allowed under constant supervision by a fully trained PhD student or postdoc on a 250 mg scale if all relevant safety data (friction and impact sensitivity are known) and if the reaction has been carried out in our labs at least 5 times without any problems (this needs to be documented).

For work-up and any manipulation of energetic materials (250 – 500 mg scale in the lab) the following safety clothing is mandatory:

leather jacket (or equivalent)
SS & Kevlar gloves and wrist protectors
earthened shoes
face shield

No private visitors (who are not members of the LMU chemistry department) are allowed at any time in any of the research labs).

In case of an accident with injuries please report immediately to 112 (but inform the gate – 77790 – immediately thereafter to allow access for emergency vehicles:

Now describe the kind of injury and state the number of injured people.

Also state:	where	Haus D, Labor D3…..
	what happened	"Arbeitsunfall mit Personenschaden"
	kind of injury	……
	number of injured people	……

4.3 Steel Sleve Test Procedure

LMU LUDWIG-MAXIMILIANS-UNIVERSITÄT MÜNCHEN

DEPARTMENT CHEMIE UND BIOCHEMIE
ENERGETIC MATERIALS RESEARCH
PROF. DR. THOMAS M. KLAPÖTKE
www.cup.uni-muenchen.de/ac/klapoetke/index.php

Department Chemie und Biochemie, Butenandtstr. 5-13, 81377 München

AK Klapötke

Prof. Dr. Thomas M. Klapötke

Telefon +49 (0)89 2180-77491
Telefax +49 (0)89 2180-77492

tmk@cup.uni-muenchen.de

www.cup.uni-muenchen.de

Postanschrift
Butenandtstr. 5-13
81377 München

Ihr Zeichen, Ihre Nachricht vom Unser Zeichen

München, 06.03.2008

Arbeitsanweisung Koenen Test

Die Prüfung der thermischen Empfindlichkeit am Lehrstuhl KLapötke nach dem Koenen-Test (Stahlhülsenverfahren) erfolgt strikt gemäß der WIWEB-Standardarbeitsanweisung 410/001 vom 01.06.1997 (Kopien erhältlich vom Sekr. Klapötke).

Zusätzlich gelten folgende Arbeitsanweisungen:

1. Bei der Durchführung des Tests (ab Pressen der Substanz) bis zur Explosion (bzw. bei nicht erfolgter Explosion bis zum sicheren Entfernen der zu untersuchenden Substanz aus der Stahlhülse) muss sowohl der AK-Leiter (Prof. Kapötke) als auch der für den Test verantwortliche wiss. Mitarbeiter (Herr Steemann) anwesend sein.
2. Die Teilnahme von Personen, die nicht feste Mitglieder des AK (Klapötke) sind, bedarf der vorherigen schriftlichen Genehmigung durch den AK-Leiter.
3. Während der Testvorbereitung (Einfüllen der Substanz in die Stahlhülse, Pressen, Einbringen in die Testapparatur) dürfen sich max. zwei Personen des Testteams in der Autoklavenstation aufhalten. Das Test-Team besteht aus: AK-Leiter: T. M. Klapötke, Test-Leiter: F. X. Steemann, High-Speed-Operator: N. Mayr, Substanz-Erzeuger: XXX).
4. Die Durchführung des Tests ist auf Seite – 2 - beschrieben.

Dienstgebäude
Butenandtstr. 9
Haus D
81377 München

Öffentliche Verkehrsmittel
U6 Großhadern
Bus 266 oder 268
Waldhüterstraße

Dienstzimmer D3.080
Tel.: +49 (0)89 2180-77491
Fax: +49 (0)89 2180-77492

Sekretariat D3.082
Tel.: +49 (0)89 2180-77494
Fax: +49 (0)89 2180-77492

Durchführung des Koenen Tests

1. Aufbau in der Autoklavenkammer und optische Funktionsprüfung der Koenen-Test-Apparatur durch den Test-Leiter.
2. Funktionsprüfung aller Halogenlampen durch den Test-Leiter (Lampen ab jetzt an).
3. Aufbau, Einstellung und Funktionsprüfung der High-Speed-Kamera durch den High-Speed-Operator (PC und Operation von außerhalb der Autoklavenstation (Flur-Bereich vor der Autoklavenstation).
4. Zweimalige Funktionsprüfung der Piezo-Zündung aus dem an die Autoklaavenstation angrenzenden Labor aller vier Bunsenbrenner durch den Testleiter.
5. NUR wenn 1 – 4 okay, weiter mit 6.
6. Füllen der Stahlhülse im Abzug der Autoklavenstation durch den Substanz-Erzeuger in Anwesenheit des Testleiters oder des AK-Leiters. Zu diesem Zeitpunkt befinden sich nicht mehr und nicht weniger als zwei Personen in der Autoklavenstation. Der Befüller der Stahlhülse trägt entsprechende Sicherheitsausrüstung, mindestens aber: leitfähige Schuhe, Ledermantel, Vollvisiergesichtsschutz, Ohrenschutz, Kevlar Handschuhe und Handgelenkschützer.
7. Pressen der Substanz in der Stahlhülse bei 80 N in der mittleren Autoklavenkammer bei verschlossener Tür durch ein Mitglied des Test-Teams unter Anwesenheit eines zweiten Mitglieds des Testteams. Zu diesem Zeitpunkt befinden sich nicht mehr und nicht weniger als zwei Personen in der Autoklavenstation.
8. Entnehmen der Stahlhülse aus der Pressapparatur und verschrauben mit dem Deckel in der Autoklavenstation (Schraubstock) durch den AK-Leiter und Einbringen in die Testapparatur (Zugang von außen). Der AK-Leiter trägt entsprechende Sicherheitsausrüstung, mindestens aber: leitfähige Schuhe, Ledermantel, Vollvisiergesichtsschutz, Ohrenschutz, Kevlar Handschuhe und Handgelenkschützer. Zu diesem Zeitpunkt befindet sich nur der AK-Leiter in der Autoklavenstation, die Tür zum angrenzenden Flurbereich ist offen. Die ausblasbare Tür zur Druckausgleich der Testkammer bleibt ca. 10 cm offen.
9. Schließen der Tür zum Flurbereich, nahezu Schließen (bis auf ca. 5 cm) der Tür zwischen der Autoklavenstation um dem angrenzenden Labor. Ab jetzt bis Testende befinden sich keine Personen in der Autoklavenstation oder in einer der Autoklavenkammern.
10. Information der Wache über den geplanten Stahlhülsentest in DU: 77790.
11. Rückfrage durch den AK-Leiter an den Test-Leiter und den High-Speed-Operator, ob alles in Ordnung ist.
12. NUR wenn 11. okay, weiter mit 13.

13. Gas-Auf durch den AK-Leiter (die Tür des an die Autoklavenstation angrenzenden Labors zum Flurbereich ist offen) und nach 1 Sek, count-down: 5, 4, 3, 2, 1, 0. Bei 0 Zündung durch Piezo-Züner, Wiederholung bei +1 und + 2 Sek.
14. Abwarten bis Explosion, max. aber 5 Minuten.
15. Gas-Aus durch den AK-Leiter.
16. Information der Wache über den erfolgten Stahlhülsentest in DU: 77790.
17. Ausschalten aller Halogen-Lampen, vorher Autoklavenkammer nicht betreten und Stahltür nicht berühren.
18. Falls Explosion, weiter mit 19, falls keine Explosion, weiter mit 24.
19. Öffnen der Tür zwischen Autoklavenstation und Flurbereich.
20. Kurze optische Prüfung durch den Test-Leiter oder AK-Leiter in der Autoklavenkammer, ob alles in Ordnung ist; ggf. Abhilfe schaffen
21. Abwarten bis toxische Dämpfe abgezogen sind.
22. Betreten der Autoklavenkammer durch den Test-Leiter oder Substanzerzeuger und Beginn der Auswertung des Experiments.
23. Prüfen, ob unumgesetzter Explosivstoff vorhanden (auf Stahl-Tisch etc.). Ggf. sachgerechte Entsorgung durchführen.
24. Abwarten für 30 Minuten.
25. Entnehmen der Stahlhülse durch ein Mitglied des Test-Teams (geeignete Schutzkleidung) und sachgerechte Entsorgung der ggf. verbleibenden Substanz.

4.4 Summary of Standard Operation Procedures [a)]

1. Könen-Test (Steel Sleeve)

a. Vorschrift: „Prüfung der thermischen Empfindlichkeit (Stahlhülsenverfahren)“; Standardarbeitsanweisung 410/001 des Wehrwissenschaftlichen Instituts für Werk-, Explosiv- und Betriebsstoffe (WIWEB) i.d.F.v. 28. Mai 1997 ;geläufiger: EG A.14[1]
b. Ziel: Test der Explosionsfähigkeit einer Verbindung i.S.d. Sprengstoffgesetztes (SprengG)
c. Probenvorbereitung: Die nichtwiederverwendbare Stahlhülse wird im Falle von Feststoffen unter Anpressen mit einer Kraft von 80 N bis zu einer Füllhöhe von 15 mm unterhalb des Hülsenrandes befüllt. Im Falle einer zu testenden Flüssigkeit – bzw. eines Gels – wird die Testsubstanz in die Hülse eingegossen, bis eine Lunker-freie Füllhöhe von 60 mm erreicht ist.

   Substanzen mit einer Reibeempfindlichkeit von $F < 80$ N sollen nicht angepresst werden!

   Die Hülse wird mit der (u.U.) wiederverwendbaren Verschraubung verschlossen ohne Substanz zwischen Bund und Platte oder im Gewinde einzuschließen.
d. Durchführung: Die Stahlhülse wird von vier Bunsenbrennern gleichmäßig erhitzt, die Heizgeschwindigkeit liegt im Temperaturbereich von 135 bis 285 °C zwischen 185 K/min und 215 K/min. Es wird erhitzt, bis Explosion bzw. Zersetzung

[1] EG A.14: Prüfverfahren nach Anhang I Teil A.14 der Richtlinie 92/69/EWG der Kommission vom 31. Juli 1992 zur Siebzehnten Anpassung der Richtlinie 67/548/EWG zur Angleichung der Rechts- und Verwaltungsvorschriften für die Einstufung, Verpackung und Kennzeichnung gefährlicher Stoffe an den technischen Fortschritt (ABl. EG Nr. L 383 S. 113 und Nr. L 383 A S. 1 (S. 87))
Und: Recommendations on the Transport of Dangerous Goods: Tests and criteria, 1990, United Nations, New York. a) The author of this thesis is indebted to and thanks Dr. F.X. Steemann for providing the summary of standard operation procedures mentionend in section 4.4.

eintritt, oder im Falle ausbleibender Zersetzung über einen Zeitraum von 5 Minuten.

e. Auswertung:

Splitterbildtyp	Beschreibung	Ergebnis
0	Hülse unverändert	
A	Hülsenboden ausgebeult	
B	Hülsenboden und –wände ausgebeult	
C	Hülsenboden abgeplatzt	
D	Hülse aufgerissen	
E	Hülse in zwei Teile zerlegt	
F	Hülse in drei oder mehr überwiegend große Teile zerlegt, die evtl. noch zusammenhängen	Explosion
G	Hülse in viele überwiegend kleine Teile zerlegt, Verschluß unbeschädigt	Explosion
H	Hülse in viele überwiegend kleine Teile zerlegt, Verschluß ausgebeult oder zerlegt	Explosion

Damit gelten Splitterbildtypen F, G und H als „positiver" Könen-Test. Die thermische Empfindlichkeit der Substanz wird nach dem Düsendurchmesser bei der Explosion (kritischer Durchmesser) bewertet:

Bewertung	Düsendurchmesser bei Explosion
Unempfindlich	< 2 mm
Wenig empfindlich	≥ 2 mm und < 10 mm
Empfindlich	≥ 10 mm und < 16 mm
Sehr empfindlich	≥ 16 mm und < 20 mm
Äußerst empfindlich	≥ 20 mm

2. Determination of the Impact Sensitivity

a. Vorschrift: NATO Standardization Agreement 4489 (STANAG 4489), Explosives, Impact Sensitivity Tests, September 17, **1999**
Geläufiger: EG A.14[1]

b. Ziel: Test der Schlagempfindlichkeit einer Verbindung mithilfe des BAM-Geräts

c. Probenvorbereitung: Eine Probenmenge von etwa 40 mm³ wird im Falle eines Feststoffes als ein Häufchen in der Mitte des

Metallstempels aufgetragen und der obere Stempel leicht angedrückt, bis er den Haufen berührt. Bei insb. leichtflüssigen Flüssigkeiten kann u.U. das Problem auftreten, dass bei dem Aufprall des Fallgewichts die Probensubstanz zwischen Stempel und Fassung gepresst wird. Für diese Fälle enthält die hier zitierte STANAG-Vorschrift kein besonderes Vorgehen, nach EG A.14[1] ist ein Abstand von 1 mm zwischen den Stempeln zu belassen. Wird z.B. Schleifpapier als zusätzliche Unterlage zwischen Stempel und Probe eingefügt, sollte dies gesondert angegeben werden und auf mögliche Auswirkungen auf das Testergebnis hingewiesen werden.

d. Durchführung: Die Fallhöhe des Gewichtes (1kg, 5 kg, 10 kg) wird in 10 cm Inkrementen verringert, pro Versuch ist eine neue Probe einzusetzen. Messungen unterhalb einer Fallhöhe von 10 cm sind nach STANAG nicht vorgesehen.

   Nach EG A.14[1] werden pro Fallhöhe sechs Versuche durchgeführt: Es werden sechs Einzelversuche unter Verwendung des Fallgewichts von 10 kg und Anwendung einer Fallhöhe von 0,40 m (40 J) ausgeführt. Wenn es während der sechs Versuche bei 40 J zu einer Explosion kommt, sind weitere sechs Einzelversuche mit einem Fallgewicht von 5 kg und einer Fallhöhe von 0,15 m (7,5 J) auszuführen. In geeigneten Inkrementen wird die Fallhöhe der Einzelversuche verringert, bis sechs Versuche negativ verlaufen. Dieser Wert gilt als Schlagempfindlichkeit nach EG A.14[1]. Nach STANAG ist der 50%-Wert ausgehend von dem wie eben beschrieben ermittelten Wert zu bestimmen, indem mit jeweils 30 Einzelversuchen die Fallhöhe gefunden wird, bei welcher 50% der Versuche positiv ausfallen (Bruceton-Methode, „aufwärts“ und „abwärts“ gemessen). Zeigen dabei zehn Einzelversuche konsistent eine höhere oder niedrigere Fallhöhe an, ist ein neuer Startwert zu messen.

e. Auswertung: Als positiver Verlauf wird eine Zersetzung in Gestalt von Explosion, Entflammung oder Knall gedeutet.

Unterhalb einer Fallenergie von 40 J gilt eine Substanz als schlagempfindlich gem. Richtlinie EG A.14[1]; ist keiner von sechs Versuchen positiv, ist der Stoff bei der aktuellen Fallenergie nicht empfindlich nach EG A.14[1].

3. Determination of the Friction Sensitivity

a. Vorschrift: NATO Standardization Agreement 4487 (STANAG 4487), Explosives, Friction Sensitivity Tests, August 22, **2002**
   Geläufiger: EG A.14[1]
b. Ziel: Test der Reibempfindlichkeit einer Verbindung mithilfe des BAM-Geräts
c. Probenvorbereitung: Porzellanplatte wird mit Riffelung quer zur Bewegungsrichtung des Porzellanstempels eingespannt. Eine Probenmenge von etwa 10 mm^3 wird vor und unter den Porzellanstempel auf die Porzellanplatte aufgebracht, so dass der Stempel über die Probe gezogen wird.
d. Durchführung: Jeder Einzelversuch hat zwischen unbenutzten Oberflächen zu erfolgen, d.h. neben einer bestehenden Reibspur oder auf einer neuen Platte und mit einer unbenutzten Seite des Stempels. Es werden sechs Einzelversuche unter Verwendung einer Belastung von 360 N ausgeführt. Wenn es während der sechs Versuche zu einer positiven Reaktion kommt, sind weitere sechs Einzelversuche mit einer Belastung von 120 N auszuführen. Der höchste Belastungswert, bei welchem in sechs Versuchen kein positiver Testverlauf zu beobachten ist, gilt als Reibeempfindlichkeit.
   Nach STANAG wird der 50%-Wert ermittelt, indem ausgehend von dem Ergebnis der „1 aus 6"-Methode statistisch nach Bruceton in 25 bis 30 Versuchen gemessen wird, bis 50% der Versuche positiv verlaufen.
e. Auswertung: Als positiver Verlauf wird eine Zersetzung in Gestalt von Explosion, Entflammung oder Knall (nach STANAG auch Knistern) gedeutet.

Unterhalb einer Reibekraft von 120 N gilt eine Substanz als reibeempfindlich gem. Richtlinie EG A.14[1].

4. Determination of the Electrostatic Discharge Sensitivity

a. Vorschrift: NATO Standardization Agreement 4239 (STANAG 4239), Electrostatic Discharge, Munitions Test Procedures, October 13, **1997**
b. Ziel: Test der Empfindlichkeit einer Verbindung gegenüber elektrostatischer Entladung mithilfe des ESD-Geräts[2]
c. Probenvorbereitung: Gem. Benutzerhandbuch zum ESD-Gerät.
d. Durchführung: Der Kondensator wird bis auf den Stellwert aufgeladen und dann über die Probe entladen. Es werden mindestens 20 Einzelversuche für Personen-verursachte Entladung (25 kV, 15 kV, 10 kV, 5 kV mit jeweils 5000 Ω und 500 Ω bei jeweils 500 pF, Abweichungen von ±5% zulässig) und mindestens 10 Einzelversuche für Helikopter-verursachte Entladung (250 kV, 200 kV, 150 kV, 100 kV, 50 kV, 25 kV mit jeweils Gesamtstromkreiswiderstand bei Entladung mit ±5% Genauigkeit und 1000 pF ±10% gemessen) durchgeführt. Dabei genügt es, die Entladung bei jedem Einzelversuch an einer anderen Stelle der Probe herbeizuführen (Probe muss nicht immer wieder ausgetauscht werden). Die Auf- und Entladungszeit soll im Falle der Personen-verursachten Entladung anhand der 10%- und 90%-Werte ermittelt und notiert werden, ebenso die Testergebnisse.
e. Auswertung: STANAG 4239 gibt keine genaue Auskunft darüber, ob ein 50%-Wert zu ermitteln ist, oder ob ein positiver Testverlauf Empfindlichkeit gegenüber der jew. Entladungsstärke bedeutet. Letzteres erscheint jedoch sinnvoll.

[2] Die STANAG 4239 bezieht sich hauptsächlich auf ein Prüfverfahren für Munitionssorten mit elektro-explosiven Bauteilen (EED) und ähnlichen elektrischen/elektronischen Subsystemen.

ANHANG:

EG A.14:

Prüfverfahren nach Anhang I Teil A.14 der Richtlinie 92/69/EWG der Kommission vom 31. Juli 1992 zur Siebzehnten Anpassung der Richtlinie 67/548/EWG zur Angleichung der Rechts- und Verwaltungsvorschriften für die Einstufung, Verpackung und Kennzeichnung gefährlicher Stoffe an den technischen Fortschritt (ABl. EG Nr. L 383 S. 113 und Nr. L 383 A S. 1 (S. 87))

A.14.1. Methode

A.14.1.1. Einleitung

Die Methode stellt ein Prüfschema dar zur Feststellung, ob feste oder pastenförmige Stoffe bei Flammenzündung (thermische Empfindlichkeit) oder bei Einwirkung von Schlag oder Reibung (mechanische Empfindlichkeit) und ob Flüssigkeiten bei Flammenzündung oder bei Einwirkung von Schlag eine Explosionsgefahr darstellen.
Die Methode besteht aus drei Teilen:

a. Prüfung der thermischen Empfindlichkeit (1);
b. Prüfung der mechanischen Empfindlichkeit bei Schlagbeanspruchung (1);
c. Prüfung der mechanischen Empfindlichkeit bei Reibbeanspruchung (1).

Die Methode liefert Ergebnisse, mit denen die Möglichkeit der Auslösung einer Explosion bei Einwirkung bestimmter, nicht außergewöhnlicher Beanspruchungen festgestellt werden kann. Sie dient nicht zur Feststellung, ob ein Stoff unter beliebigen Bedingungen explosionsfähig ist.
Die Methode eignet sich zur Feststellung, ob ein Stoff unter den besonderen, in der Richtlinie festgelegten Bedingungen eine Explosionsgefahr darstellt (thermische und mechanische Empfindlichkeit). Sie beruht auf der Verwendung mehrerer Arten von Apparaturen, die international weit verbreitet sind (1) und die im allgemeinen aussagekräftige Ergebnisse ergeben. Dabei wird eingeräumt, daß die

Methode keine endgültige Lösung darstellt. Es können andere als die genannten Apparaturen verwendet werden, wenn diese international anerkannt sind und die Ergebnisse in angemessener Form mit denen aus den genannten Apparaturen korreliert werden können.
Die Prüfungen brauchen nicht vorgenommen zu werden, wenn verfügbare thermodynamische Daten (z.B. Bildungs-, Zersetzungsenthalpie) und/oder das Fehlen bestimmter reaktiver Gruppen (2) in der Strukturformel zweifelsfrei erkennen lassen, daß sich der Stoff nicht unter Bildung von Gasen oder Freisetzung von Wärme schnell zersetzen kann (d.h. die Substanz keine Explosionsgefahr darstellt). Eine Prüfung der mechanischen Empfindlichkeit bei Reibbeanspruchung ist für Flüssigkeiten nicht erforderlich.

A.14.1.2. Definitionen und Einheiten

Explosionsgefährlich:

Stoffe, die durch Flammenzündung zur Explosion gebracht werden können oder die gegen Schlag oder Reibung in den genannten Apparaturen empfindlich sind (oder die in alternativen Apparaturen eine höhere mechanische Empfindlichkeit zeigen als 1,3-Dinitrobenzol).

A.14.1.3. Referenzsubstanzen

1,3-Dinitrobenzol, kristallin, gesiebt auf Korngröße 0,5 mm, technisches Produkt für die Prüfung der Schlag- und Reibempfindlichkeit.
Perhydro-1,3,5-trinitro-1,3,5-triazin (RDX, Hexogen, Cyclonit - CAS 121-82-4), umkristallisiert aus wäßrigem Cyclohexanon, naßgesiebt durch ein Sieb 250 im und als Rückstand auf einem Sieb 150 µm gewonnen, anschließend bei 103 ± 2 °C (über 4 Stunden) getrocknet für die zweite Reihe der Prüfung auf Schlag- und Reibempfindlichkeit.

A.14.1.4. Prinzip der Methode

Um sichere Bedingungen für die Ausführung der drei Empfindlichkeitsprüfungen zu finden, ist die Durchführung von Vorversuchen erforderlich.

A.14.1.4.1. Prüfung auf die Sicherheit des Umgangs mit der Substanz

Aus sicherheitstechnischen Gründen werden vor Durchführung der Hauptprüfungen sehr kleine Proben (etwa 10 mg) der Prüfsubstanz ohne Einschluß mit einer Gasbrennerflamme erhitzt, in einem geeigneten Gerät einem Schlag ausgesetzt und unter Verwendung eines Reibstiftes und eines Widerlagers oder in einer beliebigen Reibmaschine gerieben. Das Ziel dieser Vorversuche ist festzustellen, ob der Stoff so empfindlich und so explosiv ist, daß zur Vermeidung von Verletzungen des Prüfenden bei der Durchführung der vorgeschriebenen Empfindlichkeitsprüfungen, insbesondere der Prüfung der thermischen Empfindlichkeit, besondere Schutzmaßnahmen vorzusehen sind.

A.14.1.4.2. Thermische Empfindlichkeit

Für die Prüfung wird die Prüfsubstanz in einer Stahlhülse erhitzt, die durch Düsenplatten mit Öffnungen verschiedenen Durchmessers verschlossen ist. Auf diese Weise wird bestimmt, ob der Stoff unter intensiver thermischer Beanspruchung bei definiertem Einschluß explodieren kann.

A.14.1.4.3. Mechanische Empfindlichkeit (Schlag)

Die Prüfung besteht darin, die Prüfsubstanz dem Schlag eines festgelegten Fallgewichtes aus einer festgelegten Höhe auszusetzen.

A.14.1.4.4. Mechanische Empfindlichkeit (Reibung)

Bei dieser Prüfung werden feste oder pastenförmige Substanzen der Reibung zwischen standardisierten Oberflächen unter festgelegten Bedingungen der Belastung und der relativen Bewegung ausgesetzt.

A.14.1.5. Qualitätskriterien

Nicht festgelegt.

A.14.1.6. Beschreibung der Methode

A.14.1.6.1. Thermische Empfindlichkeit (Flammenzündung)

A.14.1.6.1.1. Apparatur

Die Apparatur besteht aus einer nicht wiederverwendbaren Stahlhülse mit deren wiederverwendbarer Verschraubung (Abbildung 1), die in eine Heiz- und Schutzvorrichtung eingesetzt wird. Jede Hülse wird aus Blech im Tiefziehverfahren hergestellt (siehe Anlage) und hat einen inneren Durchmesser von 24 mm, eine Länge von 75 mm und eine Wanddicke von 0,5 mm. Am offenen Ende sind die Hülsen mit einem Bund versehen, an dem sie mit der Düsenplatte verschlossen werden können. Der Verschluß besteht aus einer druckfesten Düsenplatte mit einer zentrischen Bohrung, die mit der aus Gewindering und Mutter bestehenden Verschraubung fest mit einer Hülse verbunden wird. Gewindering und Mutter bestehen aus Chrom-Mangan-Stahl (siehe Anlage), der bis 800 °C zunderfest ist. Die Düsenplatten sind 6 mm dick, bestehen aus warmfestem Stahl (siehe Anlage) und stehen mit verschiedenen Öffnungsdurchmessern zur Verfügung.

A.14.1.6.1.2. Versuchsbedingungen

Normalerweise wird die Substanz im Auslieferungszustand geprüft, obwohl in einigen Fällen, z.B. bei gepreßten, gegossenen oder anderweitig

verdichteten Stoffen, vor der Prüfung ein Zerkleinern erforderlich werden kann.

Bei Feststoffen wird die Menge des pro Prüfung zu verwendenden Materials durch ein zweistufiges Probeverfahren für die Befüllung bestimmt. Dabei wird eine gewogene Hülse mit 9 cm^3 Prüfsubstanz gefüllt und die Prüfsubstanz unter Anwendung einer Kraft von 80 N, bezogen auf den Gesamtquerschnitt der Hülse, angedrückt. Aus sicherheitstechnischen Gründen oder in solchen Fällen, wo der Aggregatzustand der Probe durch Druck verändert werden kann, können andere Füllverfahren angewendet werden; wenn z.B. die Substanz sehr reibempfindlich ist, empfiehlt sich das Andrücken nicht. Wenn der Stoff sich als kompressibel erweist, wird weitere Substanz hinzugefügt und angedrückt, bis die Hülse bis zu einer Höhe von 55 mm vom Rand gefüllt ist. Danach wird die Gesamtmenge bestimmt, die für die Füllung bis zum Niveau von 55 mm unter dem Rand benötigt wurde, und es werden zwei weitere gleichgroße Portionen zugegeben, wobei auch diese unter Anwendung einer Kraft von je 80 N angedrückt werden. Schließlich wird Substanz entweder zugefügt (unter Andrücken) oder ggf. entnommen, bis die Hülse bis zu einer Höhe von 15 mm unter dem Rand gefüllt ist. Dann wird eine zweite Probebefüllung durchgeführt, die mit einer angedrückten Menge von einem Drittel der Gesamtmenge der ersten Probebefüllung beginnt. Danach werden zwei weitere solche Portionen unter Anwendung von 80 N hinzugefügt und die Höhe der Substanz in der Hülse durch Hinzufügen oder Entnehmen bis auf 15 mm under dem Rand gebracht. Die bei der zweiten Probebefüllung ermittelte Feststoffmenge wird für jeden der eigentlichen Versuche verwendet, wobei das Füllen mit drei gleichgroßen Mengen vorgenommen wird, deren jede durch Anwendung der erforderlichen Kraft auf 9 cm^3 komprimiert wird. (Dies kann durch Verwendung von Abstandsringen erleichtert werden.)

Flüssigkeiten und gelatinöse Substanzen werden in die Hülse bis zu einer Höhe von 60 mm eingefüllt, wobei im letzteren Fall besondere Sorge dafür zu tragen ist, daß keine Lunker gebildet werden. Der Gewindering wird von unten auf die Hülse aufgeschoben, die geeignete Düsenplatte eingesetzt und die Mutter nach Aufbringen eines Schmiermittels auf Molybdändisulfid-

Basis angezogen. Es muß darauf geachtet werden, daß keine Substanz zwischen dem Bund und der Platte oder im Gewinde eingeschlossen ist.
Zum Aufheizen wird Propangas verwendet, das aus einer handelsüblichen Stahlflasche mit Druckminderer (60 bis 70 mbar) entnommen und über einen Durchflußmesser und einen Verteiler gleichmäßig vier Brennern zugeführt wird (was durch Beobachtung der Flammen der einzelnen Brenner festgestellt werden kann). Die Brenner sind entsprechend Abbildung 1 an dem Schutzkasten angeordnet. Die vier Brenner haben zusammen einen Verbrauch von etwa 3,2 l Propan pro Minute. Die Verwendung alternativer Heizgase und Brenner ist möglich, doch muß die Heizgeschwindigkeit der in Abbildung 3 genannten entsprechen. Für alle Apparaturen ist die Heizgeschwindigkeit regelmäßig unter Verwendung von Hülsen mit Dibutylphthalatfüllung zu kontrollieren (vgl. Abbildung 3).

A.14.1.6.1.3. Versuchsausführung

Jeder Versuch wird fortgeführt, bis die Stahlhülse entweder zerlegt oder fünf Minuten erhitzt worden ist. Ein Versuch, der zu einer Zerlegung der Hülse in drei oder mehr Teile führt (diese können in einigen Fällen noch durch schmale Metallstreifen miteinander verbunden sein - vgl. Abbildung 2), wird als Explosion eingestuft. Ein Versuch mit weniger Teilen oder überhaupt keiner Zerlegung wird nicht als Explosion eingestuft.
Zunächst wird eine erste Reihe mit drei Versuchen unter Verwendung einer Düsenplatte mit einem Öffnungsdurchmesser von 6,0 mm durchgeführt; wenn es hier zu keiner Explosion kommt, folgt eine zweite Reihe, ebenfalls mit drei Versuchen, mit einer Düsenplatte von 2,0 mm Öffnungsdurchmesser. Tritt während einer dieser Versuchsreihen eine Explosion ein, kann auf die Durchführung weiterer Versuche verzichtet werden.

A.14.1.6.1.4. Auswertung

Das Versuchsergebnis wird als positiv eingestuft, wenn es in einer der genannten Versuchsreihen zu einer Explosion kommt.

A.14.1.6.2. Mechanische Empfindlichkeit (Schlag)

A.14.1.6.2.1. Apparatur (Abbildung 4)

Die wesentlichen Teile eines typischen Fallhammers sind der Block aus Gußstahl mit Fuß, der Amboß, die Säule, die Führungsschienen, die Fallgewichte, die Auslösevorrichtung und ein Probenhalter. Der Stahlamboß -100 mm (Durchmesser) x 70 mm (Höhe) ist oben auf einen Stahlblock - 230 mm (Länge) x 250 mm (Breite) x 200 mm (Höhe) - mit Fuß - 450 mm (Länge) x 450 mm (Breite) x 60 mm (Höhe) aufgeschraubt. Eine Säule aus nahtlos gezogenem Stahlrohr ist in einer Halterung befestigt, die auf der Rückseite des Stahlblocks angeschraubt ist. Der Fallhammer ist mit vier Steinschrauben auf einem massiven Betonsockel - 60 cm x 60 cm x 60 cm - so verankert, daß die Führungsschienen absolut senkrecht stehen und das Fallgewicht leicht geführt wird. Fallgewichte zu 5 kg und 10 kg aus massivem Stahl stehen zur Verfügung. Der Schlageinsatz jedes Gewichts besteht aus gehärtetem Stahl, HRC 60 bis 63, und hat einen Mindestdurchmesser von 25 mm.
Die zu untersuchende Probe ist in eine Stempelvorrichtung einzuschließen, die aus zwei koaxial übereinanderstehenden Stahlstempeln und einem Hohlzylinder aus Stahl als Führungsring besteht. Die Stahlstempel, Abmessung 10 (-0,003, -0,005) mm Durchmesser und 10 mm Höhe, müssen polierte Flächen, abgerundete Kanten (Krümmungsradius 0,5 mm) und eine Härte HRC 58 bis 65 haben. Der Hohlzylinder muß einen äußeren Durchmesser von 16 mm, eine geschliffene Bohrung von 10 (+0,005, +0,010) mm und eine Höhe von 13 mm haben. Die Stempelvorrichtung ist auf einen Zwischenamboss (26 mm Durchmesser, 26 mm Höhe) aus Stahl zu stellen und durch einen Zentrierring mit einem Lochkranz zum Abströmen der Explosionsschwaden zu zentrieren.

A.14.1.6.2.2. Versuchsbedingungen

Die Probe muß ein Volumen von 40 mm^3 oder ein der verwendeten Alternativapparatur angepaßtes Volumen haben. Feststoffe sind im trockenen Zustand zu prüfen und wie folgt vorzubereiten:

a. Pulverförmige Substanzen sind zu sieben (Maschenweite 0,5 mm); der gesamte Siebdurchgang ist zur Prüfung zu verwenden;
b. Gepreßte, gegossene oder anderweitig verdichtete Substanzen sind zu zerkleinern und zu sieben; zur Prüfung ist die Siebfraktion 0,5 bis 1 mm Durchmesser zu verwenden; sie muß für die Originalsubstanz repräsentativ sein.

Substanzen, die in der Regel pastenförmig geliefert werden, sollten, wenn möglich, im trockenen Zustand geprüft werden, auf jeden Fall aber nach Entfernen der größtmöglichen Menge an Verdünnungsmittel. Bei der Prüfung flüssiger Substanzen ist zwischen dem oberen und dem unteren Stahlstempel ein Abstand von 1 mm zu halten.

A.14.1.6.2.3. Versuchsausführung

Es werden sechs Einzelversuche unter Verwendung des Fallgewichts von 10 kg und Anwendung einer Fallhöhe von 0,40 m (40 J) ausgeführt. Wenn es während der sechs Versuche bei 40 J zu einer Explosion kommt, sind weitere sechs Einzelversuche mit einem Fallgewicht von 5 kg und einer Fallhöhe von 0,15 m (7,5 J) auszuführen. Bei Verwendung einer anderen Apparatur wird die Probe mit der gewählten Referenzsubstanz unter Benutzung einer anerkannten Auswertungsmethode (z.B. up-and-down technique usw.) verglichen.

A.14.1.6.2.4. Auswertung

Das Prüfergebnis wird als positiv eingestuft, wenn es mit der beschriebenen Apparatur zumindest in einem der genannten Versuche zu einer Explosion (eine Entflammung und/oder ein Knall steht einer Explosion gleich) kommt oder wenn bei Verwendung einer alternativen Apparatur die Probe empfindlicher ist als 1,3-Dinitrobenzol oder Hexogen (RDX).

A.14.1.6.3. Mechanische Empfindlichkeit (Reibung)

A.14.1.6.3.1. Apparatur (Abbildung 5)

Der Reibapparat besteht aus einer Grundplatte (Gußstahl), auf der die Reibvorrichtung, bestehend aus einem feststehenden Porzellanstift und einem beweglichen Porzellanplättchen, montiert ist. Das Porzellanplättchen ist in einem Schlitten befestigt, der in zwei Gleitschienen geführt wird. Der Schlitten wird mit einem Elektromotor über eine Schubstange, eine Exzenterscheibe und ein geeignetes Getriebe so angetrieben, daß das Porzellanplättchen unter dem Porzellanstift eine einmalige Hin- und Rückbewegung von 10 mm Länge ausführt. Der Porzellanstift kann z.B. mit 120 oder 360 N belastet werden.
Die flachen Porzellanplättchen sind aus rein weißem technischem Porzellan gefertigt (Rauhtiefe 9 µm bis 32 µm) und haben die Abmessungen 25 mm (Länge) x 25 mm (Breite) x 5 mm (Höhe). Der zylindrische Porzellanstift ist ebenfalls aus rein weißem technischem Porzellan gefertigt. Er ist 15 mm lang, hat einen Durchmesser von 10 mm und eine rauhe sphärische Endfläche mit einem Krümmungsradius von 10 mm.

A.14.1.6.3.2. Versuchsbedingungen

Die Probe muß ein Volumen von 10 mm^3 oder ein der verwendeten Alternativapparatur angepaßtes Volumen haben.
Feststoffe sind im trockenen Zustand zu prüfen und wie folgt vorzubereiten:

a. Pulverförmige Substanzen sind zu sieben (Maschenweite 0,5 mm); der gesamte Siebdurchgang ist zur Prüfung zu verwenden;
b. Gepreßte, gegossene oder anderweitig verdichtete Substanzen sind zu zerkleinern und zu sieben; zur Prüfung ist die Siebfraktion < 0,5 mm Durchmesser zu verwenden.

Pastenförmige Substanzen sollten, wenn möglich, im trockenen Zustand geprüft werden. Falls das nicht = möglich ist, muß die Paste, nach Entfernen der größtmöglichen Menge an Verdünnungsmittel, als 0,5 min - dicker, 2 mm breiter und 10 mm langer Film, der mit einem speziellen Formteil hergestellt wird, geprüft werden.

A.14.1.6.3.3. Versuchsausführung

Der Porzellanstift wird auf die zu untersuchende Probe gesetzt und belastet. Bei Durchführung des Versuchs muß der Schwammstrich des Porzellanplättchens quer zu dessen Bewegungsrichtung liegen. Es ist darauf zu achten, daß der Stift auf der Probe steht und daß soviel Prüfsubstanz vor dem Stift liegt, daß bei der Plättchenbewegung genügend Prüfsubstanz unter den Stift gelangt. Pastenförmige Substanzen werden mittels einer Lehre (Dicke: 0,5 mm) mit einer Öffnung von 2 mm x 10 mm auf das Plättchen aufgetragen. Das Porzellanplättchen wird unter dem Porzellanstift in einer Zeit von 0,44 s je 10 mm hin- und herbewegt. jeder Oberflächenbezirk des Plättchens und des Stiftes darf nur einmal verwendet werden; die beiden Enden eines jeden Stiftes können für zwei Versuche, und die beiden Oberflächen eines jeden Plättchens können für je drei Versuche benutzt werden.
Es werden sechs Einzelversuche unter Verwendung einer Belastung von 360 N ausgeführt. Wenn es während der sechs Versuche zu einer positiven Reaktion kommt, sind weitere sechs Einzelversuche mit einer Belastung von 120 N auszuführen. Bei Verwendung einer anderen Apparatur wird die Probe mit der gewählten Referenzsubstanz unter Benutzung einer anerkannten Auswertungsmethode (z.B. up-and-down technique usw.) verglichen.

A.14.1.6.3.4. Auswertung

Das Prüfergebnis wird als positiv eingestuft, wenn es mit dem beschriebenen Reibapparat zumindest in einem der genannten Versuche zu einer Explosion (ein Knistern und/oder ein Knall oder eine Entflammung stehen einer Explosion gleich) kommt oder wenn bei Verwendung einer alternativen Reibprüfung die äquivalenten Kriterien erfüllt werden.

A.14.2. Daten

Grundsätzlich gilt ein Stoff als im Sinne dieser Richtlinie explosionsgefährlich, wenn bei der Prüfung auf thermische, Schlag- oder Reibempfindlichkeit ein positives Ergebnis erzielt wird.

A.14.3. Bericht

A.14.3.1. Prüfbericht

Im Prüfbericht ist, wenn möglich, folgendes anzugeben:

- die Bezeichnung, die Zusammensetzung, die Reinheit, der Feuchtigkeitsgehalt usw. der Prüfsubstanz;
- der Aggregatzustand der Probe und die Angabe, ob die Probe zerkleinert und/ oder gesiebt worden ist;
- die Beobachtungen während der Prüfungen auf thermische Empfindlichkeit (z.B. Probenmasse, Anzahl der Splitter usw.);
- die Beobachtungen während der Prüfungen auf mechanische Empfindlichkeit (z.B. größere Rauchentwicklung oder vollständige Zersetzung ohne einen Knall, Flammen, Funken, Knistern usw.);
- die Ergebnisse jedes Einzelversuchs;
- bei Anwendung einer Alternativapparatur: die wissenschaftliche Begründung sowie die Beweisführung für die Vergleichbarkeit der Ergebnisse zwischen der beschriebenen und der Alternativapparatur;
- alle nützlichen Hinweise auf Versuche mit ähnlichen Substanzen, die für die richtige Interpretation der erhaltenen Versuchsergebnisse von Bedeutung sein können;
- alle zusätzlichen Bemerkungen, die für die Interpretation der Ergebnisse von Bedeutung sind.

A.14.3.2. Interpretation und Bewertung der Ergebnisse

Im Prüfbericht sind alle Ergebnisse anzugeben, die als falsch, anormal oder nicht repräsentativ angesehen werden. Wird ein Versuchsergebnis nicht in die Bewertung einbezogen, so ist dies zu begründen, und es sind die

Ergebnisse anderer oder zusätzlicher Versuche aufzuführen. Kann die Abnormität eines Ergebnisses nicht erklärt werden, muß das Ergebnis als solches akzeptiert und der Stoff entsprechend eingestuft werden.

A.14.4. Literatur

(1) Recommendations on the Transport of Dangerous Goods: Tests and criteria, 1990, United Nations, New York.
(2) Bretherick, L., Handbook of Reactive Chemical Hazards, 4. Auflage, Butterworths, London, ISBN 0-750-60103-5, 1990.
(3) Koenen, H., Ide, K.H. und Swart, K.H., Explosivstoffe, 1961, Bd. 3, 6-13 und 30-42.
(4) NF T 20-033 (Sept. 35). Chemical products for industrial use - Determination of explosion risk.

Anlage zu RL 67/548/EWG Anhang V A.14

Beispiel für Werkstoffspezifikation zur Prüfung auf thermische Empfindlichkeit (vgl. DIN 1623)
(1) Hülse: Werkstoffspezifikation Nr. 1.0336.505 g
(2) Düsenplatte: Werkstoffspezifikation Nr. 1.4373
(3) Gewindering und Mutter: Werkstoffspezifikation Nr. 1.3817

Abbildung 1

Apparatur für die Prüfung auf thermische Empfindlichkeit

(alle Abmessungen in mm)

Abb. 1a Stahlhülse und Verschraubung

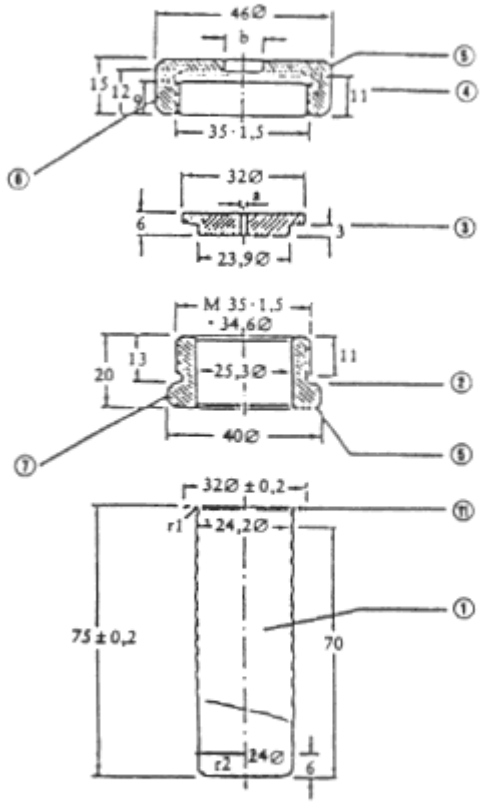

(1) Hülse
(1a) äußerer Flansch
(2) Gewindering; reibungsarmes Gewinde
(3) Düsenplatte a = 2,0 oder 6,0 mm Durchm.
(4) Mutter b = 10 mm Durchmesser
(5) abgefaste Fläche
(6) 2 Flächen für Schlüsselweite 41

Abb. 1b Heiz- und Schutzvorrichtung

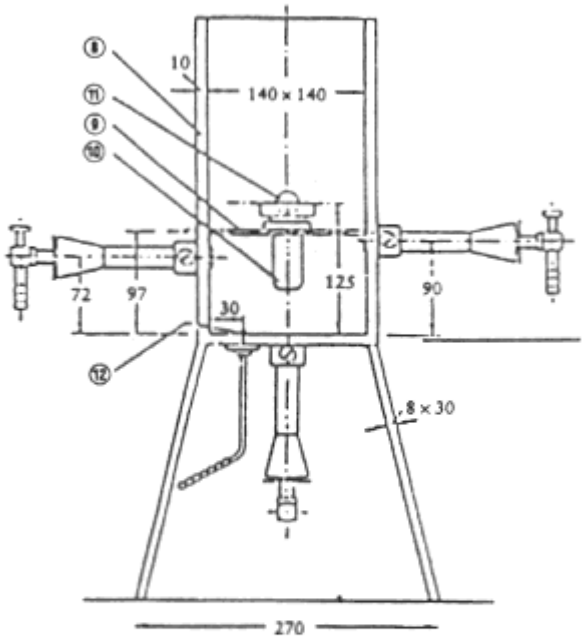

(7) 2 Flächen für Schlüsselweite
(8) splitterfester Kasten
(9) 2 Haltestangen für Hülse
(10) Hülse, montiert
(11) Lage des hinteren Brenners; andere Brenner sichtbar
(12) Lockflamme

Abbildung 1: Apparatur für die Prüfung auf thermische Empfindlichkeit

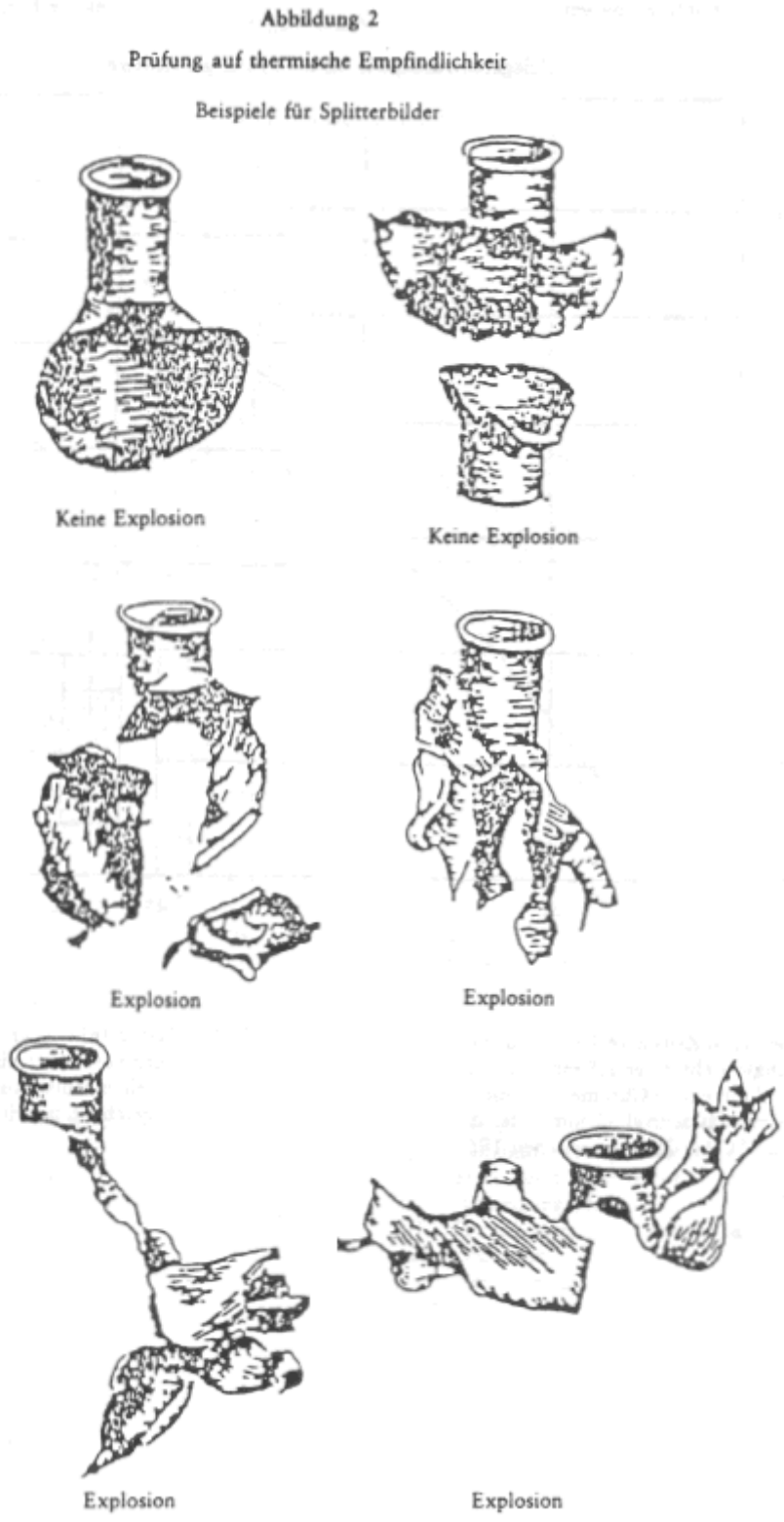

Abbildung 2: Prüfung auf thermische Empfindlichkeit; Beispiele für Splitterbilder

Abbildung 3

Kalibrierung der Heizgeschwindigkeit für die Prüfung auf thermische Empfindlichkeit

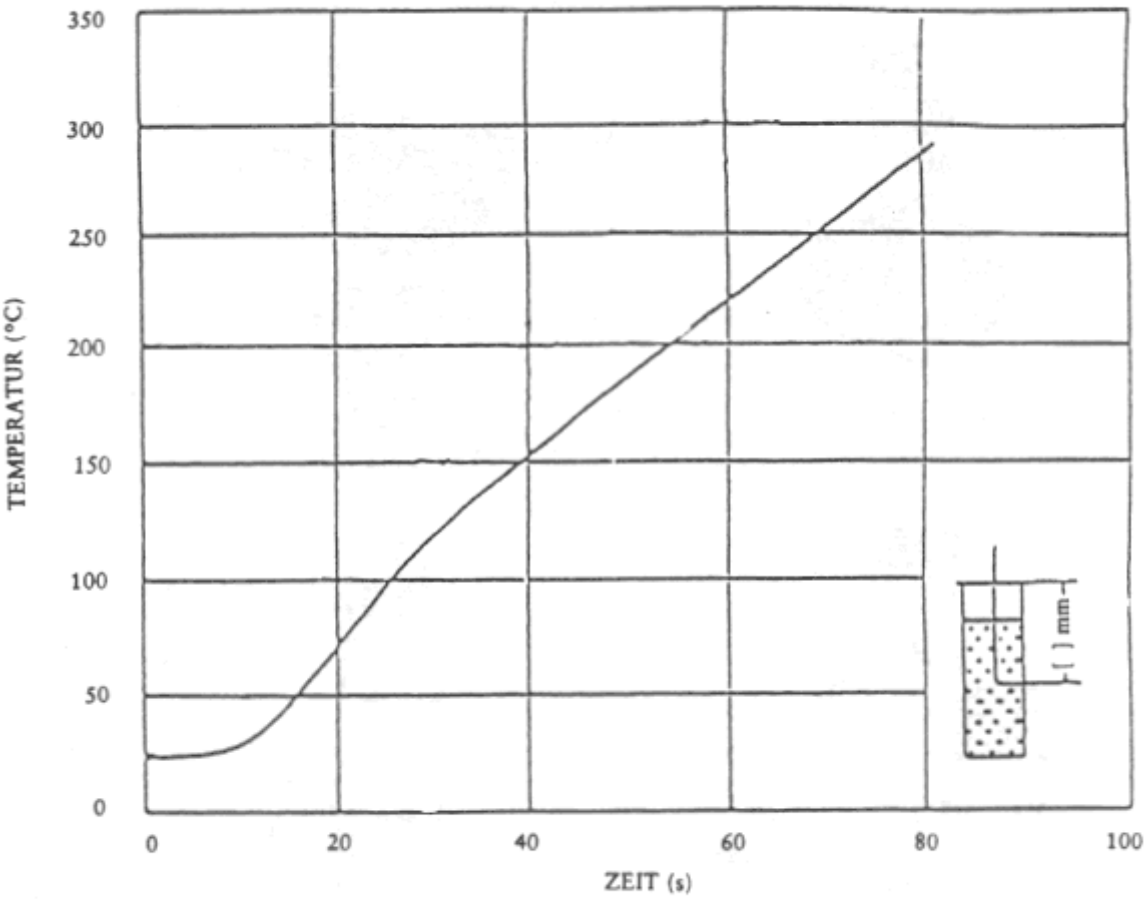

Temperatur-/Zeitkurve bei Erwärmung von Dibutylphthalat (27 cm^3) in einer (mit einer Düsenplatte mit Öffnungsdurchmesser 1,5 mm) verschlossenen Hülse bei einem Propanverbrauch von 3,2 l/min. Die Temperatur wird mit einem Chromel-/Alumel-Thermoelement (Durchmesser: 1 mm) in einer Hülse aus rostfreiem Stahl gemessen, das zentral 43 mm unter dem Hülsenrand angebracht ist. Die Heizgeschwindigkeit muß im Bereich von 135 °C bis 285 °C zwischen 185 K/min und 215 K/min liegen.

Abbildung 3: Kalibrierung der Heizgeschwindigkeit für die Prüfung auf thermische Empfindlichkeit

Abb. 4a Fallhammer, Vorder- und Seitenansicht; Gesamtansicht

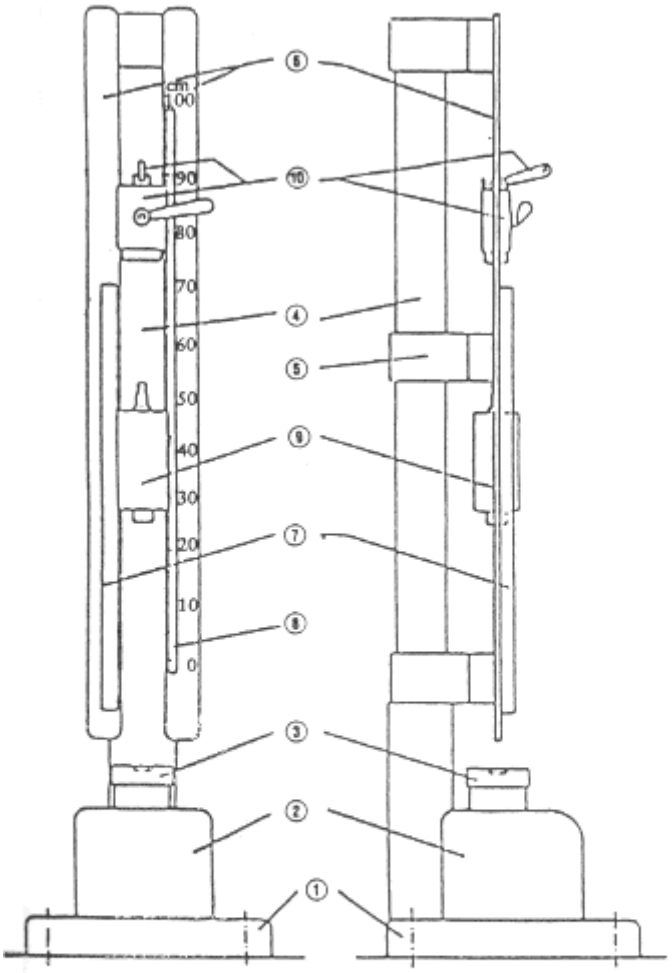

Abbildung 4: Apparatur zur Prüfung auf Schlagempfindlichkeit
Abb. 4a: Fallhammer, Vorder- und Seitenansicht; Gesamtansicht

Abb. 4b Fallhammer, unterer Teil

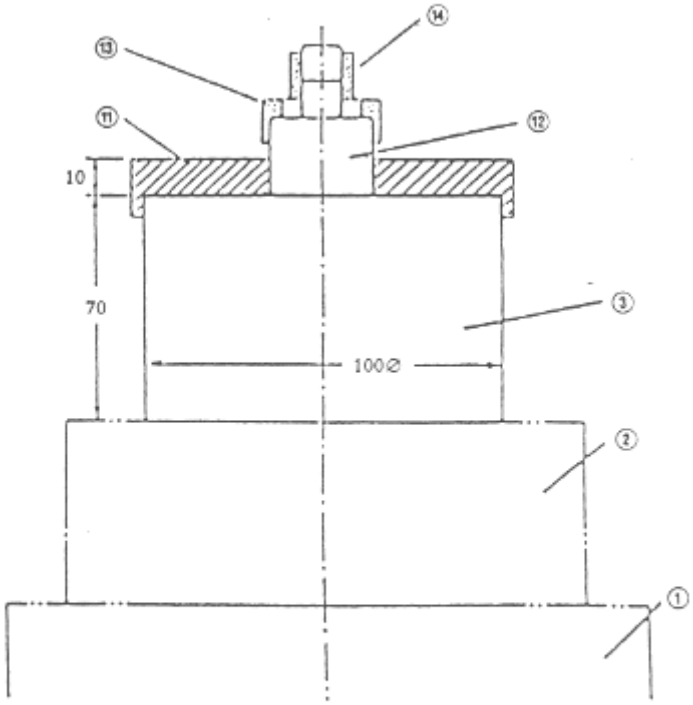

(9) Fallhammer (Fallgewicht)
(10) Halte- und Auslösevorrichtung
(11) Befestigungsplatte
(12) Zwischenamboß (austauschbar), 26 Durchmesser × 26
(13) Zentrierring mit Öffnungen
(14) Stempelvorrichtung

Abb. 4b: Fallhammer unterer Teil

Abb. 4c Stempelvorrichtung für pulver- oder pastenförmige Substanzen

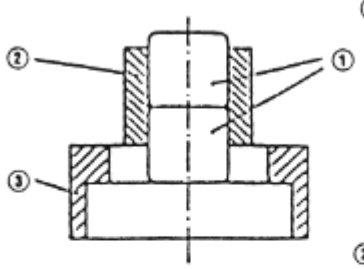

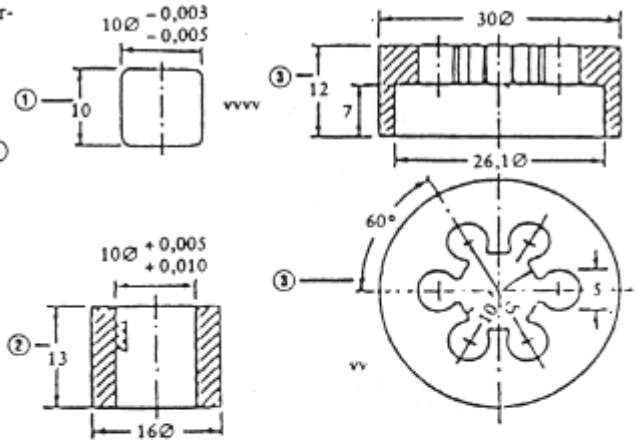

(1) Stahlstempel
(2) Führungsring für Stahlstempel
(3) Zentrierring mit Öffnungen
(a) Aufriß
(b) Grundriß
(4) Gummiring
(5) Flüssigkeit (40 mm³)
(6) flüssigkeitsfreier Raum

Abb. 4d Stempelvorrichtung für Flüssigkeiten

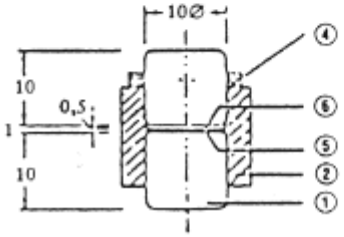

Abb. 4c/4d: Stempelvorrichtung für pulver- oder pastenförmige Substanzen/ -für Flüssigkeiten

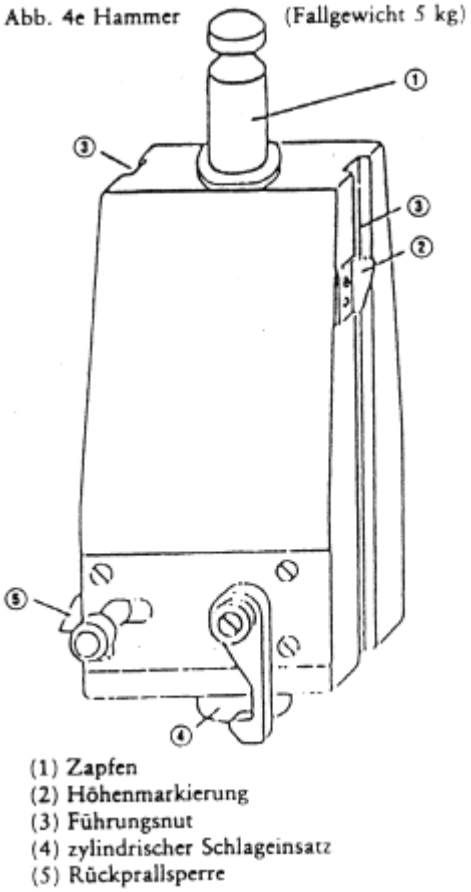

Abb. 4e: Hammer

Abbildung 5

Apparatur zur Prüfung auf Reibempfindlichkeit

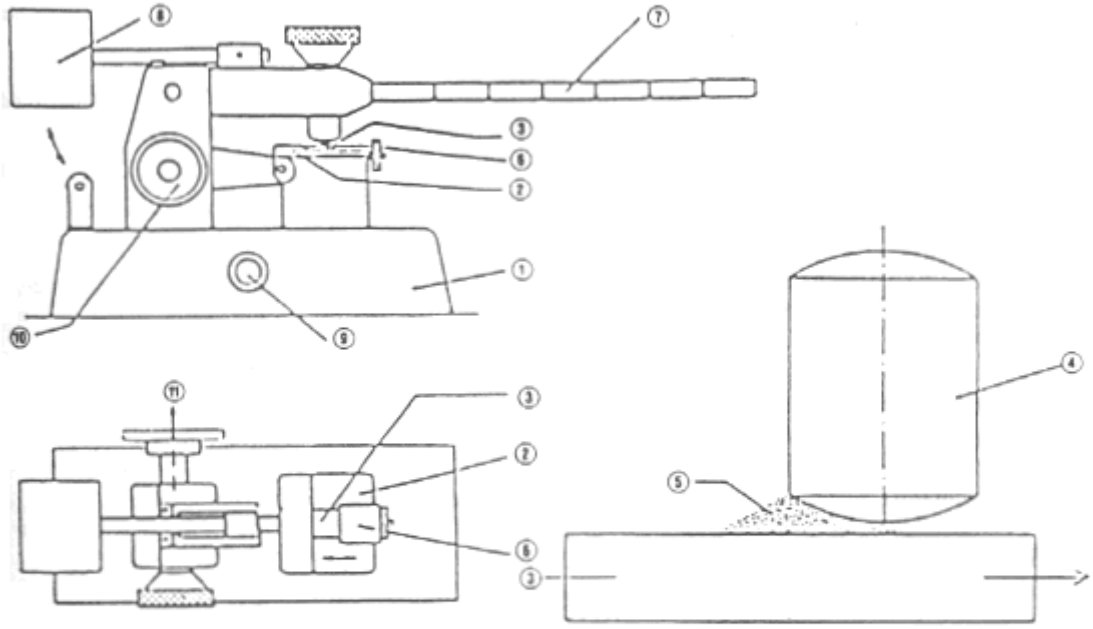

Abb. 5a Reibapparat;
Aufriß und Grundriß
(1) Stahlfuß
(2) Schlitten
(3) Porzellanplättchen, 25 mm × 25 mm × 5 mm, auf dem Schlitten befestigt
(4) fester Porzellanstift, 10 Durchm. × 15 mm
(5) Prüfsubstanz, etwa 10 mm^3

Abb. 5b Ausgangsstellung des Stiftes auf der Probe
(6) Stifthalter
(7) Belastungsarm
(8) Gegengewicht
(9) Schalter
(10) Rad zum Fahren des Schlittens in Ausgangsstellung
(11) zum Elektromotor

Abbildung 5: Apparatur zur Prüfung auf Reibempfindlichkeit
Abb. 5a Reibapparat; Aufriß und Grundriß
Abb. 5b Ausgangsstellung des Stiftes auf der Probe

4.5 Explosives Hazard Classification Procedures

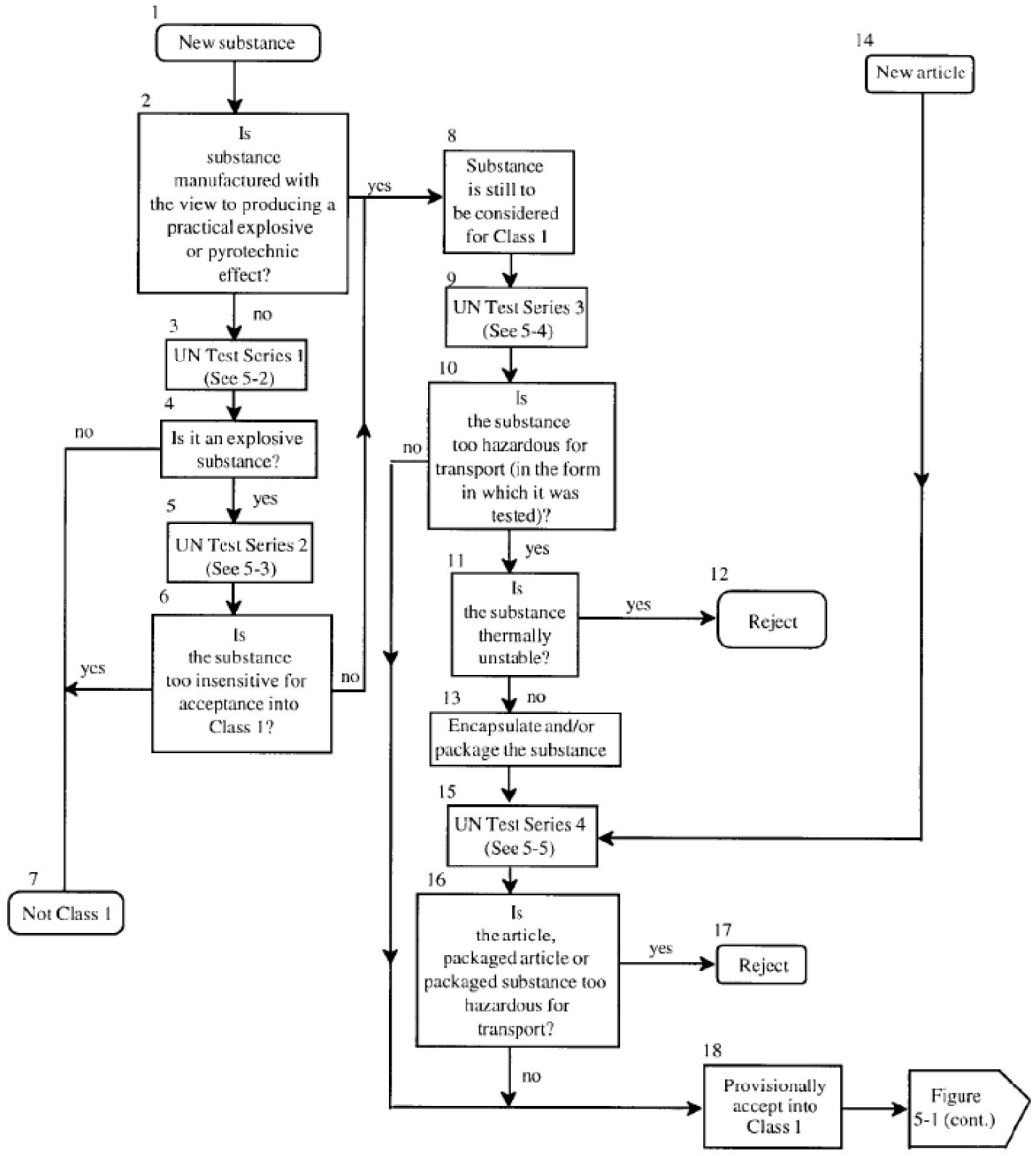

Figure 5-1. UN hazard classification procedures for articles and substances.

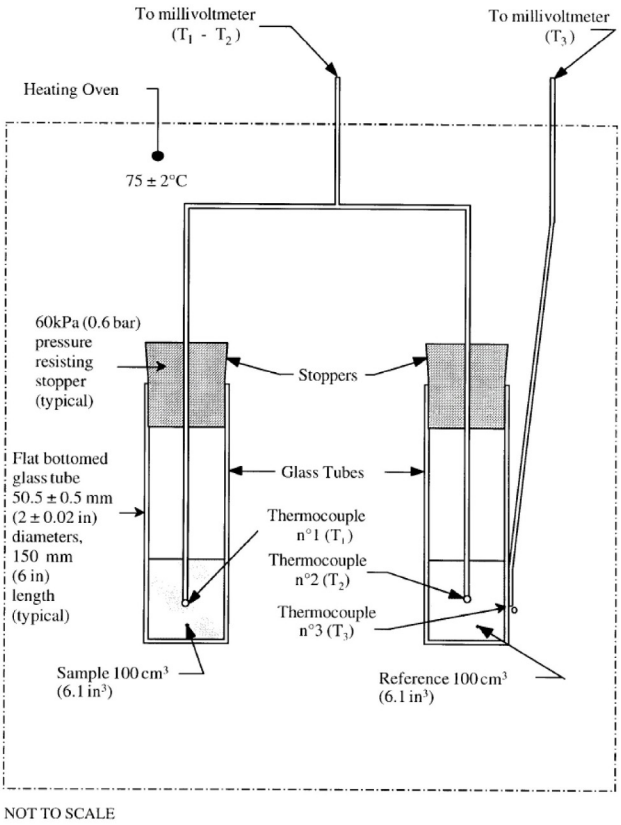

Figure 5-13. Thermal stability test configuration (UN 3c).

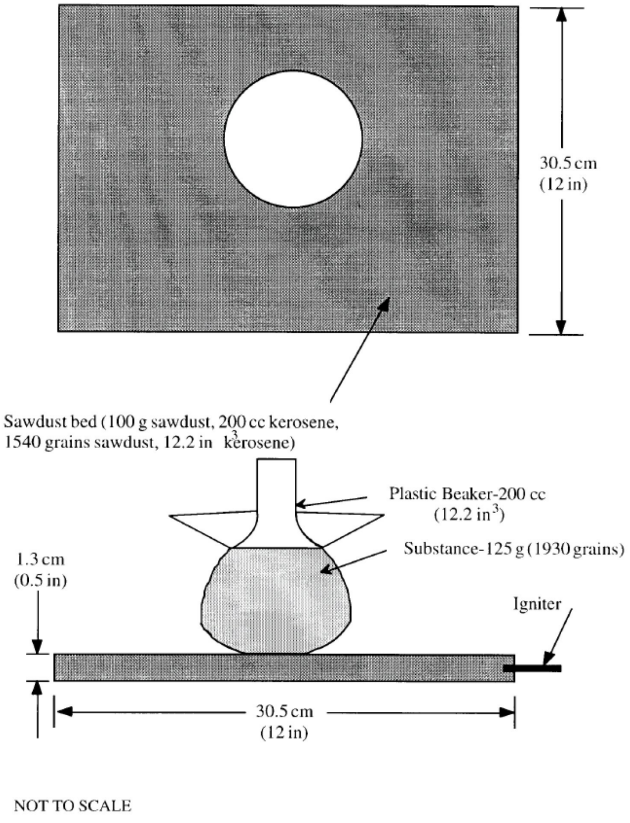

Figure 5-14. Small scale burning test configuration (UN 3d).

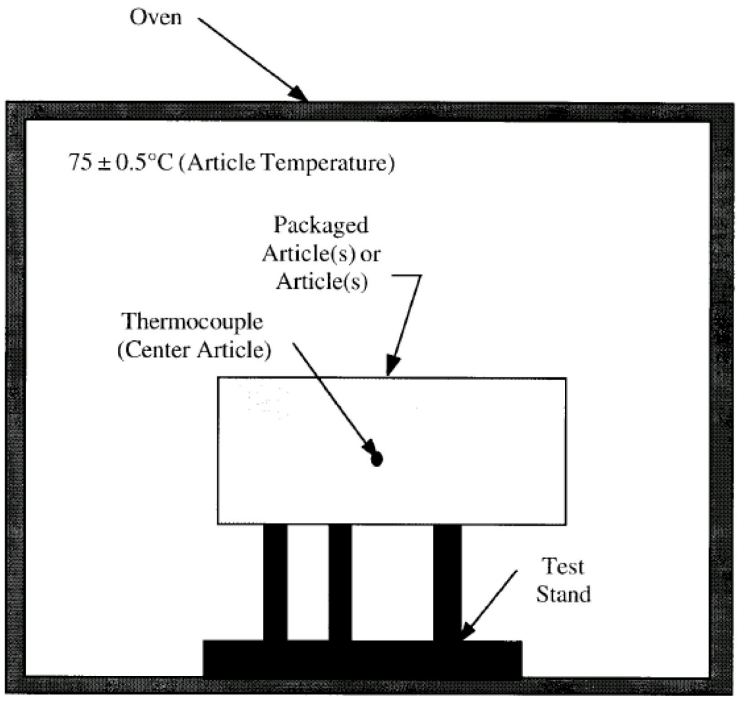

Figure 5-15. Thermal stability test for articles (UN 4a).

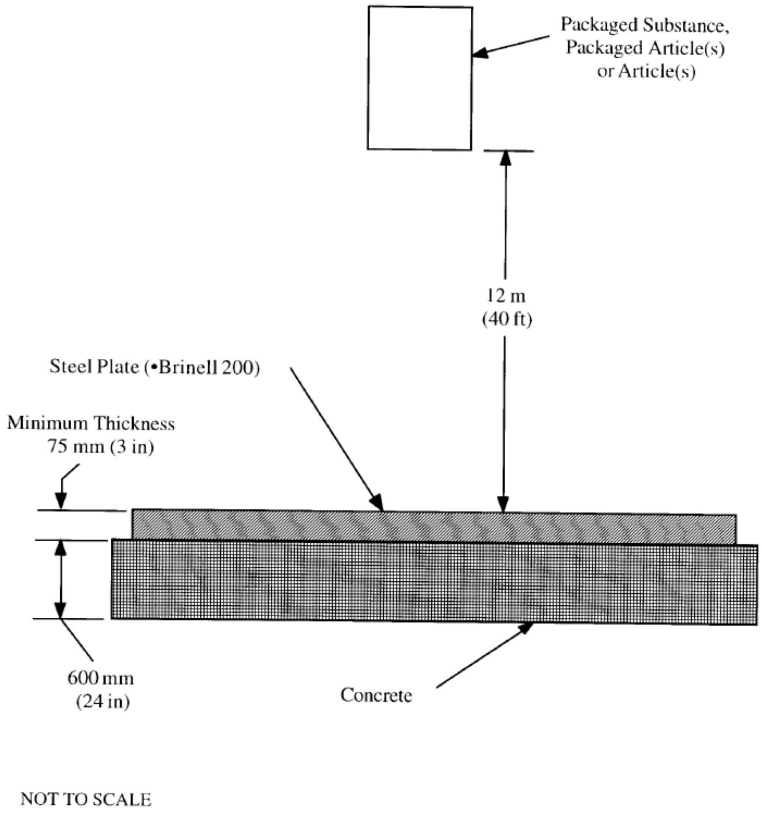

Figure 5-17. Twelve meter drop test configuration (UN 4b).

Test results according to: DEPARTMENT OF DEFENSE AMMUNITION AND EXPLOSIVES HAZARD CLASSIFICATION PROCEDURES

Test #	Test	+ / -	Comment
UN 3a	Impact sensitivity		
UN 3b	Friction sensitivity		
UN 3c	Thermal stability		
UN 3d	Small scale burning		
UN 4a (i)	Thermal stability for articles and packaged articles		
UN 4b (ii)	12 m free fall		

Munich, ……

Name:……

Signature: ……

Appendix 1 to section II N of the Army Research Laboratory (ARL) interim hazard classification (ICH) request

Molecular structure (Lewis-type drawing):

Chemical name:

Abbreviation (if any):

Formula (CHNO):

m.p. / °C: …….. (DSC @ 5°C / min)
$T_{dec.}$ / °C: …….. (DSC @ 5°C / min)
density / g cm^{-3}: .....
IS / J: ..... grain size: ..... µm
FS / N: ..... grain size: ..... µm
ESD / J: ..... grain size: ..... µm
hygroscopic (yes / no): …….
water-stable: (yes / no): …….
water-soluble: …….

4.6 Frequency Analyses

The vibrational spectra of 1,5-BTMSD and 1,1,5-TTMSD were calculated using density functional methods. The Becke3LYP hybrid functional was used combined with a correlation consistent basis set (cc-pVDZ). The equilibrium geometries were optimized on the same level. The SCF convergence criteria were set *tight* and the size of the integration grid *ultrafine*. The harmonic vibrational frequencies were corrected by multiplication with a correction factor of 0.970 in order to account for anharmonicity effects. The calculations were performed with the program package Gaussian 03, Revision D.01. For the evaluation of the intensity of IR bands following abbreviations were used: vs (very strong, 100 – 75% of the maximal intensity), s (strong, 75 – 50%), m (medium, 50 – 25%) and w (weak, 25 – 0%). The Raman intensities are given as percentage of the maximal intensity.

Frequency Analysis of 1,5-BTMSD

Vibrational frequency (calculated, unscaled, cm^{-1})	Vibrational frequency (calculated, scaled, cm^{-1})	Calculated IR Intensity (arb. u.)	Exptl. IR frequencies (cm^{-1})	Exptl. Raman shifts (cm^{-1})	Tentative assignment
3565	**3458**	39.05			$\nu(N^5H)$
3464	**3360**	6.13	3334 (vs)	3328 (16)	$\nu(N^6H)$
3128	**3034**	3.38			
3124	**3030**	3.52			
3123	**3029**	3.32			
3122	**3029**	4.87			
3117	**3024**	11.75			
3113	**3020**	6.90			
3110	**3017**	30.95	2903 (vs)		$\nu_{as}(CH_3)$
3109	**3016**	17.03	2557 (m)		$\nu_{as}(CH_3)$
3107	**3014**	0.17			
3107	**3014**	0.30			
3104	**3011**	18.59			
3102	**3009**	1.39			
3034	**2943**	3.36		2964 (41)	$\nu_s(CH_3)$
3030	**2939**	7.79			
3029	**2938**	9.32			
3028	**2937**	8.78			
3027	**2936**	5.32			
3026	**2936**	7.08		2904 (50)	$\nu_s(CH_3)$
			2411 (m)		
1637	**1587**	455.37	1656 (vs)		
1522	**1476**	15.54	1585 (vs)	1587 (20)	$\nu(C^1\text{-}N^6)$

1450	**1407**	3.76	1483 (s)	1485 (6)	$\delta_{as}(CH_3)$
1448	**1404**	17.35	1428 (vs)	1419 (14)	δ_{as} (CH_3)
1441	**1397**	19.95			
1440	**1397**	1.73			
1436	**1393**	2.49			
1434	**1391**	0.37			
1433	**1390**	2.35			
1432	**1389**	0.94			
1430	**1387**	0.70			
1429	**1386**	0.85			
1427	**1384**	46.17	1378 (vs)		δ(NH)
1421	**1378**	0.41			
1420	**1378**	0.23			
1369	**1328**	2.90			
1362	**1321**	126.18	1352 (vs)		$N(N^4\text{-}N^5)$
1279	**1240**	11.49	1289 (vs)	1289 (21)	δ_s (CH_3)
1276	**1238**	17.43	1250 (vs)	1264 (6)	δ_s (CH_3)
1272	**1234**	28.81			
1269	**1231**	20.71			
1269	**1231**	38.97			
1267	**1229**	30.62			
1219	**1182**	29.97	1209 (vs)	1209 (14)	δ(NH)
1134	**1100**	9.69	1102 (vs)	1103 (17)	ν(ring)
1107	**1074**	51.75			
1007	**976**	24.54	987 (vs)	988 (5)	ν(ring)
887	**861**	93.45	877 (vs)	896 (6)	$\delta(CH_3)$
875	**849**	198.96		856 (12)	$\delta(CH_3)$
873	**847**	126.65			
868	**842**	230.77	848 (vs)	840 (12)	ρ(C-H)
863	**837**	103.43			
862	**836**	58.47			
853	**827**	50.97			
818	**793**	0.99			
790	**766**	12.55			
780	**757**	24.32			
775	**751**	24.27	760 (vs)		$\delta(CH_3)$
769	**746**	19.49	715 (s)		$\delta(CH_3)$
754	**731**	6.65			
700	**679**	20.86	696 (s)	698 (14)	ν(Si-C)
697	**676**	2.69			
696	**675**	0.51			
694	**674**	1.09			
693	**672**	9.41			
690	**669**	1.68			
688	**667**	9.77	650 (s)		skeleton vib.
680	**660**	0.56			
654	**634**	6.91		625 (100)	skeleton vib
			616 (s)		
606	**588**	44.57	585 (m)		
601	**583**	1.31			
566	**549**	43.75			

				522 (13)	
488	**474**	47.99	494 (w)		
429	**416**	25.02			
353	**342**	6.82		375 (10)	
315	**306**	16.78		315 (20)	
302	**293**	10.84			

Frequency Analysis of 1,1,5-TTMSD

Vibrational frequency (calculated, unscaled, cm^{-1})	Vibrational frequency (calculated, scaled, cm^{-1})	Calculated IR intensity (arb. u.)	Exptl. IR frequencies (cm^{-1})	Exptl. Raman shifts (cm^{-1})	Tentative assignment
3571	**3464**	32.9	3237 (m)		ν(NH)
3127	**3033**	2.7	3181 (s)		$\nu_{as}(CH_3)$
3112	**3019**	12.3			
3111	**3017**	16.3			
3110	**3017**	36.5			
3109	**3016**	18.2			
3104	**3011**	28.9			
3102	**3009**	6.6			
3034	**2943**	5.0	2958 (m)	2962 (50)	$\nu_s(CH_3)$
3033	**2942**	6.0			
3030	**2940**	7.3			
3030	**2939**	11.7			
3029	**2938**	2.1			
3029	**2938**	8.7			
3028	**2937**	11.1			
3027	**2936**	5.3			
3026	**2936**	3.4	2903 (w)	2902 (100)	$\nu_s(CH_3)$
1625	**1576**	393.5	1580 (s)	1580 (9)	$\nu(N^5\text{-}C^1)$
1508	**1462**	24.7	1454 (w)	1452 (10)	δ(NH)
			1440 (w)		
1452	**1408**	3.4			
1450	**1406**	4.6			
1448	**1405**	12.6		1413 (15)	$\delta(CH_3)$
1362	**1322**	75.7	1309 (w)		$\nu(N^2\text{-}N^3)$
1352	**1312**	79.0	1298 (m)	1299 (11)	$\delta(NH) + \nu(N^3\text{-}N^4)$
1277	**1238**	35.6			
1271	**1233**	44.6			
1269	**1231**	64.7	1256 (vs)		$\rho(CH_3)$
1269	**1230**	12.4			

1268	**1230**	15.4			
1267	**1229**	24.4	1204 (m)	1205 (8)	$\rho(CH_3)$
1211	**1175**	37.8	1165 (m)		$\delta(NH) + \delta(ring)$
			1097 (m)	1105 (11)	$\nu(N^1\text{-}N^2) + \nu(N^3\text{-}N^4)$
1133	**1099**	9.7			
1105	**1072**	38.5	1031 (m)	1034 (6)	$\delta(NH) + \delta(ring)$
1007	**977**	19.7	982 (w)	983 (7)	$\delta(ring)$
			936 (s)		
903	**876**	374.1		899 (5)	$\delta(N^6{}_{\text{out of plane}})$
901	**874**	153.8	884 (s)		Skeleton vibration
876	**850**	370.1			$\rho(CH_3)$
874	**848**	135.1			
864	**838**	100.5			
839	**814**	87.5	840 (vs)		$\rho(CH_3)$
776	**753**	19.3	759 (m)	759 (11)	$\delta(CH_3)$
772	**749**	25.2			
759	**736**	21.3			
696	**675**	6.4	690 (w)	692 (19)	$\nu_{as}(Si(CH_3)_3)$
690	**669**	4.6			
687	**667**	12.6			
682	**662**	5.1		644 (49)	$\nu_{as}(Si(CH_3)_3)$
672	**652**	7.6	638 (m)	621 (32)	$\nu_{as}(Si(CH_3)_3)$
620	**601**	16.5			
604	**586**	4.5	576 (w)		$\nu_s(Si(CH_3)_3)$
604	**586**	9.4			
523	**507**	1.3	525 (w)	531 (14)	$\delta(N^6{}_{\text{in plane}})$

4.7 Single Crystal X-ray Structures

compound name	Potassium nitroformate	Ammonium nitroformate
compound, abbrev.	KNF	ANF
formula, moiety	K, CN_3O_6	NH_4, CN_3O_6
formula, sum	KCN_3O_6	CH_4NO_6
M / g mol^{-1}	189.14	168.08
crystal system	monoclinic	tetragonal
space group	$P2_1/n$ (no.14)	$P4_12_12$ (no.92)
a / Å	7.541(5)	6.7617(1)
b / Å	8.041(5)	6.7617(1)
c / Å	9.031(5)	12.7877(4)
α / °	90	90
β / °	99.334(5)	90
γ / °	90	90
V / Å^3	540.4(6)	584.66(2)
$\rho_{calc.}$ / g cm^{-3}	2.325(3)	1.9095(1)
F(000)	376	344
cell formula Z	4	4
space group Z	4	4
Z´	1	1
diffractometer	Oxford Xcalibur 3 CCD	Oxford Xcalibur 3 CCD
$\lambda_{Mo\ K\alpha}$ / Å	0.71073	0.71073
μ / mm^{-1}	0.197	0.197
T / K	200	100
reflections, collected	2580	2710
reflections, independent	998	588
R_{int}	0.0436	0.0173
parameter	100	72
R_1 [I > 2σ(I)]	0.0325	0.0209
wR_2 [I > 2σ(I)]	0.0663	0.0507
R_1 [all data]	0.0480	0.0243
wR_2 [all data]	0.0718	0.0523
S	1.048	1.096
$\Delta\rho_{max, min}$ / e Å^3	0.264, 0.246	0.210, 0.152
deposition no.	CSD - 417762	CSD - 417767

compound name	Hydrazinium nitroformate	Melaminium nitroformate
compound, abbrev.	HNF	MNF
formula, moiety	N_2H_5, CN_3O_6	$C_3H_7N_6$, CN_3O_6
formula, sum	$CH_5N_5O_6$	$C_4H_7N_9O_6$
M / g mol^{-1}	183.10	277.19
crystal system	monoclinic	monoclinic
space group	$P2_1/n$ (no.14)	$P2_1/n$ (no.14)
a / Å	8.0447(8)	5.8220(3)
b / Å	5.4420(5)	23.2249(18)
c / Å	14.5015(12)	7.2508(4)
α / °	90	90
β / °	98.785(8)	101.129(6)
γ / °	90	90
V / Å^3	627.4(1)	961.9(1)
$\rho_{calc.}$ / g cm^{-3}	1.938	1.6407(13)
F(000)	376	568
cell formula Z	4	4
space group Z	4	4
Z´	1	1
diffractometer	Oxford Xcalibur 3 CCD	Oxford Xcalibur 3 CCD
$\lambda_{Mo\ K\alpha}$ / Å	0.71073	0.71073
μ / mm^{-1}	0.196	0.175
T / K	100	100
reflections, collected	2734	5434
reflections, independent	1033	2057
R_{int}	0.0451	0.0373
parameter	343	200
R_1 [I > 2σ(I)]	0.0416	0.0588
wR_2 [I > 2σ(I)]	0.0560	0.1066
R_1 [all data]	0.0858	0.0864
wR_2 [all data]	0.0660	0.1164
S	1.004	1.113
$\Delta\rho_{max, min}$ / e Å^3	0.218, 0.247	0.301, 0.289
deposition no.	CSD - 417768	CSD - 417766

compound name	Melaminium nitroformate	Melaminium nitroformate, Dimethylsulfate, 1:1
compound, abbrev.	MNF	MNF · DMSO
formula, moiety	$C_3H_7N_6$, CN_3O_6	$C_3H_7N_6$, CN_3O_6 · $(CH_3)_2SO$
formula, sum	$C_4H_7N_9O_6$	$C_6H_{13}N_9O_7S$
M / g mol^{-1}	277.19	355.32
crystal system	monoclinic	triclinic
space group	$P2_1$ (no.4)	$P\bar{1}$ (no.2)
a / Å	9.2736(6)	9.966(5)
b / Å	7.2249(4)	10.920(5)
c / Å	15.660(1)	15.751(5)
α / °	90	108.257(5)
β / °	97.884(6)	90.342(5)
γ / °	90	116.274(5)
V / Å^3	1039.3(1)	1438.5(1)
$\rho_{calc.}$ / g cm^{-3}	1.771	1.6407(13)
F(000)	568	736
cell formula Z	4	4
space group Z	2	2
Z´	2	2
diffractometer	Oxford Xcalibur 3 CCD	Oxford Xcalibur 3 CCD
$\lambda_{Mo\ K\alpha}$ / Å	0.71073	0.71073
μ / mm^{-1}	0.162	0.282
T / K	100	100
reflections, collected	4182	11548
reflections, independent	1475	5583
R_{int}	0.0215	0.0434
parameter	343	420
R_1 [I > 2σ(I)]	0.0344	0.0662
wR_2 [I > 2σ(I)]	0.0783	0.1542
R_1 [all data]	0.0497	0.0956
wR_2 [all data]	0.0831	0.1683
S	0.962	0.957
$\Delta\rho_{max, min}$ / e Å^3	0.382, 0.244	0.019, 0.317
deposition no.	CSD - 417765	CSD - 417764

compound name	Melaminium nitroformate, Methanol, 1:1	Guanidinium nitroformate, Hydrate, 1:1
compound, abbrev.	MNF · MeOH	GNFH
formula, moiety	$C_3H_7N_6$, $CN_3O_6 \cdot CH_3OH$	CH_6N_3, $CN_3O_6 \cdot H_2O$
formula, sum	$C_5H_{11}N_9O_7$	$C_2H_8N_6O_7$
M / g mol^{-1}	309.23	228.14
crystal system	monoclinic	monoclinic
space group	$P2_1/c$ (no.14)	$C2/c$ (no.15)
a / Å	10.8294(19)	8.1859(4)
b / Å	5.8091(11)	14.3541(7)
c / Å	19.646(3)	7.7556(5)
α / °	90	90
β / °	95.82(1)	101.132(2)
γ / °	90	90
V / Å^3	1229.5(4)	894.1(1)
$\rho_{calc.}$ / g cm^{-3}	1.6706(5)	1.6948(2)
F(000)	640	472
cell formula Z	4	8
space group Z	4	4
Z′	1	0.5
diffractometer	Oxford Xcalibur 3 CCD	Nonius Kappa CCD
$\lambda_{Mo K\alpha}$ / Å	0.71073	0.71073
μ / mm^{-1}	0.152	0.167
T / K	100	200
reflections, collected	9950	5277
reflections, independent	1928	1021
R_{int}	0.1163	0.0937
parameters	193	87
R_1 [I > 2σ(I)]	0.1034	0.0513
wR_2 [I > 2σ(I)]	0.2025	0.1293
R_1 [all data]	0.1424	0.0645
wR_2 [all data]	0.2294	0.1395
S	1.223	1.072
$\Delta\rho_{max, min}$ / e Å^3	0.305, 0.308	0.293, 0.433
deposition no.	CSD - 417763	CSD - 417769

compound name	Aminoguanidinium nitroformate	Diaminoguanidinium nitroformate
compound, abbrev.	AGNF	DAGNF
formula, moiety	CH_7N_4, CN_3O_6	CH_8N_5, CN_3O_6
formula, sum	$C_2H_7N_7O_6$	$C_2H_8N_8O_6$
M / g mol^{-1}	225.15	240.16
crystal system	triclinic	monoclinic
space group	P-1(no.2)	$P2_1/n$ (no.14)
a / Å	5.0690(7)	10.980(1)
b / Å	7.5590(10)	7.7524(8)
c / Å	11.3200(11)	11.415(1)
α / °	84.567(9)	90
β / °	84.425(9)	105.336(8)
γ / °	79.609(11)	90
V / Å^3	423.2(1)	937.1(2)
$\rho_{calc.}$ / g cm^{-3}	1.7665(4)	1.7022(3)
F(000)	232	496
cell formula Z	2	4
space group Z	2	4
Z´	1	1
diffractometer	Oxford Xcalibur 3 CCD	Oxford Xcalibur 3 CCD
$\lambda_{Mo\ K\alpha}$ / Å	0.71073	0.71073
μ / mm^{-1}	0.170	0.162
T / K	200	200
reflections, collected	4264	9138
reflections, independent	1657	1832
R_{int}	0.0169	0.0324
parameter	164	178
R_1 [I > 2σ(I)]	0.0312	0.0465
wR_2 [I > 2σ(I)]	0.0748	0.1022
R_1 [all data]	0.0346	0.0602
wR_2 [all data]	0.0773	0.1107
S	1.086	1.172
$\Delta\rho_{max, min}$ / e Å^3	0.181, 0.278	0.282, 0.194
deposition no.	CSD - 417771	CSD - 417772

compound name	Triaminoguanidinium nitroformate	Melaminium dinitrate
compound, abbrev.	TAGNF	MDN
formula, moiety	CH_9N_6, CN_3O_6	$C_3H_8N_6$, $2(NO_3)$
formula, sum	$C_2H_9N_9O_6$	$C_3H_8N_8O_6$
M / g mol^{-1}	255.18	252.17
crystal system	triclinic	monoclinic
space group	P-1(no.2)	$P2_1/c$ (no.14)
a / Å	8.020(2)	7.758(5)
b / Å	8.347(2)	9.804(5)
c / Å	8.515(2)	12.094(5)
α / °	105.49(2)	90
β / °	95.03(2)	100.526(5)
γ / °	111.10(2)	90
V / Å^3	501.7(2)	904.4(8)
$\rho_{calc.}$ / g cm^{-3}	1.6892(7)	1.8521(16)
F(000)	264	520
cell formula Z	2	4
space group Z	2	4
Z´	1	1
diffractometer	Oxford Xcalibur 3 CCD	Oxford Xcalibur 3 CCD
$\lambda_{Mo\ K\alpha}$ / Å	0.71073	0.71073
μ / mm^{-1}	0.159	0.173
T / K	200	200
reflections, collected	2634	10088
reflections, independent	1962	2084
R_{int}	0.019	0.0694
parameter	190	186
R_1 [I > 2σ(I)]	0.0379	0.0647
wR_2 [I > 2σ(I)]	0.0970	0.1402
R_1 [all data]	0.0476	0.0896
wR_2 [all data]	0.1041	0.1575
S	1.070	1.185
$\Delta\rho_{max, min}$ / e Å^3	0.215, 0.301	0.273, 0.318
deposition no.	CSD - 417770	-

compound name	Guanidinium nitrate, Azidoformamidinium nitrate, 1:1	Guanidinium diaminopicrate
compound, abbrev.	GN · AFN	GDAP
formula, moiety	CH_4N_5, CH_6N_3, $2(NO_3)$	$C_6\ H_4\ N_5\ O_7$, $C\ H_6\ N_3$
formula, sum	$C_2H_{10}N_{10}O_6$	$C_7\ H_{10}\ N_8\ O_7$
M / g mol^{-1}	270.20	318.23
crystal system	monoclinic	monoclinic
space group	$P2_1/c$ (no.14)	$C2/c$
a / Å	11.7413(4)	12.688(3)
b / Å	6.8897(3)	13.536(3)
c / Å	13.6195(4)	6.8422(14)
α / °	90.00	90
β / °	102.593(3)	102.45(3)
γ / °	90.00	90
V / Å^3	1075.23(7)	1147.4(5)
$\rho_{calc.}$ / g cm^{-3}	1.6692(1)	1.8422(8)
$F(000)$	560	656
cell formula Z	4	4
space group Z	4	8
Z´	1	0.5
diffractometer	Oxford Xcalibur 3 CCD	Nonius Kappa CCD
$\lambda_{Mo\ K\alpha}$ / Å	0.71073	0.71073
μ / mm^{-1}	0.156	0.164
T / K	100	200
reflections, collected	5638	2157
reflections, independent	2110	1119
R_{int}	0.0217	0.0248
parameter	203	123
R_1 [I > 2σ(I)]	0.0260	0.0562
wR_2 [I > 2σ(I)]	0.0582	0.1450
R_1 [all data]	0.0375	0.0783
wR_2 [all data]	0.0604	0.1628
S	0.922	1.032
$\Delta\rho_{max,\ min}$ / e Å^3	0.165, 0.202	0.511, 0.399
deposition no.	-	-

compound name	Aminoguanidinium diaminopicrate	Diaminoguanidinium diaminopicrate
compound, abbrev.	AGDAP	DAGDAP
formula, moiety	$C_6 H_4 N_5 O_7$, $C H_7 N_4$	$C_6 H_4 N_5 O_7$, $C H_8 N_5$
formula, sum	$C_7 H_{11} N_9 O_7$	$C_7 H_{12} N_{10} O_7$
M / g mol^{-1}	333.25	348.27
crystal system	monoclinic	monoclinic
space group	$P2_1/c$	$P2_1/n$
a / Å	9.6745(10)	14.111(5)
b / Å	7.2308(10)	6.656(5)
c / Å	18.0315(18)	14.171(5)
α / °	90.00	90.000(5)
β / °	91.525(9)	103.257(5)
γ / °	90.00	90.000(5)
V / Å^3	1260.9(3)	1295.5(12)
$\rho_{calc.}$ / g cm^{-3}	1.7555(4)	1.7856(17)
$F(000)$	688	720
cell formula Z	4	4
space group Z	4	4
Z´	1	1
diffractometer	Oxford Xcalibur 3 CCD	Oxford Xcalibur 3 CCD
$\lambda_{Mo K\alpha}$ / Å	0.71073	0.71073
μ / mm^{-1}	0.156	0.158
T / K	200	200
reflections, collected	6265	11771
reflections, independent	2474	2560
R_{int}	0.0659	0.1412
parameter	253	
R_1 [I > 2σ(I)]	0.0710	0.0624
wR_2 [I > 2σ(I)]	0.1316	0.0827
R_1 [all data]	0.1324	0.1691
wR_2 [all data]	0.1638	0.1163
S	1.094	1.011
$\Delta\rho_{max, min}$ / e Å^3	0.497, 0.273	0.326, 0.293
deposition no.	-	-

compound name	Triaminoguanidinium diaminopicrate, hydrate	1,2,4,5-Tetrahydro-3,6-diamino-1,2,4,5-tetrazinium chlorid
compound, abbrev.	TAGDAP · H_2O	4H-ATCl
formula, moiety	C_6 H_4 N_5 O_7, C H_9 N_6, H_2 O	C_2 H_8 N_6, 2(Cl)
formula, sum	C_7 H_{15} N_{11} O_8	C_2 H_8 Cl_2 N_6
M / g mol^{-1}	381.30	187.04
crystal system	monoclinic	triclinic
space group	$P2_1/n$	P-1 (no.2)
a / Å	12.8432(5)	7.2122(6)
b / Å	6.8676(3)	7.3472(5)
c / Å	17.1507(7)	7.4770(6)
α / °	90.00	100.661(6)
β / °	108.969(4)	98.192(6)
γ / °	90.00	110.426(7)
V / Å^3	1430.58(10)	355.54(5)
$\rho_{calc.}$ / g cm^{-3}	1.7704(1)	1.7472(2)
F(000)	792	192
cell formula Z	4	2
space group Z	4	2
Z´	1	1
diffractometer	Oxford Xcalibur 3 CCD	Oxford Xcalibur 3 CCD
$\lambda_{Mo\ K\alpha}$ / Å	0.71073	0.71073
μ / mm^{-1}	0.158	0.845
T / K	100	100
reflections, collected	8809	3353
reflections, independent	3241	1266
R_{int}	0.0392	0.0210
parameter		115
R_1 [I > 2σ(I)]	0.0407	0.0243
wR_2 [I > 2σ(I)]	0.0792	0.0583
R_1 [all data]	0.0761	0.0337
wR_2 [all data]	0.0917	0.0613
S	0.988	1.047
$\Delta\rho_{max, min}$ / e Å^3	0.303, 0.236	0.274, 0.226
deposition no.	-	-

compound name	1-Methyl-5-(*N*-methyl)-aminotetrazolium perchlorate	2,2,2-Trinitroethanol
compound, abbrev.		TNE
formula, moiety	$C_3 H_8 N_5$, Cl O_4	$C_2 H_3 N_3 O_7$
formula, sum	$C_3 H_8$ Cl $N_5 O_4$	$C_2 H_3 N_3 O_7$
M / g mol^{-1}	213.59	181.07
crystal system	orthorhombic	monoclinic
space group	$P2_12_12_1$ (no.19)	$P2_1/c$ (no.14)
a / Å	5.7472(2)	6.1242(4)
b / Å	12.0965(4)	18.8223(7)
c / Å	12.4377(4)	11.7466(4)
α / °	90	90.00
β / °	90	104.962(3)
γ / °	90	90.00
V / Å^3	864.68(5)	1308.14(11)
$\rho_{calc.}$ / g cm^{-3}	1.6408(1)	1.8388(2)
F(000)	440	736
cell formula Z	4	8
space group Z	4	4
Z´	1	2
diffractometer	Oxford Xcalibur 3 CCD	Oxford Xcalibur 3 CCD
$\lambda_{Mo K\alpha}$ / Å	0.71073	0.71073
μ / mm^{-1}	0.437	0.190
T / K	100	100
reflections, collected	2366	13153
reflections, independent	1488	2566
R_{int}	0.0183	0.0300
parameter	126	241
R_1 [I > 2σ(I)]	0.0313	0.0371
wR_2 [I > 2σ(I)]	0.0889	0.0874
R_1 [all data]	0.0347	0.0432
wR_2 [all data]	0.0909	0.0919
S	1.081	1.130
$\Delta\rho_{max, min}$ / e Å^3	0.380, 0.473	0.214, 0.181
deposition no.	-	

compound name	Bis-(2,2,2-trinitroethyl)-amine	N^1-(2,2,2-Trinitroethyl)-1*H*-tetrazole-1,5-diamine
compound, abbrev.	BTNA	TTD
formula, moiety	$C_4 H_5 N_7 O_{12}$	$C_3 H_5 N_9 O_6$
formula, sum	$C_4 H_5 N_7 O_{12}$	$C_3 H_5 N_9 O_6$
M / g mol^{-1}	343.15	263.16
crystal system	orthorhombic	orthorhombic
space group	*Pbca* (no.61)	$Pna2_1$
a / Å	12.8907(3)	14.9692(6)
b / Å	11.7069(3)	10.0155(5)
c / Å	16.0622(5)	6.3729(3)
α / °	90	90.00
β / °	90	90.00
γ / °	90	90.00
V / Å^3	2423.95(11)	955.45(8)
$\rho_{calc.}$ / g cm^{-3}	1.8806(1)	1.8295(2)
$F(000)$	1392	536
cell formula Z	8	4
space group Z	8	4
Z´	1	1
diffractometer	Oxford Xcalibur 3 CCD	Oxford Xcalibur 3 CCD
$\lambda_{Mo K\alpha}$ / Å	0.71073	0.71073
μ / mm^{-1}	0.190	0.171
T / K	200	100
reflections, collected	13680	5914
reflections, independent	2305	1704
R_{int}	0.0246	0.0517
parameter	229	175
R_1 [I > 2σ(I)]	0.0392	0.0354
wR_2 [I > 2σ(I)]	0.1163	0.0616
R_1 [all data]	0.0470	0.0650
wR_2 [all data]	0.1095	0.0705
S	1.060	0.944
$\Delta\rho_{max, min}$ / e Å^3	0.238, 0.230	0.276, 0.273
deposition no.	CCDC - 699142	CCDC - 699140

compound name	N^1,N^5-Bis-(2,2,2-trinitroethyl)-1H-tetrazole-1,5-diamine	(E)-1-methyl-1-(1*H*-tetrazol-5-yl)-2-(2,2,2-trinitroethylidene)-hydrazine
compound, abbrev.	BTTD	MTTH
formula, moiety	$C_5H_6N_{12}O_{12}$	$C_4H_5N_9O_6$
formula, sum	$C_5H_6N_{12}O_{12}$	$C_4H_5N_9O_6$
M / g mol^{-1}	426.22	275.17
crystal system	monoclinic	orthorhombic
space group	$P2_1/c$ (no.14)	*Pbca*(no.61)
a / Å	9.9710(7)	9.7012(4)
b / Å	6.4861(4)	12.8504(7)
c / Å	23.1501(13)	17.3758(9)
α / °	90	90
β / °	94.464(5)	90
γ / °	90	90
V / Å^3	1492.64(16)	2166.14(19)
$\rho_{calc.}$ / g cm^{-3}	1.8967(2)	1.6876(1)
F(000)	864	1120
cell formula Z	4	8
space group Z	4	8
Z´	1	1
diffractometer	Oxford Xcalibur 3 CCD	Oxford Xcalibur 3 CCD
$\lambda_{Mo\ K\alpha}$ / Å	0.71073	0.71073
μ / mm^{-1}	0.184	0.155
T / K	100	100
reflections, collected	8094	8573
reflections, independent	2944	1784
R_{int}	0.0525	0.1493
parameter	280	172
R_1 [I > 2σ(I)]	0.0844	0.0779
wR_2 [I > 2σ(I)]	0.1145	0.1570
R_1 [all data]	0.1243	0.1457
wR_2 [all data]	0.1264	0.1942
S	1.216	1.076
$\Delta\rho_{max, min}$ / e Å^3	0.327, 0.334	0.423, 0.425
deposition no.	CCDC - 699136	-

compound name	1-Methyl-5-(1-methyl-2-(2,2,2-trinitroethyl)hydrazinyl)-1H-tetrazole	2-(5-(1-Methyl-2-(2,2,2-trinitroethyl)hydrazinyl)-1H-tetrazol-1-yl)ethanol
compound, abbrev.	MMTHT	MTHTE
formula, moiety	$C_5H_9N_9O_6$	$C_5H_{11}N_9O_7$
formula, sum	$C_5H_9N_9O_6$	$C_5H_{11}N_9O_7$
M / g mol^{-1}	291.21	321.21
crystal system	triclinic	monoclinic
space group	$P\bar{1}$ (no.2)	$P2_1/c$ (no.14)
a / Å	7.2651(13)	13.0419(4)
b / Å	7.5773(16)	7.3020(2)
c / Å	11.695(7)	14.8002(5)
α / °	102.89(3)	90
β / °	103.82(3)	112.118(4)
γ / °	99.387(17)	90
V / Å^3	593.3(4)	1305.73(7)
$\rho_{calc.}$ / g cm^{-3}	1.6301(11)	1.6341(1)
F(000)	300	664
cell formula Z	2	4
space group Z	2	4
Z´	1	1
diffractometer	Oxford Xcalibur 3 CCD	Oxford Xcalibur 3 CCD
$\lambda_{Mo\ K\alpha}$ / Å	0.71073	0.71073
μ / mm^{-1}	0.146	0.147
T / K	100	100
reflections, collected	5201	8966
reflections, independent	2299	2813
R_{int}	0.0225	0.0237
parameter	217	243
R_1 [I > 2σ(I)]	0.0293	0.0286
wR_2 [I > 2σ(I)]	0.0678	0.0682
R_1 [all data]	0.0426	0.0425
wR_2 [all data]	0.0716	0.0732
S	0.943	1.017
$\Delta\rho_{max, min}$ / e Å^3	0.204, 0.229	0.231, 0.218
deposition no.	-	-

compound name	1-(^{4}N-2,2,2-Trinitroethyl)-2,5-hydroxymethyl-triazine	N^3,N^6-Bis-(2,2,2-trinitroethyl)-3,6-diamino-1,2,4,5-tetrazine
compound, abbrev.	THMT	BTAT
formula, moiety	$C_5H_9N_7O_8$	$C_6H_6N_{12}O_{12}$
formula, sum	$C_5H_9N_7O_8$	$C_6H_6N_{12}O_{12}$
M / g mol^{-1}	307.20	438.23
crystal system	monoclinic	orthorhombic
space group	$P2_1/n$ (no.14)	$Pna2_1$
a / Å	9.1753(4)	23.3824(8)
b / Å	10.3168(4)	5.9271(2)
c / Å	13.0862(5)	11.1373(3)
α / °	90.00	90
β / °	105.975(4)	90
γ / °	90.00	90
V / Å^3	1190.90(9)	1543.52(9)
$\rho_{calc.}$ / g cm^{-3}	1.7134(1)	1.8858(1)
F(000)	632	888
cell formula Z	4	4
space group Z	4	4
Z´	1	1
diffractometer	Oxford Xcalibur 3 CCD	Oxford Xcalibur 3 CCD
$\lambda_{Mo\ K\alpha}$ / Å	0.71073	0.71073
μ / mm^{-1}	0.158	0.181
T / K	100	100
reflections, collected	7201	11060
reflections, independent	2702	2339
R_{int}	0.0313	0.0219
parameter	226	279
R_1 [I > 2σ(I)]	0.0315	0.0269
wR_2 [I > 2σ(I)]	0.0620	0.0685
R_1 [all data]	0.0593	0.0329
wR_2 [all data]	0.0690	0.0710
S	0.899	1.029
$\Delta\rho_{max, min}$ / e Å^3	0.256, 0.279	0.326, 0.200
deposition no.	-	CCDC - 699141

compound name	S-Ethyl-2,2,2-trinitroethyl-thioformate	Bis-(2,2,2-trinitroethyl)-carbonate
compound, abbrev.		BTC
formula, moiety	$C_5 H_7 N_3 O_8 S$	$C_5 H_4 N_6 O_{15}$
formula, sum	$C_5 H_7 N_3 O_8 S$	$C_5 H_4 N_6 O_{15}$
M / g mol^{-1}	269.21	388.14
crystal system	triclinic	orthorhombic
space group	*P*-1 (no.2)	*Pbca* (no.61)
a / Å	7.9304(6)	10.8828(2)
b / Å	11.8342(11)	11.4746(2)
c / Å	12.2221(12)	20.9073(4)
α / °	67.067(9)	90.00
β / °	88.073(7)	90.00
γ / °	87.634(7)	90.00
V / Å^3	1055.29(16)	2610.81(8)
$\rho_{calc.}$ / g cm^{-3}	1.6944(3)	1.9750(1)
$F(000)$	552	1568
cell formula Z	4	8
space group Z	2	8
Z´	2	1
diffractometer	Oxford Xcalibur 3 CCD	Oxford Xcalibur 3 CCD
$\lambda_{Mo K\alpha}$ / Å	0.71073	0.71073
μ / mm^{-1}	0.346	0.204
T / K	100	100
reflections, collected	6814	12846
reflections, independent	6814	3795
R_{int}	0.0893	0.0247
parameter	324	251
R_1 [I > 2σ(I)]	0.0356	0.0272
wR_2 [I > 2σ(I)]	0.0658	0.0617
R_1 [all data]	0.0690	0.0445
wR_2 [all data]	0.0717	0.0681
S	0.788	0.993
$\Delta\rho_{max, min}$ / e Å^3	0.320, 0.238	0.377, 0.244
deposition no.	-	

compound name	2,2,2-Trinitroethyl-azidoformate	Bis-(2,2,2-trinitroethyl)-hydrazodicarboxylate, Acetone, 1:1
compound, abbrev.	TAF	BTHC · Acetone
formula, moiety	$C_3 H_2 N_6 O_8$	$C_6 H_6 N_8 O_{16}$, $C_3 H_6 O$
formula, sum	$C_3 H_2 N_6 O_8$	C9 H12 N8 O17
M / g mol^{-1}	250.11	504.27
crystal system	monoclinic	triclinic
space group	$P2_1/c$ (no.14)	$P\bar{1}$ (no.2)
a / Å	7.3139(3)	10.1798(13)
b / Å	13.0430(6)	10.4185(17)
c / Å	18.8050(7)	11.256(3)
α / °	90.00	63.448(19)
β / °	91.273(4)	70.392(13)
γ / °	90.00	89.865(12)
V / Å^3	1793.46(13)	990.4(4)
$\rho_{calc.}$ / g cm^{-3}	1.8526(1)	1.6910(7)
F(000)	1008	516.0
cell formula Z	8	2
space group Z	4	2
Z′	2	1
diffractometer	Oxford Xcalibur 3 CCD	Oxford Xcalibur 3 CCD
$\lambda_{Mo K\alpha}$ / Å	0.71073	0.71073
μ / mm^{-1}	0.184	0.166
T / K	100	100
reflections, collected	8785	29458
reflections, independent	3244	6588
R_{int}	0.0657	0.0329
parameter	323	355
R_1 [I > 2σ(I)]	0.0830	0.0366
wR_2 [I > 2σ(I)]	0.1016	0.0849
R_1 [all data]	0.1341	0.0718
wR_2 [all data]	0.1166	0.1006
S	1.312	1.044
$\Delta\rho_{max, min}$ / e Å^3	0.374, 0.488	0.361, 0.294
deposition no.	CCDC - 699137	CCDC - 699138

compound name	Bis-(2,2,2-trinitroethyl)-hydrazodicarboxylate, Ethylacetate, 1:1	2-amino-4,6-dimethyl -1,3,5-triazine, Guanidine, 1:1
compound, abbrev.	BTHC · EtOAc	ADMT · Guanidine
formula, moiety	$C_6 H_6 N_8 O_{16}$, $C_4 H_8 O_2$	$C_5H_8N_4$, $C_1H_5N_3$
formula, sum	$C_{10} H_{14} N_8 O_{18}$	$C_6H_{13}N_7$
M / g mol^{-1}	534.29	183.23
crystal system	triclinic	monoclinic
space group	P-1 (no.2)	$P2_1/c$ (no.14)
a / Å	10.2012(7)	9.9182(3)
b / Å	11.3283(4)	4.8503(2)
c / Å	11.4482(6)	18.8708(7)
α / °	63.977(4)	90
β / °	64.955(6)	91.382(3)
γ / °	87.713(4)	90
V / Å^3	1059.65(10)	907.54(6)
$\rho_{calc.}$ / g cm^{-3}	1.6746(2)	1.3411(1)
F(000)	548	392
cell formula Z	2	4
space group Z	2	4
Z′	1	1
diffractometer	Oxford Xcalibur 3 CCD	Oxford Xcalibur 3 CCD
$\lambda_{Mo K\alpha}$ / Å	0.71073	0.71073
μ / mm^{-1}	0.163	0.094
T / K	100	100
reflections, collected	9707	4341
reflections, independent	4140	1755
R_{int}	0.0201	0.0193
parameter	349	170
R_1 [I > 2σ(I)]	0.0361	0.0327
wR_2 [I > 2σ(I)]	0.1014	0.0770
R_1 [all data]	0.0452	0.0499
wR_2 [all data]	0.1055	0.0837
S	1.102	0.969
$\Delta\rho_{max, min}$ / e Å^3	0.384, 0.370	0.145, 0.196
deposition no.	CCDC - 699139	CCDC - 642807

a) ADMT = 2-amino-4,6-dimethyl-1,3,5-triazine

compound name	2-amino-4,6-dimethyl -1,3,5-triazine, 2 Guanidine, 1:2	N^5-trimethylsilyl-1,5-diamino-1H-tetrazole
compound, abbrev.	ADMT · 2 Guanidine	5-TMSD
formula, moiety	$C_5H_8N_4$, 2($C_1H_5N_3$)	$C_4H_{12}N_6Si$
formula, sum	$C_7H_{18}N_{10}$	$C_4H_{12}N_6Si$
M / g mol^{-1}	242.31	172.29
crystal system	monoclinic	monoclinic
space group	$P2_1/c$ (no.14)	$P2_1/c$ (no.14)
a / Å	6.5743(2)	12.767(3)
b / Å	23.7968(7)	5.9889(12)
c / Å	7.8931(2)	11.752(2)
α / °	90.00	89.951(17)
β / °	96.373(2)	90.773(17)
γ / °	90.00	89.991(16)
V / Å^3	1227.22(6)	898.4(3)
$\rho_{calc.}$ / g cm^{-3}	1.3115(1)	1.2738(4)
F(000)	520	368
cell formula Z	4	4
space group Z	4	4
Z´	1	1
diffractometer	Oxford Xcalibur 3 CCD	Oxford Xcalibur 3 CCD
$\lambda_{Mo\ K\alpha}$ / Å	0.71073	0.71073
μ / mm^{-1}	0.094	0.214
T / K	100	100
reflections, collected	12408	774
reflections, independent	2148	327
R_{int}	0.0385	0.1090
parameter	204	112
R_1 [I > 2σ(I)]	0.0412	0.0680
wR_2 [I > 2σ(I)]	0.0992	0.1441
R_1 [all data]	0.0691	0.0966
wR_2 [all data]	0.1144	0.1599
S	1.024	1.187
$\Delta\rho_{max, min}$ / e Å^3	0.201, 0.247	0.192, 0.223
deposition no.	CCDC - 642808	-

b) ADMT = 2-amino-4,6-dimethyl-1,3,5-triazine

compound name	N^1,N^5-bis(trimethylsilyl)-1,5-diamino-1H-tetrazole	N^1-(propan-2-ylidene)-1,5-diamino-1H-tetrazole
compound, abbrev.	1,5-BTMSD	1-PYD
formula, moiety	$C_7 H_{20} N_6 Si_2$	$C_4 H_2 D_6 N_6$
formula, sum	$C_7 H_{20} N_6 Si_2$	$C_4 H_2 D_6 N_6$
M / g mol^{-1}	244.47	146.18
crystal system	monoclinic	monoclinic
space group	$P2_1/n$ (no.14)	$P2_1/c$ (no.14)
a / Å	14.6063(7)	7.4859(3)
b / Å	6.4066(3)	7.4334(2)
c / Å	15.0847(9)	11.9822(4)
α / °	90.00	90.00
β / °	100.568(5)	97.308(3)
γ / °	90.00	90.00
V / Å^3	1387.63(12)	661.34(4)
$\rho_{calc.}$ / g cm^{-3}	1.1702(1)	1.4681(1)
F(000)	528	296
cell formula Z	4	4
space group Z	4	4
Z´	1	1
diffractometer	Oxford Xcalibur 3 CCD	Oxford Xcalibur 3 CCD
$\lambda_{Mo K\alpha}$ / Å	0.71073	0.71073
μ / mm^{-1}	0.239	0.102
T / K	100	100
reflections, collected	13361	6449
reflections, independent	4562	2163
R_{int}	0.0433	0.0217
parameter	216	123
R_1 [I > 2σ(I)]	0.0359	0.0342
wR_2 [I > 2σ(I)]	0.0750	0.0839
R_1 [all data]	0.0787	0.0500
wR_2 [all data]	0.0931	0.0892
S	0.988	0.995
$\Delta\rho_{max, min}$ / e Å^3	0.487, 0.601	0.231, 251
deposition no.	-	-

compound name	N^1,N^1-bis-(trimethylsilyl)-1,5-diamino-1H-tetrazole	N^1,N^1,N^5-tris(trimethylsilyl)-1,5-diamino-1H-tetrazole
compound, abbrev.	1,1-BTMSD	1,1,5-TTMSD
formula, moiety	$C_7 H_{20} N_6 Si_2$	$C_{10}H_{28}N_6Si_3$
formula, sum	$C_7 H_{20} N_6 Si_2$	$C_{10}H_{28}N_6Si_3$
M / g mol^{-1}	244.47	316.65
crystal system	triclinic	monoclinic
space group	P-1 (no.2)	$P2_1/c$ (no.14)
a / Å	6.3649(10)	9.5490(4)
b / Å	8.0322(16)	17.1449(6)
c / Å	14.026(2)	11.8672(4)
α / °	93.961(14)	90.00
β / °	97.427(13)	94.643(4)
γ / °	105.416(15)	90.00
V / Å^3	681.5(2)	1936.48(12)
$\rho_{calc.}$ / g cm^{-3}	1.1914(3)	1.0861(1)
F(000)	264	688
cell formula Z	2	4
space group Z	2	4
Z′	1	1
diffractometer	Oxford Xcalibur 3 CCD	Oxford Xcalibur 3 CCD
$\lambda_{Mo K\alpha}$ / Å	0.71073	0.71073
μ / mm^{-1}	0.244	0.244
T / K	100	100
reflections, collected	4812	14750
reflections, independent	1870	4281
R_{int}	0.1030	0.0494
parameter	144	176
R_1 [I > 2σ(I)]	0.0879	0.0403
wR_2 [I > 2σ(I)]	0.1214	0.0813
R_1 [all data]	0.1530	0.0818
wR_2 [all data]	0.1425	0.1001
S	1.177	1.030
$\Delta\rho_{max, min}$ / e Å^3	0.411, 0.371	0.333, 0.274
deposition no.	-	-

compound name	3,4,6-Trichlor-pyridazine	3,4,5,6-Tetrachlor-pyridazine
compound, abbrev.	3,4,6-TCP	3,4,5,6-TCP
formula, moiety	C_4 H Cl_3 N_2	C_4 Cl_4 N_2
formula, sum	C_4 H Cl_3 N_2	C_4 Cl_4 N_2
M / g mol^{-1}	183.42	217.86
crystal system	orthorhombic	tetragonal
space group	*Pbca* (no.61)	$P4_12_12$ (no.92)
a / Å	10.571(5)	5.2649(2)
b / Å	7.243(5)	5.2649(2)
c / Å	17.302(5)	52.351(2)
α / °	90.0	90
β / °	90.0	90
γ / °	90.0	90
V / Å^3	1324.7(12)	1451.10(10)
$\rho_{calc.}$ / g cm^{-3}	1.8394(17)	1.9944(1)
F(000)	720	848
cell formula Z	8	8
space group Z	8	4
Z´	1	2
diffractometer	Oxford Xcalibur 3 CCD	Oxford Xcalibur 3 CCD
$\lambda_{Mo\ K\alpha}$ / Å	0.71073	0.71073
μ / mm^{-1}	1.280	1.542
T / K	100	100
reflections, collected	12166	13078
reflections, independent	1278	1299
R_{int}	0.0264	0.0972
parameter	86	91
R_1 [I > 2σ(I)]	0.0292	0.0770
wR_2 [I > 2σ(I)]	0.0713	0.1411
R_1 [all data]	0.0301	0.0772
wR_2 [all data]	0.0720	0.1412
S	1.169	1.138
$\Delta\rho_{max, min}$ / e Å^3	0.206, 0.240	0.382, 0.383
deposition no.	-	-

compound name	4-Azido-3,6-dichlor-pyridazine	4,6-Dichloro-3(2H)-pyridazinone
compound, abbrev.	4-A,3,6-DCP	DCP
formula, moiety	C_4 H Cl_2 N_5	C_4 H_2 Cl_2 N_2 O
formula, sum	C_4 H Cl_2 N_5	C_4 H_2 Cl_2 N_2 O
M / g mol^{-1}	190.00	164.98
crystal system	orthorhombic	monoclinic
space group	$P2_12_12_1$ (no.19)	$P2_1/n$ (no.14)
a / Å	4.4512(6)	5.1841(2)
b / Å	10.5426(12)	8.8456(4)
c / Å	14.9866(17)	13.5868(5)
α / °	90.0	90.00
β / °	90.0	100.264(4)
γ / °	90.0	90.00
V / Å^3	703.28(15)	613.07(4)
$\rho_{calc.}$ / g cm^{-3}	1.7945(4)	1.7874(1)
F(000)	376	328
cell formula Z	4	4
space group Z	4	4
Z´	1	1
diffractometer	Oxford Xcalibur 3 CCD	Oxford Xcalibur 3 CCD
$\lambda_{Mo\ K\alpha}$ / Å	0.71073	0.71073
μ / mm^{-1}	0.854	0.962
T / K	100	100
reflections, collected	7079	8850
reflections, independent	1374	2054
R_{int}	0.0431	0.0412
parameter	104	90
R_1 [I > 2σ(I)]	0.0353	0.0342
wR_2 [I > 2σ(I)]	0.0740	0.0706
R_1 [all data]	0.0374	0.0655
wR_2 [all data]	0.0753	0.0813
S	1.101	1.042
$\Delta\rho_{max, min}$ / e Å^3	0.232, 0.202	0.430, 0.314
deposition no.	-	-

compound name	Mercuryfulminate	Hexaazidocyclo-triphosphazene
compound, abbrev.	$Hg(CNO)_2$	P_3N_{21}
formula, moiety	$C_2 N_2 O_2 Hg$	P_3N_{21}
formula, sum	$C_2 N_2 O_2 Hg$	P_3N_{21}
M / g mol^{-1}	284.63	387.12
crystal system	orthorhombic	triclinic
space group	*Cmce* (no.64)	*P*-1 (no.2)
a / Å	5.3549(2)	7.1953(9)
b / Å	10.4585(5)	7.3718(9)
c / Å	7.5579(4)	12.9942(15)
α / °	90.00	87.432(10)
β / °	90.00	78.955(10)
γ / °	90.00	89.592(10)
V / Å^3	423.27(3)	675.80(14)
$\rho_{calc.}$ / g cm^{-3}	4.467	1.9024(4)
$F(000)$	488	384
cell formula Z	4	2
space group Z	8	2
Z´	0.5	1
diffractometer	Oxford Xcalibur 3 CCD	Oxford Xcalibur 3 CCD
$\lambda_{Mo\ K\alpha}$ / Å	0.71073	0.71073
μ / mm^{-1}	36.220	0.486
T / K	100	100
reflections, collected	4428	6935
reflections, independent	257	2657
R_{int}	0.0418	0.0438
parameter	23	217
R_1 [I > 2σ(I)]	0.0111	0.0388
wR_2 [I > 2σ(I)]	0.0241	0.0947
R_1 [all data]	0.0202	0.0505
wR_2 [all data]	0.0250	0.1027
S	0.906	1.062
$\Delta\rho_{max, min}$ / e Å^3	0.478, 0.621	0.351, 0.340
deposition no.	CSD - 417930	CSD - 416415

compound name	Chlortrinitromethane
compound, abbrev.	Cl-TNM
formula, moiety	$C\,Cl\,N_3\,O_6$
formula, sum	$C\,Cl\,N_3\,O_6$
M / g mol^{-1}	185.49
crystal system	monoclinic
space group	$P2_1/c$ (no.14)
a / Å	10.3347(5)
b / Å	5.7397(1)
c / Å	10.3885(2)
α / °	90.00
β / °	106.53(1)
γ / °	90.00
V / Å^3	590.76(4)
$\rho_{calc.}$ / g cm^{-3}	2.0856(1)
$F(000)$	368
cell formula Z	4
space group Z	4
Z´	1
diffractometer	Oxford Xcalibur 3 CCD
$\lambda_{Mo\,K\alpha}$ / Å	0.71073
μ / mm^{-1}	0.639
T / K	100
reflections, collected	6349
reflections, independent	1031
R_{int}	0.0916
parameter	100
R_1 [I > 2σ(I)]	0.0305
wR_2 [I > 2σ(I)]	0.0774
R_1 [all data]	0.0323
wR_2 [all data]	0.0792
S	1.056
$\Delta\rho_{max,\,min}$ / e Å^3	0.319, 0.348
deposition no.	CSD - 705645

4.8 Bibliography

Scientific Journals

16* The unique role of the nitro group in intramolecular interactions: chloronitromethanes,
Laura Macaveiu, Michael Göbel, Thomas M. Klapötke, Jane S. Murray, and Peter Politzer,
Struct. Chem. **2010**, *21*, 139-146.

15 Does $[I_3]^+$ act as an '$[I]^+$' donor to CH_3CN and N_2O? Structure of $[H_3CCN\text{-}I\text{-}NCCH_3]^+[AsF_6]^-$,
Margaret-Jane Crawford, Michael Göbel, Thomas M. Klapötke, Konstantin Karaghiosoff, and Jan Welch,
Inorg. Chem. **2009**, *48*, 9983-9985.

14* Reaction force analyses of nitro-aci tautomerizations of trinitromethane, the elusive trinitromethanol, picric acid and 2,4-dinitro-1H-imidazole,
Jane S. Murray, Pat Lane, Michael Göbel, Thomas M. Klapötke, and Peter Politzer,
Theor. Chem. Acc. **2009**, *124*, 355-363.

13* Chlorotrinitromethane and its exceptional short carbon chlorine bond,
Michael Göbel, Boris H. Tchitchanov, Jane S. Murray, Peter Politzer and Thomas M. Klapötke,
Nature Chem. **2009**, 1, 229-235.

12* Electrostatic intra- and intermolecular interactions and their significance on structure, acidity and tautomerisation of trinitromethane.
Jane S. Murray, Pat Lane, Michael Göbel, Thomas M. Klapötke, and Peter Politzer,
J. Chem. Phys. **2009**, 130(10), 104304-1 – 104304-6.

11* (Feature Article / VIP)
Development and testing of energetic materials: the concept of high densities based on the trinitroethyl functionality,
Michael Göbel and Thomas M. Klapötke,
Adv. Funct. Mater. **2009**, 19, 347-365.

Note. * published as part of this thesis.

10 Preparation and characterization of bis-[4-dimethylamino-2-pyrimidyl]dichalcogenides (S, Se, Te): X-ray crystal structure of bis-[4-dimethylamino-2-pyrimidyl]diselenide and its physicochemical behaviour in microemulsion media,
Khuldip K. Bhasin, Ekta Arora, Khushwinder Kaur, Sung-Kyu Kang, Michael Göbel, Thomas M. Klapötke and S. K. Mehta,
Tetrahedron **2009**, *65(1)*, 247-252.

9 (Cover Picture / VIP)
The synthesis of azadirachtin: a potent insect antifeedant,
Steven V. Ley, Antonio Abad-Somovilla, James C. Anderson, Carles Ayats, Rolf Bänteli, Edith Beckmann, Alistair Boyer, Maria G. Brasca, Abigail Brice, Howard B. Broughton, Brenda J. Burke, Ed Cleator, Donald Craig, Alastair A. Denholm, Ross M. Denton, Thomas Durand-Reville, Luca B. Gobbi, Michael Göbel, Brian Lawrence Gray, Robert B. Grossmann, Claire E. Gutteridge, Norbert Hahn, Sarah L. Harding, David C. Jennens, Lynn Jennens, Peter J. Lovell, Helen J. Lovell, Mary L. de la Puente, Hartmuth C. Kolb, Win-Jan Koot, Sarah L. Maslen, Catherine F. McCusker, Amos Mattes, Andrew R. Pape, Andrea Pinto, Dinos Santafianos, James S. Scott, Stephen C. Smith, Andrew Q. Somers, Christopher D. Spilling, Frank Stelzer, Peter L. Toogood, Richard M. Turner, Gemma E. Veitch, Anthony Wood, Cornelia Zumbrunn,
Chem. Eur. J. **2008**, *14(34)*, 10683-10704.

8* (Cover Picture)
Exceeding the oxygen content of liquid oxygen:
bis(2,2,2-trinitroethyl)carbonate,
Michael Göbel and Thomas M. Klapötke,
Acta Crystallogr., Sect. C: Cryst. Struct. Commun. **2008**, *64(2)*, o58-o60.

7 γ-FOX-7: Structure of a high energy density material immediately prior to decomposition,
Margaret J. Crawford, Jürgen Evers, Michael Göbel, Thomas M. Klapötke, Peter Mayer, Gilbert Oehlinger, Jan M. Welch,
Propellants, Explos., Pyrotech. **2007**, *32(6)*, 478-495.

6* 2,2,2-Trinitroethanol,
Michael Göbel and Thomas M. Klapötke,
Acta Crystallogr., Sect. C: Cryst. Struct. Commun. **2007,** *63(9)*, o562-o564.

5* First structural characterization of guanidine, $HN=C(NH_2)_2$,
Michael Göbel and Thomas M. Klapötke,
Chem. Commun. **2007**, 3180-3182.

4* (Cover Picture / open access)
The crystal and molecular structure of mercury fulminate (Knallquecksilber),
Wolfgang Beck, Jürgen Evers, Michael Göbel, Gilbert Oehlinger and Thomas M. Klapötke,
Z. Anorg. Allg. Chem. **2007,** *633(9)*, 1417-1422.

3* (Cover Picture)
Potassium-, ammonium-, hydrazinium-, guanidinium-, aminoguanidinium-, diaminoguanidinium-, triaminoguanidinium- and melaminiumnitroformate – synthesis, characterization and energetic properties,
Michael Göbel and Thomas M. Klapötke,
Z. Anorg. Allg. Chem. **2007**, *633(7)*, 1006-1017.

2* (Cover Picture)
First structurally characterised binary P-N molecule: the highly energetic compound P_3N_{21},
Michael Göbel, Konstantin Karaghiosoff, Thomas M. Klapötke,
Angew. Chem. **2006**, *118(36)*, 6183-6186; *Angew. Chem. Int. Ed.* **2006**, *45*, 6037-6040.

1 Crystal structures of the potassium and silver salts of nitroform,
Michael Göbel, Thomas M. Klapötke, Peter Mayer,
Z. Anorg. Allg. Chem. **2006**, *632(6)*, 1043-1050.

Seminar Proceedings

9* (Cover Picture)
Towards elucidating the exotic chemical reactivity of matter under extreme conditions,
Michael Göbel and Thomas M. Klapötke,
Swiss Society for Crystallography (SGK/SSCr) Newsletter **2009**, *78*, 16-17.
(ISSN 1662-5358 printed edition., ISSN 1662-534X electronic edition)

8* A structural isomer of CL-20:
synthesis, characterization and energetic properties of BTAT,
Michael Göbel and Thomas M. Klapötke,
New Trends in Research of Energetic Materials, Proceedings of the Seminar, 12th, Czech Republic, Apr. 01-03, **2009** (Pt. 2), 542-547.

7* An insensitive melt castable explosive with positive oxygen balance: synthesis, characterization and energetic properties of BTHC,
Michael Göbel and Thomas M. Klapötke,
New Trends in Research of Energetic Materials, Proceedings of the Seminar, 12th, Czech Republic, Apr. 01-03, **2009** (Pt. 2), 548-555.

6* From molecular structure to explosive performance parameters: properties of the homologous series of guanidinium salts of 3,5-diaminopicirc acid,
Michael Göbel, Thomas M. Klapötke, Anthony J. Bellamy, Luigi Cassioli, Alessandro E. Contini,
New Trends in Research of Energetic Materials, Proceedings of the Seminar, 11th, Pardubice, Czech Republic, Apr. 9-11, **2008** (Pt. 2), 574-580.

5* Development and testing of high density energetic materials containing superior amounts of oxygen,
Michael Göbel and Thomas M. Klapötke,
New Trends in Research of Energetic Materials, Proceedings of the Seminar, 10th, Czech Republic, Apr. 09-11, **2008**, 150-154.

4* Synthesis and characterization of N-trinitroethyl derivatives of nitrogen containing compounds,
Michael Göbel and Thomas M. Klapötke,
New Trends in Research of Energetic Materials, Proceedings of the Seminar, 10th, Czech Republic, Apr. 25-27, **2007**, 149-153.

3* Synthesis and characterization of the oxygen rich energetic material melaminium dinitrate (MDN),
Roland Friedemann, Michael Göbel, Thomas M. Klapötke, Susanne Scheutzow
New Trends in Research of Energetic Materials, Proceedings of the Seminar, 10th, Czech Republic, Apr. 25-27, **2007** (Pt. 2), 875-876.

2 Stable salts of methylated 5-aminotetrazoles,
Michael Göbel, Konstantin Karaghiosoff, Thomas M. Klapötke, Carlos Miró, Jan M. Welch,
New Trends in Research of Energetic Materials, Proceedings of the Seminar, 9th, Czech Republic, Apr. 19-21, **2006**, 202-213.

1* Guanidinium nitroformate salts: possible new oxidizers for high performance, halogen free solid propellants,
Michael Göbel, Thomas M. Klapötke, P. C. Thumbs,
New Trends in Research of Energetic Materials, Proceedings of the Seminar, 9th, Czech Republic, Apr. 19-21, **2006**, 127-134.

Letter

3 Danger with primary amines and methylene chloride,
Andreas Böhm, Michael Göbel, Thomas M. Klapötke, Susanne Scheutzow and Johann Weis,
Chemistry in Australia **2007**, 74(8), 2.

2 Gefahr bei primären Aminen und Dichlormethan,
Andreas Böhm, Michael Göbel, Thomas M. Klapötke, Susanne Scheutzow and Johann Weis,
Nachr. Chem. **2007**, *55*, 864.

1 Visualisierung einzelner Viren auf ihrem Infektionsweg in lebende Zellen,
Michael Göbel, Thomas Endreß, Christoph Bräuchle,
Laborwelt **2002**, *(4)*, 4-7.

Poster

8* Reaction force analysis of nitro / aci tautomerization,
Jane S. Murray, Pat Lane, Michael Göbel, Thomas M. Klapötke and Peter Politzer,
12th *International Annual Conference on New Trends in Research of Energetic Materials*, Pardubice, Czech Republic, *Apr. 01-03*, 2009.

7* (Award)
A structural isomer of CL-20:
synthesis, characterization and energetic properties of BTAT,
Michael Göbel and Thomas M. Klapötke,
12th *International Annual Conference on New Trends in Research of Energetic Materials*, Pardubice, Czech Republic, *Apr. 01-03*, 2009.

6* An insensitive melt castable explosive with positive oxygen balance:
synthesis, characterization and energetic properties of BTHC,
Michael Göbel and Thomas M. Klapötke,
12th *International Annual Conference on New Trends in Research of Energetic Materials*, Pardubice, Czech Republic, *Apr. 01-03*, 2009.

5* From molecular structure to explosive performance parameters: properties of the homologous series of guanidinium salts of 3,5-diaminopicric acid,
Michael Göbel, Thomas M. Klapötke,
11th *International Annual Conference on New Trends in Research of Energetic Materials*, Pardubice, Czech Republic, April 09 – 11, 2008.

4* Synthesis and characterization of the oxygen rich energetic material melaminium dinitrate (MDN),
Roland Friedemann, Michael Göbel, Thomas M. Klapötke, Susanne Scheutzow
10th International Annual Conference on New Trends in Research of Energetic Materials, Pardubice, Czech Republic, April 25 – 27, 2007.

3* (Award)
P_3N_{21},
Michael Göbel, Thomas M. Klapötke,
13. Vortragstagung der Wöhler Vereinigung für Anorganische Chemie, Aachen, September 18 – 19, 2006.

2* New energetic materials: guanidinium nitroformate salts,
Michael Göbel, Thomas M. Klapötke,
Gordon Research Conference on Energetic Materials, New Hampshire, USA, June 18 – 23, 2006.

1 (Award)
Crystal structures of the potassium and silver salts of nitroform,
Michael Göbel, Thomas M. Klapötke, Peter Mayer,
8th International Annual Conference on New Trends in Research of Energetic Materials, Pardubice, Czech Republic, April 19 – 21, 2005.

Talks

11* (Martin Summerfield Best Paper Award)
High-nitrogen and high-oxygen explosives as possible replacements for RDX,
Thomas M. Klapötke, Michael Göbel, Jörg Stierstorfer,
8th International Symposium on Special Topics in Chemial Propulsion, Cape Town, South Africa, November 2 – 6, 2009.

10* (Invited Talk)
Energetic materials research – Kunst oder Wissenschaft?
Michael Göbel,
Deutsches Krebsforschungszentrum (DKFZ), Heidelberger Life-Science Lab, Heidelberg, Germany, October 23, 2009.

9* (Invited Talk)
Towards elucidating the exotic chemical reactivity of matter under extreme conditions,
Michael Göbel and Thomas M. Klapötke,
Annual Meeting of the Swiss Society of Crystallography, Fribourg, Switzerland, September 8, 2009.

8* Development and testing of energetic materials: The concept of high densities based on the trinitroethyl functionality,
Michael Göbel and Thomas M. Klapötke,
EDA Workshop on Energetic Materials with Higher Performance, EMHP and Formulation and Production of New Energetic Materials, FPNEM, FOI, Kista, Stockholm, Sweden, April 22, 2008.

7* Development and testing of high density energetic materials containing superior amounts of oxygen,
Michael Göbel and Thomas M. Klapötke,
11th International Annual Conference on New Trends in Research of Energetic Materials, Pardubice, Czech Republic, April 09 – 11, 2008.

6* (Award)
Synthesis and characterization of N-trinitroethyl derivatives of nitrogen containing compounds,
Michael Göbel and Thomas M. Klapötke,
10th International Annual Conference on New Trends in Research of Energetic Materials, Pardubice, Czech Republic, April 25 – 27, 2007.

5* Recent aspects of academic and applied research in azide chemistry,
Thomas M. Klapötke, Michael Göbel, Vikas Verma,
IC07 – Conference of the Inorganic Chemistry Division Royal Australian Chemical Institute – Hobart, Tasmania, February 4 – 8, 2007.

4* New highly energetic materials based on C-N and P-N heterocycles,
Thomas M. Klapötke, Michael Göbel, Margaret J. Crawford, Jan M. Welch, Jörg Stierstorfer, Vikas Verma, Jan J. Weigand, Anton Hammerl,
IRIS – 11, Oulu, Finland, 30 July – 04. August, 2006.

3* Nitro compounds, tetrazoles and azides: the last five months at LMU munich,
Margaret J. Crawford, Michael Göbel and Thomas M. Klapötke,
University of Melbourne, Australia, May 22, 2006.

2 Stable salts of methylated 5-aminotetrazoles,
Michael Göbel, Konstantin Karaghiosoff, Thomas M. Klapötke, Carlos Miró, Jan M. Welch,
9th International Annual Conference on New Trends in Research of Energetic Materials, Pardubice, Czech Republic, April 19 – 21, 2006.

1 (Award)
Guanidinium nitroformate salts: possible new oxidizers for high performance, halogen free solid propellants,
Michael Göbel, Thomas M. Klapötke,
9th International Annual Conference on New Trends in Research of Energetic Materials, Pardubice, Czech Republic, April 19 – 21, 2006.

Press / Books

10* *Chemie der hochenergetischen Materialien*, Klapötke, T.M. (Ed.), de Gruyter, Berlin, 2009, 132-137.

9* When atoms are getting close: shortest carbon-chlorine single bond detected until now,
Press release, Ludwig-Maximilian University Munich, May (4) 2009.

8* Explosive future, *Materials Views* 2009, *March*, p. A3.

7* Wenn Grün die Umwelt gefährdet,
Forschungsnewsletter *EINSICHTEN*, Ludwig-Maximilan University Munich, October 2008, p.61.

6* Explosives Geheimnis gelüftet,
Frankfurter Allgemeine Zeitung, September (26) 2007, 224, p. N2.

5* Das letzte Geheimnis des Knallquecksilbers,
Neue Zürcher Zeitung, September (5) 2007.

4* Mercury fulminate revealed,
Chemical & Engineering News, September (3) 2007, p. 10.

3* Trendbericht Festkörperchemie,
Nachr. Chem. 2007, *55*, p. 244.

2* Trendbericht Anorganische Chemie,
Nachr. Chem. 2007, *55*, p. 225.

1* *High Energy Density Materials*; Mingos, D.M.P; Klapötke, T.M., Eds.; Structure and Bonding; Springer: Berlin Heidelberg, 2007; Vol. 125, pp. 77 & 96-99.

4.9 Curriculum Vitae

Personal Details

Name	Michael Göbel
Place of birth	Landau / Pfalz
Date of birth	25.04.1977
Nationality	German
Marital status	Unmarried

Education

06/05 – 12/09	**Ludwig-Maximilian University, Munich** Research Group of Prof. T.M. Klapötke Dissertation: *Energetic materials containing the trinitromethyl pseudohalide functionality*
09/04 – 03/05	**Ludwig-Maximilian University, Munich** Research Group of Prof. T.M. Klapötke Diploma thesis: *Versuche zur Darstellung von 1,1,1,4,4,4-Hexanitro-2-butin sowie Strukturaufklärung von Salzen des Trinitromethans*
07/04	**Ludwig-Maximilian University, Munich** Diploma in Chemistry, final examinations
09/01 – 12/01	**University of Cambridge, UK** Research Group of Prof. S.V. Ley, Advanced study period
11/00	**Ludwig-Maximilian University, Munich** Diploma in Chemistry, preliminary examinations
10/99	**Ludwig-Maximilian University, Munich** Official enrolment within the degree programme 'Diplom-Chemie'
04/99 – 09/99	**Ludwig-Maximilian University, Munich** Guest student within the degree programme 'Diplom-Chemie'
10/97 – 10/99	**Georg-Simon-Ohm Fachhochschule, Nuremberg** Diploma in Chemical Engineering, preliminary examinations (February 1999)
08/96 – 08/97	**Civilian Service** at the ‚Ökumenische Sozialstation für den Landkreis Weilheim-Schongau'
07/96	**Fachoberschule, Weilheim / Oberbayern** A-levels

4.10 Acknowledgements

I am indebted to and thank Prof. Dr. Thomas M. Klapötke. Under his supervision it was possible to develop ideas and translate them into results. His always generous and supporting attitude together with a tremendous leap of faith towards my person is very much appreciated and I am most grateful and glad I had the opportunity to work in his group.

I would like to express my gratitude to Prof. Dr. W. Beck. I feel honoured I had the chance to listen to and work with him on many topics including but not limited to mercury fulminate and I would like to thank him for being co-referee of this thesis.

I am thankful to Prof. Dr. J. Evers, Prof. Dr. I.-P. Lorenz, Prof. Dr. P. Knochel and Prof. Dr. A. Kornath for their immediate attendance to act as examiners in my *viva-voce*.

I am indebted for aid in the preparation of this thesis to many of my colleagues, friends and to many teachers in chemistry, including

Dr. Anthony J. Bellamy, Dr. Richard Betz, Franziska Betzler, Dr. Sebastian M. Braun, Dr. habil. Margaret-Jane Crawford, Camilla Evangelisti, Dagmar Ewald, Dennis Fischer, Dr. Gerd Fischer, Niko Fischer, Roland Friedemann, Dr. Anton Hammerl, Stefan Huber, Prof. Dr. Konstantin Karaghiosoff, Marcos Kettner, Prof. Dr. Peter Klüfers, Prof. Dr. Bettina V. Lotsch, Franz Martin, Dr. Peter Mayer, Norbert Mayr, Dr. Carlòs Miro-Sabaté Richard Moll, Dr. Jane S. Murray, Anian Nieder, Dr. Oliver Oeckler, Gilbert Oehlinger, Alexander Penger, Dr. Kurt Pohlborn, Prof. Dr. Peter Politzer, Davin Piercey, Hendrik Radies, Sebastian Rest, Magdalena Rusan, Irene Scheckenbach, Dr. Matthias Scherr, Susanne Scheutzow, Prof. Dr. Wolfgang Schnick, Dr. Stefan Sproll, Dr. Franz X. Steemann, Dr. Jörg Stierstorfer, Karina Tarantik, Boris H. Tchitchanov, Peter C. Thumbs, Vikas Verma, Dr. Jan J. Weigand, Dr. Jan Welch, and I am glad to express my gratitude to them.

The Cusanuswerk is thanked for a scholarship.

Above all, I am indebted to my parents, grandparents and family who continuously encouraged and supported me.

4.11 References

(1) Official Energy Statistics from the U.S. Government, Energy Information Administration (EIA), annual power data for 2007, http://www.eia.doe.gov/cneaf/electricity/epa/epat2p2.html

(2) J.B. Bdzil, T.D. Aslam, R. Henninger, J.J. Quirk, *Los Alamos Science* **2003**, *28*, 96.

(3) C.J. Wu, L.E. Fried, L.H. Yang, N. Goldman, S. Bastea, *Nature Chem.* **2009**, *1*, 57.

(4) M.R. Manaa, E.J. Reed, L.E. Fried, N. Goldman, *J. Am. Chem. Soc.* **2009**, DOI: 10.1021/ja808196e

(5) W.C. Davies, *Los Alamos Science* **1981**, *2*, 48.

(6) The New York Times, April 7, 2009, p. A1.

(7) J. Akhavan (2004) *The Chemistry of Explosives*, 2nd edn. The Royal Society of Chemistry, Great Britain, p. 41.

(8) M. Dé Fourneaux, *Overview of National Policies*, ADPA IM Symposium, Williamsburg, June 6-9, 1994.

(9) UN Recommendations on the Transport of Dangerous Goods: series 7 Tests and Criteria.

(10) T.M. Klapötke (2007) *Nichtmetallchemie*. In: E. Riedel (ed.) *Moderne Anorganische Chemie*, 3rd edn. Walter de Gruyter, Berlin.

(11) P. Noble, Jr., F.G. Borgardt, W.L. Reed, *Chem. Rev.* **1964**, *64*, 19.

(12) a) M.J. Kamlet, NAVORD Report 6207, 14 Feb 1959, Naval Surface Weapons Center; b) M.J. Kamlet, H.G. Adolph, *J. Org. Chem.* **1968**, *33*, 3073.

(13) K.F. Mueller, R.H. Renner, W.H. Gilligan, H.G. Adolph, M.J. Kamlet, *Combust. Flame* **1983**, *50*, 341.

(14) J. Akhavan, *The Chemistry of Explosives*, RSC Paperbacks, Cambridge, 1998.

(15) H. Bircher, Chimia **2004**, *58(6)*, 357.

(16) C.H. Johannson, P.A. Persson, *Detonics of High Explosives*. Academic Press, London & New York, 1970.

(17) I.B. Akst, *Heat of Detonation, the Cylinder Test, and Performance in Munition*, 9th Symposium on Detonation, Portland, USA, 1989.

(18) M.J. Kamlet, in a seminar at the White Oak Laboratory, NSWC, 1987.

(19) T.M. Klapötke, J. Stierstorfer, *Dalton Trans.* **2009**, 643.

(20) M. DéFourneaux, *About the Misuse of Detonation Velocities for the Characterisation of High Explosives*, 25th International Conference on 'Energetic Materials – Analysis, Characterization and Test Techniques' ICT, Karlsruhe (Germany), June 28 – July 1, 1994.

(21) A.J. Sanderson, *Journal de Physique* **1995**, 5, C4-573.

(22) M.J. Kamlet, S.J. Jacobs, *J. Chem. Phys.* **1968**, 48, 23.

(23) O. Schischkoff, *Ann. Chem.* **1857**, *101*, 216.

(24) L.A. Kaplan, in *Chemistry of the Nitro and Nitroso Groups*, H. Feuer (Ed.), Interscience Publishers, New York, **1970**.
(25) M.G.A. Shvekhgeimer, *Russ. Chem. Rev.* **1998**, *67(1)*, 35.
(26) F.D. Chattaway, *J. Chem. Soc.* **1910**, *97*, 2099.
(27) P. Liang, *Org. Syn.* **1955**, *3*, 803; P. Liang, *Org. Syn.* **1921**, *21*, 105.
(28) K.J. Orton, P.V. McKie, *J. Chem. Soc.* **1920**, *117*, 283.
(29) T. Urbanski, *Chemistry and Technology of Explosives* **1964**. I. Pergamon Press. pp. 589-594.
(30) Pictet, Genequand, *Ber.* **1903**, *36*, 2225.
(31) A. Hantzsch, *Ber.* **1906**, *39*, 2478.
(32) Pictet, Khotinsky, *Ber.* **1907**, *40*, 1163.
(33) a) Claessen, Ger. pat. 184.229; b) Claessen, *Chem. Abstr.* **1907**, *1*, 2524.
(34) a) R. Schenck, Ger. pat, 211.198, 211,199; b) R. Schenck, *Chem. Abstr.* **1909**, *3*, 2205.
(35) a) Bayer & Co, Brit. pat. 24.299; b) Bayer & Co, Ger. pat. 224.057; c) Bayer & Co, Chem. Abstr. 1911, *5*, 2305; d) Berger, Compt. Rend. 1910, 151, 813; e) Berger, Bull. Soc. Chim. France 1911, 9, 26.
(36) W. Will, *Chem. Ber.* **1914**, *47*, 961.
(37) P.V. McKie, *J. Soc. Chem. Ind.* **1925**, *44*, 430T.
(38) P.V. McKie, *J. Chem. Soc.* **1927**, 962.
(39) A. Langlet, N.V. Latypov, U. Wellmar, P. Goede, *Propellants Explos. Pyrotech.* **2004**, *29(6)*, 344.
(40) J.G. Tschinkel, *J. Ind. Eng. Chem.* **1956**, *48*, 732.
(41) A.G. Anderson, Jr., R. Scotoni, Jr., E.J. Cowles, G. Fritz, *J. Org. Chem.* **1957**, *22*, 1193.
(42) C.W. Plummer, U.S. Patent 2.991.315, *Chem. Abstr.* **1962**, *56*, 2330e.
(43) a) H. Meyer, *Analyse und Konstitutionsermittlung organischer Verbindungen*, Julius Springer, Vienna 1938, 6th ed. p. 773; b) Ruzicka, Huyser, Pfeiffer, Seidel, *Ann.* **1929**, *471*, 21.
(44) T. Urbanski, *Chemistry and Technology of Explosives* **1964**. I. Pergamon Press. p. 593.
(45) a) R. Schenck, *Zeitsch. Angew. Chem.* **1920**, *33*, 245; b) R. Schenck, *Chem. Zeit.* **1920**, *44*, 497;
c)www.rsc.org/delivery/_ArticleLinking/DisplayArticleForFree.cfm?doi=CA9201805457&JournalCode=CA
(46) E. Rüst, A. Ebert, K. Egli, *Unfälle beim chemischen Arbeiten*, Rascher, **1948**, p. 23.
(47) H. Feuer, T. Kucera, *J. Am. Chem. Soc.* **1955**, 77, 5740.
(48) T.N. Hall, *Tetrahedron* **1963**, *19*, 115.
(49) S.V. Lieberman, E.C. Wagner, *J. Org. Chem.* **1949**, *14*, 1001.
(50) E.R. Alexander, E.J. Underhill, *J. Am. Chem. Soc.* **1949**, *71*, 4014.
(51) H. Feuer, W.A. Swarts, *J. Org. Chem.* **1962**, *27*, 1455.

(52) V.I. Slovetskii, V.A. Tartakovskii, S.S. Novikov, *Izv. Akad. Nauk SSSR, Otd. Khim. Nauk* **1962**, 1400.
(53) W. Beck, J. Evers, M. Göbel, G. Oehlinger, T.M. Klapötke, *Z. Anorg. Allg. Chem.* **2007**, 1417.
(54) W. Beck, T.M. Klapötke, *J. Mol. Struct.* **2008**, *848*, 94.
(55) G.S. Hammond, W.D. Emmons, C.O. Parker, B.M. Graybill, J.H. Waters, N.F. Hawthorne, *Tetrahedron* **1963**, *19*, 177.
(56) P.O. Tawney, U.S. Patent 3.040.105 **1962**; *Chem. Abstr.* **1962**, *57*, 13609.
(57) D.R. Levering, *J. Org. Chem.* **1962**, *27*, 2930.
(58) R.B. Kaplan, H. Shechter, *J. Am. Chem. Soc.* **1961**, *83*, 3535.
(59) C.W. Plummer, *U.S. Patent* 2,991,315 **1961**; *Chem. Abstr.* **1967**, *67*, 53650.
(60) S.S. Novikov, L.I. Khmelnitskii, O.V. Lebedev, *Izv. Akad. SSSR* **1960**, 1783; *Chem. Abstr.* **1961**, *55*, 19832.
(61) A.V. Shastin, T.I. Godovikova, S.P. Golova, V.S. Kuz'min, L.I. Khmel'nitskii, B.L. Korsunskii, *Mendeleev Commun.* 1995, *5*, 17.
(62) L. Hunter, *J. Chem. Soc.* **1923**, *123*, 543.
(63) C.O. Parker, W.D. Emmons, A.S. Pangano, H.A. Rolewicz, K.S. McCallum, *Tetrahedron* **1962**, *17*, 79.
(64) G. Darzens, M. Levy, *Compt. Rend.* **1949**, *229*, 1081.
(65) M.H. Gold, M.B. Frankel, G.B. Linden, K. Klager, *J. Org. Chem.* **1962**, *27*, 334.
(66) A.I. Shreibert, N.V. Elaskov, A.P. Khardin, V.I. Ermarchenko, *Zh. Organ. Khim.* **1967**, *3*, 1755.
(67) D.J. Glover, *Tetrahedron* **1963**, *19*, 219.
(68) F.G. Borgardt, A.K. Seeler, P. Noble, Jr., *J. Org. Chem.* **1966**, *31*, 2806.
(69) H. Feuer, E.H. White, M. Pier, *J. Org. Chem.* **1961**, *26*, 1639.
(70) E. Schmidt, *Chem. Ber.* **1919**, *52*, 400.
(71) S. Iyer, N. Slagg, in: Structure and Reactivity. (1988) J.F. Liebman, A. Greenberg (Eds.), VCH, New York, Chapter 7.
(72) C.B. Storm, J.R. Stine, J.F. Kramer, in: Chemistry and Physics of Energetic Materials. (1990) S.N. Bulusu (Ed.), Kluwer, Dordrecht, Chapter 27.
(73) T.B. Brill, K. James, *Chem. Rev.* **1993**, *93*, 2667.
(74) B.M. Rice, J.J. Hare, *J. Phys. Chem. A* **2002**, *106*, 1770.
(75) M. Pospisil, P. Vávra, M.C. Concha, J.S. Murray, P. Politzer, *J. Mol. Model.* **2009**, DOI 10.1007/s00894-009-0587-x.
(76) J.F. Liebman, in: The Chemistry The Chemistry of Amino, Nitroso, Nitro and Related Groups, Supplement F2, Chapter 8, 371.
(77) B.T. Fedoroff, O.E. Sheffield, *Encyclopedia of Explosives and Related Items* **1962**, *7*, I38.
(78) B.T. Fedoroff, O.E. Sheffield, *Encyclopedia of Explosives and Related Items* **1962**, *9*, T266.
(79) B.T. Fedoroff, O.E. Sheffield, *Encyclopedia of Explosives and Related Items* **1962**, *7*, I39.

(80) T.S. Pivina, K.V. Sukhachev, N.S. Zefirov, *Proceedings of the 5th International Conference of the 'Groupe de Travail de Pyrotechnie'*, p.71, June 6, 1993.

(81) Gaussian 03, Revision A.1, M.J. Frisch, G.W. Trucks, H.B. Schlegel, G.E. Scuseria, M.A. Robb, J.R. Cheeseman, J.A. Montgomery, Jr., T. Vreven, K.N. Kudin, J.C. Burant, J.M. Millam, S.S. Iyengar, J. Tomasi, V. Barone, B. Mennucci, M. Cossi, G. Scalmani, N. Rega, G.A. Petersson, H. Nakatsuji, M. Hada, M. Ehara, K. Toyota, R. Fukuda, J. Hasegawa, M. Ishida, T. Nakajima, Y. Honda, O. Kitao, H. Nakai, M. Klene, X. Li, J.E. Knox, H.P. Hratchian, J.B. Cross, C. Adamo, J. Jaramillo, R. Gomperts, R.E. Stratmann, O. Yazyev, A.J. Austin, R. Cammi, C. Pomelli, J.W. Ochterski, P.Y. Ayala, K. Morokuma, G.A. Voth, P. Salvador, J.J. Dannenberg, V.G. Zakrzewski, S. Dapprich, A.D. Daniels, M.C. Strain, O. Farkas, D.K. Malick, A.D. Rabuck, K. Raghavachari, J.B. Foresman, J.V. Ortiz, Q. Cui, A.G. Baboul, S. Clifford, J. Cioslowski, B.B. Stefanov, G. Liu, A. Liashenko, P. Piskorz, I. Komaromi, R.L. Martin, D.J. Fox, T. Keith, M.A. Al-Laham, C.Y. Peng, A. Nanayakkara, M. Challacombe, P.M.W. Gill, B. Johnson, W. Chen, M.W. Wong, C. Gonzalez, and J.A. Pople, Gaussian, Inc., Pittsburgh PA, 2003.

(82) C.B. Storm, J. Stine, J.F. Kramer, *Sensitivity Relationships in Energetic Materials*, Los Alamos Technical Report LA-UR-89-2936, 1989.

(83) M.J. Kamlet, *6th Symposium on detonation*, San Diego, California, 1976.

(84) J.S. Murray, P. Politzer, *Computational studies of energetic nitramines*, Proceedings of the NATO advanced study institute on chemistry and physics of the molecular processes in energetic materials, 1989.

(85) H. Nefati, J.J. Legendre, C. Michot, *Proceedings of the 5th International Conference of the 'Groupe de Travail de Pyrotechnic'*, p.79, June 6, 1993.

(86) A. Delpuech, J. Cherville, C. Michaud, 7th Symposium on Detonation, p.65, June 16, 1981.

(87) L. Brunet, J.M. Lombard, B. Blaise, L. Morin-Allory, *Proceedings of the 5th International Conference of the 'Groupe de Travail de Pyrotechnic'*, p.89, June 6, 1993.

(88) J.S. Murray, P. Lane, P. Politzer, *J. Mol. Phys.* **1995**, *85*, 1.

(89) A. Meents, B. Dittrich, S.K.J. Johans, V. Thome, E.F. Weckert, *Acta Cryst.* **2008**, *B64*, 42.

(90) B. Vogelsanger, *Chimia* **2004**, *58(6)*, 402.

(91) T. Urbanski, in *Chemistry and Technology of Explosives*, Vol. 4, Technical University Warsaw, 1985.

(92) P. Folly, *Chimia* **2004**, *58(6)*, 394.

(93) G.B. Manelis; G.M. Nazin; Y.I. Rubtsov; V.A. Strunin, in *Thermal Decomposition and Combustion of Explosives and Propellants*, Taylor & Francis Group, London and Berlin, **2003**.

(94) A. Hammerl, T. M. Klapötke, H. Nöth, M. Warchhold, G. Holl, M. Kaiser, U. Ticmanis, *Inorg. Chem.* **2001**, *40*, 3570.

(95) R.N. Rogers, *Thermochim. Acta* **1975**, *11*, 131.

(96) Systag AG
(97) Joint Technical Bulletin TB 700-2 NAVSEAINST 8020.8B TO 11A-1-47 DLAR 8220.1, Department of Ammunition and Explosives Hazard Classification Procedures, Headquarters Departments of the Army, the Navy, the Air Force, and the Defense Logistics Agency, Washington DC (USA), January, 5th 1998.
(98) A. Hantzsch, A. Rinckenberger, *Ber.* **1899**, *32*, 628.
(99) O.E. Dragomir, *Dissertation*, Techn. Univ. Delft, **2009**.
(100) SciFinder Database Enquiry 02/2007
(101) H.S Jadhav, M.B. Talawar, D.D. Dhavale, S.N. Asthana, V.N. Krishnamurthy, *Indian Journal of Chemical Technology* **2005**, *12(2)*, 187.
(102) N.I. Golovina, L.O. Atovmyan, *Zh. Strukt. Khim. (Russ.)* **1967**, *8*, 307.
(103) A.M. Krishnan, P. Sjoberg, P. Politzer, J.H. Boyer, *J. Chem. Soc. Perkins Trans. 2*, **1989**, 1237.
(104) A. Gunasekaran, J.H. Boyer, *Heteroatom Chemistry* **1992**, *3*, 611.
(105) B. Dickens, *Chem. Commun.* **1967**, *5*, 246.
(106) N.I. Golovina, L.O. Atovmyan, *Zh. Strukt. Khim. (Russ.)(J. Struct. Chem.)* **1966**, 7, 235.
(107) N.V. Grigor'eva, N.V. Margolis, I.N. Shokhor, V.V. Mel'nikov, I.V. Tselinskii, *Zh. Strukt. Khim. (Russ.)(J. Struct. Chem.)* **1966**, 7, 278.
(108) N.V. Grigor'eva, N.V. Margolis, I.N. Shokhor, I.V. Tselinskii, V.V. Mel'nikov, *Zh. Strukt. Khim. (Russ.)(J. Struct. Chem.)* **1968**, *9*, 550.
(109) B. Dickens, *J. Res. Nat. Bur. Stand. A*, **1970** 74**,** 309.
(110) N.V. Podberezskaya, V.P. Doronina, V.V. Bakakin, I.I. Yakovlev, *Zh. Strukt. Khim. (Russ.)(J. Struct. Chem.)* **1984**, *25*, 182.
(111) K.D. Scherfise, F. Weller, K. Dehnicke, *Z. Naturforsch. B* **1985**, *40*, 906.
(112) H.L. Ammon, C.S. Choi, A. Bashir-Hashemi, R.M. Moriarty, J.S. Khosrowshahi, *Acta Crystallogr.* **1989**, *C45*, 319.
(113) H.L. Ammon, C.S. Choi, R.S. Damvarapu, S. Iyer, J. Alster, *Acta Crystallogr.* **1990**, *C46*, 295.
(114) N.V. Podberezskaya, N.V. Pervukhina, V.P. Doronina, *Zh. Strukt. Khim.(Russ.)(J. Struct. Chem.)* **1991**, *32*, 34.
(115) H. Bock, R. Dienelt, H. Schodel, Z. Havlas, *Chem.Commun.* **1993**, 1792.
(116) H. Schodel, R. Dienelt, H. Bock, *Acta Crystallogr.* **1994**, *C50*, 1790.
(117) H. Bock, T. Hauck, C. Nather, Z. Havlas, *Z. Naturforsch.* **1994**, *49*, 1012.
(118) J.C. Bryan, M.N. Burnett, A.A. Gakh, *Acta Crystallogr.*, **1998**, *C(54)9*, 1229.
(119) M. Göbel, T.M. Klapötke, P. Mayer, *Z. Anorg. Allg. Chem.* **2006**, *632(6)*, 1043.
(120) M. Göbel, T.M. Klapötke, P.C. Thumbs, *New Trends in Research of Energetic Materials, Proceedings of the Seminar, 9th, Pardubice, Czech Republic, Apr. 19-21, 2006* (**2006**), *(Pt. 1)*, 127.
(121) A. Gunasekaran, J.H. Boyer, *Heteroatom Chemistry* **1992**, *3*, 611.
(122) P.S. Dendage, D.B. Sarwade, S.N. Asthana, H. Singh, *J. Energ. Mat.* **2001**, *19*, 41.

(123) A.M. Krishnan, P. Sjoberg, P. Politzer, J.H. Boyer, *J. Chem. Soc. Perkins Trans. 2*, **1989**, 1237.
(124) J.C. Bryan, M.N. Burnett, A.A. Gakh, *Acta Crystallogr.*, **1998**, *C(54)9*, 1229.
(125) H.M. Niemeyer, *J. Mol. Struct.* **1978,** *50*, 123.
(126) K.E. Edgecombe, R.J. Boyd, *Can. J. Chem.* **1983,** *61*, 45.
(127) B. Dickens, *Chem. Commun.* **1967**, *5*, 246.
(128) B. Dickens, *J. Res. Nat. Bur. Stand. A*, **1970** *74,* 309.
(129) N.V. Podberezskaya, V.P. Doronina, V.V. Bakakin, I.I. Yakovlev, *Zh. Strukt. Khim. (Russ.)(J. Struct. Chem.)* **1984**, *25*, 182.
(130) K.D. Scherfise, F. Weller, K. Dehnicke, *Z. Naturforsch. B* **1985**, *40*, 906.
(131) H.L. Ammon, C.S. Choi, R.S. Damvarapu, S. Iyer, J. Alster, *Acta Crystallogr.* **1990**, *C46*, 295.
(132) N.V. Podberezskaya, N.V. Pervukhina, V.P. Doronina, *Zh. Strukt. Khim.(Russ.)(J. Struct. Chem.)* **1991**, *32*, 34.
(133) H. Schodel, R. Dienelt, H. Bock, *Acta Crystallogr.* **1994**, *C50*, 1790.
(134) H. Bock, T. Hauck, C. Nather, Z. Havlas, *Z. Naturforsch.* **1994**, *49*, 1012.
(135) J.C. Bryan, M.N. Burnett, A.A. Gakh, *Acta Crystallographica*, **1998**, *C(54)9*, 1229.
(136) M. Göbel, T.M. Klapötke, P.C. Thumbs, New Trends in Research of Energetic Materials, Proceedings of the Seminar, 9th, Pardubice, Czech Republic, Apr. 19-21, 2006 (**2006**), (Pt. 1), 127.
(137) B. Dickens, *Chem. Commun.* **1967**, *5*, 246.
(138) B. Dickens, *J. Res. Nat. Bur. Stand. A*, **1970** *74,* 309.
(139) D.V. Jahagirdar, R.M. Kharwadkar, *Ind. J. Chem.* **1981**, *20A*, 635.
(140) J.C. Bryan, M.N. Burnett, A.A. Gakh, *Acta Crystallogr.*, **1998**, *C(54)9*, 1229.
(141) Gaussian 03, Revision A.1, M.J. Frisch, G.W. Trucks, H.B. Schlegel, G.E. Scuseria, M.A. Robb, J.R. Cheeseman, J.A. Montgomery, Jr., T. Vreven, K.N. Kudin, J.C. Burant, J.M. Millam, S.S. Iyengar, J. Tomasi, V. Barone, B. Mennucci, M. Cossi, G. Scalmani, N. Rega, G.A. Petersson, H. Nakatsuji, M. Hada, M. Ehara, K. Toyota, R. Fukuda, J. Hasegawa, M. Ishida, T. Nakajima, Y. Honda, O. Kitao, H. Nakai, M. Klene, X. Li, J.E. Knox, H.P. Hratchian, J.B. Cross, C. Adamo, J. Jaramillo, R. Gomperts, R.E. Stratmann, O. Yazyev, A.J. Austin, R. Cammi, C. Pomelli, J.W. Ochterski, P.Y. Ayala, K. Morokuma, G.A. Voth, P. Salvador, J.J. Dannenberg, V.G. Zakrzewski, S. Dapprich, A.D. Daniels, M.C. Strain, O. Farkas, D.K. Malick, A.D. Rabuck, K. Raghavachari, J.B. Foresman, J.V. Ortiz, Q. Cui, A.G. Baboul, S. Clifford, J. Cioslowski, B.B. Stefanov, G. Liu, A. Liashenko, P. Piskorz, I. Komaromi, R.L. Martin, D.J. Fox, T. Keith, M.A. Al-Laham, C.Y. Peng, A. Nanayakkara, M. Challacombe, P.M.W. Gill, B. Johnson, W. Chen, M.W. Wong, C. Gonzalez, and J.A. Pople, Gaussian, Inc., Pittsburgh PA, 2003.
(142) Test methods according to the UN Recommendations on the Transport of Dangerous Goods, Manual of Tests and Criteria, fourth revised edition, United

Nations Publications, New York and Geneva, **2003**, ISBN 92-1-139087-7, Sales No. E.03.VIII.2.; 13.4.2 Test 3(a)(ii) BAM Fallhammer.

(143) Y.A. Lebedev, E.A. Miroshnichenko, Y.K. Knobel, *Termokhimiya nitrosoedinenii [Thermochemistry of nitrocompounds]*, Nauka, Moscow, **1970**, 168.

(144) T.S. Kon´kova, Yu.N. Matyushin, *Russ. Chem. Bull.* **1998**, *47*, 2371.

(145) M. Sućeska, *Propellants, Explos., Pyrotech.* **1991**, *16*, 197.

(146) M. Sućeska, *Proc. of 30th Int. Annual Conference of ICT*, June 29 – July 2, Karlsruhe, Germany, **1999**, 50.

(147) M. Sućeska, *Propellants Explosives and Pyrotechniques* **1999**, *24*, 280.

(148) M. Sućeska, *Proc. of 32nd Int. Annual Conference of ICT*, July 3-6, Karlsruhe, Germany, **2001**, 110.

(149) M. Sućeska, *Materials Science Forum* **2004**, *465*, 325.

(150) P.S. Dendage, D.B. Sarwade, S.N. Asthana, H. Singh, *J. Energ. Mat.* **2001**, *19*, 41.

(151) J.H. Köhler, *Explosivstoffe*, 9. Ed., Wiley-VCH, New York, **1998**, 344.

(152) M. Sućeska, *Materials Science Forum* **2004**, *465*, 325.

(153) J.H. Köhler, *Explosivstoffe*, 9. Ed., Wiley-VCH, New York, **1998**, 166.

(154) Test methods according to the UN Recommendations on the Transport of Dangerous Goods, Manual of Tests and Criteria, fourth revised edition, United Nations Publications, New York and Geneva, **2003**, ISBN 92-1-139087-7, Sales No. E.03.VIII.2.; 13.4.2 Test 3(a)(ii) BAM Fallhammer.

(155) HF-Vacuum-Pruefer, type VP 24.

(156) B. Dickens, *Chem. Commun.* **1967**, *5*, 246.

(157) A. Gunasekaran, J.H. Boyer, *Heteroatom Chemistry* **1992**, *3*, 611.

(158) R. Tanbug, K. Kirschbaum, A.A. Pinkerton, *J. Chem. Crystallogr.* **1999**, *29*, 4.

(159) R. Friedemann, M. Göbel, T.M. Klapötke, S. Scheutzow, New Trends in Research of Energetic Materials, Proceedings of the Seminar, 10th, Czech Republic, Apr. 25-27, **2007**, 875.

(160) M.L. Hobbs, M.R. Baer, Calibration of the BKW-EOS with a large product species data base and measured CJ properties, Proc. of the 10th Symp. (Int.) on Detonation, ONR 33395-12, Boston, MA, July 12-16 1993, 409.

(161) J.N. Varghese, A.M. O'Connell, E.N. Maslen, *Acta Cryst.* **1977**, B33, 2102.

(162) R. Tanbug, K. Kirschbaum, A.A. Pinkerton, *J. Chem. Crystallogr.* **1999**, *29*, 4.

(163) A. Martin, A.A. Pinkerton, *Acta Cryst.* **1995**, *C51*, 2174.

(164) Y. Wang, B. Wei, Q. Wang, *J. Cryst. Spectrosc. Res.* **1990**, *20*, 79.

(165) U. Müller, H. Bärnighausen, *Acta Cryst.* **1970**, *B26*, 1671.

(166) M. Göbel, T.M. Klapötke, *Chem. Commun.* **2007**, 3180.

(167) H. Henke, H. Bärnighausen, *Acta Cryst.* **1972**, *B28*, 1100.

(168) A. Dworkin, R. Naumann, C. Seigfred, J.M. Karty, *J. Org. Chem.* **2005**, *70*, 7605; and references therein.

(169) R.L. Livingston, C.N.R. Rao, *J. Phys. Chem.* **1960**, *64*, 756.

(170) H. Henke, H. Bärnighausen, *Acta Cryst.* **1972**, *B28*, 1100.
(171) A.J. Bellamy, L. Cassioli, A.E. Contini, *New Trends in Research of Energetic Materials, Proceedings of the 8th Seminar (Part 1), Czech Republic, Apr. 19-21*, **2005**, 472.
(172) Experimental value, M. Sućeska, *Materials Science Forum* **2004**, *465*, 325.
(173) S.K. Bhattacharjee, H.L. Ammon, *Acta Cryst.* **1981**, *B37*, 2082.
(174) S. Sorriso, in:The Chemistry of Amino, Nitroso, Nitro and Related Groups, S. Patai (Ed.), Supplement F, Part 1, Chapter 1.
(175) A. Domenicano, A. Vaciago, C.A. Coulson, *Acta Cryst.* **1975**, *B31*, 221.
(176) A. Domenicano, A. Vaciago, C.A. Coulson, *Acta Cryst.* **1975**, *B31*, 1630.
(177) A. Domenicano, A. Vaciago, C.A. Coulson, *Tetrahedron Lett.* **1976**, *13*, 1029.
(178) L.S. Bartell, *J. Chem. Phys.* **1960**, *32*, 827.
(179) L.S. Bartell, *Tetrahedron* **1962**, *17*, 177.
(180) L.S. Bartell, *J. Chem. Educ.* **1968**, *45*, 754.
(181) O.L. Carter, A.T. McPhail, G.A. Sim, *J. Chem. Soc. (A)* **1966**, 822.
(182) L. Nygaard, I. Bojesen, T. Pedersen, J. Rastrup-Andersen, *J. Mol. Struct.* **1968**, *2*, 209.
(183) R.J. Gillespie, R.S. Nyholm, *Quart. Rev.* **1957**, *11*, 339.
(184) R.J. Gillespie, *J. Chem. Educ.* **1963**, *40*, 295.
(185) R.J. Gillespie, *J. Chem. Soc.* **1963**, 4672.
(186) R.J. Gillespie, *Angew. Chem. Int. Ed.* **1967**, *6*, 819.
(187) R.J. Gillespie, *J. Chem. Educ.* **1970**, *47*, 18.
(188) R.J. Gillespie, *Molecular Geometry*, Van Nostrand-Reinhold, London, 1972.
(189) E.G. Cox, D.W.J. Cruickshank, J.A.S. Smith, *Proc. R. Soc. Sect. A* **1958**, *247*, 1.
(190) H.H. Cady, A.C. Larson, *Acta Cryst.* **1965**, *18*, 485.
(191) S.K. Bhattacharjee, H.L. Ammon, *Acta Cryst.* **1981**, *B37*, 2082.
(192) M.D. Coburn, D.G. Ott, *J. Heterocycl. Chem.* **1990**, *27*, 1941.
(193) J. Sauer, in : Comprehensive Heterocyclic Chemistry, Ch. 6.21
(194) S.F. Nelsen, Y. Kim, *J. Org. Chem.* **1991**, *56*, 1045.
(195) J.C.A. Boeyens, *J. Cryst. Molec. Struct.* **1978**, *8*, 317.
(196) J.D. Coates, L.A. Achenbach, *Nat. Rev. Microbiol.* **2004**, *2*, 569.
(197) a) M.J. Kamlet, NAVORD Report 6207, 14 Feb **1959**, Naval Surface Weapons Center. b) M.J. Kamlet, H.G. Adolph, *J. Org. Chem.* **1968**, *33*, 3073. c) V. Grakauskas, K. Baum, US Patent 3423419, **1969**. d) V. Grakauskas, K. Baum, *J. Org. Chem.* **1969**, *34*, 3927.
(198) a) T.M. Klapötke, C.M. Sabaté, *Chem. Mater.* **2008**, *20(11)*, 3629. b) C. Darwich, T.M. Klapötke, C.M. Sabaté, *Chem. Eur. J.* **2008**, *14*, 5756. c) J. Stierstorfer, T.M. Klapötke, A. Hammerl, B. Chapman, *Z. Anorg. Allg. Chem.* **2008**, *634*, 1051. d) M. Göbel, T.M. Klapötke, *Z. Anorg. Allg. Chem.* **2007**, *633(7)*, 1006. e) Y. Guo, H. Gao, B. Twamley, J.M. Shreeve, *Adv. Mat.* **2007**, *19*, 2884. f) M. Göbel, K. Karaghiosoff, T.M. Klapötke, *Angew. Chem. Int. Ed.* **2006**, *45(36)*, 6037. g) M. Hiskey, A. Hammerl, G. Holl, T.M.

Klapötke, K. Polborn, J. Stierstorfer, J.J. Weigand, *Chem. Mater.* **2005**, *17*, 3784. h) H. Xue, J.M. Shreeve, *Adv. Mat.* **2005**, *17*, 2142.

(199) J. Hine, W.C. Bailey, *J. Org. Chem.* **1961**, *26*, 2098.

(200) Th. N. Hall, *Tetrahedron* **1963**, *19(1)*, 115.

(201) I.B. Starchenkov, V.G. Andrianov, A.F. Mishnev, *Chemistry of Heterocyclic Compounds* **1997**, *33*, 216.

(202) A.B. Sheremetev, V.O. Kulagina, L.V. Batog, O.V. Lebedev, I.L. Yudin, T.S. Pivina, *Proceedings of the International Pyrotechnics Seminar* **1996**, *22*, 377.

(203) A.V. Kalinin, E.T. Apasov, Y.A. Strelenko, S.L. Ioffe, V.A. Tartakovsky, *Izvestiya Akademii Nauk, Seriya Khimicheskaya* **1993**, *4*, 736.

(204) a) R. Schenck; G.A. Wetterholm, *U.S. Pat. 2,731,460* (1956).
b) R. Schenck; G.A. Wetterholm, *Chem. Abstr.* **1956**, 50, 7125.

(205) A.A. Kozyro, V.V. Simirsky, A.P. Krasulin, V.M. Sevruk, G.J. Kabo, M.L. Gopanik, Y.V. Grigotiev, *Zh. Fiz. Khim.* **1990**, *64*, 656.

(206) A. Gao, Y. Oyumi, T.B. Brill, *Combust. Flame* **1991**, *83*, 345.

(207) D. Moderhack, K.H. Goos, L. Preu, *Chem. Ber.* **1990**, *123*, 1575.

(208) N.N. Makhova, A.B. Sheremetev, I.V. Ovchinnikov, I.L. Yudin, A.S. Ermakov, P.V. Bulatov, D.B. Vinogradov, D.B. Lempert, G.B. Manelis, *International Annual Conference of ICT* **2004**, 140/1.

(209) X.X. Zhou, Y.Z. YU, *Kogyo-kayaku* **1991**, *52(4)*, 251.

(210) T.P. Russell, T.M. Allen, Y.M. Gupta, *Chem. Phys. Lett.* **1997**, *267*, 351.

(211) R. Gilardi, C. George, J. L. Flipper-Anderson, *Acta Cryst.* **1988**, *C44*, 1686.

(212) M.D. Coburn, D.G. Ott, *J. Heterocycl. Chem.* **1990**, *27*, 1941.

(213) Ger. Pat. 934 694, 1955; *Chem. Abstr.* **1959**, *53*, 17513b.

(214) I.V. Ovchinnikov, A.S. Kulikov, M.A. Epishina, N.N. Makhova, V.A. Tartakovsky, *Russ. Chem. Bull.* **2005**, *54*, 1346.

(215) N.K. Sundholm, T.C. Richards, D.L. Schoene, Naugatuch Chem Div, US Rubber Co, Progress Report (15 Feb. 1950 to 15 Apr. 1950), NORD 10121, p.4.

(216) J.M. Dyke, G. Levita, A. Morris, J.S. Ogden, A.A. Dias, M. Algarra, J.P. Santos, M.L. Costa, P. Rodrigues, M.M. Andrade, M.T. Barros, *Chem. Eur. J.* **2005**, *11*, 1665.

(217) R.C. Farmer, *J. Chem. Soc.* **1920**, 1603.

(218) C.N. Hinshelwood, *J. Chem. Soc.* **1921**, 721.

(219) J.M. Rosen, J.C. Dacons, NOLTR 62-192, 15 Nov 1962, Naval Surface Weapons Center.

(220) Y.A. Lebedev, E.A. Miroshnichenko, Y.K. Knobel, *Termokhimiya nitrosoedinenii (Thermochemistry of nitrocompounds)* **1970**, 168.

(221) G.A. Petersson, T.G. Tensfeldt, J.A. Montgomery, Jr., *J. Chem. Phys.* **1991**, *94*, 6091.

(222) J.W. Ochterski, G.A. Petersson, J.A. Montgomery, Jr., *J. Chem. Phys.* **1996**, *104*, 2598.

(223) J.A. Montgomery, Jr., M.J. Frisch, J.W. Ochterski, G.A. Petersson, *J. Chem. Phys.* **2000,** 112, 6532.

(224) L.A. Curtiss, K. Raghavachari, P.C. Redfern, J.A. Pople, *J. Chem. Phys.* **1997**, *106(3)*, 1063.

(225) M.S. Westwell; M.S. Searle; D.J. Wales; D. II. Williams, *J. Am. Chem. Soc.* **1995**, *117*, 5013.

(226) J. Chao, F.D. Rossini, *J. Chem. Eng. Data* **1965**, *10*, 374.

(227) N.D. Lebedeva, V.L. Ryadnenko, I.N. Kuznetsova, *Russ. J. Phys. Chem. (Engl. Transl.)* **1968**, *42*, 962.

(228) C. Lenchitz, R.W. Velicky, G. Silvestro, L.P. Schlosberg, *J. Chem. Thermodyn.* **1971**, *3*, 689.

(229) V.I. Pepekin, Y.N. Matyushin, Y.A. Lebedev, Thermochemistry of N-nitro- and N-nitrosoamines of the alicyclic series, Bull. Acad. Sci. USSR, Div. Chem. Sci. **1974**, 1707.

(230) G. Krien, H.H. Licht, J. Zierath, *Thermochim. Acta* **1973**, *6*, 465.

(231) R.L. Simpson, P.A. Urtiew, D.L. Ornellas, G.L. Moody, K.J.Scribner, D.M. Hoffman, *Propellants, Explos., Pyrotech.* **1997**, 22, 249.

(232) V.A. Ostrovskii, M.S. Pevzner, T.P. Kofman, I.V. Tselinskii, *Targets Heterocycl. Syst.* **1999** , *3*, 467.

(233) M.F. Cheng, H.O. Ho, C.S. Lam, S. Chow, C.S. Li, *J. Serb. Chem. Soc.* **2002**, *67(4)*, 257.

(234) M. Göbel, T.M. Klapötke, *Acta Cryst.* **2007**, *C63*, o562.

(235) M. Göbel, T. M. Klapötke, *Acta Cryst.* **2008**, *C64*, o58.

(236) J. Köhler, R. Meyer, A. Homburg, *Explosivstoffe*, 10th ed. 2008, Wiley VCH, Weinheim.

(237) M. Sućeska, *Propellants, Explos., Pyrotech.* **1991**, *16*, 197.

(238) M. Sućeska, *Proc. of 30th Int. Annual Conference of ICT*, June 29 – July 2, Karlsruhe, Germany, **1999**, 50.

(239) M. Sućeska, *Propellants, Explos., Pyrotech.* **1999**, *24*, 280.

(240) M. Sućeska, *Proc. of 32nd Int. Annual Conference of ICT*, July 3-6, Karlsruhe, Germany, **2001**, 110.

(241) M. Sućeska, *Materials Science Forum* **2004**, *465*, 325.

(242) M.L. Hobbs, M.R. Baer, *Calibration of the BKW-EOS With a Large product Species Data Base and Measured C-J Properties, Proc. of the 10th Symp. (International) on Detonation*, ONR 33395-12, Boston, MA, July 12-16 1993, p. 409.

(243) EG A.14: Prüfverfahren nach Anhang I Teil A.14 der Richtlinie 92/69/EWG der Kommission vom 31. Juli 1992 zur Siebzehnten Anpassung der Richtlinie 67/548/EWG zur Angleichung der Rechts- und Verwaltungsvorschriften für die Einstufung, Verpackung und Kennzeichnung gefährlicher Stoffe an den technischen Fortschritt (ABI. EG Nr. L 383 S. 113 und Nr. L 383 A S. 1 (S. 87)) as well as

Recommendations on the Transport of Dangerous Goods: Tests and criteria, 1990, United Nations, New York.

(244) A. Bondi, *J. Phys. Chem.* **1964**, *68*, 441.

(245) H.E. Ungnade, L.W. Kissinger, *Tetrahdron* **1963**,*19*, 121.

(246) R.D. Shannon, *Acta Cryst.* **1976**, *A32*, 751.

(247) M.D. Lind, *Acta Cryst.* **1970**, *B26*, 590.

(248) F.H. Allen, J.P.M. Lommerse, V.J. Hoy, J.A.K. Howard, G.R. Desiraju, *Acta Cryst.* **1997**, *B53*, 1006.

(249) J.P.M. Lommerse, A.J. Stone, R. Taylor, F.H. Allen, *J. Am. Chem. Soc.* **1996**, *118*, 3108.

(250) F.H. Allen, C.A. Baalham, J.P.M. Lommerse, P.R. Raithby, *Acta Cryst.* **1998**, *B54*, 320.

(251) I.B. Starchenkov, V.G. Andrianov, A.F. Mishnev, *Chemistry of Heterocyclic Compounds* **1997**, *33*, 216.

(252) A.B. Sheremetev, V.O. Kulagina, L.V. Batog, O.V. Lebedev, I.L. Yudin, T.S. Pivina, *Proceedings of the International Pyrotechnics Seminar* **1996**, *22*, 377.

(253) A.V. Kalinin, E.T. Apasov, Y.A. Strelenko, S.L. Ioffe, V.A. Tartakovsky, *Izvestiya Akademii Nauk, Seriya Khimicheskaya* **1993**, *4*, 736.

(254) R.L. Collin, W.N. Lipscomb, *Acta Cryst.* **1951**, *4*, 10.

(255) K.H. Linke, H.G. Kalker, *Z. Anorg. Allg. Chem.* **1977**, *434* , 165.

(256) A. Héroux, F. Brisse, *Acta Cryst.* **1997**, *C53*, 1318.

(257) *Holleman-Wiberg, Lehrbuch der Anorganischen Chemie*, 102nd ed., Walther de Gruyter, Berlin, New York, **2007**, p.2006.

(258) R. Goddard, O. Heinemann, C. Kruger, *Acta Cryst.* **1997**, *C53*, 590.

(259) C. Krieger, H. Fischer, F.A. Neugebauer, *Acta Cryst.* **1987**, *C43*, 1320.

(260) M.E. Hill, US Patent 3.375.266, 1956.

(261) T.N. Hall, *J. Org. Chem.* **1968**, *33*, 4557.

(262) F.H. Allen, *Acta Cryst.* **2002**, *B58*, 380.

(263) *Holleman-Wiberg, Lehrbuch der Anorganischen Chemie*, 101st ed., de Gruyter, Berlin **1995**, p. 504.

(264) P. Geißler, T.M. Klapötke, H.J. Kroth, *Spectrochim. Acta* **1995**, *Part A*, *51A*, 1075.

(265) F.H. Allen, *Acta Cryst.* **2002**, *B58*, 380.

(266) A. Héroux, F. Brisse, *Acta Cryst.* **1997**, *C53*, 1318.

(267) F.H. Allen, *Acta Cryst.* **2002**, *B58*, 380.

(268) M. Göbel, T.M. Klapötke, *Adv. Funct. Mater.* **2009**, *19*, 347.

(269) F.H. Allen, O. Kennard, *Chem. Des. Autom. News* **1993**, *8*, 31.

(270) C.P. Butts, L. Eberson, K.L. Fulton, M.P. Hartshorn, W.T. Robinson, D.J. Timmerman-Vaughan, *Acta Chem. Scand.* **1996**, *50*, 991.

(271) Adolf, **1996**, private communication to the Cambridge Structural Database, refcode NABMIM.

(272) Y. Oyumi, A.L. Rheingold, T.B. Brill, *Propellants, Explos., Pyrotech.* **1987**, *12*, 46.

(273) S.K. Bhattacharjee, H.L. Ammon, *Acta Crystallogr.* **1982**, *B38*, 2503.

(274) T.M. Klapötke, B. Krumm, M. Scherr, G. Spieß, F.X. Steemann, *Z. Anorg. Allg. Chem.* **2008**, *634*, 1244.

(275) Y. Oyumi, T. B. Brill, A.L. Rheingold, *J. Phys. Chem.* **1985**, *89*, 4824.

(276) L.O. Atovmyan, N.I. Golovina, L.T. Eremenko, N.G. Zhitomirskaya, G.V. Oreshko, M.A. Fadeev, *Izv. Akad. Nauk SSSR, Ser. Khim. (Russ.) (Russ. Chem. Bull.)* **1984**, 549.

(277) N.I. Golovina, L.O. Atovmyan, N.V. Chukanov, G.V. Oreshko, R.F. Trofimova, M.A. Fadeev, L.T. Eremenko, *Zh. Strukt. Khim. (Russ.) (J. Struct. Chem.)* **1990**, *31*, 126.

(278) L.O. Atovmyan, R.G. Gafurov, N.I. Golovina, L.T. Eremenko, B.S. Fedorov, *Zh. Strukt. Khim. (Russ.)(J. Stuct. Chem.)* **1980**, *21*, 135.

(279) L.T. Eremenko, L.O. Atovmyan, N.I. Golovina, G.V. Oreshko, M.A. Fadeev, *Chem. Commun.* **1984**, 709.

(280) C. Jinhua, M. Shaoping, Z. Xiaotong, *Jiegou Huaxue (Chin.) (Chinese J. Struct. Chem.)* **1983**, *2*, 41.

(281) S.K. Bhattacharjee, H.L. Ammon, *Acta Crystallogr.* **1981**, *B37*, 2082.

(282) M.J.Frisch, G.W. Trucks, H.B. Schlegel, G.E. Scuseria, M.A.Robb, J.R. Cheeseman, J.A. Montgomery Jr., T. Vreven, K.N.Kudin, J.C. Burant, J.M. Millam, S.S. Iyengar, J. Tomasi, V. Barone, B. Mennucci, M. Cossi, G. Scalmani, N. Rega, G.A.Petersson, H. Nakatsuji, M. Hada, M. Ehara, K. Toyota, R. Fukuda, J. Hasegawa, M. Ishida, T. Nakajima, Y. Honda, O. Kitao, H. Nakai, M. Klene, X. Li, J.E. Knox, H.P. Hratchian, J.B. Cross, V. Bakken, C. Adamo, J. Jaramillo, R. Gomperts, R.E. Stratmann, O.Yazyev, A.J. Austin, R. Cammi, C. Pomelli, J.W. Ochterski, P.Y.Ayala, K. Morokuma, G.A. Voth, P. Salvador, J.J. Dannenberg, V.G.Zakrzewski, S. Dapprich, A.D. Daniels, M.C. Strain, O. Farkas, D.K. Malick, A.D. Rabuck K. Raghavachari, J.B. Foresman, J.V. Ortiz, Q. Cui, A.G. Baboul, S. Clifford, J. Cioslowski, B.B. Stefanov, G. Liu, A. Liashenko, P. Piskorz, I. Komaromi, R.L. Martin, D.J. Fox, T. Keith, M.A. Al-Laham, C.Y.Peng, A. Nanayakkara, M. Challacombe, P.M.W. Gill, B. Johnson, W. Chen, M.W. Wong, C. Gonzalez, J.A. Pople. Gaussian 03, Revision D.01. Gaussian, Inc Wallingford CT. 2004.

(283) CrysAlis CCD, Oxford Diffraction Ltd., Version 1.171.27p5 beta (release 01-04-2005 CrysAlis171.NET.

(284) CrysAlis RED, Oxford Diffraction Ltd., Version 1.171.27p5 beta (release 01-04-2005 CrysAlis171.NET.

(285) A. Altomare, G. Cascarano, C. Giacovazzo, A. Guagliardi, *J. Appl. Crystallogr.* **1993**, *26*, 343.

(286) G.M. Sheldrick, SHELXL-97, University of Göttingen, **1997**.

(287) L.J. Farrugia, *J. Appl. Crystallogr.* **1999**, *32*, 837.

(288) A.L. Spek, Platon, Utrecht University, Utrecht, The Netherlands, 1999.

(289) NATO standardization agreement (STANAG) on explosives, impact sensitivity tests, no. 4489, Ed. 1, Sept. 17, 1999.

(290) WIWEB-Standardarbeitsanweisung 4-5.1.02, Ermittlung der Explosionsgefährlichkeit, hier der Schlagempfindlichkeit mit dem Fallhammer, Nov. 8, 2002.
(291) NATO standardization agreement (STANAG) on explosives, friction sensitivity tests, no. 4487, Ed. 1, Aug. 22, 2002.
(292) WIWEB-Standardarbeitsanweisung 4-5.1.03, Ermittlung der Explosionsgefährlichkeit oder der Reibeempfindlichkeit mit dem Reibeapparat, Nov. 8, 2002.
(293) R.C. West, S.M. Selby, *Handbook of Chemistry and Physics*, The Chemical Rubber Co., Cleveland, 1967, 48th edn, p. D22.
(294) N.S. Marans, R.P. Zelinski, *J. Am. Chem. Soc.* **1950**, *72*, 5329.
(295) H. Feuer, T.J. Kucera, *J. Org. Chem.* **1960**, *25*, 2069.
(296) K.G. Ship, M.E. Hill, NAVORD 6752, 1960.
(297) W.J. Murray, C.W. Sauer, US Patent 3.006.957, 1957; *Chem. Abstr.* **1962**, 56, 2330c.
(298) H.E. Ungnade, L.W. Kissinger, *Tetrahedron* **1963**, *19*, 121.
(299) M.D. Coburn, D.G. Ott, *J. Heterocycl. Chem.* **1990**, *27*, 1941.
(300) M.E. Hill, *Preparation and Properties of Bis(Trinitroethyl)Carbonate*, NAVORD 3656 (1953).
(301) M.E. Hill, Development of the Synthesis of Bis(Trinitroethyl)Carbonate, BTNEC, A New Oxygen Rich High Explosive, NAVORD 3469 (1955).
(302) W.H. Gilligan, S.L. Stafford, *Synthesis* **1979**, *8*, 600.
(303) J.M. Welch, *Dissertation*, Ludwig-Maximilan Univ., **2008**.
(304) M.J. Crawford, J. Evers, M. Göbel, T.M. Klapötke, P. Mayer, G. Oehlinger, J.M. Welch, *Propellants, Explos., Pyrotech.* **2007**, *32(6)*, 478.
(305) M. Göbel, T.M. Klapötke, *Z. Anorg. Allg. Chem.* **2007**, *633(7)*, 1006.
(306) A.T. Mixon, J. Cioslowski, *J. Am. Chem. Soc.* **1991**, *113*, 6760.
(307) J. Cioslowski, S.T. Mixon, E.D. Fleischmann, *J. Am. Chem. Soc.* **1991**, *113*, 4751.
(308) M.A. Pietsch, M.B. Hall, *J. Phys. Chem.* **1994**, *98*, 11373.
(309) K.Y. Mathews, D.W. Ball, *J. Mol. Struct. (Theochem)* **2009**, *90(2)*, 15-20.
(310) S.J. Angyal, W.K. Warburton, *J. Chem. Soc.* **1951**, 2492.
(311) R.W. Alder, M.R. Bryce, N.C. Goode, N. Miller, J. Owen, *J. Chem. Soc., Perkin Trans. 1* **1981**, 2840.
(312) H.A. Staab, T. Saupe, *Angew. Chem.* **1988**, *100*, 895; *Angew. Chem., Int. Ed. Engl.* **1988**, *27*, 865.
(313) L. Pauling, *The Nature of the Chemical Bond*, 3rd ed.; Cornell University Press: Ithaca, NY, 1960, p.286.
(314) P. Gund, *J. Chem. Educ.* **1972**, *49*, 100.
(315) P. Kollman, J. McKelvey, P. Gund, *J. Am. Chem. Soc.* **1975**, *97*, 1640.
(316) J.F. Capitani, L. Pedersen, *Chem. Phys. Lett.* **1978**, *54*, 547.
(317) A.M. Sapse, L.J. Massa, *J. Org. Chem.* **1980**, *45*, 719.

(318) T. Ohwada, A. Itai, T. Ohta, K. Shudo, *J. Am. Chem. Soc.* **1987**, *109*, 7036.
(319) N. Sreerama, S. Vishveshwara, *J. Mol. Struct.* **1989**, *194*, 61.
(320) M. L. Williams, J. E. Gready, *J. Comput. Chem.* **1989**, *10*, 35.
(321) K. B. Wiberg, *J. Am. Chem. Soc.* **1990**, *112*, 4177.
(322) A. Gobbi, G. Frenking, *J. Am. Chem. Soc.* **1993**, *115*, 2362.
(323) N. de Vries, C. E. Costello, A.G. Jones and A. Davidson, *Inorg. Chem.* **1990**, *29*, 1348.
(324) W.P. Fehlhammer, R. Metzner and W. Sperber, *Chem. Ber.* **1994**, *127*, 829.
(325) P.J. Bailey, K.J. Grant, S. Pace, S. Parsons and L.J. Stewart, *J. Chem. Soc., Dalton Trans.* **1997**, 4263.
(326) H.J. Kabbe, K. Eiter, F. Möller, *Liebigs Ann. Chem.* **1967**, *704*, 140.
(327) M. Becker, M. Jansen, *Acta Crystallogr.* **1999**, *C55*, IUC 9900094.
(328) A. Gobbi, G. Frenking, *J. Am. Chem. Soc.* **1993**, *115*, 2362.
(329) V.A. Ostrovskii, G.I. Koldobskii, R.E. Trifonov, in: Comprehensive Heterocyclic Chemistry, 2008, Ch. 6.07, 257.
(330) F.R. Benson, in: Heterocyclic Compounds, R.C. Elderfield (Ed.), Wiley, New York, 1967, Vol. 8, p.8.
(331) A. Hammerl, *Dissertation*, Ludwig-Maximilan Univ., Munich 2001.
(332) J.J. Weigand, *Dissertation*, Ludwig-Maximilan Univ., Munich 2005.
(333) J. Stierstorfer, *Dissertation*, Ludwig-Maximilan Univ., Munich 2009.
(334) P. Cmoch, L. Stefaniak, E. Melzer, S. Baloniak, G.A. Webb, *Magn.Reson.Chem.* **1999,** *37*, 493.
(335) J. Benito, Ernesto de Jesus, F. de la Mata, J. C. Flores, R. Gomez, Gomez-Sal, *J.Organomet.Chem.* **2002,** *664*, 258.
(336) R. M. Gauvin, C. Lorber, R. Choukroun, B. Donnadieu, J. Kress, *Eur.J.Inorg.Chem.* **2001,** 2337.
(337) Y. Hamada, Y. Yamamoto, H. Shimizu, *J.Organomet.Chem.* **1996,** *510*, 1.
(338) M. Schorr, W. Schmidt, *Phosphorus, Sulfur Silicon Relat. Elem.* **1992,** *68*, 25.
(339) W.Verboom, W.Visser, D.N.Reinhoudt, *Synthesis* **1981,** 807.
(340) U. Wannagat, H.Bürger, C.Krüger, J.Pump, *Z.Anorg.Allg.Chem.* **1963,** *321*, 208.
(341) A.S.Gordetsov, S.V.Zimina, L.N.Martynkova, E.M.Moseeva, S.E.Skobeleva, T.K.Postnikova, V.L.Tsvetkova, R.P.Zaharova, *Metalloorganicheskaya Khimiya* **1992,** *5*, 811.
(342) J. Benito, Ernesto de Jesus, F. de la Mata, J. C. Flores, R. Gomez, Gomez-Sal, *J.Organomet.Chem.* **2002,** *664*, 258.
(343) Y. Hamada, Y. Yamamoto, H. Shimizu, *J.Organomet.Chem.* **1996,** *510*, 1.
(344) R. M. Gauvin, C. Lorber, R. Choukroun, B. Donnadieu, J. Kress, *Eur.J.Inorg.Chem.* **2001,** 2337.
(345) U. Wannagat, H.Bürger, C.Krüger, J.Pump, *Z.Anorg.Allg.Chem.* **1963,** *321*, 208.

(346) A.S.Gordetsov, S.V.Zimina, L.N.Martynkova, E.M.Moseeva, S.E.Skobeleva, T.K.Postnikova, V.L.Tsvetkova, R.P.Zaharova, *Metalloorganicheskaya Khimiya* **1992,** *5*, 811.
(347) U. Wannagat, H.Bürger, C.Krüger, J.Pump, *Z.Anorg.Allg.Chem.* **1963,** *321*, 208.
(348) F. Brotzel, Y.C. Chu, H. Mayr, *J. Org. Chem.* **2007**, *72*, 3679.
(349) M. Schorr, W. Schmidt, *Phosphorus, Sulfur Silicon Relat. Elem.* **1992,** *68*, 25.
(350) J. Benito, Ernesto de Jesus, F. de la Mata, J. C. Flores, R. Gomez, Gomez-Sal, *J.Organomet.Chem.* **2002,** *664*, 258.
(351) W. Broser, W. Harrer, *Angew. Chem.* **1965**, *77*, 1139.
(352) E. Boston, R. Maggi, K. Friedrich, M. Schlos, *Eur. J. Inorg. Chem.* **2001**, 3985.
(353) M. Schorr, W. Schmidt, *Phosphorus, Sulfur Silicon Relat. Elem.* **1992,** *68*, 25.
(354) E. Boston, R. Maggi, K. Friedrich, M. Schlos, *Eur. J. Inorg. Chem.* **2001**, 3985.
(355) I. Gronde, N.W. Mitzel, *Z. Anorg. Allg. Chem.* **2009**, *635*, 1313.
(356) A.S. Lyakhov, P.N. Gaponik, S.V. Voitekhovich, *Acta Cryst.* **2001**, *C57*, 185.
(357) P.N. Gaponik, V.P. Karavai, *Khimiya Geterotsiklicheskikh Soedinenii* **1984**, *12*, 1683.
(358) R. N. Butler, *Adv .Heterocyclic Chem.*, **1977**, 21, 323.
(359) E. Cubero, M. Orozco, F. J. Luque, *J. Am. Chem. Soc.*, **1998**, 120, 4723.
(360) H. A. Dabbagh, W. Lwowski, *J. Org. Chem.*, **2000**, 65, 7284.
(361) V. P. Krivopalov, A. U. Denisov, U. V. Gaitlov, V. I. Mamatiuk, *Dokl. Akad. Nauk SSSR*, **1988**, 300, 115.
(362) S. Baloniak, A. A. Katrusiak, *Pol. J. Chem.*, **1994**, 68, 683.
(363) A. S. Katrusiak, M. Gdaniec, A. A. Katrusiak, *Pol. J. Chem.*, **1997**, 71, 488.
(364) Itai, Kamiya, *Chem. Pharm. Bull.* (Tokyo) **1963**, *11*, 348.
(365) R.D. Allan, J.R. Greenwood, T.W. Hambley, J.R. Hanrahan, D.E. Hibbs, S. Itani, H.W. Tran, P. Turner, *Org. Biomol. Chem.* **2004**, *2*, 1782.
(366) G. Pattison, G. Sandford, E.V.B. Wallace, D.S. Yufit, J.A.K. Howard, J.A. Christopher, D.D. Miller, *J. Heterocyclic Chem.* **2008**, *45*, 143.
(367) Itai, Kamiya, *Chem. Pharm. Bull.* (Tokyo) **1963**, *11*, 348.
(368) C.J. Pennino, B.F. Goodrich Company (New York), U.S. Patent 2.846.433, **1958**.
(369) A. Dooms-Goossens, K. De Boulle, J. Snauwaert, H. Degreef, *Contact Dermatitis* **1986**, *14*, 64.
(370) R. Mizzoni, P. E. Spoerri, *J. Am. Chem. Soc.* **1954**, *94*, 2201.
(371) P. Coad, R.A. Coad, S. Clough, J. Hyepock, R. Salisbury, C.Wilkins, *J. Org. Chem.* **1963**, *28*, 218.
(372) R.D. Chambers, J.A.H. MacBride, W.K.R. Musgrave, *J. Chem. Soc.* **1968**, 2116.
(373) P. Coad, R.A. Coad, S. Clough, J. Hyepock, R. Salisbury, C.Wilkins, *J. Org. Chem.* **1963**, *28*, 218.
(374) R. Schönbeck, E. Kloimstein, *Monatshefte für Chemie* **1968**, *99*, 15.
(375) F. Kurzer: „Fulminic Acid in the History of Organic Chemistry“, *J. Chem. Educ.* **2000**, *77*, 851.

(376) H. Wieland: „Die Knallsäure“, Sammlung Chemischer und Chemisch-Technischer Vorträge, Enke **1909**, Vol. *14*, p. 385.

(377) Ch. Grundmann, P. Grünanger: „The Nitrile Oxides“, Springer, Berlin **1971**.

(378) M. Winnewisser, B.P. Winnewisser: „Why it took 174 years to understand the structure of fulminic acid?“, *Chem. Listy* **1976**, *70*, 785.

(379) J.H. Teles, G. Maier, B.A. Hess, L.J. Schaad, M. Winnewisser, B. Winnewisser, *Chem. Ber.* **1989**, *122*, 753.

(380) N.H. Toftlund, *Dansk Kemi.* **1996**, *77*, 17; *Chem.Abstr.* **1997**, 121, 143725.

(381) F. Kurzer: „The Life and Work of Edward Charles Howard FRS“, Annals of Science **1999**, *56*, 113.

(382) E. Howard, *Philosophical Transactions R. Soc.* **1800**, *90* I, 204.

(383) For a review of Liebig's work on metal fulminates: W. Beck: „The First Chemical Achievements and Publications by Justus von Liebig (1803-1873) and Some Further Developments in Metal Fulminates and Related Areas of Chemistry“, *Eur. J. Inorg. Chem.* **2003**, 4275.

(384) J. Liebig, J.L. Gay-Lussac: „Analyse der Fulminate d'argent“, *Ann. Chim. Phys.* **1824**, *XXV*, 285; J. Liebig, J.L. Gay-Lussac: “Zerlegung des knallsauren Silberoxydes”, *Poggendorffs Annalen der Physik* **1824**, *1*, 87.

(385) R. Scholl, *Ber. Dtsch. Chem. Ges.* **1990**, *23*, 3509.

(386) I.U. Nef, *Ann. Chem.* **1894**, *280*, 264.

(387) L. Wöhler, *Ber. Dtsch. Chem. Ges.* **1905**, *38*, 1351; **1910**, *43*, 754.

(388) H. Wieland: „Die Knallsäure“, Sammlung Chemischer und Chemisch-Technischer Vorträge, Enke **1909**, Vol. *14*, p. 385.

(389) Berthelot, Vielle, *Comptes rendus* **1880**, 946.

(390) H. Wieland: „Die Knallsäure“, Sammlung Chemischer und Chemisch-Technischer Vorträge, Enke **1909**, Vol. *14*, p. 385.

(391) For Wieland's work on fulminic acid see: F. Klages, *Naturwissenschaften* **1942**, *30*, 351.

(392) R. Huisgen, M. Christl, *Angew. Chem.* **1967**, *79*, 471; *Angew. Chem. Int. Ed. Engl.* **1967**, *6*, 456; *Chem. Ber.* **1973**, *106*, 3291; M. Christl, R. Huisgen **1973**, *106*, 3345.

(393) Berthelot, Vielle, *Comptes rendus* **1880**, 946.

(394) H. Wieland, *Ber. Dtsch. Chem. Ges.* **1907**, *40*, 418; **1910**, *43*, 3362; also see: L.Wöhler, Ber. Dtsch. Chem. Ges. **1910**, 43, 754.

(395) R. Knoll, „Das Knallquecksilber und ähnliche Sprengstoffe“, A. Hartleben's Verlag, Wien und Leipzig **1908**.

(396) A. Nobel, *J. Soc. Arts* **1875**, *23*, 611.

(397) J. Boileau in „Explosives“, Ullmanns Encyclopedia of Industrial Chemistry **2003**, Wiley-Interscience.

(398) F.D. Miles, J. Chem. Soc. 1931, 2532; Strukturbericht Band II, 1928-1932, C. Hermann, O. Lohrmann, H. Philipp, Akademische Verlagsgesellschaft MBH Leipzig

1937, S. 880; H.G. Otto, Zeitschrift für das gesamte Schieß- und Sprengstoffwesen 1943, 38, 85.

(399) A. Suzuki, *J. Ind. Explosives Soc.* Japan **1953**, *14*, 142; *Chem. Abstr.* **1955**, *49*, 58514; Z. Iqbal, A.D. Yoffe, *Proc. Roy. Acad. Soc.* **1967**, *302*, 48.

(400) F.D. Miles, *J. Chem. Soc.* **1931**, 2532; *Strukturbericht Band II*, 1928-1932, C. Hermann, O. Lohrmann, H. Philipp, Akademische Verlagsgesellschaft MBH Leipzig **1937**, S. 880; H.G. Otto, *Zeitschrift für das gesamte Schieß- und Sprengstoffwesen* **1943**, *38*, 85.

(401) *International Centre for Diffraction Data*, 12 campus Boulevard, Newton Square, PA, 19073-3273 USA, Powder Diffraction File Mercury Fulminate, 00-002-0287.

(402) M.E. Brown, G.M. Swallowe, *Thermochimica Acta* **1981,** *49*, 333.

(403) R.C. Seccombe, C.H.L. Kennard, *J. Organomet. Chem.* **1969**, *18*, 243; J. Hvoslef, *Acta. Chem. Scand.* **1958**, *12*, 1568; O. Reckeweg, A. Simon, *Z. Naturforsch.* **2002**, *57b*, 895.

(404) For a review of Liebig's work on metal fulminates: W. Beck: „The First Chemical Achievements and Publications by Justus von Liebig (1803-1873) and Some Further Developments in Metal Fulminates and Related Areas of Chemistry", *Eur. J. Inorg. Chem.* **2003**, 4275.

(405) J. Liebig: „Über das Knallsilber und das Knallquecksilber", Buchners Repertorium der Pharmacie **1823**, Vol. *XV*, p. 361; J. Liebig: „Über das Knall-Silber und Knall-Quecksilber und über ihre, und anderer Knall-Metalle wahre Natur", *Gilbert Annalen der Physik und Chemie* **1823**, Vol. *LXXV*, p. 393; J. Liebig: „Sur l'Argent et le Mercure fulminans", *Ann. Chim. Phys.* **1823**, *XXIV*, 294; presented by Gay-Lussac at the Royal Academy in Paris, Sept. **1823**.

(406) W. Beck, K. Feldl, *Angew. Chem.* **1966**, *78*, 746; *Angew. Chem. Int. Edn. Engl.* **1966**, *5*, 722; W. Beck, P. Swoboda, K. Feldl, R. S. Tobias, *Chem. Ber.* **1971**, *104*, 533.

(407) M. Winnewisser, H.K. Bodensch, *Z. Naturforsch.* **1967**, *22a*, 1724; M. Winnewisser, R. Schermaul, Berichte der Justus Liebig-Gesellschaft, Bd. 3, **1994**; G. Schulze, O. Koja, B.P. Winnewisser, M. Winnewisser, *J. Mol. Structure* **2000**, *307*, 517 and references therein.

(408) For a review of Liebig's work on metal fulminates: W. Beck: „The First Chemical Achievements and Publications by Justus von Liebig (1803-1873) and Some Further Developments in Metal Fulminates and Related Areas of Chemistry", *Eur. J. Inorg. Chem.* **2003**, 4275.

(409) W. Beck, *J. Organomet. Chem. Rev. Sect. A* **1971**, *7*, 159.

(410) D. Britton, J.D. Dunitz, *Acta Crystallogr.* **1965**, *19*, 662; J.C. Barrick, D. Canfield, B. C. Giessen, *Acta Crystallogr.* **1979**, *B35*, 464; D. Britton, *Acta Crystallogr.* **1991**, *C47*, 2646.

(411) W. Weigand, U. Nagel, W. Beck, *J. Organomet. Chem.* **1986**, *314*, C55.

(412) W.P. Bosman, W. Bos, J.M.M. Smits, P.T. Beurskens, J.J. Bour, J.J. Steggerda, *Inorg. Chem.* **1986**, *25*, 2093.

(413) W. Ponikwar, P. Mayer, H. Pietrowski, P. Swoboda, C.J. Oetker, W. Beck, *Z. Anorg. Allg. Chem.* **2002**, *628*, 15.
(414) W. Ponikwar, E. Schuierer, W. Beck, *Z. Anorg. Allg. Chem.* **2000**, *626*, 1282.
(415) P. Mayer, W. Ponikwar, P. Swoboda, W. Beck, *Z. Anorg. Allg. Chem.* **2000**, *626*, 2038.
(416) W. Beck, T.M. Klapötke, *Z. Naturforsch.* **2001**, *56b*, 1376.
(417) L. Türker, S. Erkoc, J. Mol. Structure: *THEOCHEM* **2004**, *712*, 139.
(418) J.R. Rodriguez-Carvajal, *FullProf, A Program for Rietveld Refinement and Pattern Matching Analysis*, Abstracts of the Satellite Meeting on Powder Diffraction of the XV Congress of the IUCR, p.127, Toulouse, France, **1990**.
(419) J.R. Rodriguez-Carvajal, *FullProf, A Program for Rietveld Refinement and Pattern Matching Analysis*, Abstracts of the Satellite Meeting on Powder Diffraction of the XV Congress of the IUCR, p.127, Toulouse, France, **1990**, p. 1839.
(420) P. Nockemann, U. Cremer, U. Ruschewitz and G. Meyer, *Z. Anorg. Allg. Chem.* **2003**, *629*, 2079.
(421) F.D. Miles, *J. Chem. Soc.* **1931**, 2532; *Strukturbericht Band II*, 1928-1932, C. Hermann, O. Lohrmann, H. Philipp, Akademische Verlagsgesellschaft MBH Leipzig **1937**, S. 880; H.G. Otto, *Zeitschrift für das gesamte Schieß- und Sprengstoffwesen* **1943**, *38*, 85.
(422) G.M. Sheldrick, SHELXS-97, University of Göttingen, Germany, **1997**.
(423) *Holleman-Wiberg, Lehrbuch der Anorganischen Chemie*, 101st ed., de Gruyter, Berlin **1995**, p.1842.
(424) For a review of Liebig's work on metal fulminates: W. Beck: „The First Chemical Achievements and Publications by Justus von Liebig (1803-1873) and Some Further Developments in Metal Fulminates and Related Areas of Chemistry", *Eur. J. Inorg. Chem.* **2003**, 4275.
(425) W.P. Bosman, W. Bos, J.M.M. Smits, P.T. Beurskens, J.J. Bour, J.J. Steggerda, *Inorg. Chem.* **1986**, *25*, 2093.
(426) U. Nagel, K. Peters, H. G. von Schnering, W. Beck, *J. Organomet. Chem.* **1980**, *185*, 427.
(427) W. Ponikwar, P. Mayer, H. Pietrowski, P. Swoboda, C.J. Oetker, W. Beck, *Z. Anorg. Allg. Chem.* **2002**, *628*, 15.
(428) P. Mayer, W. Ponikwar, P. Swoboda, W. Beck, *Z. Anorg. Allg. Chem.* **2000**, *626*, 2038.
(429) P. Klüfers, H. Fuess, S. Haussühl, *Z. Kristallogr.* **1981**, *156*, 255.
(430) R.L DeKock, E.J. Baerends., *J. Am. Chem. Soc.* **1984**, *106*, 3387.
(431) *Holleman-Wiberg, Lehrbuch der Anorganischen Chemie*, N. Wiberg, Walther de Gruyter, Berlin, New York, **1995**, p.1842.
(432) U. Müller, *Z. Anorg. Allg. Chem.* **1973**, *399*, 183.
(433) Houben-Weyl, Methoden der Organischen Chemie, Vol. VIII, Thieme, Stuttgart **1952**, p. 355; E. Beckmann, *Ber. Dtsch. Chem. Ges.* **1886**, *19*, 993.

(434) F.D. Miles, *J. Chem. Soc.* **1931**, 2532; *Strukturbericht Band II*, 1928-1932, C. Hermann, O. Lohrmann, H. Philipp, Akademische Verlagsgesellschaft MBH Leipzig **1937**, S. 880; H.G. Otto, *Zeitschrift für das gesamte Schieß- und Sprengstoffwesen* **1943**, *38*, 85.

(435) a) Horstmann, S.; Irran, E.; Schnick, W., *Angew. Chem. Int. Ed.* **1997**, *36(17)*, 1873. b) K. Landskron, H. Huppertz, J. Senker, W. Schnick, *Angew. Chem.* **2001**, *113*, 2713; *Angew. Chem. Int. Ed.* **2001**, *40*, 2643.

(436) E.H. Kober, H.F. Lederle, G.F. Ottmann, USA Patent US 32918645 **1966**.

(437) X. Zeng, W. Wang, F. Liu, M. Ge, Z. Sun, D. Wang, *European Journal of Inorganic Chemistry* **2006**, *(2)*, 416.

(438) P. Volgnandt, A. Schmidt, *Z. Anorg. Allg. Chem.* **1976**, *425(2)*, 189.
The authors state that phosphorus pentachloride reacts with excess of sodium azide not to phosphorus pentaazide as reported earlier, but to sodium hexaazidophosphate.

(439) Ch. Grundmann, R. Rätz, *Z. Naturforschg.* **1954**, *10b*, 116.

(440) F. Räuchle, M. Gayoso, *Annales de Fisica* **1970**, *66*, 241.

(441) J. Müller, H. Schröder, *Z. Anorg. Allg. Chem.* **1979**, *450*, 149.

(442) R. Haiges, S. Schneider, T. Schroer, K.O. Christe, *Angew. Chem. Int. Edn.* **2004,** *43(37)*, 4919.

(443) I.C. Tornieporth-Oetting, T.M. Klapötke, *Angew. Chem.* **1995**, *107*, 559; *Angew. Chem. Int. Edn. Engl.* **1995**, *34*, 511.

(444) T.M. Klapötke, *Chem. Ber.* **1997**, *130*, 443.

(445) I.C. Tornieporth-Oetting, T.M. Klapötke in *Combustion Efficiency and Air Quality*, (Hrsg.: I. Hargittai, T. Vidoczy), Plenum Press, New York, **1995**, S. 51.

(446) B. Thomas, G. Seifert, G. Großmann, *Z. Chem.* **1980**, *20*, 217.

(447) J.B. Foresman, A. Frisch, *Exploring Chemistry with Electronic Structure Methods*, 2nd Ed., Gaussian, Inc. ISBN 0-9636769-3-8, 64.

(448) G.J.Bullen, *Journal of the Chemical Society* **1971**, [Section] A: Inorganic, Physical, Theoretical, *(10)*, 1450.

(449) T. Urbański (Ed.), in: *Nitro Compounds* **1964**, Tetrahedron 20, Suppl. 1.

(450) L.A. Kaplan, in: The Chemistry of the Nitro and Nitroso Groups, Part 2. H. Feuer (Ed.) Wiley-Interscience, p. 289.

(451) T. Urbański, in: *Chemistry and Technology of Explosives* **1984**, Vol 4. Pergamon Press, New York, p. 245.

(452) Ger. Pat. 934 694, 1955; *Chem. Abstr.* **1959**, *53*, 17513b.

(453) J.S. Murray, P. Lane, M. Göbel, T.M. Klapötke, P. Politzer P, *J. Chem. Phys.* **2009**, *130*, 104304.

(454) H. Morrison, B.H. Migdalof, *J. Org. Chem.* **1965**, *30*, 3996.

(455) A.T. Nielsen, in: The Chemistry of the Nitro and Nitroso Groups, Part 1, H. Feuer, (Ed.), Wiley-Interscience, New York, 1969, ch. 7.

(456) S. Patai, (Ed.), The Chemistry of Amine, Nitroso and Nitro Compounds and Their Derivatives, Wiley, New York, 1982.

(457) M.L. McKee, *J. Am. Chem. Soc.* **1986**, *108*, 5784.
(458) P.V. Bharatam, K. Lammertsma, in: Energetic Materials. Part 1. Decomposition, Crystal and Molecular Properties, P. Politzer, J.S. Murray, (Eds.), Elsevier, Amsterdam, 2003, ch. 3.
(459) M.J. Kamlet, H.G. Adolph, *Propell. Explos.* **1979**, *4*, 30.
(460) R. Engelke, W.L. Earl, C.M. Rohlfing, *J. Chem. Phys.* **1986**, *84*, 142.
(461) P. Politzer, J.M. Seminario, A.G. Zacarías, *Mol. Phys.* 1996, **89**, 1511.
(462) J.S. Murray, P. Lane, M. Göbel, T.M. Klapötke, P. Politzer, *Theor. Chem. Acc.* **2009**, DOI 10.1007/s00214-009-0620-2.
(463) A.T. Nielsen, in: The Chemistry of the Nitro and Nitroso Groups, Part 1, H. Feuer, (Ed.), Wiley-Interscience, New York, 1969, ch. 7.
(464) L.W. Andrew, D.L. Hammick, *J. Chem. Soc.* **1934**, 244.
(465) S.S. Novikov, V.I. Slovetskii, V.A. Tartakovskii, S.A. Shevelev, A.A. Fainzil'berg, *Dokl. Akad. Nauk SSSR* **1962**, *146*, 104; *Chem. Abstr.* **1963**, *58*, 3289.
(466) R. Hoffmann, H. Hopf, *Angew. Chem. Int. Ed.* **2008**, *47*, 4474.
(467) A.J. Stone, *Science* **2008**, *321*, 787.
(468) P. Metrangolo, F. Meyer, T. Pilati, G. Resnati, G. Terraneo, *Angew. Chem. Int. Edn.* **2008**, *47*, 6114.
(469) P. Metrangolo, G. Resnati, *Science* **2008**, *321*, 918.
(470) L. Birckenbach, K. Huttner, W. Stein, *Chem. Ber.* **1929**, *62*, 2065.
(471) V.I. Pepkin, Yu.N. Matyushin, G.Kh. Khisamutdinov, V.I. Slovetskii, A.A. Fainzil'berg, *Khimicheskaya Fizika* **1993**, *12*, 1399.
(472) G.Kh. Khisamutdinov, V.I. Slovetsky, M.Yu. Golub, S.A. Shevelev, A.A. Fainzil'berg, *Russ. Chem. Bull.* **1997**, *46*, 324.
(473) C.O. Parker, W.E. Emmons, H.A. Rolewicz, K.S. McCallum,*Tetrahedron* **1962**, *17*, 79.
(474) A.K. Macbeth, D.D. Pratt, *J. Chem. Soc.* **1921**, *119*, 354.
(475) W. Will, *Chem. Ber.* **1914**, *47*, 961.
(476) D.V. Levchenkov, A.B. Kharitonkin, V.A. Shlyapochnikov, *Russ. Chem. Bull.* **2001**, *50*, 385.
(477) V.A. Shlyapochnikov, D.V. Levchenkov, A.B. Kharitonkin, *Russ. Chem. Bull.* **2001**, *50*, 1173.
(478) S.G. Vulfson, A.P. Timosheva, A.N. Vereshchagin, B.A. Arbuzov, *J. Mol. Struct.* **1977**, *40*, 225.
(479) V.A. Shlyapochnikov, A.A. Fainzil'berg, S.S. Novikov, *Izvestiya Akademii Nauk SSSR* **1961**, *3*, 519.
(480) N.I. Sadova, N.I. Popik, L.V. Vilkov, Ju.A. Pankrushev, V.A. Shlyapochnikov, *Chem. Commun.* **1973**, *19*, 708.
(481) N.I. Sadova, N.I. Popik, L.V. Vilkov, *Zhurnal Strukturnoi Khimii* **1976**, *17*, 298.
(482) J. Demaison, G. Wlodarczak, H.D. Rudolph, In *Advances in Molecular Structure Research*, Vol. 3; Hargittai, I.; Hargittai, M., Eds.; JAI Press: Greenwich, **1997**, 1.

(483) J. Demaison, L. Margulès, J.E. Boggs, *Struct. Chem.* **2003**, *14*, 159.
(484) A.N. Shidlovskaya, Ya.K. Syrkin, S.S. Novikov, A.A. Fainzil'berg, V.V. Sevost'yanova, V.I. Gulevskaya, *Dokl. Akad. Nauk SSSR* **1960**, *132*, 1367.
(485) T.E. Levow, Union Carbide Corporation. Novel organofunctional silicon compounds Substituted with Halogen and Process for making same. US Patent 3694480, **1972**.
(486) M.I. Dakhis, A.A. Levin, V.A. Shlyapochnikov, *Zhurnal Strukturnoi Khimii* **1971**, *14*, 162.
(487) J.T. Larkins, J.M. Nicholson, F.E. Saalfeld, *Organic Mass Spectrometry* **1971**, *5*, 265.
(488) A.K. Macbeth, D.D. Pratt, *J. Chem. Soc.* **1921**, *119*, 354.
(489) M.F. Zimmer, E.E. Barcody, M. Schwartz, M.P. McAllister, *J. Chem. Eng. Data* **1964**, *9*, 527.
(490) A. Reed, P.v.R. Schleyer, *J. Am. Chem. Soc.* **1987**, *109*, 7362.
(491) A.E. Reed, L.A. Curtiss, F. Weinhold, *Chem. Rev.* **1988**, ***88***, 899.
(492) R.D. Harcourt, T.M. Klapötke, Pauling Three-electron bonds and increased valence structures as components of the "Intellectual Heritage" of Qualitative Valence Bond Theory *Research Trends* **9**, 11-22 (2006).
(493) J.R. Witt, D. Britton, C. Mahon, *Acta Crystallogr.* **1972**, *B28*, 950.
(494) D.R. Huntley, G. Markopoulos, P.M. Donovan, L.T. Scott, R. Hoffmann, *Angew. Chem. Int. Edn.* **2005**, *44*, 7549.
(495) V. Schomaker, D.R. Stevenson, *J. Am. Chem. Soc.* **1941**, *63*, 37.
(496) H.O. Pritchard, H.A. Skinner, *Chem. Rev.* **1955**, *55*, 745.
(497) L.P. Hammet, *Chem. Rev.* **1935**, *17*, 125.
(498) L.P. Hammet, *J. Am. Chem. Soc.* **1937**, *59*, 96.
(499) R.W. Taft, In: *Steric effects in organic chemistry*, ed. By Newman, M.S., Chapt. 13, Wiley, New York, **1956**.
(500) D. Datta, *J. Phys. Org. Chem.* **1991**, *4*, 96.
(501) J.E. Huheey, *J. Org. Chem.* **1966**, *31*, 2365.
(502) R.F. Stewart, *J. Chem. Phys.* **1972**, *57*, 1664.
(503) *Chemical applications of atomic and molecular electrostatic potentials* (1981) Politzer, P.; Truhlar, D.G. (eds) Plenum Press, New York.
(504) R.F.W. Bader, M.T. Carroll, J.R. Cheeseman, C. Chang, *J. Am. Chem. Soc.* **1987**, *109*, 7968.
(505) P. Politzer, P. Lane, M.C. Concha, Y. Ma, J.S. Murray, *J. Mol. Model.* **2007**, *13*, 305.
(506) J.S. Murray, P. Lane, P. Politzer, *J. Mol. Model.* **2009**, *15*, 723.
(507) T. Clark, M. Hennemann, J.S. Murray, P. Politzer, *J. Mol. Model.* **2007**, *13*, 291.
(508) P. Politzer, J.S. Murray, P. Lane, *Int. J. Quant. Chem.* **2007**, *107*, 3046.
(509) T. Di Paolo, C. Sandorfy, *Can. J. Chem.* **1974**, *52*, 3612.
(510) R.E. Rosenfield, Jr., R. Parthasarathy, J.D. Dunitz, *J. Am. Chem. Soc.* **1977**, *99*, 4860.
(511) P. Murray-Rust, W.D.S. Motherwell, *J. Am. Chem. Soc.* **1979**, *101*, 4374.

(512) P. Auffinger, F.A. Hays, E. Westhof, P. Shing Ho, *Proc. Nat. Acad. Sci. USA* **2004**, *101*, 16789.

(513) T. Brinck J.S. Murray, P. Politzer, *Int. J. Quant. Chem., Quantum Biol. Symp.* **1992**, *19*, 57.

(514) J.S. Murray, M.C. Concha, P. Lane, P. Hobza, P. Politzer, *J. Mol. Model.* **2008**, *14*, 699.

(515) W. Wang, N.B. Wang, W. Zheng, A. Tian, *J. Phys. Chem. A* **2004**, *108*, 1799.

(516) J. Hine, W.C. Bailey, Jr., *J. Org. Chem.* **1960**, *26*, 2098.

(517) A. Brändström, *J. Chem. Soc., Perkin Trans. 2* **1999**, 1855.

(518) L. Macaveiu, M. Göbel, T.M. Klapötke, J.S. Murray, P. Politzer, *Struct. Chem.* **2009**, *in press.*

(519) W. Caminati, E.B. Wilson, *J. Mol. Spectrosc.* **1980**, *81*, 507.

(520) M. Göbel, B.H. Tchitchanov, J.S. Murray, P. Politzer, T.M. Klapötke, *Nature Chem.* 2009, *1*, 229.

(521) C.B. Hübschle, P. Luger, *J. Appl. Cryst.* **2006**, *39*, 901.

(522) A.K. Macbeth, D.D. Pratt, *J. Chem. Soc.* **1921**, *119*, 354.